

Imperial College London
Department of Chemical Engineering

Iterative Synthesis of Uniform Poly(ethylene glycol) via Organic Solvent Nanofiltration

Marc Schaepertoens

First submitted September 2017

Revised June 2019

Supervised by Prof. Andrew G. Livingston

Submitted in part fulfilment of the requirements for the degree of Doctor of Philosophy

Copyright declaration

The copyright of this thesis rests with the author. Unless otherwise indicated, its contents are licensed under a Creative Commons Attribution-NonCommercial 4.0 International License (CC BY-NC 4.0).

Under this licence, you may copy and redistribute the material in any medium or format. You may also create and distribute modified versions of the work. This is on the condition that: you credit the author and do not use it, or any derivative works, for a commercial purpose.

When reusing or sharing this work, ensure you make the licence terms clear to others by naming the licence and linking to the licence text. Where a work has been adapted, you should indicate that the work has been changed and describe those changes.

Please seek permission from the copyright holder for uses of this work that are not included in this licence or permitted under UK Copyright Law.

Declaration of originality

The work contained in this thesis is my own, except where noted otherwise and all external sources are appropriately referenced. Where required, permission has been sought for use of external content (p. 411).

Please consult the Acknowledgements for details on materials provided by colleagues and the technical services used for analytical work.

Abstract

This thesis describes the synthesis of uniform, heterobifunctional poly(ethylene glycol) via organic solvent nanofiltration, a scalable and cost-effective membrane-based technology that allows reactions and purifications to be carried out in liquid medium throughout and provides access to oligomers of commercially relevant length. This membrane-based strategy contrasts with established routes via chromatography, extraction and solid phase synthesis.

The preparation of uniform oligomers relies on the stepwise addition of building blocks, one at a time, over many synthetic extension cycles. To ensure uniformity, the growing oligomer requires purification from excess building block and reaction debris after each extension. In this strategy, intermediate and final products en route to the desired poly(ethylene glycol) oligomer are freed from impurities by diafiltration.

In order to facilitate the removal of impurities during diafiltration, multiple oligomers are synchronously grown on a soluble, multivalent anchor. The attachment of multiple growing oligomers onto the anchor leads to a fast-growing product complex with enough size to be well-retained by a membrane. On the other hand, the separable impurities consisting of much smaller building block and reaction debris can readily pass through the membrane, resulting in an efficient separation. To enhance discrimination, the anchor is enlarged, and the size of the functional groups on the building block minimized. Further, the anchor is designed to be sufficiently distinct and readily detectable by UV.

A two-stage diafiltration process then allowed the synthesis of uniform, mono-methyl Eg_{60} (mPEG-2700) with excellent quality (dispersity $\mathcal{D} = 1.0006$, oligomer purity = 97 %) from an Eg_{12} building block in four chain extension cycles.

It is demonstrated that deprotection and purification may be accomplished jointly via nanofiltration with a poly(ether ether ketone) membrane that is sufficiently stable towards acidic deprotection conditions and that spent diafiltration solvent may be partially recovered by membrane-based solvent recovery in a closed loop.

Acknowledgements

The author is grateful for the guidance and teachings of Dr. Piers R. J. Gaffney, Dr. Jeong F. Kim, Dr. György Székely, Dr. Jerry Y. Y. Heng and Prof. Andrew G. Livingston.

For technical support, the author gratefully acknowledges Dr. Lisa Haigh (mass spectrometry), Peter R. Haycock (NMR), Dr. Andrew J. P. White (X-ray crystallography) (all Department of Chemistry, Imperial College London) as well as Dr. Mark F. Wyatt and the EPSRC UK National Mass Spectrometry Facility at Swansea University (high resolution mass spectrometry).

The poly(ether ether ketone) (PEEK) membranes used in this thesis were produced by João Da Silva Burgal. The poly(benzimidazole) (PBI) membranes were produced by Irina B. Valtcheva during the early stages of this work, and later by György Székely. An updated version of the PBI membrane was provided by Patrizia Marchetti, Piers R. J. Gaffney and Ruiyi Liu towards the end of the project.

Financial support was provided by the EPSRC under grant codes EP/K502856/1 (Doctoral Training Award for Marc Schaeperstoens) and EP/M003949/1 ("Iterative Synthesis with Organic Solvent Nanofiltration for Precision Manufacture of High Value Sequence-Controlled Polymers (ItSyN)"). The author thanks the Department of Chemical Engineering for the award of the DTA.

For their company and camaraderie, the author thanks the colleagues at the Livingston group, Pembroke Gardens, Volleyball and the Schäpertöns family.

Prof. Andrew G. Livingston and Dr. Piers R. J. Gaffney reviewed the thesis, Mahmood M. M. Abdulsalam Ebrahim contributed to proof-reading and Joshua J. May proof-read the final version. All remaining errors are my own.

Table of contents

Copyright declaration.....	2
Declaration of originality	3
Abstract.....	4
Acknowledgements	5
Table of contents.....	6
List of abbreviations and nomenclature	10
General abbreviations.....	10
Analytical abbreviations	10
Chemical nomenclature and abbreviations	11
Technical nomenclature	12
General introduction	13
1. Chapter 1: Iterative Synthesis of Uniform Poly(ethylene glycol).....	17
1.1. Introduction.....	17
Sequence-defined and uniform oligomers.....	19
Oligomers and polymers	20
1.1.1. Synthetic strategies towards sequence-defined oligomers.....	21
Strategies utilizing a protecting group.....	21
Protecting group-free strategies	24
1.1.2. Poly(ethylene glycol) as a model system	33
Applications of poly(ethylene glycol).....	33
Cost and benefit of disperse and uniform PEG	36
1.1.3. Synthesis of uniform poly(ethylene glycol)	38
Ether formation via Williamson ether synthesis.....	38
Side reactions of Williamson ether synthesis.....	38
1.1.4. Starting materials for uniform PEG synthesis	40
Indirect synthesis from lower homologues.....	40
Purity of Eg ₄ starting material	40
1.1.5. Chain extension strategies and growth mathematics	42
Unidirectional linear extension.....	44
Bidirectional linear extension	46
Chain doubling	51
Chain tripling	59
1.1.6. Examples of separation strategies for uniform oligomer synthesis	61
1.1.6.1. Chromatography as a separation technique.....	61
1.1.6.2. Extraction as a separation technique	62
1.1.6.3. Crystallization as a separation technique – a route via macrocyclic sulfates	65
1.1.7. The homostar approach.....	70

1.2.	Materials and methods.....	74
1.3.	Results and discussion	76
1.3.1.	Uniform PEG synthesis.....	79
1.3.1.1.	Building block preparation.....	79
1.3.1.2.	Hub attachment	81
1.3.1.3.	Chain extension cycles (extension and deprotection)	82
1.3.2.	Analysis of homostar purity via HPLC and MALDI-ToF	85
1.4.	Conclusion.....	89
2.	Chapter 2: Chain extension kinetics	91
2.1.	Introduction.....	91
2.2.	Materials and methods.....	92
2.2.1.	Methodology for chain extension reactions.....	92
2.2.2.	Reaction monitoring and sampling	92
2.2.3.	HPLC analysis.....	95
2.2.4.	Data processing	95
2.2.5.	Simulation of chain extension kinetics	100
2.2.6.	Mathematical description of the chain extension kinetics.....	102
2.3.	Results and discussion	103
2.3.1.	Extension from Eg_8 to Eg_{16}	103
2.3.2.	Summary of reaction parameters, reaction rate coefficients and analysis	113
2.3.3.	Potential improvements of the kinetic study	116
	Induction time and alkoxide formation	116
	Change in solvent composition and molarity.....	117
	Reaction rate and mechanism of dimer formation.....	118
	UV analysis and functional group contributions	119
2.4.	Conclusion.....	120
3.	Chapter 3: Utilizing membrane separation in the synthesis of monodisperse PEGs	121
3.1.	Introduction.....	121
3.1.1.	Comparison between solid phase synthesis and liquid phase synthesis.....	121
3.1.2.	Utilizing nanofiltration in the synthesis of uniform, sequence-defined oligomers.....	123
3.1.3.	The membrane filtration spectrum and transport phenomena	127
	Organic solvent nanofiltration	129
	The solution-diffusion model.....	129
	Membrane parameters and characterization	131
	Concentration polarization	132
3.1.4.	Membrane processes	135
	Mathematical description of diafiltration	137
3.1.5.	Improving membrane process performance.....	139
	Membrane performance	139

Process configuration	143
Tuning molecular architecture	144
3.2. Materials and methods.....	146
3.2.1. Membrane preparation.....	146
Poly(ether ether ketone) membranes	146
Polybenzimidazole membranes.....	146
Membrane installation	147
3.2.2. Membrane screening	148
3.2.3. Diafiltration.....	150
Diafiltration apparatus set-up and operation	150
Diafiltration preparation	152
Monitoring diafiltration progress.....	153
3.3. Results and discussion	157
3.3.1. Protecting group size decrease.....	157
3.3.2. Leaving group size decrease	161
3.3.3. Hub size increase	164
3.3.4. Deprotection of Thp during nanofiltration	167
3.3.5. Trial synthesis of Eg ₁₆ with combined nanofiltration and deprotection	173
3.3.6. Membrane re-screening for synthesis of Eg ₆₀	183
3.3.7. Synthesis of Eg ₆₀ on Hub ³ with ThpO–Eg ₁₂ –OTs building block.....	189
3.4. Conclusion.....	196
4. Chapter 4: Solvent recovery during diafiltration	197
4.1. Introduction.....	197
Model system	199
4.2. Materials and methods.....	200
4.2.1. Process set-up.....	200
4.2.2. Mathematics	201
4.2.3. Membranes.....	202
4.3. Results and discussion	205
4.4. Conclusion.....	209
Overall conclusion and outlook.....	210
5. Chapter 5: Experimental.....	214
5.1. General experimental	214
5.2. Hubs.....	215
NMR Annotation	215
5.3. Building blocks	224
5.4. Eg ₁₂ homostars.....	230
5.5. Chain extension, diafiltration and deprotection	232
5.6. Functionalization and hub cleavage	238

5.7. Other compounds.....	239
Appendix A – Historical methods towards uniform PEG	240
Synthesis of uniform oligo(ethylene glycol) from 1936 to 1970.....	240
Synthesis of uniform oligo(ethylene glycol) from 1970 onwards	242
Appendix B – Functionalization and hub disassembly for Eg ₅₆	248
Appendix C – Industrial synthesis of Eg ₁ – Eg ₄	249
Appendix D – Kinetics from Eg ₁₆ to Eg ₅₆	251
Extension from Eg ₁₆ to Eg ₂₄	251
Extension from Eg ₂₄ to Eg ₃₂	256
Extension from Eg ₃₂ to Eg ₄₀	261
Extension from Eg ₄₀ to Eg ₄₈	266
Appendix E – HPLC spectra for the synthesis of Eg ₆₀	275
Appendix F – Membrane cell assembly	277
Appendix G – Diafiltration apparatus	282
Equipment list	282
Diafiltration set-up.....	283
Appendix H – X-ray crystallography.....	287
X-ray crystal structure of Hub ² –CH ₂ OH (42c).....	287
X-ray crystal structure of Hub ³ –CH ₂ OH (43c).....	288
X-ray crystal structure of Hub ³ –CH ₂ Br (43d).....	290
Appendix I – Mass spectra for the synthesis of Eg ₆₀	291
Appendix J – NMR spectra for the synthesis of Eg ₆₀	328
Permissions for use of figures and tables	411
References.....	413

List of abbreviations and nomenclature

General abbreviations

BB	Building block
HS	Homostar
mPEG	Mono-methoxylated poly(ethylene glycol)
MWCO	Molecular weight cut-off
OSN	Organic solvent nanofiltration
PBI	Polybenzimidazole
PEEK	Poly(ether ether ketone)
PEG	Poly(ethylene glycol)
PTFE	Polytetrafluoroethylene
SPS	Solid phase synthesis

Analytical abbreviations

a.u.	Arbitrary units
COSY	Correlation spectroscopy (2D NMR)
DAD	Diode array detector
DEPT-135	Distortionless enhancement by polarization transfer (NMR)
ELSD	Evaporative light scattering detector
ESI	Electrospray ionization
FID	Flame ionization detector
GC	Gas chromatography
GPC	Gel permeation chromatography
HMBC	Heteronuclear multiple-bond correlation spectroscopy (2D NMR)
HPLC	High performance liquid chromatography
HSQC	Heteronuclear single-quantum correlation spectroscopy (2D NMR)
MALDI-TOF	Matrix-assisted laser desorption ionization time-of-flight mass spectrometry
MS	Mass spectrometry
NMR	Nuclear magnetic resonance spectroscopy
m/z	Mass-to-charge ratio
PDI	Polydispersity index (see dispersity, \bar{D})
S/N	Signal-to-noise ratio
TLC	Thin-layer chromatography
UV	Ultraviolet

Chemical nomenclature and abbreviations

Ac	Acetyl
Bn	Benzyl
BnOip	Benzyloxyisopropyl
Bz	Benzoyl
DBX	α,α' -Dibromo- <i>p</i> -xylene
DCA	Dichloroacetic acid
DMF	<i>N,N</i> -Dimethylformamide
DMSO	Dimethyl sulfoxide
Dmtr	4,4'-Dimethoxytrityl
E2	Bimolecular elimination
Eg _n	Oligomer consistent of n units of ethylene glycol
Fg	Generic functional group
Lg	Generic leaving group
M ⁿ , M ¹ , M ² , ...	Generic monomers
Mip	Methoxyisopropyl
Ms	Methanesulfonyl, or mesyl
MsOH	Methanesulfonic acid
NMI	<i>N</i> -Methylimidazole
OMs	Methanesulfonate, or mesylate
OTs	<i>p</i> -Toluenesulfonate, or tosylate
Pg	Generic protecting group
Pmb	<i>p</i> -Methoxybenzyl
py	Pyridine
R ¹ , R ² , ...	Generic organic substituents
rt	Room temperature
S _N 2	Bimolecular nucleophilic substitution
THF	Tetrahydrofuran
Thp	Tetrahydropyranyl
Trt	Triphenylmethyl, or trityl
Ts	<i>p</i> -Toluenesulfonyl, or tosyl
TsOH	<i>p</i> -Toluenesulfonic acid

Technical nomenclature

A	Active membrane area
B	Membrane permeance
c_i	Concentration of solute i
c_i^t	Concentration of solute i at time t
c_{ip}	Concentration of solute i on the membrane permeate side
c_{ib}	Concentration of solute i in the bulk on the membrane retentate side
γ_{ip}	Separation factor of impurity i over product p during diafiltration
D	Diffusivity
\mathcal{D}	Dispersity
F_0, F_P	Feed flowrate, permeate flowrate
F_{1r}	Return flowrate from stage 1 to feed tank
J_v	Volumetric flux through a membrane
k	Reaction rate coefficient
k'	Pseudo-first order reaction rate coefficient
M_w	Mass-average molar mass
M_n	Number-average molar mass
P_1, P_2, P_s, \dots	Pressure in membrane stage 1, 2, s , ...
ΔP	Transmembrane pressure
$\Delta \Pi$	Osmotic pressure difference
r_{21}	Recycle ratio
\mathbb{R}_i	Membrane rejection
t	Time
T_m	Melting point
T_g	Glass transition temperature
T_b	Boiling point
V	Volume
\dot{V}	Volumetric flowrate
V_1, V_2, V_s, \dots	Volume in membrane stage 1, 2, s , ...
V_P^t / V_s	Diafiltration volume

General introduction

Uniform and sequence-defined polymers provide substantial benefits over their disperse counterparts. For several natural polymers such as deoxyribonucleic acid (DNA), ribonucleic acid (RNA) and peptides, the exact sequence of base pairs or amino acids is crucial to their function. For other macromolecules such as poly(ethylene glycol), the extent of dispersity influences their physical properties and may go as far as determining in vivo behaviour.

In contrast to conventional polymer synthesis, the preparation of sequence-defined oligomers relies on the stepwise addition of building blocks, one at a time, over many synthetic extension cycles. To ensure uniformity of the final product, the growing oligomer must be purified from excess building block and reaction debris after each extension cycle. Sequence-defined oligomers are therefore substantially more costly to produce in comparison to conventional polymers as a result of the repeated purifications necessary between extension cycles.

Technology does exist to synthesize sequence-defined oligomers to industrially relevant lengths. For example, solid phase synthesis (SPS), developed by Robert B. Merrifield (Nobel Prize in Chemistry 1984), has been used since the 1960s to synthesize oligonucleotides, peptides and other sequence-defined oligomers on a solid matrix in an iterative fashion. Purification is made easier as the growing oligomers are immobilized on the solid support and excess reagent after extension cycles can simply be washed away. The technology does however suffer from several drawbacks, chiefly a lack of continuous scalability due to the limitations of the solid beds used and a related lack of economies of scale. Chromatography, a technology often used for the purification of synthetic oligomers such as poly(ethylene glycol), is in principle linearly scalable and can be combined with reactions in a homogeneous liquid but also lacks meaningful economies of scale. Both technologies work by separating on a heterogeneous medium.

Extraction is an alternative which does in principle allow the purifications in a fully liquid system with the associated benefits of processability and provides economies of scale. However, particularly for systems where the growing oligomer and the reaction debris and building blocks do not exhibit good separation and distribution across the aqueous and organic phase, separation is complicated. The problem becomes exacerbated for oligomers with surfactant properties such as poly(ethylene glycol) (PEG), which distribute increasingly evenly across both aqueous and organic phases with increasing chain length and impede de-mixing after extraction with a tendency to form emulsions.

Specific to PEG, as of 2017 the longest oligomers synthesized using chromatography or extraction for purification between chain extensions are Eg₆₄ and Eg₂₄ respectively. These oligomers are therefore also much shorter than the lengths typically required for pharmaceutical applications (5-20 kDa).

Problem Statement: There is currently no established, scalable and cost effective technology platform enabling the synthesis of poly(ethylene glycol) oligomers towards commercially relevant chain lengths.

A membrane-based technology, organic solvent nanofiltration (OSN), would enable reactions and purifications to be carried out in a liquid medium throughout and promises to be a more scalable and cost-effective alternative. OSN also promises to enable synthesis of oligomers with sufficient length to be of commercial relevance. To successfully prepare uniform oligomers with this purification technology, the synthetic chemistry used during building block preparation and chain extension must be compatible with the membrane-based separation. The chemistry is therefore chosen to be synergistic and to facilitate the purification and the individual process steps are optimized with the goal of a working process with the potential for large scale implementation in mind.

While the problem statement extends to other oligomers such as oligonucleotides and peptides for which the work of colleagues¹ is ongoing, this thesis focuses on the synthesis of uniform, heterobifunctional poly(ethylene glycol) via organic solvent nanofiltration.

This thesis is divided into four chapters, followed by an experimental chapter.

Chapter 1 introduces the motivation for obtaining uniform (monodisperse) polymers and the current perspective on uniform and sequence-defined oligomers in general. The first chapter then moves on to the synthesis of poly(ethylene glycol) and discusses the specific challenges related to its synthesis.

Different iterative growth strategies are compared for their speed of growth, the oligomer length increase per chain extension cycle, and the ease of product purification.

Ultimately an approach is chosen, whereby multiple oligomers are attached to and grown on a single anchor. This approach, the homostar approach, provides a large size differential between the growing oligomer product and the building block and reaction debris to be separated. It is then demonstrated that synthesis of an oligomer comprising 56 units of ethylene glycol (56-mer, Eg₅₆) is feasible with known chemistry and that the chosen growth strategy is potentially suitable for nanofiltration, but the purifications in Chapter 1 are still only chromatography-based.

Aims:

- Select a growth strategy suitable for purification by nanofiltration
- Establish that the synthetic chemistry of all steps involved in the preparation of a uniform oligo(ethylene glycol) is feasible

Chapter 2 details a kinetic study carried out alongside the preparative synthesis towards Eg₅₆ described in Chapter 1. In preparation for attaining commercially relevant chain lengths, it is necessary to check whether the reaction kinetics of chain extension remain sufficiently fast or become slower with increasing chain length.

Aims:

- Quantify the chain extension kinetics and gain an understanding of kinetics with increasing chain length
- Identify and quantify kinetics of significant side reactions

Chapter 3 begins with a review of the iterative synthesis of uniform and sequence-defined oligomers via OSN to date. It is then identified that the chemistry used for the synthesis of Eg₅₆ described in Chapter 1 requires modifications to facilitate purification of the growing oligo(ethylene glycol) oligomer by OSN. The three key functional elements – protecting group, leaving group and hub – of the molecules to be separated are then optimized for nanofiltration in conjunction with the overall strategy.

Based on the adapted building blocks and a new hub, the successful purification of the growing oligomeric PEG product from the building block and reaction debris via OSN is then demonstrated. As proof of concept, a nearly uniform mono-methyl Eg_{60} oligomer (mPEG-2700) with excellent quality (dispersity $D = 1.0006$, oligomer purity = 97 %) is then assembled in four iterative chain extensions from a 12-mer building block, replacing chromatographic purification entirely with membrane-based separation.

Aims:

- Adapt the homostar and building block chemistry to optimize purification by OSN
- Demonstrate successful purification of a growing oligo(ethylene glycol) over several extension cycles
- Extend an oligomer towards commercially relevant length

Chapter 4 discusses the implications of high solvent consumption during product purification by nanofiltration. The problem is not specific to purifying uniform oligomers but is a feature of the washing process used. The recovery of washing solvent is in principle also possible via OSN but must use a tighter membrane which ideally retains all impurity and only permeates solvent. However, membranes with an ideal separation profile for this solvent recovery application are difficult to find in practice. To enable solvent recovery by nanofiltration with imperfect membranes that do not fully retain all impurity, a process adaption is devised.

Aims:

- Trial an integrated membrane-based solvent recovery for a two-stage cascade in a closed-loop set-up based on prior work
- Demonstrate successful purification of the product by diafiltration even when the solvent recovery membrane unit cannot fully retain all impurities.

The overarching goal of the project is to prepare uniform heterobifunctional oligo(ethylene glycol) of commercially relevant length via iterative synthesis using OSN as the purification technique and doing so in a cost-effective and scalable manner which translates well to a potential industrial process.

1. Chapter 1: Iterative Synthesis of Uniform Poly(ethylene glycol)

1.1. Introduction

Most synthetic polymers exhibit an inherent size distribution as a result of their manufacturing process. In a typical polymerization process, upon initiation, a quantity of monomer is allowed to polymerize, and monomers can combine successively to form the polymer chain. The exact mechanism of polymerization varies depending on the monomer, e.g. step-growth or chain-growth, but the concept is similar in that monomers combine continuously until the reaction is complete. An example of a step-growth polymerization typical of a condensation polymer with a single bifunctional monomer is shown below (Figure 1).

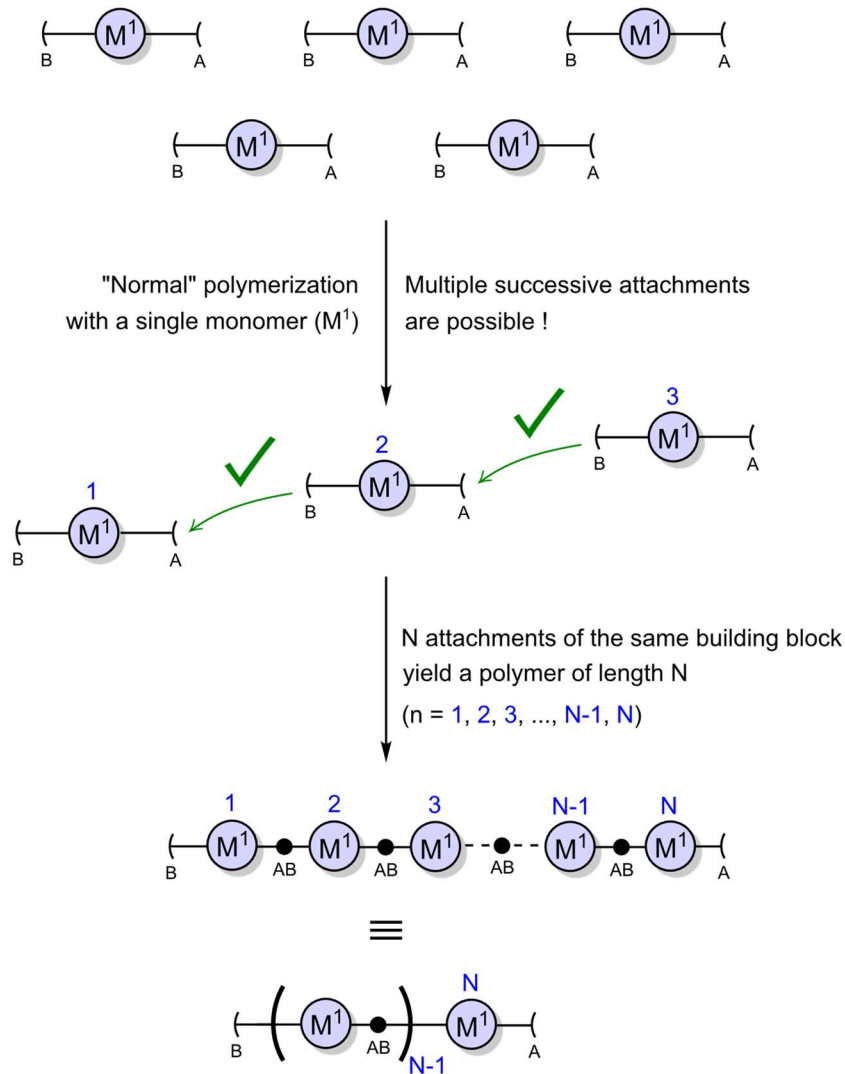


Figure 1. Step-growth polymerization where multiple successive attachments of a single bifunctional monomer (M^1) form the polymer chain. The monomer has two different complementary sites, A and B, which can combine ($B \rightarrow A$) to form the polymer while two similar sites ($A \rightarrow A$ and $B \rightarrow B$) cannot combine.

Due to the statistics of an unhindered polymerization, some monomers will combine faster than others so that the polymer chains in the mixture do not grow at the same rate. The product is therefore a polymer with a mixture of different chain lengths, typically with a Gaussian distribution.

One measure of size distribution, i.e. distribution of molar masses in polymers, is dispersity (previously referred to as polydispersity index, PDI), more specifically molar-mass dispersity (\mathcal{D}), the ratio of the mass-average molar mass, relative molecular mass, or molecular weight (M_w), to the number-average molar mass, relative molar mass, or molecular weight (M_n).²

$$\mathcal{D} = \frac{M_w}{M_n}; \mathcal{D} \geq 1$$

Equation 1

(Note that the mass-average and number-average molar mass, M_w and M_n respectively, should not be confused with the abbreviation for a generic monomer, M^1 , in Figure 1.)

Much of the physical behaviour and properties of polymers are affected by their dispersity. For example, polymers typically do not exhibit sharp melting (T_m) and glass transition points (T_g) as their behaviour changes over a temperature range as a result of dispersity.

To improve upon properties by narrowing the size distribution, ways have been found to synthesize polymers with relatively low dispersity, for example through living polymerization. Living polymerization is a variant of chain-growth polymerization characterized by a rapid chain initiation, i.e. much faster chain initiation than chain propagation, and by the absence of chain transfer or chain termination reactions. As such, all active species are formed simultaneously and all then react continuously at an approximately similar rate until all monomer units are used up, and without termination until the active species are quenched. For some important polymers such as poly(ethylene glycol) (PEG) which is used widely in the pharmaceutical industry as a non-toxic, non-immunogenic ingredient, \mathcal{D} values as low as 1.05 are now the norm for polymers smaller than 30 kDa, and \mathcal{D} values around 1.1 are considered acceptable for higher molecular weights.³ However, even with dispersity values of around 1.05, samples may still contain a double digit figure of chains with different length for each chain of the desired size, i.e. specified M_w . A typical sample of PEG manufactured via living anionic polymerization with \mathcal{D} of 1.03 for a M_w of approx. 2,200 Da still contains less than 10 % of the denominated target species (Figure 2).

Most industrially produced synthetic polymers are therefore not exactly defined in their size and properties but this usually does not impede their function.

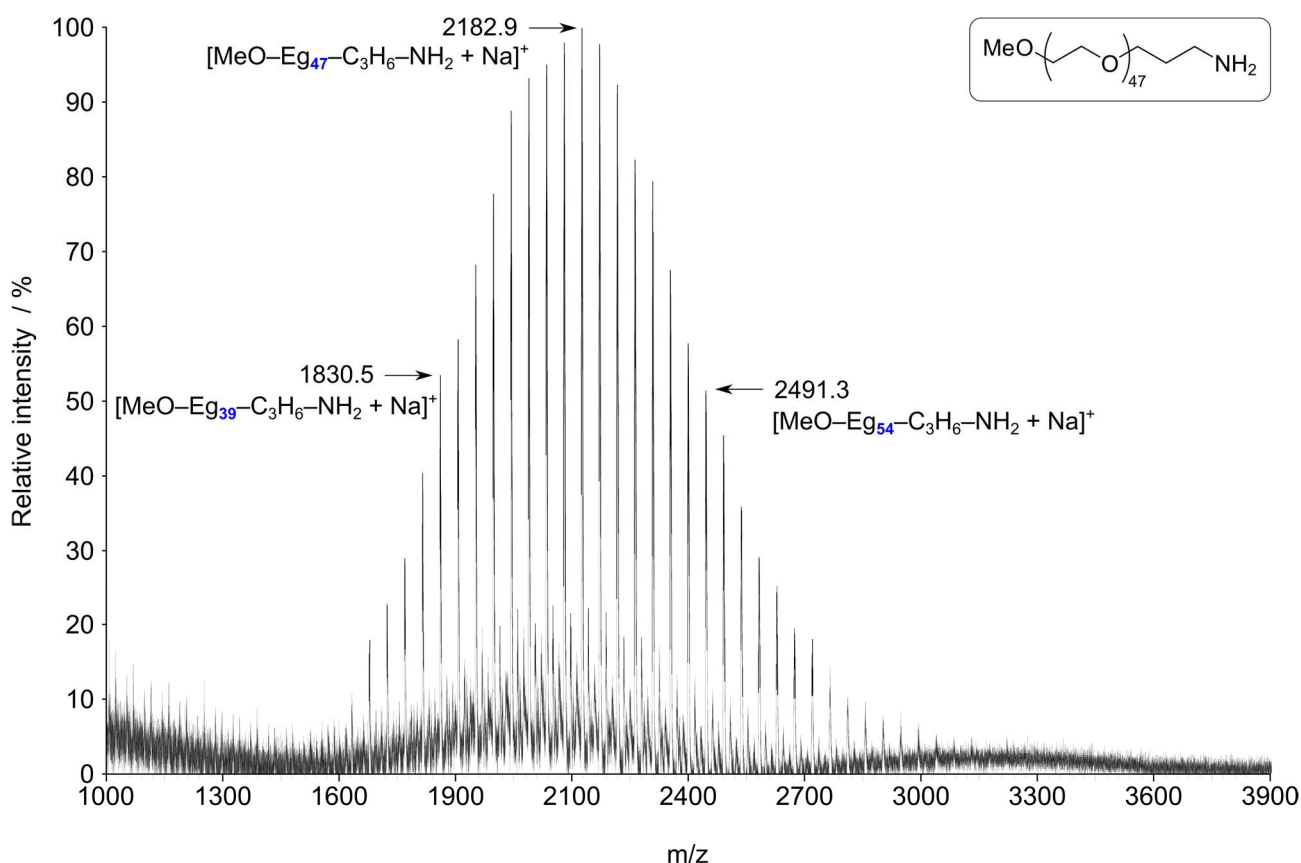


Figure 2. MALDI-ToF mass spectrum of a sample of α -methoxy ω -aminopropyl PEG-2000 purchased from NOF Corporation (JP). Despite the relatively low dispersity of 1.03 for a standard polymer, the product contains less than 10 % of the $\text{MeO-Eg}_{47}\text{-C}_3\text{H}_6\text{NH}_2$ target species. Adapted from ⁴ with permission from John Wiley & Sons.

Sequence-defined and uniform oligomers

There are in contrast some polymers for which an exact definition of size and sequence is critical to their function. Biopolymers such as deoxyribonucleic acid (DNA), ribonucleic acid (RNA), polypeptides and polysaccharides are the foundation of life. For DNA and RNA, sequence-definition is the prerequisite for their function. Strikingly, nature can synthesize these biopolymers in a very precise fashion and the universal genetic code of all life on earth relies on exact replication and transcription of these two polymers comprising a combination of only four monomers, or base pairs – adenine, guanine, cytosine and either thymine for DNA or uracil for RNA.

DNA and RNA are therefore examples of sequence-defined polymers as the exact sequence of bases is well-defined. Their precise sequence-definition is crucial to their functionality.

A distinction can be drawn between sequence-defined and uniform polymers in that a sequence-defined polymer refers to a macromolecule comprising more than one monomer in a defined sequence while uniformity or non-uniformity is a reference to whether the bulk polymer, i.e. the assembly of chains

constituting the polymer, exhibit dispersity (non-uniform) or are all of the same length (uniform). A collection of sequence-defined oligomers will therefore also necessarily be of uniform molecular size, while a uniform polymer comprising many chains of the same length but assembled from only one monomer would not exhibit sequence-definition.

Oligomers and polymers

Lastly, a distinction should be made between polymers and oligomers. An oligomer (Ancient Greek: ὀλίγος (olígos, “few”, “small”, “little”) and μέρος (méros, “part”)) is, according to the International Union of Pure and Applied Chemistry (IUPAC), “a molecule of intermediate relative molecular mass, the structure of which essentially comprises a small plurality of units [...] in contrast to a polymer, where the number of monomers is, in principle, not limited.”⁵ As a result, oligomer syntheses are discussed here conceptually as an (often small) sequence of several individual addition steps rather than one continuous reaction which yields a fully polymerized product.

1.1.1. Synthetic strategies towards sequence-defined oligomers

There are various ways of synthesizing and replicating defined sequences by mimicking their biosynthesis, e.g. by templating, as practised during polymerase chain reaction. However, the focus here will be on the ways of manufacturing sequence-defined oligomers using synthetic chemistry.

The defining feature of all strategies towards sequence-defined oligomers is that monomers are not allowed to attach twice successively in the same reaction step as is common in normal polymerizations as previously shown in Figure 1. Instead, multiple attachments are actively prevented by using protecting groups, orthogonal functional group chemistries, or by more exotic means such dormant reactive groups and exploiting vastly different reaction activation energies with temperature swings.

As a result, sequence-defined polymers are typically grown in a stepwise, or iterative fashion, whereby each unit of a sequence is inserted one at a time. Of course, this makes the synthesis of a sequence-defined oligomer much more cumbersome and resource-intensive. While Chapter 1 details only the synthetic challenges of making a uniform oligomer from poly(ethylene glycol), Chapter 3 is dedicated to finding a way of mitigating the additional cost of purification between each iterative cycle by using nanofiltration.

Strategies utilizing a protecting group

A common tool to prevent the reaction of a functional group in synthetic chemistry is the use of a protecting group (Pg). A protecting group acts as a mask and temporarily passivates a functional group so that it is no longer reactive. An important feature of a protecting group is that it can be selectively removed again without affecting other sections of the molecule. The conceptually simplest strategy towards a sequence-defined oligomer making use of a protecting group consists of one type of heterobifunctional monomer with two different reactive sites. One site of the monomer is active and ready for attachment to an existing chain, and the other site is inactive. The inactive site is masked by a protective group which prevents further monomer attachment at this site in the same reaction step. The attachment of monomer to a growing oligomer is the first part of a chain extension cycle.

After complete reaction, i.e. successful attachment of monomer to all reactive sites of an existing oligomer mixture, the reaction is quenched. Prior to the next extension, the inactive sites still masked by protective groups need to be deprotected and thereby made available for further extension in the next chain extension cycle. The deprotection, or reactivation of the chain terminus for next extension, marks the second part of the chain extension cycle. A complete chain extension cycle can be repeated multiple times to give a uniform, sequence-defined monomer of the desired length (Figure 3).

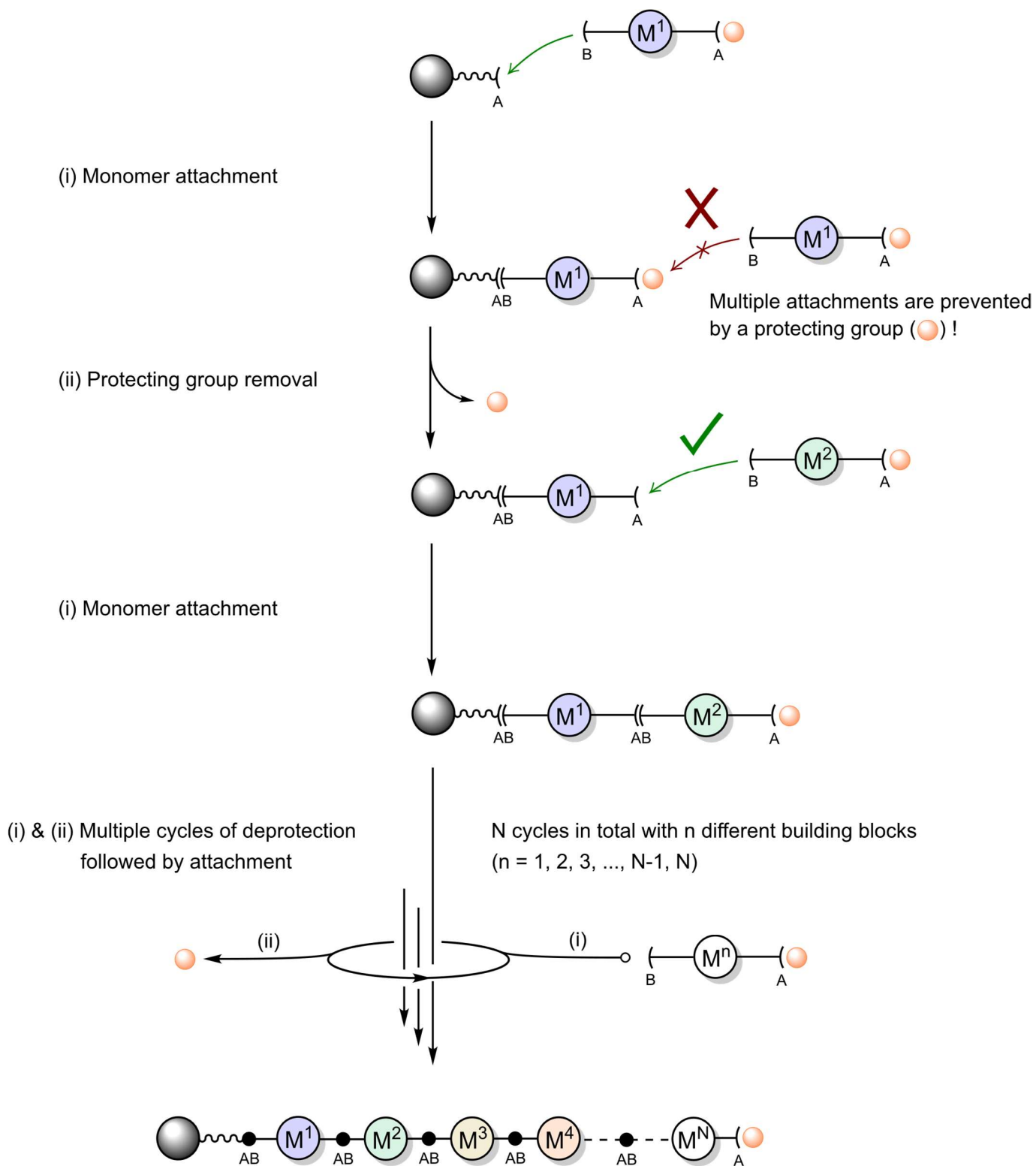


Figure 3. Iterative strategy for preparing a sequence-defined polymer with protected building blocks of type AB on a solid support (grey sphere). Monomers (M^n) may vary but have similar heterobifunctional terminal functionality: two different complementary sites, A and B, which can combine ($B \rightarrow A$) to form the polymer but only after the protecting group (small orange sphere) has been removed from the terminus. If all M^n are equal, a uniform oligomer is obtained, and if M^n are different that oligomer will also be sequence-defined. Protecting group = ●.

Crucially, all residual monomer and debris from the previous reaction step must be removed prior to the next extension reaction. This is because the deprotection affects the product oligomer as well as any residual excess monomer from the previous extension step. Any leftover monomer from the previous step would no longer contain a protective group on one end and would therefore lead to double coupling in the next extension step as another monomer could attach to the unprotected end of these deprotected monomers as shown in Figure 4.

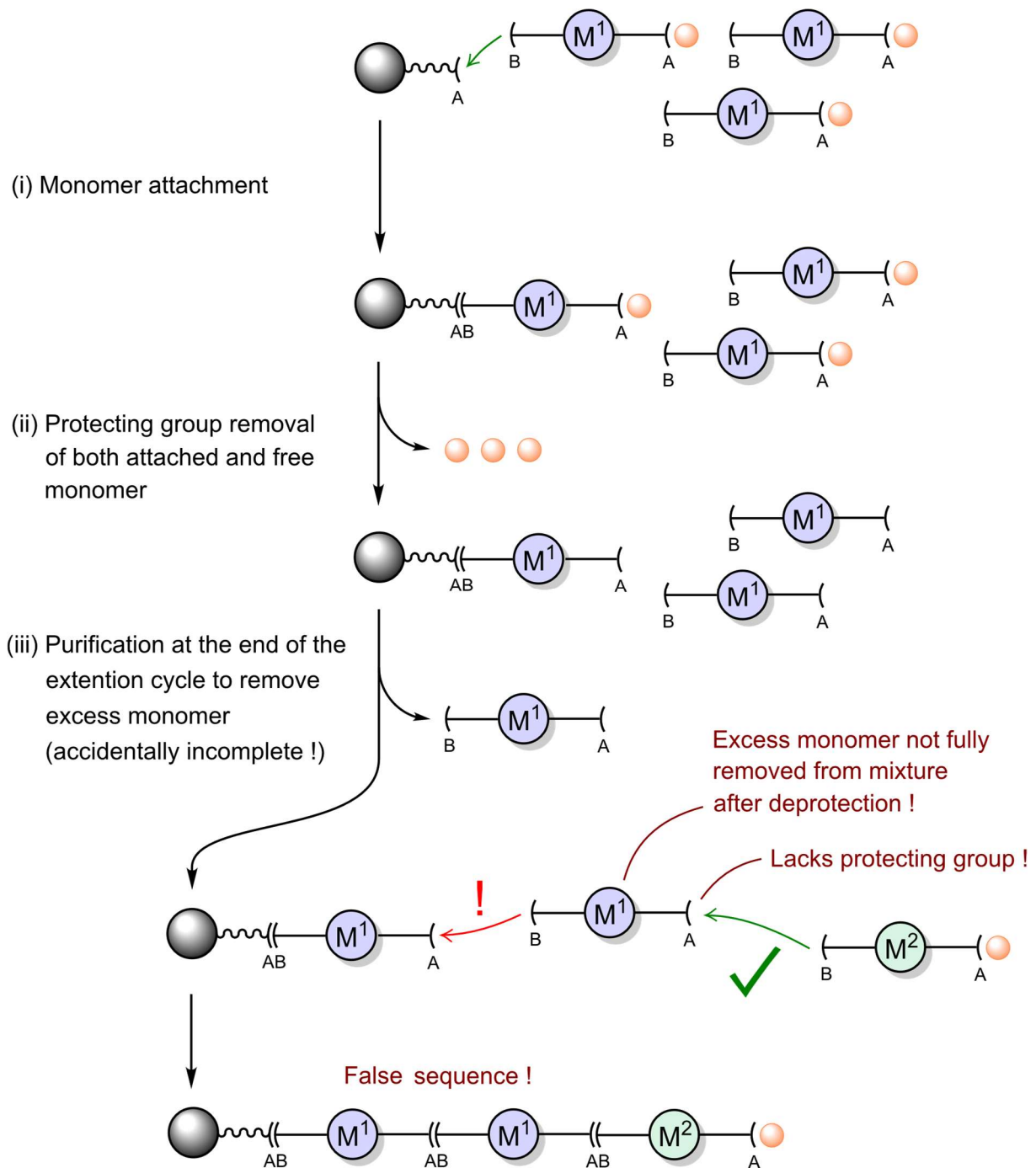


Figure 4. Incomplete removal of monomer after protecting group removal leads to undesired double coupling of monomer during the subsequent chain extension cycle yielding a false sequence.

Separation of the excess monomer may in theory be performed prior to, jointly with or after deprotection and needs to take into account the reaction and deprotection debris. The choice of how exactly to purify this mixture depends on multiple factors including the separation technique employed and this separation problem will be one of the central themes in this thesis.

For the synthesis of uniform poly(ethylene glycol) in this work, a protecting group strategy is used and several alternative protecting group-free approaches are outlined below for completion.

Protecting group-free strategies

Sequence-defined polymers may also be obtained via protecting group free strategies. These include approaches utilizing orthogonal building block functionalities and approaches where a dormant site on a building block is activated after building block attachment, a similar concept to using a protecting group. Another strategy, which upon closer inspection yields copolymers, exploits different activation energies and uses two different temperatures for attachment of two different building blocks. A last example showcased exploits an internal rearrangement of a boronate ester within a temperature cycle and relies on different stabilities of reagents and products at temperatures between $-78\text{ }^{\circ}\text{C}$ and room temperature.

Two homobifunctional monomers

The simplest protecting group-free approach makes use of two different monomers with similar terminal functionality each. Expressed similarly to the previous example, the monomers possess AA and BB functionality respectively, where sites A can only couple to sites B (Figure 5). Because each monomer is homobifunctional (having similar functionality on each terminus), neither monomer can couple to itself. Therefore, chain extension is only possible by alternating addition of each monomer.⁶

There is one serious drawback to the technique: because an added monomer has similar functionality on each terminus, it can cross-link two growing chains (Figure 6). An extension strategy with homobifunctional monomers is therefore only workable in confined circumstances. Either extending chains must be kept physically separate from each other, e.g. by growing on a heterogeneous, solid support, or local concentrations of monomer must be in large excess, perhaps in combination with a high dilution technique. Even then, a small proportion of cross-linking will statistically occur in the latter case. The approach is therefore less suitable in homogeneous reactions where participants are well-mixed. There, the selectivity of the reaction would be inversely related to the excess of monomer used, necessitating the use of large excesses of monomer or affording a loss of selectivity, both undesirable in a larger scale setting. Strictly speaking, this strategy yields co-oligomers (oligomeric copolymers) as

alternating functional groups will be orientated towards each terminus of the chain in alternating fashion, similarly to Nylon (Polyamide) 6,6 in comparison to Nylon (Polyamide) 6.

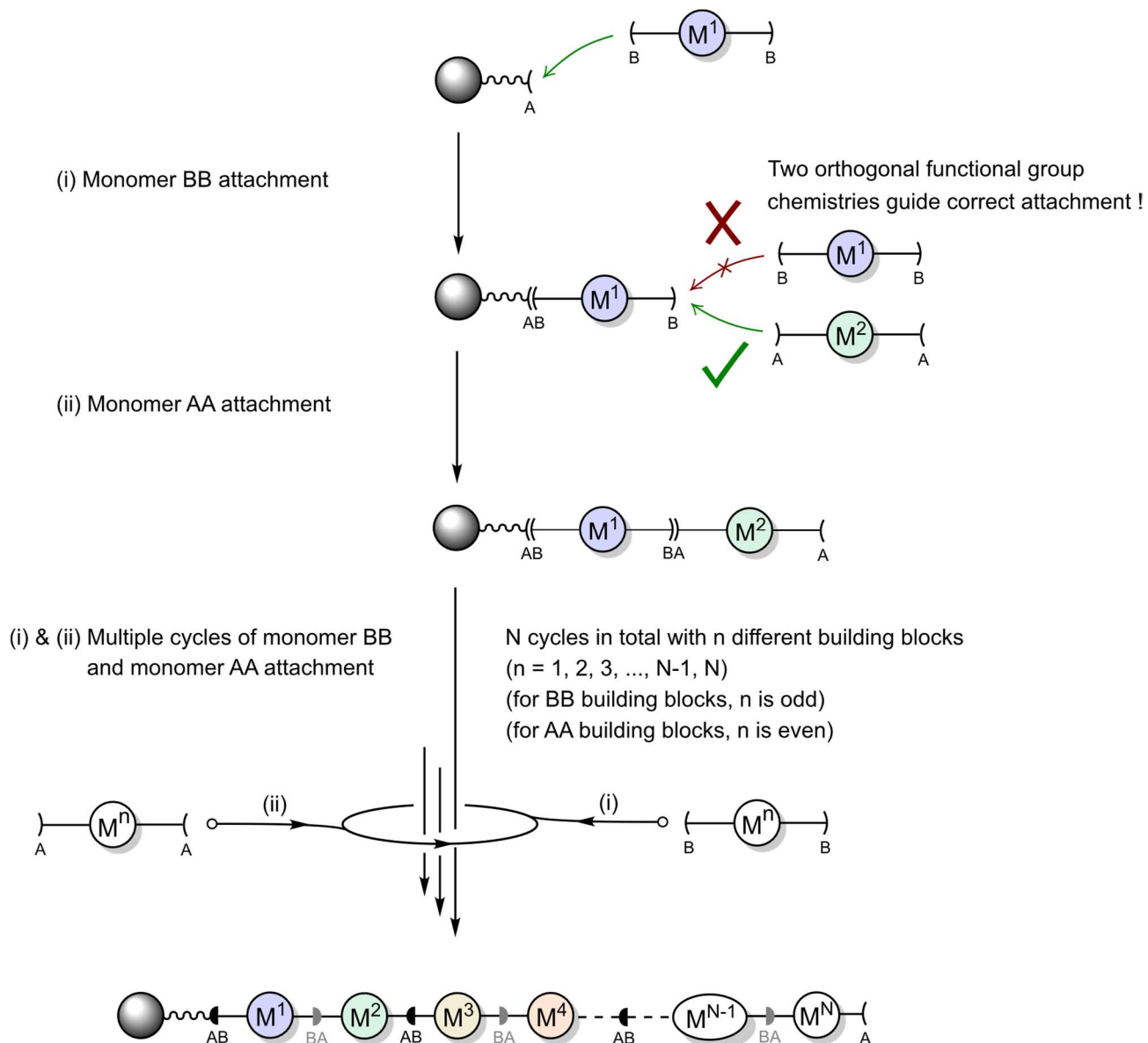


Figure 5. Iterative strategy for preparing a sequence-defined polymer with non-protected building blocks of type AA and type BB on a solid support (grey sphere). Monomers (M^n) may have different cores but have similar, homobifunctional terminal functionality: either two sites A and A, or two sites B and B, which can combine intermolecularly ($B \rightarrow A$) to form the oligomer with alternating orientation of the functional groups (small black and grey half-circles). If all M^n are equal, a uniform co-oligomer is obtained, and if M^n are different that co-oligomer will also be sequence-defined.

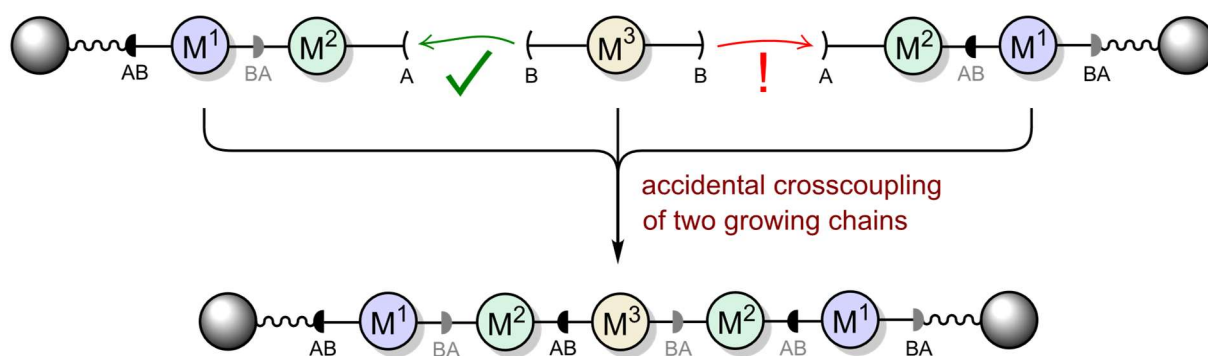


Figure 6. Undesirable side reaction during iterative extension with type AA and type BB building blocks (as shown in Figure 5) if local excess of monomer is not sufficiently high.

Two heterobifunctional monomers with four different functional groups in total

A more sophisticated way of avoiding the use of a functional group is to use two heterobifunctional monomers with selective functionalities that only allow coupling of one functional group of one monomer to one functional group of another monomer. In theory, this necessitates each functional group to be orthogonal to itself and another intramolecular functional group while being selective to one functional group on another monomer and orthogonal to the second functional group on this other monomer. Thereby self-coupling is prevented and selective coupling to the other type of monomer ensured. Expressed similarly to the above examples, the two different monomers have BC and DA type functionality respectively and coupling is only possible between $C \rightarrow B$ and $D \rightarrow A$. The approach using these four different functionalities is exemplified in Figure 7 where it is shown that the two different monomers may also contain different core groups.⁶

Because two different monomers are utilized, this approach will yield co-oligomers and cannot be used to grow homo-oligomers having the same functionality between each monomer unit. In practice, monomers fulfilling such a diverse set of selectivity and orthogonality criteria are also difficult to design.

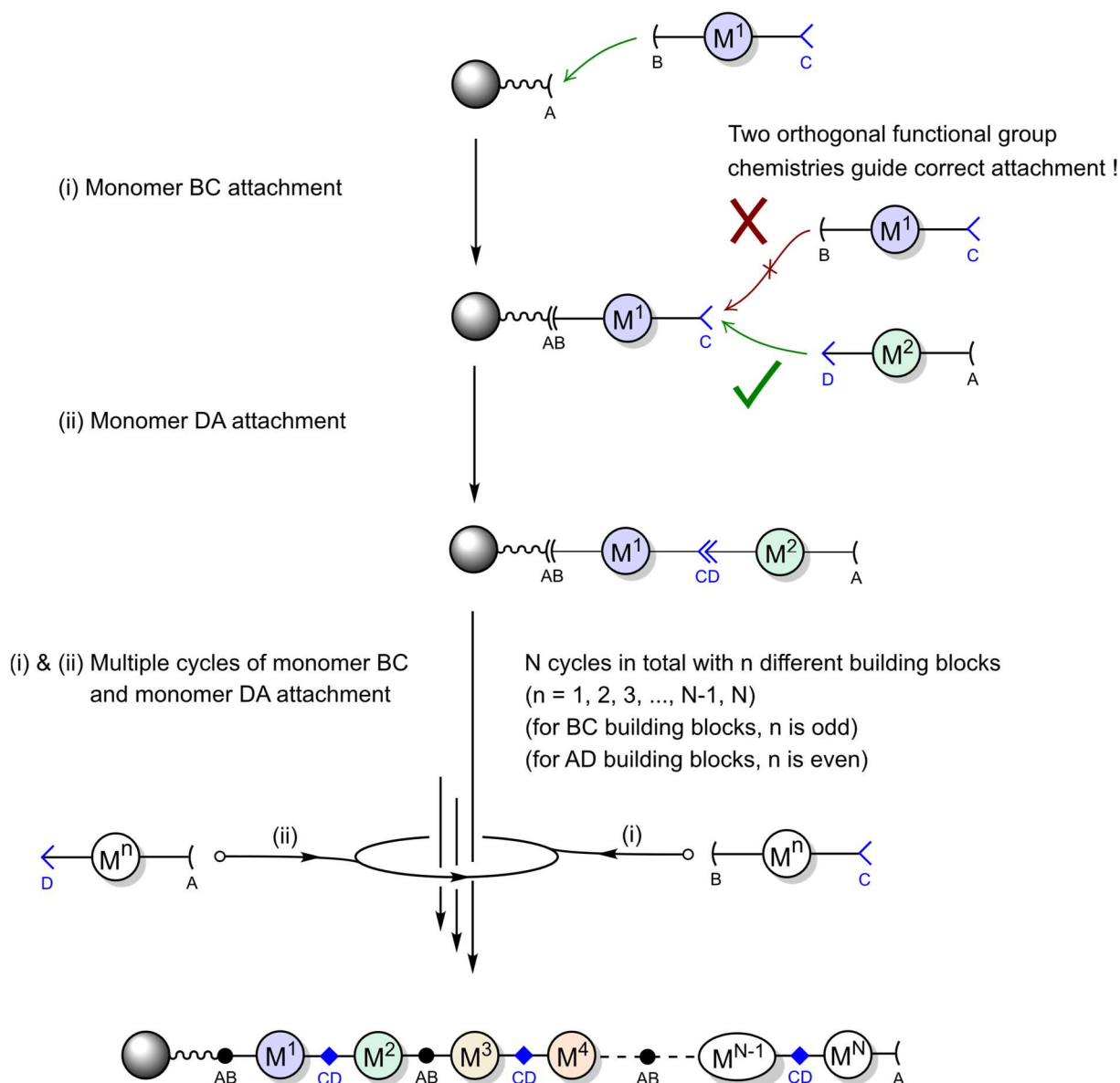


Figure 7. Iterative strategy for preparing a sequence-defined polymer with non-protected building blocks of type BC and type DA on a solid support (grey sphere). Two dissimilar monomers ($M^{n,\text{odd}}$) and ($M^{n,\text{even}}$) must have dissimilar, heterobifunctional terminal functionality: each functional group is compatible to only one other functional group on the other, alternating monomer but orthogonal to itself, the other intramolecular functional group and the other intermolecular functional group on the alternating monomer. The only couplings allowed are therefore $B \rightarrow A$ and $D \rightarrow C$. The strategy will yield a co-oligomer with alternating functional groups (small black circles and blue turned squares). If all M^n have similar cores, a uniform co-oligomer is obtained, and if M^n are different that co-oligomer will also be sequence-defined.

Functional group interconversion of dormant reactive groups

A strategy which is conceptually very similar to using protecting groups, makes use of a dormant reactive group on a monomer. The dormant reactive group needs to be activated in a separate reaction step prior to further chain extension. This strategy is therefore an analogue of the protective group approach previously described – rather than unmasking a reactive functional group by removing a protective group, the reactive character of a terminal is reinstated or freshly created by activation or functional group interconversion. There should be no obvious merits over a protecting group-based strategy as no reaction steps are saved and, in both strategies, a further reaction step is needed after successful monomer coupling to provide a reactive site for the next monomer attachment cycle.

Exemplary of the route via dormant reactive groups is the synthesis of a thiophene oligomer on a solid support⁷ (Figure 9) and the synthesis of ether oligomers in liquid phase.⁸ In the former case, thiophene oligomers were synthesized via alternating attachment of a substituted or unsubstituted thiophene monomer to a bromide functionality via Stille coupling, and bromination of the newly attached ring to provide an attachment point for the next monomer.

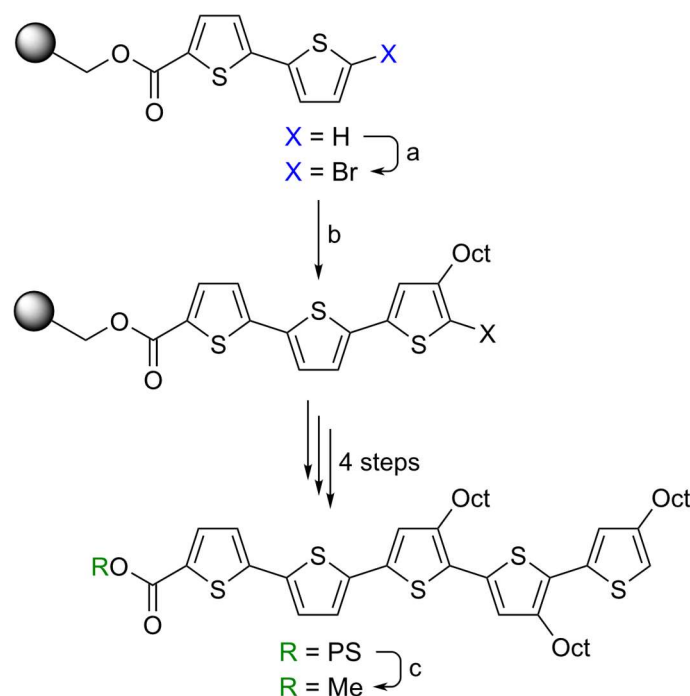


Figure 8. Synthesis of a thiophene oligomer via a strategy using dormant reactive groups. *Reagents and conditions:* a, N-bromosuccinimide, DMF, rt; b, 2-(trimethylstannyl)-4-octylthiophene, Pd(PPh₃)₂Cl₂, DMF, 80 °C; c, NaOMe, THF, reflux, 1 h, then MeI, 18-Crown-6, reflux, 3 h. Adapted from ⁷ with permission of The Royal Society of Chemistry.

In the latter example, ether oligomers were synthesized via Mitsunobu coupling between benzyl alcohol or a benzylic alcohol with a hydroxyaromatic aldehyde or ketone as a nucleophile, followed by re-generation of a benzyl or benzylic alcohol for the next coupling from the aldehyde or ketone functionality

via reduction (NaBH_4).⁸ Coupling was viable with a multitude of building blocks, including ortho- and bis-ortho-substituted phenols as well as substituted acetophenones which yield chiral products after reduction, but not with salicylaldehyde.

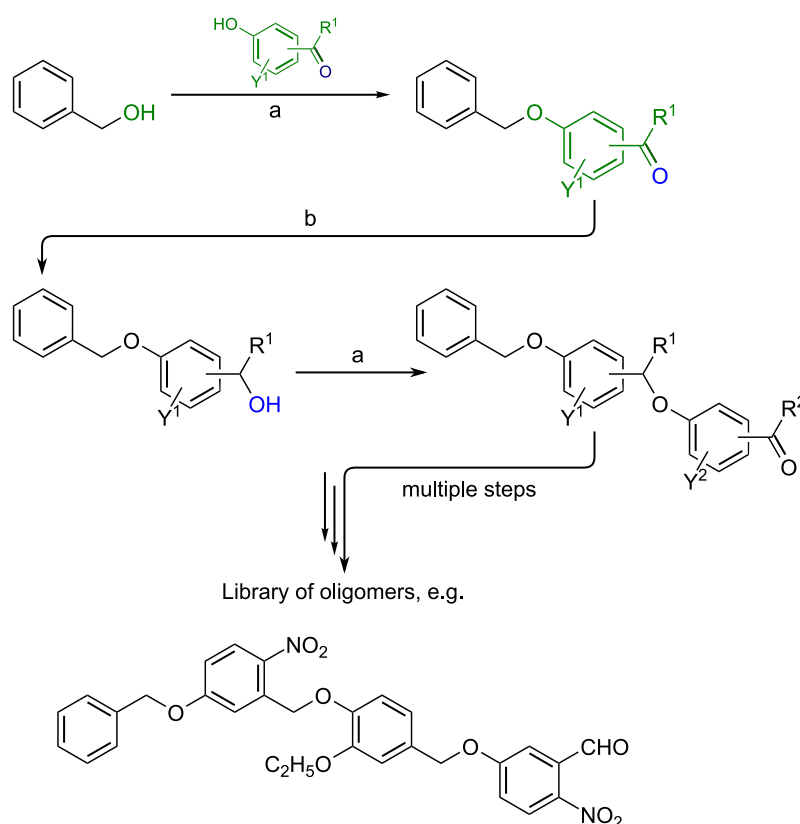


Figure 9. Iterative coupling strategy for the preparation of aromatic ether oligomers. a) Mitsunobu coupling: Phenol, PPh_3 , diisopropyl azodicarboxylate, THF, 0-25 °C b) Reduction: NaBH_4 , MeOH $\text{R}^n = \text{H}$ or Me; $\text{Y}^n = \text{CH}_3$, OCH_3 , OC_2H_5 , NO_2 and combinations thereof. Adapted with permission from ⁸. Copyright (2004) American Chemical Society.

Exploiting a reactivity difference via temperature change

Another approach that is more distinct from protecting group techniques relies on a change in reaction kinetics of the second site of the monomer upon attachment on the first site. An example is the synthesis of triazine-based polymers⁹ which relies on a step change in reactivity with each added substituent group on cyanuric chloride, i.e. with each removal of an electron-withdrawing chloride group. The different monomers are made by attaching one side group to cyanuric chloride leaving two further reactive sites. When a monomer is attached to one of these two reactive sites via a free amine group on the growing oligomer, the third and last reactive site is significantly deactivated so that much higher temperature is needed to affect further monomer attachment. In the words of the authors: “Each substitution deactivates remaining sites such that higher temperatures are required for each substitution around the ring, from -20 to 5 °C for the first reaction, rising from 18 °C to 35 °C for the next reaction, and temperatures above

60 °C for the third.⁹ Therefore, excess monomer can be separated off and a diamine spacer inserted at elevated temperature to provide another amine site for the next cycle. However, even in this scenario a second reaction is needed to generate the new reactive site and this approach is therefore comparable to the dormant reactive site strategy.

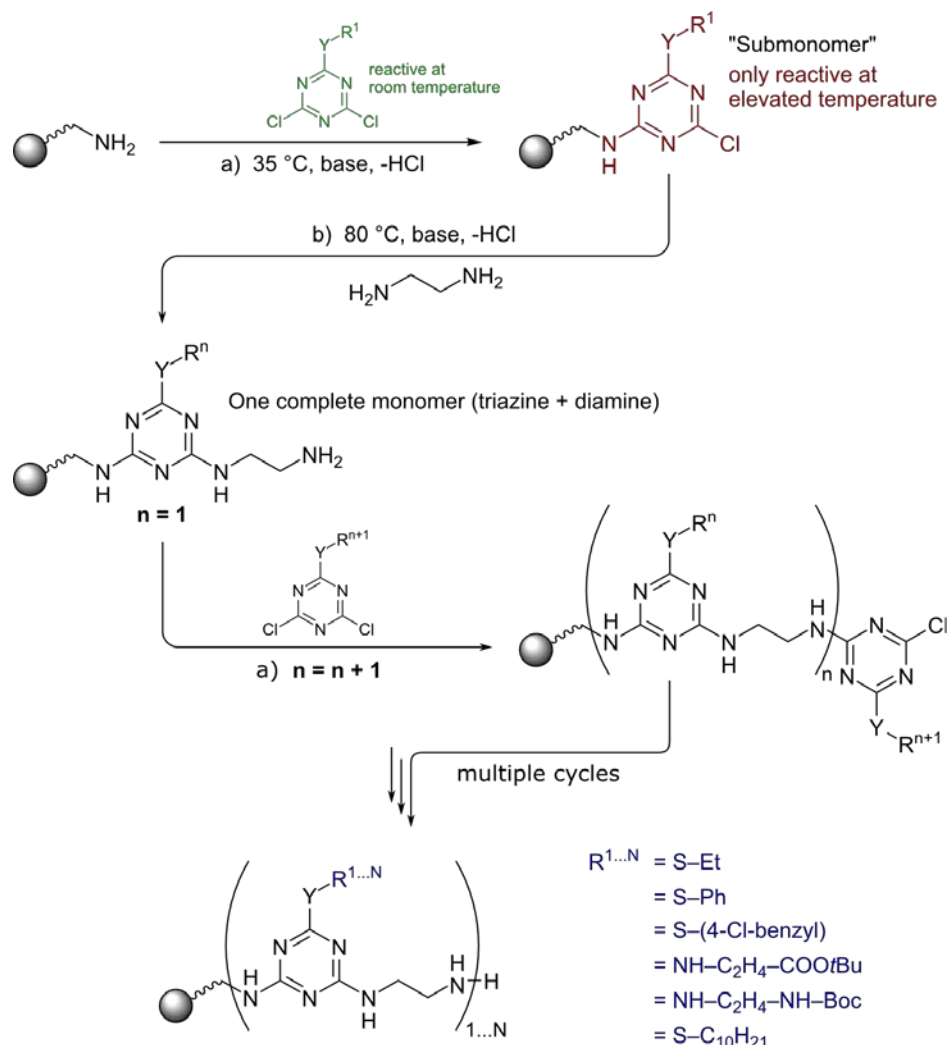


Figure 10. Solid phase synthesis of a triazine-based polymer exploiting a difference in reactivity between a monosubstituted and a twice substituted cyanuric acid derivative. Adapted from ⁹ under a CC BY-NC-ND license.

Exploiting differing reactant stability and product intermolecular rearrangement via a temperature cycle

One impressive example of a protecting group-free approach is a controlled iterative homologation of a boronic ester (Figure 11).¹⁰ Therein, a chiral lithiated hindered benzoate (generated in situ from its stannane with *n*-BuLi at -78 °C) is coupled to a boronic ester to form a boronate complex. The product mixture is aged at -42 °C for a period of time to allow excess lithiated benzoate to decompose, followed

by warming to room temperature (+20 °C) to allow for 1,2-migration to give the homologated/elongated product with reformation of a boronic ester ready for further elongation. Instead of a protecting group, this approach therefore uses a temperature cycle and finely tuned reactivity with an internal rearrangement to generate the coupling site for the next cycle. The approach was used to synthesize oligomers of what could probably be referred to as poly(methyl methylene) with controlled tacticity (isotactic, syndiotactic and a tailored combination thereof). The overall 44-58 % yield of 10-mer (after 9 couplings) with a reported oligomer purity of up to 97 % and a calculated enantiomeric ratio of the major diastereoisomer of 10²⁹:1 is impressive. However, this approach is clearly limited to monomers which are tailored to undergo very specific rearrangements to restore a functional group, and in this case also relies on a temperature cycle involving relatively low temperatures (down to -78 °C).

An analogue natural iterative chain extension process mentioned by Burns et al. is the enzyme-catalyzed formation of polyketides where a thioester is passed from one module to another (Figure 12).¹¹

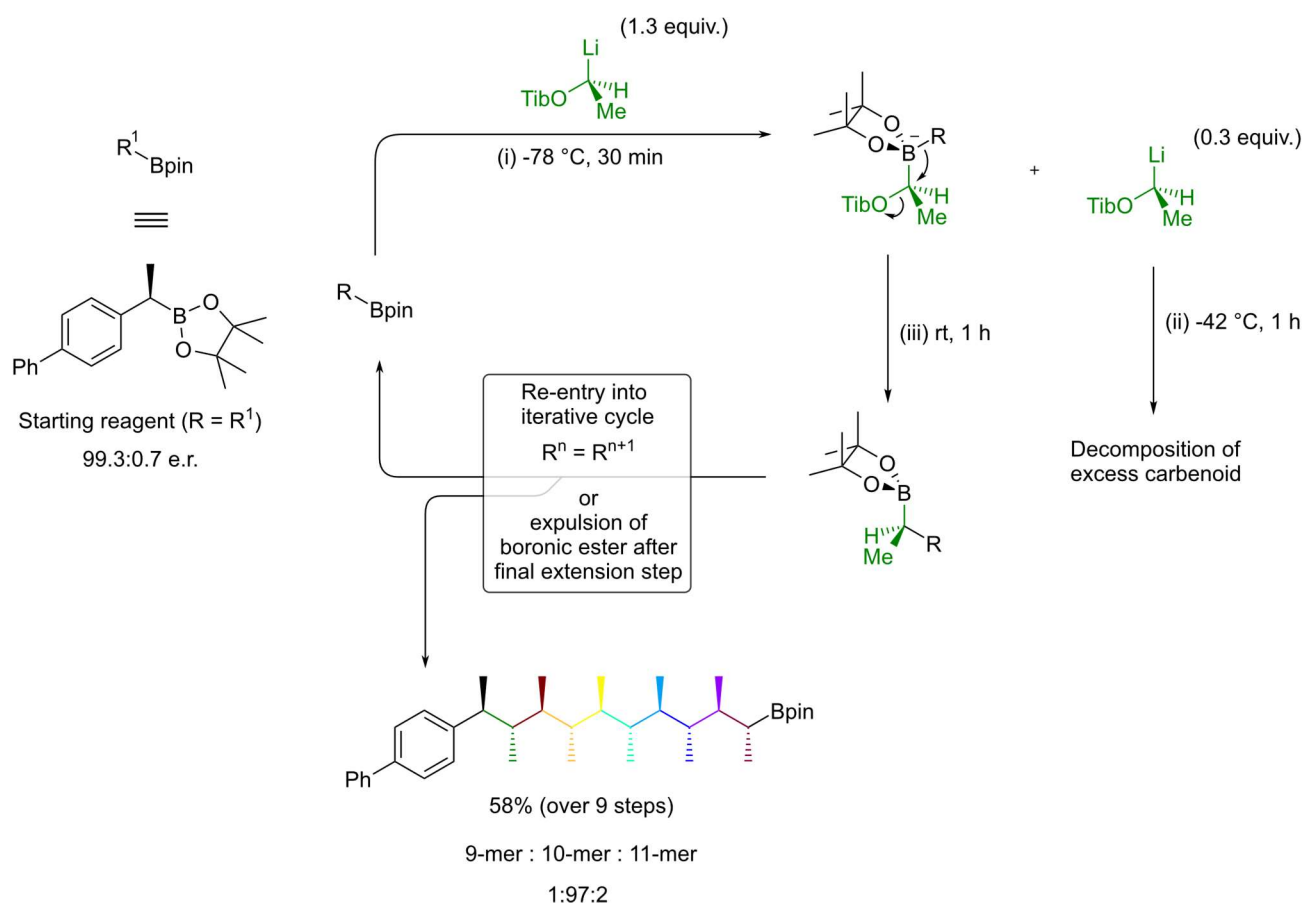


Figure 11. Iterative homologation of boronic esters via (i) coupling of a chiral lithiated hindered benzoate generated in situ with a boronic ester, (ii) ageing of the mixture for 1 h at -42 °C to decompose excess lithiated benzoate and (iii) internal rearrangement of the boronate complex to yield the elongated product boronic ester ready for further chain extension. Tib = 2,4,6-triisopropylbenzoate. pin = pinacol. rt = room temperature. Adapted from ⁹ with permission from Nature Publishing Group.

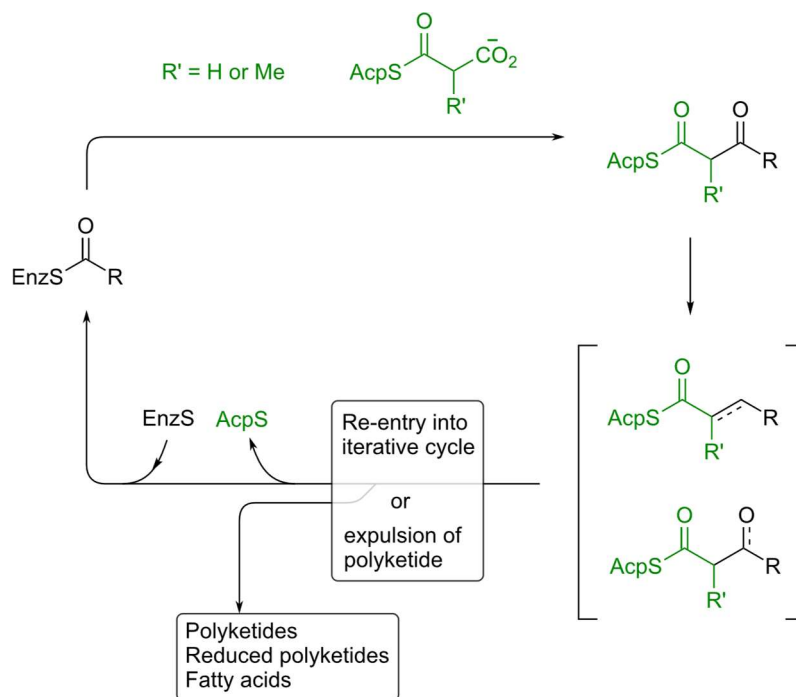


Figure 12. Example of polyketide biosynthesis where successive cycles of chain extension and functional-group interconversions generate a diverse array of complex molecules. Acp = acyl carrier protein; Enz = enzyme. Adapted from ¹⁰ with permission from Nature Publishing Group.

1.1.2. Poly(ethylene glycol) as a model system

The synthetic strategies described in the previous section apply to a wide range of polymers. In order to demonstrate successful synthesis of an oligomer, and to study the feasibility of purifying intermediate products en route to a uniform oligomer with nanofiltration, a suitable model system was required. The criteria were: a non-toxic polymer which had been well-studied, whose synthesis involved inexpensive starting materials, and which had available reference compounds, ideally in both disperse and uniform versions. Other desirable features of the polymer were sufficient stability under standard conditions, that it should not be overly sensitive to oxidation or other side reactions, and constituent monomers which could be reliably coupled with established protocols. The polymer was to command enough relevance in industrial applications to justify research into viable methods of scaling up synthesis and purification and be used in applications in which a uniform sample could provide substantial benefits over a disperse sample.

A suitable candidate was found in poly(ethylene glycol) (PEG) (Figure 13). PEG is a polyether which is well soluble in a wide range of aqueous and organic media and is also used as a dispersant. PEG is non-toxic and physically and environmentally benign and the handling of non-functionalized PEG requires no further measures beyond the use of standard laboratory personal protective equipment. Conveniently, starting materials for PEG synthesis are available inexpensively and in sufficient quantity up to the tetramer (four units of ethylene glycol), or Eg₄. Extensive research into the synthesis of uniform PEG is available and a small number of commercial suppliers for uniform PEGs exist.

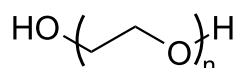


Figure 13. Poly(ethylene glycol), a pharmaceutically relevant polymer.

Applications of poly(ethylene glycol)

Poly(ethylene glycol) is widely used in the pharmaceutical industry to increase serum/ drug elimination half-life of pharmaceutically active molecules, e.g. proteins, by covalent attachment of these molecules to PEG (PEGylation). The features of PEGylation, in line with its widespread use, have been reviewed extensively^{3,12-18} and are summarized by Jevševar et al. as follows:

“Conjugation of PEG to protein results in a new macromolecule with significantly changed physicochemical characteristics. These changes are typically reflected in alterations of receptor binding affinity, *in vitro* and *in vivo* biological activity, absorption rate and bioavailability, biodistribution, [pharmacokinetic] and pharmacodynamic profiles, as well as reduced immunogenicity and reduced toxicity. The main drawback of PEGylation is usually reduced biological activity *in vitro*,

which is compensated in vivo by significantly improved [pharmacokinetic] behaviour. Generally, the longer the PEG chain, the longer the elimination half-life of the PEG-protein conjugate. In addition to PEG length, its shape greatly influences absorption and elimination half-life. Various sources have confirmed that branched PEGs extend elimination half-life more than linear PEGs of the same nominal molecular weight^{19, 20}.

In their disperse form, PEGs have been widely used by the pharmaceutical industry since 1990 when the first PEGylated protein was approved (Table 1). It is noticeable that almost all approved drugs have used monomethoxy-PEGs larger than 5 kDa, often significantly larger in the range of 20 kDa to 40 kDa. This is because, particularly for large drug molecules, a minimum length of PEG is required to achieve the desired effects. The recently approved small molecular drug Movantik® (PEGylated α -naloxol) is the only notable exception, with a methoxy-PEG conjugate comprising only 7 units of ethylene glycol (Eg₇). The drug itself has a mass of only 329 Da, and together with the PEG conjugate has a mass of 652 Da. In contrast to other PEGylated drugs where the goal is to e.g. increase serum half-life, the PEGylation of naloxol is chiefly intended to prevent the drug from crossing the blood-brain barrier. It is conceivable that this recent development opens up a market for the use of PEG conjugates smaller than 5 kDa, but to date the majority of PEGylation applications require PEGs in excess of 5 kDa, equivalent to around 110 units of ethylene glycol.

Table 1. U.S. Food and Drug Administration (FDA) and/or European Medicines Agency (EMA) approved PEGylated drugs since 1990 (up to 2015). Compiled from literature sources^{3,12,17,21,22} and FDA and EMA documents available online.

Brand name ^[a]	Generic name	M _w of drug (kDa)	M _w of PEG (kDa)	Number of PEGs per drug molecule	Indication	Year approved ^[b]
Adagen	pegadamase	96-126	5	11-17	Severe combined immunodeficiency	1990
Oncaspar	pegaspargase	483-548	5	69-82	Acute lymphoblastic leukemia	1994
PegIntron	pegylated interferon alpha 2b	31	12	1	Hepatitis C	2000
Somavert	pegvisomant	42-52	5	4-6	Acromegaly	2002
Neulasta	pegfilgrastim	39	20	1	Neutropenia	2002
Macugen	pegaptanib	50	40	1 (branched)	Wet form of age-related macular degeneration	2004
Mircera	methoxy polyethylene glycol-epoetin beta	60	30	1	Anemia/chronic renal failure	2007
Pegasys	pegylated interferon alpha 2a	60	40	1 (branched)	Chronic, moderate to severe RA, Crohn's disease, axial spondyloarthritis and psoriatic arthritis	2008
Cimzia	certolizumab pegol	48	40	1	Crohn's disease, rheumatoid arthritis, psoriatic arthritis, ankylosing spondylitis	2008
Krystexxa	pegloticase	540	10	9 per homotetramer (4)	Chronic gout	2010
Omontys	peginesatide ^[c]	45	40	1 (branched)	Anemia/chronic renal failure	2012
Plegridy	pegylated interferon beta-1	44	20	1	Relapsing forms of multiple sclerosis	2014
Movantik	pegylated α -naloxol	0.33	0.32 ^[d]	1	opioid-induced constipation	2014
Adynovate	pegylated recombinant human factor VIII	280	20	2-8	hemophilia A	2015

[a] All brand names are registered trademarks

[b] Where the drug was approved in the US and Europe, and where the drug was approved for more than one indication, the earliest date is given

[c] recalled

[d] pegylated α -naloxol is currently the only drug PEGylated with a PEG chain length smaller than 5 kDa.

Cost and benefit of disperse and uniform PEG

Disperse PEG is produced industrially via living anionic polymerization from ethylene oxide. In this context, poly(ethylene glycol) is also referred to as poly(ethylene oxide) (PEO), because the route uses ethylene oxide as the monomer. PEG produced in this way typically exhibit a dispersity of less than 1.1, often less than 1.05. As shown previously, a polymer sample with a dispersity of 1.03 still comprises chains of more than 30 different lengths (Figure 2). This equates to more than 30 different distinct species in a mass spectrometric analysis, of which fewer than 10 % are the most abundant or advertised species.

Compared to living anionic polymerization, iterative synthesis of a uniform polymer of similar size is significantly more expensive as a result of the multitude of synthetic steps involved. An approximate comparison reveals a price difference of around 10^2 - 10^3 (Table 2). Uniform PEG is currently produced at relatively small scales by small independent suppliers, e.g. Quanta BioDesign (US), Polypure (NO) and Exactmer (UK). Meanwhile, conventional suppliers produce approximately 500 kton of disperse PEG per year, of which 50 % accounts for the medical uses. As a result, there is a difference in bulk availability, presumably due to lower demand for uniform PEG. It appears that the market for uniform PEG is not yet fully established and is somewhat supply-driven while the precise industrial benefits of uniform PEG are being established. The list of suppliers advertising PEGs which are of low dispersity but not uniform includes Nektar Therapeutics (US) (formerly Shearwater Corporation (US)), NOF Corporation (JP), SunBio (KR), Dr. Reddys (IN) (formerly Chirotech Technology Ltd. (UK)), JenKem (CN) and Creative PEGWorks (US). These suppliers offer PEG up to and above the lengths of approximately 40 kDa typically needed for PEGylation of pharmaceuticals.

Table 2. Approximate price comparison between disperse and uniform PEGs with M_w around 2,000.

Supplier	M_w of PEG (Da)	Functionality (R^1 -Eg _n - R^2)	Price ^[a] ($\text{£}\cdot\text{g}^{-1}$)	Type
Sigma-Aldrich	≈ 2,000	MeO-Eg _{≈45} -OH	0.60	disperse
JenKem Technology (US)	≈ 2,000	MeO-Eg _{≈45} -NH ₂ ·HCl	40	disperse
Polypure (NO)	1,252	HO-Eg ₂₈ -OH	110	uniform
Quanta BioDesign (US)	2,147	MeO-Eg ₄₈ -OH	855	uniform
Quanta BioDesign (US)	2,146	MeO-Eg ₄₈ -NH ₂	1,100	uniform
Exactmer (UK)	4,965	MeO-Eg ₁₁₂ -OH	1,500	uniform

[a] Prices were looked up between 2017-2019 and refer to purchasable quantities between 1-10 g. For simplicity, exchange rates were approximated as $\text{£} : \$: \text{€} = 1:1:1$.

While it is not yet established that uniform PEG used for PEGylation would hold significant advantages over disperse PEG with regard to in situ behaviour, there are some definite physical characteristic advantages. For example, when a drug of a given molecular weight is PEGylated with a disperse PEG, the resultant product is also disperse and thus poorly defined. But if a uniform PEG was coupled with the same drug, it would result in a well-defined product with better analysability and characterization. For example, quality control of a uniform PEG via chromatographic or mass spectrometric analysis is much simplified (Figure 14). Beyond better characterizability, uniform PEG would also feature a sharper T_m and generally behave less like a polymer. For example, uniform oligomers should provide a more predictable and more uniform assembly at the nanoscale. It is also conceivable that the use of better defined or uniform PEG could become a factor during regulatory approval.²³

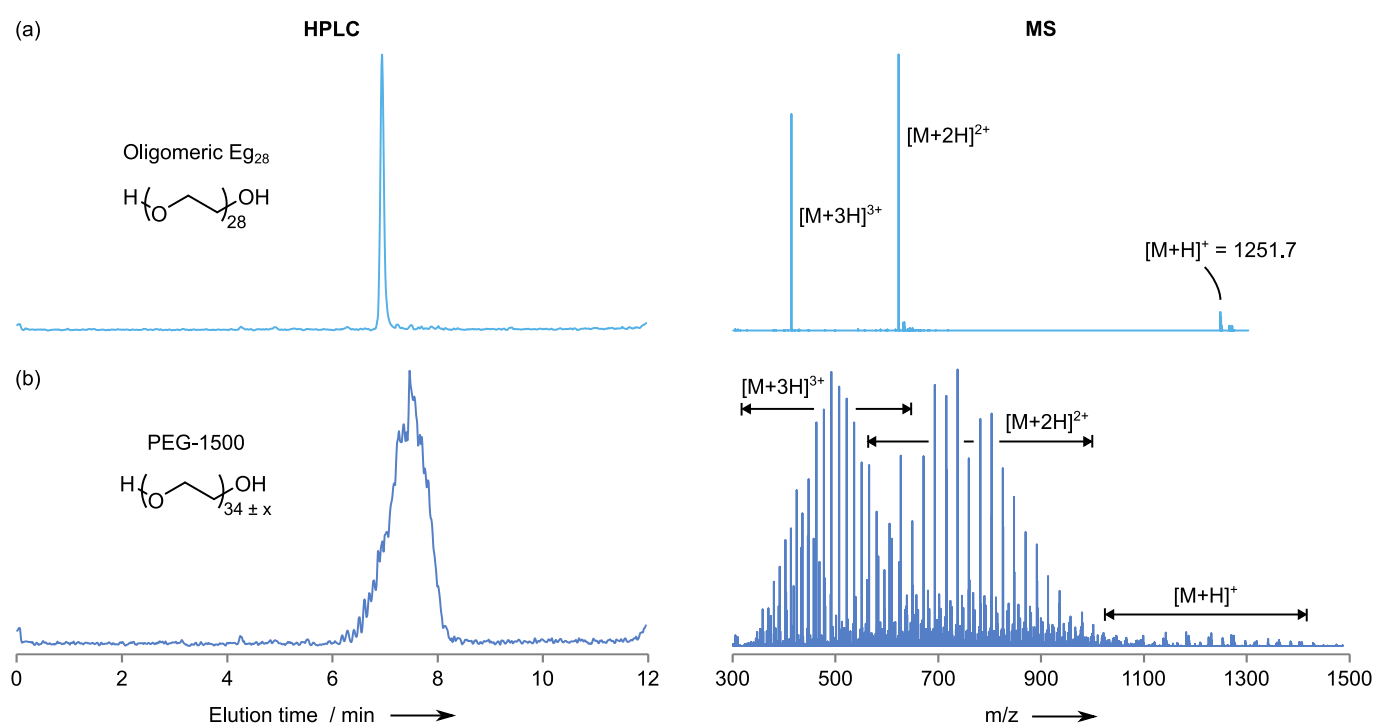


Figure 14. High-performance liquid chromatography (left) and mass spectrometry (right) show superior characterizability of the (a) uniform E₉₂₈ oligomer versus (b) a disperse PEG-1500 polymer mixture. Adapted from ²⁴ with permission from Polypure AS.

1.1.3. Synthesis of uniform poly(ethylene glycol)

Ether formation via Williamson ether synthesis

In contrast to disperse samples of PEG which are produced via polymerization of ethylene oxide, uniform oligomeric PEGs are typically synthesized via Williamson etherification (also referred to as Williamson synthesis²⁵ or Williamson ether synthesis²⁶). Williamson ether synthesis is a nucleophilic substitution reaction of S_N2 type, where an alkoxide reacts with an alkylating agent containing a nucleofuge, a leaving group (Lg) which retains the lone pair upon migration (Figure 15). Typical nucleofuges on the alkylating agent are primary halides and alkyl sulfonates, e.g. chloride (–Cl), bromide (–Br), methanesulfonate (or mesyl, –OMs) and toluenesulfonate (or tosyl, –OTs).

Because both reaction participants, alkoxide and alkylating agent, can be derived from alcohols, Williamson ether synthesis can indirectly be used to join two molecules with terminal alcohol groups such as polyether oligomers (Figure 16).

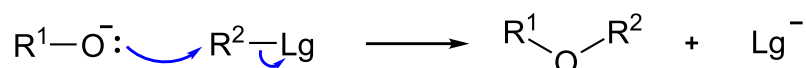


Figure 15. Williamson ether synthesis of an alkoxide with an alkylating agent. R¹, R² denote alkyl groups, preferably primary or secondary. Lg denotes a leaving group.

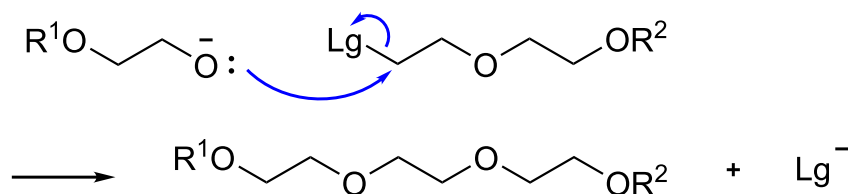


Figure 16. Joining of two polyether oligomers via Williamson ether synthesis.

Side reactions of Williamson ether synthesis

A common side reaction to etherification as with other S_N2 reactions is the competing E2 elimination (Figure 17). Particularly with poor leaving groups such as chloride, commonly used in the early attempted syntheses of uniform PEGs, E2 competition is substantial. Elimination can be mitigated by using good leaving groups such as bromides and sulfonate esters as is often done in more recent work.

Another common side reaction is the hydrolysis of the leaving group with hydroxide (Figure 18). Hydroxide may arise either indirectly from trace water which yields free hydroxide in the presence of a

strong base, or via contamination of an impure sample of base with hydroxide, e.g. trace potassium hydroxide (KOH) in lower commercial grades of potassium tert-butoxide (KOtBu).

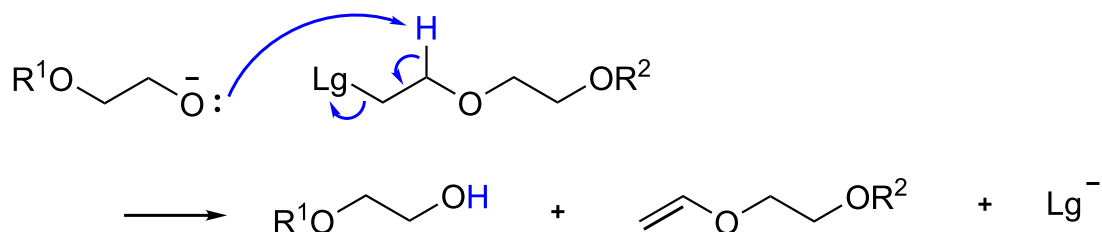


Figure 17. E2 elimination, a common side reaction during $\text{S}_{\text{N}}2$ etherifications, yields the vinyl ether by abstracting the β -proton neighbouring the carbon on which the leaving group (Lg) resides.

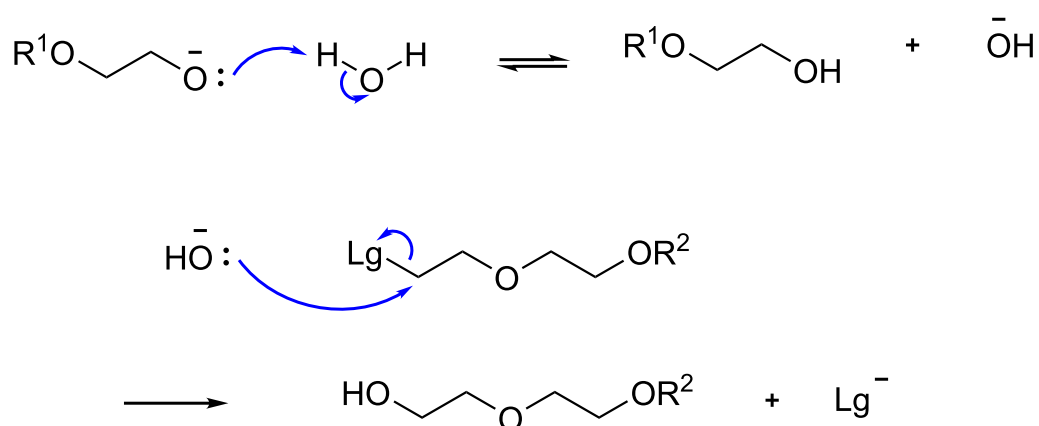


Figure 18. Hydrolysis of the alkylating agent during Williamson ether synthesis with hydroxide from trace water or impure base.

Lastly, alkoxides may depolymerize to expel small ether molecules and yield a shorter alkoxide lacking one or multiple units of ethylene glycol (Figure 19). As such, leaving alkoxides in solution for prolonged periods of time affects product quality.

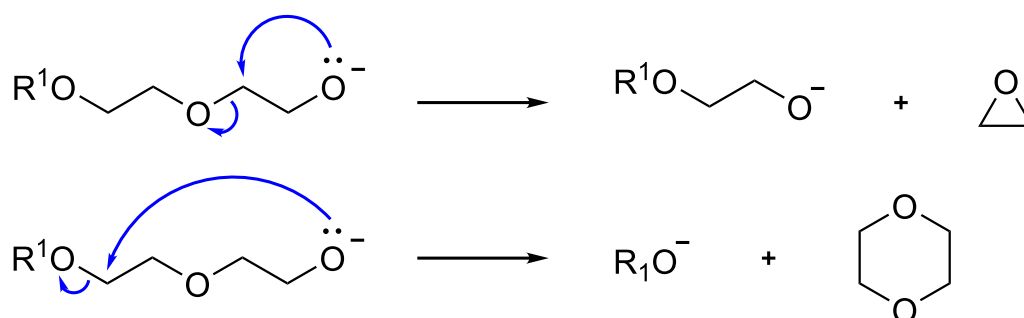


Figure 19. Depolymerization of alkoxides during Williamson ether synthesis to form ethylene oxide (top) and 1,4-dioxane (bottom).

1.1.4. Starting materials for uniform PEG synthesis

Indirect synthesis from lower homologues

Instead of using the simplest monomer, monoethylene glycol (Eg_1), to build upon, most synthetic routes toward uniform PEG start from a slightly longer oligomer that is commercially available to save reaction steps. Longer oligomers are typically assembled from ethylene glycol homologues between Eg_2 and Eg_6 with tetra(ethylene glycol) (Eg_4) most commonly used. Eg_4 is the longest oligomer readily available in quantities over 1 kg and offers a good compromise of purity, chain length and price (Table 3). Longer oligomers are still readily available up to Eg_8 but at higher expense. From around Eg_8 onwards, uniform oligomers are only available from specialist suppliers.

Table 3. Costs of oligo(ethylene glycol)s available from Sigma-Aldrich in 2017.

Eg_n	Largest available quantity / g	Price / £.g^{-1}	Purity / %
1	2,800	0.04	≥ 99
2	2,800	0.02	99
3	2,800	0.02	99
4	20,000	0.02	99
5	25	8.48	98
6	25	6.42	97
7		Not available as the diol	
8	5	70.1	97
9		Not available as the diol	

Purity of Eg_4 starting material

For the synthesis of uniform oligomers, the purity of the starting material is crucial. Any impurities in the starting material will necessarily be carried forward into the product unless some form of separation is achieved during building block synthesis. With depolymerization recognized as a common problem in uniform PEG synthesis, it is important to have an exact understanding of starting material purity. This allows a comparison of the attained final product purity to the highest possible theoretical purity that

could have been achieved for a given starting material, because shorter and longer oligomers in the starting material are necessarily carried over into the product.

For example, when assembling a longer oligomer from Eg_4 starting material with 99.5 % purity and containing 0.5 % shorter Eg_3 oligomer as impurity, an Eg_{100} product would after 24 extensions possess a maximum purity of 88.2 %. With a starting material purity of 99.8 %, the maximum attainable purity at Eg_{100} would be 95.1 %. Product oligomer purity close to this theoretical value would therefore suggest an almost flawless oligomer synthesis while a purity much lower than this theoretical value would point towards synthetic challenges irrespective of starting material quality.

1.1.5. Chain extension strategies and growth mathematics

From the various synthetic strategies available for synthesis of uniform oligomers (Section 1.1.1), a protecting group-based strategy was eventually selected for the synthesis of uniform PEG. Of the strategies available, several could be ruled out from the outset due to their specific compatibility with chemistries unsuitable for polyethers. Strategies with different building block functionalities e.g. BC/DA were not chosen because the desired poly(ethylene glycol) homopolymer was to consist of a single monomer type with ether connectivity throughout. The requirements for high purity and working in a homogeneous liquid setting in preparation for purification via nanofiltration ultimately dictated that only an approach using protecting groups would be suitable.

When synthesizing uniform oligomers via a protecting group-based strategy, four different routes of chain extension can be chosen and these differ with regard to their theoretical speed of oligomer growth, or with the quantity of additional chain length added per extension step. They can be divided into two linear and two multiplicative strategies (Figure 20): (a) unidirectional linear extension, (b) bidirectional linear extension, (c) chain doubling and (d) chain tripling.

Across the different routes exists a trade-off between the speed of chain growth and the ease of purification between chain extensions. For example, the linear growth strategies afford a slower growing oligomer but yield product mixtures which are comparatively easy to purify. On the other hand, the multiplicative doubling and tripling routes grow the oligomer exponentially fast but pose increasingly difficult purification challenges between chain extension steps as the oligomer lengthens. As a result, there are several practical implications for the successful implementation of each strategy. Below, all four traditional routes are first discussed in detail. It is then explained why a modification of a linear growth route was eventually chosen despite the theoretically inferior growth mathematics.

Because most routes towards uniform PEG currently rely on chromatographic separation, an overview of alternative purification methods is given with an outlook towards replacing the purification of intermediates between chain extension steps by nanofiltration. Besides chromatography, alternative purification methods notably include extraction and crystallization for which several examples of successful syntheses towards uniform PEG are given in the penultimate section of the introduction (Section 1.1.6). A review of historical attempts at synthesizing uniform, oligomeric PEG is presented in Appendix A.

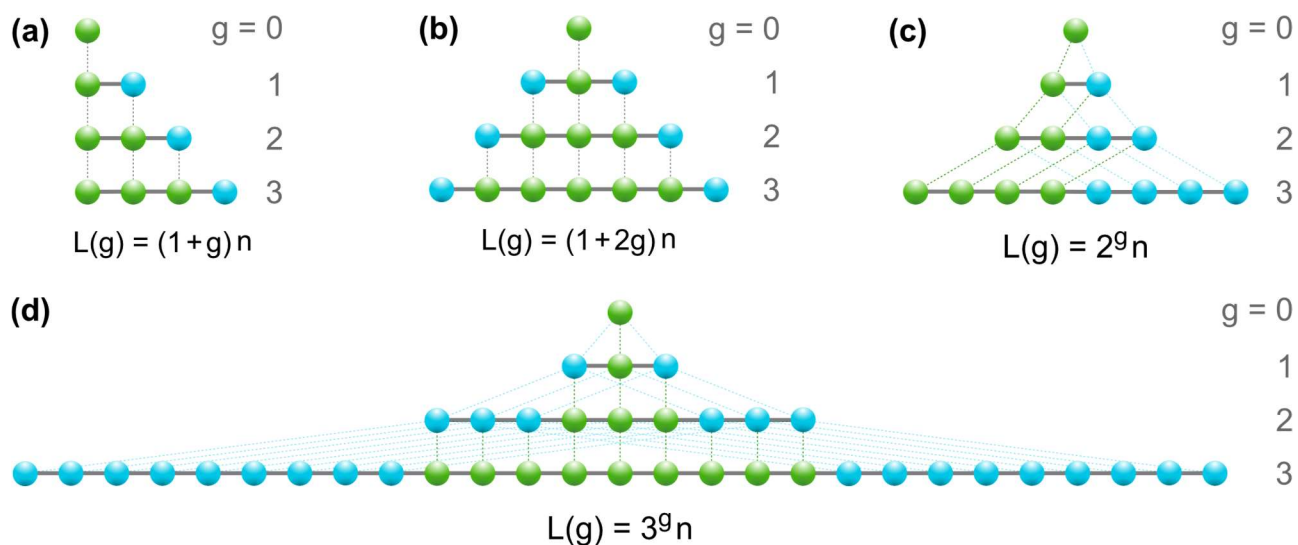


Figure 20: Speed of growth of the different chain extension routes in a protecting group-based strategy: (a) unidirectional linear extension, (b) bidirectional linear extension, (c) chain doubling, (d) chain tripling. $L(g)$ = length of the product chain in generation g , n = length of the building block, g = extension generation. ● = starting building block, or building block from previous chain extension, ● = freshly added building block during chain extension. Adapted from ²⁷ with permission from John Wiley & Sons.

Unidirectional linear extension

In unidirectional linear extension, the same building block is repeatedly added on only one side of a growing chain (Figure 21), making this route the conceptually simplest one. The unidirectional extension route relies on two different, at least partially orthogonal protecting groups, one 'semi-permanent' and one temporary. The semi-permanent protecting group renders inert the terminus that is not being extended throughout the synthesis while the temporary protecting group is removed once in each extension cycle to re-activate the terminus for further extension. However, the semi-permanent protecting group may also be removed at the very end of the extension, once the desired chain length is attained.

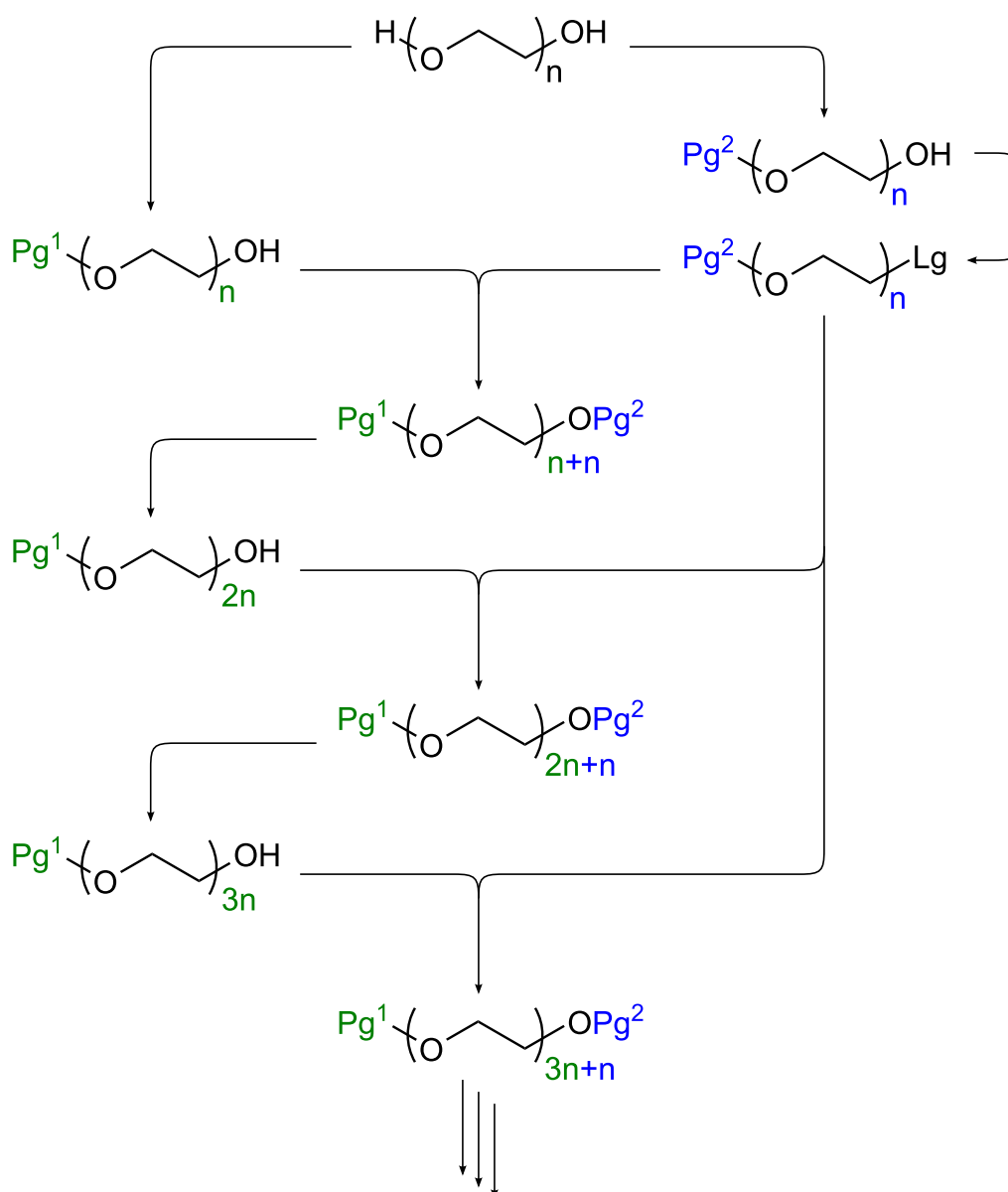


Figure 21. Unidirectional linear chain extension with two orthogonal protecting groups, Pg^1 and Pg^2 , and a leaving group, Lg .

One key requirement shared by all extension strategies is that both the temporary and the semi-permanent protecting group must be stable toward the chain extension conditions. In unidirectional linear extension, another key requirement is that the semi-permanent protecting group is stable towards the conditions used for removing the temporary protecting group, while the reverse must not necessarily apply.

As a result of the orthogonal protecting groups used, a unidirectional linear growth route inherently yields oligomers with heterobifunctionality, a much sought-after feature in PEG oligomers, as the protecting groups may be replaced by the desired functional groups toward the end of the synthesis. On the other hand, the unidirectional linear route exhibits disadvantageous growth mathematics, as an oligomer will only extend by one length of building block per chain extension cycle. Up to lengths of Eg_{16} , unidirectional linear extension has frequently been used to assemble building blocks which are then used in faster growth strategies such as chain doubling. Unidirectional linear extension is not often chosen as a strategy towards higher lengths because of its inferior growth mathematics.

Position of the nucleophile and nucleofuge

One side reaction competing with the desired Williamson etherification is E2 elimination (Figure 17) which generates vinyl ether side product by eliminating the leaving group on the chain terminus during chain extension. Depending on the type of leaving group, the vinyl ether side product can be difficult to distinguish and to remove from the product by chromatographic techniques. In linear strategies this problem is overcome by placing the leaving group on the building block. Thereby, vinyl ethers are formed from excess building block and do not reduce the reaction yield of growing oligomer by terminating fractions of the growing product. More importantly, the formed vinyl ether will be of similar size to the building block and may usually be removed jointly alongside other debris when purifying the product. Placing the leaving group on the building block is also opportune because it can be added to the building block at scale in a single step, rather than adding a leaving group to the growing oligomer prior to each further cycle of chain extension.

Bidirectional linear extension

In bidirectional linear extension strategies, like in unidirectional linear extension, the same sized building block is repeatedly added, but on both sides of the growing chain. Because building blocks are added to both sides of the growing oligomer, this strategy requires no semi-permanent protecting group and only one type of temporary protecting group.

Bidirectional linear extension strategies offer faster growth than their unidirectional equivalent but with one significant disadvantage: attachment of the same building block on both end of a chain necessarily yields a homobifunctional product with similar functionality on either terminus.

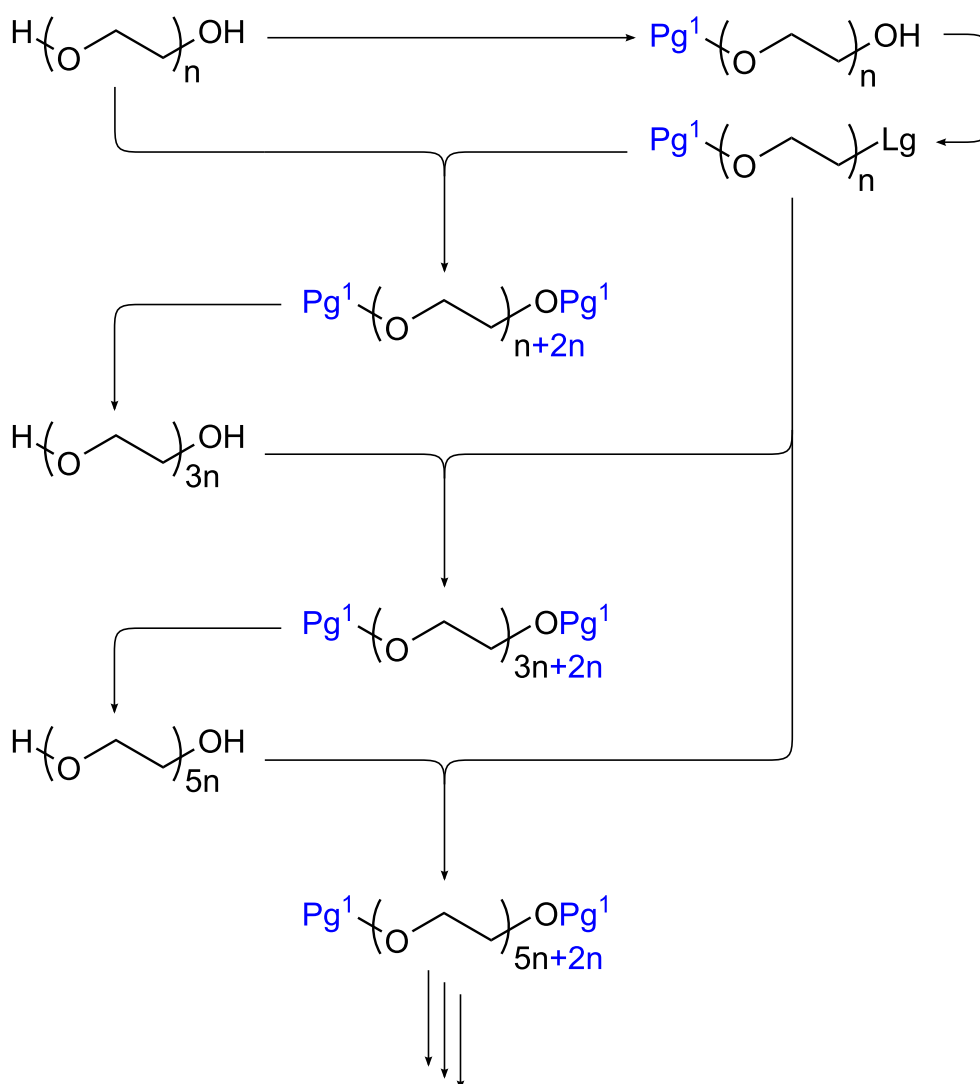
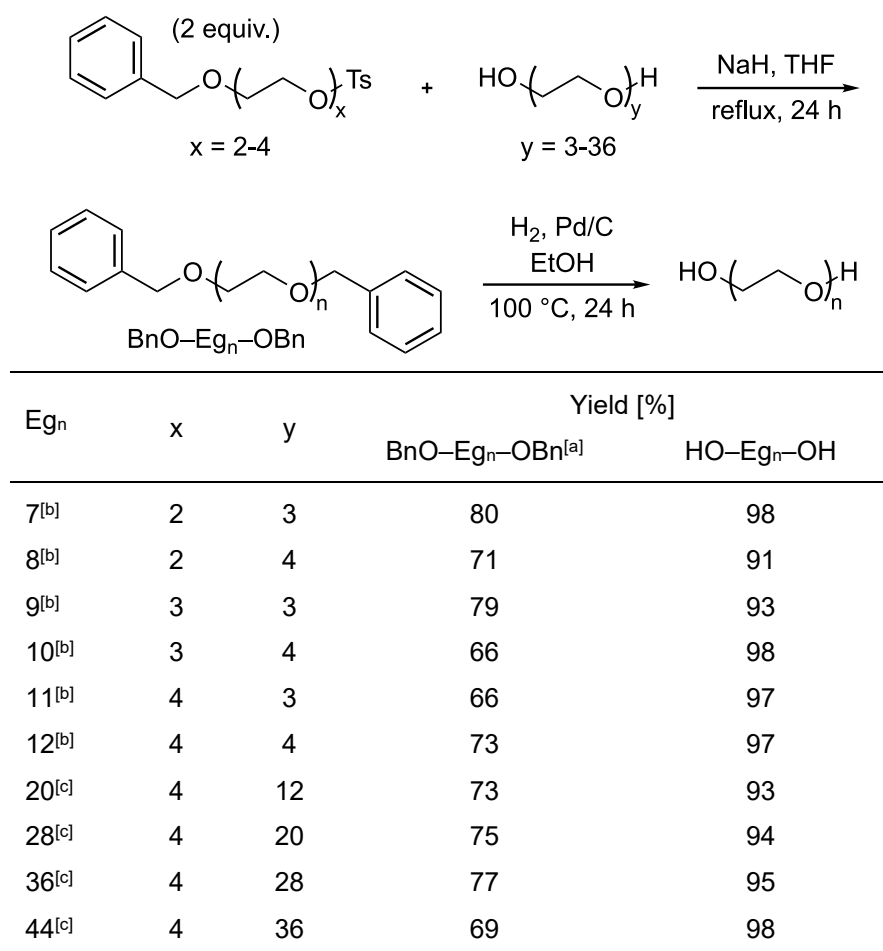


Figure 22. Bidirectional linear chain extension with one temporary protecting group, Pg^1 , and a leaving group, Lg .

Three very similar syntheses using bidirectional linear extension have been demonstrated: up to Eg_{44} by Ahmed & Tanaka in 2006²⁸, up to Eg_{29} by Niculescu-Duvaz et al. in 2008²⁹ and up to Eg_{22} by Maranski et

al. in 2014³⁰. All routes used benzyl ether as the protecting group and tosylate ester as the leaving group in their building blocks (BnO–Eg_n–OTs). Both Ahmed & Tanaka and Maranski et al. used Eg₄ as building block and the former also used Eg₄ diol as starting material whereas Maranski and co-workers appear to have used Eg₆ diol, presumably assembled from multiples of Eg₂. Niculescu-Duvaz et al. used Eg₆ as starting material for the building block and coupled this to an Eg₅ diol, presumably to make odd-numbered PEGs, in what would otherwise appear to be an unnecessary complication of the route. Niculescu-Duvaz et al. thus obtain Eg₁₇ after the first, and Eg₂₉ after the 2nd extension.

Table 4. Synthesis of uniform oligo(ethylene glycol) via bidirectional linear extension. Reproduced with permission from ²⁸. Copyright (2006) American Chemical Society.



[a] BnO–Eg_n–OBn yields are calculated based on starting oligoethylene glycols.

[b] Coupling: Eg_y (5 mmol), BnO–Eg_x–OTs (15 mmol), NaH (100 mmol), THF (250 mL), reflux, 24 h; Hydrogenolysis: BnO–Eg_n–OBn (5 mmol), 5 wt % Pd/C (200 mg), H₂ (8 atm), EtOH (130 mL), 100 °C, 24 h.

[c] Coupling: Eg_y (1 mmol), BnO–Eg_x–OTs (3 mmol), NaH (20 mmol), THF (70 mL), reflux, 24 h; Hydrogenolysis: BnO–Eg_n–OBn (1 mmol), 5 wt % Pd/C (200 mg), H₂ (8 atm), EtOH (100 mL), 100 °C, 24 h.

Ahmed & Tanaka used concentrations of 20 mM diol, 60 mM tosylate up to Eg₁₂ and lower concentrations of 14 mM diol, 43 mM tosylate from Eg₁₂ to Eg₄₄. For all reactions a large excess of NaH (20 eq., 10 eq. per hydroxyl) was used and the reactions were refluxed in THF for 24 h after dropwise addition of the tosylate in THF to the mixture of diol and NaH in THF. After quenching, the product was purified by gel permeation chromatography (GPC).²⁸

The Eg₄₄ product was the longest PEG oligomer synthesized at the time with a reportedly high degree of uniformity, but some synthetic details deserve attention. A large excess (20 eq., 10 eq. per hydroxyl) of NaH base is used and the formed free alkoxide is then left to stir in solution while the tosylate nucleofuge building block is slowly added. Regarding the main reaction, a large excess of strong base should serve little purpose as only the hydroxyls on the PEG diol need to be deprotonated to yield the respective alkoxides. With NaH as base, the formation of alkoxide is also irreversible so that a much smaller excess should suffice. Any further excess of base does not serve the main reaction but potentially promotes the competing E2 elimination. However, NaH does not exhibit high solubility in most solvents, so the problem may not be severe. Either way, a near stoichiometric use of base, or multiple substoichiometric additions, should lower the rate of competing elimination of building block nucleofuge, assuming all added base was in solution.

The conditions used for chain extension after complete addition of the reactants are also forcing (reflux in THF for 24 hours), reminiscent of some of the earlier work with chloride as a much weaker nucleofuge. This may be necessary because of the relatively low concentrations of diol and tosylate from Eg₁₂ onwards, and the generally low tosylate to hydroxyl ratio of 3:2, leading to a low concentration of both diol and tosylate towards the end of the reaction.

While the alkoxide is active and has not chain extended with a protecting group terminated building block, it is available for depolymerization. As a result, it is desirable to achieve significant conversion before using forcing conditions to push chain extension to completion. It may therefore be helpful to run the reaction nearer to room temperature for several hours and only then use more forcing temperatures. Overall, the long reaction time under forcing conditions suggests depolymerization may have taken place. The authors make no mention of depolymerization being a problem for uniformity although this had been recognized previously, e.g. by Boden et al. in 1997³¹. The work-up procedure using gel permeation chromatography is also unlikely to have resolved these shorter (-Eg₁, -Eg₂, etc.) homologues. The authors may not have judged the challenges associated with depolymerization to be a priority and their Eg₄₄ product may not be completely uniform as a result. Because no mass spectra are reproduced in the supporting information or main text, the product purity cannot be verified independently.

While the overall yields for chain extension are acceptable in the region of 66 – 80 %, their products may potentially contain entrained solvent residue. The intermediate Eg_{20} diol product is reported as a colourless liquid but comparative data of PEGs in the region of 1000 Da (DOW Carbowax™ 1000, PEG1000 of Sigma-Aldrich) suggest that the compound should be a solid with a melting range of 33-40 °C, indicative of traces of solvent in the product. PEGs hold on to solvent and are difficult to dry fully and as a result, elemental analysis results should also be viewed with caution.

There are several other examples of bidirectional coupling towards shorter oligomers: Eg_{12} by Keegstra et al. in 1992³² (Figure 23), Eg_{14} by Chen & Baker in 1999³³, Eg_{12} by Lumpi et al. in 2009³⁴ and Eg_{12} by Gothard & Grzybowski in 2012³⁵.

The syntheses are similar in their approach, all using trityl ether as the protecting group and tosylate as the leaving group. Each work details the synthesis of $TrtO-Eg_6-OTrt$ as the smallest prepared oligomer from $TrtO-Eg_2-OH$ and $TsO-Eg_2-OTs$ as a basic example or intermediate for further use. Notably, both reactants, $TrtO-Eg_2-OH$ and $TsO-Eg_2-OTs$, can be recrystallized for purification, presumably allowing attaining high oligomer purities. Further, Chen et al.³³ report that $TsO-Eg_3-OTs$ can still be crystallized successfully, extending this method to synthesize high purity oligomers from crystallizable starting materials to Eg_7 . While $TrtO-Eg_3-OH$ is rarely used, $TrtO-Eg_4-OH$ is frequently reported to be a viscous oil so is presumably not crystallizable. Similarly, there is evidence that compounds including and beyond $TsO-Eg_4-OTs$ are not crystallizable³⁶.

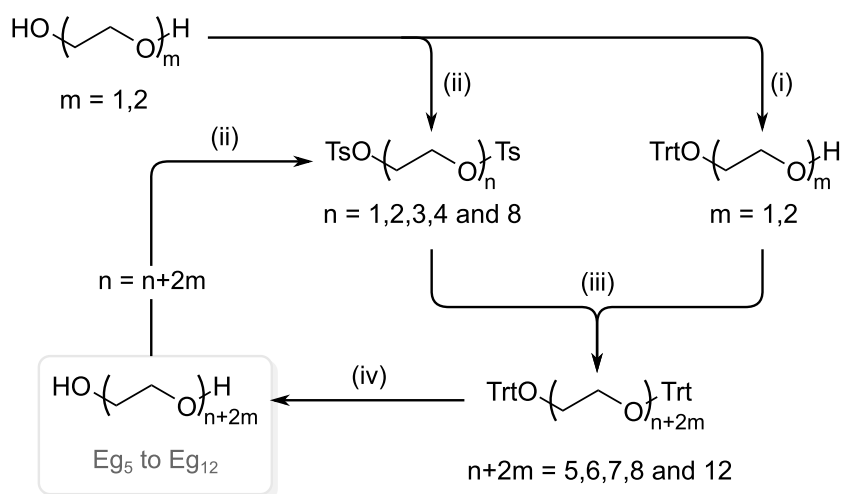


Figure 23. Bidirectional linear extension by Keegstra et al. (1992). (i) $TrCl$, pyridine; (ii) $TsCl$, KOH , CH_2Cl_2 ; (iii) NaH , THF; (iv) H_2 , Pd/C , CH_2Cl_2 . Adapted with permission from ³². Copyright (1992) American Chemical Society.

In their synthesis toward Eg_{12} , Lumpi et al. also detail a high yielding acidic cleavage of trityl ethers with 80 % $AcOH$ (40 °C, 2h) as an alternative to palladium-catalyzed hydrogenolysis. Earlier in 2009, French

et al.²⁷ had similarly cleaved trityl with trifluoroacetic acid as the catalyst and triisopropylsilane as a trapping agent for the trityl cation to prevent the reverse reaction.

Among the examples of bidirectional linear extension was also a particularly exotic one where chain extension by a single unit was carried out with isopropyl bromoacetate (Figure 24). The resultant carboxylate ester acts as a dormant reactive group, but reactivation by reduction was laborious. Due to the use of LiAlH₄ for reduction, the difficulty of removing the generated by-products after deprotection led to low yields.³⁷ The authors dismissed the strategy for continuous extension, but the reaction with isopropyl bromoacetate or an analogue can instead be used for introducing carboxylic acid terminal functionality on PEGs.

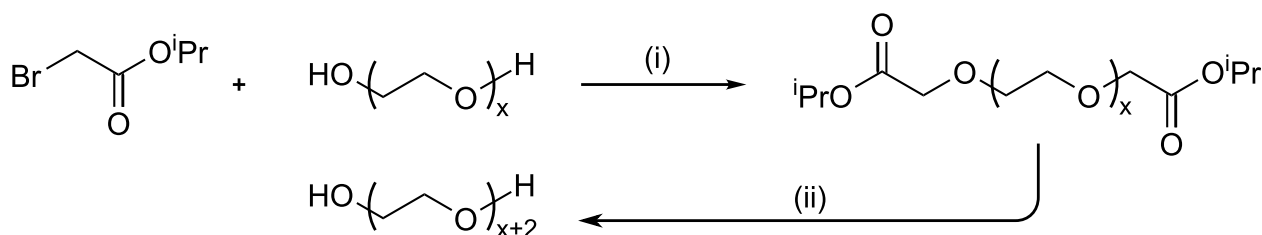


Figure 24. Bidirectional linear chain extension with carboxylate ester as protecting group. a) NaH, THF, 0 °C, 2 h, then rt, 16 h. b) LiAlH₄, THF, 0 °C, 2 h. Adapted from ³⁷ with permission from Georg Thieme Verlag KG.

Burkett & Chan eventually settled on allyl ether as protecting group on the building block instead and chain extended a bistosylate oligomer with freshly powdered KOH in the presence of 20 mol% tetrabutylammonium bromide under thermal conditions (Figure 25) to extend towards Eg₁₂.³⁷

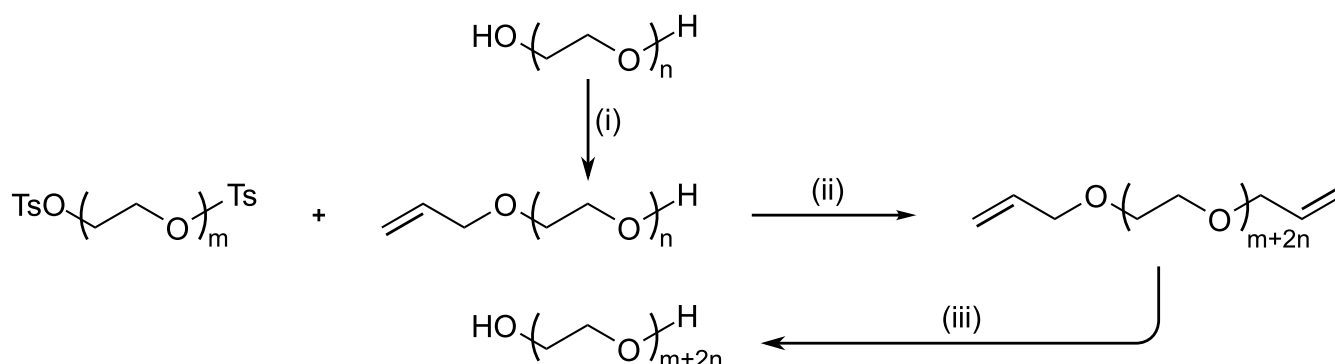


Figure 25. Bidirectional linear chain extension with allyl ether as protecting group. a) t-BuOK, allyl bromide, THF, rt, 24 h, n = 1-4. b) KOH, tetrabutylammonium bromide (20 mol%), toluene, 110 °C, 120 min, m = 1-4. c) 10 % Pd/C, TsOH (5 mol%), MeOH-H₂O (24:1), reflux, 2-24 h. Adapted from ³⁷ with permission from Georg Thieme Verlag KG.

Chain doubling

Chain doubling is a mathematically superior chain extension strategy as it attains longer chain lengths faster by growing chains exponentially rather than linearly. In chain doubling, two different building blocks with mutually orthogonal temporary protecting groups (Pg^1 and Pg^2) are needed to maintain the heterobifunctional character of the product after each extension. As a result of using two orthogonal temporary protecting groups, the product after extension will have a different protecting group at either chain terminus.

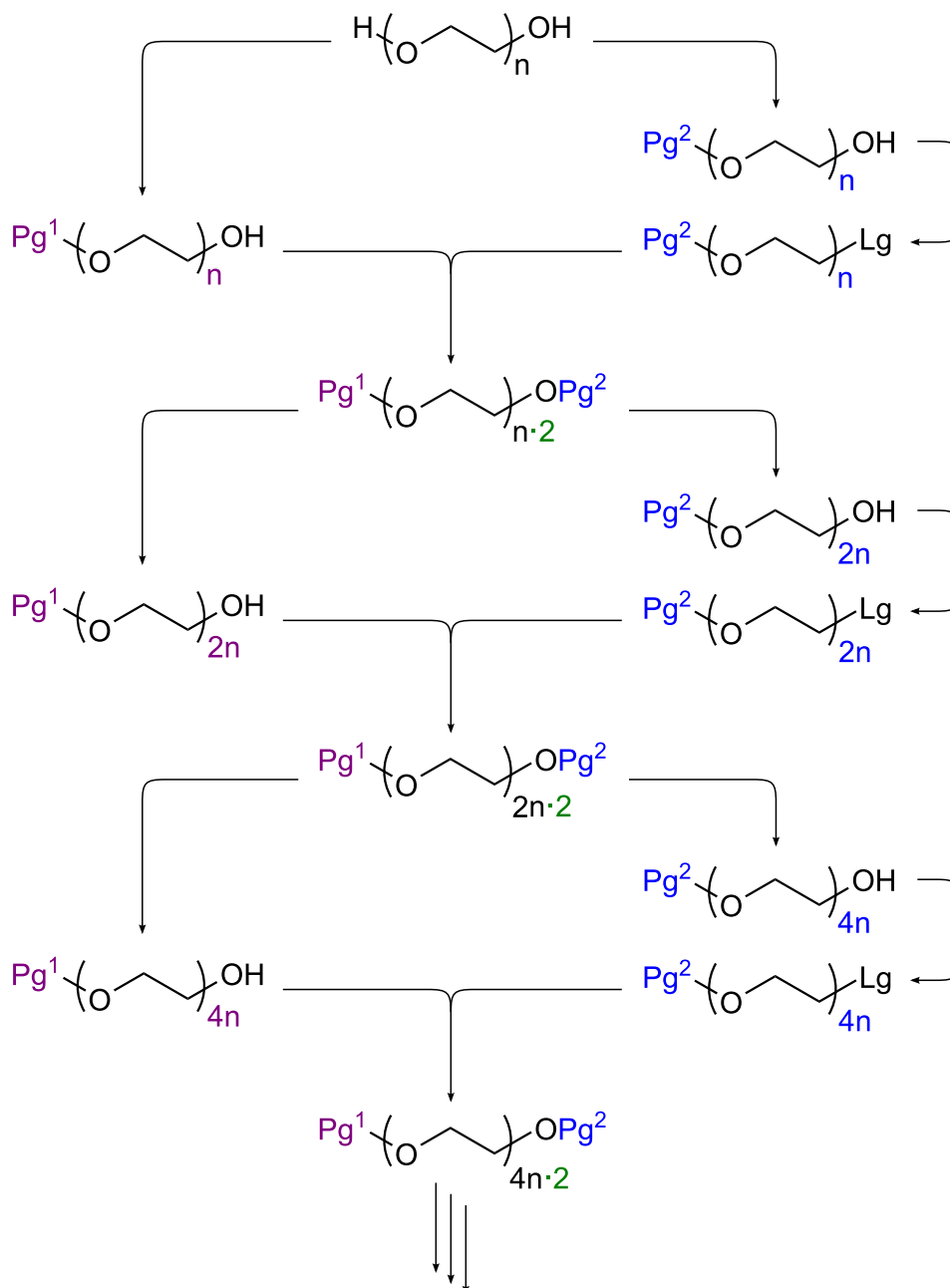


Figure 26. Chain doubling chain extension with two orthogonal temporary protecting groups, Pg^1 and Pg^2 and a leaving group, Lg.

In chain doubling, the two building blocks for chain extension are prepared from the product of the previous extension step ($\text{Pg}^1\text{-Eg}_n\text{-Pg}^2$) by splitting and desymmetrizing the product batch. From the first fraction of the product batch, Pg^2 is removed to yield $\text{Pg}^1\text{-Eg}_n\text{-OH}$. From the remaining fraction, the other protecting group, Pg^1 , is removed and replaced with a leaving group to yield $\text{Lg-Eg}_n\text{-Pg}^2$. Two building blocks with different protecting groups are thereby recreated from the heterobifunctional product obtained after each chain extension. These two building blocks may then be coupled once more in the following chain doubling step. Due to the need to assemble the building block anew after each chain extension step, the purifications and functional group interconversions between chain extensions require more steps in a chain doubling than in a linear strategy where the building block is similar in each chain extension step and can be prepared at scale for all chain extensions of a synthesis. In chain doubling, desymmetrization also becomes more difficult with each extension cycle as the product oligomer grows longer and the products become harder to distinguish by their end groups.

Critically, chain doubling strategies require full orthogonality between two temporary protecting groups. In chain doubling, both protecting groups must be removable individually without affecting the other protecting group. This is in contrast with the unidirectional linear strategy where two protecting groups are also used but where only one protecting group is temporary while the other is semi-permanent. In unidirectional linear extension, the temporary protecting group must be removable without affecting the semi-permanent protection but not vice versa because the semi-permanent protecting group only needs removing after the chain has been extended to the desired length. In practice, with etherification reactions under strongly basic conditions, the two protecting group types typically chosen are acid labile and hydrogenolytically labile protecting groups. However, while an acid labile protecting group can usually be removed without affecting a hydrogenolytically cleavable benzyl ether or equivalent, acid labile protecting groups are not always stable under hydrogenolytic conditions. It follows that the requirement for mutual orthogonality in chain doubling is substantially more difficult than the one-way orthogonality requirement of unidirectional linear extension.

In chain doubling, the relative size of the functional group termini diminishes with each extension and does so for both reagents and product. While reagents and products become increasingly dissimilar in linear strategies as the product increases in size while the same sized building block is continuously added, the opposite is true for a chain doubling strategy where both reagents and product double in size with each chain extension cycle. As products and reagents become increasingly alike due to the diminishing effect of the termini, the purification eventually requires separation of one large polyether from another, with the product chain always double the size as the reagent. This is particularly detrimental to strategies via extraction where partition relies on polarity features of one of the functional chain termini whose distinguishing character diminishes over time relative to the growing polyether

chain. But the diminishing contribution from functional groups can also negatively affect other separation techniques such as chromatography, crystallization and nanofiltration.

The doubling of the polyether chain with each extension step also has practical implications for the reaction kinetics. In order to keep the reaction rate constant, the concentration of the reactive chain termini of both reactants would have to remain roughly constant. With the inevitable increase in molecular weight and thus polyether content in the product, the ratio of terminal functional groups to polyether chain halves with each chain doubling. In order to keep the molar concentration of the chain termini in the reaction mixture constant over several chain doubling cycles, the volume of solvent must be scaled back accordingly. An increasing fraction of the reaction volume being taken up by the growing polyether is a fate that all iterative extension strategies share as the PEG oligomers grow longer. The only alternative would be to keep constant the mass ratio of reactant to solvent and accept a reduction in reactant molar concentration and the resultant slower reaction.

To date, only three examples of a chain doubling strategy have been demonstrated. An early example by Boden et al. in 1997 yielded a second generation Eg_{12} product using benzyl thioether (cleaved with Na in liq. NH_3) and tetrahydropyranyl (Thp) as orthogonal protecting groups. Two more recent examples, resulting in second and third generation doubling products respectively, were published by Loiseau et al. in 2003³⁸ up to Eg_{24} and by French et al. in 2009²⁷ up to Eg_{16} (and up to Eg_{32} with difficulty after desymmetrization was not completely selective at the Eg_{16} stage). Both examples used an acid labile protecting group and a hydrogenolytically cleavable protecting group as orthogonal pendants. While benzyl ether was used as the hydrogenolytically cleavable protecting group in both examples, French et al. used either *t*-butyl ether or trityl ether as the acid labile protecting group while Loiseau et al. used tetrahydropyranyl (Thp), or *p*-methoxybenzyl (Pmb) which can be oxidatively cleaved with one-electron oxidants.

French et al. use Eg_4 starting material and make extensive use of automated flash chromatography to separate truncated homologues ($-Eg_1$) from the Eg_8 and Eg_{16} doubling products. Here it was noted that *t*-butyl-protected Eg_8 lacked the chromatographic resolution necessary for complete removal of the truncated impurity, while trityl-protected substrates allowed superior chromatographic separation. Truncated homologues are a result of trace Eg_3 in the Eg_4 starting material as well as of base-catalyzed depolymerization of the polyether chain during chain extension.^{27,31,38} French et al. noted 3 % Eg_7 contaminant from depolymerization during chain doubling to Eg_8 after first treating the alcohol building block with NaH in dry THF, followed by dropwise addition of the tosylate building block. It was further noted that “the level of depolymerized contaminant increased with the prolonged existence of the intermediate alkoxide”²⁷. Thus, care was taken in the subsequent doubling to Eg_{16} to minimize the concentration of alkoxide by use of a softer base, $KOtBu$, which was also added gradually. While the authors state that the contaminating Eg_7 impurity of the Eg_8 α -benzyl ω -trityl ether was “readily

[emphasis added] separated by normal-phase flash chromatography²⁷, the experimental section details chromatographic elution of 25 g batches with 12 column volumes each with a fraction of the material containing > 0.25 % Eg₇ re-columned once more. 30.3 g (62 %) were recovered containing only 0.07 % Eg₇ with an additional 5.5 g (11 %) recovered at a lower unspecified purity. While the above is a testament to the excellent quality control of the authors and the need to minimize depolymerization, the relatively low overall recovery and rigorous chromatographic protocol suggest that purification is not in fact straightforward.

A similar separation was performed at the Eg₁₆ level, yielding 99.0 % oligomer purity ($\text{D} = 1.0000023$) after chain doubling presumably with NaH in DMF, and a remarkable 99.8 % oligomer purity via slow addition of base without subsequent separation of the Eg₁₅ via reverse phase chromatography.²⁷ While slow addition of base leads to a lower level of depolymerization, a higher level of tosylate elimination was observed. This is presumably due to the longer overall reaction time and the equilibrium between the polyether alkoxide and the t-butyl alkoxide, allowing a fraction of the base to be in a state where it is available to cause elimination but not chain extension. In the described procedure, 1 eq. of alcohol and 1 eq. of tosylate were coupled with 1.3 eq. of base added over a period of 20 hours using a syringe pump. The total reaction time and corresponding conversion is not separately specified, but the protocol suggests a relatively slow reaction. French et al. used a 1:1 ratio of tosylate to alcohol in their coupling reactions resulting in the reaction rate decreasing to zero in second order fashion with both reactants depleting simultaneously as the reaction approaches complete conversion.

Overall, any chain doubling strategy will always be susceptible to a lack of kinetic efficacy for which there is no convenient solution. In a chain doubling strategy, using an excess of one of the building blocks to obtain more pseudo-first order character and have the reaction rate decrease more slowly towards the end of the reaction means losing increasingly valuable product from a prior generation, if the excess cannot be recovered. The problem of losing product from a prior doubling generation when employing excess reactant in a chain doubling strategy also becomes more pronounced with each extension cycle as the reactants become longer and more valuable. This contrasts with linear strategies where the same building block can be prepared in bulk and used for all chain extension steps and employing and losing an excess of that relatively inexpensive building block can be better tolerated. On the other hand, using an excess of one reactant to drive the reaction to completion in a chain doubling strategy is also less useful, as both reactants will have similar size and be similarly easy or difficult to remove from the product. This contrasts with linear strategies where the building block will be much easier to remove from the product than incompletely extended product lacking one length of building block.

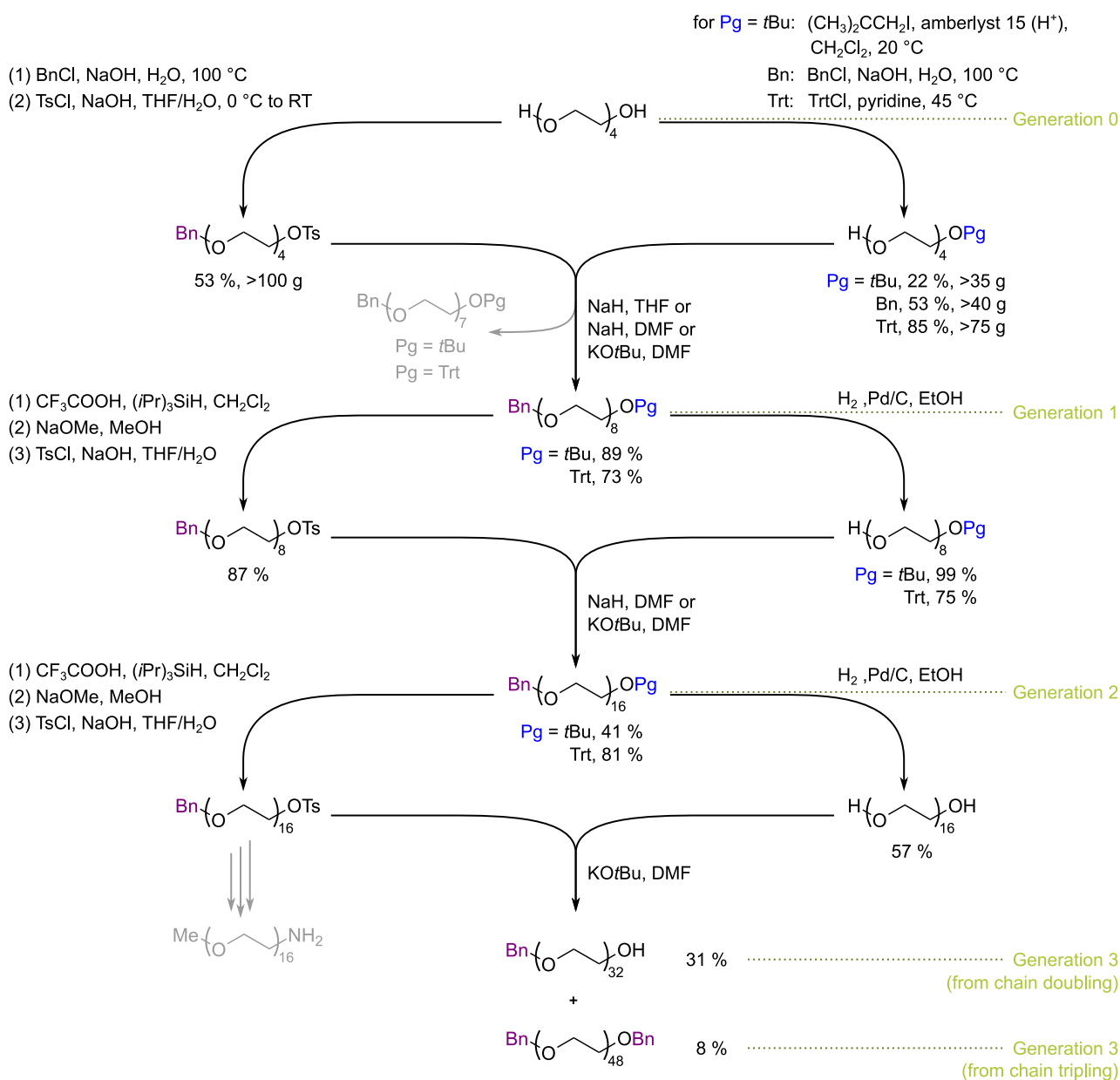


Figure 27. Synthesis of highly pure heterobifunctional BnO–Eg₃₂–OH oligomer via chain doubling and homobifunctional BnO–Eg₄₈–OBn via chain tripling by French et al. (2009). Trt = trityl, Ts = para-toluenesulfonyl, Pg = protecting group. Adapted from 27 with permission from John Wiley & Sons.

Boden et al.³¹ had previously detailed two different modes of depolymerization, noting that “the rather forcing conditions required for this reaction mean that there is almost always some base-catalyzed depolymerization [...]. Hence the reaction of H(OCH₂CH₂)₃ONa with CH₃(OCH₂CH₂)₃Cl requires 100 °C for about 3 days and the [Eg₆] product is contaminated with ca. 15 % [Eg₅] as well as smaller amounts of [Eg₄] materials, a mixture which is all but impossible to separate by fractional distillation. Another well-known depolymerization of PEG chains involves the elimination of [Eg₂] (dioxan) units in, for example, thionyl chloride chlorination of polyethylenoxy alcohols, a reaction which is suppressed in the presence of pyridine.”

Loiseau et al. observed similar problems of chain depolymerization, during chlorination of a monobenzyl-protected Eg_6 species using thionyl chloride and, in contrast to Boden et al., with or without pyridine. The authors note that GC-MS analysis of a crude reaction mixture revealed the presence of the desired product $Bn(OCH_2CH_2)_6Cl$ (36 %), accompanied by a significant amount of the truncated $Bn(OCH_2CH_2)_4Cl$, corresponding to a loss of two ethylenoxy units.³⁸ In a similar chlorination of the Eg_9 oligomer, a truncated Eg_8 homologue with loss of only one ethylenoxy unit was detected. As a result, Loiseau et al. resorted to the use of tosylates as superior nucleofuges and this is now the established protocol with chloride replaced by sulfonate leaving groups (OMs, OTs, etc.) in most of the recent syntheses of uniform PEG. In their optimized protocol, Loiseau et al. eventually arrived at an Eg_{24} oligomer, completely uniform within the limit of detection.

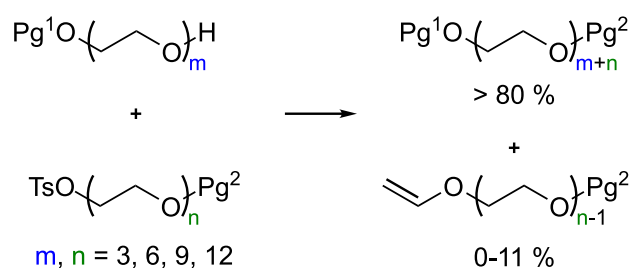
Regarding protecting group orthogonality, the hydrogenolytic deprotection of the benzyl ether at the Eg_{16} level in the above example of French et al. simultaneously results in a significant level of trityl cleavage. During benzyl deprotection, French et al. note that in cases where trityl protection was also present, regular monitoring by thin-layer chromatography (TLC) or HPLC was used to determine when all starting material had been consumed as they generally found the diol easier to remove from the product than left over starting material.²⁷ The lack of complete orthogonality is therefore apparent to the authors, and in their case presented an obstacle to further chain doubling as the heterobifunctionality of the building block could not be maintained past Eg_{16} . Similarly, Loiseau et al. noted regarding their synthesis of heterobifunctional Eg_{24} , that the benzylic protecting groups were stable under the acidic conditions required for the deprotection of the Thp group, but not vice versa.³⁸ They concluded that selective monodeprotection of these bifunctional molecules should be performed in the following order: Thp > Pmb > Bn. This obstacle highlights the systematic difficulty of maintaining a chain doubling strategy with two mutually orthogonal protecting groups. With regard to chain tripling, their preference for separating the diol rather than the diprotected starting material from the partially deprotected product also highlights the difficulty of separating chain extension products with similar chain length only based on their end group functionality, particularly as chains become longer. Several authors have attributed the cleavage of Thp acetals and triethylsilyl ethers under various hydrogenolysis conditions to the in situ generation of acid from residual $PdCl_2$ in commercial grades of Pd/C with supplier-dependent disparity.³⁹⁻⁴¹ According to another report, however, $Pd(OAc)_2$ itself does not generate significant quantities of acid in situ.⁴²

Vinyl ether formation

In chain doubling strategies, the nucleofuge necessarily needs to reside on one of the two building blocks at each step and must be added each time to one of the two building blocks in each extension cycle. As a result, vinyl ether side product is formed from one of the similarly sized reagents and complicates excess building block recovery. The relative quantities of main product and vinyl side

product in an extension reaction with tosylate as the leaving group have been quantified in detail by Loiseau et al. (Table 5).³⁸

Table 5. Synthesis of unsymmetrical Eg₉ to Eg₂₄ chains^[a] and the corresponding formation of vinyl ether by-products. Reproduced with permission from ³⁸. Copyright (2004) American Chemical Society.



Entry	Pg ¹ (m)	Pg ² (n)	Product	Yield ^[b] (%)
1	Pmb (6)	Thp (3)	PmbO(CH ₂ CH ₂ O) ₉ Thp	80 (11)
2	Bn (3)	Thp (6)	BnO(CH ₂ CH ₂ O) ₉ Thp	84 (6)
3	Bn (6)	Thp (3)	BnO(CH ₂ CH ₂ O) ₉ Thp	81 (7)
4	Bn (3)	Pmb (6)	BnO(CH ₂ CH ₂ O) ₉ Pmb	83 (8)
5	Pmb (6)	Bn (3)	BnO(CH ₂ CH ₂ O) ₉ Pmb	87 (3)
6	Pmb (6)	Thp (6)	PmbO(CH ₂ CH ₂ O) ₁₂ Thp	86 (4)
7	Pmb (6)	Bn (6)	BnO(CH ₂ CH ₂ O) ₁₂ Pmb	84 (9)
8	Bn (6)	Pmb (6)	BnO(CH ₂ CH ₂ O) ₁₂ Pmb	83 (5)
9	Bn (6)	Thp (6)	BnO(CH ₂ CH ₂ O) ₁₂ Thp	85 (6)
1	Thp (3)	Pmb (9)	ThpO(CH ₂ CH ₂ O) ₁₂ Pmb	81 (9)
2	Pmb (3)	Bn (9)	PmbO(CH ₂ CH ₂ O) ₁₂ Bn	88 (0)
3	Bn (3)	Pmb (9)	PmbO(CH ₂ CH ₂ O) ₁₂ Bn	84 (5)
4	Thp (3)	Bn (9)	ThpO(CH ₂ CH ₂ O) ₁₂ Bn	83 (7)
5	Pmb (6)	Bn (9)	PmbO(CH ₂ CH ₂ O) ₁₅ Bn	87 (4)
6	Bn (3)	Pmb (12)	PmbO(CH ₂ CH ₂ O) ₁₅ Bn	81 (0)
7	Thp (6)	Bn (9)	ThpO(CH ₂ CH ₂ O) ₁₅ Bn	88 (0)
8	Thp (9)	Bn (9)	ThpO(CH ₂ CH ₂ O) ₁₈ Bn	81 (7)
9	Thp (6)	Bn (12)	ThpO(CH ₂ CH ₂ O) ₁₈ Bn	80 (7)
10	Pmb (9)	Bn (9)	PmbO(CH ₂ CH ₂ O) ₁₈ Bn	85 (8)
11	Pmb (6)	Bn (12)	PmbO(CH ₂ CH ₂ O) ₁₈ Bn	91 (3)
12	Thp (9)	Pmb (9)	ThpO(CH ₂ CH ₂ O) ₁₈ Pmb	90 (4)
13	Pmb (12)	Bn (12)	PmbO(CH ₂ CH ₂ O) ₂₄ Bn	83 (0)

[a] Reaction conditions: the alcohol was stirred with 1.8 equiv of NaH in THF for 20 to 24 h, prior to the addition of the tosylate, and reacted further for 3 days.

[b] Isolated yields after purification. Value in parentheses correspond to % yield of the vinyl ether side product.

From an economic point of view, loss of excess building block to elimination is less problematic for the comparatively short and relatively low value building block in linear strategies, whereas loss in chain doubling strategies represents loss of a fraction of increasingly valuable product at each extension stage.

Detrimental effect of trace hydroxide or water in chain doubling strategies

There is one further crucial aspect of chain doubling that has not been discussed in the literature to the author's knowledge. The successful chain doubling strategy relies on the orthogonality of the protecting groups and on the product of each chain doubling reaction to retain these two different protecting groups. However, any trace water or hydroxide will indirectly result in a minor quantity of homobifunctional side product with the same protecting group on each terminus (Figure 28). Particularly for longer chain lengths, these homobifunctional and heterobifunctional chains with similar length will be very difficult to separate. If the homobifunctional side product were not separated, it would be carried forward as the diol and cause chain tripling during the next chain extension step. This chain tripling product would also be homobifunctional (Pg^2 on both ends) and 50 % longer than the main product, once again posing a separation challenge, albeit a slightly less difficult one.

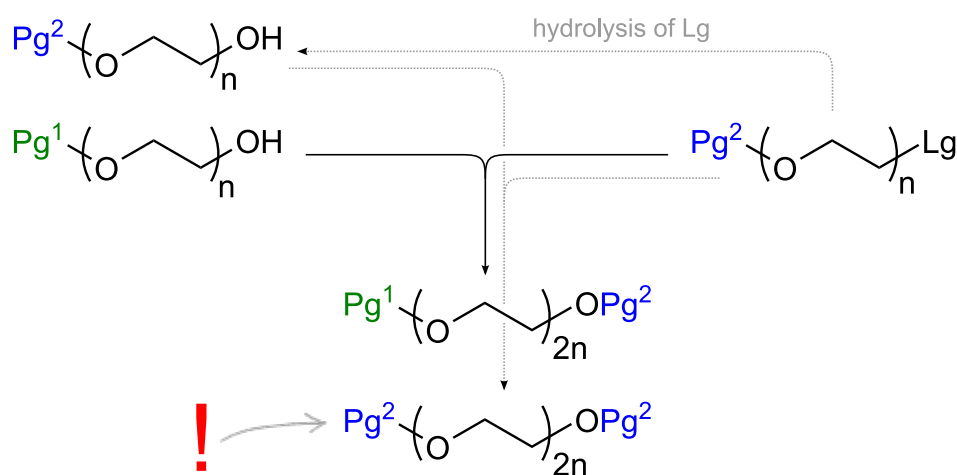


Figure 28. Chain doubling chain extension with two orthogonal protecting groups, Pg^1 and Pg^2 and a leaving group, Lg. Trace hydroxide or water in the presence of strong base leads to hydrolysis of the leaving group on the activated building block and the resultant building block is also available for coupling. This ultimately leads to two molecules of the same building block combining to yield a homobifunctional product with similar protecting groups on either terminus.

Analysis for chain doubling strategies

Chain doubling strategies require more extended analysis and quality control when analysing two different length reagents additional to the changing product at each extension level. As a result, many different species need tracking, calibrating and accounting for during reaction and downstream separation. When using an acid labile protecting group without a UV chromophore as well as a UV active

nucleofuge such as a tosylate, it would appear sensible to combine these on one building block and leave the alcohol functionality on the building block on which the UV active benzylic ether or equivalent protecting group resides, so that both building blocks may be tracked by UV. The product is UV traceable even if only one of the protecting groups contains a UV chromophore.

Chain tripling

In chain tripling, two equivalents of building block derived from the product of the previous extension step are added to a third fragment of product, also from the previous step (Figure 29). The same building block is therefore attached at either end leading necessarily to a homobifunctional product with two similar protecting groups on either side of the chain. Thus, it is not possible to remove one protecting group selectively and reassemble two different building blocks for the next coupling step as is possible in chain doubling. Partial deprotection of homobifunctional extension product will yield a statistical mixture of unreacted doubly protected product, singly protected product, and fully deprotected product. Separation of the resultant mixture is very challenging and will become more difficult with increasing chain length as the distinguishing character of the termini diminishes. If separation of the mixture is possible, a leaving group may be added to the other side of the singly protected product. The resultant building block may then be reacted with the fully deprotected product in the next chain tripling, while the unreacted still doubly protected starting material from the previous step is not immediately useful. While theoretically the fastest growth strategy, chain tripling is therefore only practicable with a significant effort spent at desymmetrizing the homobifunctional product after each extension step.

In a rare example, French et al. performed chain tripling at the end of their synthesis (Figure 27). They opted to fully deprotect the Eg_{16} building block with trifluoroacetic acid (TFA) to yield the diol after substantial trityl cleavage had already occurred during attempted monodeprotection of the benzyl ether protecting group during hydrogenolysis. The last step of their synthesis was thus a chain tripling trial between $\text{HO-Eg}_{16}\text{-OH}$ and $\text{BnO-Eg}_{16}\text{-OTs}$. Judging by the reaction yields with both $\text{BnO-Eg}_{32}\text{-OH}$ (21 %) as well as $\text{BnO-Eg}_{48}\text{-OBn}$ (8 %) formed, kinetic efficacy was low.²⁷

Overall, chain tripling is not commonly practised due to the homobifunctional product formed after each extension step, which is difficult to heterodifunctionalize and separate. It may therefore reasonably be used as the final chain extension step, where a homobifunctional product is needed, but is likely to be practically unworkable in other cases.

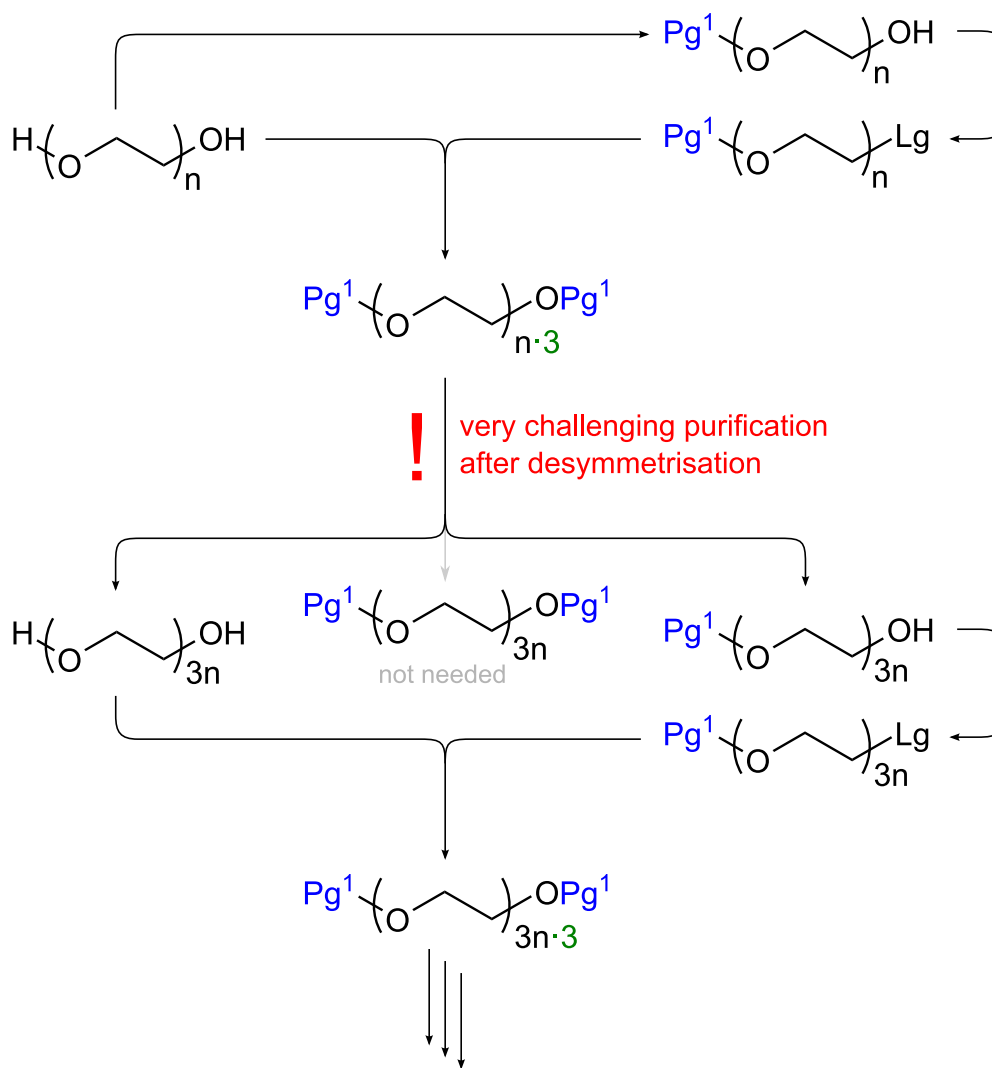


Figure 29. Chain tripling chain extension with a protecting group, Pg^1 , and a leaving group, Lg .

1.1.6. Examples of separation strategies for uniform oligomer synthesis

Because uniform oligomers are synthesized in an iterative fashion, many individual extension cycles are needed to reach the target length. In order to ensure uniformity, reaction debris and excess monomer need to be separated after each extension step resulting in large number of purifications en route to the final oligomer. Because Williamson ether synthesis requires no expensive catalysts and can be run in common solvents with inexpensive base, the cost of uniform PEG synthesis is driven by the purification between extension cycles.

The separation can be further divided into purification after chain extension and purification after building block preparation, particularly for the linear synthesis routes. In a linear strategy, a single type of building block is manufactured at the start of the synthesis and then used for all chain extensions. As a result, the linear routes are particularly improved by methods that allow straightforward and economic building block synthesis in bulk. The separation after chain extensions is a challenge that all strategies share and where the method of separation often depends on oligomer chain length.

For most syntheses demonstrated in the literature to date, chromatography is still the first choice, particularly for purifications of longer oligomers past Eg_{16} . But several recent advances demonstrate that much research is devoted to finding viable and economically beneficial alternatives to chromatography, particularly for building block synthesis. Where a hydrophobic leaving group still represents a large part of the molecule, it was demonstrated that extraction is feasible up to Eg_{16} . And for smaller oligomers, a route via macrocyclic sulfates utilizing crystallization has shown much promise. These three different separation techniques – chromatography, extraction and crystallization, each a potential alternative to nanofiltration, are outlined alongside several examples below.

1.1.6.1. Chromatography as a separation technique

Most growing uniform oligomers can be separated from their precursors via chromatography and for most substrates that are non-crystallizable and require mild conditions, chromatography remains the standard technique for purifications in the pharmaceutical industry. With simulated moving bed chromatography and multicolumn counter current solvent gradient purification, even difficult mixtures can be separated industrially and technical feasibility is usually 'only' a question of column length. However, chromatography is typically an expensive separation technique when compared to alternatives such as distillation or extraction. While linearly scalable, chromatography requires the preparation and maintenance of solid beds with the associated limitations of axial dispersion and limited mass transfer. If uniform PEG synthesis is to succeed industrially, more economical separation techniques will likely have to be employed. Where not otherwise mentioned, previous studies of uniform PEG have used chromatography as their means of separation.

1.1.6.2. Extraction as a separation technique

In a chromatography-free strategy designed to facilitate extractive separations, Wawro et al.^{43,44} used trityl as protecting and tosylate as leaving group, with both functional groups and particularly the leaving group acting as hydrophobic tags. In their strategy, only one active species is carried forward from each step with all other by-products protected on either terminus and thus inert to further extension. At the end of their synthesis, all symmetric biprotected by-products are eventually transformed into hydrophilic PEGs of different lengths and removed by extraction with brine, leaving only the desired product in the organic layer with the leaving group acting as the hydrophobic anchor (Figure 30). The building block functional asymmetry is introduced in the first step.

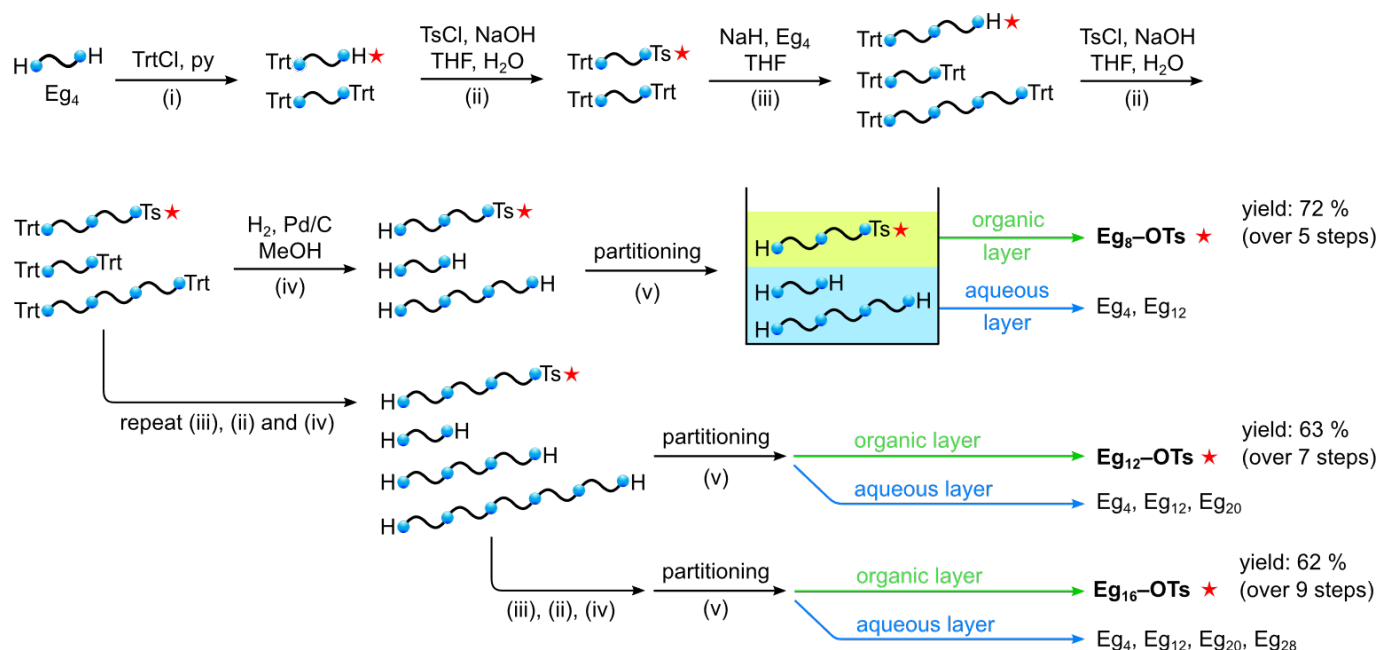
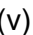



Figure 30. Chromatography-free synthesis of Eg₈, Eg₁₂ and Eg₁₆ oligo(ethylene glycol) mono-p-toluenesulfonates via extraction. (i) Asymmetric protection with triphenylmethyl chloride (trityl chloride, TrtCl), excess Eg₄, pyridine, rt (ii) leaving group activation with 4-toluenesulfonyl chloride (tosyl chloride, TsCl), THF:H₂O, 0 °C (iii) chain elongation with Eg₄, NaH, THF, 40 °C and (iv) hydrogenolytic cleavage of the trityl ether, followed by (v) partition between ethyl acetate and saturated brine.  = Eg₄,  = terminal oxygen or oxygen between Eg₄ sections, ★ = target species. Intermediate compounds prior to partition (v) were not isolated in pure state. Adapted from ⁴⁴ under a CC BY-NC 3.0 License.

The strategy crucially relies on the clean partition of unsubstituted, free PEG diols into the aqueous phase, with simultaneous retention of p-toluenesulfonate esters in the organic layer. The strategy is demonstrated up to Eg₁₆, i.e. up to HO–Eg₁₆–OTs. In their protocol⁴³, the authors give a detailed account of the strategy up to Eg₈, and speculate that the method can be applied up to HO–Eg₂₄–OTs, acknowledging that “oligomers longer than PEG₂₄-Ts do not have sufficiently high affinity to the organic layer and are lost during extraction.”⁴⁴

The extrapolation to successful synthesis of $\text{Eg}_{24}\text{-OTs}$ was made based on successful retention of a 2 % solution of PEG1000-OTs in EtOAc when extracting with an equal volume of 100 % sat. brine (Figure 31). Extraction with different strengths of brine show that partition is no longer clean below 100 % saturation, and that a fraction of the longer oligomers, from about $\text{HO-Eg}_{16}\text{-OTs}$ and longer, partially reside in the aqueous phase when partitioning with 75 % brine. In their synthesis of $\text{HO-Eg}_8\text{-OTs}$, the actual concentration in the organic layer is much higher at approx. 11.5 % w/v (33.5 – 35.5 g in 300 mL EtOAc), and at least two washes are made with only 50 % saturated brine.

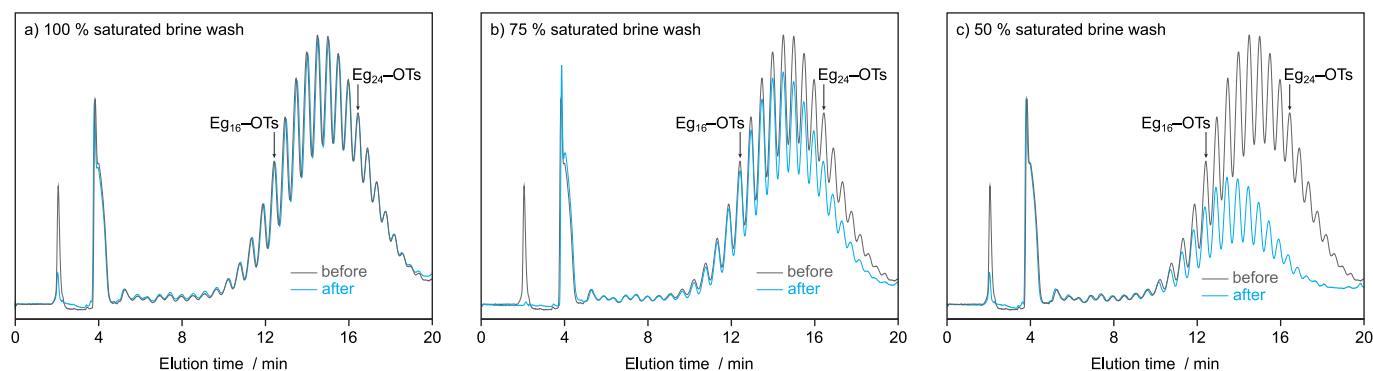
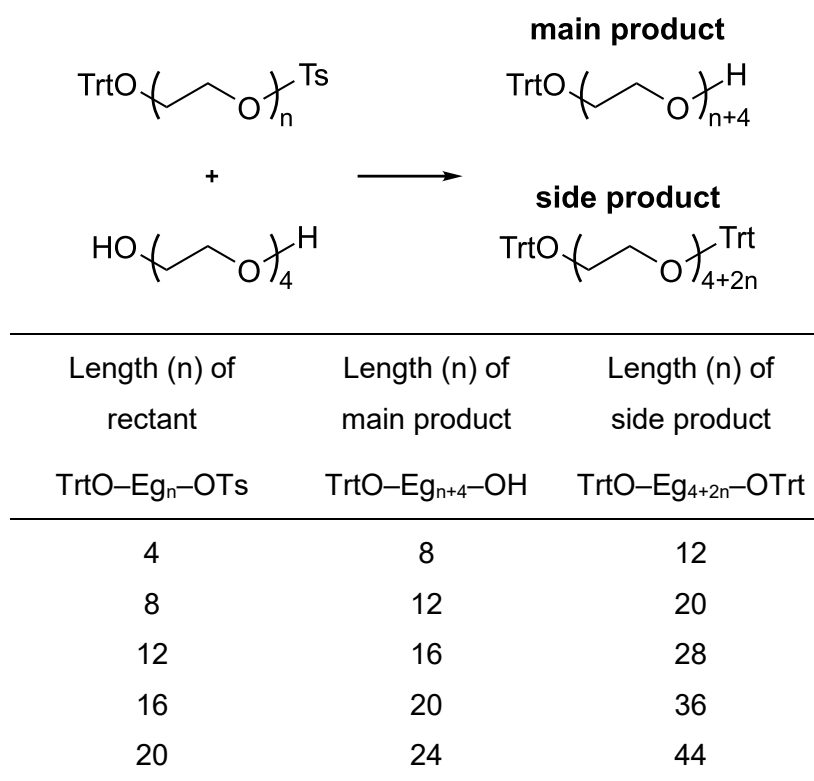


Figure 31. HPLC chromatogram of PEG1000-OTs before (grey) and after partition (blue) between ethyl acetate and brine. A 2 % solution of PEG1000-OTs in EtOAc was extracted with an equal volume of (a) 100 % saturated brine, (b) 75 % saturated brine and (c) 50 % saturated brine. Analysis performed with Cosmosil 5C₁₈-AR-II column, 4.6 × 150 mm at 40 °C, eluted with 50-65 % (v/v) MeOH : H₂O linear gradient during 20 min, with a constant flow rate of 0.8 mL min⁻¹. Reproduced from ⁴³ under a CC BY-NC 3.0 License.

There is a second complication in using extraction with unidirectional linear extension strategy that makes use of a large excess of tetragol during chain extension as opposed to a second protecting group. Despite the large excess of the alcoholic reagent, there will be a small degree of statistical dimer formation, e.g. during extension from $\text{TrtO-Eg}_4\text{-OTs}$ with a large excess of $\text{HO-Eg}_4\text{-OH}$, $\text{TrtO-Eg}_8\text{-OH}$ will be the main extension product, but contaminated by a small amount of $\text{TrtO-Eg}_{12}\text{-OTrt}$. The diol side product after deprotection of the first extension mixture, $\text{HO-Eg}_{12}\text{-OH}$, may still extract into the aqueous phase sufficiently well. However, the dimer side product chain becomes increasingly long with each further generation in the fashion (Table 6).

With the extension from $\text{TrtO-Eg}_{20}\text{-OTs}$ to $\text{TrtO-Eg}_{24}\text{-OH}$, extraction after deprotection would therefore not only have to remove all Eg_4 but also all Eg_{44} diol side-product into the aqueous phase, while retaining all Eg_{24} tosylate, arguably a difficult partition. The problem of the dimer side product could be avoided by using a temporary protecting group additional to the semi-permanent trityl protection, rather than relying on a large excess of tetragol in each chain extension step.

Table 6. Unidirectional chain extensions of building blocks with a large excess of Eg₄ instead of using Eg₄ with an orthogonal protecting group. A common side reaction when the second protecting group is omitted is the attachment of two units of activated building block to a single Eg₄.



As a potent surfactant, PEG will eventually interfere with extraction and impose a limit on how far a synthetic route based on purification by extraction can proceed. Wawro et al.'s contribution is valuable in that it provides a chromatography-free, scalable route to building blocks of lengths up to Eg₁₆ from where strategies based on other purification techniques can proceed. Independent of the exact oligomer length reached, an extractive strategy of this type will be limited to building blocks where a hydrophobic leaving group provides sufficient retention of the product in the organic phase after deprotection, and where diol can still simultaneously be removed into the aqueous layer.

There are a few further examples of extractive techniques in uniform PEG synthesis and beyond relying on elaborate functional groups such as fluorohydrocarbons.^{45,46}

1.1.6.3. Crystallization as a separation technique – a route via macrocyclic sulfates

Another method suitable for producing lower length building blocks is a strategy via macrocyclic sulfates described in two similar publications by Zhang et al. in 2015^{47,48}. The strategy was touted as highly efficient by the authors and afforded uniform Eg₆₄, the longest uniform PEG oligomer at the time, but is comparable to other approaches in extension cycle yield. The key advantage of the approach appears to be the use of a cyclic sulfate as building block, which opens the potential for recrystallization as a purification technique. With a few exceptions of very short, functionalized oligomers, e.g. TsO–Eg₂–OTs, most linear PEG derivatives cannot be crystallized. As a result, the removal of shorter and longer homologues from trace contaminated PEG starting material, e.g. Eg₃ and Eg₅ in Eg₄, is difficult. The rigidity provided through the transformation of PEG into a cyclic sulfate circumvents this limitation.

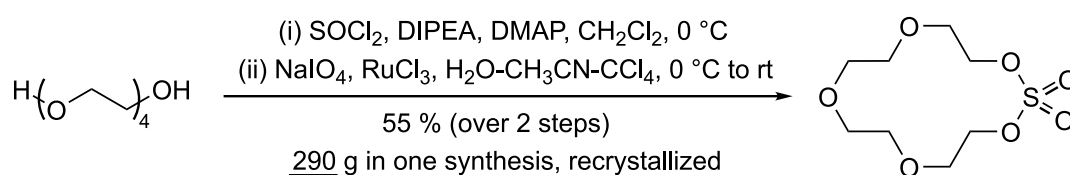


Figure 32. Large-scale preparation of the macrocyclic sulfate of Eg₄. DIPEA = N,N-diisopropylethylamine, or Hünig's base. DMAP = 4-dimethylaminopyridine Reproduced from ⁴⁷ with permission from WILEY-VCH.

Zhang et al. demonstrated that macrocyclic sulfates can be recrystallized at scale (Figure 32) and that they can be synthesized from homologues of varying length from Eg₂ to at least Eg₂₀ (Table 7). There appears to be a drop in isolated yield from a maximum of 84 % for Eg₄ down to approx. 50 % for the Eg₁₆ and Eg₂₀ homologues, with a simultaneous eight-fold reduction of concentration and increase in reaction temperature. It may reasonably be suspected that selective recrystallization of these macrocycles therefore also has its limits, perhaps around Eg₁₂ to Eg₁₆. The side products formed during the first reaction step are presumably cyclic dimers where the intermediate chlorosulfite nucleofuge generated from SOCl₂ is attacked intermolecularly by another starting molecule, rather than intramolecularly by the other end of the chain on which the nucleofuge resides. As a result, a high dilution (low concentration) is needed to favour the intramolecular pathway towards the monomeric cycle and avoid formation of linear species and macrocycles containing multiple connected chains. Incidentally, this high dilution reaction potentially lends itself well to combination with an integrated membrane system as demonstrated by Ormerod et al. in their formation of a cyclic peptide via OSN.⁴⁹ While the use of CCl₄ in this instance can presumably be avoided with alternative solvents such as CH₂Cl₂, as demonstrated in a similar reaction on a different linear substrate⁵⁰, the oxidation uses relatively costly RuCl₃ as catalyst.

Table 7. Macrocyclization of various oligo(ethylene glycols) from Eg₂ to Eg₂₀.^[a] Reproduced from ⁴⁷ with permission from WILEY-VCH.

Eg _n	Concentration [mol·L ⁻¹]	T [°C]	t ^[b] [h]	Yield (%)	
				Sulfite	Sulfate
2	0.041	0	1	76	96
3	0.041	0	1	71	98
4	0.041	0	1	84	87
5	0.041	0	1	81	86
6	0.041	0	1	79	94
7	0.021	10	1	72	96
8	0.021	10	1	82 ^[c]	75
9	0.021	10	12	71	89
10	0.005	10	12	57	84
12	0.005	10	72	63 ^[d]	83
16	0.005	10	40	51	69
20	0.003	25	24	49	62

[a] Reactions were performed on 1-5 g scales.

[b] Reaction time after dropwise addition of SOCl₂.

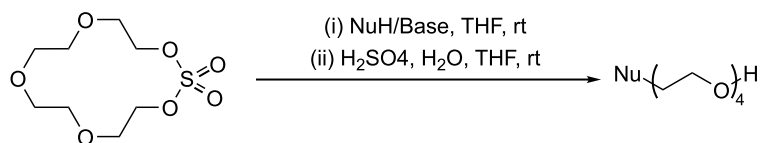
[c] A yield of 53 % was obtained at 0.041 mol·L⁻¹ Eg₈.

[d] A yield of 59 % was obtained at 0.010 mol·L⁻¹ Eg₁₂.

While Zhang et al. described their process as leaving group and protecting group free, it is noticeable that they are in fact combined in the macrocyclic sulfate. During nucleophilic attack the sulfate acts as the leaving group and after attachment of the nucleophile it continues to reside on the other end of the chain as a sulfonate anion that acts as a protecting group until it is removed with H₂SO₄/H₂O in the second reaction step. The strategy allows a wide variety of functional groups to be inserted in this fashion (Table 8).

Zhang et al. then demonstrated the synthesis to Eg₃₆ via bidirectional extension with cyclic Eg₄ building block as well as synthesis of Eg₆₄ via unidirectional extension with Eg₈ building block (Figure 33). Reaction conditions and yields of either strategy are similar to other uni- and bidirectional coupling strategies, and it is suspected that trace water would also lead to dimer formation.

Table 8. Nucleophilic ring-opening of Eg₄ macrocyclic sulfate to yield a variety of linear monofunctionalized PEGs.^[a] Reproduced from ⁴⁷ with permission from WILEY-VCH.



Entry	NuH / Base	Product	Yield [%]
1	BnOH / NaH	BnO-(CH ₂ CH ₂ O) ₄ -H	93
2	BnO-(CH ₂ CH ₂ O) ₄ -H / NaH	BnO-(CH ₂ CH ₂ O) ₈ -H	88
3	ⁿ C ₈ F ₁₇ (CH ₂) ₃ OH / NaH	ⁿ C ₈ F ₁₇ (CH ₂) ₃ O-(CH ₂ CH ₂ O) ₄ -H	76
4	ⁿ C ₈ H ₁₇ OH / NaH	ⁿ C ₈ F ₁₇ O-(CH ₂ CH ₂ O) ₄ -H	80
5	/ NaH		94
6 ^[b]	MeONa	MeO-(CH ₂ CH ₂ O) ₄ -H	70
7	KO ^t Bu	^t BuO-(CH ₂ CH ₂ O) ₄ -H	48
8			99
9	/ NaH		92
10	/ NaH		83
11	/ K ₂ CO ₃		72
12	AcONa	AcO-(CH ₂ CH ₂ O) ₄ -H	99
13	BzONa	BzO-(CH ₂ CH ₂ O) ₄ -H	99
14	AcSK	AcS-(CH ₂ CH ₂ O) ₄ -H	88
15	TrtSH	TrtS-(CH ₂ CH ₂ O) ₄ -H	84
16	EtO ₂ C-CH ₂ -CO ₂ Et / K ₂ CO ₃		34
17	BnNH ₂ / NaH		80
18	NaN ₃	N ₃ -(CH ₂ CH ₂ O) ₄ -H	97
19 ^[b,c]	NaF	F-(CH ₂ CH ₂ O) ₄ -H	88

[a] All reactions were performed on 1 g scales.

[b] DMF was used as solvent.

[c] The reaction was run at 120 °C.

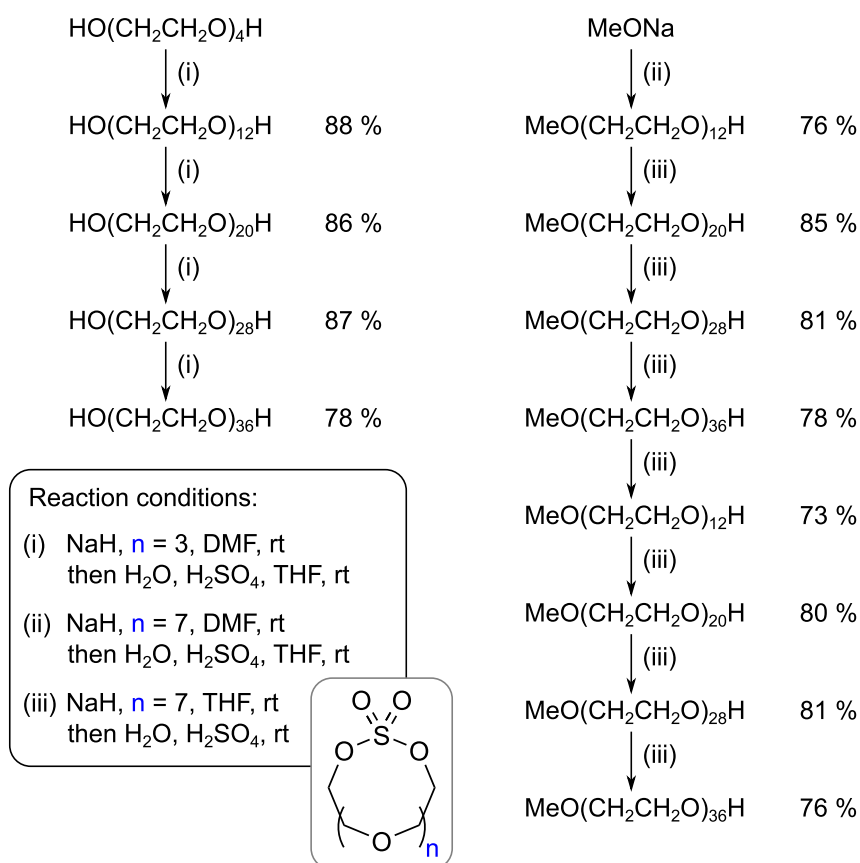


Figure 33. (Left) Bidirectional linear extension towards uniform unfunctionalized Eg₃₆ and (right) unidirectional linear extension towards MeO–Eg₆₄ from macrocyclic Eg₄ and Eg₈ sulfates respectively. Adapted from ⁴⁷ with permission from WILEY-VCH.

MALDI-ToF analysis in the accompanying supporting information to Zhang et al.'s work reveals that as far as is visible in the excerpts, there is no contamination of +Eg₁ in any of the species. Up to MeO–Eg₅₆–OH, there is also only a very low level of –Eg₁ impurity, perhaps in the region of 1–2 %, although there is a marked increase from MeO–Eg₅₆–OH to MeO–Eg₆₄–OH. When looking at Eg₅₆, consisting of 14 combined units of Eg₄, an impurity level of, for example, 1.4 % of shorter homologue would indicate only approximately 0.1 % contamination of Eg₃ in the Eg₄ starting material, assuming absolutely no depolymerization took place in any of the reactions. The fact that the –Eg₁ impurity did increase from compound MeO–Eg₅₆–OH to MeO–Eg₆₄–OH however indicates that some depolymerization may take place under these conditions (if the discrepancy cannot be traced to an analytical error). The level of impurity, at least up to Eg₅₆, is therefore very low when compared to typically expected level in other strategies as commercial samples of tetragol do not provide 99.9 % purity. To the author's knowledge, no suppliers for tetragol with 99.9 % purity exist. It is therefore plausible that the crystallization of the building block does reduce the level of undesired trace homologues derived from the tetragol starting material, as expected.

The authors reported dispersity values of the final species of 1.00005 (MeO–Eg₅₆–OH), and 1.00003 (MeO–Eg₆₄–OH). While the results at least up to MeO–Eg₅₆–OH are certainly impressive regarding the content of shorter –Eg₁ homologue, these values should be treated with caution. First, it is unlikely that purity should have increased with an additional chain extension step, particularly when the level of –Eg₁ impurity is noticeably higher. But more importantly, the major contaminant deriving from the chain extension cycles rather than the starting material, would be the lack of attachment of a unit of building block. This contamination may be the result of either an incomplete chain extension reaction or incomplete deprotection in the prior step. These chain errors are in fact visible at a level of approximately 5 %, higher than the level of –Eg₁ impurity, in the MALDI-ToF spectrum for the two preceding species, MeO–Eg₄₀–OH and MeO–Eg₄₈–OH. In the spectra of the final two species, the MALDI-ToF spectra excerpts in the supporting information only show a range of 331.4 Da and 347.6 Da downfield of the main peak respectively with a –Eg₈ impurity expected at approx. 352.2 Da downfield of the main peak.

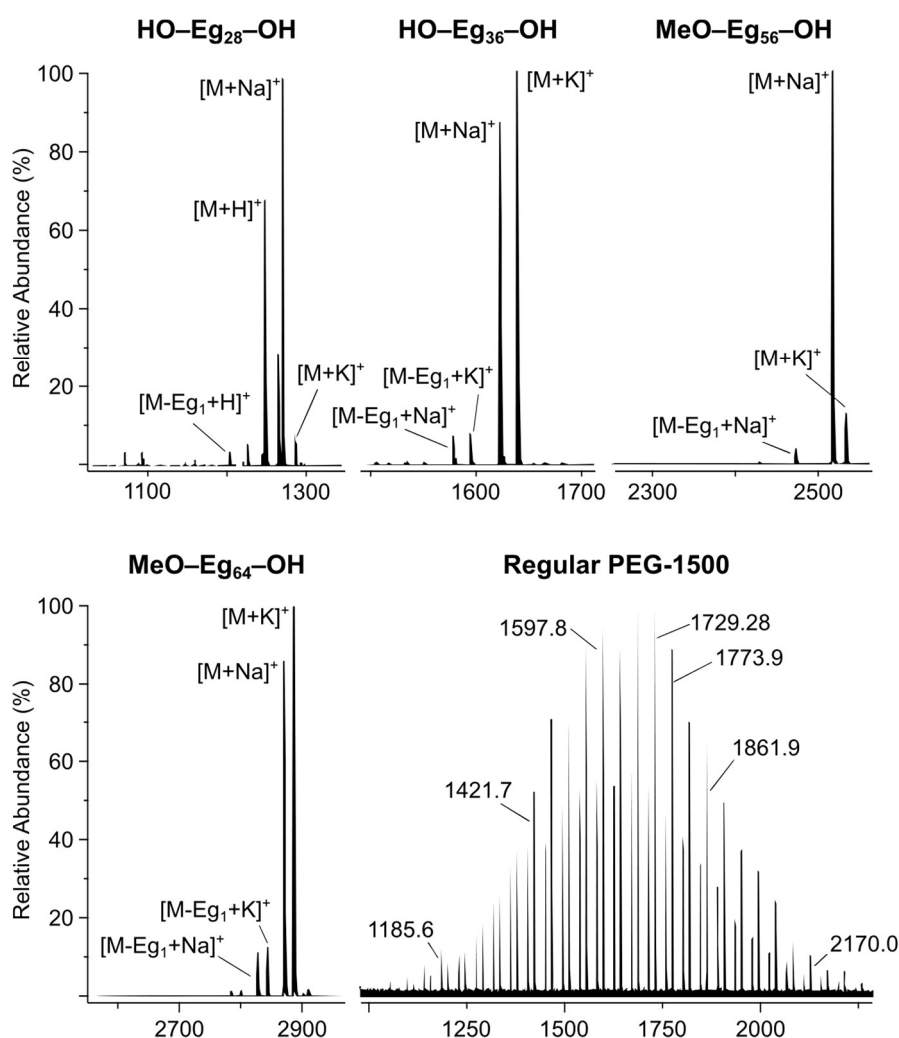


Figure 34. MALDI-TOF mass spectrometry of uniform diol PEGs, HO–Eg₂₈–OH and HO–Eg₃₆–OH and monomethoxy PEGs MeO–Eg₅₆–OH and MeO–Eg₆₄–OH, in comparison to bulk standard PEG1500. Reproduced from ⁴⁷ with permission from WILEY-VCH.

It is possible that the -Eg₈ impurities have been accidentally overlooked in the MALDI-ToF spectra of the final two species and were perhaps not included in the dispersity value calculation. Generally, it is a regular occurrence that the lack of published full range MALDI-ToF spectra makes an independent assessment of product purity impossible.

It therefore appears that the real strength of Zhang et al.'s approach is the synthesis of building block with potentially much higher oligomer purity than possible via traditional approaches that required extensive chromatographic purification to remove the \pm Eg₁ homologues. The purification via recrystallization, perhaps in combination with extraction, could thus potentially allow chromatography-free scaled-up synthesis of large quantities of building block up to lengths of around Eg₁₂ or Eg₁₆. The macrocyclic sulfate building blocks could then be converted into linear building blocks in a final step and used for any other route towards longer PEGs in regular fashion.

1.1.7. The homostar approach

For the synthesis of Eg₅₆ oligomer, a modified version of the unidirectional, linear extension route was used. Rather than growing chains individually, several oligomer chains are attached to a trivalent hub acting as anchor and grown as a combined molecule (Figure 35). Due to the star-shaped point-symmetrical molecule formed from attaching to the hub multiple chains which grow from the hub centre in different directions, this strategy was termed the 'homostar' approach. (In Greek, ὁμός means the same, equal or like). The properties of star-shaped polymers with arms constituted of PEG have been reviewed.⁵¹

The homostar approach is conceptually very similar to the unidirectional linear extension strategy outlined on p. 44 but it is a modification of this strategy because several growing chains are attached to a hub. In the homostar strategy, the hub simultaneously acts as the semi-permanent protecting group (see Pg¹ in Figure 21) and as an anchor. The homostar approach has a key advantage over the traditional unidirectional extension method because several chains grow as a single molecule at the same time. As a result, the product molecule increases in molecular size much faster and the fast-increasing size differential allows the product to be more readily distinguished from the reagents and side products during purification. The approach is thus particularly attractive for membrane applications such as nanofiltration that allow molecular sieving based at least partially on a size.

Before using the homostar approach in an extension strategy relying chiefly on nanofiltration for purification between extension steps, it was critical to establish the chain extension chemistry itself. In the following discussion, the synthesis of a heterobifunctional Eg₅₆ oligomer is outlined, with

chromatography used as a primary separation means before complementing the strategy with nanofiltration in a later chapter.

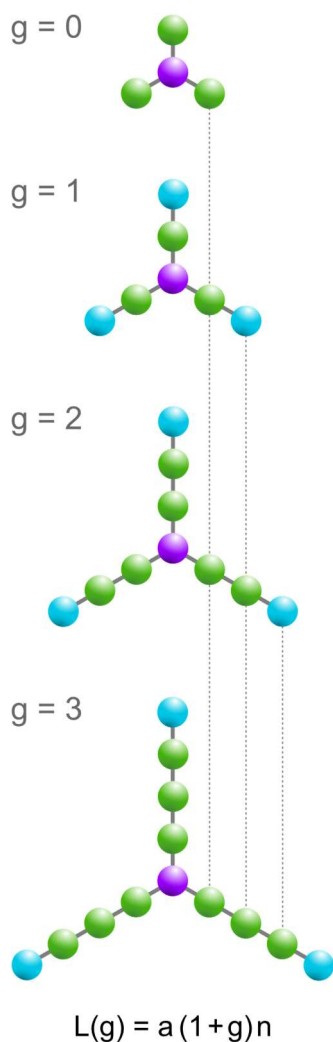


Figure 35. Speed of growth of the homostar strategy, with unidirectional linear extension on a multivalent hub. $L(g)$ = length of the product chain in generation g , n = length of the building block, g = the extension generation, a = number of attachment sites on the multivalent hub. (In this example, 3 chains are grown simultaneously). ● = starting building block, or building block from previous chain extension, ● = freshly added building block during chain extension, ● = multivalent hub. Adapted from ⁵² with permission from The Royal Society of Chemistry.

In summary, Table 9 captures some of the advantages and disadvantages of each extension strategy and highlights the benefits of the homostar approach. A list of the products and the various synthetic strategies towards uniform PEG oligomers is shown in Table 10.

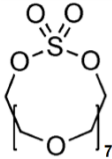
Table 9. Extension and purification characteristics of the different chain extension strategies.

	Linear unidirectional	Linear bidirectional	Chain doubling	Chain tripling	Homostar approach
Building block preparation	Same building block in each step; may be prepared at scale		Two different building blocks in each step, each different in every extension step		Same in each step, may prep. at scale
Heterobifunctionality after each extension	Yes	No	Yes	No	Yes
Rate of oligomer growth	Linear	Linear	Exponential	Exponential	Linear
Size of product vs. building block	Increases by 1 length of building block per step	Increases by 2 lengths of building block per step	Always a ratio of 2	Always a ratio of 3	Increases by 3 lengths of building block per step ^[a]
No. of reaction steps per extension / additional separation steps	2: extension, deprotection		4: extension; deprotection of Pg ¹ , deprotection of Pg ² and replacement with Lg	At least 3: extension; partial deprotection, addition of Lg	2: extension, deprotection
Reaction kinetics	May use excess building block as required		Any excess building block must come from the product of the previous extension, thus increasingly valuable building block lost as excess		May use excess building block as required
Ease of separation after chain extension	Comparatively easy	Comparatively easy	Medium	Very challenging ^[b]	Comparatively easy

[a] While each chain only increases by 1 length of building block like in linear, unidirectional extension, the product molecule grows by however many chains are attached to the multivalent hub (3 lengths in the case of a trivalent hub).

[b] See Figure 29

Table 10. Overview of the synthetic strategies towards uniform PEG oligomers to date.

Mode	Attained length Eg _N (generation)	Building block(s) Fg ¹ -Eg _n -Fg ²	Starting material Eg _n	Reference
Bidirectional linear	44 (5)	BnO-Eg ₄ -OTs	Eg ₄	Ahmed & Tanaka 2009 ³³
Chain doubling	11 (2)	BnO-Eg _n -OH BnO-Eg _n -OTs HO-Eg _n -OThp	Eg ₂ , Eg ₃ , Eg ₄	Burns, Field, Hashimoto, Petteys, Ridley, Samankumara Sandanayake 1999 ⁴⁴
Chain doubling	24 (3)	BnO-Eg _n -OTs HO-Eg _n -OPmb (PmbO-Eg _n -OTs) (HO-Eg _n -OThp)	Eg ₃ , Eg ₆	Loiseau, Hii, Hill 2003 ³²
Chain doubling	12 (2)	BnS-Eg _n -OH Cl-Eg _n -OThp	Eg ₃	Boden, Bushby, Clarkson, Evans, Knowles, Marsh 1997 ³⁶
Bidirectional non- linear	28 (2)	TsO-Eg ₄ -OTs HO-Eg _n -OH	Eg ₄	Harada, Li, Kamachi 1994 ⁴⁵
Chain doubling	32 (3)	BnO-Eg _n -OTs HO-Eg _n -OTrt	Eg ₄	French, Thompson, Davis 2009 ⁴²
Unidirectional linear	64 (7 from Eg ₈)	Macro- cyclic Eg ₈ sulfate 	Eg ₄	Zhang, Li, Shi, Xia, Chen, Yang, Jiang 2015 ²⁸
Bidirectional linear	24 (3)	HO-Eg ₆ -OH BnO-Eg ₄ -OTs MeO-Eg ₂ -OTs	Eg ₂ , Eg ₄ , Eg ₆	Maranski, Andreev, Bruce 2014 ³⁵

1.2. Materials and methods

Two different batches of Eg₄ starting material were purchased from Sigma-Aldrich over the course of this work and used as received with purity quantified via gas chromatography (GC) with flame ionization detection (FID) by the supplier (Table 11). Batch MKBK3234V was used for the final synthesis of Eg₅₆ and because Eg₅₆ is a combination of 14 units of Eg₄, a maximum molar purity of 92.0 % can be achieved after 14 couplings with an Eg₄ starting material oligomer purity of 99.41 % ($\approx 0.9941^{14}$).

Table 11. Summary of Eg₄ starting material purities by GC-FID as obtained from Sigma-Aldrich (Product: 110175-1KG). GC area-% is approximated to be equal to the mass-% of each species. Molar purity accounts for the difference in molecular weight from Eg₃ to Eg₅.

LOT (Date)		M _w	GC Area (area-%)	Purity (mole-%)
MKBK3234V (03/2012)	Eg ₃	150.17	0.44	0.57
	Eg ₄	194.23	99.24	99.41
	Eg ₅	238.28	0.03	0.02
MKBS7714V (03/2014)	Eg ₃	150.17	0.29	0.38
	Eg ₄	194.23	99.60	99.58
	Eg ₅	238.28	0.05	0.04

Reagents were purchased from *Sigma-Aldrich* and used as supplied. Sublimed potassium tert-butoxide (KO^t-Bu) was used. All solvents were purchased from *VWR* (UK), acetonitrile was purchased from *Merck* (DE). CH₂Cl₂, MeCN, THF and DMF were dried and stored over baked 4Å molecular sieves. Flash chromatography was conducted in a 9 cm diameter, porosity 3 glass sinter funnel with Geduran® (Si 60) for normal phase columns, and silanized silica for reverse phase columns (*Merck*, DE). Thin layer chromatography was carried out using silica gel 60 F₂₅₄ aluminium-backed plates (*Merck*, DE); compounds were visualized using UV light, KMnO₄ stain, or for Dmtr ethers trifluoroacetic acid vapour was blown over the plate.

Mass spectra were recorded on Micromass MALDI micro MX, or Micromass LCT Premier (ESI) mass spectrometers at the Department of Chemistry, Imperial College London. Mass spectrometry samples were not spiked and 6-Aza-2-thiothymine (10 mg·mL⁻¹) was used as matrix.

¹H- and ¹³C-NMR spectra were recorded on a Brüker AV-400 spectrometer. Chemical shifts in ppm are referenced with respect to residual solvent signals: δ_H (CHCl₃) 7.25 ppm, δ_H (CHD₂OD) 3.31 ppm; δ_C (CDCl₃) 77.50 ppm, δ_C (CD₃OD) 49.15 ppm. The splitting patterns for ¹H-NMR spectra are denoted as follows; s (singlet), d (doublet), t (triplet), q (quartet), quin (quintet), m (multiplet), b (broad) and

combinations thereof. Coupling constants (J) are in Hertz (Hz). ^{13}C -NMR assignments (C, CH, CH_2 and CH_3) and ^1H -NMR assignments, where given, were established with the aid of DEPT-135, HSQC and COSY experiments. CDCl_3 was purchased from VWR and CD_3OD from Merck. All NMR of Dmtr-derivatives was conducted in the presence of a small amount of Et_3N , and these purified compounds were always stored with a trace of added Et_3N .

Parts of this chapter have been published in two journal articles.^{4,52} For full experimental details, please consult the Supporting Information therein.

1.3. Results and discussion

Parts of this chapter have been published in two journal articles.^{4,52}

- Szekely, G.; Schaepertoens, M.; Gaffney, P. R. J.; Livingston, A. G., Iterative synthesis of monodisperse PEG homostars and linear heterobifunctional PEG. *Polymer Chemistry* (2014), 5, 694-697.
- Szekely, G.; Schaepertoens, M.; Gaffney, P. R. J.; Livingston, A. G., Beyond PEG2000: Synthesis and Functionalization of Monodisperse PEGylated Homostars and Clickable Bivalent Polyethyleneglycols. *Chemistry – A European Journal* (2014), 20 (32), 10038-10051.

The goal of this foundational work was to synthesize uniform PEG based on the homostar growth strategy and to demonstrate that the approach fulfilled all synthetic requirements before demonstrating the route with nanofiltration as the purification technology. Planning to synthesize oligomers beyond Eg₂₄ where alternative separations such as extraction may no longer be feasible, chromatography was first used as a tested and reliable means of purification between chain extensions in this synthesis of Eg₅₆.

Prior to chain extension, however, it was necessary to prepare enough building block of high quality and to prepare a first generation central homostar species ready for extension by attaching the first round of chains to a hub. Thereafter, chain extension can commence up to the desired length, followed by cleavage from the hub. The oligomer may optionally be functionalized at one terminus prior to cleavage from the hub, and once after at the other terminus. Broadly, the strategy can thus be divided into four parts:

- 1) Building block preparation
- 2) First generation homostar formation (hub attachment)
- 3) Chain extension (multiple cycles), consisting of
 - a. Etherification
 - b. Deprotection
- 4) Functionalization and hub cleavage

Based on the published work^{4,52}, the requirements for success with regard to each step are summarized below. The overall strategy is sketched out in Figure 37.

I. Building block preparation

Preparing in an economic fashion large quantities of PEG building block, $\text{Pg}^1\text{-Eg}_M\text{-Lg}$ (where m is the length of starting material and M is the final length of building block after elongation), from a commercial oligomer that is sufficiently uniform. The building block may be elongated prior to chain extension and a balance found between the number of elongation and chain extensions steps to attain the final product length. For example, by elongating the building block once to double the size of the starting material, the number of later chain extensions may be halved.

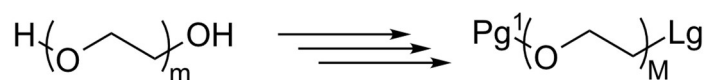


Figure 36. Multi-step preparation of $\text{Pg}^1\text{-Eg}_M\text{-Lg}$ building block from $\text{HO-Eg}_m\text{-OH}$ starting material.

It is important that the cost of building block preparation is not economically prohibitive and its synthesis scalable as a homostar strategy with optimized purification between chain extensions would be rendered impotent if the building block preparation became limiting.

II. First generation homostar formation

Preparing on a suitable hub a first generation homostar, $\text{Hub}(-\text{Eg}_M\text{-OH})_a$ (where a is the number of attachment sites on the hub), ready for chain extension. The functional linkage between the hub and the PEG chain must be stable to the chain extension (Step III) and deprotection conditions (Step IV) as it simultaneously acts as the semi-permanent protecting group.

The structure and valency of the hub should be chosen to balance the rate of growth with ease of analysis. Fewer arms lead to a slower growth of product and will later lead to a more difficult separation via nanofiltration, while too many arms may complicate analysis, for example in mass spectrometry, due to excessive fragmentation. In NMR, a symmetrical hub will generally facilitate analysis and a hub containing a UV chromophore allows tracking by UV and provides a linear quantification method when a non-UV absorbing protecting group is used or when the homostar is temporarily deprotected.

III. Williamson etherification

Ensure completion of and optimize the Williamson ether synthesis with $\text{Pg}^1\text{-Eg}_M\text{-Lg}$ building block: $\text{Hub}(-\text{Eg}_n\text{-OH})_a \rightarrow \text{Hub}(-\text{Eg}_{n+M}\text{-OPg}^1)_a$. Ideally, unconsumed building block should be recovered.

IV. Deprotection

Ensure unblocking of the protecting group, $\text{Hub}(-\text{Eg}_n\text{-OPg}^1)_a$ to $\text{Hub}(-\text{Eg}_n\text{-OH})_a$, is quantitative and orthogonal to the semi-permanent protection chemistry (described in Step II) linking the PEG oligomers to the hub core (Figure 1, step 4).

V. Functionalization

After chain extension to the full length homostar, functionalize the chain termini into a pharmaceutically useful end group compatible with hub disassembly in Step VI: $\text{Hub}(-\text{Eg}_n-\text{OH})_a \rightarrow \text{Hub}(-\text{Eg}_n-\text{R}^1)_a$

VI. Homostar disassembly and functionalization

Disassemble the full-length homostar, $\text{Hub}(-\text{Eg}_n-\text{R}^1)_a$ to yield 'a' multiples of $\text{HO}-\text{Eg}_n-\text{R}^1$, where R^1 is a functional group that distinguishes one end of the PEG from the other; a second functional group, R^2 , may then be appended to yield $\text{R}^2-\text{Eg}_n-\text{R}^1$

VII. Depolymerization

Minimize the extent to which any of the above reactions, particularly the chain extension in Step III, reduce oligomer purity, e.g. through depolymerization.

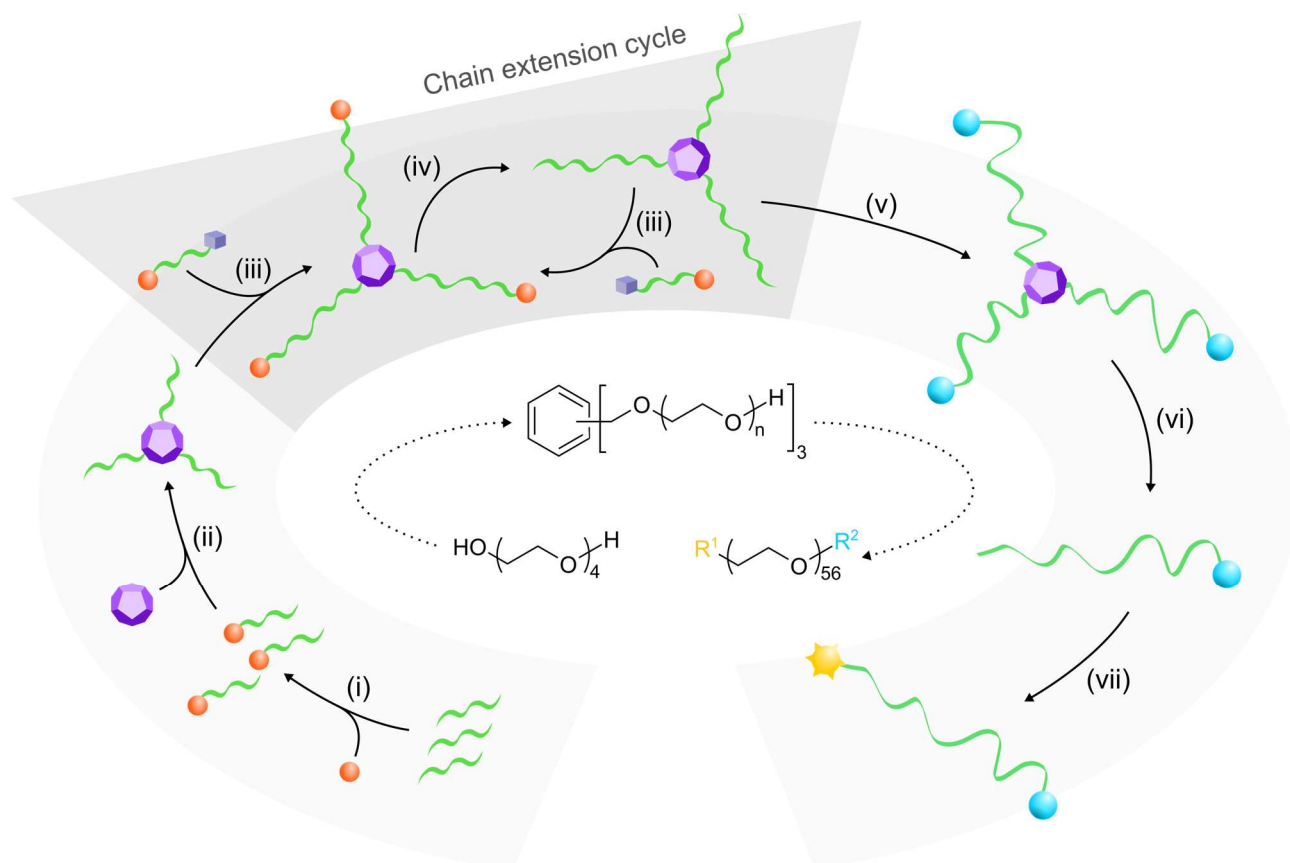


Figure 37. Key steps in the synthesis of uniform PEG via a homostar strategy: (i) Assembly of building block, (ii) assembly of homostar, (iii) chain extension, (iv) unblocking of the temporary protecting group, (v) functionalization of the outer terminus, (vi) disassembly of the homostar to liberate the individual PEG oligomers, and optionally (vii) functionalization of the liberated terminus. $\text{HO}-\text{Eg}_n-\text{OH}$; Pg ; Lg ; R^1 and R^2 = non-identical functional groups. Adapted from ⁴ with permission from John Wiley & Sons.

1.3.1. Uniform PEG synthesis

1.3.1.1. Building block preparation

The first part of the strategy concerns itself with building block preparation. This first implementation of the homostar strategy for PEGs was anticipated to rely heavily on chromatographic separation. The 4,4'-dimethoxytrityl (Dmtr) protecting group was therefore suitable – its hydrophobicity serves as a useful distinguishing feature for the poly(ethylene glycol) chain during chromatographic separation and the Dmtr group also possesses appropriate lability under acidic conditions.

Building block was prepared from tetra(ethylene glycol) (or tetragol, Eg_4 , $HO-Eg_4-OH$, **1**) according to Figure 38. First, a large excess of **1** (5-10 eq.) was protected with 4,4'-dimethoxytrityl chloride (**2**) in the presence of Et_3N as acid scavenger. Tetragol contains two equivalent hydroxyl end groups, both of which are equally susceptible to protection. The use of a large excess of tetragol therefore statistically favours the monoprotected product, $DmtrO-Eg_4-OH$ (**3**), but production of a small quantity (ca. 5-10 %) of biprotected side product, $DmtrO-Eg_4-ODmtr$ (**4**), cannot be avoided. While the biprotected side product is inert to further reaction and may remain in the product mixture, excess reagent (**1**) must be removed.

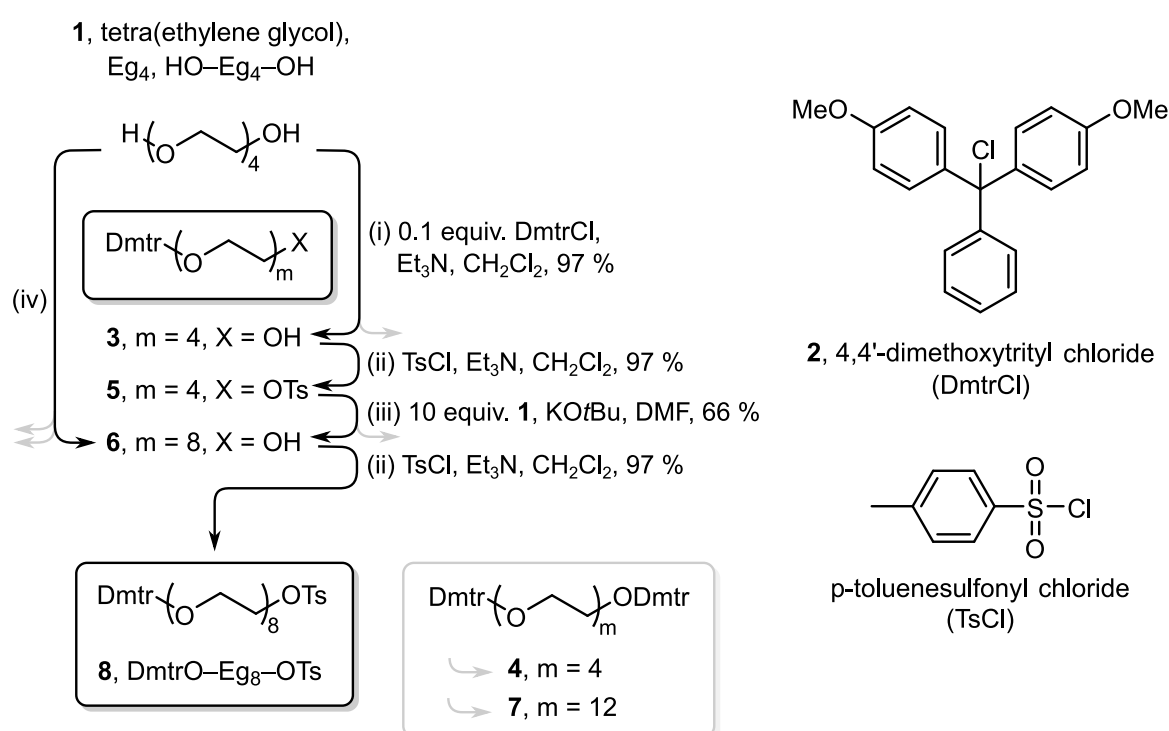


Figure 38. Synthesis of $DmtrO-Eg_8-OTs$ (**8**) building block from Eg_4 starting material. (i) Monoprotection with **2** using a large excess of Eg_4 , (ii) activation of the unprotected hydroxyl terminus by leaving group insertion, (iii) building block elongation with a large excess of Eg_4 . (iv) Optionally the procedure may be telescoped by carrying forward crude product and separating only Eg_4 where necessary up to **6**, without purification of intermediates **3** and **5**. Adapted from ⁴ with permission from John Wiley & Sons.

Due to the hydrophobicity of the Dmtr protecting group, separation is feasible by either reverse phase chromatography⁴ or extraction^{43,44} and the former technique was chosen. The use of extraction as a separation technique in building block preparation up to Eg₁₆ has been previously discussed (Section 1.1.6.2 on page 62). Selective adsorption of tetragol onto CaCl₂, i.e. formation of the metal complex in Et₂O⁵³, under sufficiently dry conditions is also feasible, although the procedure requires fine-tuning. Another alternative to using a large excess of reagent, stoichiometric Ag(I) may be used for heterobifunctionalizing short chains.⁵⁴

After protection of one end of the chain, the other chain terminus was activated with p-toluenesulfonyl chloride (TsCl), in the presence of Et₃N as an acid scavenger and, optionally, N-methylimidazole (NMI), to yield the toluenesulfonate ester, DmtrO–Eg₄–OTs (**5**). The use of NMI as a catalyst for the toluenesulfonate ester formation with TsCl in conjunction with Et₃N as base is documented⁵⁵, but the introduction of NMI also poses a removal problem. Typically, removal of the conjugate acid under slightly acidic conditions via extraction would be feasible, but the procedure must not affect the acid labile protecting group. With primary alcohols, introduction of an OTs moiety is also feasible without NMI as a catalyst. Alternatively, relevant sulfonate ester formations with methanesulfonyl chloride (MsCl) are reported to proceed smoothly without catalyst even for secondary alcohols.⁵⁵

Following activation, it is critical to quench and/or remove any excess TsCl reagent from the product mixture as PEGs bearing acid-labile protecting groups have been reported to undergo concomitant unblocking during treatment with sulfonyl chlorides.^{28,38} It is possible that the observed decomposition was caused by traces of TsCl remaining in the apparently pure product after concentration, and that residual TsCl may have reacted to release HCl and thus caused deprotection during storage, rather than deprotection occurring concomitantly during tosylation. Excess TsCl was therefore quenched via N-methylimidazole-catalyzed hydrolysis by stirring the product mixture in a monophasic mixture of THF:H₂O in the presence of NaHCO₃, prior to aqueous work-up. It is important to ensure that no hydrolysis of the tosylate ester occurs here as the non-activated species and resultant side products will be difficult to separate during the following steps. It was not finally determined whether the TsCl quench under aqueous conditions simultaneously resulted in a small degree of toluenesulfonate ester hydrolysis. If so, the quench would be counterproductive as the removal of DmtrO–Eg₄–OH (**3**) from DmtrO–Eg₄–OTs (**5**) would likely pose a more difficult separation problem than the removal of TsCl from **5**. For example, the chromatographic separation of **3** from **5** should be more difficult than the separation of TsCl from **5** on a normal phase medium. Wawro et al.'s work on the multigram chromatography-free synthesis of octa(ethylene glycol) p-toluenesulfonate⁴³ does suggest that a clean quench of the excess TsCl is possible when using appropriate conditions.

After activation, DmtrO–Eg₄–OTs (**5**) is extended by another length of Eg₄ by etherifying with tetragol in the presence of a strong base, either KOtBu (2 eq.) or NaH (2 eq.). Once again, a large excess of

tetragol (5-10 eq.) is used to statistically favour the desired product. The main product, DmtrO–Eg₈–OH (**6**), includes a free hydroxyl and is therefore susceptible to reaction with the DmtrO–Eg₄–OTs (**5**) reactant, similarly to tetragol (HO–Eg₄–OH). Reaction of **5** with **6** (perhaps better thought of as extension of tetragol with **5** on both sides) leads to formation of the undesired diprotected side product, DmtrO–Eg₁₂–ODmtr (**7**). Like **4**, **7** is inert to further reaction as it has a Dmtr protective group on either chain terminus and thus does not require immediate separation and may be carried forward in the mixture. However, the side reaction should be reduced from an economic standpoint until use and separation of excess tetragol become costlier than the loss of DmtrO–Eg₄–OTs (**5**) reagent to the side reaction.

The extended building block is then once more activated to give the final building block, DmtrO–Eg₈–OTs (**8**) which may be used in the subsequent chain extension steps.

1.3.1.2. Hub attachment

The second part of the strategy concerns itself with attachment of the building block to the hub. Before chain extension can commence, a starting point for attachment, the first generation homostar, needs to be assembled from a suitable hub reagent and the non-activated building block, DmtrO–Eg₈–OH (**6**). Commercially available 1,3,5-tris-(bromomethyl)benzene (**9**) was reacted with a small excess of **6** (4 eq.) in the presence of KO^tBu (3.5 eq.) to yield the first generation homostar (Figure 39). This reaction proceeds to completion rapidly (< 5 min) and later work has shown that a smaller excess of building block can generally be used (≤ 3.3 eq.). The use of a smaller excess of **6** not only conserves material but also simplifies the post-reaction work-up.

In this version of the hub attachment reaction, the alkoxide of the non-activated building block acts as the nucleophile attacking the benzyl bromide moiety on the hub reagent. As a result of the nucleofuge residing on the hub reagent, traces of hydroxide introduced either directly via impurities in the base used or indirectly via trace water will result hydrolysis of the hub benzyl bromide moiety. This leads to formation of homostar side products containing fewer than three attached arms, e.g. two hub sites possess successfully attached arms and one side group persists as the hydroxymethyl moiety. It is therefore critical to use a high grade of base, e.g. sublimed KO^tBu (lower grades e.g. 98 % typically contain KOH as a major contaminant), and dry the building block reagent rigorously to remove traces of H₂O. The reaction mixture is separable via reverse phase chromatography (whereas normal phase chromatography gave poor separation). If present, it is critical that any homostar side product bearing fewer than three arms is removed at this point to preserve monodispersity as any benzyl alcohol groups would be available for later chain extension. For hub attachment, the reverse attack pathway is conceivable, e.g. between 1,3,5-tris-(hydroxymethyl)benzene and DmtrO–Eg₈–OTs (**8**), but is comparatively very slow.

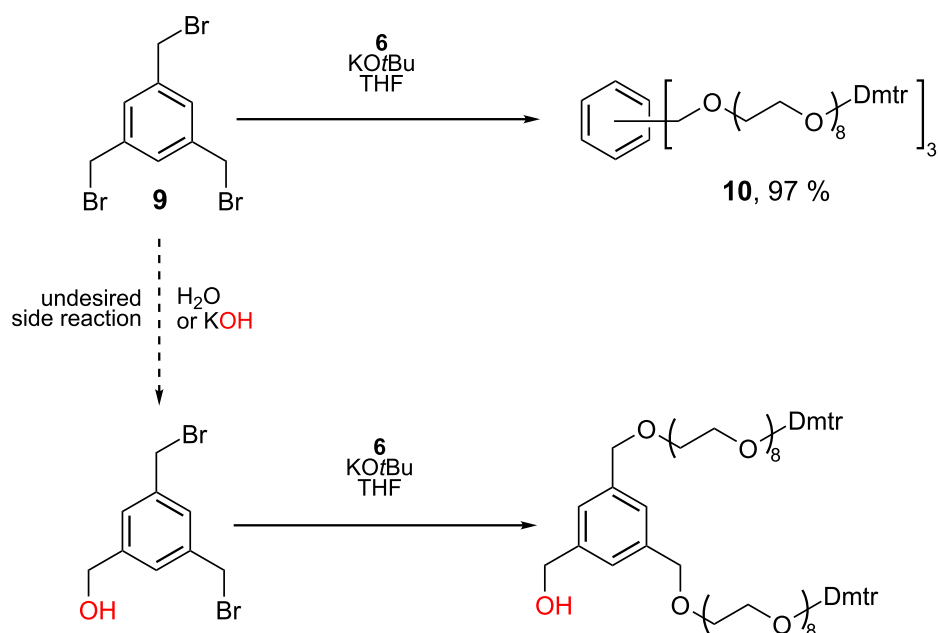


Figure 39. Hub attachment with 1,3,5-tris(bromomethyl)benzene and **6** to yield the first generation homostar and detrimental side reaction with trace H₂O or hydroxide to yield the two-armed species with incomplete attachment of arms. (one-armed side product is not shown.)

1.3.1.3. Chain extension cycles (extension and deprotection)

The third part of the strategy concerns the chain extension of the homostar side-arms and is the key towards obtaining the desired length of PEG. The protecting group on one terminus of each building block ensures that a building block can attach to the hydroxyl group on each arm only once per step via its activated terminus. After a chain extension step, the protected termini consisting of the Dmtr protecting groups need to be deprotected before another chain extension can commence. The chain extension cycle therefore consists of a) chain extension and b) deprotection (Figure 40). Because the first set of chains has already been attached during hub attachment, the next part-step is deprotection. The protected first generation homostar is treated with Cl₂HCOOH (dichloroacetic acid, or DCA) (1.3 eq.) in CH₂Cl₂ which liberates an intense orange-red colour corresponding to formation of the Dmtr⁺ cation. In hydroxylic solvent, such as methanol, this colour would rapidly dissipate by transfer of the Dmtr⁺ cation to the solvent. However, the acid-catalyzed deprotection of Dmtr with alcoholic solvent is reversible and does not reach completion, even with a large molar excess of the alcohol.⁴ Because any trace of incomplete deprotection would adversely affect oligomer dispersity, pyrrole (3.3 eq. per arm) was used as a cation trap to force the reaction to completion.⁵⁶ No decomposition of the hub linkage was ever detected under the above deprotection conditions, but reaction time lengthened from 30 to 120 min with increasing chain length.⁴ It was hypothesized that the increasing volume fractions of polyether could partially buffer the acid. To overwhelm the buffering, the DCA concentration may be increased while the concentration of pyrrole should be kept as low as practically possible to minimize the generation of polypyrrole.⁴ For further discussion on the subsequent work-up, the reader is referred to Szekeley et al.⁴

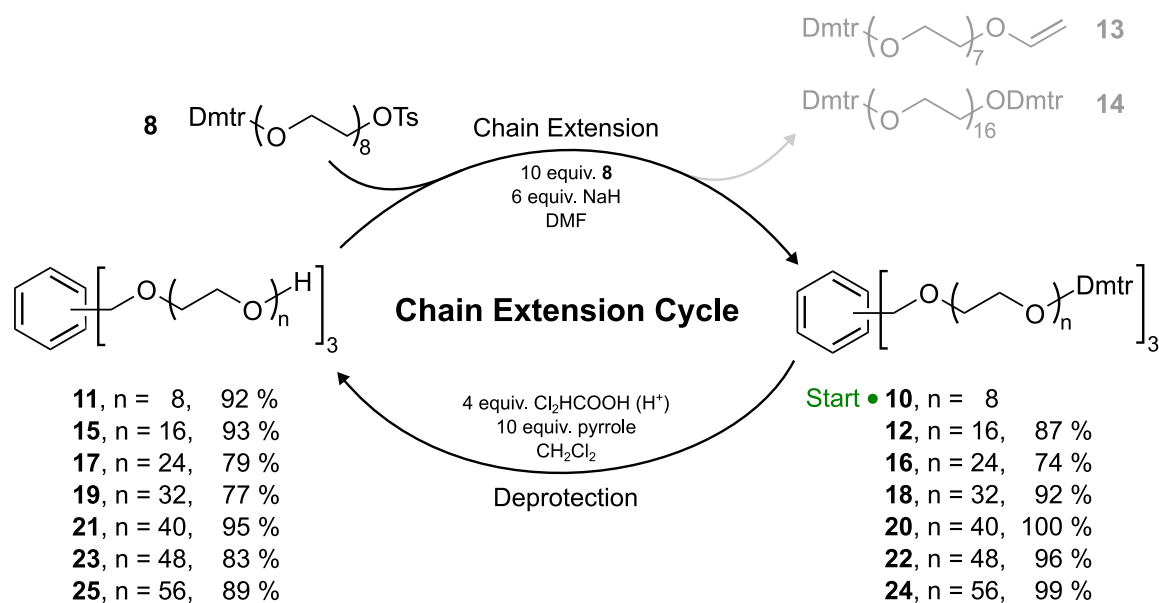


Figure 40. Homostar chain extension cycle, consisting of chain extension and deprotection. Chain extension yields the extended protected homostar as well as vinyl ether and building block dimer side products. Adapted from ³ with permission from John Wiley & Sons

The first chain extension cycle on the first generation deprotected homostar initiates via etherification with excess DmtrO–Eg₈–OTs (**8**) (10 eq., 3.3 eq. per arm), in a suitable non-protic solvent in the presence of a strong base capable of deprotonating the homostar hydroxyl chain termini to generate the alkoxide species. In the literature, a combination of either NaH or KO^tBu as base (6 eq.), and either N',N'-Dimethylformamide (DMF) or tetrahydrofuran (THF) as solvent were typically chosen. Throughout the final synthesis described here, a combination of NaH and DMF was used. While no systematic studies were carried out, it was observed that PEGs exhibit very high solubility and a slightly higher reaction rate in DMF. The generation of alkoxide from the chain terminal primary alcohol (pK_a ≈ 16) with NaH [pK_a(H₂) ≈ 35] is also irreversible while the reaction with KO^tBu [pK_a(^tBuOH) ≈ 18] is reversible. In early trials of the chain extension reaction, KO^tBu (6 eq.) was used as base instead of NaH and approximately a sixth of the recoverable building block was typically converted to vinyl ether (**13**). In contrast, this elimination by-product was almost undetectable in etherifications promoted by sodium hydride, which was used as the base from then on.^{4,27}

It was quickly apparent during etherification reactions under these conditions that reaction kinetics were slow. In general, the etherification reactions here were complete in the order of hours or days, rather than seconds or minutes. Because complete reaction is critical to maintaining uniformity of the PEG oligomer, it was necessary to successively increase the reaction temperature from room temperature to 40 °C and the reaction time from several hours to 36 h. A kinetic study of these etherifications is presented in the following chapter.

Overall, six chain extensions were carried out after the initial hub attachment to reach a target length of Eg₅₆. The average yields of etherification and detritylation were 86 % and 92 % respectively, resulting in an acceptable average chain extension cycle yield of 79 % (Table 12 and Table 13). Both procedures included two lower yielding steps at lower chain length and refinement of the chromatographic work-up led to higher yields towards the end of the synthesis run at higher chain length. Yield loss is attributed largely to the chromatographic work-up as reactions were monitored to completion via HPLC with enough building block and base still present in each case. Functionalization and hub disassembly were then be carried out as reported⁴, with a summary given in Appendix B.

Table 12. Summary of the scale and yield of homostar chain extension reactions. Reproduced from ⁴

Product homostar	Triol homostar reactant			Extended product homostar			Yield [%]
	Mass [g]	M _w [Da]	Mole [mmol]	Mass [g]	M _w [Da]	Mole [mmol]	
Eg ₁₆ (12)	2.500	1225.4	2.04	6.030	3189.8	1.89	93
Eg ₂₄ (16)	3.700	2282.7	1.62	5.450	4247.1	1.28	79
Eg ₃₂ (18)	2.382	3340.0	0.71	2.780	5304.4	0.52	77
Eg ₄₀ (20)	2.000	4397.2	0.45	2.609	6361.6	0.41	95
Eg ₄₈ (22)	1.982	5454.5	0.36	2.085	7414.2	0.28	83
Eg ₅₆ (24)	1.653	6511.8	0.25	1.898	8476.2	0.22	89

[a] The spectroscopic data for the compounds can be found in the Supporting Information of Szekely et al.⁴

Table 13. Summary of the scale and yield of the homostar deprotection reactions. Reproduced from ⁴

Product homostar	Protected homostar reactant			Deprotected triol homostar			Yield [%]
	Mass [g]	M _w [Da]	Mole [mmol]	Mass [g]	M _w [Da]	Mole [mmol]	
Eg ₈ (11)	5.947	2132.5	2.78	3.131	1225.4	2.55	92
Eg ₁₆ (15)	5.960	3189.8	1.86	3.720	2282.7	1.63	87
Eg ₂₄ (17)	5.450	4247.1	1.28	3.160	3340.0	0.94	74
Eg ₃₂ (19)	2.720	5304.4	0.51	2.070	4397.2	0.47	92
Eg ₄₀ (21)	2.379	6361.6	0.37	2.067	5454.5	0.37	101 ^[b]
Eg ₄₈ (23)	2.050	7414.2	0.27	1.733	6511.8	0.26	96
Eg ₅₆ (25)	1.487	8476.2	0.17	1.317	7569.1	0.17	99

[a] The spectroscopic data for the compounds can be found in the Supporting Information of Szekely et al.⁴

[b] High M_w PEG species are difficult to dry fully. Sample may have contained residual solvent.

1.3.2. Analysis of homostar purity via HPLC and MALDI-ToF

A critical requirement for maintaining chain uniformity is to ensure completeness of the chain extension and deprotection reactions. Reactions were monitored both by HPLC and mass spectrometry (MS). HPLC was run with a reverse phase C₁₈ stationary phase connected to a diode array detector (Agilent G1315B DAD) and an enhanced light scattering detector (ELSD). Tracking of the homostar species is helped by the shift in elution time on the reverse phase HPLC with the addition of each building block due to the transfer of the hydrophobic Dmtr protecting group. The mono-, di- and fully tri-extended homostar can therefore be resolved and the presence/absence of incompletely chain extended intermediates detected.

All protected species including the DmtrO–Eg₈–OTs building block, the DmtrO–Eg₁₆–ODmtr building block dimer as well as the partially and fully extended homostars could be readily tracked by their UV absorption at 260 nm due to the large extinction coefficient of the Dmtr ether. However, prior to extension, the homostar triol only comprises a benzyl ether core with a comparatively weak UV absorption. For this purpose, an ELSD detector was used downstream of the UV detector. The operation principle of ELSD is that the liquid eluent is mixed with an inert carrier gas and dispersed into a fine mist through a nebulizer. The mist is passed through a heated drift tube where the mobile phase is evaporated off until only components less volatile than the mobile phase, ideally only dried analyte, remain. In a detection region, a beam of light is shone through the resultant particles and the scattering quantified. Because the detector response is non-linear and requires calibration for quantitative analysis, this technique was only used for qualitative assessment of homostar triol disappearance. Further, with sensitivity towards the full length of the chain rather than just the UV active end groups, ELSD served as a useful additional check on all polyether species in the mixture, becoming particularly useful with higher homostar M_w.⁵⁷ Where preparative chromatography was used during building block preparation, HPLC analysis was also useful to confirm that all PEG-related contaminants that could affect dispersity such as tetragol had been removed.

While HPLC is useful in tracking reactions and detecting completion of chain extension and deprotection reactions, it cannot readily resolve polyether homologues, oligomers with slightly different length, when they possess similar functionality. For example, HPLC cannot resolve a three-armed Eg₅₆ homostar (e.g. **24** or **25**) containing 168 monomeric units from its homologues containing one more, or one less unit (\pm Eg₁). At these chain lengths, even resolution of a shortmer containing one fewer added Eg₈ building block from a prior extension ($-$ Eg₈) is challenging.

Mass spectrometry was therefore essential to quantify oligomer purity after each chain extension step. For the analysis of the homostars, matrix-assisted laser desorption/ionization (MALDI) with a time of flight detector (MALDI-ToF) was used. In MALDI, the analyte is co-crystallized with a laser absorbing

matrix which increases its propensity to ionize with minimal fragmentation and often fewer multi-charged ions than with other techniques e.g. electrospray ionization (ESI). After ablation and desorption triggered through pulsed laser irradiation, the analyte is ionized by protonation or deprotonation and after acceleration quantified by their time of flight.

MALDI-ToF allows quantification under a confined set of circumstances. Absolute quantification of concentration or comparison between samples is usually complicated by the variability in the co-crystallization process. But relative quantification is possible where the propensity of all species in the mixture to ionize can be assumed equal, e.g. where the molecular weight and chemical functionality are similar. In these cases, the relative signal intensities of all species can be compared to obtain an estimate of molar purity. For large homostars, this assumption is close to valid, as an Eg₅₆ homostar lacking an Eg₁ unit would be only be approximately 0.6 % smaller by molecular weight while a homostar lacking one Eg₈ building block would be 4.6 % smaller.

Here homostars may also possess higher intrinsic sensitivity to departures from uniformity. With three oligomer chains joined into a single three-armed homostar, the likelihood of detecting a chain length impurity in one of the arms is theoretically enhanced because the number of individual analyzed molecules is approximately three times smaller than if the chains were analyzed individually after cleavage from the hub. Equally, the relative difference in mass between the main species and an impurity would decrease approximately threefold making relative quantification more accurate. However, ionization becomes more difficult with increasing analyte M_w overall.

During MALDI analysis, the deprotected homostar triols at length Eg₄₈ (**23**) and Eg₅₆ (**25**) yielded poor signal-to-noise (S/N) ratios even after repeated attempts and did not allow identification of minor impurities. In comparison, the protected tris-Dmtr ether homostars at length Eg₄₀ (**20**) and above yielded higher S/N spectra, perhaps due to better incorporation of the Dmtr group into the matrix or because the Dmtr group itself helps in absorbing laser irradiation and thereby assists ionization. The downside of analysing the Dmtr protected homostars was often a partial fragmentation of the main species with loss one, two or three Dmtr groups. Illustrative is the difference of the protected and deprotected homostars at length Eg₄₈ (**22** and **23** respectively). The protected tris(Eg₄₈-ODmtr) homostar (**22**) (Figure 41 a), fully defragmented in this example, shows high S/N and allows identification of minor impurities, while the same spectrum of the triol (**23**) (Figure 41 b) exhibits poor S/N. The spectral quality shown is representative of the higher M_w triols Eg₄₈ and Eg₅₆ while spectra of Eg₄₀ and below gave better results (see Supporting Information of Szekely et al.⁴).

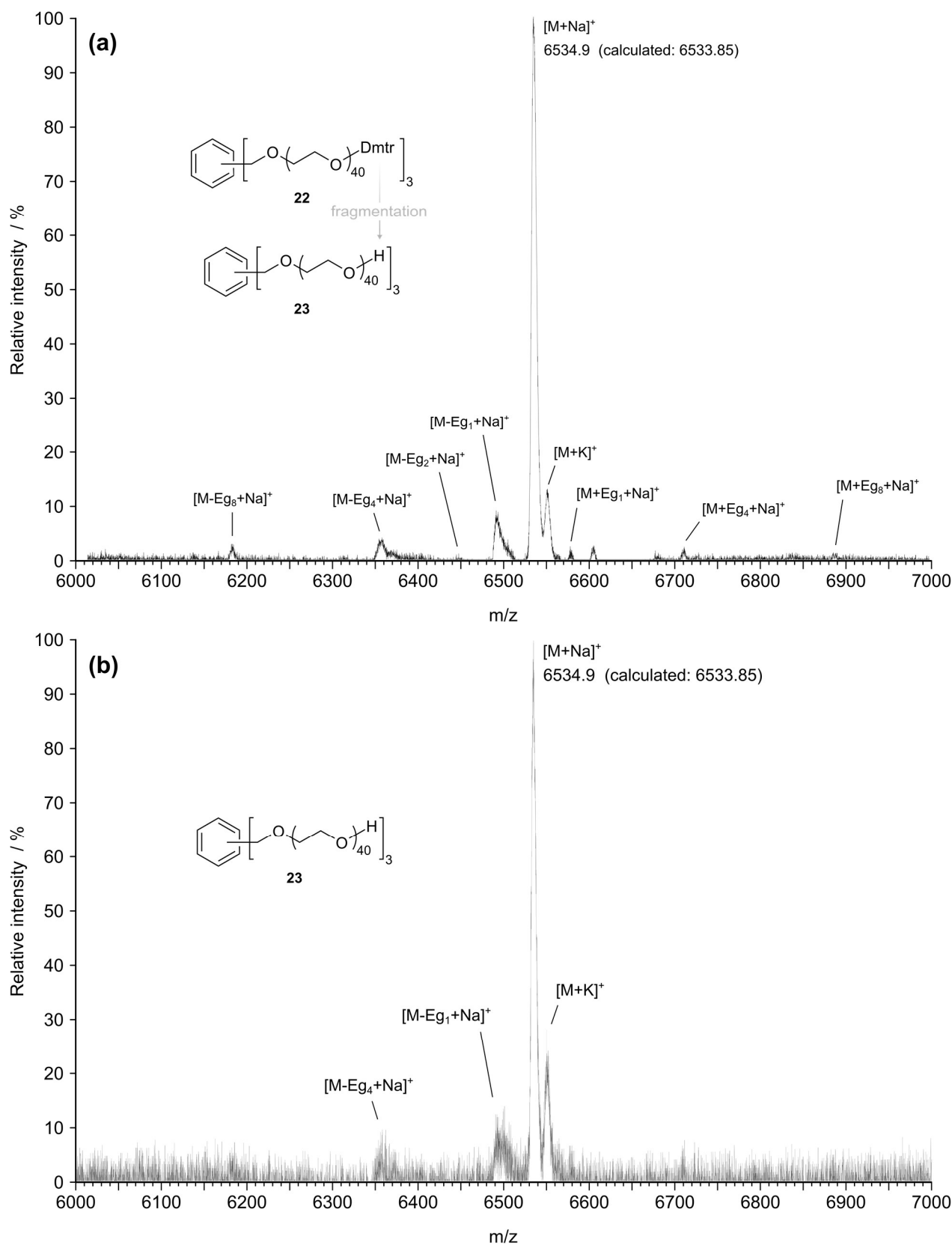


Figure 41. MALDI-ToF mass spectrum of (a) tris(Eg₄₈-ODmtr) homostar **22** showing complete fragmentation by detritylation to tris(Eg₄₈-OH) homostar **23** with good S/N and (b) tris(Eg₄₈-OH) homostar **23** itself with poor S/N. Adapted from ⁴ with permission of John Wiley & Sons.

While impurity analysis at length Eg_{56} was difficult, the high S/N of the spectrum of tris(Eg_{48} -ODmtr) homostar (**22**) fully deprotected in situ allowed a detailed quality assessment of the synthesis. The two main species present are the sodium base peak $[M + Na]^+$ (100 % relative intensity) and potassium adduct $[M + K]^+$. Multiple adducts are visible in this case because no salts were added during the sample preparation process to favour exclusive formation of a single adduct. The main impurity is lacking one unit of monomer $[M - Eg_1 + Na]^+$ (9 %) which may derive from starting material or depolymerization during chain extension. With Eg_4 starting material of 99.41 % molar purity containing 0.57 % Eg_3 , this departure from uniformity likely stems from the starting material, as a concatenation of 36 units of Eg_4 (12 per chain) on the Eg_{48} homostar should contain roughly 18.6 % $[1 - (1 - 0.0057)^{36}]$ of shortmer lacking one monomer unit. In fact, the detected level of this impurity should be roughly twice as high if the supplier estimate of purity was correct. Depolymerization therefore does not appear to have occurred to a significant degree during synthesis. Similarly, the 0.02 % of Eg_5 in the starting material should have led to about 0.7 % of $[M + Eg_1 + Na]^+$ which is approximately consistent with the level visible.

The remaining impurities are by-products of the synthesis. Of the shorter homologues, $[M - Eg_4 + Na]^+$ (4 %) lacking one tetragol unit must derive from low levels of DmtrO- Eg_4 -OTs (**5**) contaminating the activated DmtrO- Eg_8 -OTs (**8**) building block after tosylation. DmtrO- Eg_4 -OTs (**5**) in turn must have stemmed from a very low level of DmtrO- Eg_4 -OH (**3**) contaminating the DmtrO- Eg_8 -OH (**6**) after building block elongation, which was incompletely separated by chromatography post reaction. $[M - Eg_8 + Na]^+$ (3 %) is a result of incomplete chain extension which can be caused by either incomplete reaction during a chain extension or by incomplete detritylation in a prior deprotection, as a still protected site cannot be extended. Because reactions were monitored by HPLC, it is thought that these shortmers were formed at a low level over multiple chain extension and deprotection cycles as a single poor coupling should have been detected.

Of the longer homologues, both $[M + Eg_4 + Na]^+$ (2 %) and $[M + Eg_8 + Na]^+$ (1 %) are detected. The latter likely derives from slight detritylation of the DmtrO- Eg_8 -OTs (**8**) building block which was prepared in bulk at the beginning of the synthesis, stocked and used over time. The resultant formation of deprotected HO- Eg_8 -OTs causes double coupling during chain extension. The $M + Eg_4$ impurity could have been explained similarly, by the presence of coincidentally shorter and deprotected building block, were it not for the relatively higher intensity of this peak. If the impurity was generated from HO- Eg_4 -OTs derived from leftover DmtrO- Eg_4 -OTs in the DmtrO- Eg_8 -OTs building block, the ratio of HO- Eg_4 -OTs to HO- Eg_8 -OTs in the building block sample should be small, and the peak ratio of the impurities, $[M + Eg_4 + Na]^+$ and $[M + Eg_8 + Na]^+$, should be consistent therewith. Because it is not, the $M + Eg_4$ impurity must instead stem from contamination of the building block with DmtrO- Eg_{12} -OTs, which derives from double coupling caused by HO- Eg_4 -OTs during building block synthesis. HO- Eg_4 -OTs in turn must have been caused by a low level of deprotection of DmtrO- Eg_4 -OTs at the very start of the synthesis.

1.4. Conclusion

In Chapter 1, it was demonstrated that the synthesis of uniform oligo(ethylene glycol) up to Eg_{56} via the homostar approach is feasible. Impurity analysis by MALDI revealed that one main source of oligomer impurity was the Eg_4 starting material. The use of alternative starting material sources, or of a separation technique during building block synthesis that also achieves oligomer purification such as crystallization is therefore worth considering. At the same time, chain impurities also arose from all synthetic steps as impurities could be traced back to the building block synthesis and potentially to its storage as well as the chain extension and deprotection reactions.

For an industrial process to work on this basis, the reaction would likely need to be fine-tuned. First, to be economical, an industrial synthesis would likely need to make do with a smaller excess of building block. At the current level of excess (10 eq. of building block, 3.3 eq. per arm), the building block utilization is only 30 %. In theory the remaining 70 % (excluding any side products derived from building block) could be recovered. However, the idea of recovering the building block after reaction runs counter to the principle of the homostar approach. The homostar approach is so effective precisely because it facilitates purification of a large product from a much smaller building block. But the difference in size between the building block and its two side products, vinyl elimination product and dimer, is much smaller in comparison, resulting in a more difficult separation. If building block were to be recovered chromatographically, that recovery would likely become the economically limiting step of the overall separation, rendering innovations with regard to separability of the homostar post chain extension void. Ultimately, the strategy should therefore be improved with regard to building block preparation and building block input factor during chain extension.

The dimethoxytrityl protecting group may also be an inefficient choice. While readily traceable, the Dmtr group is one of the larger acid labile protecting groups weighing in at 303 Da, equivalent to almost seven units of ethylene glycol. About 35 % of a $\text{Dmtr-Eg}_8\text{-OTs}$ building block therefore consist of the protecting group which needs to be carried through the building block preparation, the reaction and separation steps but does not contribute to the length of the final product. A reduction in protecting group size, e.g. towards smaller acetal type protecting groups, could therefore increase mass efficiency, and reduce cost. A similar reasoning could be applied to the tosylate leaving group which could be replaced, for example, by the smaller mesylate.

Overall, the process described in Chapter 1 is limited in both cost and scalability by the use of chromatography as the separation tool. For the relatively cheap starting materials used in uniform PEG synthesis, a quick cost calculation reveals that the vast majority (> 90 %) of the cost is in the chromatographic separation, through solvent use and labour. This production cost is reflected in the high prices currently charged for homo- and heterobifunctional uniform PEG. At the same time, while the

typical minimum size for effective PEGylation is 5,000 Da, this region has so far only been accessed with branched products. This suggests that there are limitations to the current strategies for linear PEGs. The quest for uniform PEGs of pharmaceutically useful length therefore requires an entirely different separation approach, and a strategy designed around such a separation. That approach could be organic solvent nanofiltration (OSN), a membrane-based separation technique.

In Chapter 3, OSN will be used to improve the purifications within the chain extension cycle, both after chain extension and after deprotection. Prior to implementing nanofiltration however, the kinetics of chain extension were investigated to obtain an estimate of reaction speed and impurity accrual (e.g. M – Eg₈) over time.

2. Chapter 2: Chain extension kinetics

2.1. Introduction

In order to obtain a uniform PEG product, chain extension reactions must be significantly more than 99 % complete after each step, or shorter homologues will quickly accumulate over multiple cycles. Because the separation of incompletely extended homostar from the homostar main product is much more difficult than the removal of building block, building block dimer and debris, understanding the homostar chain extension is a priority. If there is a 1 % shortfall in conversion during an extension cycle, leading to incompletely extended homostar that is not separable, it could lead to approximately 5 % of shorter impurity after only 5 cycles. The monitoring of the chain extension reactions to completion was therefore critical to ensuring uniformity of the product PEG. In order to better understand how fast chain extensions proceed, a kinetic study was carried out alongside the synthesis run from Eg₈ to Eg₅₆ described in Chapter 1.

Each chain extension consists of three main reactions from the reactant triol to the fully extended homostar in which each of the homostar's three arms homostar are extended. Each chain extension step is an etherification reaction that obeys S_N2 characteristics and these extension steps occur in series (Figure 42). The first, second and third extension are assigned the individual rate constants, k_1 , k_2 and k_3 .

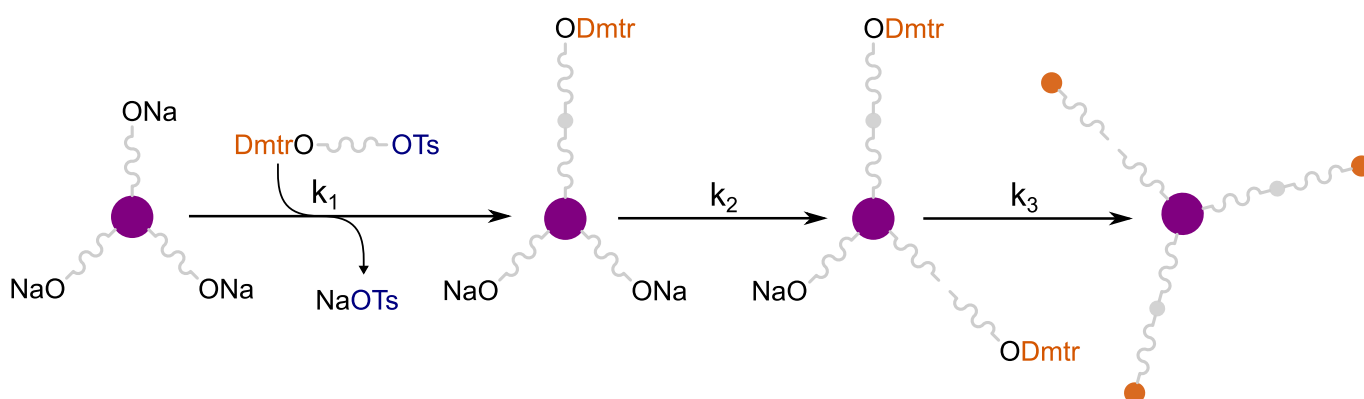


Figure 42. (a) Chain extension from reactant triol homostar, via intermediate singly and doubly extended homostars, to fully extended product.

2.2. Materials and methods

2.2.1. Methodology for chain extension reactions

The kinetic study was carried out on a synthetic scale alongside the synthesis of Eg₅₆ described in Chapter 1. Reactant triol homostar and building block were azeotropically dried (three times) with MeCN in separate flasks, with a trace of Et₃N added to the building block prior to the first drying step. The homostar was dried in a two-armed flask, with one arm connected to a Schlenk line supplied with argon via a Young's tap, and the other arm stopped closed. NaH (60 wt% suspension in mineral oil) was three times washed and dried with n-hexane under a stream of argon to give a free-flowing powder. The building block was then dissolved in a minimum quantity of N,N-dimethylformamide (DMF) solvent and transferred into the two-armed flask containing the homostar. The flask having contained the building block was then twice more rinsed with DMF and the rinsing solution transferred. The quantities of DMF for transfer and rinsing were chosen to obtain the correct final volume of DMF for the reaction after transfer.

The reaction flask was then immersed in a silicone oil bath, heated to the reaction temperature and stirred for several minutes. Only then was NaH added against a flow of argon through the side arm of the two-necked flask and the flask closed once more. The addition of NaH marks the start of the reaction and, upon addition, a timer was simultaneously started with assistance of a second person.

2.2.2. Reaction monitoring and sampling

Samples (50 μ L) were taken from the reaction mixture through the side arm with a micropipette against a brisk stream of argon, and samples were quenched by injection into a GC vial filled with dilute aqueous solution of NH₄Cl (450 μ L) (2 eq. of NH₄Cl per mol of NaH). The GC vial was immediately capped and shaken to affect complete quenching, with assistance by a second person where necessary. By addition into the quenching solution, the samples were diluted 1:10 (50 μ L of reaction mixture in 500 μ L total volume). The sampling volume was deliberately small to minimize the impact on the isolated product yields, although this required dilution for HPLC analysis in turn.

Samples were taken from 00:01:14 onwards at intervals regularly spaced on a logarithmic time scale (Table 14). Short sampling intervals at the beginning of the reaction necessitated the assistance of a second person for capping and shaking of samples. Sampling on a logarithmic time scale was chosen due to the exponential nature of the S_N2 reaction, with sampling more closely spaced at the beginning of the reaction when the change in concentration is faster.

Table 14. Sampling table over 36 h for kinetic studies during chain extension.

Sample	Time [hh:mm:ss]
1	00:01:14
2	00:01:32
3	00:01:54
4	00:02:21
5	00:02:54
6	00:03:36
7	00:04:27
8	00:05:30
9	00:06:49
10	00:08:26
11	00:10:27
12	00:12:56
13	00:16:00
14	00:19:48
15	00:24:31
16	00:30:20
17	00:37:33
18	00:46:29
19	00:57:31
20	01:11:12
21	01:28:07
22	01:49:04
23	02:15:00
24	02:47:06
25	03:26:49
26	04:15:59
27	05:16:50
28	06:32:10
29	08:05:23
30	10:00:46
31	12:23:36
32	15:20:22
33	18:59:09
34	23:29:58
35	29:05:08
36	36:00:00

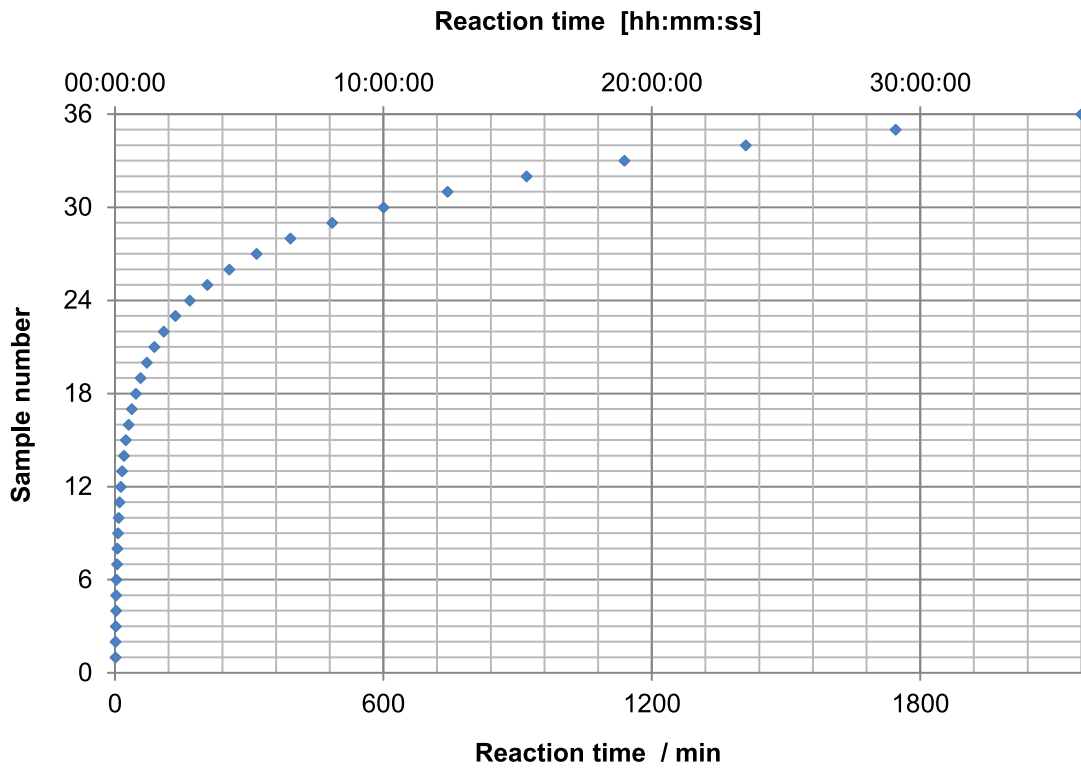


Figure 43. Kinetic sampling points over 36 h visualized on a linear scale.

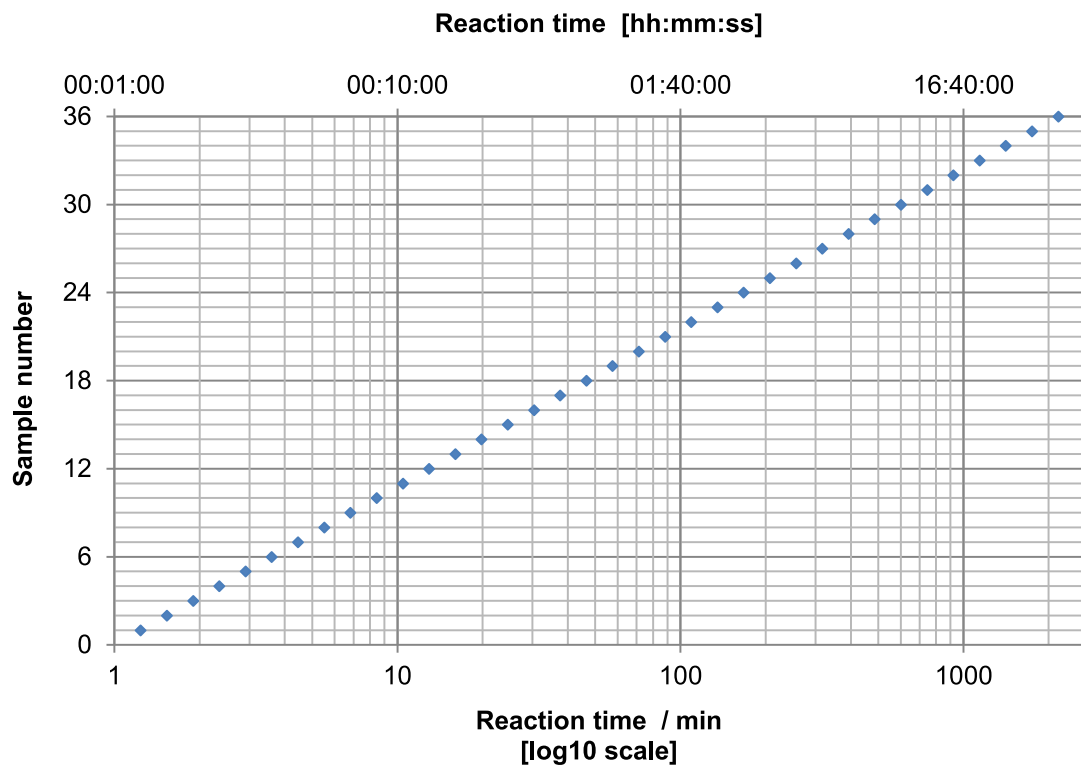


Figure 44. Kinetic sampling points over 36 h visualized on a logarithmic scale.

2.2.3. HPLC analysis

Samples were analyzed with an Agilent 1100 Series HPLC system equipped with a quaternary pump, an autosampler and a diode array detector (Agilent G1315B DAD). For chain extensions from Eg₂₄ to Eg₃₆ and onwards, a Phenomenex Aeris Widespore 3.6 mm XB-C₁₈ 150 mm x 4.6 mm column was used with a flowrate of 0.8 mL·min⁻¹ and a column temperature of 30 °C. A binary solvent system of methanol and 5 mM diethylammonium acetate in deionized water was used. A linear gradient was run from 50 to 90 % methanol over 20 min, followed by a hold at 90 % methanol for 5 min, and a re-equilibration period of 5 min at 50 % methanol. The sample injection volume was 50 µL.

Downstream of the UV detector was installed a Varian 385-LC Evaporative Light Scattering Detector (ELSD) operated as follows: 40 °C evaporation temperature, 55 °C nebulization temperature, 1.5 SLM N₂ flow rate.

2.2.4. Data processing

Quantification of Dmtr containing species

The study was helped by the structure of the building blocks including very hydrophobic Dmtr protecting groups. As a result of these, homostar triol reactant, the singly and doubly extended intermediate products, and the fully extended homostar possess very different retention times on a C₁₈ stationary phase during HPLC analysis. With each extended arm, the retention time increases due to the addition of a chain terminal lipophilic Dmtr ether. In contrast, the unprotected homostar reactant possesses comparatively little hydrophobic character and elutes early on. This degree of separation provided a useful basis for the kinetic study.

HPLC traces were collected, the peaks assigned and integrated at 260 nm for quantification. Present in all traces were six species: the four homostar species – unreacted triol, singly, doubly and fully extended homostar – as well as DmtrO–Eg₈–OTs (**8**) building block and DmtrO–Eg₁₆–ODmtr (**14**) building block dimer.

The quantification for this kinetic study relies on the conservation of Dmtr ether groups across the five Dmtr-containing species during chain extension, excluding the homostar triol which lacks a Dmtr ether. The starting triol possesses a benzyl ether group absorbing only weakly at 260 nm and the only other group on one of the six reaction participants exhibiting UV absorbance at 260 nm is the tosylate ester on the building block.

The concentration of the five species containing at least one Dmtr ether was derived from their integrated peak area at 260 nm using the following set of assumptions:

- The UV extinction coefficient of the Dmtr ether group at 260 nm is constant over the molar concentration range in question.
- The contribution of the tosylate ester group towards UV absorbance at 260 nm is considered negligible compared to the contribution of the Dmtr ether.
- It follows that the UV peak integral of each Dmtr ether containing species is proportional to the number of moles of that species after accounting for the number of Dmtr groups per molecule.
- It also follows that the sum of the integrals of the five Dmtr ether containing species is assumed to remain constant over the course of the reaction as these are assumed to consist only of the Dmtr ether contribution.

(Strictly, the assumption is incorrect because there is a minor contribution from the tosylate ester which is expelled during chain extension to form a tosylate salt which elutes elsewhere and will no longer contribute towards the integral total of the five Dmtr containing species. While the expulsion of tosylate ester only occurs for the approximate one third of building block which reacts, its loss nevertheless leads to a small decrease in the net UV absorbance of all Dmtr containing species as the reaction proceeds.)

- The density of building block and homostar reactant is assumed equal to that of tetragol ($1.125 \text{ g}\cdot\text{mL}^{-1}$) and there is no density change upon mixing, so that the volumes of DMF solvent, homostar triol and building block give the total reaction volume when added together.

With these assumptions, the following process is then applied to each collection of 36 HPLC traces representing a single chain extension:

- 1) A full table of all HPLC traces for a reaction is compiled. The peaks for the six reaction participants are identified, and integrated. (The identification of the triol position was often helped by consulting the ELSD traces.)
- 2) The integrals of the five Dmtr containing species are summed and an integral total for the Dmtr containing species thus calculated for each sample trace.
- 3) For the collection of 36 Dmtr integral sums per chain extension are calculated: mean, median and standard deviation around the mean.
- 4) The normalized values for all 36 traces are then calculated, whereby the Dmtr integral sum of each individual trace is divided by the mean of the 36 Dmtr integral totals. This step yields normalized values scattered around 1 and helps to identify outliers far removed from the average value. (For visual aid, the integral sums or normalized values for all traces can be plotted alongside each other.) All outlying samples are excluded from further analysis.

- 5) Some relative error is inevitably introduced during pipetting when removing the sample from the reaction mixture. Another source of relative error is the injection of the sample for HPLC analysis. To eliminate this relative error and make all samples taken from a reaction mixture quantitatively comparable to each other, all peak integrals of an individual trace are scaled according to the deviation of the Dmtr integral sum of that trace from the mean of all 36 Dmtr integral sums. For example, if the average integral sum for the five Dmtr containing species across all 36 samples was 10,000 arbitrary units (a.u.) and one sample deviated upwards, with a total UV integral of 10,200 a.u., all individual peak integrals of that sample, even that of the triol, are scaled down accordingly by dividing by a factor of 1.02 (or 10,200/10,000). After applying this step to all traces, the Dmtr integral sums of each trace should now be equal to the mean Dmtr integral sum across all traces.
- 6) The molar quantities of the five key species are then back-calculated from the Dmtr integral sum and the theoretical molar quantity of building block weighed in at the beginning of the reaction, which constitutes the single source of Dmtr ether during chain extension.
- 7) For example, for the first chain extension from Eg_8 to Eg_{16} the molar quantities of the five Dmtr containing species are calculated as follows:
- The Dmtr integral sum for the five Dmtr containing species is 14,500 arbitrary units (a.u.).
 - The moles of DmtrO– Eg_8 –OTs building block weighed in were 20.4 mmol.
 - 1 mmol of Dmtr ether is therefore equivalent to 711 a.u. By dividing all UV peak integrals for the individual species by a factor of $711 \text{ mmol} \cdot (\text{a.u.})^{-1}$, the corresponding moles of Dmtr ether are obtained.
 - The moles of each individual species are then obtained by accounting for the number of Dmtr ether groups per molecule.
For example, for the diextended homostar and DmtrO– Eg_{16} –ODmtr dimer, each containing two equivalents of Dmtr, the moles of Dmtr ether need to be divided by a factor of 2 to obtain the moles of the species. For the triextended homostar containing three equivalents of Dmtr, the moles are divided by three.
- 8) Lastly, by dividing the molar quantity of each Dmtr containing species by the reaction volume, assumed to be the sum of the total reactant volume and the solvent volume, the molar concentration of all Dmtr containing species is obtained.
For example, the total reaction volume for the chain extension from Eg_8 to Eg_{16} was 58.2 mL. For the DmtrO– Eg_8 –OTs building block, the calculated molar starting concentration is 0.35 M (20.4 mmol / 58.2 mL). As the building block contains only one Dmtr ether, 14,500 a.u. are equivalent to 0.35 M of building block. For a species containing two Dmtr ethers, 14,500 a.u. are equivalent to 0.175 M of that species.

While the UV traces at 260 nm were used for quantification, ELSD traces were only used for qualitative guidance since calibrations would have otherwise had to be performed for many different homostar species. Particularly the isolation of pure intermediate homostars for calibration was deemed impractical.

Quantification of homostar triol

The unreacted homostar triol concentration cannot be estimated in similar fashion, as it lacks a Dmtr group, and must therefore be estimated via the benzyl ether UV absorbance. The triol is harder to quantify accurately as its maximum integral under similar conditions to those used for the Dmtr containing species is smaller by at least a factor of ten due to the low absorbance of the benzyl ether hub at 260 nm. At these relatively low triol peak areas, the overlap of even small peaks caused large relative errors and made triol quantification difficult.

In theory, several methods are available for quantifying the homostar triol. If NaH is added last, as done in this study, one method is the sampling of the reaction mixture prior to starting the reaction. Sampling was in fact performed here in triplicate to estimate the starting integral of triol and back-calculate starting concentration of triol from the theoretically added homostar triol mass, but this measurement yielded mixed results. First, the three samples did not always yield similar values, suggesting variability in the HPLC injection. Further, a variable induction period upon addition of NaH meant that the starting triol concentration could not always be aligned with the data points derived from sampling during reaction on a single curve.

ELSD would have been an alternative means of quantification with higher sensitivity toward the large fraction of polyether in the molecule not detectable by UV but would have required calibration for each generation of triol and is itself prone to error due to its strong non-linearity if peak shapes vary between calibration and sampling. For the first few chain extensions the combination of short homostar chain length and choice of HPLC column also led to poor retention and caused the reactant triol to elute early on, overlapping with the solvent front and salt peaks (NaOTs as a reaction by-product, NH_4Cl from quenching) which are also detected by ELSD.

Ultimately, the homostar triol peak integral at the start of the reaction ($t = 0$ min) was estimated by backwards extrapolation. The fit was manually performed by visual inspection and due to the induction period a linear fit often looked most suitable over the first few minutes. The apparent concentration at each sampling point was then back-calculated proportionally using the peak integral and concentration at t_0 .

The theoretical starting concentrations back-calculated from the masses of reactants and solvents weighed in and the corresponding average Dmtr integral sum and estimated starting Hub¹ peak area are

shown in Table 15. Due to a change of HPLC method after extension to Eg₂₄ and other factors such as adjustment of HPLC injection volumes between extensions, there is not a clear trend in the average Dmtr integral sum or estimated Hub¹ peak area. If analytic conditions were comparable throughout, quantification of Dmtr containing species and homostar triol always yielded the correct peak area and weighing in and transfer of building block always yielded the correct mass balance, then peak areas should be proportional to the theoretical starting concentrations by the same factor in each chain extension.

Table 15. Starting concentrations of homostar triol and building block and corresponding peak areas

	$c_{\text{HS-triol}}^{t=0}$ mM	$c_{\text{BB}}^{t=0}$ mM	Concentration factor ^[a] no units	Average Dmtr integral sum a.u.	Estimated Hub ¹ peak area (t = 0) a.u.
Eg ₈ → Eg ₁₆	0.035	0.350	1.000	14489.2	113.7
Eg ₁₆ → Eg ₂₄	0.034	0.340	0.940	11619.0	45.6
Eg ₂₄ → Eg ₃₂	0.033	0.330	0.885	23213.7	86.5
Eg ₃₂ → Eg ₄₀	0.032	0.319	0.831	15972.1	170.9
Eg ₄₀ → Eg ₄₈	0.031	0.310	0.783	17751.0	119.4
Eg ₄₈ → Eg ₅₆	0.030	0.301	0.738		

[a] Concentration factor is the ratio of the concentration product ($c_{\text{HS-triol}}^{t=0} \cdot c_{\text{BB}}^{t=0}$) for a chain extension relative to the concentration product for the extension from Eg₈ to Eg₁₆. The concentration factor does not need to be additionally applied to the reaction rate coefficients as it is already included within the simulation by using the different starting concentrations.

2.2.5. Simulation of chain extension kinetics

The rate of decrease of homostar triol concentration was used to obtain an initial estimate of the reaction rate for the first chain extension step. Given the large excess of building block, it can be assumed that the reaction rate is pseudo first order and an exponential decline fitted to obtain the pseudo first order rate constant, k' , as given by the integrated first order rate law (Equation 2). By dividing k' by the average building block concentration over the time interval, an estimate of the real second order rate constant for the reaction of triol, k_1 , is obtained (Equation 3).

$$c_{\text{HS-triol}}^t \approx c_{\text{HS-triol}}^{t=0} \cdot e^{-k't}$$

Equation 2

$$k_1 \approx \frac{k'}{\left(\frac{c_{\text{BB}}^{t=0} + c_{\text{BB}}^t}{2}\right)}$$

Equation 3

Using the obtained rate constant as a starting estimate, concentration profiles for each chain extension were simulated for the system of equations shown in section 2.2.6 and manually fitted to suit the concentrations obtained from the integrated data sets. Where the profiles of the triol and Dmtr containing species could not be jointly fitted, a good fit of the Dmtr containing species was given priority. For simulation of the concentration profiles, a MATLAB script was used into which the various parameters could be input, namely induction time (t_{ind}), the starting concentrations of homostar triol ($c_{\text{HS-triol}}^{t=0}$) and building block ($c_{\text{BB}}^{t=0}$), as well as the four kinetic constants (k_1, k_2, k_3 for chain extension; k_4 for building block dimerization). The concentration profiles were then simulated numerically.

Because the moles of homostar must be conserved, the simulation of the reaction kinetics requires that the starting concentration of homostar triol and concentration of the fully extended homostar are equal. Because the two concentrations are estimated by different methods as described above, this would lead to disagreement in the starting and final molar concentrations. After obtaining the initial reaction rate estimate, the homostar triol starting concentration is therefore adjusted to be equal to the final concentration of fully extended homostar. Because the concentration of fully reacted homostar reaches a plateau in each data set upon completion of the reaction, its value can be obtained with relative accuracy. The starting triol concentration is then adjusted to a similar molar concentration for the kinetic simulation.

The method of adjusting the triol concentration in the simulation to suit the Dmtr containing species was chosen as it is simpler than scaling the experimental concentrations of all Dmtr containing species. In

reality, a discrepancy in the molar concentration is much more likely to arise from inaccuracies introduced from transfer of the building block. The molar excess of DmtrO–Eg₈–OTs building block added to the reaction mixture will vary slightly above or below 10, while the homostar as the limiting reagent is accurately weighed provided it is fully dried and is not transferred between flasks. But the starting triol concentration is harder to estimate accurately because the triol peak integral is small and because the triol disappears quickly upon starting the reaction while the sum of the Dmtr peak integrals stays approximately constant throughout the reaction.

During simulation and fitting, precedence was given to a good fit for the Dmtr containing species over the homostar triol. As a result, the experimental concentrations for all Dmtr containing species will always show good agreement with the kinetics simulation while the concentrations of the triol will sometimes show disagreement. This occurs in cases where the starting concentrations of triol and the final concentration of fully extended homostar, calculated from their respective peak areas, are not equal. In practice, this arises when the building block and starting triol were not added in a molar ratio of 1:10 and slightly differ from the reported theoretical quantities, or where triol peaks overlap and cannot be quantified accurately.

In this synthetic protocol, homostar triol and building block were mixed with solvent prior to addition of NaH. Because alkoxide formation upon addition of NaH is not instantaneous, an induction period was always observed. It was attempted to keep this induction period to a minimum by washing the NaH powder with n-hexane prior to addition, but some variability was nevertheless observed between reactions. This induction period (t_{ind}) was accounted for in the simulation and adjusted for each chain extension.

2.2.6. Mathematical description of the chain extension kinetics

The following system of equations is used for simulating the chain extension reactions:

$$\begin{aligned}\frac{d[c_1]}{dt} &= (-k_1[c_1]) \cdot [c_5] \\ \frac{d[c_2]}{dt} &= (+k_1[c_1] - k_2[c_2]) \cdot [c_5] \\ \frac{d[c_3]}{dt} &= (+k_2[c_2] - k_3[c_3]) \cdot [c_5] \\ \frac{d[c_4]}{dt} &= (+k_3[c_3]) \cdot [c_5] \\ \frac{d[c_5]}{dt} &= (-k_1[c_1] - k_2[c_2] - k_3[c_3] - 2 \cdot k_4) \cdot [c_5] \\ \frac{d[c_6]}{dt} &= +k_4 \cdot [c_5]\end{aligned}$$

Equation 4-9

$k_1, k_2, k_3, k_4 > 0$; all constant

$[c_1], [c_2], [c_3], [c_4], [c_5], [c_6] \geq 0$; all variable with time

$[c_1]$ to $[c_4]$ are the concentrations of unreacted triol, monoextended homostar, diextended homostar and fully triextended homostar respectively and $[c_5]$ and $[c_6]$ are the concentrations of DmtrO–Eg₈–OTs (**8**) building block and DmtrO–Eg₁₆–ODmtr (**14**) building block dimer respectively.

$[c_1]$: Hub¹(–Eg_n–OH)₃

$[c_2]$: Hub¹(–Eg_n–OH)₂(–Eg_{n+8}–ODmtr)₁

$[c_3]$: Hub¹(–Eg_n–OH)₁(–Eg_{n+8}–ODmtr)₂

$[c_4]$: Hub¹(–Eg_{n+8}–ODmtr)₃

$[c_5]$: DmtrO–Eg₈–OTs (**8**)

$[c_6]$: DmtrO–Eg₁₆–ODmtr (**14**)

k_1, k_2 and k_3 (M⁻¹·min⁻¹) are the reaction rate coefficients for each of the three individual chain extension steps, all S_N2 type. k_4 (min⁻¹) is an arbitrary reaction rate coefficient for the formation of dimer from building block. The experimental data often gave a good fit for a first order reaction for dimer formation, so the above rate equation was chosen although the exact mechanism has not been investigated.

2.3. Results and discussion

The raw data and analysis for the chain extension from Eg_8 to Eg_{16} is shown in detail in Section 2.3.1 below. The remaining chain extensions from Eg_{16} to Eg_{56} are detailed in Appendix D.

2.3.1. Extension from Eg_8 to Eg_{16}

The reaction from $\text{Hub}^1(-Eg_8-OH)_3$ (**11**) to the next generation homostar, $\text{Hub}^1(-Eg_{16}-ODmtr)_3$ (**12**), proceeds in three successive reaction steps via two partially extended intermediates. Each chain extension step is an etherification reaction that obeys S_N2 characteristics and each reaction step is assigned an individual reaction rate constant (Figure 45a). The first, second and third extension are assigned the individual rate constants, k_1 , k_2 and k_3 . Simultaneously a side reaction occurs through which $\text{DmtrO}-Eg_8-OTs$ building block (**8**) is continuously degraded and converted to $\text{DmtrO}-Eg_{16}-ODmtr$ building block dimer (**14**) (Figure 45b). The building block degradation mechanism is not investigated in detail here and the formation is described from building block as a first order reaction with rate constant k_4 , in first approximation. The formation of alkoxide from the reaction of the hydroxide chain termini of the homostar with NaH is considered fast with respect to the other reaction steps in first approximation.

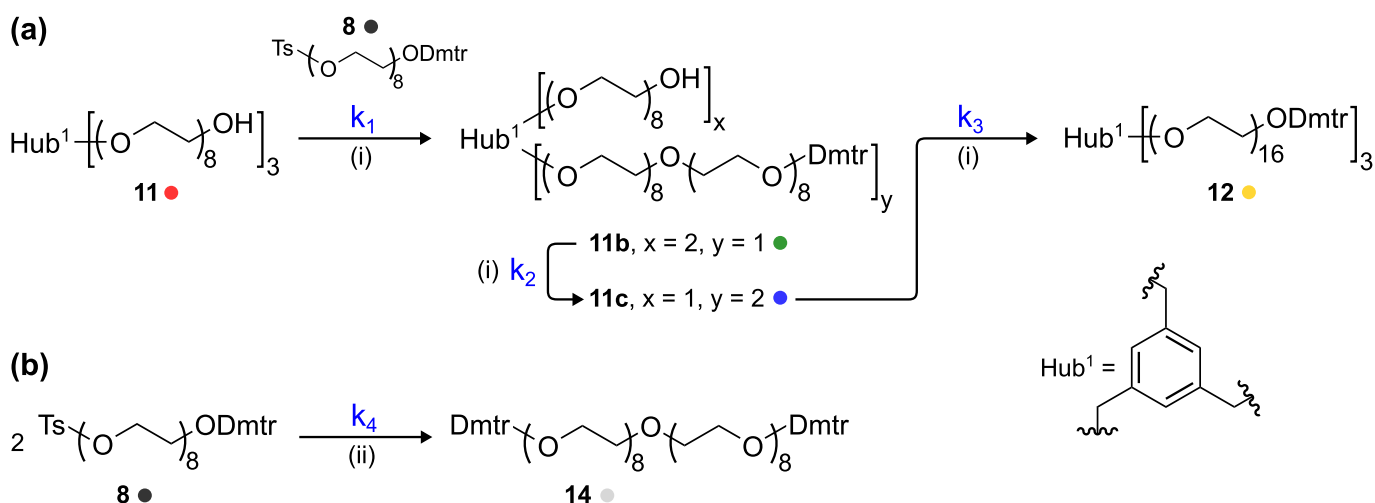


Figure 45. (a) Chain extension from the first generation homostar triol, $\text{Hub}^1(-Eg_8-OH)_3$ (**11**, ●), via intermediate singly (**11b**, ●) and doubly extended (**11c**, ●) homostars, to the second generation homostar, $\text{Hub}^1(-Eg_{16}-ODmtr)_3$ (**12**, ●) and (b) side reaction of $\text{DmtrO}-Eg_8-OTs$ (**8**, ●) building block to generate $\text{DmtrO}-Eg_{16}-ODmtr$ dimer (**14**, ●). (i) 10 eq. **8**, 6 eq. NaH, DMF (ii) Exact reaction mechanism unknown. Annotated colours correspond to the simulated chain extension profiles in the following section.

Waterfall plots of the HPLC traces taken over the course of the reaction (12.5 h) with ELSD and UV (260 nm) detection (Figure 46, top and bottom respectively) reveal a central peak eluting around 12.5 min corresponding to the DmtrO–Eg₈–OTs building block (**8**). Expansions of the plot (Figure 47 and Figure 48) give a more detailed view of either side of the main peak.

In Figure 46, eluting earlier than **8** (to the left of the building block main peak), are visible the solvent front and reaction debris such as sodium tosylate (NaOTs) salt (2.8-3.2 min), the Eg₈ homostar triol (**11**) (3.8 min, ●) and the Eg₈ homostar with one extended arm, Hub¹(–Eg₈–OH)₂(–Eg₁₆–ODmtr)₁ (**11b**) (8.4 min, ●). Eluting later than **8** (to the right of the building block main peak), are visible the doubly extended homostar, Hub¹(–Eg₈–OH)₁(–Eg₁₆–ODmtr)₂ (**11c**) (14 min, ●), DmtrO–Eg₁₆–ODmtr building block dimer (**14**) (15.8 min, ●) and fully extended homostar, Hub¹(–Eg₁₆–ODmtr)₃ (**12**) (18.2 min, ●).

The analysis of the UV traces reveals a similar picture and all Dmtr ether containing species can be readily identified but it is much harder to locate the homostar triol in the UV spectra due to the low extinction coefficient of the hub benzyl ether (Figure 47, compare top and bottom). Hence, the ELSD spectra were usually used as a location aid and for confirmation.

A comparison of the UV and ELSD spectra also reveals peaks which were not identified as part of the kinetic study. Identification of these peaks e.g. by an HPLC coupled with mass spectrometric analysis could have given valuable information into side products and impurities formed during the reaction, or into impurities already present on the HPLC column prior to analysis. A peak of relatively constant size is visible (ELSD but no UV) at about 5.3 minutes. Another constant peak is visible around 11.2 minutes (ELSD and UV) and a peak around 11.5 minutes (ELSD and UV) increases in size (Figure 47) and these could be DmtrO–Eg₈–Cl and building block vinyl ether elimination side-product (**13**) respectively. DmtrO–Eg₈–Cl can be generated during tosylation of building block with TsCl when the chloride liberated during the reaction exchanges with the tosyl leaving group.

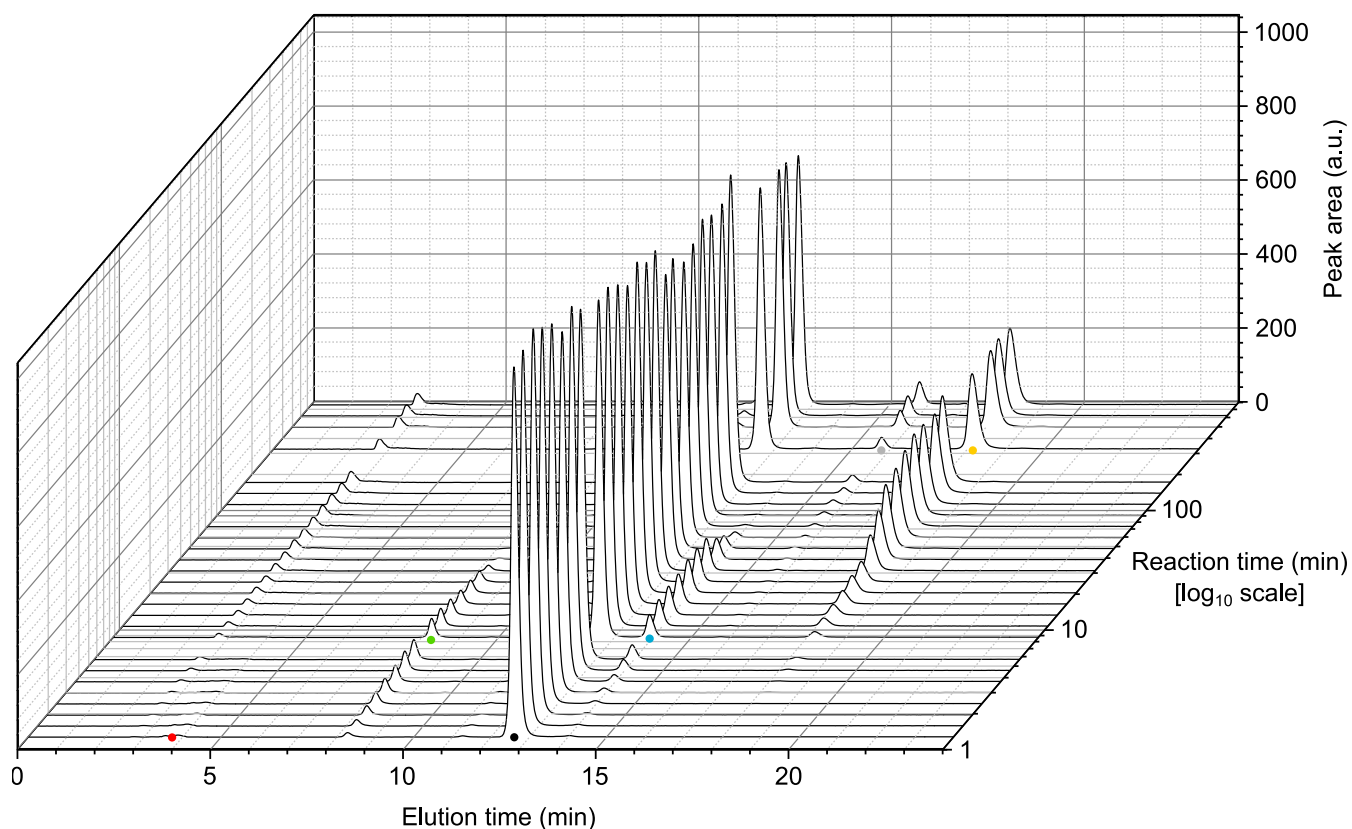
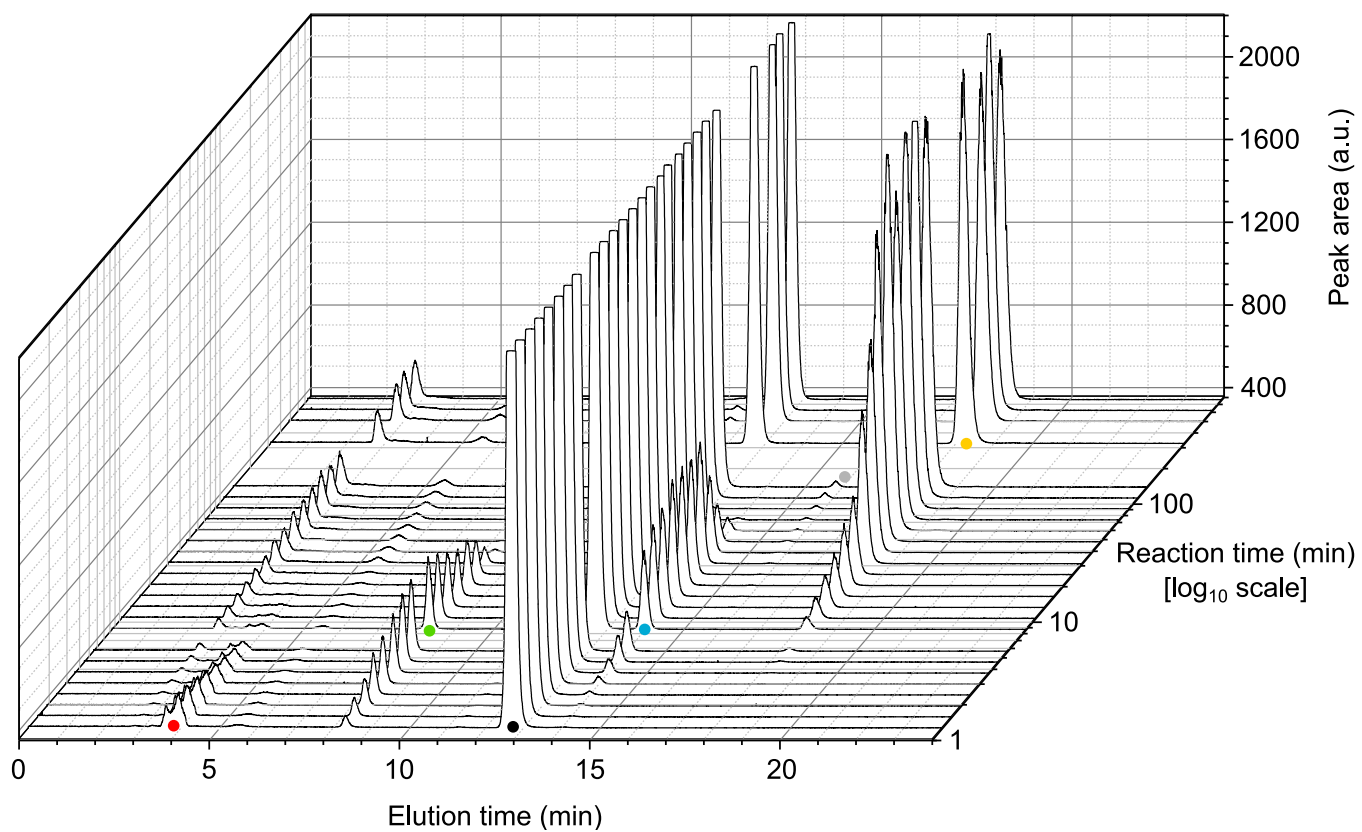


Figure 46. Waterfall plot of HPLC traces with (top) ELSD and (bottom) UV (260 nm) detection for the chain extension from Eg_8 to Eg_{16} over 750 min (12.5 h). NaOTs (2.8 min), **11** (3.8 min, ●), **11b** (8.4 min, ●), **8** (12.5 min, ●), **11c** (14 min, ●), **14** (15.8 min, ●), **12** (18.2 min, ●). Reaction time (z-axis) is shown on a \log_{10} scale. Regions on either side of the main peak are shown enlarged in Figure 47 and Figure 48.

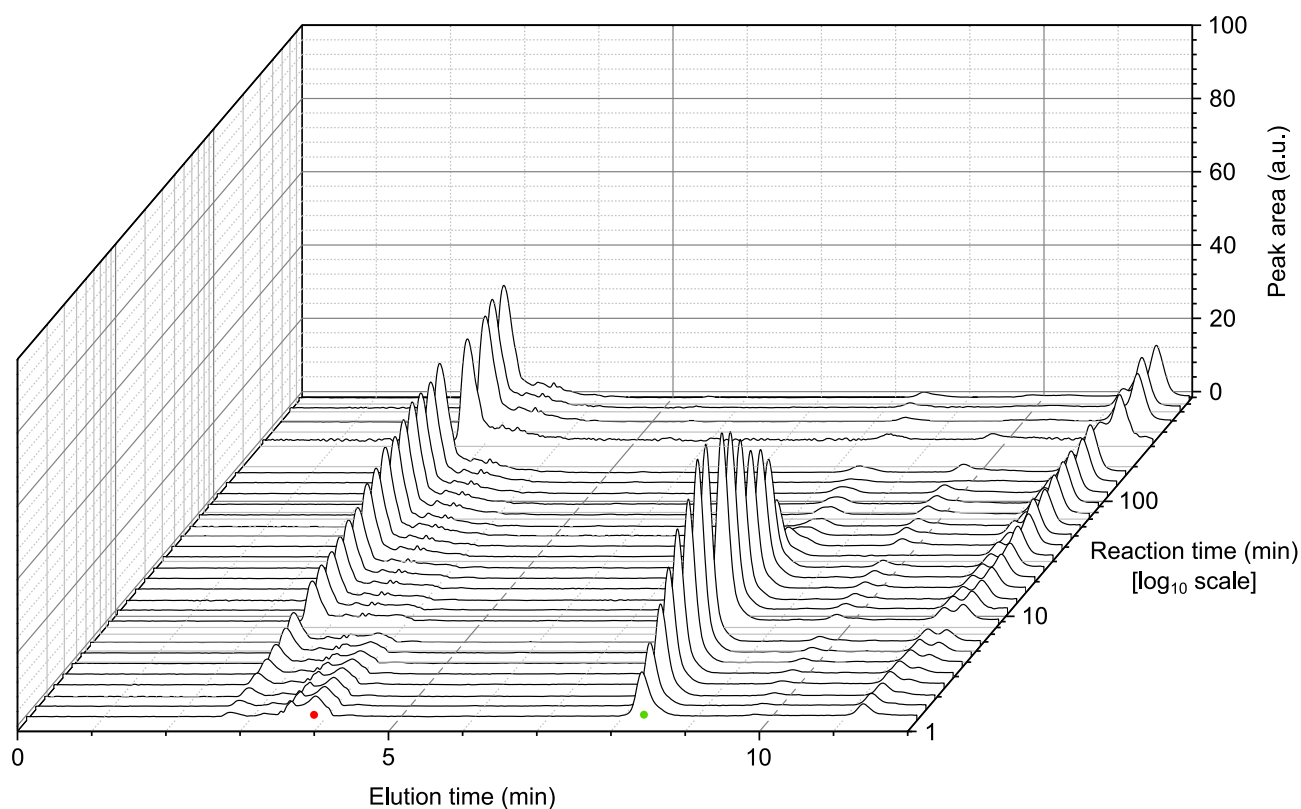
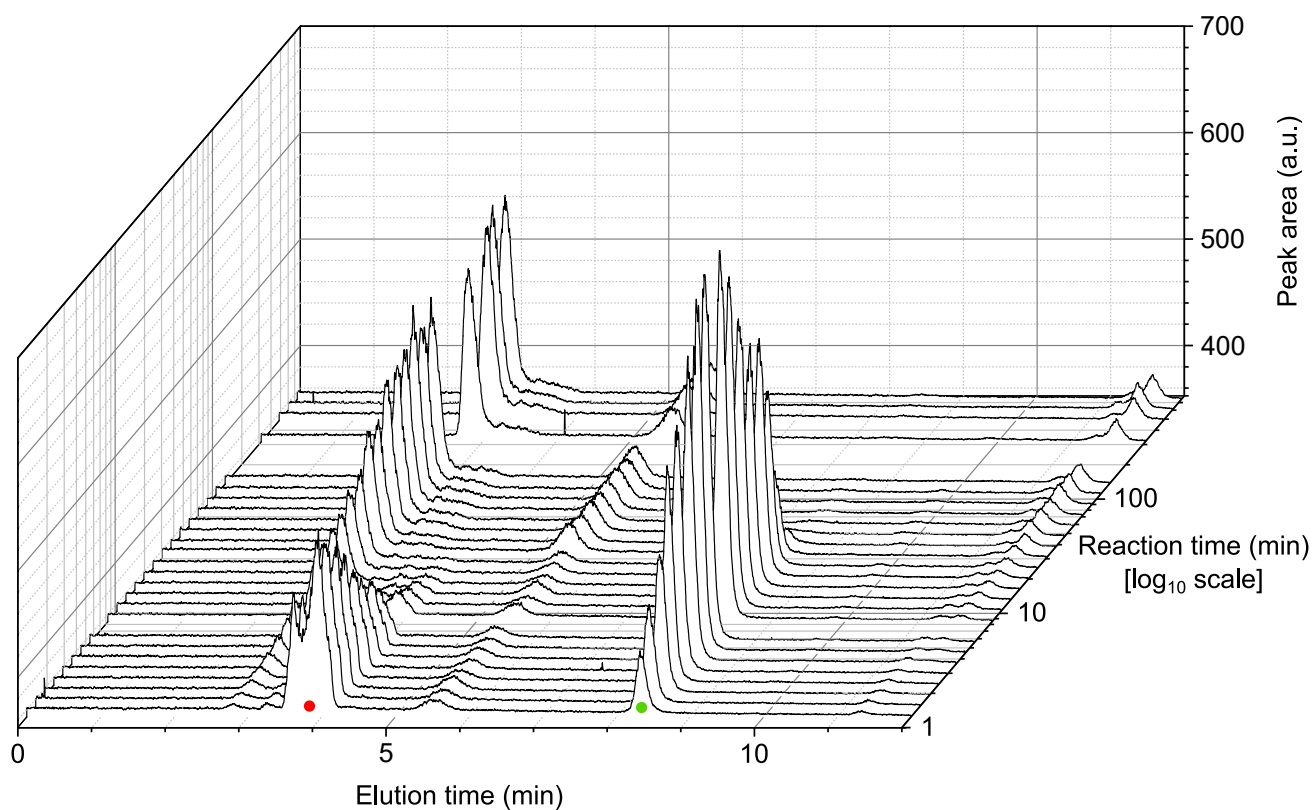


Figure 47. Enlarged from Figure 46. HPLC traces with (top) ELSD and (bottom) UV (260 nm) detection for the chain extension from Eg_8 to Eg_{16} . Homostar triol (**11**) (3.8 min, ●) partially overlapped with earlier eluting peaks consisting of reaction debris such as NaOTs salts (2.8-3.2 min) but integration was still possible in this case.

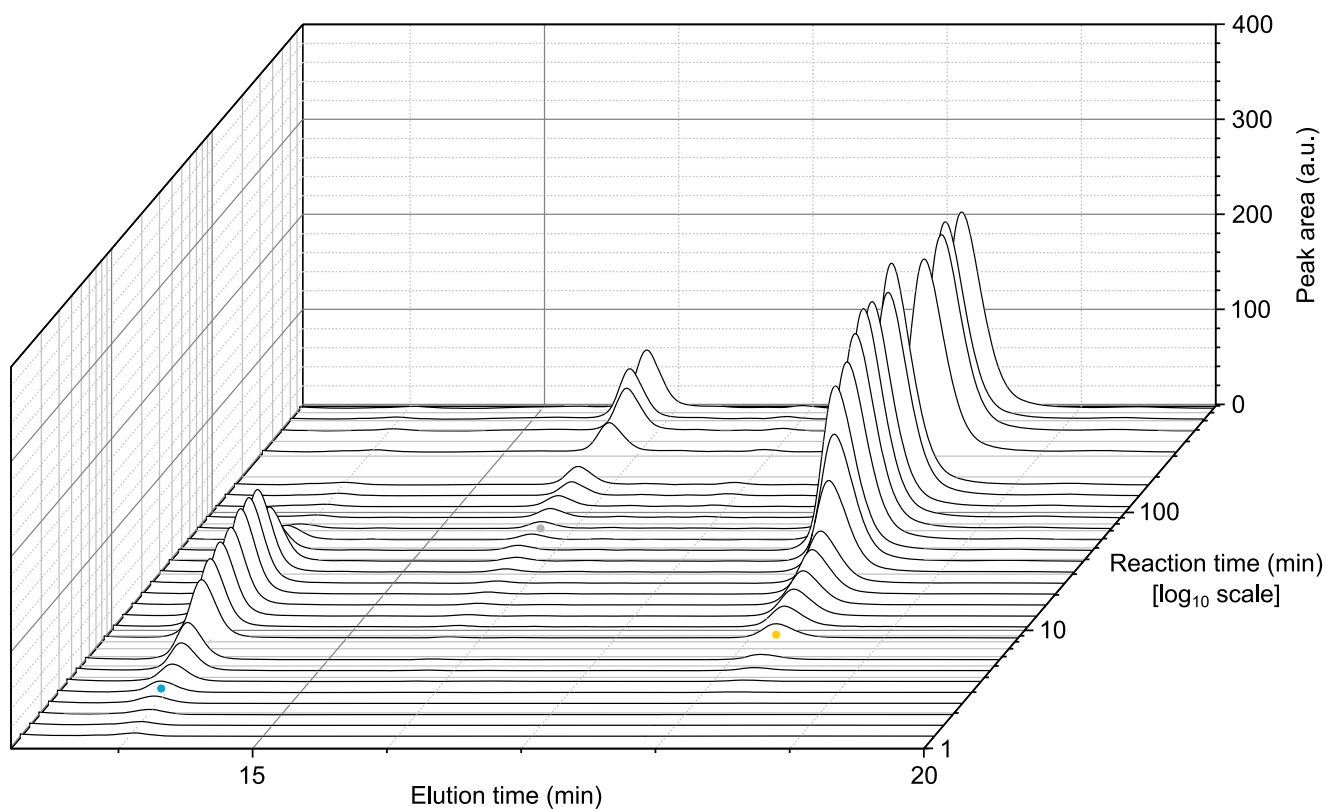
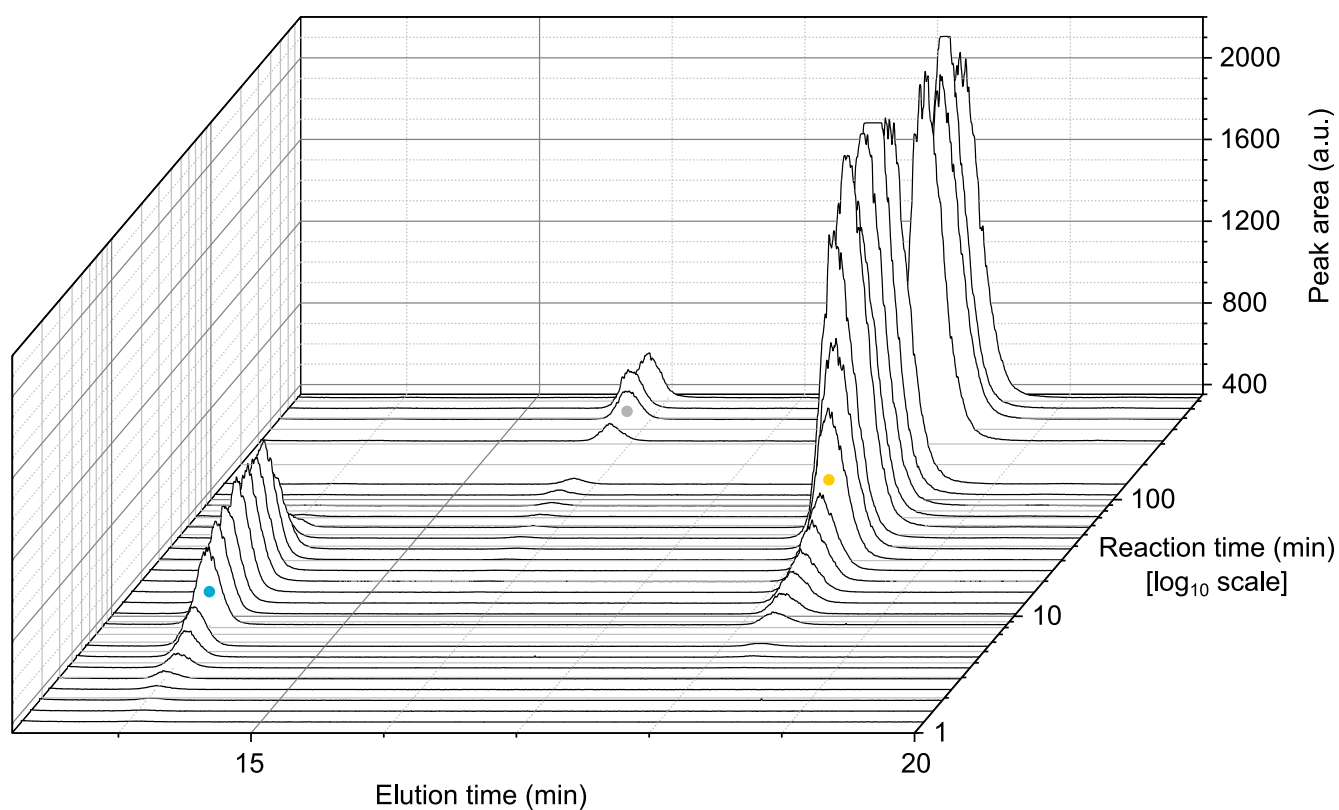


Figure 48. Enlarged from Figure 46. HPLC traces with (top) ELSD and (bottom) UV (260 nm) detection for the chain extension from Eg_8 to Eg_{16} . DmtrO- Eg_{16} -ODmtr dimer (**14**) (15.8 min, ●) concentration increases towards the end of the reaction.

While the homostar triol (**11**) was not easily detectable by UV and the peak overlapped slightly with what are presumably tosylate salts eluting close to the solvent front, integration was still possible. The integrated peak areas for the triol were translated into concentration values by means of the starting concentration at t_0 , as shown in Figure 49. The data shows good agreement with an exponential fit over the entire range. The pseudo first order rate coefficient could therefore be extracted directly from Figure 49 ($k' \approx 0.143 \text{ min}^{-1}$). The average concentration of building block over the time period of the exponential fit was 0.324 M, so the second order rate constant is around $0.4 \text{ M}^{-1} \cdot \text{min}^{-1}$. Because of the small peak areas for the unreacted hub triol, the rate constant estimated in this fashion should be treated with caution and used as a starting estimate for the simultaneous simulation of all rate constants.

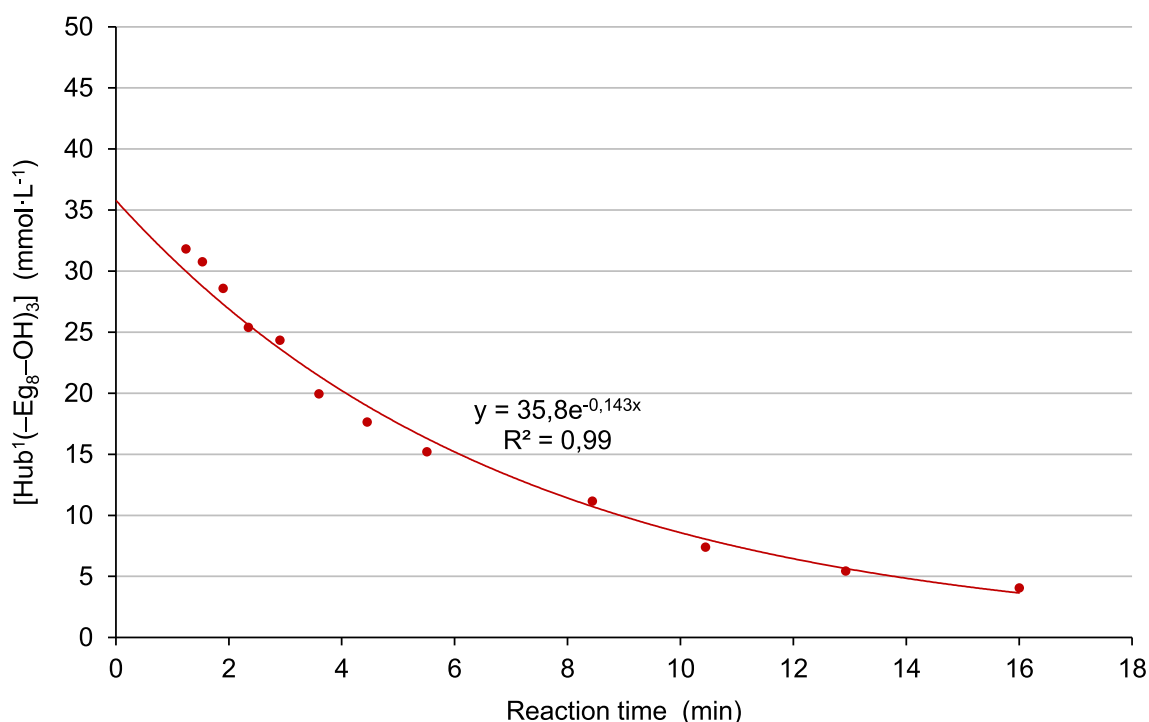


Figure 49. Concentration profile of homostar triol at the start of the reaction up to the 16th minute.

Coupled with the concentration data of the five Dmtr containing species obtained from integration of the UV traces and conversion into concentration values as described in section 2.2.4, a complete data set is obtained (Figure 50). The data points corresponding to the homostar triol (red circles) are directly equivalent to the data shown in Figure 49. The concentration profiles show the expected trend with the intermediate homostar species appearing and then disappearing in succession: as the Eg₈ homostar triol (**11**, ●) disappears at the start of the reaction, the monoextended homostar (**11b**, ●) starts to appear, peaks, then declines and is converted into the doubly extended homostar (**11c**, ●), which is finally converted into the fully extended homostar (**12**, ●). Eventually, the concentrations of the triol and both partially extended homostars tend towards zero and the fully extended Hub¹(-Eg₁₆-ODmtr)₃ (**12**, ●) plateaus as the reaction reaches completion. It is evident that as long as building block and strong base

are present and the reaction is not quenched, building block (**8**, \blacklozenge) continues to be converted to DmtrO–Eg₁₆–ODmtr building block dimer (**14**, \blackplus) after the reaction is complete after around the 200th minute.

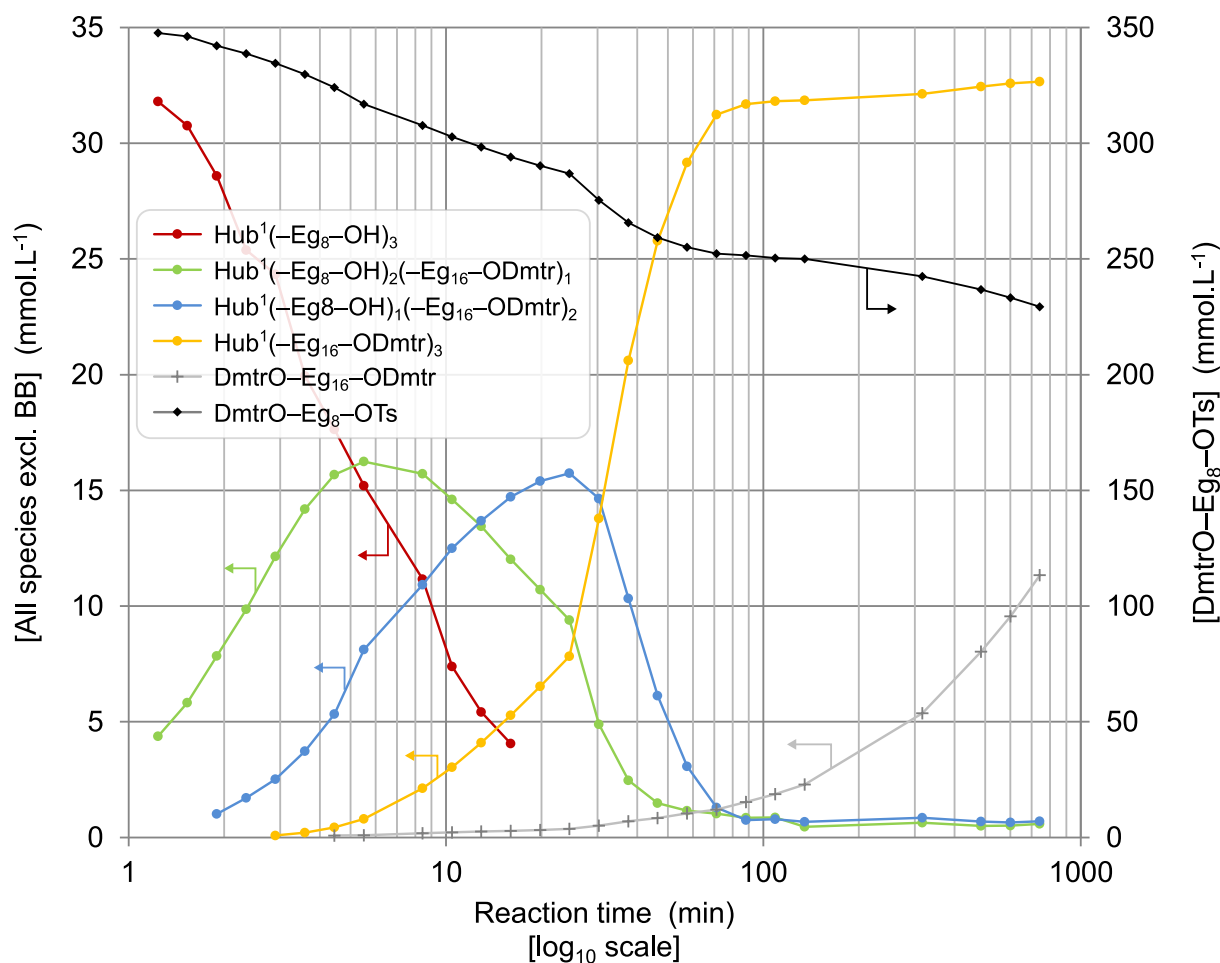


Figure 50. Concentration data points for the chain extension from Eg₈ to Eg₁₆. Connections between data points are for visualization only.

The same concentration data set is then overlaid with simulated concentration curves obtained via an ordinary differential equation solver in MATLAB with the system of equations described in section 2.2.6 (Figure 51). The rate constant for the first extension step from the triol, $k_1 = 0.4 \text{ M}^{-1} \cdot \text{min}^{-1}$, was used as the starting estimate for all extensions (k_1, k_2, k_3) but it quickly emerged that the reaction constant declined with each extended arm ($k_1 > k_2 > k_3$). For the overall chain extension from Eg₈ to Eg₁₆, using as starting concentrations $c_{\text{HS-triol}}^{t=0} = 33 \text{ mmol} \cdot \text{L}^{-1}$, $c_{\text{BB}}^{t=0} = 350 \text{ mmol} \cdot \text{L}^{-1}$, an acceptable fit was obtained with reaction rate constants $k_1 = 0.70 \text{ M}^{-1} \cdot \text{min}^{-1}$, $k_2 = 0.40 \text{ M}^{-1} \cdot \text{min}^{-1}$, $k_3 = 0.20 \text{ M}^{-1} \cdot \text{min}^{-1}$ for the first, second and third arm extension respectively. It was necessary to fit an induction time delay of 0.75 min to account for the induction period and it is notable that the Dmtr containing species exhibit a better fit than the homostar triol which could not be brought into agreement simultaneously. A temporary drop in reaction rate is apparent around the 20th to 40th minute, presumably due to a discontinuation of the magnetic stirring in the silicone oil bath responsible for maintaining the reaction temperature at 30 °C.

The need for fitting an induction time indicates that the formation of the alkoxide from the hydroxide chain termini on the homostar with NaH is not sufficiently fast to be negligible.

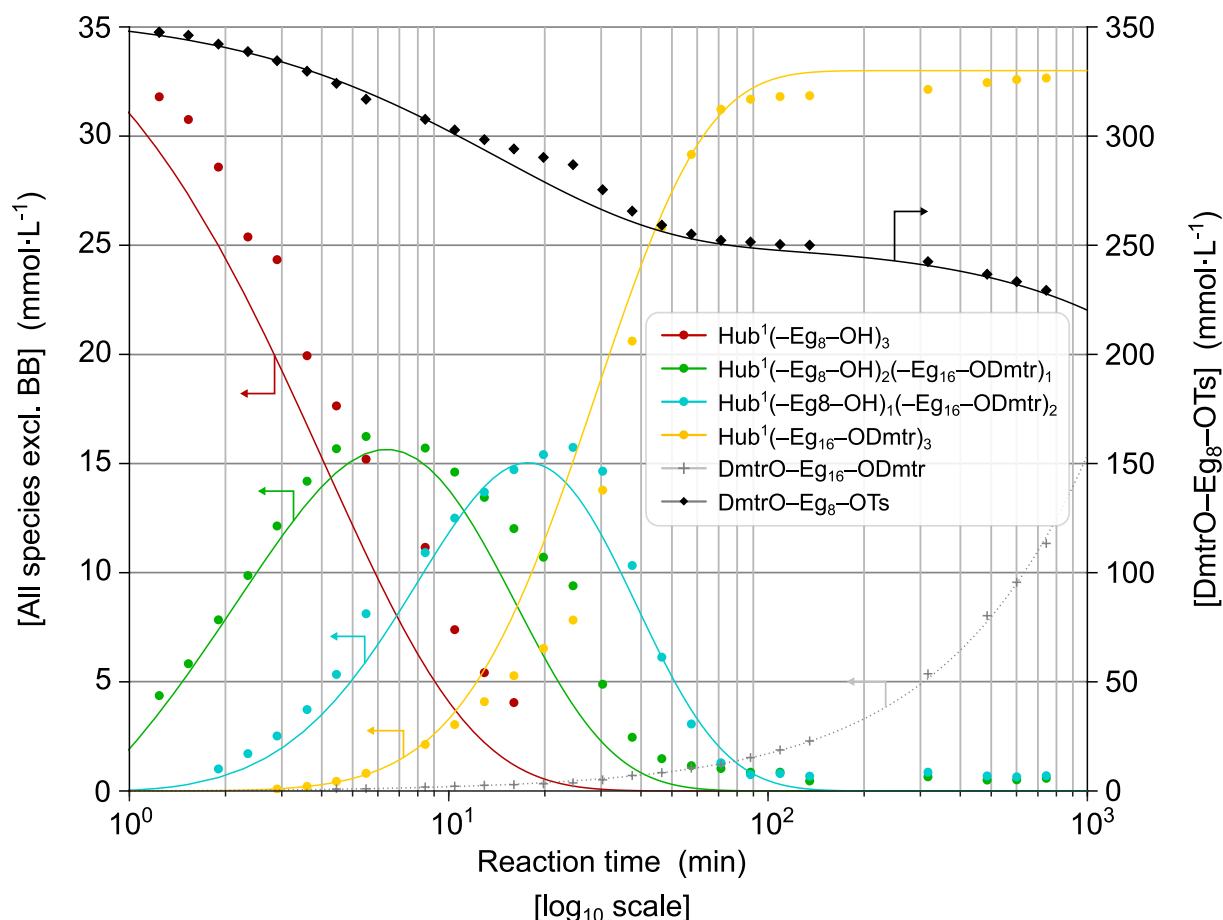


Figure 51. Simulated concentration profiles for the chain extension from Eg_8 to Eg_{16} : $t_{ind} = 0.75$ min, $k_1 = 0.70 \text{ M}^{-1} \cdot \text{min}^{-1}$, $k_2 = 0.40 \text{ M}^{-1} \cdot \text{min}^{-1}$, $k_3 = 0.20 \text{ M}^{-1} \cdot \text{min}^{-1}$, $k_4 = 6.5 \cdot 10^{-5} \text{ min}^{-1}$, $c_{HS\text{-triol}}^{t=0} = 33 \text{ mmol} \cdot \text{L}^{-1}$, $c_{BB}^{t=0} = 350 \text{ mmol} \cdot \text{L}^{-1}$. A temporary drop in reaction rate is apparent around 20-40 min, due to a discontinuation of the magnetic stirring in the silicone oil bath responsible for maintaining the reaction temperature at $30 \text{ }^\circ\text{C}$.

A decrease in the reaction rate constant with each extended arm can be rationalized with the Arrhenius equation (Equation 10), where k is a rate constant, T is the absolute temperature in Kelvin, A is the pre-exponential factor, E_a is the activation energy and k_B is the Boltzmann constant, and where E_a and $k_B T$ have similar units and A has units similar to the rate constant which vary depending on the order of the reaction (min^{-1} for the chain extensions constants k_1 , k_2 and k_3).

$$k = A \cdot e^{\left(-\frac{E_a}{k_B T}\right)}$$

Equation 10

For the extension from Eg_8 to Eg_{16} (as for any individual chain extension reaction studied here), the temperature of the reaction remains similar over the course of the reaction, and the extension of each

arm follows a similar chemical mechanism thus requiring a similar activation energy, E_a . Independent of the exact activation energy and temperature, the exponential term of the Arrhenius equation for the extension of any two arms during a chain extension should therefore be similar. When comparing the Arrhenius equation for two specific reaction rate constants (corresponding to the extension of successive arms), the exponential terms therefore cancel. It follows that the ratio of the rate constants must be proportional to the ratio of the pre-exponential factors (Equation 11).

$$\frac{k_1}{k_2} = \frac{A_1}{A_2}$$

Equation 11

While the exponential term describes the probability that a given collision in correct orientation will lead to a successful reaction when the two reaction partners can overcome the activation energy, the pre-exponential factor, A , describes the frequency of collisions in the correct orientation. For a given overall number of collisions at a given temperature and concentration, the fraction of collisions in proper orientation must therefore differ between two arm extensions to lead to different reaction rate constants.

For the extension of successive homostar arms, this should be the case. With the attachment of the first arm, an individual homostar molecule loses one of its three sites available for extension. This corresponds to a loss of a third of available reaction sites per molecule and so for a given total number of collisions, the number of collisions in proper orientation should decrease by a similar proportion, roughly 1/3, according to theory. Upon attachment of the second arm, the pre-exponential factor should further halve as the fraction of collisions in proper orientation for a successful reaction decreases further with only one site per molecule now left available for reaction. It follows that the ratio of the rate constants for the individual arm extensions should be expected in the ratio of $k_1:k_2:k_3 = 3:2:1$ provided no additional factors have an influence.

The difference in rate constant between each extended arm becomes more visually accessible when comparing the concentration profiles of the intermediate homostar species for a hypothetical chain extension with values similar to those obtained previously ($k_1 = 0.60 \text{ M}^{-1}\cdot\text{min}^{-1}$, $k_2 = 0.40 \text{ M}^{-1}\cdot\text{min}^{-1}$, $k_3 = 0.20 \text{ M}^{-1}\cdot\text{min}^{-1}$; Figure 52a) with a hypothetical reaction in which the rate constants are equal ($k_1 = k_2 = k_3 = 0.40 \text{ M}^{-1}\cdot\text{min}^{-1}$; Figure 52b). It is apparent that in the hypothetical example with equal rate constants, the concentration of the doubly extended homostar peaks much lower than the concentration of monoextended homostar whereas the concentrations peak at similar values in the real example. (This pattern is apparent throughout all the chain extensions up to E_{g56} without exception; in some cases, the doubly extended homostar concentration actually peaks slightly higher.)

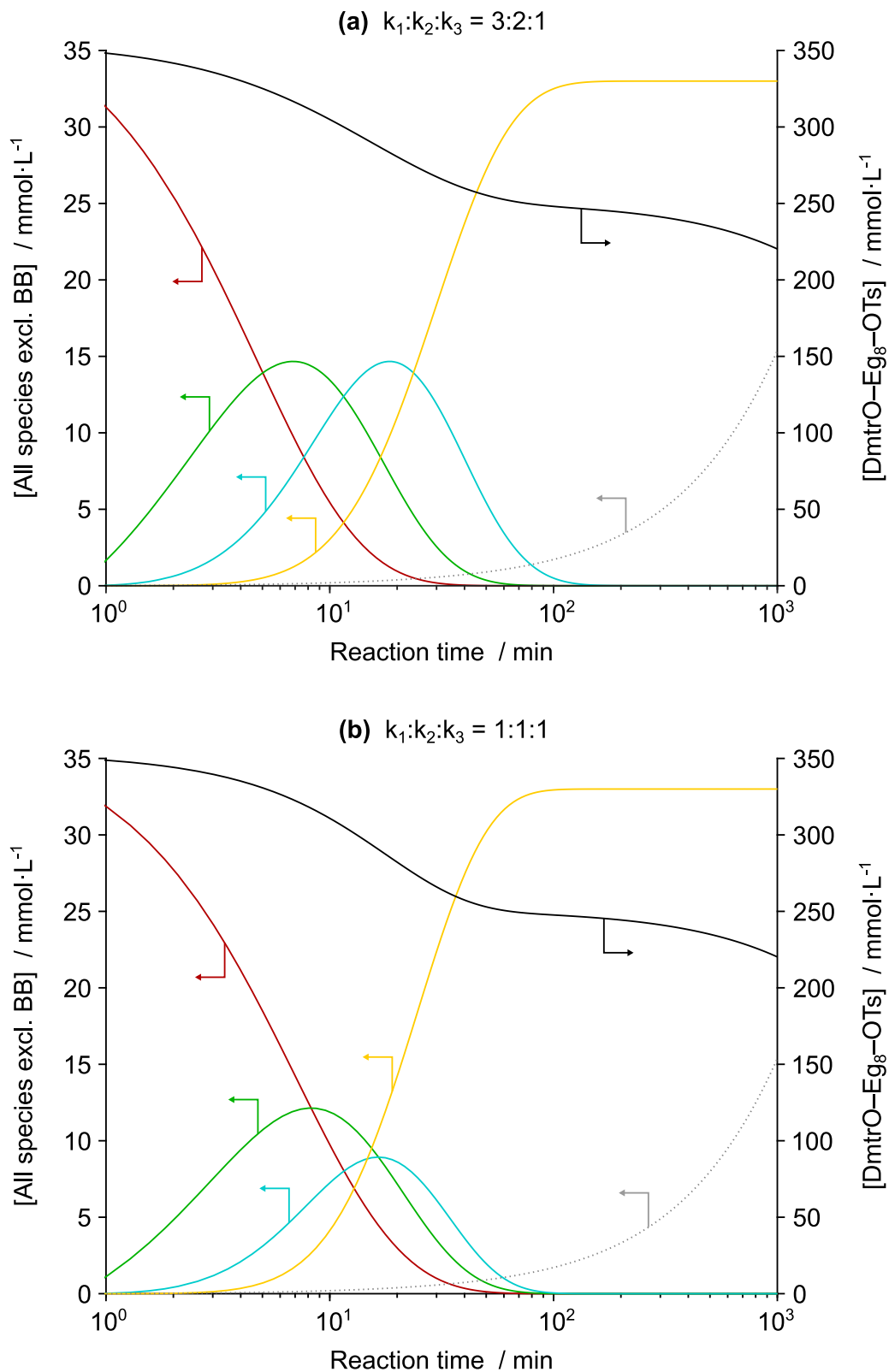


Figure 52. Comparison of simulated concentration profiles for two hypothetical chain extensions (a) with $k_1:k_2:k_3$ in the ratio 3:2:1 ($k_1 = 0.60 \text{ M}^{-1}\cdot\text{min}^{-1}$, $k_2 = 0.40 \text{ M}^{-1}\cdot\text{min}^{-1}$, $k_3 = 0.20 \text{ M}^{-1}\cdot\text{min}^{-1}$) and (b) with $k_1:k_2:k_3$ in the ratio 1:1:1 ($k_1 = k_2 = k_3 = 0.40 \text{ M}^{-1}\cdot\text{min}^{-1}$). The remaining parameters were kept similar to those obtained for the chain extension from Eg_8 to Eg_{16} (Figure 51): $t_{\text{ind}} = 0.75 \text{ min}$, $k_4 = 0.65 \cdot 10^{-4} \text{ min}^{-1}$, $c_{\text{HS-triol}}^{t=0} = 33 \text{ mmol}\cdot\text{L}^{-1}$, $c_{\text{BB}}^{t=0} = 350 \text{ mmol}\cdot\text{L}^{-1}$.

2.3.2. Summary of reaction parameters, reaction rate coefficients and analysis

A similar analysis was then carried out for the remaining chain extensions up to Eg₄₈. A summary of the reaction conditions, simulation parameters and deduced reaction rate coefficients is shown in Table 16 and Table 17.

It is apparent that the trend of decreasing reaction rate constant for extension of successive arms persists and that, similar to the chain extension from Eg₈ to Eg₁₆, the rate coefficients k_1 , k_2 and k_3 decrease in ratio of roughly 3:2:1 for all chain extensions up to Eg₄₈. Further, it is evident that there is a collective decrease (-65 % to -75 %) for all reaction rate coefficients, including for the formation of dimer, between the first chain extension (Eg₈ to Eg₁₆) and the second (Eg₁₆ to Eg₂₄). Thereafter, the normalized reaction rate coefficients stay approximately constant with increasing chain length up to Eg₄₈ when accounting for different reaction temperatures. The lack of significant further decline in reaction rate from extension past Eg₁₆ can perhaps be rationalized as follows: the Eg₈ homostar triol reactant is still sufficiently small and the arms sufficiently short so that each arm is mainly solvated by the DMF solvent, and the chain extension follows the kinetics of a fully solvated small molecule. After extension to Eg₁₆, the arms are perhaps sufficiently long to create a local environment partially influenced by the polyether arms with slower reaction characteristics. Overall, the observation that reaction rate coefficients do not significantly decline beyond Eg₂₄ is critical because it tentatively suggests that further extension beyond Eg₅₆ is in principle not limited by reaction kinetics.

In an alternative hypothetical scenario, each extended arm could have caused partial shielding and sterical hindrance of the remaining reactive alkoxides and thus slowed reaction of the remaining arms beyond the statistical reduction of correctly oriented collisions expected in accordance with the Arrhenius equation. Even more prohibitive for a successful synthesis of longer PEG oligomers would have been a transition into an altogether different reaction regime limited significantly by mass transfer as observed in polymer kinetics. Such a change may still occur but has not been observed up to Eg₄₈. Given that such a transition does not occur here, and the reactions behave as expected in accordance with the Arrhenius equation, it suggests that individual arms act and react independently without strongly affecting each other.

The decline in reaction rate between extension to Eg₁₆ and extension to Eg₂₄ should also not be over-interpreted without repeats as the collective fit of the data for the first extension was only mediocre with a poor fit of the triol and the reaction temperature dropped temporarily between the 20th and 40th minute introducing additional error. The temporary temperature drop is reflected in a decrease of reaction rate around 20-40 min and was caused by a discontinuation of the magnetic stirring in the silicone oil bath responsible for maintaining the reaction temperature at 30 °C.

Table 16. Summary of reaction rate coefficients, i.e. MATLAB simulation parameters and reaction rate coefficients.

t_{ind}	$c_{\text{HS-triol}}^{t=0}$	$c_{\text{BB}}^{t=0}$	Concentration factor ^[a]	T	Reaction rate coefficients				Reaction rate coefficients, temperature normalized (30 °C) ^[b]				
					k_1	k_2	k_3	k_4	k_1	k_2	k_3	k_4	
min	mol·L ⁻¹	mol·L ⁻¹	no units	°C	M ⁻¹ ·min ⁻¹	M ⁻¹ ·min ⁻¹	M ⁻¹ ·min ⁻¹	min ⁻¹ ·10 ³	M ⁻¹ ·min ⁻¹	M ⁻¹ ·min ⁻¹	M ⁻¹ ·min ⁻¹	min ⁻¹ ·10 ³	
Eg ₈ → Eg ₁₆	0.8	0.033	0.35	1.00	30	0.70	0.40	0.20	0.065	0.70	0.40	0.20	0.065
Eg ₁₆ → Eg ₂₄	1.7	0.031	0.34	0.90	30	0.20	0.14	0.05	0.023	0.20	0.14	0.05	0.023
Eg ₂₄ → Eg ₃₂	9.0	0.029	0.33	0.81	40	0.25	0.19	0.10	0.055	0.13	0.10	0.05	0.028
Eg ₃₂ → Eg ₄₀	1.5	0.033	0.32	0.90	40	0.38	0.24	0.13	0.060	0.19	0.12	0.06	0.030
Eg ₄₀ → Eg ₄₈	1.1	0.030	0.31	0.79	50	0.67	0.45	0.25	0.120	0.17	0.11	0.06	0.030
Eg ₄₈ → Eg ₅₆	no reliable interpretation possible due to sparse and discontinuous sampling												

[a] Concentration factor is the ratio of the concentration product ($c_{\text{HS-triol}}^{t=0} \cdot c_{\text{BB}}^{t=0}$) for a particular chain extension relative to the concentration product for the extension from Eg₈ to Eg₁₆.

[b] The calculation for the normalized reaction coefficients makes the simplistic assumption that the reaction rate doubles every 10 °C around rt.

Table 17. Mass, volume, molality and weight ratio data for the chain extension reactions

	Homostar triol		Building block		Total reactants		Solvent		Total mixture		Molality triol	$m_{\text{reactants}} / m_{\text{solvent}}$	$m_{\text{reactants}} / m_{\text{total}}$
	mmol	g	mmol	g	g	mL	g	mL	g	mL	mmol·g ⁻¹	g·g ⁻¹	g·g ⁻¹
Eg ₈ → Eg ₁₆	2.04	2.500	20.4	16.9	19.4	17.2	38.9	41.0	58.2	58.2	0.052	0.50	0.33
Eg ₁₆ → Eg ₂₄	1.62	3.700	16.2	13.4	17.1	15.2	30.8	32.5	47.9	47.7	0.053	0.55	0.36
Eg ₂₄ → Eg ₃₂	0.71	2.382	7.1	5.9	8.3	7.3	13.5	14.2	21.7	21.5	0.053	0.61	0.38
Eg ₃₂ → Eg ₄₀	0.45	2.000	4.5	3.7	5.7	5.1	8.5	9.0	14.3	14.1	0.053	0.67	0.40
Eg ₄₀ → Eg ₄₈	0.36	1.982	3.6	3.0	5.0	4.4	6.8	7.2	11.8	11.6	0.053	0.73	0.42
Eg ₄₈ → Eg ₅₆	0.25	1.653	2.5	2.1	3.7	3.3	4.7	5.0	8.5	8.3	0.053	0.78	0.44

For the chain extension from Eg₄₈ to Eg₅₆, the reaction was run in a narrow two-armed tube resembling a test tube rather than a round-bottomed flask due to the small total reaction volume (8.3 mL). As a result of the narrow neck, effervescence resulting from addition of NaH could not sufficiently dissipate and resulted in a foam atop the reaction mixture for much of the reaction time. For a lack of clean access to the reaction mixture, it was decided not to regularly sample this reaction and only five samples were taken over the course of the reaction to obtain a qualitative impression of reaction completion. The collected data from five samples was in that case not sufficient for generating concentration profiles from which reaction rate constants could be deduced.

Most of the reactions exhibited an induction time of several minutes (0.8-1.7 min) except for the chain extension from Eg₂₄ to Eg₃₂ (9.0 min). The longer induction time for the extension to Eg₃₂ may have been the result of an inconsistency during NaH preparation leading to a less immediate accessibility and dispersion of the NaH base. Some induction time is always expected because sodium hydride is not soluble in organic solvents⁵⁸ and alkoxide formation can therefore only occur at the solid interface. As a result, the induction time should also be influenced by the particle size distribution of the NaH base used.

In general, rather than no reaction occurring before the induction time, it is usually the case that the homostar reactant triol concentration only follows the expected exponential trend after the simulated induction time while following an approximately linear decline beforehand. Instead of splitting the simulation of the concentration curves into a linear part prior to the in-built induction time (t_{ind}) and an exponential part thereafter, it was accepted that the concentration data would show a poorer fit with the simulated exponential curves for the first few minutes.

Lastly, analysis was complicated in two cases by the overlap of two Dmtr containing species in the HPLC chromatograms. During chain extension from Eg₁₆ to Eg₂₄, the HPLC peaks of the doubly extended homostar and the building block overlapped, and during extension from Eg₂₄ to Eg₃₂ the peak of the mono-extended homostar overlapped with the building block peak. In those cases, the concentrations of the two concerned species were combined in the concentration data and simulated jointly. Further, in those cases both the simulated fit of the joint concentration and the simulated profiles of the individual concentrations are shown. (When species overlap and are simulated, care needs to be taken to account for potentially different number of Dmtr ether groups per molecule of each species.)

The retention on the reverse phase column used for analysis is dominated by the Dmtr ether groups in each molecule. If all other group contributions in each species were negligible, one would expect the mono-extended homostar and the building block as well as the doubly extended homostar and the building block dimer to elute at similar times along the chromatogram. In fact, the contributions of the polyether fraction of each species are not negligible and cause lesser or stronger retention depending on the interaction with the RP-HPLC column and choice of mobile phase. As a result of the polyether chain

length continuously increasing, the homostar species shift along the chromatogram and inevitably overlap with the building block or building block dimer peak at one point or another, as these stay at the same elution time throughout. Overall, the additional large quantity of polyether usually distinguished the homostars from the building block and the building block dimer sufficiently. A full resolution of all species over the course of multiple chain extensions, however, can therefore only be achieved when relying on more than one HPLC method to avoid overlap.

2.3.3. Potential improvements of the kinetic study

Induction time and alkoxide formation

With regard to the speed of alkoxide formation, it is unclear whether complete alkoxide formation is in fact fast and occurs within several minutes of adding NaH. In earlier work, Lumpi et al.³⁴ monitored the conversion of TrtO–Eg₄–OH to the corresponding alkoxide with excess NaH (1.25 eq.) by means of an attenuated total reflectance (ATR-IR) in-line probe (Figure 53) to shorten reaction times of earlier protocols (Keegstra et al.³²) where the reactant alcohol was pre-mixed with NaH for a period of 24 h. Their results suggest that full conversion to the alkoxide may take between 90 min and 4 h which stands in contrast to the much shorter induction period observed in this work. An overview of the concentration profiles throughout this kinetic study suggests that alkoxide formation is significantly faster, as the reaction itself is often complete within 90 min, at lower concentrations of substrate. Lumpi et al. used THF as solvent and the substrate (TrtO–Eg₄–OH) was more hydrophobic and more concentrated (0.8 M), perhaps diminishing the already sparse solubility of NaH and impeding alkoxide formation. Perhaps, NaH is better soluble in the DMF-polyether solvent-substrate system.

Based on their ATR-IR data, Lumpi et al. concluded that the time for pre-mixing could be significantly reduced in comparison to previous protocols, but with pre-mixing still performed for several hours. However, it is questionable whether any premixing between alcohol and base to generate alkoxide should be performed at all, if a base is used which does not show substantial side reaction with the building block leaving group. Pre-formation of the alkoxide was avoided here to minimize the concentration of active alkoxide and prevent the formation of shorter homologues by depolymerization.

Nevertheless, it would have been useful to perform an experiment to assess the change or elimination of the induction period by running at least one experiment with similar concentrations, but with different order of reactant addition, whereby homostar triol and NaH are premixed in DMF and allowed to preform alkoxide for several hours. Building block dissolved in DMF can then be added last as a liquid medium and should mix rapidly under stirring, thereby leading to a shorter or no induction period in theory with all alkoxide having formed at the point of building block addition.

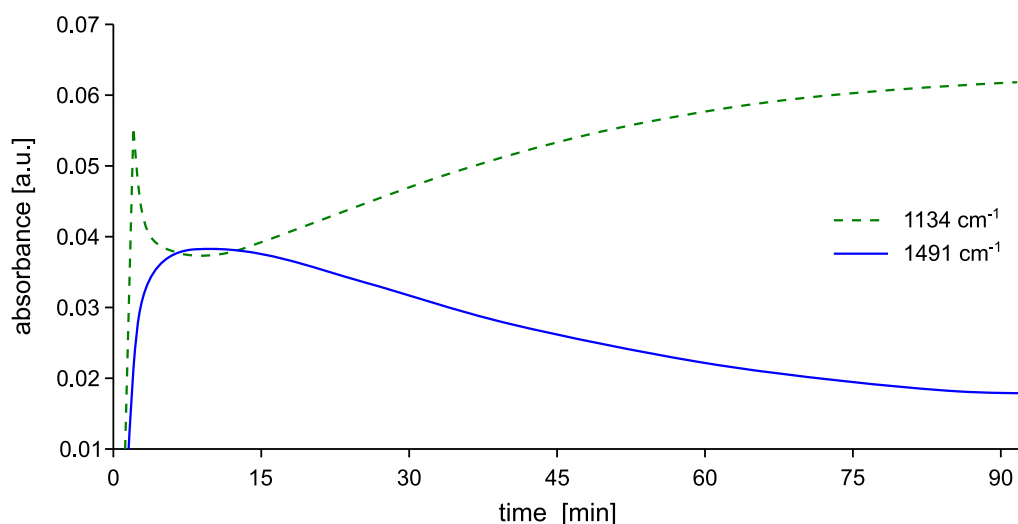


Figure 53. ATR-IR in-line monitoring for the deprotonation of TrtO-Eg₄-OH (0.8 M) with NaH (1 M, i.e. 500 mmol worth of solid in 500 ml as a suspension) in THF. Distortions for $t \leq 10$ min are attributed to equilibration effects (temperature and concentration) by Lumpi et al. Reproduced from ³⁴ with permission from Elsevier.

Change in solvent composition and molarity

This kinetic study was run with a small gradual drift in concentration with each chain extension. Because this kinetic study was carried out alongside a synthesis run and had to be run at practical concentrations to ensure completion of the reaction, molality was deliberately kept constant but as a result the solvent composition and molarity changed. This is because the reactants themselves represent a significant proportion of the reaction medium in these reactions. During the study, solvent quantities were calculated on a mole per mole basis (260 eq. of DMF; equivalent to approx. 20 mL of DMF per mmol of reactant homostar triol), i.e. molality was kept constant. As a result of the increase in the polyether fraction per mole of homostar with each chain extension step and the slightly different assumed density of polyether and DMF, the concentration of reactant with respect to solvent decreased.

Another implication of the increasing molecular weight of the homostars and the thus increasing ratio of polyether is the change of the solvent environment. Table 17 highlights that the mass fraction of polyether reactants (building block + homostar) with respect to the total reaction mixture mass increases from around 33 % to 44 %, due to the increasing molecular weight of the homostar. The resultant change in reaction medium itself may have an influence on the reaction kinetics. DMF is more polar than PEG itself, as exemplified by a comparison with solvents resembling PEG (Table 18). For example, triethylene glycol dimethyl ether, THF and 1,4-dioxane all possess lower relative permittivity and a lower dipole moment than DMF. As a result, there are reported differences²⁷ for chain extensions between DMF and THF and it can reasonably be expected that the increasing fraction of self-solvating polyether will negatively affect the kinetics at some point.

Table 18. Selected organic solvents together with their physical constants, arranged in order of decreasing E_T^N value, as empirical parameter of solvent polarity^{59,60}. Reproduced in part from ⁶¹ with permission from John Wiley & Sons.

Solvent	$T_{mp} / ^\circ\text{C}$	$T_{bp} / ^\circ\text{C}$	$\epsilon_r^{[a]}$	$\mu \cdot 10^{30} / \text{Cm}^{[b]}$	$E_T^N{}^{[c]}$
Water	0.0	100.0	78.36	6.2	1.000
N,N-Dimethylformamide (DMF)	-60.4	153.1	36.71	12.7	0.386
Triethylene glycol dimethyl ether ^[d]	-45	216	7.6	7.4	0.253
Tetrahydrofuran	-108.4	66.0	7.58	5.8	0.207
1,4-Dioxane	11.8	101.3	2.21	1.5	0.164
<i>n</i> -Hexane	-95.4	68.7	1.88	0.0	0.009

[a] Relative permittivity (“dielectric constant”) of the pure liquid at 25 °C, unless followed by another temperature in parentheses.

[b] Dipole moment in Coulombmetre (Cm), measured in benzene, tetrachloromethane, 1,4-dioxane, or *n*-hexane at 20-30 °C. 1 Debye = $3.336 \cdot 10^{-30}$ Cm.

[c] Normalized E_T^N values, derived from the transition energy at 25 °C of the long-wavelength visible absorption of a standard pyridinium *N*-phenolate betaine dye, $E_T(30)^{59,60}$.

[d] Chosen to resemble PEG.

Indirectly, the increasing polyether fraction will also eventually complicate mixing, particularly at lower temperatures. Using the melting points of commercial PEG samples as a guideline (Appendix A, Figure 124), the melting points of the homostars from Eg₂₄ onwards should be in the region above 50 °C. While the reaction mixture contains solvent as diluent, it also accumulates the by-product tosylate salts, and contains sodium hydride both dissolved and suspended, each of which should raise the viscosity and melting point. With increasing homostar chain length, the choice of concentration may therefore be constrained by other considerations, e.g. mass and heat transfer, rather than just kinetics when looking at scale-up.

Reaction rate and mechanism of dimer formation

Lastly, the rate of dimer formation was fitted with first order kinetics with respect to the building block concentration throughout, although the exact reaction mechanism was not investigated. The simulation of dimer formation, modelled as a first order reaction with respect to building block, showed good agreement with the experimental concentration data in all extensions apart from Eg₄₀ to Eg₄₈. If the building block degradation arose from slow intrusion of moisture through the flask neck during sampling, it is surprising that the reaction rate coefficient for dimer formation (k_4) stood in an approximately constant relationship ($k_1/k_4 \approx 4.5-10.5$) to the other rate coefficients in all chain extension cycles and also remained approximately constant beyond extension from Eg₁₆. This suggests that intrusion of water

throughout the reactions must have been very replicable or that a different mechanism was the cause of dimer formation.⁶²⁻⁶⁹

UV analysis and functional group contributions

While it is apparent in the UV spectra that the contribution of the benzyl ether hub is small compared to the Dmtr ether, this error could have been quantified. Similarly, the relative contribution of the tosylate group could have been quantified by measuring a deprotected sample under similar conditions.

Alternatively, screening over a larger UV wavelength around 260 nm, e.g. 240-310 nm, could have helped to identify wavelengths where the UV absorption of Dmtr ether compared to that of tosylate and benzyl ether is particularly large.

2.4. Conclusion

Overall, it can be concluded from this kinetic study that further chain extension beyond E_{g56} may reasonably be expected to work given that the inherent reaction rate stays approximately constant beyond extension to E_{g24} . The absence of further decline beyond E_{g24} also suggests that greater chain lengths can be attained, although other factors such as mixing and heat transfer may necessitate raising temperature or diluting the reaction medium eventually. Similarly high molar concentrations cannot be maintained indefinitely as a concentration limit will be reached at lower temperatures with an ever increasing weight fraction of poly(ethylene glycol) and the relative solvent volume will therefore have to decrease. It is therefore unavoidable that the solvent composition changes over time and contains increasing fractions of polyether if the mixture is to be maintained equally concentrated. The problem of reactant solubility could then be circumvented by raising the reaction temperature above the melting point of poly(ethylene glycol) around 60 °C but this may negatively affect selectivity. At temperatures around 60 °C, the reaction could conceivably be run neat, or with very little added solvent.

Base-catalyzed depolymerization and leaving group elimination as well as the formation of dimer remain concerns but have not been kinetically investigated here. If chain extension reactions were to become slower beyond E_{g56} , but with a similar level of dimer formation observed, the relatively more pronounced degradation of building block could severely affect process economics. It is therefore imperative that the exact mechanism of dimer formation from building block is understood so that preventative measures can be taken. If the side reaction relies on the presence of hydroxide, the route by which it enters the reaction, e.g. sealing, drying or quality of base used, will need to be improved. If dimer is formed from other routes, for example from interaction with solvent, this could necessitate a solvent switch.

While the kinetic study revealed that reactions at higher chain lengths can be carried through to completion, the necessary conversion in the order of 99.9 % or higher remains challenging and requires long reaction times in excess of one hour. These chain extensions can therefore likely only be run in batch, which is in principle not limiting when considering that downstream processing of these mixtures will likely also be non-continuous.

The choice of downstream separation for purification of these challenging mixtures is key and in the following chapter, a route via organic solvent nanofiltration (OSN), a membrane-based separation platform, is proposed as an alternative to the techniques used previously such as chromatography and extraction.

3. Chapter 3: Utilizing membrane separation in the synthesis of monodisperse PEGs

3.1. Introduction

As described for the synthesis of Eg₅₆ (Chapter 1), the key challenge for preparing longer uniform oligomers besides reactivity for increasing chain length (Chapter 2) is the separation of the growing oligomers. To validate the synthetic chemistry, chromatography was used for purification of the growing oligomer product in the synthesis of Eg₅₆. But because chromatography suffers from several drawbacks, the goal was to use a membrane-based separation technique compatible with organic solvents, organic solvent nanofiltration (OSN), to overcome this separation challenge in the synthesis of uniform PEG. The homostar strategy used in Chapter 1, where multiple chains are grown on a hub, was deliberately chosen to facilitate this separation by creating a fast-growing product homostar while using a small building block in each chain extension.

Another method often used in the synthesis of defined oligomers such as oligonucleotides and peptides is synthesis on a solid support. OSN should improve upon the comparatively high cost of chromatography and solid phase synthesis and at the same time avoid mass transfer and reactivity problems of solid phase synthesis by allowing operation in a homogeneous, liquid phase throughout. For a better understanding, a comparison between the two competing technologies is given below.

3.1.1. Comparison between solid phase synthesis and liquid phase synthesis.

Since the 1960s, following Robert B. Merrifield's development of synthesizing peptides on a solid matrix^{70,71} (Nobel Prize in Chemistry 1984)⁷², solid phase synthesis (SPS) has been the standard operation for synthesizing oligonucleotides, peptides and other sequence-defined molecules in an iterative fashion. In solid phase synthesis, the first monomer of the growing oligomer is immobilized on a solid matrix, initially polystyrene beads but many other types of matrix have since been developed, and purification between different reaction steps is carried out by simply washing a bed of the packed beads. The method had replaced complicated purification steps as well as increased the yield significantly into the region of 99.5 %. With automated solid phase synthesizers since developed, solid phase synthesis can be utilized to produce a large variety of sequence-defined oligomers up to length of around 70 monomers (beyond which coupling of multiple smaller oligomers becomes favourable) at kilogram scale.

However, solid phase synthesis also has several drawbacks. Current automated synthesizers are limited to about kilogram scale and there is no reasonable perspective for exponential scaling of the current

synthesizers, i.e. multiples of the same unit would scale linearly, and there is little scope to expand current synthesizers. One reason for the limitation is that packed beds only scale up to a point, beyond which channelling and other non-uniformities start to negatively impact on mass transfer e.g. during purification and reaction. In other words, freshly introduced monomers as well as washing solvent during purification cease to reach all regions of the bed equally well which starts to impose limits on scalability as expanding bed size risks introducing dead regions that result in impurities. Solid phase synthesis also has an intrinsic limit of mass intensity as oligomers can only be grown on the functionalized surface of the beads, while the internal volume of the beads and the voidage of the packed bed is dead space where no oligomer can be grown.

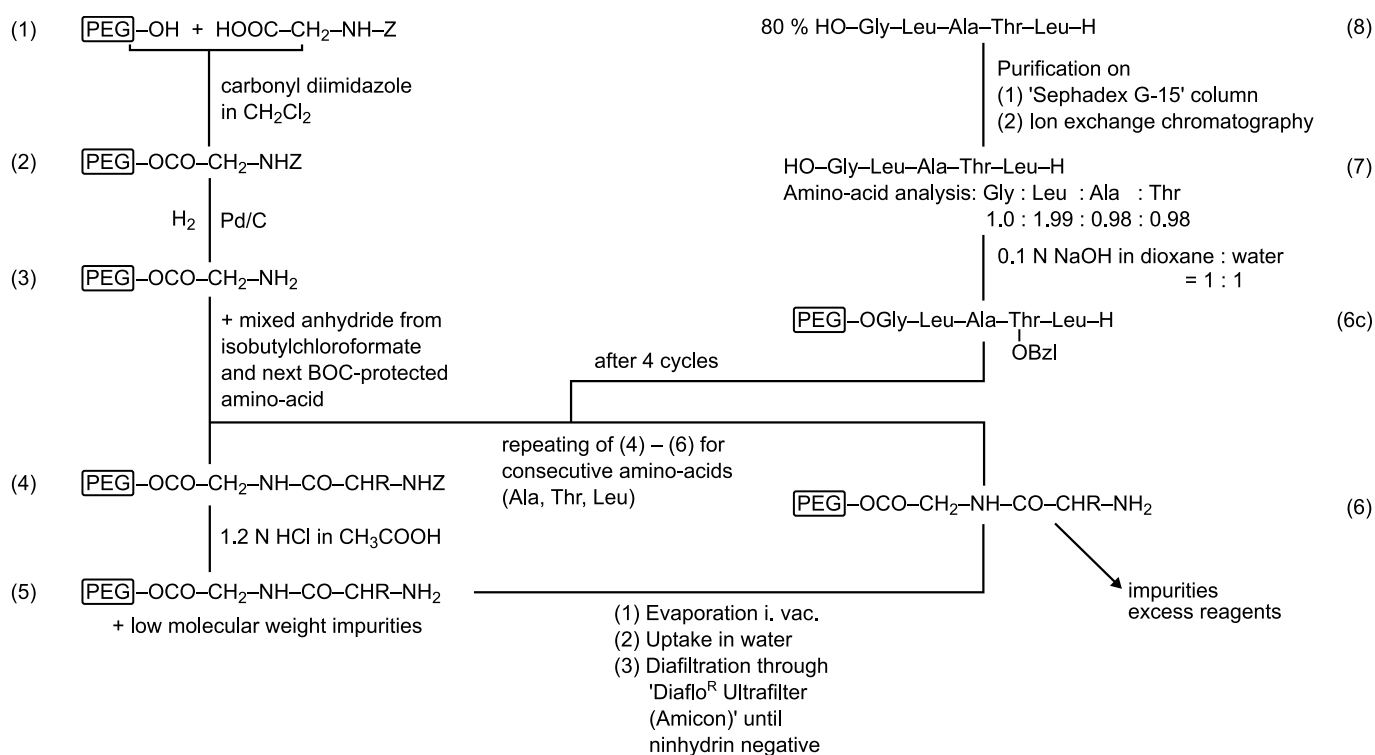
With the potential onset of RNA oligomer drugs, and for scalability of oligomer synthesis in general, it would therefore be desirable to grow oligomers in a similar fashion but in a homogeneous liquid medium provided purification is feasible. Besides scalability, there are other advantages to liquid phase synthesis:

- **Analysability/Traceability:** In a homogeneous liquid medium, reaction progress could be accurately monitored. It is not easily possible to monitor reaction progress and success in solid phase synthesis as analysis requires taking out a sample of bead and cleaving off it the oligomer that has hitherto been grown. There is a risk that due to heterogeneity in the bed, the analyzed sample is not representative of the entire bed. In a homogeneous liquid medium, both reaction progress and purification progress can be monitored in situ.
- **Reaction kinetics and reagent excess:** One limitation of solid phase synthesis is that reaction kinetics are limited by mass transfer to the solid phase surface and that large amounts of reagent excess must be used to ensure full completion of all reactions. In a homogeneous liquid phase, reactions are not mass transfer limited, and smaller excesses of reagent may be feasible, i.e. reaction times should be faster for similarly large excess.
- **Material transfer:** An important industrial consideration is material transfer within a plant and liquid solutions are significantly easier to transfer than solids.

Liquid phase synthesis potentially possesses significant advantages over solid phase synthesis but the high degree of purification needed for oligomer synthesis and which SPS provides is hard to match. In fact, it is only because of the much-simplified purification procedure that solid phase synthesis is so attractive in oligomer synthesis and if a way could be found to affect similar purification in a homogeneous liquid medium, this would mark significant progress.

3.1.2. Utilizing nanofiltration in the synthesis of uniform, sequence-defined oligomers

The idea of utilizing membrane separation for oligomer synthesis in a homogeneous medium as a substitute for solid phase synthesis originated in the early 1970s with a patent⁷³ and publication⁷⁴ by Bayer, Mutter and co-workers on synthesizing peptides. This early implementation was fraught with complications largely related to the instability of membranes in organic solvents at the time. With membranes only operable in water, the process needed to accommodate several additional steps for evaporation of the reaction solvent, uptake in water for diafiltration, and followed presumably by another switch back to the reaction solvent (Figure 54). Bayer & Mutter used a 10,000 Da poly(ethylene glycol) support to increase the size difference between their product and the reagent monomer. They used a linear monovalent version of the support.



Abbreviations: Z = BOC = t-Butyloxycarbonyl. PEG-OH = Polyethylene glycol, molecular weight = 10,000. Bzl = Benzyl.

Figure 54. Flow chart for the synthesis of the amino acid sequence HO-Gly-Leu-Ala-Thr-Leu. The separation after coupling and deprotection between step (5) and (6) is accomplished by ultrafiltration after uptake in water. Reproduced from ⁷⁴ with permission from Springer Nature.

Despite the lack of solvent stable membranes rendering infeasible a direct filtration of the reaction mixture at the time, Bayer & Mutter identified substantial advantages of the liquid phase method over solid phase synthesis⁷⁴:

- I. The synthesis is achieved in homogeneous solution.
- II. Better yields can be obtained due to better mass transfer compared to a heterogeneous phase.

- III. A wider range of protecting groups and coupling methods can be used.
- IV. In the context of membrane separation, a soluble anchor can be designed in line with the requirements for rejection and solubility.
- V. There is an opportunity to isolate the desired product from impurities derived from a failed coupling.
- VI. The completeness of coupling can be monitored by taking samples from the homogeneous solution.
- VII. Scaling-up of a reaction is easier when working in solution as opposed to solid beds.
- VIII. Automation and transportation are easier for liquids than solid.

Particularly, the opportunity to monitor the homogeneous solution (point VI) is crucial when synthesizing longer oligomers. In a solid phase synthesis, the reaction cannot be monitored in situ because the substrate is bound to a solid bed and the bed itself may not be homogeneous. Sampling requires removing beads from the bed and cleaving the sample off the solid support for analysis. A failed coupling step is therefore usually only detected at the end of a synthesis run when it is too late to correct. For a synthesis of a longer oligomer, this introduces the risk of continuing past a failed coupling sequence, and losing further material in subsequent couplings, before having to discard the entire batch at the end of the run.

A streamlined synthesis of a 5-membered peptide, also on a linear PEG anchor but with filtration in organic solvent, was demonstrated with a stable ceramic membrane by So et al. in 2010^{75,76} (Figure 55). The switch to a membrane stable in organic media, not available to Bayer & Mutter at the time, allowed the membrane filtration to be performed in the same solvent required for the reaction, thus simplifying the overall process. Other processes at the time often relied upon precipitation, e.g. in ether, to achieve separation. The synthesis on polymer supports has been reviewed.⁷⁷

Livingston et al. considered relatively early on how the synthesis of uniform oligomers could be performed in conjunction with membrane separation. A key innovation for the separation of reaction mixtures during uniform polymers synthesis, the homostar approach, was patented in 2011 by Livingston et al.⁷⁸ with the proposition to link several oligomers to a single branch point molecule. As previously discussed, the approach is useful because it increases the size difference between the product and reactants and makes separation via OSN more viable. Beside the work contained herein, the concept has since been demonstrated in the synthesis of 2'-Methyl-RNA phosphorothioate 9-mer⁷⁹ (Figure 56) and for uniform PEGs with sidechains⁸⁰, both on a trivalent support.

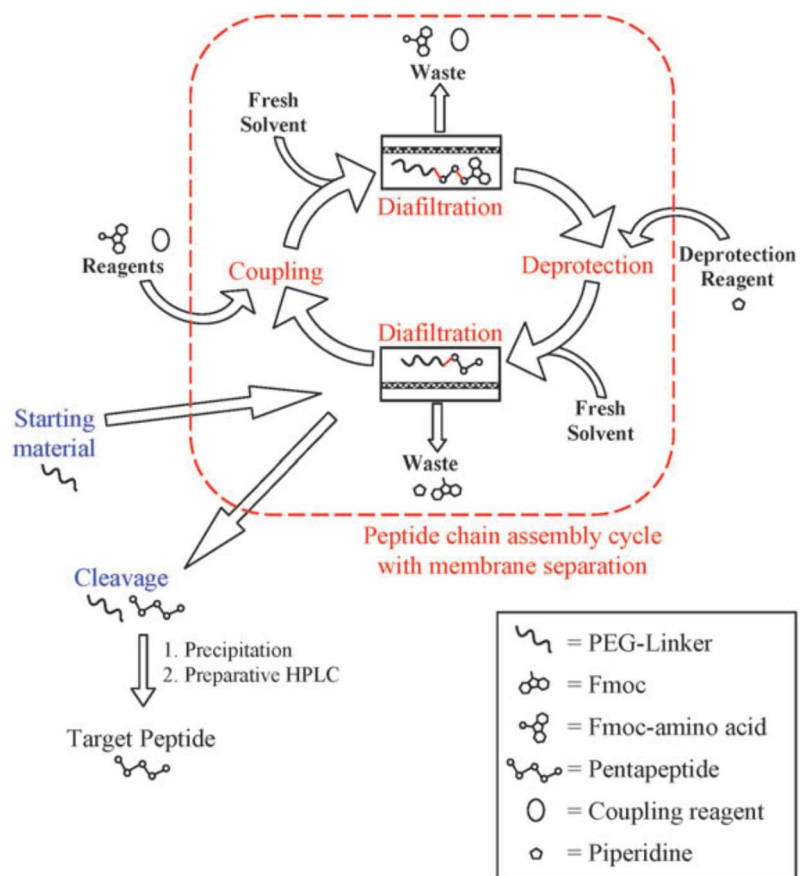


Figure 55. Schematic of membrane enhanced peptide synthesis for peptide chain assembly using nanofiltration. Reproduced from ⁷⁵ with permission from The Royal Society of Chemistry

The intention to substantially simplify the purification of reaction mixtures by nanofiltration is reflected in the synthesis of Eg₅₆ via the homostar approach (Chapter 1) which bound three growing oligomer chains onto a trivalent hub to increase the size differential. However, when attempting to separate some of the chain extension mixtures described in Chapter 1 in early nanofiltration trials, separation was found to be more difficult than expected when considering the size differential, a crude predictor of nanofiltration separation performance. The insufficient membrane selectivity during trials, combined with the need for almost complete impurity removal required for maintaining uniformity of the growing oligomer, led to low yields and long processing times during nanofiltration. The binding together of three growing oligomers into a homostar alone did not sufficiently raise selectivity in combination with the building block used.

Chapter 3 describes how these challenges were overcome for the synthesis of Eg₆₀, an oligomer similar in size to the Eg₅₆ oligomer prepared previously, using only nanofiltration for purification between chain extensions. In order to optimize nanofiltration selectivity, a two-pronged approach was used: the molecular architecture of hub and building block were fine-tuned and a two-stage membrane process was established.

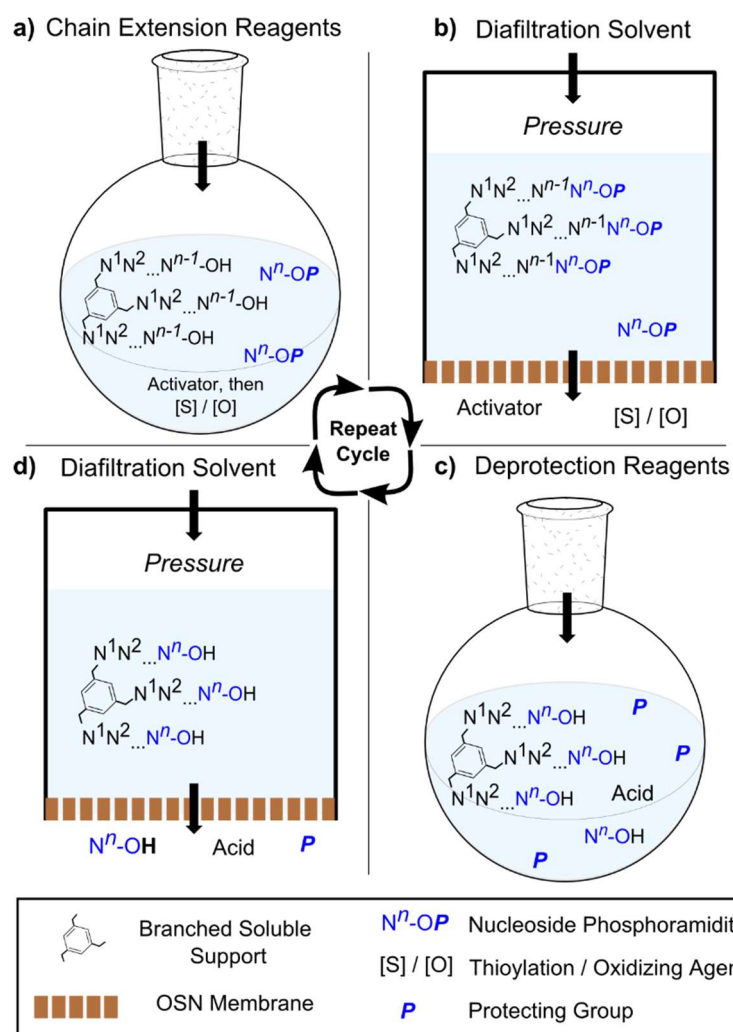


Figure 56. Liquid phase oligonucleotide synthesis coupled with OSN: a) Chain extension reaction; b) diafiltration by OSN to remove excess reagents; c) 5'-O deprotection; d) diafiltration by OSN to remove deprotection debris, then repeat cycle to the desired length. Reproduced from ⁷⁹ with permission from John Wiley & Sons.

3.1.3. The membrane filtration spectrum and transport phenomena

In the widest sense, a membrane is a filter characterized by an ability to allow one component of a mixture to pass through relatively unhindered while simultaneously preventing passage of another component.⁸¹ (In membrane terminology, the fluid passing through a membrane is typically referred to as permeate while the fraction not permeating the membrane is referred to as retentate. A solute which is preferentially retained by the membrane and is being enriched in the retentate is also referred to as being rejected.) In contrast to conventional filters, membranes allow separation on a molecular level and thus provide an alternative to standard unit operations such as distillation.⁸¹ In the context of separating on a molecular level, membranes are also described as semi-permeable barriers or as having the ability to control the rate of permeation of different chemical species.⁸²

The membranes used in chemical engineering applications are typically synthetic and often made from polymeric materials. One example of a large-scale industrial application of membranes is the desalination of brackish or sea water to produce potable water. In this application, the membranes reject in the range of 95 – 99.7 % of the dissolved ions, plus any larger species, to produce water ready for drinking. This application area of membranes is often referred to as reverse osmosis because an applied pressure pushes water through the membrane against the osmotic pressure gradient, e.g. from a concentrated saline solution to a lower concentrated water solution. These membranes therefore separate salts with diameters in the range of several Ångström and the driving force for the separation is provided in the form of applied pressure. The reverse osmosis industry is well established and total worldwide membrane module sales in 2010 were about US\$500m.⁸²

Nanofiltration occupies the separation spectrum just above reverse osmosis and usually concerns separations of molecules in the region of 100 – 2000 Da, i.e. molecules with a diameter of approximately 0.1 to 3 nm. One characteristic that reverse osmosis membranes and most nanofiltration membranes share is that they consist of non-porous, dense separation layers. In non-porous membranes, solutes are distinguished based on differences in sorption and diffusivity in the dense membrane layer rather than through pore-flow and size exclusion. Transport in these non-porous dense films can be described by the solution-diffusion model and Fick's law.

On the other side of the nanofiltration regime are ultrafiltration and microfiltration membranes which are typically microporous and usually possess connected pores passing from one side of the membrane to the other. These porous membranes are best described by a pore-flow model and Darcy's law. A summary of the different filtration ranges and the corresponding solute radii is given in Figure 57.

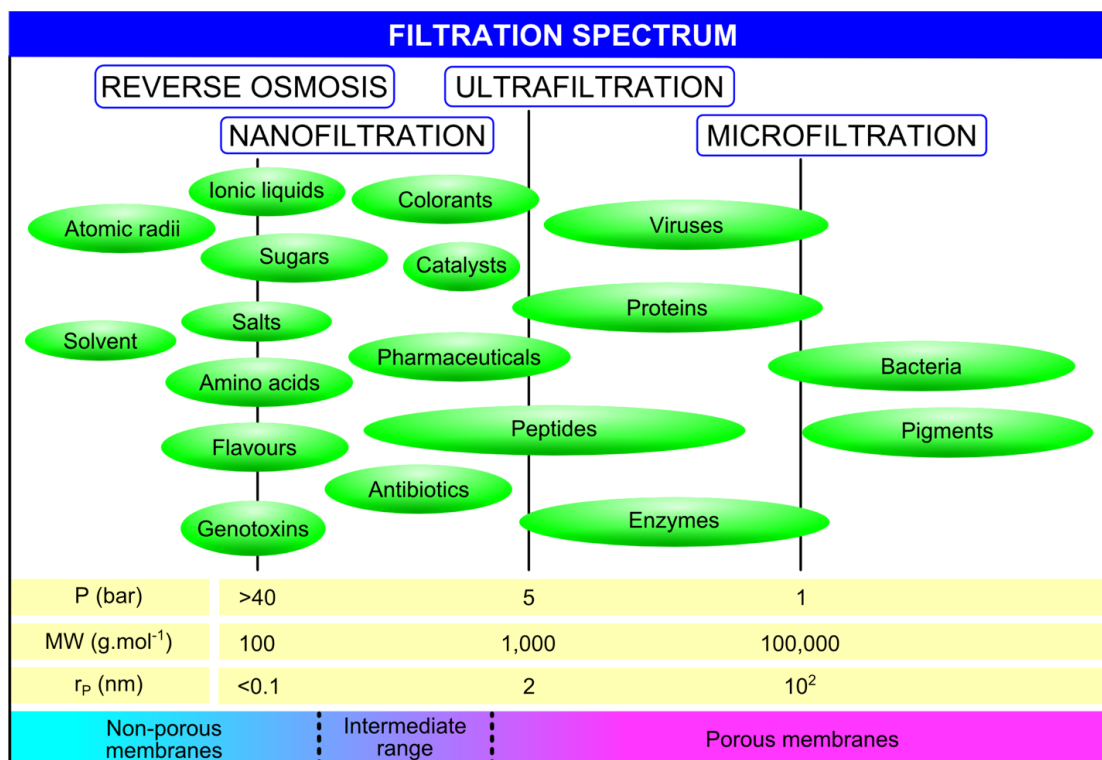


Figure 57. Classification of membrane processes according to operating pressure, retained solute/pore size (nm), molecular weight cut-off (g mol⁻¹), transport mechanism, and examples of applications. Reproduced from ⁸³ under a Creative Commons Attribution (CC-BY) License.

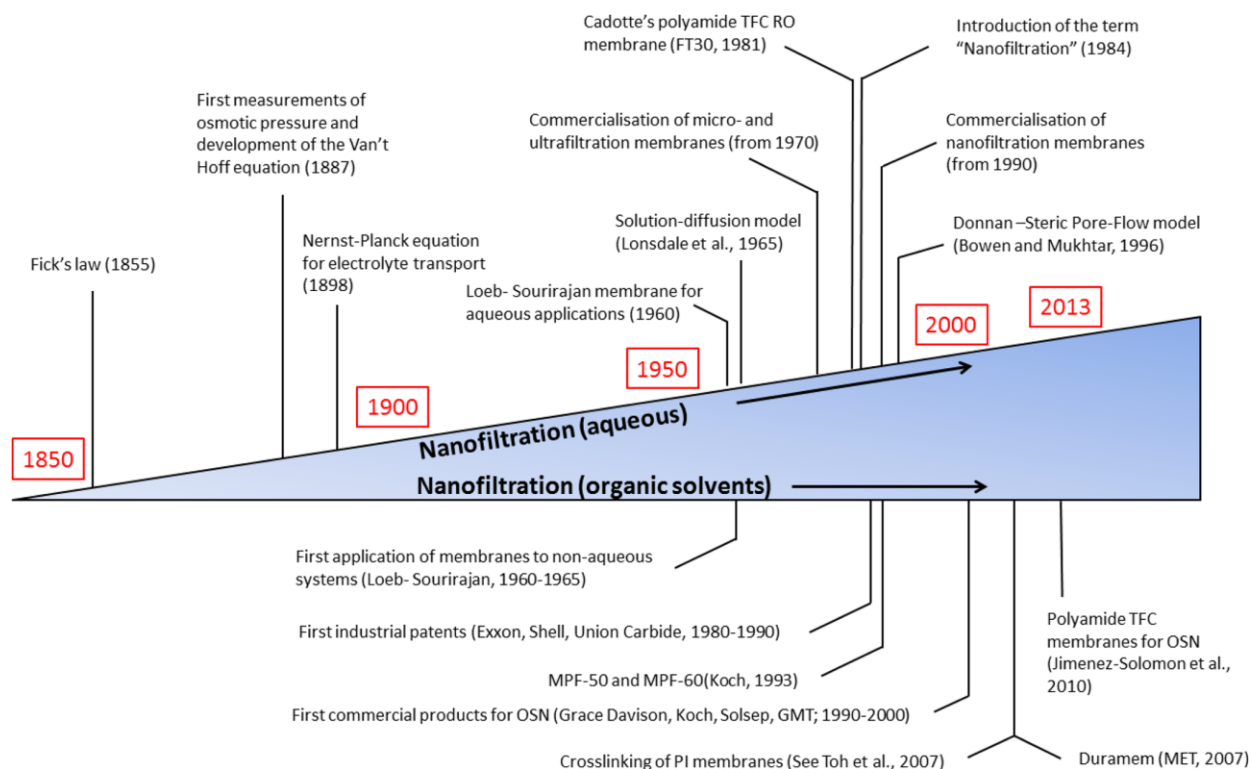


Figure 58. Summary of the most significant events, which have contributed to the development of nanofiltration over time. Reproduced from ⁸³ under a Creative Commons Attribution (CC-BY) License.

Organic solvent nanofiltration

The field of membrane separation concerned with nanofiltration in organic solvents is commonly referred to as organic solvent nanofiltration (OSN), or sometimes as organophilic nanofiltration or solvent resistant nanofiltration (SRNF). Several reviews are available^{83–85} and a brief history of the development of OSN in context with aqueous nanofiltration is shown in Figure 58. The membranes required for the separation of chain reaction mixtures for the synthesis of uniform PEG all need to distinguish between molecules in the range of around 500 – 5,000 Da in strong organic solvents. Compared to reverse osmosis and nanofiltration in aqueous systems, the field of OSN is relatively young and poses different challenges. Membrane process design in aqueous systems is often concerned with bio-fouling, scaling and similar phenomena degrading permeability of the membrane over time, but most membranes materials are generally stable in water. On the other hand, OSN membranes are typically exposed to cleaner feeds but must be stable in strong organic solvents.

The solution-diffusion model

The driving force for a membrane separation is a chemical potential gradient which encompasses the constituent forces such as pressure and concentration gradients. The two common models for membrane transport differ in how they derive the solvent and solute transport across the membrane from the chemical potential gradient. The solution-diffusion model assumes a permeant activity gradient and no pressure drop through the membrane while the pore-flow model takes as a basis a pressure gradient and assumes constant permeant activity (Figure 59). The solution-diffusion model goes back to Lonsdale et al. in 1965⁸⁶ and several reviews of membrane transport models are available.^{87–89}

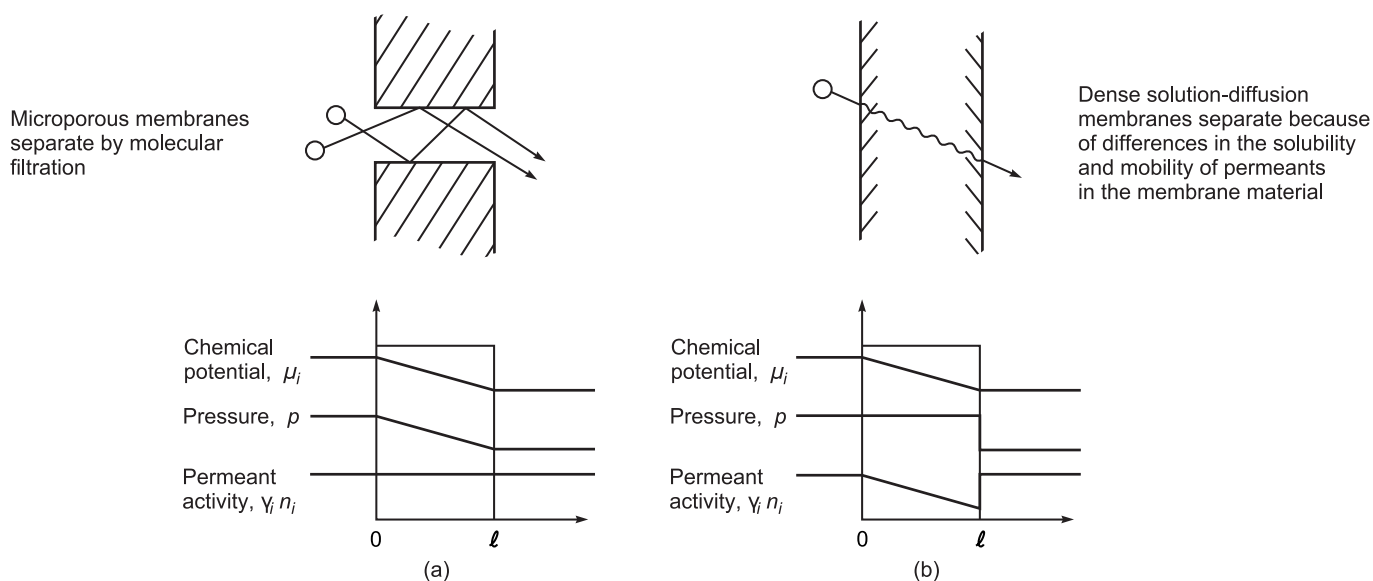


Figure 59. A comparison of the driving force gradients (chemical potential, pressure, solvent activity) of pressure-driven filtration for a one-component solution permeating through a (a) pore-flow and (b) solution-diffusion membrane. Reproduced from ⁸² with permission from John Wiley & Sons.

A simplified solution of the solution-diffusion for a binary mixture eventually leads to expressions for the flux of both components (Equation 12-13), where J_i is the flux of component i , D_i and K_i^L are diffusivity and liquid phase sorption coefficients respectively, ℓ is the thickness of the membrane c_{i_0} and c_{i_ℓ} are concentrations of component i on the feed side and permeate side membrane surface respectively, v_i is the molar volume, p_0 and p_ℓ are the pressure on the feed and permeate side of the membrane and R and T are the gas constant and temperature in Kelvin respectively.⁸²

$$J_i = \frac{D_i K_i^L}{\ell} \left(c_{i_0} - c_{i_\ell} \cdot \exp \left[\frac{-v_i (p_0 - p_\ell)}{RT} \right] \right)$$

$$J_j = \frac{D_j K_j^L}{\ell} \left(c_{j_0} - c_{j_\ell} \cdot \exp \left[\frac{-v_j (p_0 - p_\ell)}{RT} \right] \right)$$

Equation 12-13

It is apparent that the total throughput, or combined flux of both components, which determines the overall performance of the membrane, is inversely proportional to its thickness, a common finding in film theory.⁸² The other important membrane characteristic, membrane selectivity, the ability of the membrane to separate two components of a binary mixture, can be defined as the ratio of the diffusivity and liquid phase sorption coefficients (Equation 14). The sorption coefficient, K_i^L , is a term “linking the concentration of a component in the fluid phase with its concentration in the membrane polymer phase”⁸² while the diffusivity is a kinetic term “reflecting the effect of the surrounding environment on the molecular motion of the permeating components”⁸².

$$\alpha_{ij} = \frac{\frac{D_i K_i^L}{\ell}}{\frac{D_j K_j^L}{\ell}} = \left(\frac{D_i}{D_j} \right) \left(\frac{K_i^L}{K_j^L} \right)$$

Equation 14

It further follows that the quality of the separation is dependent on the applied pressure, the temperature as well as the concentration gradient across the membrane and the resultant osmotic pressure gradient. *(Because a simplified characterization of membranes is used in the following chapter, this brief discussion is included only for completion. For a detailed discussion of transport theory through membranes and the underlying assumptions, the reader is referred to the subject literature.^{82,86–89})*

Membrane parameters and characterization

In practice, it requires effort to rigorously characterize separations according to the solution-diffusion model because the required parameters, particularly diffusivity in polymers, are difficult to obtain. Instead, a simplified model is used, quantifying membrane parameters at particular process conditions, with the caveat that these parameters cannot then be universally applied to other process conditions without adjustment.

The two key parameters by which membranes are characterized here are the permeance of the membrane, which determines its throughput, and the extent to which the membrane prevents a solute from passage, described as a rejection term.

Permeance (B) [$\text{L}\cdot\text{m}^{-2}\cdot\text{h}^{-1}\cdot\text{bar}^{-1}$] relates the total volumetric flux through the membrane (J_V) [$\text{L}\cdot\text{m}^{-2}\cdot\text{h}^{-1}$], to the transmembrane pressure (ΔP) [bar] applied across the membrane, with an osmotic pressure ($\Delta\Pi$) [bar] acting in the opposite direction to the applied pressure.

$$J_V = B (\Delta P - \Delta\Pi)$$

Equation 15

For dilute solutions of a solute, the total volumetric flux is typically determined by the solvent and for the dilute, non-ionic solutes used herein the osmotic pressure can be considered negligible. Permeance is then a membrane parameter that is normalized for membrane area and pressure and in the pressure range of nanofiltration (approx. 20-50 bar) the relationship is typically linear. Permeance is experimentally determined by measuring the volumetric flowrate (\dot{V}) [$\text{L}\cdot\text{h}^{-1}$] and dividing by the membrane area (A) [m^2] and transmembrane pressure (ΔP) [bar] (Equation 16).

$$B = \frac{\dot{V}}{A \cdot \Delta P}$$

Equation 16

Membrane selectivity is described by a rejection term relating the concentration of solute on the feed and permeate side of the membrane according to Equation 17 where c_{i_0} and c_{i_p} are the concentrations of solute i on the feed and permeate side of the membrane respectively. Rejection (\mathbb{R}_i) is calculated with as a dimensionless quantity between 0 and 1 in formulae but typically plotted in units of percent ($\mathbb{R}_i \cdot 100\%$).

$$\mathbb{R}_i = \left(1 - \frac{c_{i_p}}{c_{i_0}} \right)$$

Equation 17

The rejection parameter requires further explanation because the concentration on the feed side of the membrane surface is not homogeneous due to the presence of a phenomenon termed concentration polarization.

Concentration polarization

Concentration polarization is a result of the different permeation rates of the components in a mixture. The solute in a binary mixture which permeates more slowly, or which is preferentially retained by the membrane will be enriched at the membrane surface on the feed side during normal operation. This leads to concentration of the solute on the feed side of the membrane and causes a concentration gradient between the membrane surface and the bulk solution. At the same time, the no-slip boundary condition at the membrane surface causes the formation of a boundary layer within which the flow is non-convective. As a result, the enriched solute on the membrane surface is not transported back into the bulk of the feed by convective transport through the boundary layer and the feed side is not well-mixed. Instead, the enriched solute must be transported back from the membrane surface into the bulk by back-diffusion.

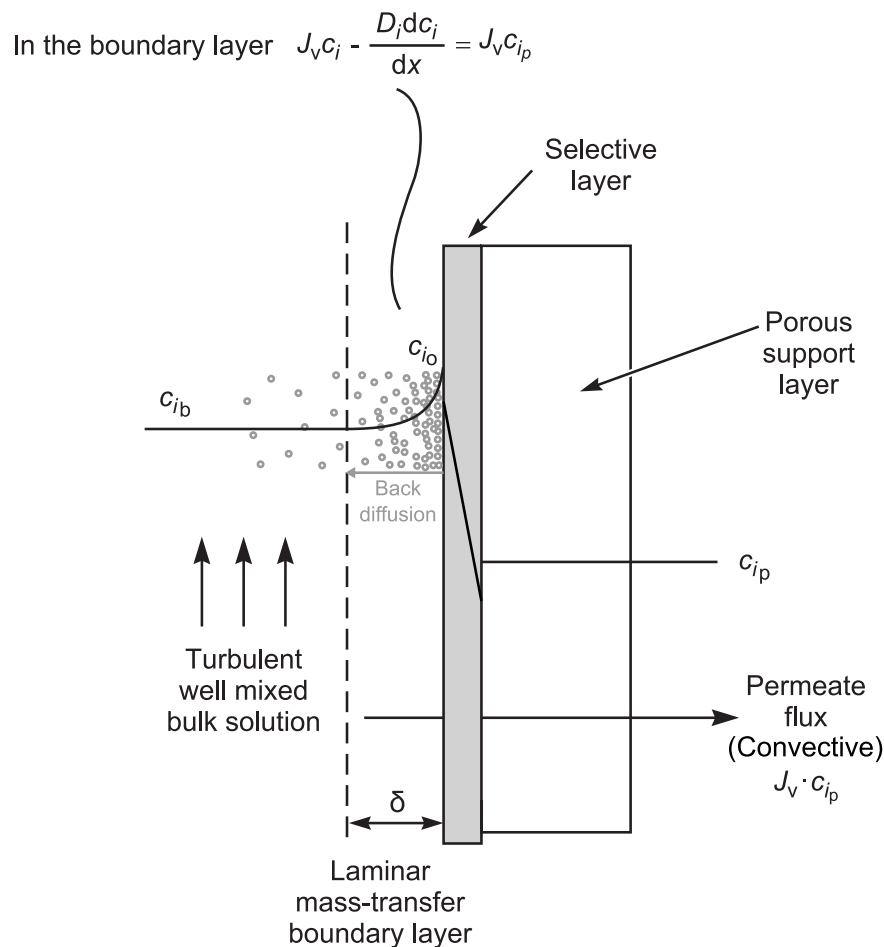


Figure 60. Concentration polarization gradient of a preferentially retained solute adjacent to a membrane. Adapted from ⁸² with permission from John Wiley & Sons and with creative input from ⁹⁰.

The net solute flux in the boundary layer is equal to the convective flux through the membrane minus the diffusive component flux acting in the opposite direction (Figure 60) and is described by Equation 18 where D_i [$\text{m}^2 \cdot \text{s}^{-1}$] is the diffusivity of the solute in the bulk medium, J_V [$\text{m} \cdot \text{s}^{-1}$ to maintain dimensional consistency] and c_i is the concentration of solute as a function of the location (x) within the boundary layer. (c_{i_p} and c_{i_p} are assumed equal as there is negligible transport resistance on the permeate side.)

$$J_V c_i - D_i \frac{dc_i}{dx} = J_V c_{i_p}$$

Equation 18.

Integration over the thickness of the boundary layer (δ) [m] with the appropriate boundary conditions yields equation Equation 19 where c_{i_b} , c_{i_0} and c_{i_p} are the concentrations of solute in the bulk, at the membrane surface and on the permeate side of the membrane respectively.⁸²

$$\frac{c_{i_0} - c_{i_p}}{c_{i_b} - c_{i_p}} = \exp\left(\frac{J_V \cdot \delta}{D_i}\right)$$

Equation 19

The solution of this equation requires knowledge of the mass transfer coefficient of the system, $k_{a,i}$ [$\text{m} \cdot \text{s}^{-1}$] given in equation Equation 20.⁹⁰

$$k_{a,i} = \frac{D_i}{\delta}$$

Equation 20

It follows that concentration polarization is more pronounced for systems with higher volumetric flux, lower temperature, higher viscosity, lower feed velocity and lower feed Reynolds number, or more generally larger boundary layer thickness as well as lower diffusivity of solute and higher rejection of the solute. Further, it is now more precisely understood that Equation 17 describes intrinsic membrane rejection, relating the concentration of a solute on the membrane *surface* to the concentration on the permeate side.

In order to reduce the effect of concentration polarization in practical applications, a sufficiently large cross-flow (Figure 61) is usually applied to the membrane surface to create turbulence and enhance performance by reducing the boundary layer thickness.

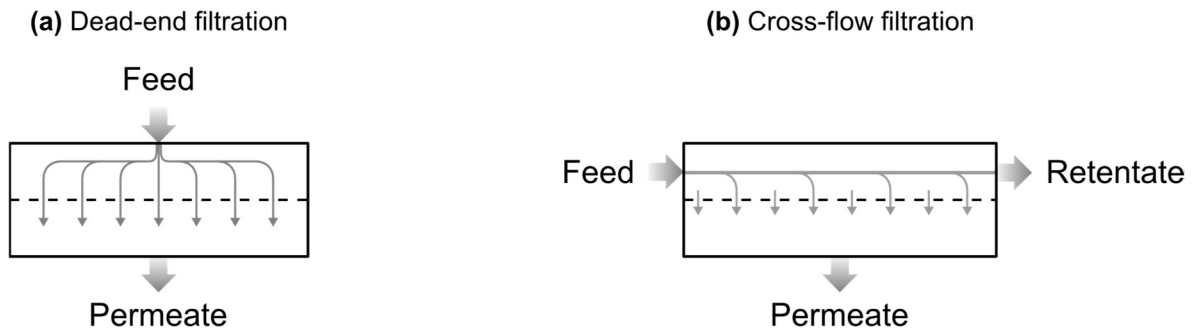


Figure 61. Schematic representation of membrane filtration system design: (a) dead-end, (b) cross-flow mode, to enhance turbulence and decrease concentration polarization.

In practice, the mass transfer coefficient of a system is not easy to obtain. Instead, a rejection term (\mathbb{R}_i) is used here whereby permeate concentrations (c_{i_p}) are directly related with the bulk concentrations on the feed side (c_{i_b}), not with the concentration on the membrane surface on the feed side (c_{i_0}).

Concentration polarization and the difference of concentration between the bulk and the membrane surface on the feed/retentate side are therefore neglected (Equation 21) which is justified by the use of dilute feed and a high cross-flow velocity. By making this simplifying assumption, we no longer quantify an intrinsic membrane rejection but obtain a rejection value that is influenced by mass transfer limitations and is therefore no longer independent of surrounding process parameters. For the rejection values obtained from screening to resemble the performance expected during purification, the process parameters should thus be kept comparable.

$$\mathbb{R}_i \approx \left(1 - \frac{c_{i_p}}{c_{i_b}} \right)$$

Equation 21

Because this work is performed in dilute systems with organic solvents possessing low viscosity and using flat-sheet membranes and deliberately high cross-flow speeds, concentration polarization should generally be low, and membrane rejections obtained during membrane screening should yield a good approximation of the expected intrinsic rejections. For sufficiently high cross-flow speeds where the recirculation flowrate far exceeds the permeate flowrate, the bulk feed and bulk retentate may also be considered well-mixed.

3.1.4. Membrane processes

There are three common batch processes for separation by membranes in the liquid phase (Figure 62):

- a) **Concentration:** A solute or mixture of solutes is concentrated by selectively removing a portion of the solvent through a membrane, leaving a more concentrated solution behind. A suitable membrane for a concentration should possess sufficiently high rejection to all solutes while ideally allowing only solvent to permeate.
- b) **Solvent exchange:** A solvent exchange using membranes works similarly to a concentration in that the membrane should possess rejection to all solutes but allow only solvent to permeate. Because the purpose is to switch solvent rather than reducing the total solution volume, the system is continuously replenished with the desired new solvent at a rate equal to the permeate flowrate exiting the system through the membrane. This membrane operation is particularly useful in cases where a higher boiling solvent needs to be replaced with a lower boiling solvent, a switch which would not typically be possible via distillation in a single step.
- c) **Purification / Diafiltration:** For a two-solute separation, a membrane needs to preferentially retain one solute while permeating another solute as well as solvent. Solvent acts as a carrier to continuously flush the more permeable component through the membrane, while the system is replenished with fresh solvent at a rate equal to the permeate flowrate. This operation is often referred to as diafiltration, or constant volume diafiltration, in the subject literature because the system volume on the feed/retentate side of the membrane is kept constant by replenishment with fresh solvent. Separation is feasible with the product being either the more permeable or the less permeable component, but in the common scenario, the product is preferentially retained, while the impurity is permeated.

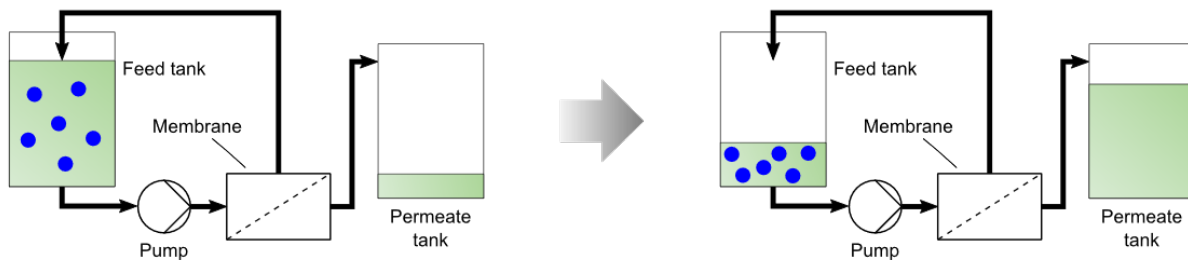
These membrane operations can be combined into multi-stage cascades^{91–98} as well as continuous operations^{95,99–102} and may be further combined with other separation techniques, e.g. distillation, crystallization and extraction, in hybrid processes.^{103–106}

The separation problem of concern (discussed in Chapter 1) where the building block, side products and reaction debris need to be separated from a growing product homostar, is well-suited to purification by diafiltration where the product is retained by the membrane, and all other species permeated (Figure 62c). While such a separation may also be carried out continuously, it would be less efficient and would not suffice for the high purity requirements required. It is also unnecessary to consider a continuous purification in this case because the high conversion requirements necessitate reactions to be carried out batch-wise. The focus is therefore on diafiltration as a batch operation.

(a) Concentration

Defining feature: at least **one solute** and **one solvent**

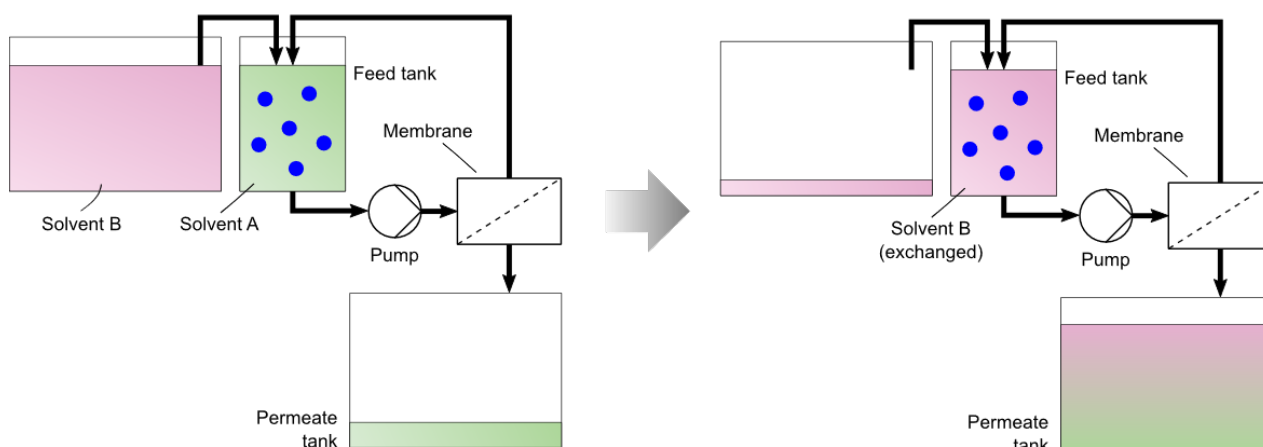
● High rejection



(b) Solvent exchange

Defining feature: at least **one solute** and **two solvents**

● High rejection



(c) Purification / Diafiltration

Defining feature: at least **two solutes** and **one solvent**

● High rejection

● Low rejection

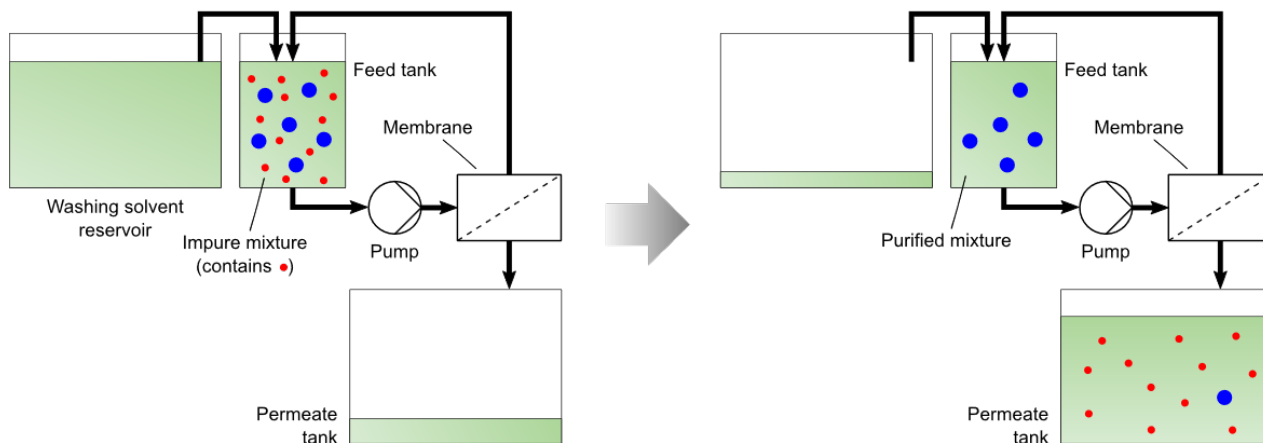


Figure 62. Membrane batch filtration processes in the liquid phase: (a) concentration, (b) solvent exchange, and (c) purification, or diafiltration. Solvent feed and permeate tanks in (b) and (c) are only approx. to scale as the solvent requirement is usually several times larger than the feed tank volume. Adapted from ¹⁰⁷ (in turn adapted from ⁸³) under a Creative Commons Attribution (CC-BY) License.

Mathematical description of diafiltration

While membranes are usually characterized in terms of their rejection (\mathbb{R}_i) (Equation 21), or the fraction of solute that is retained by the membrane, for diafiltration it is often more convenient to characterize membranes by the fraction of solute which passes ($1-\mathbb{R}_i$). This is because the effectiveness of a typical diafiltration is given by how many molecules of impurity permeate through the membrane for every molecule of product that also permeates through the membrane at the same time and is thereby lost. The equivalent term describing $1-\mathbb{R}_i$ in ultrafiltration is the sieving coefficient.⁸²

The separation effectiveness of a diafiltration may then be described by a separation factor (γ_{ip}) describing the ratio of the permeating components, impurity i and product p according to Equation 22 where \mathbb{R}_i and \mathbb{R}_p are the rejection of impurity and product respectively.

$$\gamma_{ip} = \left(\frac{1 - \mathbb{R}_i}{1 - \mathbb{R}_p} \right) = \frac{\left(\frac{c_{ip}}{c_{ib}} \right)}{\left(\frac{c_{pp}}{c_{pb}} \right)}$$

Equation 22

Assuming the diafiltration apparatus approximately resembles a continuously stirred tank reactor, the feed/retentate bulk side can be considered well-mixed. The progress of single stage diafiltration process can then be described by drawing a mass balance around the system for each component, as given in Equation 23 for impurity i, where V_S [L] is the system volume, F_p [L.h⁻¹] is the permeate flowrate, and A [m²] is the membrane area.

$$V_S \frac{dc_{ib}}{dt} = -F_p \cdot c_{ip} = -J_V \cdot A \cdot c_{ip}$$

Equation 23

Relating the permeate concentration (c_{ip}) to the bulk concentration on the feed/retentate side (c_{ib}) via the rejection (\mathbb{R}_i) (Equation 21) and rearranging, we obtain Equation 24 which can be integrated with the appropriate boundary conditions (starting concentration: $c_{ib}^{t=0}$ at time 0) to give Equation 25. The equation can be rewritten as $(J_V \cdot A \cdot t)$ equals the total permeate volume collected up to time t (V_p^t). The resultant term (V_p^t / V_S) is a dimensionless quantity which describes diafiltration progress in terms of the system turnover, i.e. how many washing volumes, or multiples of the system volume, have permeated (and been replenished with fresh solvent). This quantity (V_p^t / V_S) is often referred to as the number of diafiltration volumes or *diavolumes* but, while useful for describing single-stage systems, it cannot easily be defined for multi-stage systems.

$$\frac{dc_{ib}}{dt} = -\frac{J_V \cdot A}{V_S} \cdot (1 - \mathbb{R}_i) \cdot c_{ib}$$

Equation 24

$$\frac{c_{ib}^t}{c_{ib}^{t=0}} = \exp\left(-\frac{J_V \cdot A \cdot t}{V_S} (1 - \mathbb{R}_i)\right) = \exp\left(-\frac{V_P^t}{V_S} (1 - \mathbb{R}_i)\right)$$

Equation 25

It is apparent that the bulk concentration of every solute in the mixture follows an exponential decay from its starting concentration over time, i.e. with an increase in diafiltration volumes. The decay is more pronounced for a solute with low rejection as would be expected for a solute that is more readily washed out of the system through the membrane. This leads to the desired separation as the impurity with lower rejection is washed out of the system faster than the highly rejected product.

It follows that the yield and purity of the product p in a two-component purification by diafiltration can be defined as follows.

$$\text{Yield}(t) = \frac{c_{pb}^t}{c_{pb}^{t=0}} = \exp\left(-\frac{V_P^t}{V_S} (1 - \mathbb{R}_p)\right)$$

Equation 26

$$\text{Purity}(t) = \frac{c_{pb}^t}{c_{pb}^t + c_{ib}^t} = \frac{1}{1 + \frac{c_{ib}^t}{c_{pb}^t}} = \frac{1}{1 + \frac{c_{ib}^{t=0}}{c_{pb}^{t=0}} \cdot \exp\left(-\frac{V_P^t}{V_S} (\mathbb{R}_p - \mathbb{R}_i)\right)}$$

Equation 27

For multi-stage systems, mass balances similar to Equation 23 apply and these can be still be integrated analytically if rejections are assumed constant, i.e. independent of concentration.⁹⁷ If rejections are described as functions of the bulk concentration, the system of equations needs to be solved numerically.

3.1.5. Improving membrane process performance

Conceptually, there are three ways to improve a membrane separation and these all apply to diafiltration. First, the selectivity of the membrane itself may be improved, thus improving the separation of solutes in a single membrane stage. Also, the process configuration may be modified to make better use of an existing membrane, for example by using a multi-stage configuration. Lastly, the solute system may be adapted to better fit the membrane and configuration, for example by modifying the product to be more highly rejected or modifying the impurity to be better permeated.

Membrane performance

A separation may be improved by choosing a more selective membrane that can better discriminate between two molecules. For this purpose, it is often useful to consider the rejection of a membrane over a range of solute sizes, or a range of solute radii. A plot of rejection over solute size is referred to as a molecular weight cut-off curve because it describes the cut-off, or rejection, over a range of molecular weights. (Sometimes a discrete value for molecular weight cut-off (MWCO) is given in the literature which refers to the molecular weight of the solute which is 90 % rejected, i.e. the x-axis position where the curve crosses the 90 % rejection mark in a rejection versus molecular weight plot.)

An idealized membrane would exhibit a perfectly sharp molecular weight cut-off curve with complete rejection for the product ($R_p = 100\%$) and no rejection, or negative rejection, for the impurity ($R_i \leq 0\%$). An idealized cut-off curve exhibiting such a step change in rejection is shown in Figure 63 (grey curve). However, membranes typically exhibit sigmoidal cut-off curves and there is evidence that membranes with sharp separation curves and abrupt changes in rejection over a small molecular weight difference do not exist in this idealized form.

In an attempt to explain this phenomenon, Kim et al. adapted the transport model by Bowen and Welfoot^{108–110}, taking into account hindered diffusion to predict rejection of solutes at different pore sizes.¹¹¹ Simulating rejection as a function of solute radius for idealized membranes in which the pores are all cylindrical with uniform diameter, the authors obtain sigmoidal profiles in good agreement with experimental data¹¹². The authors conclude on this basis that “sharp separations might be difficult to achieve, even if it [were] possible to fabricate membranes with uniform cylindrical pores.”¹¹¹

Nevertheless, there are some examples of carbon molecular sieve membranes with extremely sharp cut-offs for very small molecules capable of separating the xylene isomers, specifically p-xylene from o- and m-xylene.¹¹³

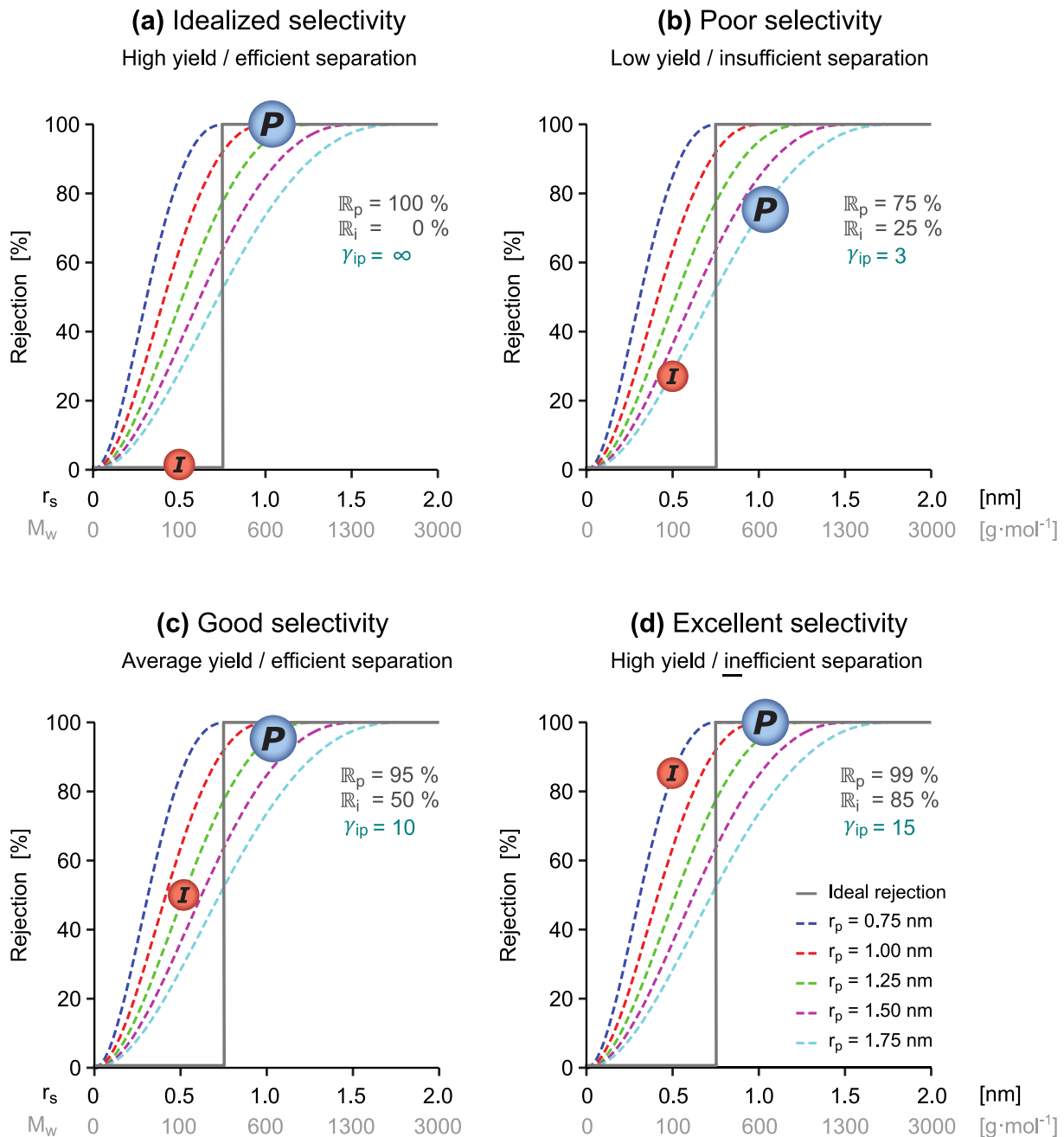


Figure 63. Scenarios for purification of product (P) from impurity (I) by diafiltration. (a) Idealized selectivity, (b) poor selectivity unsuitable for separation and (c) good selectivity. The membrane with excellent selectivity (d) allows a better separation than (c) but requires higher solvent consumption. Rejection curves are simulated in the nanofiltration region for uncharged solute of uniform size (r_s) and membranes with uniform pore sizes (r_p) between 0.75 nm and 1.75 nm using the pore-flow model assuming 10 bar pressure and 1cP solvent viscosity. The relationship between solute size (r_s) and molecular weight (M_w) is approximate. Figure reproduced from ¹⁰⁷ (an adaption from ¹¹¹).

While the difference between a membrane exhibiting idealized and poor selectivity is readily recognized (Figure 63a vs. Figure 63b), the difference between a membrane exhibiting good selectivity combined with low rejection of the impurity and a membrane exhibiting even better selectivity but high rejection of the impurity is more nuanced (Figure 63c vs. Figure 63d). The membrane with the higher separation

factor (γ_{ip}) will always afford a higher product yield for a similar attained purity, but the removal of an impurity with higher rejection will require more diafiltration volumes, i.e. a higher solvent consumption, for complete separation. This can be visualized by plotting the normalized concentration profiles of both impurity and product alongside product purity over several diafiltration volumes. (Normalized concentration is the concentration at a given time with respect to the starting concentration. For the product solute, the normalized concentration is also equivalent to its yield.) The two scenarios with good and excellent selectivity described above are here compared for a similar attained purity (99.0 %) (Figure 64). It is noticeable that the membrane with higher selectivity (Figure 64d, $\gamma_{ip} = 15$) affords a better yield (72.0 % versus 59.8 %) but requires approximately three times the diafiltration solvent (32.8 versus 10.3 diafiltration volumes) when compared to the less selective membrane with lower impurity rejection (Figure 64c, $\gamma_{ip} = 10$). The example also offers a guideline: when looking to attain high yields it is preferable to have a product rejection close to 100 % than to have an impurity rejection close to 0 %.⁸²

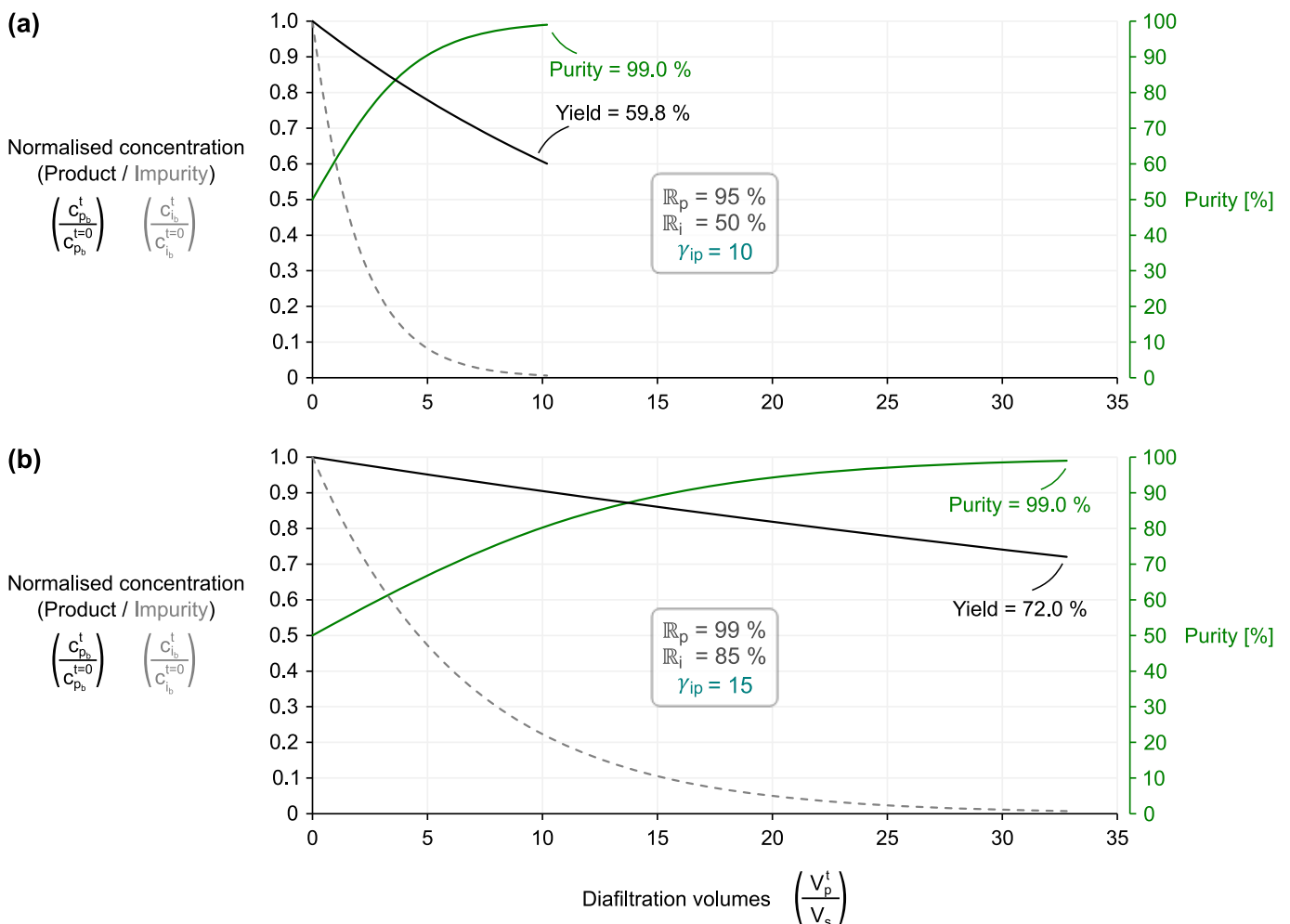


Figure 64. Simulated normalized concentration profiles for product (solid black) and impurity (dashed grey) as well as product purity (solid green) versus diafiltration volumes for two different scenarios: (a) good selectivity (as shown in Figure 63c) and (d) excellent selectivity but high impurity rejection (as shown in Figure 63c).

There thus exists in some cases a trade-off between the solvent consumption during diafiltration and the attained product yield. It should be noted that a higher solvent consumption also implies that diafiltration will take longer, or that a larger membrane area is required to process the required permeate in a similar length of time. When choosing a tighter membrane with a generally higher rejection, the effect is compounded because there is typically an inverse relationship between rejection and permeance and a tighter membrane will therefore exhibit a lower permeance already.

Lastly, the choice of membrane is restricted by the availability of membranes in the separation region of interest. In an industrial context, one is further confined to using commercially available membranes converted into industrially usable module format.^{81,82} Particularly for organic solvent nanofiltration, there is a limited number of material combinations available that fulfil separation and stability requirements at the same time.

The topic of solvent consumption is revisited in Chapter 4 in search for a solution to mitigate the high solvent consumption during diafiltration by integrating a nanofiltration-based solvent recovery unit.

Process configuration

The separation from a single membrane stage can be improved by using multiple stages in a variety of configurations. A large body of literature has been published on the use of membrane cascades.^{75,91–100,102,111,114–117}

Kim et al. describe the separation of two disperse PEG species, PEG-2000 and PEG-400 with rejections of 96 % and 60 % respectively. These two species cannot be efficiently separated with a single stage membrane separation, where a purity of 98 % can only be attained with a simultaneous yield loss of 40 %. By introducing a second stage with a similar membrane and using a recycle set-up to obtain a multi-stage effect, that yield loss can be reduced down to 6 % (Figure 65).

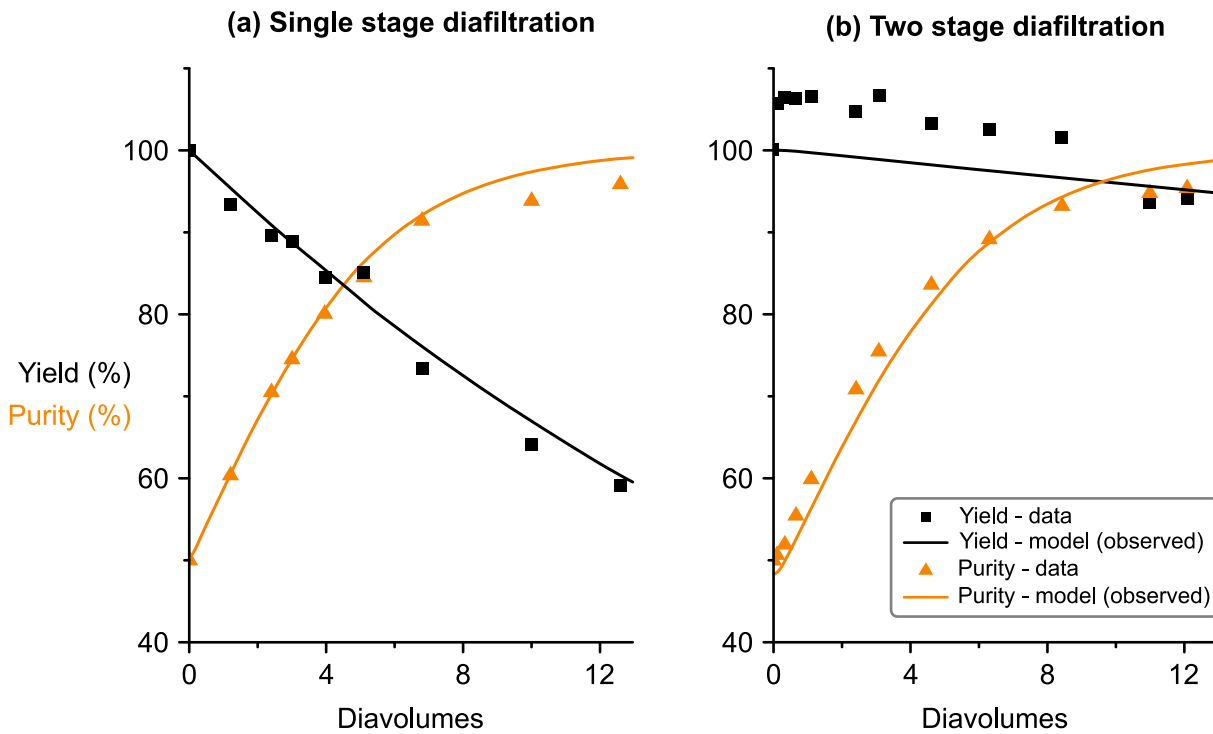


Figure 65. Separation of PEG-400 ($R = 60\%$) from PEG-2000 ($R = 96\%$). Comparison of PEG-2000 yield and purity between (a) single- and (b) two-stage diafiltration over 12 diavolumes. The yield increased from 59 % to 94 % for a similar purity of 98 %. The two-stage diafiltration was operated with a recycle ratio of 0.5. Reproduced from ¹⁰⁴ with permission from Elsevier.

Tuning molecular architecture

Lastly, changing the solutes themselves to move them further apart on a cut-off curve can increase selectivity for a given membrane. For example, a product can be anchored to a larger species to increase its rejection. A good example is ligand design during recovery of homogeneous catalysts by nanofiltration where an increase in ligand size can help retention of the catalyst complex.^{118–120} In some cases, there may also be an opportunity to tailor a process to create smaller impurities. In an industrial context, one is often tasked with separating an existing process stream with a set list of solutes at a fixed concentration. Therefore, there is usually little scope to change the membrane or solute system and the design choices often centre around process configuration.

In this synthesis of uniform PEG, however, there is scope to tune the molecular architecture of the functional groups on the termini of the building block as well as the hub. In order to maximize membrane selectivity, it is therefore expedient to consider the distinguishing features between the building block (BB) and the homostar product (HS):

- a) **Protecting group** (common to BB and HS): The effect of the protecting group (Pg) should be minimized because it is a feature common to both BB and HS. If the protecting group is large and significantly contributes to rejection of both BB and HS, it will diminish the contribution to rejection of the groups that distinguish HS and BB such as hub and leaving group. In other words, the Pg would decrease selectivity by making BB and HS more similar in terms of their rejection characteristics. The size of the Pg should therefore generally be as small as possible. However, as deprotection needs to be carried out as part of the chain extension cycle, there may be an alternative option: to remove the protecting groups prior to diafiltration, so that they no longer affect HS and BB rejection.
- b) **Leaving group** (only existent on BB): The rejection of the leaving group should generally be minimized because only the building block includes a leaving group. A decrease in leaving group rejection therefore only helps to minimize BB rejection with no effect on the rejection of product homostar. Care must be taken when changing leaving group, as it can affect the chain extension reaction.
- c) **Hub** (only existent on HS): The hub contribution to rejection should be maximized as the hub is the only distinguishing feature of the homostar aside from its increasing chain length and the bulkier geometry resulting from multiple arms. Therefore, hub size should generally be increased as much as practically possible, i.e. within the confines imposed by the required hub chemistry for attachment and disassembly, its stability towards chain extension and its solubility and affordability.

- d) **PEG oligomer** (necessarily common to both BB and HS but at different lengths with constant length on the BB and increasing length on the HS). The polymer chain chemistry cannot be changed when looking to synthesize linear uniform PEG, but there is a choice regarding the length of building block and how many chains should be attached to the hub.

The tuning of the molecular architecture and chemistry to improve nanofiltration performance will be the focus of the following discussion.

3.2. Materials and methods

3.2.1. Membrane preparation

Poly(ether ether ketone) membranes

The poly(ether ether ketone) (PEEK) membranes used in Chapter 3 were prepared as described by da Silva Burgal et al.^{121,122} PEEK membranes were prepared from a 12 wt% solution of VESTAKEEP 4000P (Evonik, DE) in 3:1 w/w MsOH:H₂SO₄, cast on a Novatexx 2471 poly(propylene) non-woven backing (Freudenberg Filtration Technologies, DE), phase-inverted in deionized water and, after solvent exchange, dried for 24 hours at 120 °C. Two different sets of membranes were prepared for screening. Both sets were prepared from the same cast but dried in different solvents, either acetone or ethanol, resulting in different molecular weight cut-offs. Drying from acetone gives a slightly looser membrane with lower overall rejection and a corresponding higher permeance, whereas the ethanol-dried membrane is tighter with higher overall rejection of all solutes and lower permeance. *All PEEK membranes used in this study were prepared by João da Silva Burgal.*

Polybenzimidazole membranes

The poly(benzimidazole) (PBI) used in the early stages of this work, and upon which the effect of increasing rejection with increasing central hub size was demonstrated (Figure 84), were prepared as described by Valtcheva et al.^{123,124} PBI dope solution (17 wt% PBI in dimethylacetamide) was prepared by dilution of a commercial PBI solution (Celazole® S26 PBI, M_w = 27,000 g mol⁻¹, from PBI Performance Products Inc., USA) containing 26 wt% PBI and 1.5 wt% LiCl as stabilizer with dimethylacetamide (Sigma-Aldrich). Membrane films were cast on a Novatexx 2471 poly(propylene) non-woven backing (Freudenberg Filtration Technologies, DE), then phase-inverted in deionized water and, after solvent exchange to acetonitrile via isopropyl alcohol, cross-linked with 3 wt% 1,4-dibromoxylene (DBX) at 80 °C for 24 hours, followed by conservation with PEG-400 until use. *Earlier sets of PBI membrane were prepared by Irina B. Valtcheva and later sets were prepared by Gyorgy Szekely.*

An updated version of the PBI membrane was later tested where the functional groups on the DBX cross-linker which had not completely reacted with the PBI polymer during cross-linking were further modified by reacting with a polyetheramine (Jeffamine® M-600 or Jeffamine® M-2005). Modification with Jeffamine® M-600 results in a looser membrane with lower overall rejection and modification with Jeffamine® M-2005 results in a tighter membrane. The preparation process is patented¹²⁵ but a detailed experimental description has not been published. *The Jeffamine-modified PBI membranes tested in this work (Figure 99) were prepared by Ruiyi Liu.*

Membrane installation

Membrane samples were cut into discs (d = 81 mm) (Figure 66) and installed into test cells (Figure 67) acting as a pressure housing. Membranes were typically installed dry without prior contact to solvent. A detailed visual guide of the test cell design and assembly procedure can be found in Appendix F on page 277.

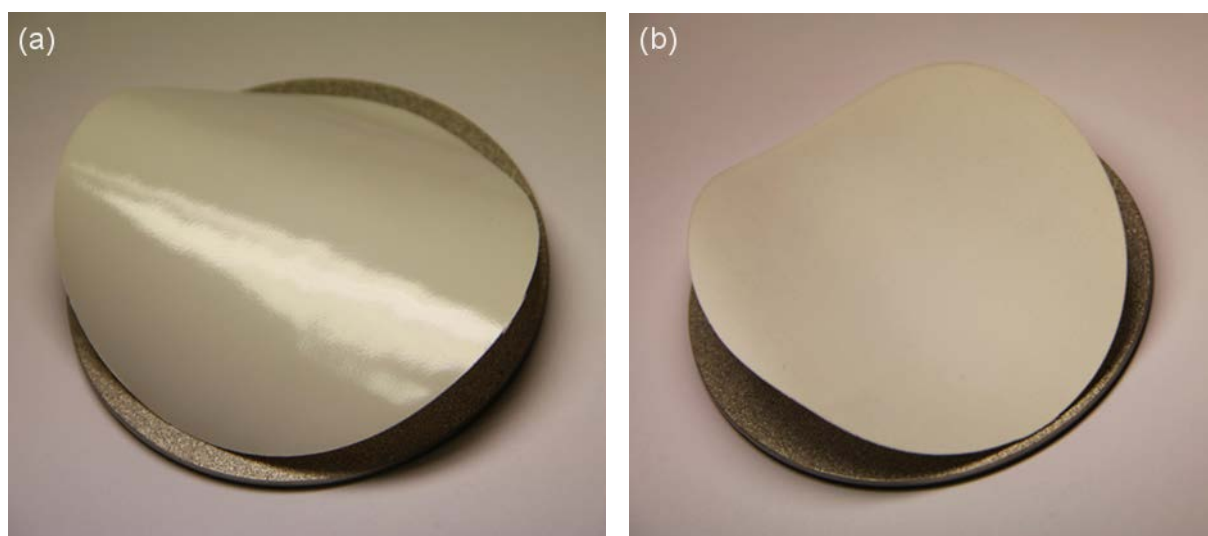


Figure 66. Membrane coupon (a) upper active layer (PEEK) and (b) rear side backing (polypropylene).

The PEEK membranes used for the diafiltration during the synthesis run towards E_{g60} (Section 3.3.6) were cut to size and first immersed in 1:4 MeOH-THF for 72 hours and then re-cut to size prior to insertion into the test cells; the membranes had swollen by 2-3 mm across an 81 mm disc, equivalent to a 3 % increase in diameter. The pre-swelling procedure prevents wrinkles from forming on the membrane due to differential swelling and thereby improves the mechanical stability of the membranes after insertion. The active membrane area after assembly is 51 cm² per pressure housing cell.



Figure 67. Assembled flat-sheet membrane pressure housing cell

3.2.2. Membrane screening

Membrane screening was performed in a set-up with two pumps, one providing pressurization and one providing circulation (Figure 68). For pressurization and recirculation, an HPLC reciprocating piston pump with a flowrate up to $100 \text{ mL}\cdot\text{min}^{-1}$ and a rotary gear pump with a flowrate of $2,400 \text{ mL}\cdot\text{min}^{-1}$ were used respectively. While the rotary gear pump was protected upstream with an inline filter, the HPLC pump was not equipped with an inlet filter to minimize pressure drop and avoid potential cavitation with the low boiling organic solvents used. The pressure housing cells holding the membranes were connected in series in the retentate loop with sufficient crossflow provided for the membrane by the recirculation pump to minimize concentration polarization (Figure 60). The recirculation flow is significantly faster than the permeate flowrate through the membrane so that the retentate side of the apparatus can be assumed well-mixed. The pressure was monitored upstream of the first and downstream of the last pressure housing cell with Bourdon tube pressure gauges and for a recirculation flowrate of $2,400 \text{ mL}\cdot\text{min}^{-1}$ the pressure drop per cell was around 0.25 bar. Screening was typically performed between 10-30 bar with the HPLC pump providing sufficient feed for all membrane cells and the excess feed not leaving the retentate loop as permeate returned to the feed tank via a back-pressure valve which was manually adjusted to set the feed/retentate side pressure.

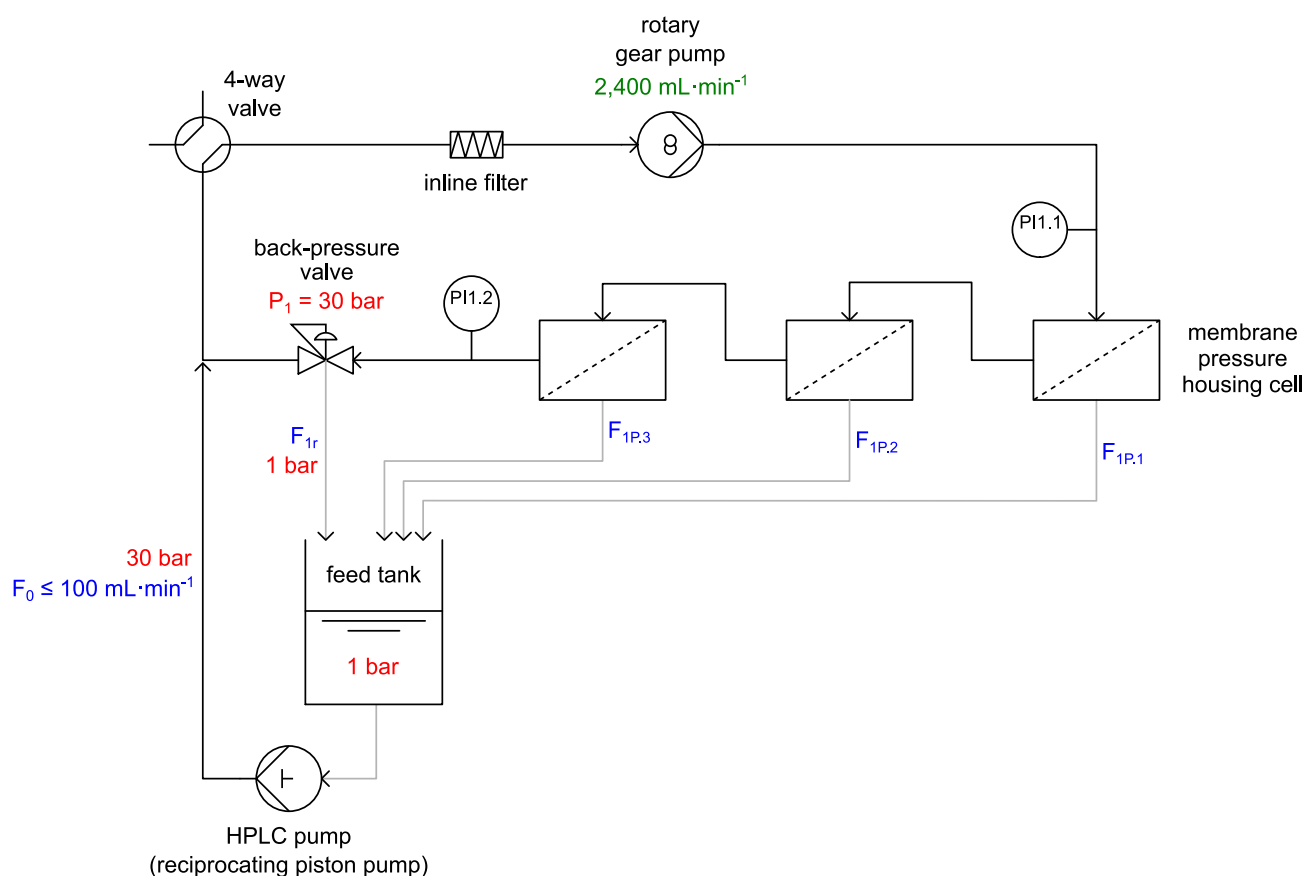


Figure 68. Membrane screening rig with two pumps and three pressure housing cells in series with manual measurement of permeate flowrate and sampling. Flexible PTFE tubing shown in light grey.

It follows that the feed flow must be at least as large as the sum of all permeate flows at the set pressure (Equation 28). In practice, the feed flow should be substantially higher than the sum of the permeate flows to provide sufficient return flow to the feed tank through the back-pressure valve (Equation 29) and prevent concentration of retained solutes in the retentate loop.

$$F_0 \geq (F_{1P.1} + F_{1P.2} + F_{1P.3} + \dots)$$

Equation 28

$$F_{1r} = F_0 - (F_{1P.1} + F_{1P.2} + F_{1P.3} + \dots)$$

Equation 29

The lines on the permeate side of the pressure housing cells and the return flow line from the back-pressure valve (F_{1r}) were built with flexible poly(tetrafluoroethylene) (PTFE) plastic tubing and permeate flowrates were measured manually with a graduated cylinder. Because flexible tubing was used, samples could be taken from the permeate lines and the return line directly into GC vials. For taking the retentate sample from the return flow line, the HPLC pump flowrate was temporarily switched down to avoid spillage. The feed tank was not always sampled as membrane rejection is calculated from the permeate and retentate concentrations (Equation 21) and the feed tank is always at least slightly less concentrated than the retentate loop unless the feed and return flowrate are extremely large compared to the sum of the permeate flows which was not the case in this set-up. When the feed tank was sampled to provide a cross-check, samples were drawn from the feed tank with a disposable syringe equipped with a needle. A small glass flask ($V \leq 200$ mL) equipped with a magnetic stirrer was used as the feed tank and the feed line from the feed tank to the HPLC pump inserted into the feed tank from above and made out as a riser pipe with flexible PTFE tubing. The feed tank was thus open to atmospheric pressure and well stirred. Permeate lines and return line were loosely inserted into the feed tank and clamped to a stand overhead.

For membrane screening, multiple coupons of flat sheet membrane (51 cm^2 membrane area per coupon) were thus screened in series under recirculation ($2.2 \text{ L} \cdot \text{min}^{-1}$) at varying pressures (10-30 bar) in a total recycle set-up. Usually, at least two coupons were screened in parallel. Where more than two coupons were screened, the arithmetic mean and standard deviation are usually shown in figures alongside the raw data. For membranes with higher permeance, fewer coupons were screened in parallel so that the sum of the permeate flows would not exceed the HPLC feed flowrate at the highest screening pressure. (Figure 68 shows three pressure housing cells connected in series as an example; a maximum of 8 pressure housing cells could be screened in parallel.) Pressures were recorded manually from the pressure indicators upstream and downstream of the cells and an average value was recorded. Where a pressure range was recorded, it indicates the pressure ripple from the single piston motion.

3.2.3. Diafiltration

Diafiltration apparatus set-up and operation

A general sketch of a single stage diafiltration apparatus was previously shown in Figure 62c. Used in this work was a two-stage diafiltration apparatus (Figure 69) whose retentate loops are each similarly set up as the retentate loop of the screening apparatus shown in Figure 68 above. Like for the screening apparatus, the first separation stage is directly pressurized by an HPLC pump from a feed tank. The second separation stage, however, is indirectly pressurized by the permeate flowing from the 1st membrane stage into the 2nd membrane stage (F_{1P}). This inflow into the 2nd stage can then further permeate the 2nd stage membranes to leave the diafiltration apparatus into the permeate tank (F_{2P}), but importantly, there is also a recycle flow from the 2nd membrane stage back to the 1st membrane stage via the feed tank. This recycle flow (F_{2r}) is critical to the performance of the two-stage set-up and can be expressed as a fraction of the permeate flow from the 1st separation stage (F_{1P}) as a recycle ratio (r_{21}) between 0 and 1 (Equation 30).

$$F_{1P} = F_{2P} + F_{2r}$$
$$r_{21} = \frac{F_{2r}}{F_{1P}} ; 0 < r_{21} < 1$$

Equation 30

In the limiting case where no recycle is used ($r_{21} = 0$), the two-stage set-up will not perform much better than a single-stage set-up. In the limiting case where almost all permeate from the first stage is recycled ($r_{21} \rightarrow 1$) and the permeate flow from the second stage is infinitesimally small, the rejection of the two-stage set-up will approach a higher value (Equation 31).¹¹⁴

$$\text{for } \mathbb{R}_{1i} = \mathbb{R}_{2i}; r_{21} \rightarrow 1: \mathbb{R}_1^{\text{Two-stage}} = 1 - \frac{C_{2P}}{C_{1r}} = 1 - (1 - \mathbb{R}_{1i})^2$$

Equation 31

The diafiltrations in this study were all run with a recycle ratio of approximately 0.5. In practice, this is achieved by modifying the 2nd stage pressure with the back-pressure valve so that 2nd stage permeate and recycle flow are equal. The recycle ratio was indirectly derived from volumetric measurements of the 2nd stage permeate (F_{2P}) and 2nd stage recycle flow (F_{2r}) using a graduated cylinder because the 1st stage permeate flow is under pressure and no inline measurement was used.

The 2nd stage permeate (F_{2P}) eventually flows out of the diafiltration apparatus into a permeate tank kept at atmospheric pressure. To keep the system volume inside the diafiltration apparatus constant, fresh

solvent must be fed into the feed tank at a rate equal to the permeate flowrate exiting the system. The solvent is fed from a fresh solvent reservoir also kept at atmospheric pressure via another HPLC pump but without a pressure gradient across the pump because both solvent reservoir and feed tank are open to atmospheric pressure. The feed tank level and system volume are thereby kept at a constant level throughout the diafiltration. Both stages are kept well-mixed on the retentate side by recirculation pumps and the 1st stage retentate loop and feed tank are kept mixed by the excess flowrate provided by the feed pressurization pump and corresponding return flow from the 1st stage to the feed tank (F_{1r}).

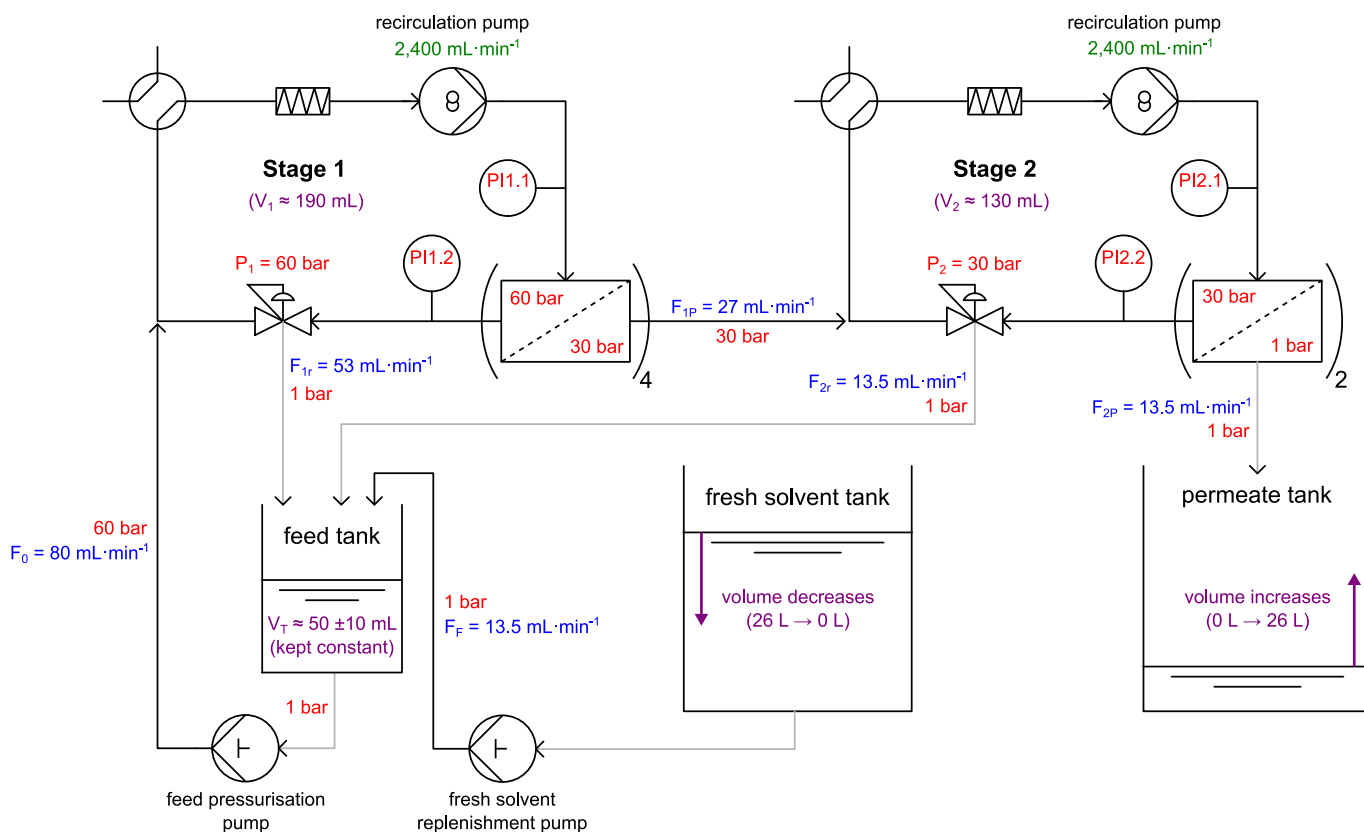


Figure 69. Schematic illustration of a two-stage diafiltration apparatus. Approximate pressures, volumes and flowrates shown for the synthesis of Eg_{60} in Section 3.3.7. For equipment labels, the reader is referred to Figure 68.

The two-stage diafiltration apparatus shown in Figure 69 is here explained using the approximate pressures, volumes and flowrates used for the synthesis of Eg_{60} in Section 3.3.7. With similar transmembrane pressures of 30 bar in each stage and a desired recycle ratio of 0.5, four and two pressure housing cells with similarly permeable membranes were installed in the 1st and 2nd stage respectively, equivalent to membrane area of 204 cm² and 102 cm², a ratio of 2:1. Over the course of a 32 h diafiltration, approximately 26 L of solvent pass through the diafiltration apparatus, depleting the feed tank and accumulating in the permeate tank. In practice, the permeate was collected in multiple 2.5 L Winchester flasks. Further details of the diafiltration apparatus can be found from p. 282 onwards.

Diafiltration preparation

In preparation for diafiltration, the solvent inside the apparatus is replaced with freshly distilled 1:4 v/v MeOH-THF to minimize contamination with THF-hydroperoxide. The volume inside the stages is washed out via the 4-way valves in each stage (Figure 70). In the open configuration, fresh solvent is fed into one side and the stage contents are simultaneously pumped out into a wash tank. A similar washing method is used to recover the product from the apparatus after nanofiltration.

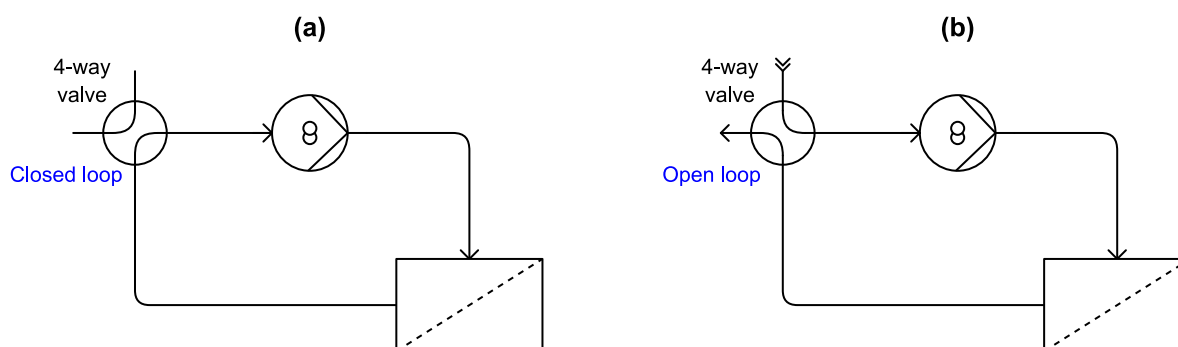


Figure 70. Use of 4-way valves (a) closed during diafiltration and (b) open for washing the retentate loops prior to and post diafiltration.

After filling the system with fresh solvent, the system is run in total recycle with the 2nd stage permeate returned to the feed tank for a period of around 30 minutes to ensure system stability. During this time, the retentate back-pressure valves are adjusted to give the desired stage pressures and flowrates. The following strategy is used:

- 1) The 1st stage back-pressure valve is adjusted to give 1st stage pressure (P_1) of 60 bar (with some fluctuation of ± 3 bar due to the pressure ripple induced by the piston motion of the HPLC pump). While P_1 is adjusted, the 2nd stage pressure (P_2) is also gradually increased to prevent the transmembrane pressure in stage 1 ($\Delta P_1 = P_1 - P_2$) exceeding 35 bar.
- 2) The 2nd stage back-pressure valve is then adjusted to give a recycle ratio of 0.5 which indirectly sets the stage 2 pressure.

F_{2r} and F_{2p} were both measured manually with a measuring cylinder in short intervals and the 2nd stage back-pressure valve adjusted until the desired recycle ratio was obtained. For the acetone-dried PEEK membranes used in Section 3.3.7, a recycle ratio of 0.5 typically corresponded to a P_2 of 27 ± 2 bar for a P_1 of 60 bar which in turn corresponded to flow rates of $27 \text{ mL} \cdot \text{min}^{-1}$ and $13.5 \text{ mL} \cdot \text{min}^{-1}$ for F_{1p} and F_{2r} respectively.

Monitoring diafiltration progress

Diafiltration progress was monitored by regular sampling of the 2nd stage recycle flow which is representative of the 2nd stage retentate loop concentration. This method of monitoring is convenient because the recycle flow downstream of the proportional relief valve is at atmospheric pressure, while the stage itself is pressurized. Sampling was scheduled to be more frequent at the beginning of the diafiltration when the change in concentration in each stage was more pronounced, due to the exponential decline of the concentration profiles. Samples were taken at half-hourly intervals for the first two hours, then hourly until the sixth hour, and every two to three hours thereafter until diafiltration was complete after 32 h. For the synthesis run towards Eg₆₀ (Section 3.3.7), samples were deliberately only taken from the 2nd stage and not from the 1st stage to conserve yield.

The concentration of ThpO–Eg₁₂–OTs (**67**) building block may be monitored by following the UV absorption at 260 nm from the toluenesulfonyl moiety. The hub may be observed at 260 nm, but also exhibits absorption at 300 nm where the toluenesulfonyl moiety ceases to absorb. It is therefore convenient to monitor UV absorption at both wavelengths, as the trace at 300 nm corresponds solely to the Hub³ containing species. However, the ThpO–Eg₂₄–OThp (**71**) dimerization side product lacks a UV chromophore. For this reason, a separate Electron Light Scattering Detector (ELSD) unit was connected downstream of the UV detector. While the UV absorption increases linearly with concentration according to the Lambert-Beer law, the ELSD response is non-linear, approximately a power function ($y = a \cdot x^b$) over a suitable interval, and therefore had to be calibrated.

Samples (0.5 mL sample taken, 30 μ L injection volume) were analyzed on an Agilent 1100 Series high performance liquid chromatography (HPLC) machine with a diode array detector (Agilent G1315B DAD) and connected to a Varian 385-LC ELSD. UV signals were gathered at 260 nm and 300 nm and ELSD traces were gathered at evaporator and nebulizer temperatures of 40 °C and 55 °C respectively, with a N₂ gas flowrate of 1.5 SLM. The HPLC column employed was an ACE 5 C₁₈-300 stationary phase (250 x 4.6 mm ID) (Advanced Chromatography Technologies Ltd., UK), a MeOH-MeCN (v/v) 1:4 solvent phase and a non-solvent phase of 5 mM ammonium acetate in deionized water. The column temperature was maintained at 30 °C, with a pump flowrate of 1 mL·min⁻¹ and a gradient from 40 % to 95 % solvent phase, see Figure 71 and Table 19 below.

Table 19. HPLC solvent gradient system.

Time / min	25 mM NH ₄ OAc in H ₂ O / %	1:4 MeOH-MeCN (v/v) / %
0	60	40
2	60	40
25	5	95
35	5	95
35.5	60	40
40	60	40

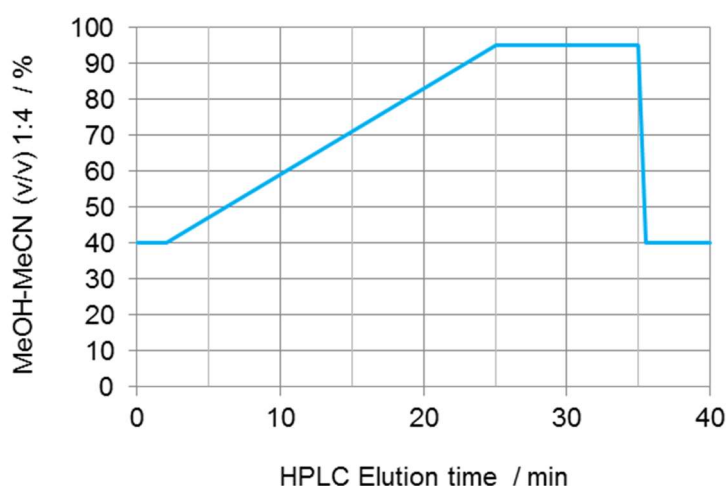


Figure 71. HPLC solvent gradient profile.

In a two-stage diafiltration apparatus, with a recycle flow from the 2nd stage to the 1st stage, the concentrations of all solutes with at least some rejection will be lower in the 2nd stage than the 1st stage. The two-stage apparatus improves upon the selectivity of a single stage because this reduction in concentration in the 2nd stage is much more pronounced for the product than for the impurity. This is because the product has higher rejection in the 1st stage than the impurity.

As a result of the above general considerations, the product homostar is concentrated almost exclusively in the 1st stage, whereas the ThpO–Eg₁₂–OTs (**67**) building block and ThpO–Eg₂₄–OThp (**71**) dimer are much more evenly distributed across the two stages. Compounds **67** and **71** can be reliably sampled from the 2nd stage recycle flow without dilution. The limit of detection is 5 a.u., equivalent to 4.7 μM of **67** or 5.4 μM of **71**, but both cease to be reliably quantifiable around 20 a.u., or at around 20 μM. With an HPLC injection volume of 30 μL, **67** and **71** are traceable for at least 6 and 18 hours of diafiltration

respectively. Compounds **67** and **71** can also be traced in the 2nd stage permeate stream for a slightly shorter time period. Permeate samples were taken for the first 9 h of diafiltration to confirm constant rejection, i.e. membrane stability, over time.

The product homostar (**61** – **79**) is more difficult to trace by monitoring the 2nd stage concentration because its absolute concentration and associated peak area are low. Due to its large UV absorption coefficient, the product can be detected, but its concentration varies strongly with small changes in recycle ratio and other system parameters. As a result, the 2nd stage concentration profiles obtained for the impurity species are typically smoother and more representative of diafiltration progress. Product concentration may be monitored by sampling the 1st stage recycle flow to the feed tank or the feed tank itself. Due to the large UV absorption coefficient, samples need to be diluted at least 1:10 and/or injection volumes lowered, at which point dilution errors become problematic. Sampling the 1st stage regularly also lowers the product yield. Therefore, having monitored both stages during the trial synthesis of Eg₁₆ homostar from Eg₄ building blocks, and having observed the expected performance, 1st stage concentrations of homostar and building block were not monitored in the final synthesis run for Eg₆₀. The dry mass yield obtained at the end of each diafiltration, after removal of solvent, and similarly after deprotection gave a good, and probably more accurate, estimate of diafiltration yield than an HPLC trace could in this case.

For the separation of the crude reaction mixture by diafiltration after chain extension to Hub³-Eg₃₆-OThp HPLC traces from the UV detector (260 nm) and the ELSD detector are shown in Figure 72 and Figure 73 below. Integration of the peak areas and conversion into concentration values via the relevant calibration yields the concentration profile shown in Figure 102.

1st stage retentate loop samples from the 1st stage proportional relief valve return flow should be taken by switching down the HPLC feed pump flow rate for a few seconds to collect approx. 200 µL of retentate into a sample vial which can then be pipetted accurately with the remainder washed back into the feed tank. Pipetting straight from the line may be inaccurate.

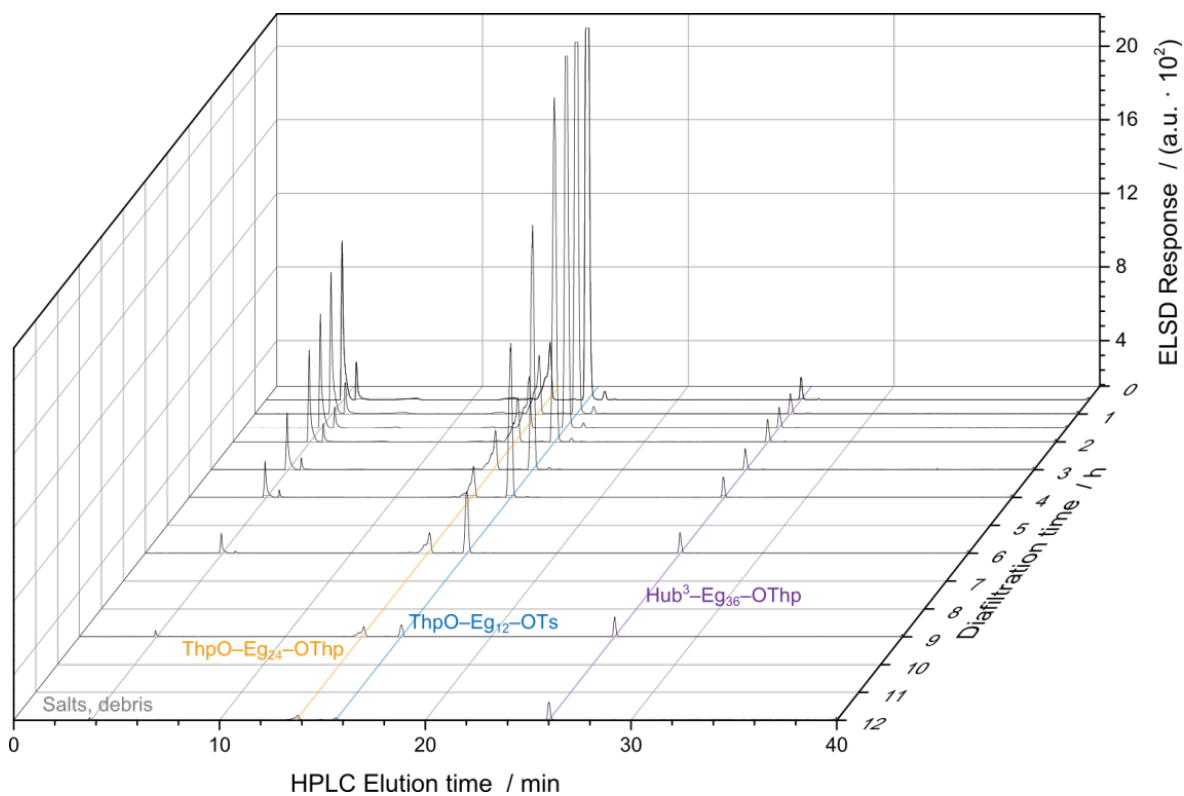


Figure 72. ELSD detector response for HPLC analysis of diafiltration progress after chain extension to Hub³-Eg₃₆-OThp (74).

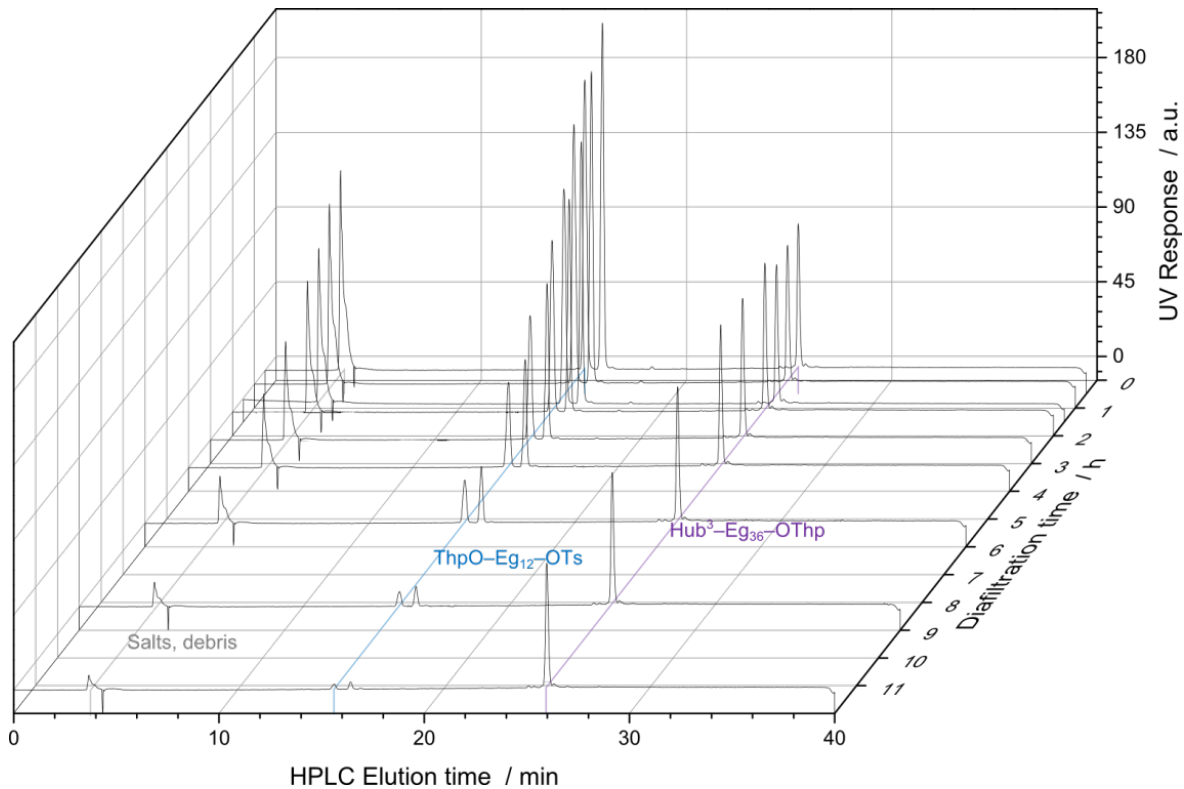


Figure 73. ELSD detector response for HPLC analysis of diafiltration progress after chain extension to Hub³-Eg₃₆-OThp (74).

3.3. Results and discussion

The following discussion details the tuning of the molecular architecture of building block and hub to improve the nanofiltration performance. The improved building block and hub are then used in a trial synthesis of Eg₁₆ where deprotection and purification are carried out jointly in the nanofiltration apparatus. A final synthesis is then carried out up to Eg₆₀ to demonstrate the viability of iterative synthesis of uniform PEG via nanofiltration.

3.3.1. Protecting group size decrease

Early nanofiltration trials were carried out with polybenzimidazole (PBI) membranes in acetonitrile solvent. The tests showed that the dimethoxytrityl protecting group (see Figure 38) dominated rejection when present in a molecule. For all molecules containing a Dmtr ether, rejection was high and largely independent of the functionality on the other terminus of the building block (Figure 74). Dmtr–Eg₄–OH (**3**), Dmtr–Eg₄–ODmtr (**4**) and Dmtr–Eg₄–OTs (**5**) all exhibit rejection in the range of 76 – 84 % at 15 bar with Dmtr–Eg₄–OH (**3**) exhibiting a slightly lower rejection than the other two species. At the same time, the three building block species are largely indistinguishable from the corresponding Hub¹(–Eg₄–ODmtr)₃ homostar (**26**), with a separation factor (Equation 22) between 3 and 4.

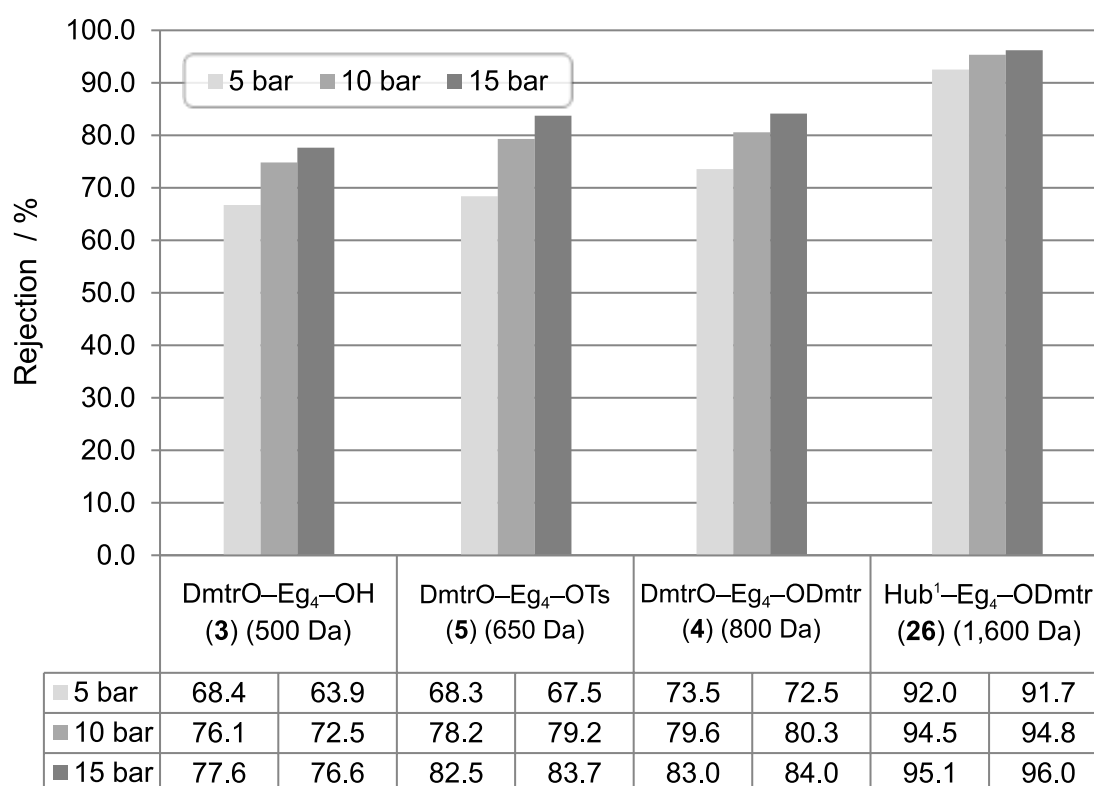


Figure 74. Rejections of tritylated building block species and the corresponding homostar with varying pressure (5, 10, 15 bar) on a 17 wt% PBI membrane (2 samples screened in parallel) in MeCN.

To maintain compatibility with the protecting group strategy, based on a hydrogenolytically cleavable hub and an acid labile temporary protecting group (Pg), an acid labile Pg with similar stability to Dmtr ethers was sought. Acetal protecting groups were potentially suitable replacements with much smaller size and three acetals were investigated (Figure 75): tetrahydropyranyl (Thp), a common protecting group in carbohydrate chemistry, 2-methoxyisopropyl (Mip), a very small acetal, and 2-benzyloxyisopropyl (BnOip), a larger analogue of Mip containing a UV chromophore.¹²⁶

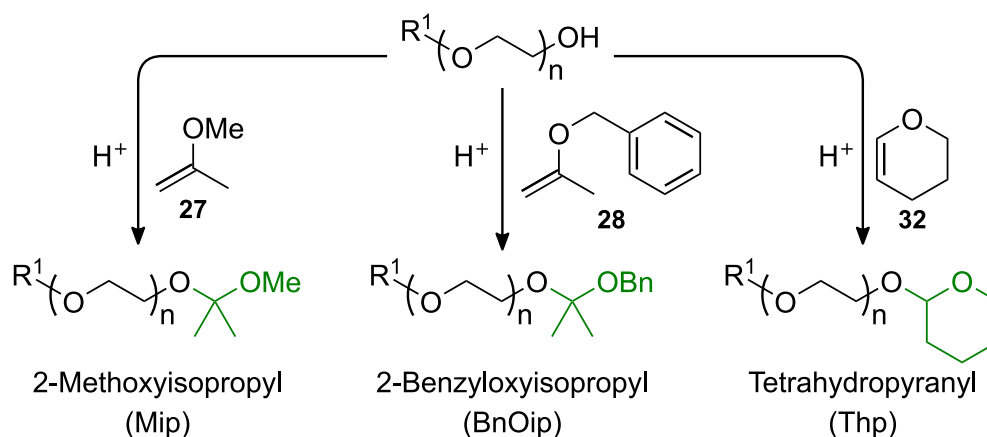


Figure 75. Three acetal protecting groups alternative to Dmtr ethers: Mip, BnOip and Thp.

The reagent for introducing the Mip protecting group, 2-methoxypropene (**27**) is available as a bulk reagent (Sigma-Aldrich, 2017: 250 g for £53). BnOip is not commonly used because the reagent needed for its introduction, 2-benzyloxypropene (benzyl isopropenyl ether¹²⁷, 1-methyl-1-benzyloxyethyl ether¹²⁶, **28**) is prohibitively expensive in comparison (Tokyo Chemical Industry, 2017: 5 mL for \$320). The BnOip acetal was particularly interesting for its chromophore and because it was reported that it could be introduced and removed under neutral conditions with Pd/C.^{128,129}

Mip and BnOip cannot be introduced like Dmtr ethers in the presence of excess tetragol because they undergo cross-acetalization. Tetragol (**1**) can further react with the desired product, MipO-Eg₄-OH (**29** in Figure 76) to yield HO-Eg₄-OC(CH₃)₂O-Eg₄-OH (**30** in Figure 76) by replacing the methoxy moiety of the protecting group to form a symmetrical acetal. The doubly Mip-protected product (**31**), the analogue of **4**, is not detected. Cross-acetalization is suppressed with Thp due to an unfavourable equilibrium for ring opening so that reaction of 3,4-dihydropyran (**32**) with excess tetragol (5 eq.) yields monoprotected ThpO-Eg₄-OH (**33**) as the major product alongside ThpO-Eg₄-OThp (**35**) as side product. For Mip and BnOip, the protecting group must therefore be introduced after the leaving group so excess **1** is first reacted with TsCl in CH₂Cl₂ with Et₃N (1.5 eq.) as acid scavenger to yield HO-Eg₄-OTs (**36**). BnOip and Mip can then be introduced by reaction with 2-methoxypropene (**27**) or 2-benzyloxypropene (**28**) in THF with trace TsOH as catalyst to yield MipO-Eg₄-OTs (**37**) and BnOipO-Eg₄-OTs (**38**) respectively.

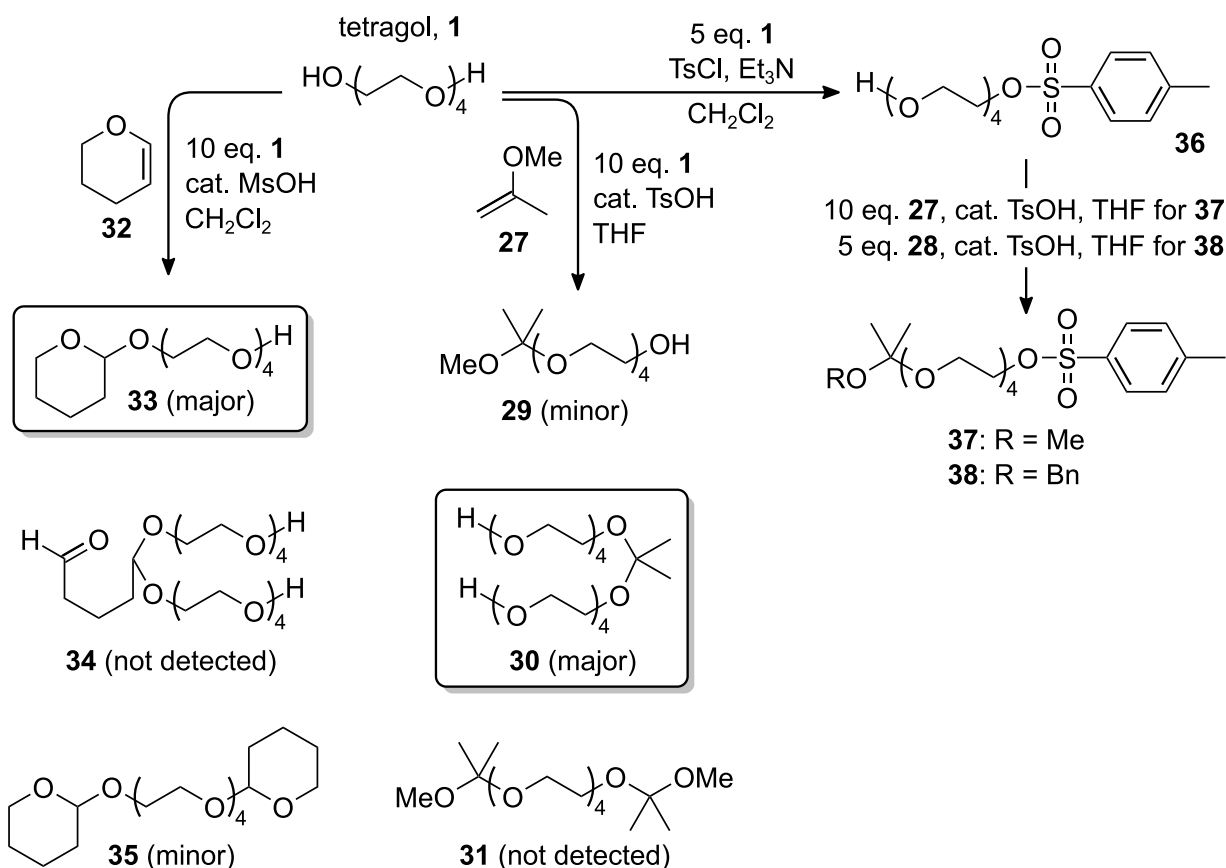


Figure 76. Indirect route to protection of tetragol with Mip and BnOip with prior addition of tosylate leaving group as direct reaction of 2-methoxypropene with excess tetragol leads to cross-acetalization.

MipO–Eg₄–OTs (**37**) and BnOipO–Eg₄–OTs (**38**) were then screened for rejection alongside unprotected HO–Eg₄–OTs (**36**) and DmtrO–Eg₄–OMs (**39**) on similar PBI membranes (c.f. Figure 74) in MeCN. Both Mip and BnOip exhibited lower rejection than dimethoxytrityl (Figure 77) and were therefore potentially suitable for a synthesis via nanofiltration. (No direct comparison was made between the rejection of Thp and the other acetals at the time, but it is assumed that Thp rejection is comparable to BnOip.)

Unfortunately, the gentle introduction and removal of BnOip with Pd/C under neutral conditions^{128,129} could not be achieved during this work. Instead polymerization of the acetal species was observed, which was attributed to acidity of the catalytic system. It is possible that protons released through the Lewis acid character of Pd are the real catalyst for the reaction.⁴² BnOip may alternatively be introduced via cross-acetalization with 2,2-dibenzyloxypropane which was prepared on a multi-gram scale from 2,2-dimethoxypropane and benzyl alcohol under reflux by distilling off methanol followed by vacuum distillation.¹³⁰ While synthesis of the reagent and protection via cross-acetalization with a large excess of 2,2-dibenzyloxypropane (10 eq.) was successful and the excess reagent could be readily recovered, benzyl alcohol is liberated as a side product and proved tedious to remove. The BnOip protecting group was eventually given up on as the high cost of reagent or additional purification effort required for its introduction did not justify the gain of a UV chromophore.

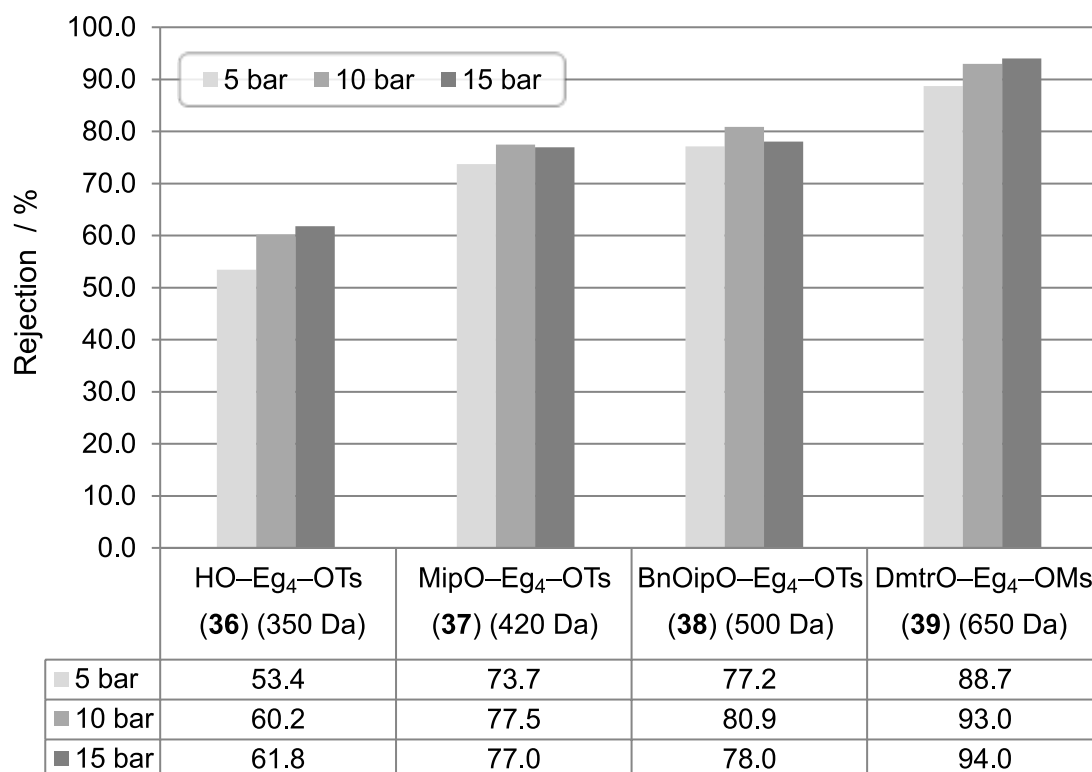


Figure 77. Rejections of alternative acetal protecting groups (Mip, BnOip versus Dmtr) with varying pressure (5, 10, 15 bar) on a 17 wt% PBI membrane (2 samples screened in parallel) in MeCN.

The Mip protecting group was easy to introduce and to remove with readily available, cheap reagents and multiple building blocks containing Mip were made and tested for rejection. However, Mip is less stable than Thp^{131,132}, and was very labile in the presence of trace acid with storage and processing requiring much care. Mip containing building blocks were stored with a trace of Et₃N and were not dried to constant mass overnight, but some partial deprotection was observed at times. Although Mip exhibited the lowest rejection from the three acetal protecting groups screened, the Mip group was eventually discarded. With the PEG backbone, hub and the potential sulfonate leaving group all being relatively robust and requiring no particular care during handling, it was deemed unwise to introduce a weak link with a Mip protecting group.

This left Thp as the acetal protecting group of choice. The cyclic nature of Thp gives it additional stability compared to the Mip and BnOip acetals and allows the group to be introduced in the presence of excess tetragol as previously shown (Figure 76).

3.3.2. Leaving group size decrease

In the next step, a change of leaving group (Lg) was considered. Given that the Lg is only present on the building block and not on the homostar, leaving group size should be minimized as much as is practicable. However, while the size and type of the leaving group affect rejection, the chemical properties of the Lg also simultaneously affect many other elements of the strategy. Modification of the leaving group therefore needs a more nuanced analysis.

First, the leaving group determines the reactivity of the building block and thus, the overall chain extension kinetics. With the information from the kinetic study available, the reaction is already relatively slow, so a reduction in leaving group reactivity may not be acceptable.

Formation of vinyl ether side product from elimination on the other hand is probably not a concern when using nanofiltration because the vinyl ether side product should always be smaller in size and molecular diameter than the building block itself. Any vinyl ether should therefore be easy to remove through the membrane alongside excess building block and reaction debris. A membrane process could therefore likely accommodate a leaving group more prone to competing elimination from a separation standpoint, although the associated higher building block input factor could be an economic concern.

The more problematic side reaction occurs with trace hydroxide to form building block dimer. Traces of hydroxide (either from water or impure base) can displace the leaving group on the building block to yield the non-activated hydroxyl analogue, and on further reaction with strong base, e.g. NaH, yield the building block alkoxide. This building block alkoxide has similar reactivity to the alkoxide chain termini of the homostar and can therefore attack another molecule of building block. As a result, two molecules of $\text{PgO-Eg}_n\text{-Lg}$ building block may combine to form a $\text{PgO-Eg}_{2n}\text{-OPg}$ dimer in the presence of trace water or base (Figure 78). (The reaction was previously described in Figure 28). The dimer side product naturally has double the length of the building block and should therefore usually be harder to remove, unless the leaving group is very large.

In this context it is important to recognize that separation via nanofiltration may be performed before or after deprotection. If by choice the separation via nanofiltration is to be accomplished in the protected state, the limiting separation will be between the protected homostar, $\text{Hub}(-\text{Eg}_n\text{-OPg})_3$ and either $\text{PgO-Eg}_n\text{-Lg}$ building block or $\text{PgO-Eg}_{2n}\text{-OPg}$ dimer, whichever is harder to remove. But if deprotection is carried out prior to or during nanofiltration, the building block would lose the protecting group on one terminus and retain the leaving group, i.e. lose only one of its end groups, while the dimer would lose the protecting group on both termini to yield the diol. The limiting separation in the deprotected state would therefore be between the deprotected homostar, $\text{Hub}(-\text{Eg}_n\text{-OH})_3$ and either $\text{HO-Eg}_n\text{-Lg}$ building block or $\text{HO-Eg}_{2n}\text{-OH}$, whichever is the harder to remove (Figure 79).

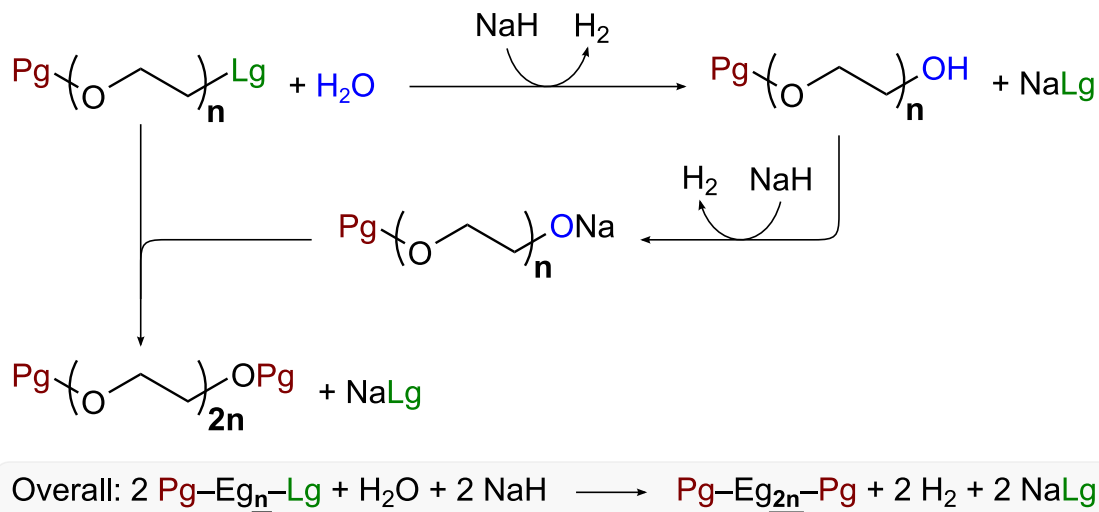


Figure 78. Formation of Pg–Eg_{2n}–Pg dimer side product from Pg–Eg_n–Lg building block caused by presence of trace water or hydroxide during etherification.

It is therefore possible that the same leaving group would not be limiting during a separation in the protected state, while being limiting during separation in the deprotected state. An eventual membrane process would be greatly aided by deprotection during nanofiltration inside the apparatus so the latter scenario should usually be considered (except if there was an intention to fully recover building block from the permeate).

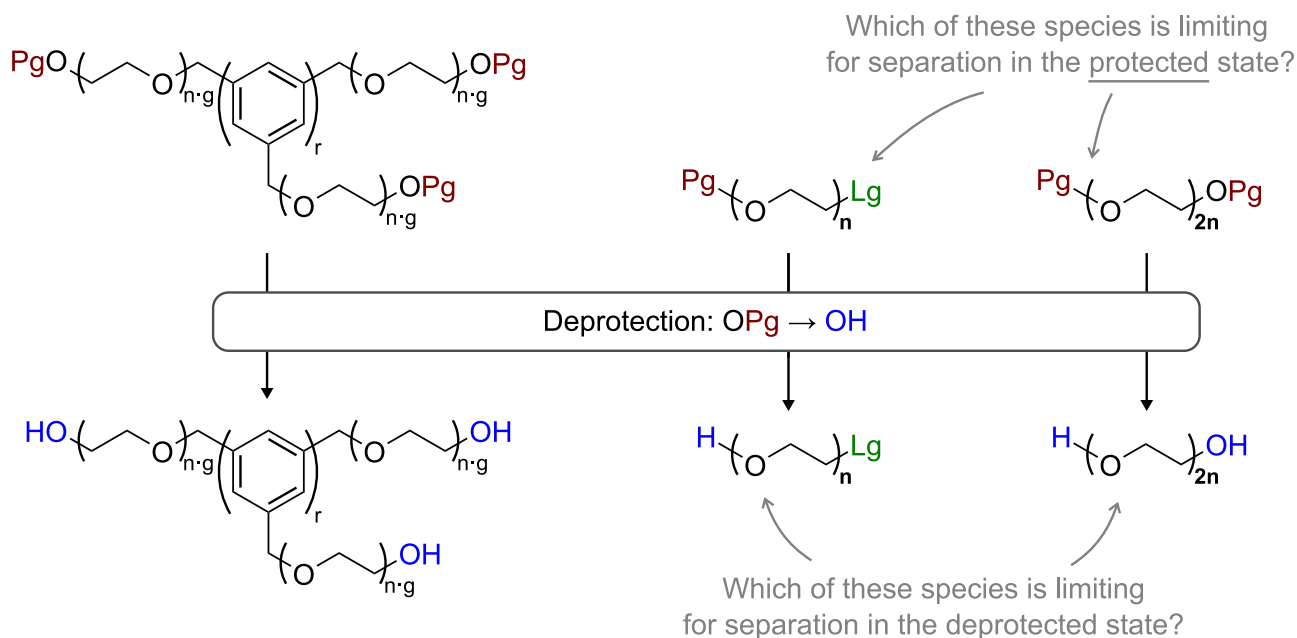


Figure 79. Homostar, building block and building block dimer in their (top) protected and (bottom) deprotected state. Deprotection causes conversion of all protected termini into hydroxyls but the leaving group on the building block is unaffected. The effect of the building block leaving group Lg on nanofiltration performance is determined by whether the building block or the dimer limit separation, and whether nanofiltration is carried out with protected or deprotected solutes.

Lastly, the difference in rejection between the building block and the dimer, in the protected or deprotected state, will also depend on the length of the building block. The dimer will always be double the length of the building block, but with increasing length of building block, the effect of the end groups will diminish. The ideal choice of leaving group and the requirement to minimize its size may therefore also vary depending on building block length.

In summary, the extent to which the leaving group size influences the performance of nanofiltration is determined by several factors, including the extent to which the reactants and reaction mixture can be kept dry, i.e. free from traces of water and hydroxide. Excluding trace water may become increasingly difficult as the growing PEG chains can sequester solvent along their entire length on a weight basis, while reactivity is determined only by the end group concentration on a molar basis.

Besides tosylate, two other common leaving groups were selected for screening: methanesulfonate (or mesylate), another sulfonate ester, and bromide. The leaving groups were each screened as the Eg₄ derivatives without protecting groups in acetonitrile with 17 wt% and 19 wt% PBI membranes (c.f. 17 wt%: Figure 74 and Figure 77..

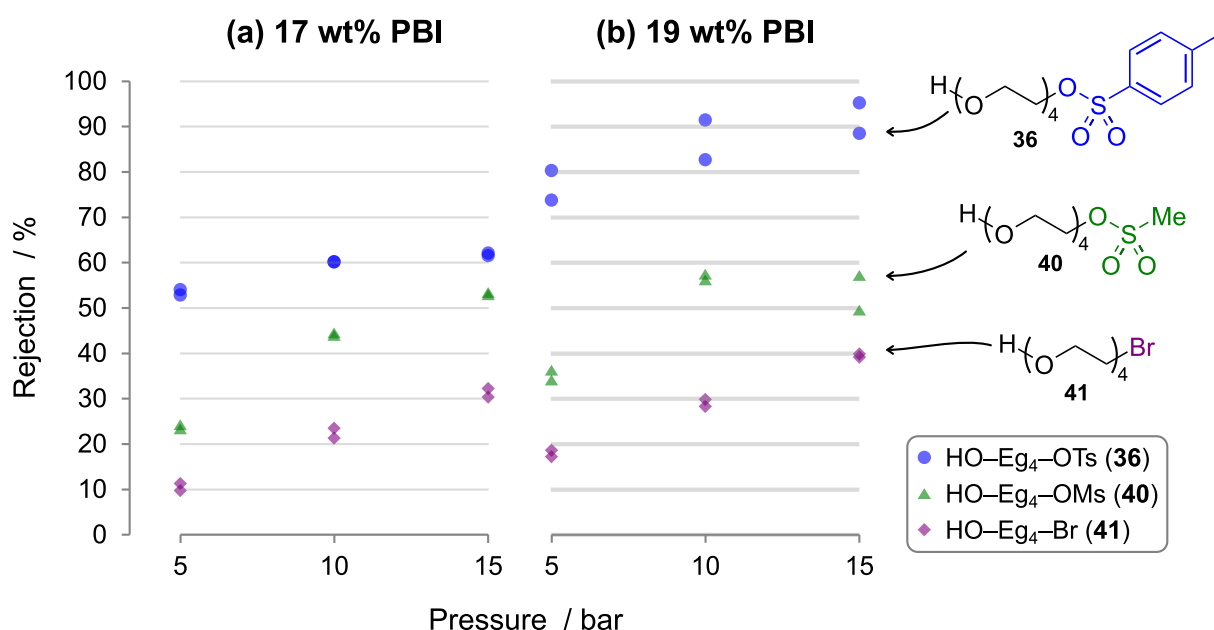


Figure 80. Rejections of building blocks with different leaving groups (OTs, OMs, Br) at varying pressure (5, 10, 15 bar) in MeCN with (a) 17 wt% and (b) 19 wt% PBI membranes (2 samples screened in parallel each).

It is evident that the Eg₄ building block with a bromide leaving group, HO-Eg₄-Br (**41**), exhibits a much lower rejection than the two building blocks with sulfonate ester leaving groups, HO-Eg₄-OTs (**36**) and HO-Eg₄-OMs (**40**), and that the methanesulfonate ester also provides at least a 10 % lower rejection than the tosyl leaving group under these conditions. Both alternative leaving groups, mesylate and

bromide, could therefore be advantageous in a membrane separation where the removal of building block rather than dimer is limiting. However, tosylate was ultimately kept as the leaving group. First, there was evidence that dimer formation could not be avoided altogether and would be limiting, potentially making a leaving group change redundant or less relevant. Both mesylate and bromide would also likely result in a slower reaction with a primary alkoxide, and there was uncertainty over possible side reactions. (For more hindered species, such as branched oligomers, there is a case for using the smaller mesylate leaving group for higher reactivity.⁸⁰) With bromide, another concern was the lack of an equally simple and mild protocol to introduce this group directly. Lastly, with the Thp protecting group lacking a UV chromophore, it was desirable to keep the UV traceability of the tosyl group.

3.3.3. Hub size increase

In a further step towards optimizing discrimination, the hub contribution to rejection was to be increased in order to better retain the homostar product during nanofiltration. Two larger homologues of the previously used hub, 1,3,5-tris-(bromomethyl)benzene (or Hub¹-CH₂Br, **9**), were prepared from commercially available tri-carboxylic acids (Figure 81). 1,3,5-Tris(4-carboxyphenyl)benzene (or Hub²-COOH, **42a**) and 1,3,5-Tris(4'-carboxy[1,1'-biphenyl]-4-yl)benzene (or Hub³-COOH, **43a**) were esterified, then reduced with LiEt₃BH, and finally brominated to give the benzyl bromide homologues of **9**, Hub²-CH₂Br (**42d**) and Hub³-CH₂Br (**43d**). Except for Hub²-CH₂Br (**42d**), all hub species were purified by crystallization in good yields and X-ray crystallography confirmed their identity (p. 287).

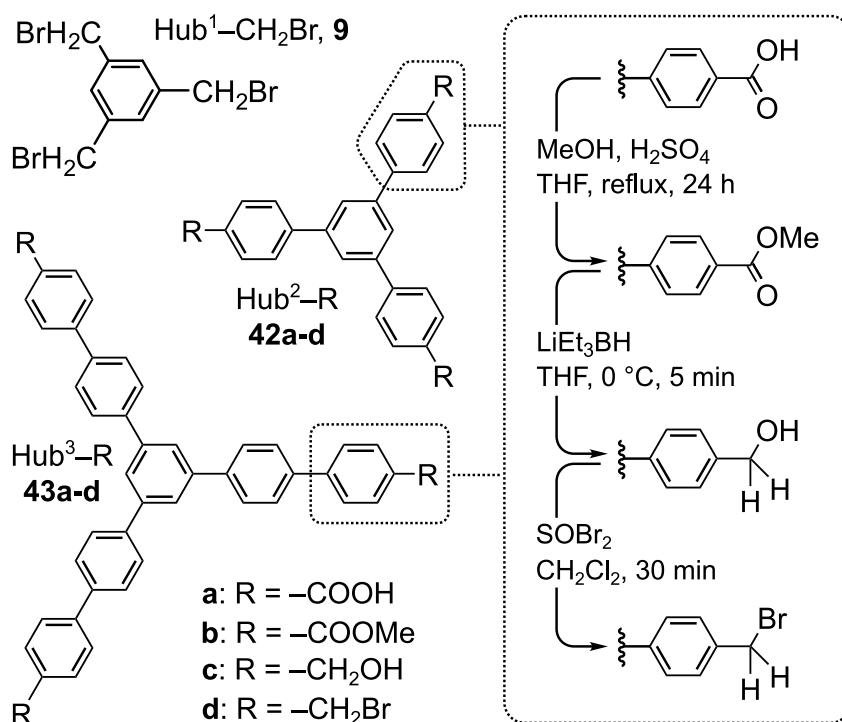


Figure 81. Synthesis of bromomethyl hubs (Hub¹, Hub², Hub³) of increasing size.

Due to the sparse solubility of some hub derivatives, particularly **43c**, and to obtain rejection results more representative of real homostars with attached PEG chains, the hubs were not screened as lone species. Instead, Eg₄ homostars were prepared by hub attachment with ThpO–Eg₄–OH (**33**) using the method previously described (Section 1.3.1.2), and then deprotected to yield the various derivatives for screening (Figure 82). It was a deliberate choice to use shorter unprotected chains to isolate the effect of the hub on rejection, although the resultant size and polarity difference compared to homostars with longer PEG chain length may be skewing the results somewhat.

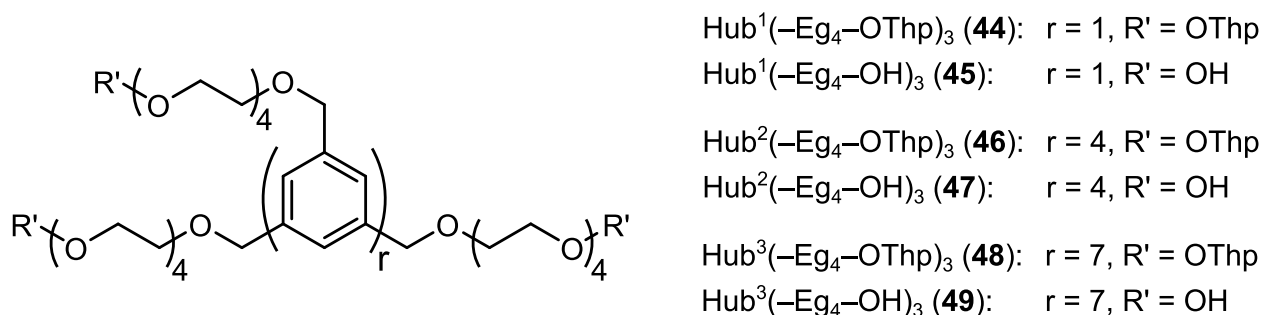


Figure 82. Eg₄ homostars of Hub¹, Hub² and Hub³ for nanofiltration screening.

An Eg₄ homostar with a geometrically different hub on the basis of tetraphenylmethane was additionally screened to compare the difference between a tetrahedral and a planar hub. Via attachment of ThpO–Eg₄–OH (**33**) to tetrakis(4-bromomethylphenyl)methane (Hub⁴–CH₂Br, **50**), Hub⁴(–Eg₄–OThp)₄ (**51**) was thus synthesized in similar fashion, followed by deprotection to yield Hub⁴(–Eg₄–OH)₄ (**52**) (Figure 83). (*Tetrakis(4-bromomethylphenyl)methane*¹³³ (**50**) was synthesized by Piers R. J. Gaffney.)

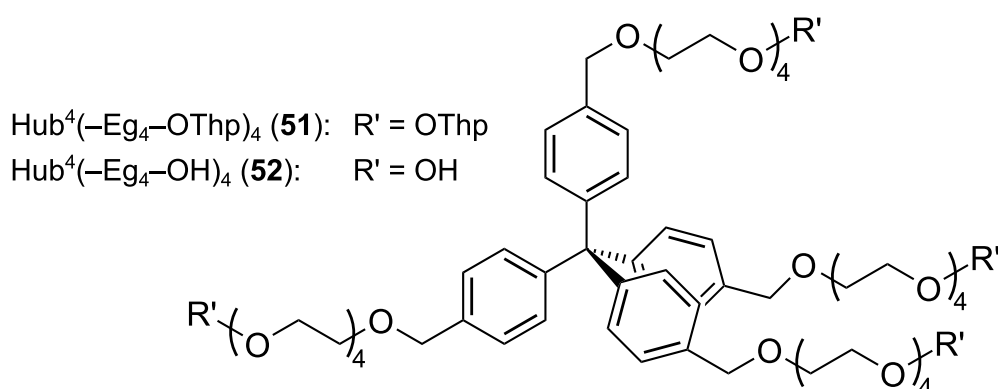


Figure 83. Eg₄ homostar of Hub⁴ for nanofiltration screening having tetrahedral hub geometry and four arms, prepared from tetrakis(4-bromomethylphenyl)methane, a derivative of tetraphenylmethane.

During membrane screening in MeCN with 17 wt% PBI membranes, the Eg₄-homostars of the larger hubs, Hub²(–Eg₄–OH)₃ (**47**) and Hub³(–Eg₄–OH)₃ (**49**) showed significantly better rejection, more than 10 percentage points higher than Hub¹(–Eg₄–OH)₃ (**45**) (Figure 84). At higher rejection values (> 90 %), a small difference of only several percentage points in rejection makes a substantial difference. When

rejections are very high, a look at the fraction of solute that permeates ($1 - R_i$), gives a more insightful answer. A change from Hub² to Hub³ results in an increase in rejection from 95.3 % to 98.8 % under these conditions at 15 bar (Figure 84). Understood as a decrease in the fraction of homostar which permeates from 4.7 % down to 1.2 %, this is a reduction in product permeation by 74 %. Similarly, the separation factor for a diafiltration would increase about four-fold (c.f. Equation 22).

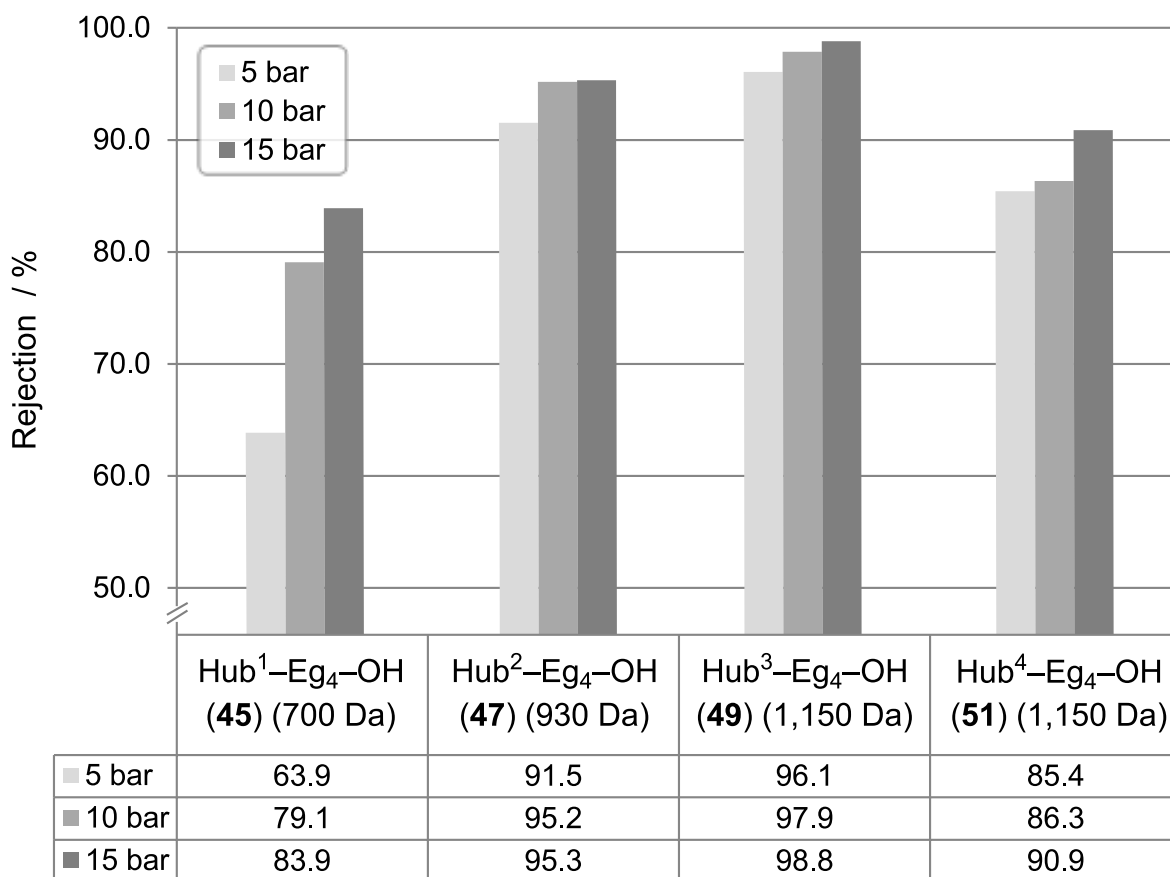


Figure 84. Rejections of Eg₄ homostars made from four different hubs with varying pressure (5, 10, 15 bar) on a 17 wt% PBI membrane (2 samples screened in parallel) in MeCN.

The tetrahedral Eg₄ homostar, Hub⁴(-Eg₄-OH)₄ (**52**), yielded lower rejection than would have been expected when only considering molecular weight. Compared to Hub³(-Eg₄-OH)₃ (**49**) with a rejection of 98.8 % at 15 bar, Hub⁴(-Eg₄-OH)₄ (**52**) has a rejection of only around 90 % despite its similar molecular weight, smaller yet than the rejection of Hub²(-Eg₄-OH)₃ (**47**) at 95 %. This is good evidence that rejection in this system is influenced by polarity effects such as the interaction of the hub centre and PEG chains with the membrane, rather than just molecular diameter or size. In the case of Hub² and Hub³, it can be rationalized that the planar hub centre is more exposed to the membrane and interacts to increase rejection. In the case of Hub⁴ on the other hand, PEG arms protrude out from the tetrahedral centre in all directions and prevent significant interaction between the membrane and the hub which appears to lead to lower rejection. (The transport through nanofiltration membranes is typically a ternary

interaction between solute, solvent and membrane and it is a well known phenomenon that rejection in systems where solute and solvent are polar to a degree is not only governed by molecular size.^{83,134–137} Overall, Hub³(–Eg₄–OH)₃ (**49**) appeared to be a good choice for increasing homostar rejection and was thus used from here on.

There was some concern whether the conjugated system of Hub³ would be susceptible to side reactions during hydrogenolysis. To confirm that the larger Hub³ was still cleavable via hydrogenolysis similar to Hub¹, a polydisperse homostar synthesized from commercially acquired mPEG-2,000 and **43d** was subjected to hydrogenolysis over Pd/C (prepared in situ¹³⁸) under H₂ atmosphere at room temperature and pressure. The reaction returned mPEG-2,000 and the tolyl derivative of **43d** in clean fashion after 24 h.

Finally, beyond the improvement in rejection, Hub³ (and Hub² to a lesser extent) offered the additional advantage that they exhibit strong UV absorption due to their conjugated system and possess a larger absorption range into higher wavelengths. For example, the Hub³ homostar has an absorption maximum around 280 nm with significant absorption at least up to 300 nm. At wavelengths around 300 nm, no other species used in this study, e.g. tosylate, interfere. The homostar can therefore be clearly distinguished from other species, and is detectable to a very low level, something that could not be achieved with the simple Hub¹ benzyl group.

3.3.4. Deprotection of Thp during nanofiltration

Settled on tetrahydropyranyl (Thp) as protecting group and tosylate as leaving group for the building block and on Hub³ as homostar core, it was now necessary to confirm under which conditions the Thp protecting group could be smoothly removed and then to combine the chemistry with diafiltration.

Thp removal is an equilibrium reaction and excess protic solvent or removal of the Thp-alcohol deprotection adduct, ideally both, are needed to push the reaction to completion. To simplify purification, it was planned to conduct acid-catalyzed Thp deprotection during nanofiltration and to remove the Thp moiety through the membrane during diafiltration alongside other debris, thereby driving the deprotection equilibrium to completion. Due to the higher relative stability of Thp compared to the Dmtr ether, it was necessary to first test what conditions were needed to affect deprotection within a reasonable time frame so that the deprotection would not become time limiting in the context of a diafiltration.

For this purpose, a deprotection trial was carried out. A stock solution made up of Hub³(–Eg₄–OThp)₃ (**48**) (10 g·L⁻¹) dissolved in MeOH was filled into HPLC vials (1 mL each) and a stock solution of toluenesulfonic acid (TsOH) in MeOH was then added to give acid concentrations between 0.1 mM and 1,000 mM. The HPLC vials were then capped and shaken for mixing. After 1 hour, the acid was

quenched by addition of dilute aqueous ammonia through the cap with a syringe and the samples were analyzed by HPLC. The deprotection of **48** proceeds via two intermediate species, singly deprotected $\text{Hub}^3(-\text{Eg}_4-\text{OThp})_2(-\text{Eg}_4-\text{OH})_1$ (**48b**) and doubly deprotected $\text{Hub}^3(-\text{Eg}_4-\text{OThp})_1(-\text{Eg}_4-\text{OH})_2$ (**48c**) to eventually yield fully deprotected $\text{Hub}^3(-\text{Eg}_4-\text{OH})_3$ (**49**). The HPLC spectra therefore show up to four species as well as a salt peak of ammonium tosylate (NH_4OTs) from acid neutralization (Figure 85). It is apparent that the more acid is added, the further deprotection proceeds prior to neutralization. A concentration of 5 mM appears to be sufficient to affect complete deprotection within one hour as no more double deprotected intermediate species (**48c**) can be detected in those spectra with all of **48** fully converted into **49**. For later diafiltration trials, a slightly higher concentration (10-50 mM) was thus chosen to allow for a margin of error.

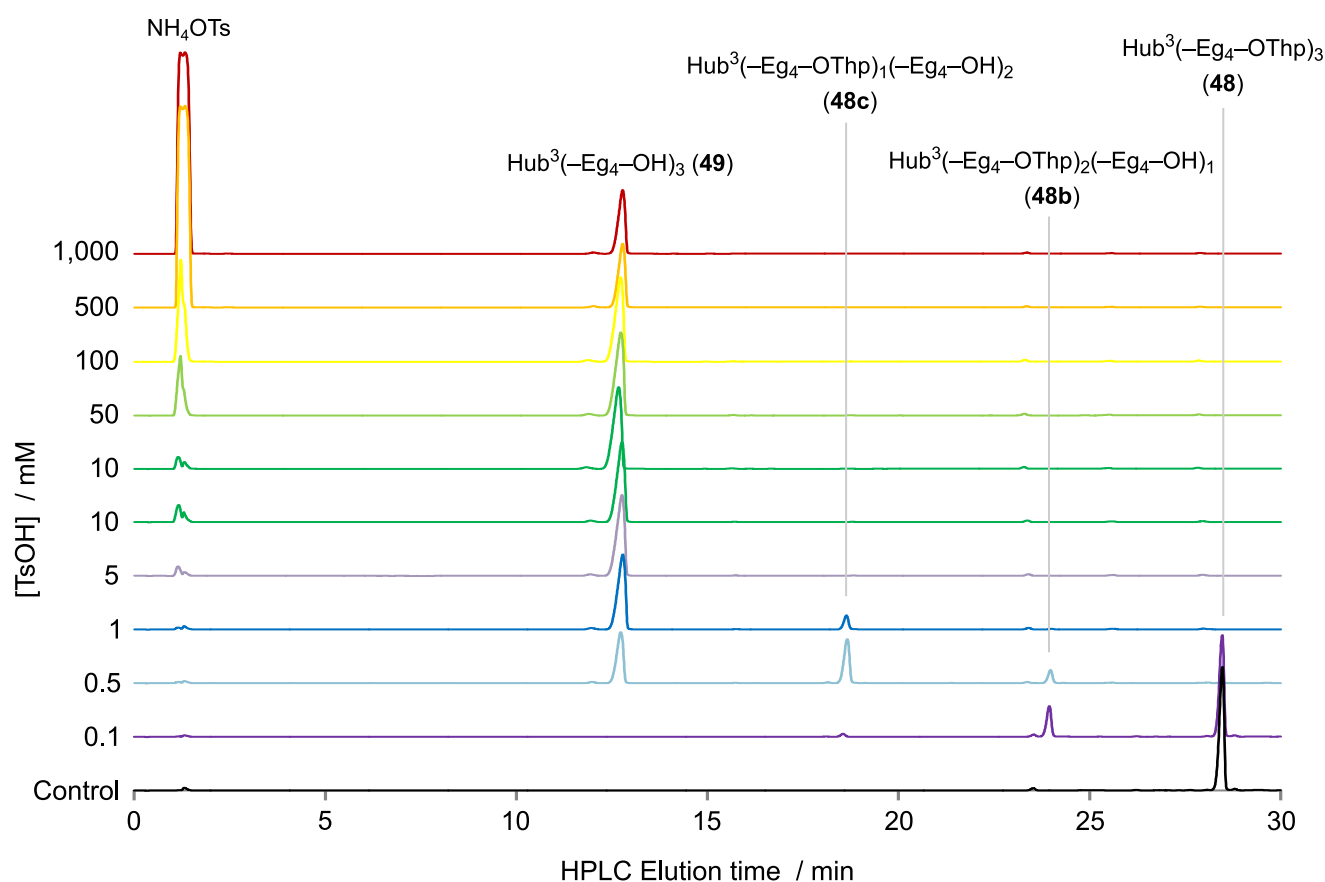
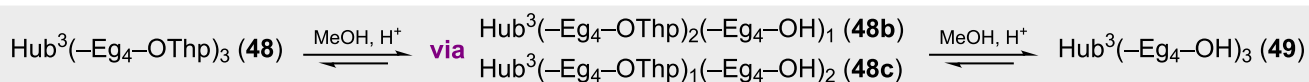
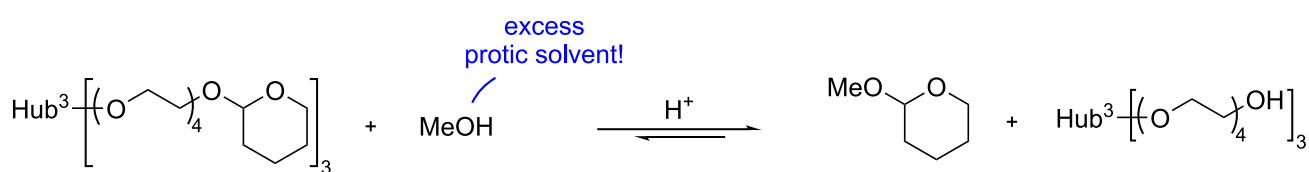


Figure 85. Deprotection trial of $\text{Hub}^3(-\text{Eg}_4-\text{OThp})_3$ (**48**) (approx. $10 \text{ g}\cdot\text{L}^{-1}$) with varying concentrations of TsOH acid catalyst (0.1 – 1,000 mM) in MeOH for 1 h with sample analysis by HPLC.

If deprotection is to be run simultaneously to diafiltration, the diafiltration needs to run with a protic solvent or a mixed solvent system having a large enough fraction of protic solvent to push the deprotection to completion. Also, the membranes need to be resistant to catalytic acid, and ideally maintain their permeability and rejection in the presence of acid. Unfortunately, permeation and rejection for the polybenzimidazole (PBI) membranes were found to vary with pH during screening, which was undesirable despite the general stability of the PBI membranes under acidic conditions in the organic solvents tested.¹²³ The result is consistent with the structure of the PBI used herein which contains two secondary amines per repeating unit on the imidazole rings and should be pH responsive as a result (Figure 86).

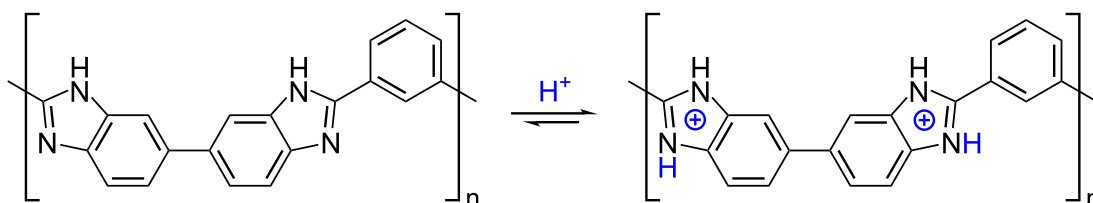


Figure 86. Structure of the poly(2,2'-[m-phenylene]-5,5'-bis-benzimidazole polybenzimidazole polymer used for the manufacture of PBI membranes and its pH responsive behaviour.

An alternative membrane made from a poly(ether ether ketone) (PEEK) polymer was eventually chosen.^{121,122} Barring some susceptibility to sulfonation, PEEK as a membrane material is both acid resistant and pH unresponsive and it was found that permeation through PEEK remained constant upon addition of acid. (PEEK has also been found stable at high temperatures and under basic conditions for OSN.¹⁰¹) Due to their structure, PEEK membranes exhibit higher permeance in aromatic solvents (e.g. toluene) as well as polar aprotic solvents (e.g. THF, DMF and acetone) while they have poorer permeance in protic solvents (e.g. H₂O, MeOH, EtOH) and apolar aliphatic solvents (e.g. hexane, heptane). Because THF exhibits good permeance through PEEK membranes¹²², but Thp removal requires a protic solvent, a mixture of 1:4 MeOH-THF (v/v) was chosen for nanofiltration. With an industrial application in mind, there were some concerns about separability and recovery of mixtures of MeOH (T_b = 64.7 °C) and THF (T_b = 66 °C), and an attempt was also made to use EtOH (T_b = 78.2 °C) but this resulted in slower deprotection.

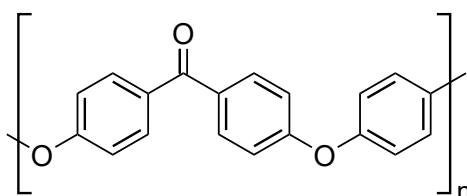


Figure 87. Structure of poly(ether ether ketone) polymer used for the manufacture of PEEK membranes.

Figure 88 shows a deprotection trial with $\text{Hub}^3(-\text{Eg}_4-\text{OThp})_3$ (**48**) inside a diafiltration apparatus with no building block present. Unblocking was initially attempted in 1:9 v/v EtOH-THF with TsOH (10 mM) (00:15 – 04:15 hours). Because unblocking was slow and had come to a halt after 4 h, further TsOH (20 mM) was added. While the reaction temporarily restarted, progress was not sufficiently fast. The solvent feed to the apparatus was then changed to 1:9 v/v H_2O -THF, in the hope that the significantly more polar protic character of water would drive the reaction. However, the reaction did not proceed at all with a feed of 10 % water. The feed was then changed to 2:8 v/v MeOH-THF with 50 mM of TsOH added, and this combination of acid and solvent affected deprotection rapidly.

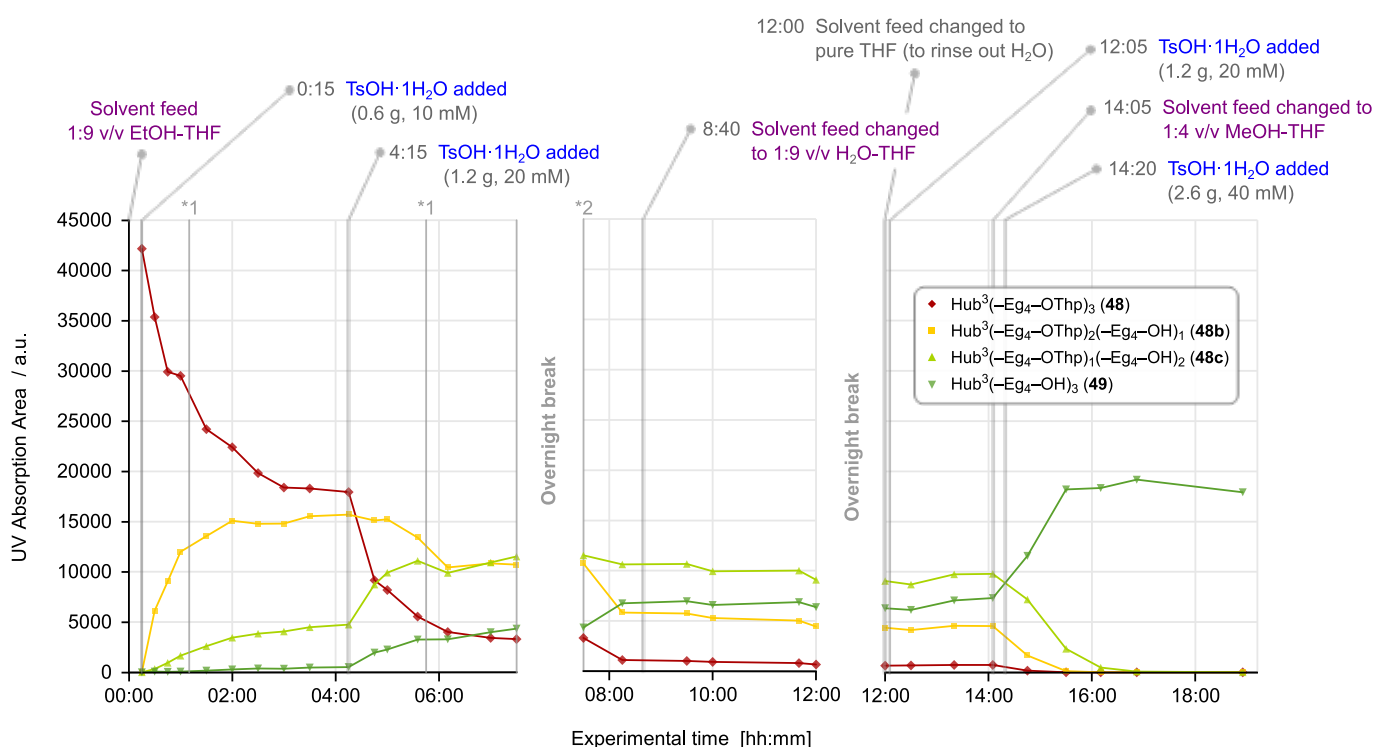


Figure 88. Deprotection trial of $\text{Hub}^3(-\text{Eg}_4-\text{OThp})_3$ (**48**) (250 mg, approx. $1 \text{ g}\cdot\text{L}^{-1}$) with various solvent mixtures: 1:9 v/v EtOH-THF (00:00 – 08:40), 1:9 v/v H_2O -THF (08:40 – 14:05) and 2:8 v/v MeOH-THF (14:05- 19:00). Only MeOH-THF led to sufficiently rapid deprotection. At 01:10 and 05:45 (marked *1), the tank overflowed and approx. 20 mL were lost in each case; the cause was the solvent pump, which was fixed at 07:30 (marked *2).

An interesting side observation was made with regard to change of solvent permeance through the membrane. When the 10 % EtOH and 20 % MeOH solutions in THF were fed into the apparatus, no appreciable change in permeance, i.e. total throughput, occurred over time. This suggests that the solvent composition permeating the membrane was stable. But when the mixture of 1:9 v/v H_2O -THF was fed into the apparatus, there was an appreciable flux decline over time (interval between 08:40 and 14:05 hours, permeance not displayed in graph). This is indicative either of a change in membrane character or a change in solvent composition on the retentate side. A quick test of the solvent ratios in retentate and permeate via NMR revealed that significant rejection of water had occurred. The PEEK

membranes had preferentially permeated THF and retained water and so water had accumulated inside the apparatus on the retentate side, leading to a decline in flux over time. At the end of the interval with 1:9 v/v H₂O-THF feed at 14:05 hours, water had accumulated to approx. 30 vol.-% in THF in the 2nd retentate stage of the diafiltration apparatus and the membranes exhibited a permeance of only around 0.6 L·m⁻²·h⁻¹·bar⁻¹, compared to a permeance of around 2.3 L·m⁻²·h⁻¹·bar⁻¹ with pure 2:8 v/v MeOH-THF solvent. While unsuitable for this diafiltration and deprotection application, the rejection of water could thus make PEEK a candidate membrane material for splitting azeotropic mixtures, e.g. the THF-H₂O, or perhaps the EtOH-H₂O azeotrope.

TsOH was later replaced by methanesulfonic acid (MsOH), a liquid, which is more readily dosed using a micropipette and weighs around 45 % less per mole (96.1 g·mol⁻¹ and 172.2 g·mol⁻¹ respectively). An overall concern was that the acid should permeate sufficiently rapidly to have fully rinsed out of the diafiltration apparatus by the time the diafiltration is complete, although this was not quantified. While the acid concentration needs to remain sufficiently high for deprotection to complete, a steady acid concentration of a fast permeating acid can more effectively be attained by repeated or continuous addition of acid over a period rather than higher retention of the acid by the membranes. This is because repeated addition can be accomplished at no significant additional cost while a high acid rejection can lead to longer diafiltration time when removal of residual acid from the product is harder. Lastly, in a multi-stage diafiltration, the distribution of acid and concentration in each stage needs to be considered.

Another deprotection trial was then run in the diafiltration apparatus with an approximate chain extension product mixture artificially made up from Hub³(-Eg₄-OThp)₃ (**48**) and ThpO-Eg₄-OTs (**53**) building block. Diafiltration was run in a two-stage system with transmembrane pressures of 30 bar in each stage, as described in the standard operating procedure on page 150. Permeate containing washed-out impurity, mostly ThpO-Eg₄-OTs (**53**) building block and reaction debris, was continuously withdrawn from the apparatus and fresh 2:8 v/v MeOH-THF continuously fed into the system at an equal rate. Samples from both the first and second retentate stage were taken to monitor concentration of **48** and **53** inside the apparatus. After 4 hours of normal diafiltration MsOH (50 mM) was added to affect deprotection. Further retentate samples were taken and diafiltration was continued for a further 5 h (to a total of 9 h) to allow any residual building block and acid to permeate.

Analysis of the concentration profiles reveals the expected exponential decline of building block, with the majority of building block (approx. 90 %) having permeated after 4 h. Also, upon addition of MsOH after 4 h, complete deprotection occurs within two hours and after 6 h only fully deprotected Hub³(-Eg₄-OH)₃ (**49**) is detected. The diafiltration and deprotection system of 2:8 v/v MeOH-THF and MsOH was therefore adopted going forward.

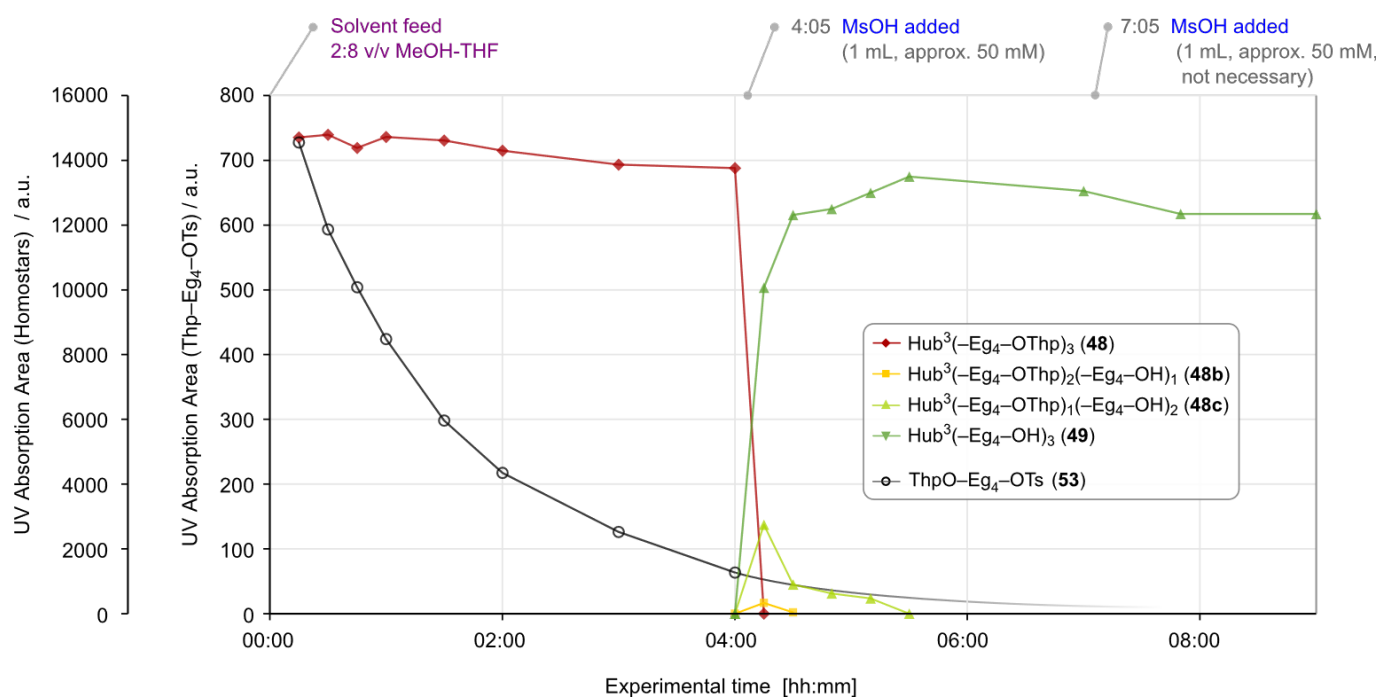


Figure 89. Integrated diafiltration-deprotection trial with a mixture of Hub³(-Eg₄-OThp)₃ (**48**) and ThpO-Eg₄-OTs (**53**). Diafiltration was run for 9 h in 2:8 v/v MeOH-THF with MsOH (1 mL, approx. 50 mM) added after 4 h for deprotection. (A further addition was made at 7 h but was not necessary in retrospect) Building block concentration is below the detection limit of HPLC after around 4 h; an extrapolation is shown for visual aid.

3.3.5. Trial synthesis of Eg₁₆ with combined nanofiltration and deprotection

With a nanofiltration system of PEEK membranes, 1:4 v/v MeOH-THF as diafiltration solvent and MsOH (50 mM) as acid for deprotection, combined nanofiltration and deprotection was tested in the synthesis of an Eg₁₆ homostar from Eg₄ building blocks over three extension cycles.

In separate 25 mL round-bottomed flasks equipped with magnetic stirrers, were placed Hub³-Eg₄-OH (**49**) (0.863 g, 0.748 mmol) and ThpO-Eg₄-OTs (**53**) (10 eq.). Each was evaporated three times from MeCN (3 mL·g⁻¹), the latter with a trace of Et₃N added prior to the first round of drying. Hub³-Eg₄-OH (**49**) was then re-dissolved in DMF (2 mL), followed by the addition of NaH (6 eq.) as a 60 % dispersion in mineral oil. ThpO-Eg₄-OTs (**53**) was also re-dissolved in DMF (5 mL) and transferred into the reaction mixture using a glass syringe. The flask which contained the building block was twice washed with DMF (2 mL each) and the rinsings also transferred. The round-bottomed flask containing the reagents in the total volume of DMF (11 mL) was then immersed in a silicone oil bath and left stirring at 40 °C for 3 h.

After 3 h, the reaction was quenched with saturated aqueous NH₄Cl (2 eq. with respect to NaH). Because diafiltration could only be run separately 7 days after the reaction due to a technical error, a clean-up procedure was performed to avoid leaving the product in wet DMF under basic conditions. Contrary to the protocol used for later extensions, DMF, water and trace ammonia were removed under high vacuum, and the mixture diluted with water (100 mL), followed by extraction into CH₂Cl₂ (3 x 100 mL). The solvent was removed on a rotary evaporator and the product concentrated under high vacuum to yield the product mixture as an oil which was stored at 4 °C until diafiltration.

For diafiltration, the product was diluted with 1:4 v/v MeOH:THF to a total volume of around 50 mL which could be accommodated in the 100 mL feed tank for nanofiltration.

The diafiltration set-up comprising two separation stages with PEEK membranes was washed and prepared with 1:4 v/v MeOH-THF at a recycle ratio of 0.5 as described in the standard procedure (p. 150). The feed tank of the diafiltration apparatus used during preparation was now replaced with the feed tank containing the diluted reaction mixture. The diafiltration was then started and run for 7 h in total. After 5 hours, MsOH (50 mM) was added to affect deprotection. Specifically, MsOH (1 mL, approx. 50 mM when considered evenly diluted across the nanofiltration apparatus) was diluted in 1:4 (v/v) MeOH:THF (10 mL) and slowly added to the feed tank over 2 min. The fresh solvent feed pump was stopped for a brief period of time to compensate for the addition of extra solvent.

During nanofiltration, samples from both retentate loops were taken approximately every 15 minutes for the first hour, every 30 minutes for the next two hours and every hour thereafter. Samples were diluted by factor of 10 (50 µL sample + 450 µL fresh solvent) for HPLC analysis due to the high UV absorption of Hub³ and to conserve yield.

After 7 hours, the apparatus was washed three times with fresh solvent, each time with 800 mL through the 1st stage and 400 mL through the 2nd stage via the four-way valves and with 300 mL to rinse the feed and permeate lines. The solvent was evaporated on a rotary evaporator, followed by removal of residual solvent under high vacuum overnight. (The time between the end of nanofiltration and the transfer of the product to drying under high vacuum is about 4 h.)

However, the resultant product mixture (1.255 g) was found to be impure and to still contain significant amounts of building block. The mixture contained 7 % of HO–Eg₄–OTs (**36**) building block reagent in its deprotected state alongside product equivalent a yield of around 88 %. Unexpectedly, the sample also contained trace 2-hydroxy-tetrahydrofuran which likely stemmed from 2-hydroperoxy-THF in turn derived from oxidation of THF. Consequently, all THF was from then on freshly distilled on a rotary evaporator immediately prior to use, with Fe(II)SO₄·7H₂O in the bottoms as antioxidant, to provide THF free from peroxides and 2-hydroxy-THF.

Table 20. Summary of the crude Hub³(–Eg₈–OH)₃ (**59**) product mixture after 7 h of diafiltration by NMR.

	Mole ratio	Mole fraction	Weight fraction	Mass (g)
Hub ³ (–Eg ₈ –OH) ₃ (59)	1.0	0.56	0.88	1.11
HO–Eg ₄ –OTs (36)	0.6	0.33	0.11	0.14
2-hydroxy-THF	0.2	0.11	0.01	0.01

The NMR samples were recombined with the crude product mixture and diafiltration was restarted for another 9 h with no further MsOH added. Thus, after 16 h of combined diafiltration time, the apparatus was once more washed as described above to yield the product, Hub³(–Eg₈–OH)₃ (**59**) (0.948 g, 75 %) as a yellowish wax.

The following two chain extensions to Hub³(–Eg₁₂–OH)₃ (**61**) via Hub³(–Eg₁₂–OThp)₃ (**60**) and to Hub³(–Eg₁₆–OH)₃ (**63**) via Hub³(–Eg₁₆–OThp)₃ (**62**) were then carried out with several modifications. Firstly, the reactions were left stirring at 40 °C for 16 h overnight. Secondly, with diafiltration carried out immediately after the reaction, debris including salts, water and DMF were not removed by extraction but it was attempted to remove these via diafiltration. After quenching with NH₄Cl_(aq) (2 eq.), the reaction mixture was thus diluted with THF (20 mL) and was left standing for several minutes to allow what are presumably ammonium salts to crystallize. The solids are then removed by filtration over a small cellulose filter paper in a glass funnel and the filter paper carefully washed with THF (approx. 20 mL). The filtrate is then diluted with methanol (approx. 10 mL) to achieve a solution with a solvent ratio of 1:4 v/v MeOH:THF and with a total volume of around 50 mL which could be accommodated in the 100 mL

feed tank for nanofiltration. The quenched, filtered and diluted reaction mixture was then installed in place of the feed tank used for diafiltration preparation and the diafiltration started.

Diafiltrations towards $\text{Hub}^3(-\text{Eg}_{12}-\text{OH})_3$ (**61**) and $\text{Hub}^3(-\text{Eg}_{16}-\text{OH})_3$ (**63**) were run for 16 hours in total with MsOH added after 8 hours. Over 16 hours of diafiltration, samples were taken from both retentate loops and both permeate lines of the second stage approximately every 30 minutes until 02h:00min, every 60 minutes until 08h:00min and every 2 hours until 16h:00min. Samples from the 1st retentate loop were again diluted by factor of 10, but samples (500 μL) from the 2nd retentate loop were no longer diluted to eliminate a potential error during quantification of 2nd stage rejection. The loss of yield from sampling the second retentate loop is still low due to the much lower concentration of homostar in the 2nd retentate loop. Permeate samples from the second stage were taken undiluted.

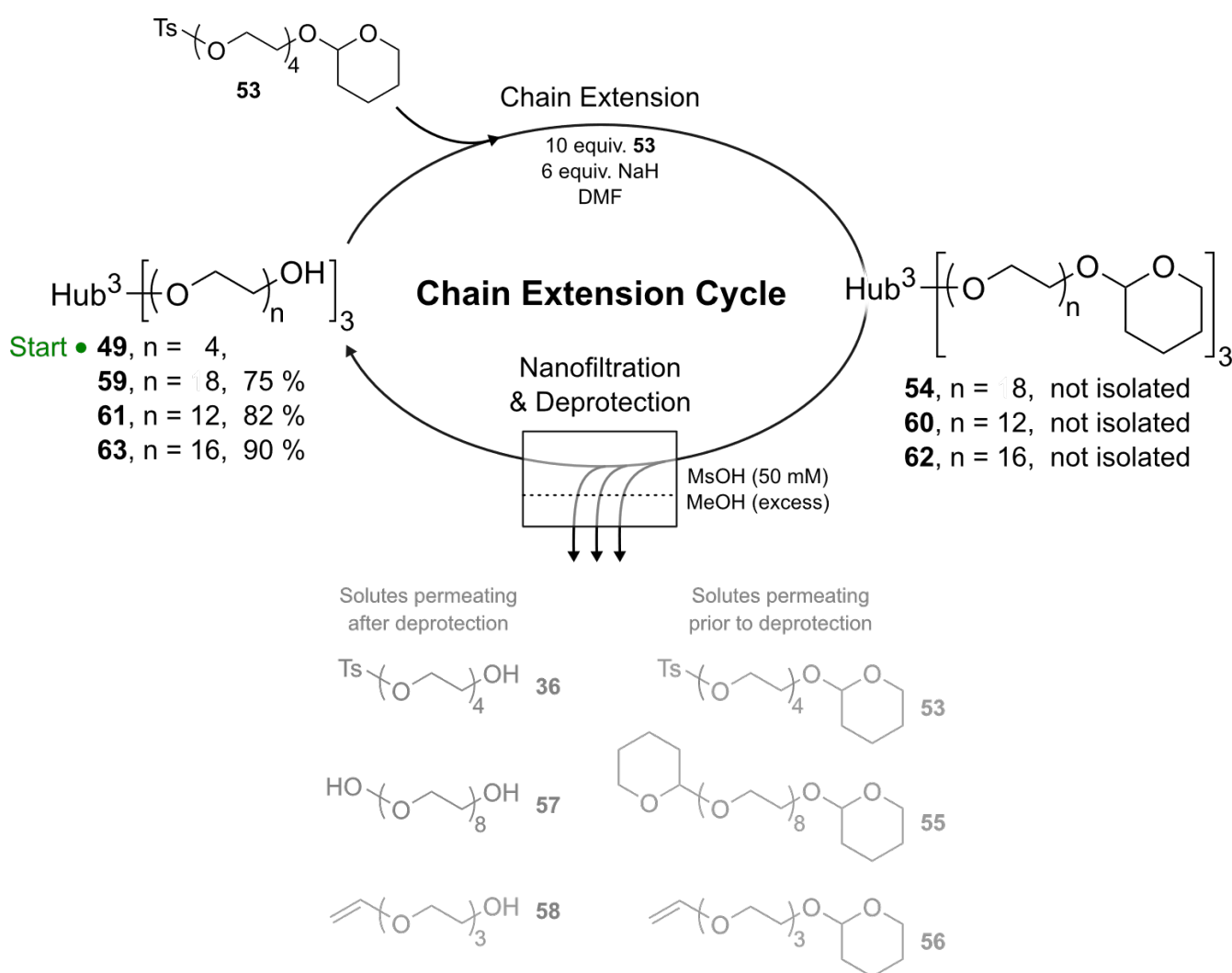


Figure 90. Trial synthesis of Eg_{16} with combined nanofiltration and diafiltration using Eg_4 building block.

After diafiltration to remove building block and debris, the isolated dry yields for $\text{Hub}^3(-\text{Eg}_{12}-\text{OH})_3$ (**61**) and $\text{Hub}^3(-\text{Eg}_{16}-\text{OH})_3$ (**63**) were 82 % and 90 % respectively with a summary of reaction parameters

given in Table 21. Over the three chain extensions, the flowrates during diafiltration were between 8.7 and 9.2 mL·min⁻¹ (8.4-8.8 L over 16 h), equivalent to a 23-fold system turnover for the diafiltration apparatus with a total volume of around 370 mL. An attempt was made at concentrating the permeate collected during the first 8 hours of diafiltration by evaporation of solvent and drying in vacuo. For the extensions to Eg₁₂ and Eg₁₆, 1.746 g and 1.126 g were recovered respectively as orange oils containing solids which solidified upon cooling at 4 °C.

Table 21. Reagent summary for etherification to Eg₁₆.

n	Hub ³ -Eg _n -OH			53		NaH ^[a]		DMF	Hub ³ -Eg _{n+4} -OH			Yield ^[b]
	g	g·mol ⁻¹	mmol	g	mmol	mg	mmol	mL	g	g·mol ⁻¹	mmol	%
4	0.863	1153.42	0.748	3.46	8.00	228	5.70	11	0.948	1682.05	0.564	75
8	0.875	1682.05	0.520	2.43	5.61	148	3.70	8	0.940	2210.69	0.425	82
12	0.861	2210.69	0.389	1.68	3.90	115	2.88	6	0.958	2739.32	0.350	90

[a] 60 wt% suspension in mineral oil.

[b] Isolated yield.

Diafiltration samples were analyzed by HPLC connected to a diode array detector and an electron light scattering detector as described on p. 153. With samples taken at least every few hours, the washing out of building block and debris could be confirmed. Using the chain extension from Eg₈ to Eg₁₂ as an example, the ELSD traces over the first 8 hours of diafiltration show the gradual decline of ThpO-Eg₄-OTs (**53**) building block between 0.5 h and 8.0 h (Figure 91, ●). Between 0.5 h and 4 h, the ThpO-Eg₈-OThp (**55**) dimer (Figure 91, ●) is also visible but ceases to be reliably detectable thereafter. The addition of MsOH for deprotection after 8 hours is apparent in the large spike of the solvent front peak eluting after 3 min (Figure 91, ●). The limit of detection for ThpO-Eg₄-OTs building block (**53**) is around 50-100 arbitrary units and, under the HPLC analysis conditions used (260 nm, 50 μL injection volume), is reached when approximately 95 % of the building block has permeated and only 5 % remains, which is around 8 h into the diafiltration and close to the time that MsOH is typically added. Deprotected building block, HO-Eg₄-OTs (**36**), and deprotected dimer, HO-Eg₈-OH (**57**), could therefore not usually be found after deprotection as they were under the detection limit. The vinyl ether elimination side-product from chain extension, ThpO-Eg₃-OCH=CH₂ (**56**) or its deprotected analogue, HO-Eg₃-OCH=CH₂ (**58**), were not detected throughout.

A comparison with the UV traces (260 nm) (Figure 92) reveals that the concentration of homostar remains relatively constant as expected, first in the protected state as Hub³(-Eg₁₂-OThp)₃ (**60**) (●) and then in the deprotected state as Hub³(-Eg₁₂-OH)₃ (**61**) (●). Due to the sampling interval between 8 h and 10 h and the relatively fast deprotection, the intermediate species Hub³(-Eg₁₂-OThp)₂(-Eg₁₂-OH)₁ (**60b**)

and $\text{Hub}^3(-\text{Eg}_{12}-\text{OThp})_1(-\text{Eg}_{12}-\text{OH})_2$ (**60c**) are not readily detected. But some Thp deprotection was visible in the form of doubly protected homostar species at the beginning of the diafiltration prior to addition of MsOH, and its peak area increases slightly with time. This is indicative of either insufficient rig washing with trace residual MsOH remaining from a prior run causing a small degree of deprotection, or membrane-catalyzed deprotection due to some sulfonic acid groups on the poly(ether ether ketone) polymer from sulfonation during membrane preparation.¹²¹ Partial deprotection would render impossible a re-run of the chain extension in the case of incomplete reaction detected after quenching and should be avoided, possibly by addition of a small quantity of organically soluble base. Lastly, the traces show that UV active solutes contained within the solvent front also permeate to a degree as the solvent front peak declines over time (Figure 92, ●).

A comparison with the UV traces collected at 300 nm (Figure 93) reveals the benefit of the conjugated system of Hub^3 possessing UV absorption at higher wavelength where all other solutes in the mixture cease to absorb. This allows a focus of all product homostar species which necessarily contain Hub^3 .

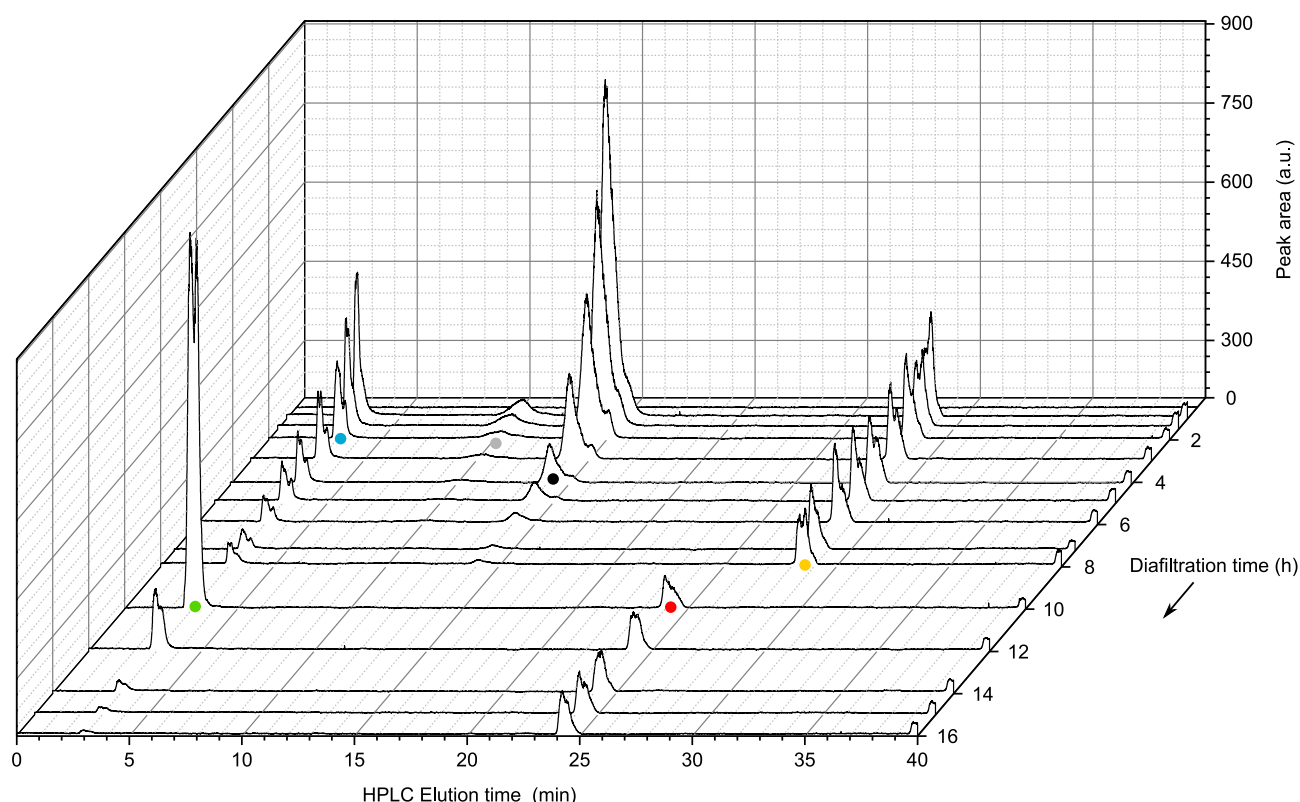


Figure 91. HPLC ELSD traces over 16 h of diafiltration after chain extension from Eg_8 to Eg_{12} . NaOTs (3 min, ●), MsOH (3 min, ●), ThpO- Eg_8 -OThp (**55**) (10.5 min, ●), ThpO- Eg_4 -OTs (**53**) (14.2 min, ●), $\text{Hub}^3(-\text{Eg}_{12}-\text{OH})_3$ (**61**) (24.2 min, ●), $\text{Hub}^3(-\text{Eg}_{12}-\text{OThp})_3$ (**60**) (28.5 min, ●).

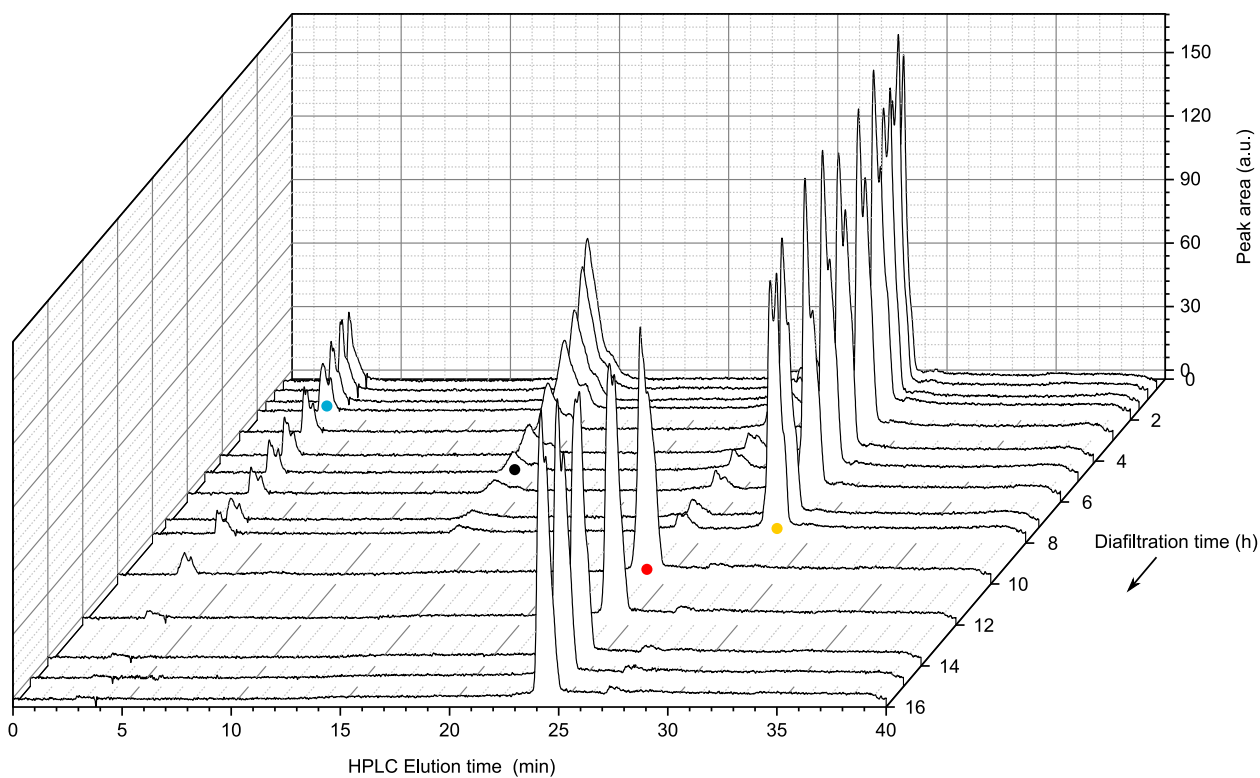


Figure 92. HPLC UV (260 nm) traces over 16 h of diafiltration after chain extension from Eg₈ to Eg₁₂. NaOTs (3 min, ●), ThpO–Eg₄–OTs (**53**) (14.2 min, ●), Hub³(–Eg₁₂–OH)₃ (**61**) (24.2 min, ●), Hub³(–Eg₁₂–OThp)₃ (**60**) (28.5 min, ●).

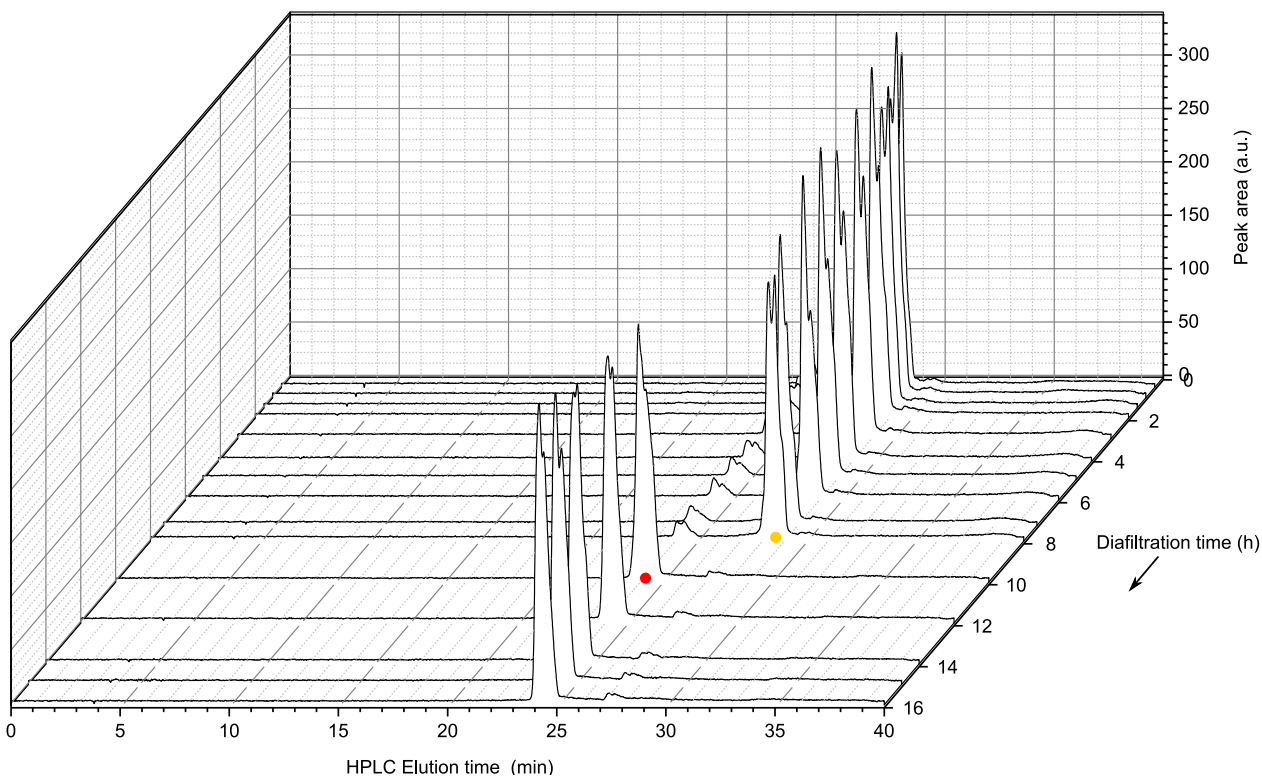


Figure 93. HPLC UV (300 nm) traces over 16 h of diafiltration after chain extension from Eg₈ to Eg₁₂. Hub³(–Eg₁₂–OH)₃ (**61**) (24.2 min, ●), Hub³(–Eg₁₂–OThp)₃ (**60**) (28.5 min, ●).

Integration of the peaks in the HPLC traces and normalizing these in relation to their maximum values, usually the starting peak areas, yields the familiar diafiltration traces (Figure 94, c.f. Figure 64). The exponential decay of the normalized peak areas for the UV traces at 260 nm of homostar and building block can be compared with Equation 25 to obtain an impression of the separation factor for this particular two-stage system under these process conditions. (The ELSD trace for ThpO–Eg₈–OThp (**55**) dimer in Figure 94b, was not calibrated and only serves as a qualitative guidance.)

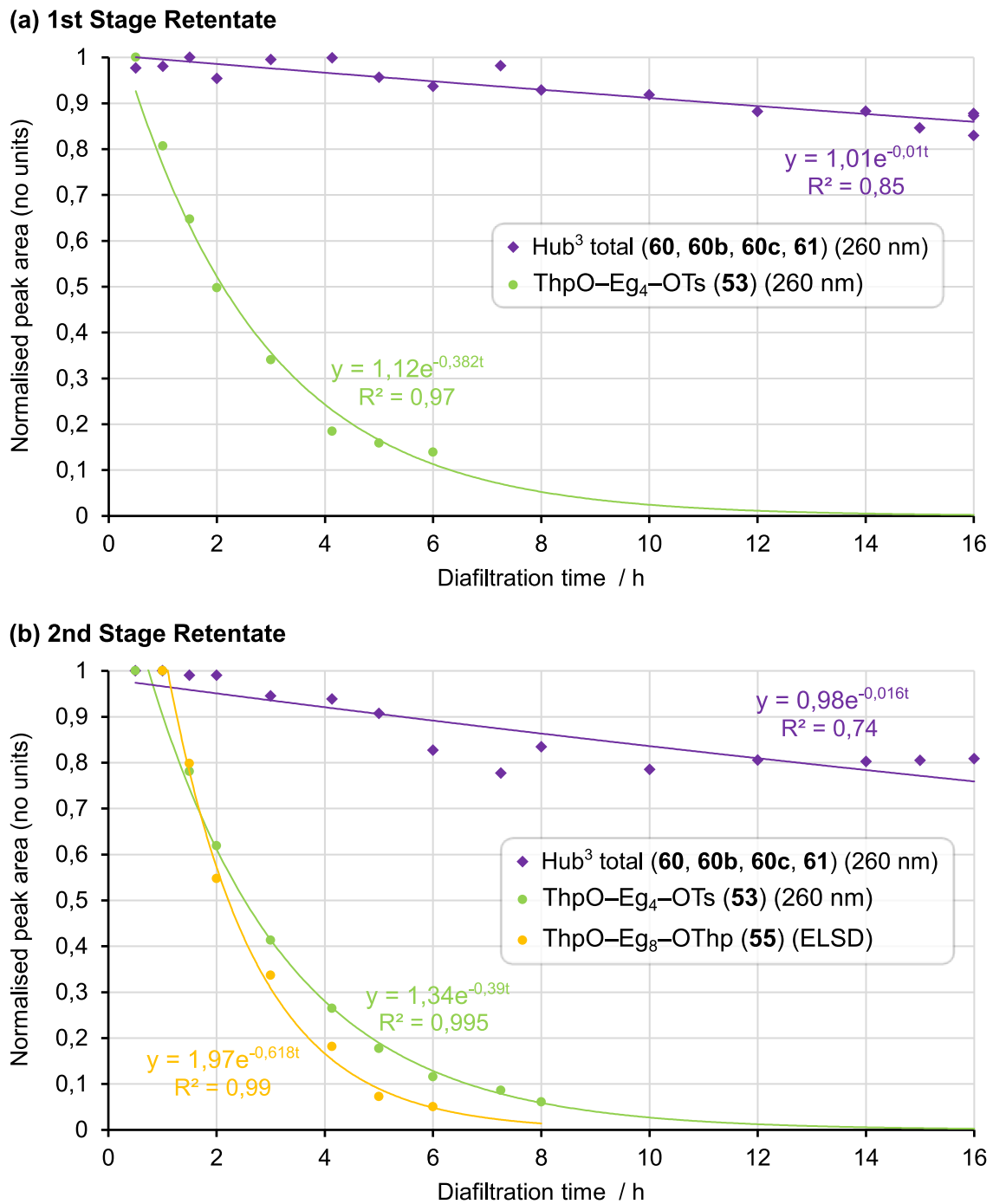


Figure 94. Normalized peak areas in the (a) 1st stage retentate and (b) 2nd stage retentate for diafiltration over 16 h during the chain extension cycle from Eg₈ to Eg₁₂.

Calibration of the UV traces for $\text{Hub}^3(-\text{Eg}_{12}-\text{OThp})_3$ (**60**) and $\text{Hub}^3(-\text{Eg}_{12}-\text{OH})_3$ (**61**) as well as $\text{ThpO}-\text{Eg}_4-\text{OTs}$ (**53**) revealed a linear relationship between UV absorption and concentration and translation of the peak areas into concentrations yields the concentration profiles (Figure 95).

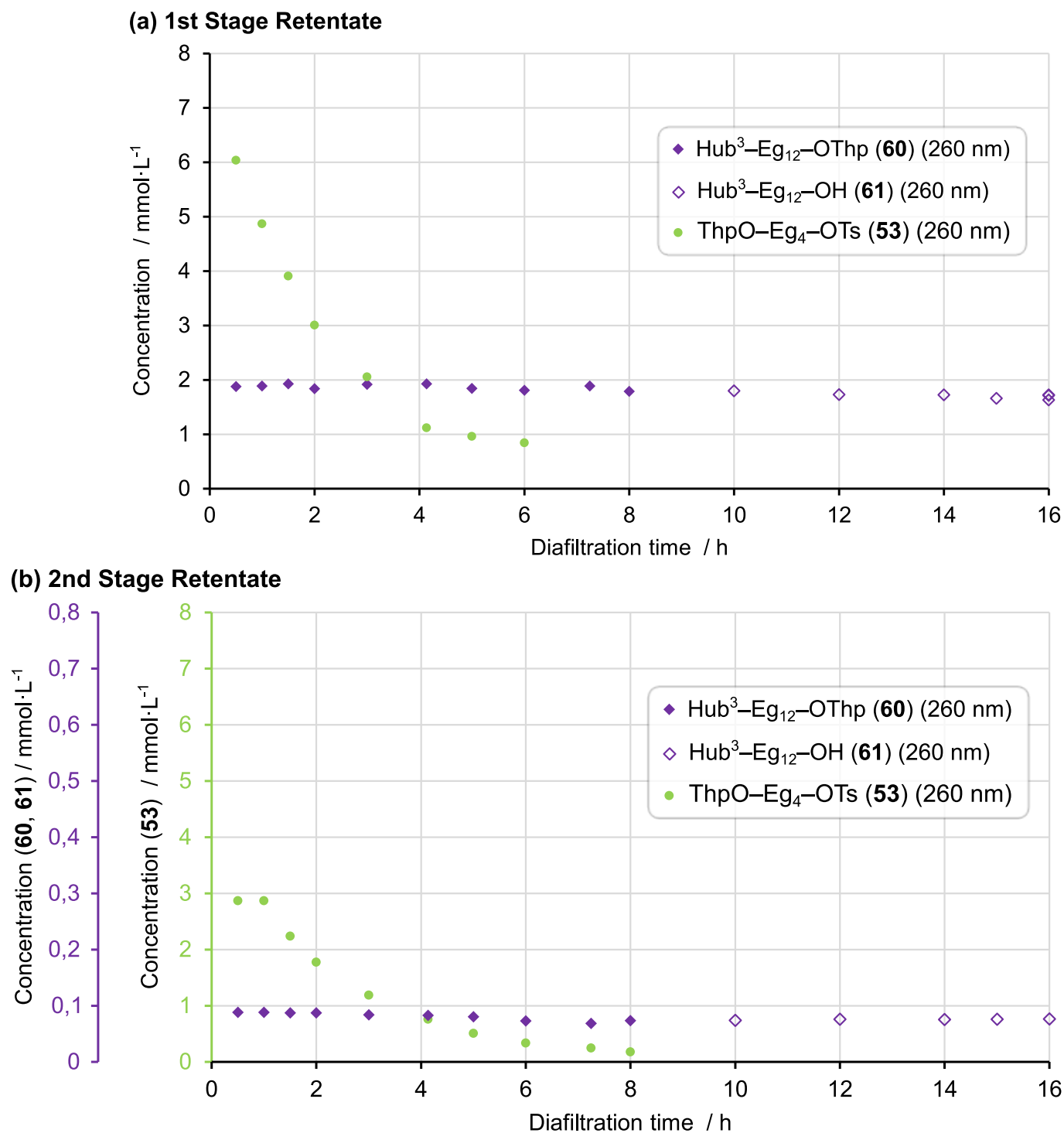
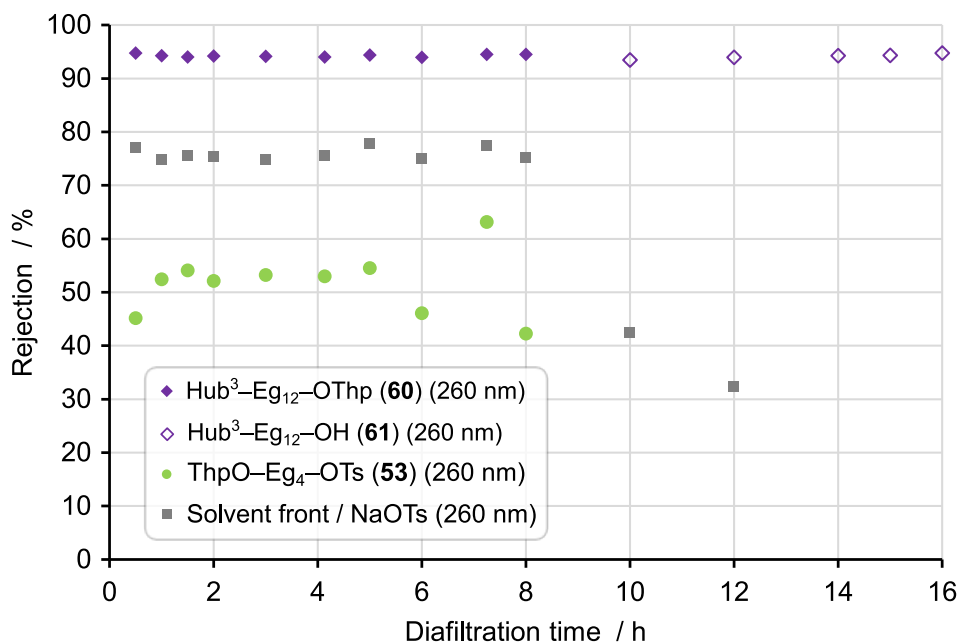


Figure 95. Concentration profiles in the (a) 1st stage retentate and (b) 2nd stage retentate for diafiltration over 16 h during the chain extension cycle from Eg_8 to Eg_{12} .

Lastly, a comparison of the 2nd stage retentate and 2nd stage permeate concentrations gave a good indication of the rejections in the second separation stage over the course of the diafiltration (Figure 96). It is apparent that homostar rejection remains constant and is thus unaffected by the addition of acid after 8 h. ThpO–Eg₄–OTs (**53**) building block rejection also remained constant within error and the data shows that solutes eluting with the solvent front, e.g NaOTs salts, can also be washed out during diafiltration, albeit more slowly than the building block due to their higher rejection.

(a) 2nd separation stage - Pressure housing cell 1 of 2



(b) 2nd separation stage - Pressure housing cell 2 of 2

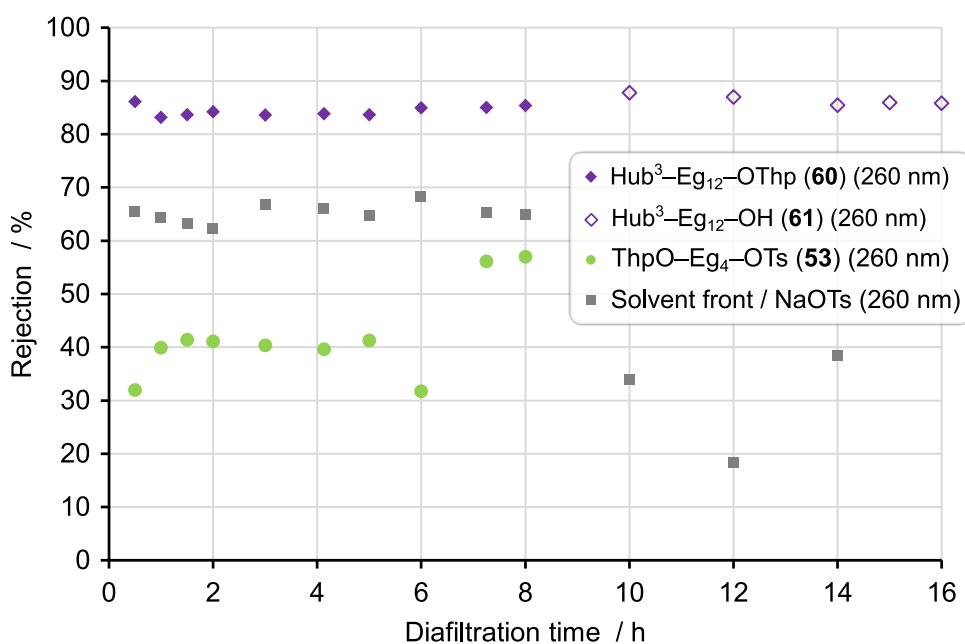


Figure 96. Rejections during diafiltration for the chain extension cycle from Eg₈ to Eg₁₂ separately recorded for the two pressure housing cells (a) 1 of 2 and (b) 2 of 2 in the 2nd separation stage.

The desired Eg_{16} homostar was ultimately obtained using combined diafiltration and deprotection in situ, but variable yields of the intermediates and brown coloration of the products suggested corrosion had occurred inside the nanofiltration apparatus. The mass spectra of the intermediates and the product $\text{Hub}^3(-\text{Eg}_{16}-\text{OH})_3$ (**63**) homostar further revealed substantial quantities of shortmer with multiples of Eg_4 building block missing. Because the reaction was run at 40 °C for 16 h overnight, incomplete or reversible deprotection of Thp was suspected as the cause.

For this reason, membrane purification and Thp deprotection were carried out separately for the final synthesis of Eg_{60} . It was apparent from the run towards Eg_{16} here that the PEEK membranes are capable of maintaining their rejection in the presence of acid and did not noticeably degrade in performance over the course of the experiments despite the harsh solvent environment of 1:4 MeOH-THF with occasional addition of 50 mM MsOH. The inability to synthesize Eg_{60} in this fashion was therefore attributed to the overall apparatus and process set-up rather than a systematic limitation of the PEEK membrane. Nevertheless, a comparison of the overall rejections, particularly for $\text{Hub}^3(-\text{Eg}_{12}-\text{OH})_3$ (**61**) between the two second stage pressure housing cells (Figure 96a versus Figure 96b) did reveal a discrepancy in rejection with the second cell performing about 10 percentage points lower across all solutes. A new set of PEEK membranes was therefore prepared for the synthesis of Eg_{60} .

3.3.6. Membrane re-screening for synthesis of Eg₆₀

For the final synthesis of uniform mono-methyl Eg₆₀, a slightly longer Eg₁₂ building block was used to increase the length gain per extension and diafiltration cycle, making Eg₆₀ attainable within four extension cycles. With the choice settled on a Thp protecting group and an OTs leaving group, the required Eg₁₂ building blocks, ThpO–Eg₁₂–OH (**66**) and ThpO–Eg₁₂–OTs (**67**), were prepared as follows: Excess tetragol (**1**) was desymmetrized by mono-protection with 3,4-dihydropyran as previously described to yield ThpO–Eg₄–OH (**33**), followed by two rounds of tosylation and unidirectional chain lengthening with excess tetragol (**1**) via ThpO–Eg₄–OTs (**53**), ThpO–Eg₈–OH (**64**) and ThpO–Eg₈–OTs (**65**) to yield the desired Eg₁₂ building blocks. Particular care was taken to fully separate from the Eg₁₂ building blocks all oligomeric impurities, both shortmers (-Eg₄) and dimers (ThpO–Eg₁₂–OThp, ThpO–Eg₂₀–OThp), although -Eg₁ could not be separated.

For the synthesis of Eg₆₀, two new batches of PEEK membranes (one acetone-dried, one EtOH-dried) were prepared. From each batch, 8 flat-sheet coupons were installed in pressure housing cells for screening. All eight samples were screened in a single stage set-up (p. 148) for quality control with the goal of realigning the pressure housing cells containing the six most selective membranes into a two-stage diafiltration set-up thereafter. To obtain a complete dataset of rejections, both protected and deprotected species were screened as a mixture: Hub³(–Eg₁₂–OThp)₃ (**60**) and ThpO–Eg₁₂–OTs (**67**) as well as Hub³(–Eg₁₂–OH)₃ (**61**) and deprotected Eg₁₂ building block, HO–Eg₁₂–OTs (**68**). The eight pressure housing cells were tested in series under recirculation (2.4 L·min⁻¹) at different pressures (10, 20 and 30 bar) in a total recycle set-up in THF-MeOH 4:1 (v/v).

With acetone-dried PEEK membranes, the first generation Eg₁₂ homostar with Hub³ exhibited high rejection in both protected and deprotected states ($\mathbb{R}_{60} = 96.1\%$, $\mathbb{R}_{61} = 96.6\%$), while protected (**67**) and deprotected building block (**68**) were retained to a lesser extent as desired ($\mathbb{R}_{67} = 72.4\%$, $\mathbb{R}_{68} = 74.8\%$) at 30 bar (see Figure 97). Although a choice was made to perform diafiltration and deprotection separately during synthesis of Eg₆₀, the similar separation factors of 7.7 and 8.1 suggest that separation should be feasible in both the protected and the deprotected state respectively.

As expected, the EtOH-dried PEEK membranes exhibited higher rejection overall and afforded homostar rejection around 99 % ($\mathbb{R}_{60} = 99.2\%$, $\mathbb{R}_{61} = 99.3\%$ at 20 bar) and building block rejection around 80 % ($\mathbb{R}_{67} = 78.4\%$, $\mathbb{R}_{68} = 81.5\%$ at 20 bar) (Figure 98), equivalent to a separation factor of over 20, more than twice as high when compared to the acetone-dried PEEK membranes. When looking to attain high yields in a diafiltration it is usually preferable to have a product rejection close to 100 % than to have an impurity rejection close to 0 %.⁸²

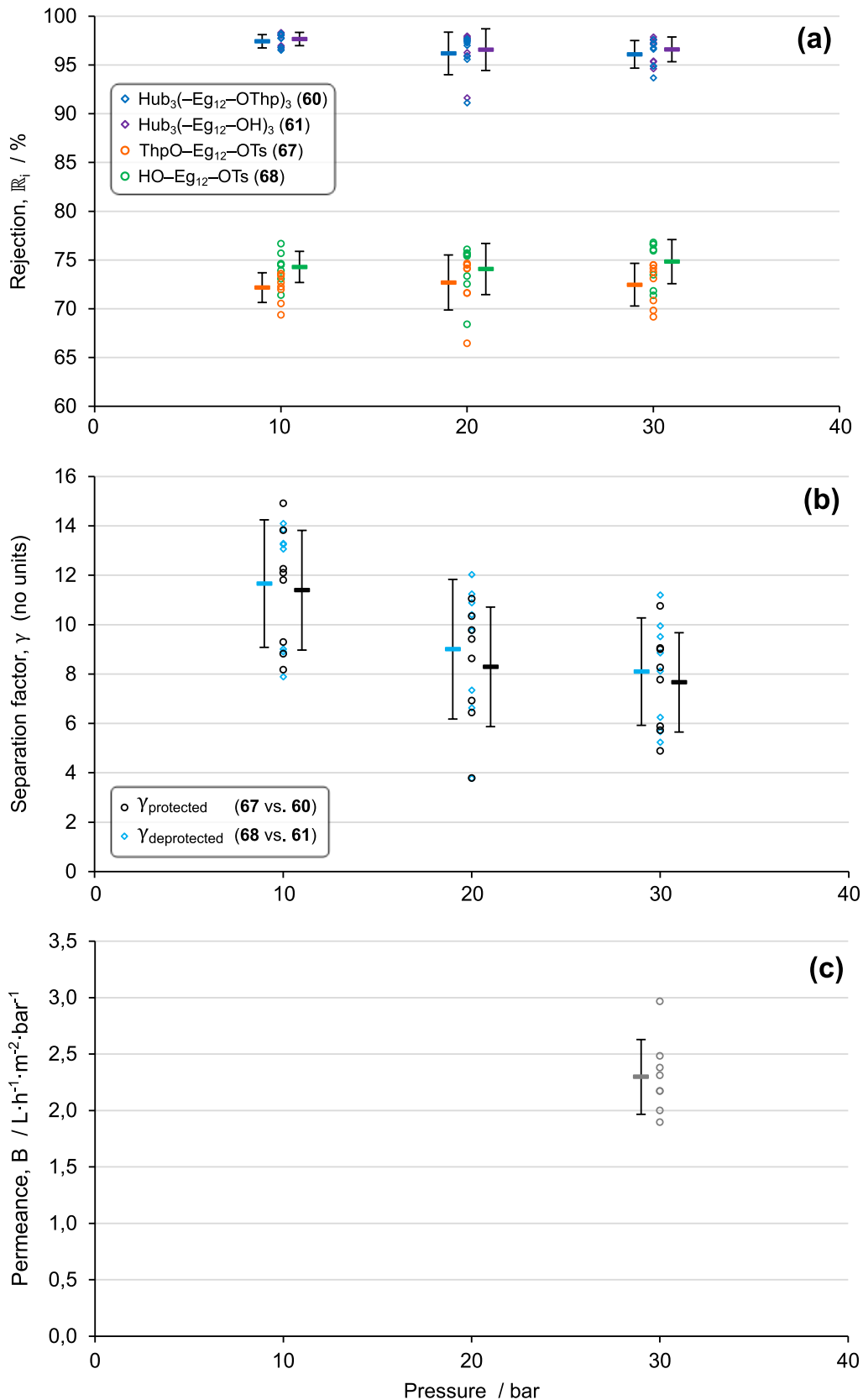


Figure 97. Screening of acetone-dried PEEK membranes (8 samples) in 1:4 v/v MeOH-THF at 10-30 bar. (a) Rejections and (b) separation factors of Eg_{12} homostars and building blocks in the protected and deprotected state alongside (c) permeance. The arithmetic mean (thick dashes in colour of the dataset) and standard deviation (black error bars) are shown.

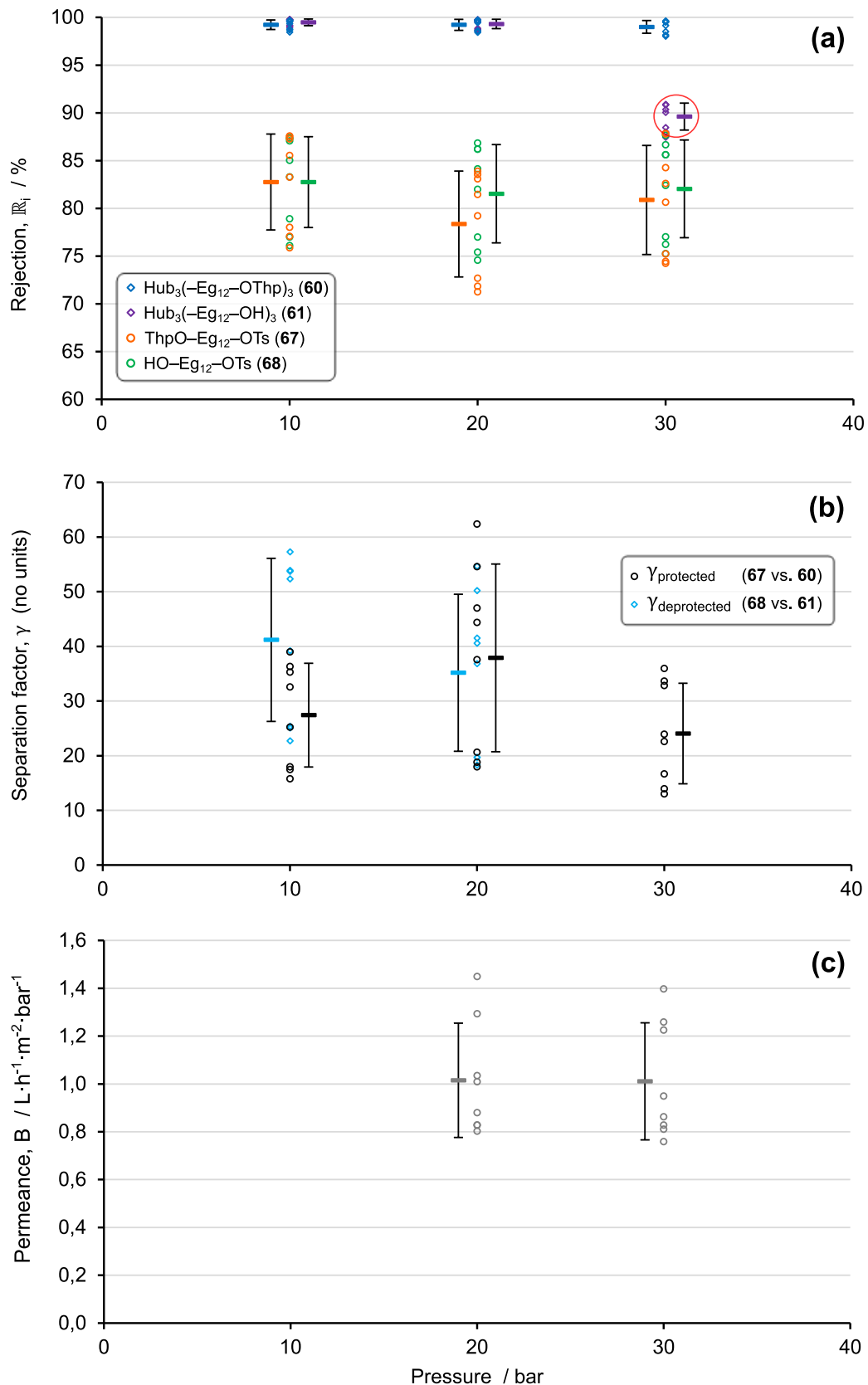


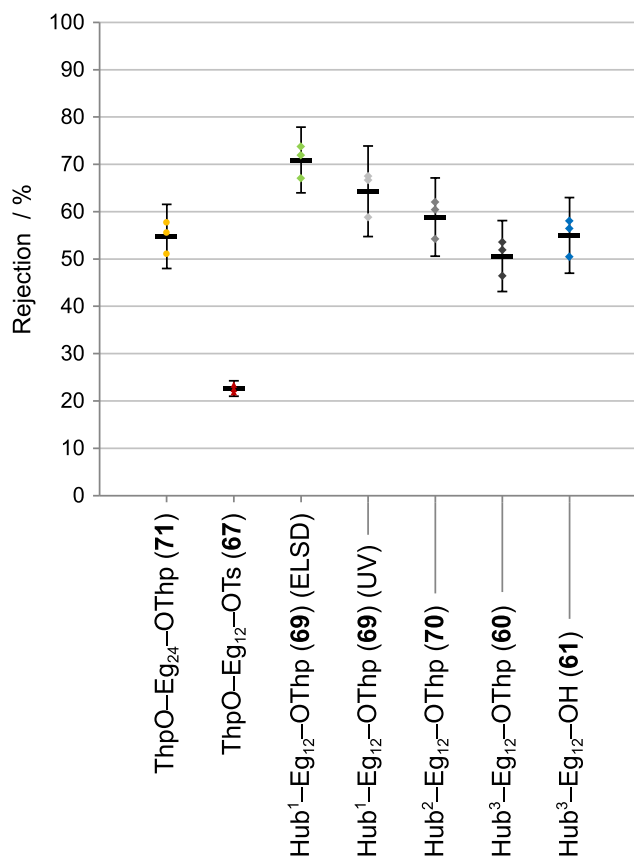
Figure 98. Screening of EtOH-dried PEEK membranes (8 samples) in 1:4 v/v MeOH-THF at 10-30 bar. (a) Rejections and (b) separation factors of Eg_{12} homostars and building blocks in the protected and deprotected state alongside (c) permeance. The arithmetic mean (thick dashes in colour of the dataset) and standard deviation (black error bars) are shown. (R_{61} at 30 bar is an outlier.)

However, with their higher overall rejection, the EtOH-dried membranes also exhibited correspondingly lower permeance, less than half the permeance as the acetone-dried membranes, $1.0 \text{ L}\cdot\text{h}^{-1}\cdot\text{m}^{-2}\cdot\text{bar}^{-1}$ compared to $2.3 \text{ L}\cdot\text{h}^{-1}\cdot\text{m}^{-2}\cdot\text{bar}^{-1}$ respectively. Combined with the higher impurity rejection, this meant that diafiltrations with the EtOH-dried would have taken much longer, approximately 1 week instead of 16 h with the available membrane area which was deemed prohibitively long. This exemplifies the dilemma which was previously explained for two selectivity scenarios in Figure 64. To make use of the EtOH-dried membrane, more membrane area would have been required to carry out the diafiltration in a similar timeframe and the separation would have required more solvent. (The EtOH-dried membranes were nevertheless tried out during the first extension to Eg_{24} but a low degree of leakage from the apparatus meant that the theoretical separation factor could not be attained in practice with a long diafiltration.)

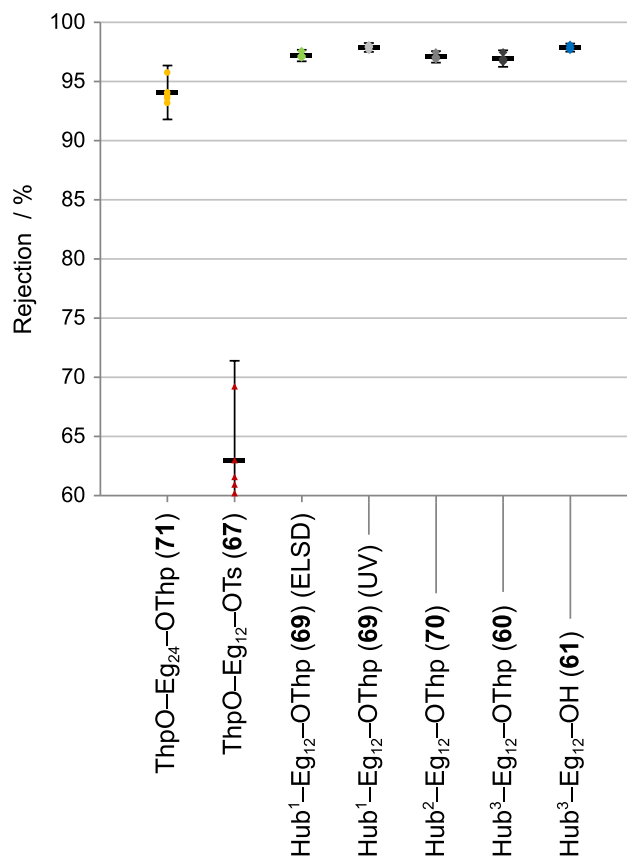
A re-screening was then performed with an updated set of PBI membranes due to concerns over $\text{ThpO}-\text{Eg}_{24}-\text{OThp}$ (**71**) dimer rejection and to verify whether the difference between Hub^1 , Hub^2 and Hub^3 persists for longer chain lengths. For this purpose, Eg_{12} homostars of Hub^1 and Hub^2 were synthesized: $\text{Hub}^1(-\text{Eg}_{12}-\text{OThp})_3$ (**69**) and $\text{Hub}^2(-\text{Eg}_{12}-\text{OThp})_3$ (**70**). Since the first screening of the Eg_4 homostar, an updated poly(ether)amine functionalized PBI membrane¹²⁵ had become available within our research group and was used instead of the original PBI membranes. Two different grades of the updated PBI membrane were prepared, one functionalized with Jeffamine M-600 and one functionalized with Jeffamine M-2005, a looser and a tighter type of membrane respectively. The membranes were tested in slightly different solvent systems, once pure MeOH and once 1:1 v/v MeOH-MeCN and the screening results for these membranes are shown in Figure 99 below. It is apparent that the loose Jeffamine M-600 functionalized PBI membrane (PBI18-DBX-(M-600)) is not suitable for the desired separation with rejections of all species below 80 % (Figure 99a). For the Jeffamine M-2005 functionalized PBI membranes (PBI18-DBX-(M-2005)), rejections of all hub species were similar around 97 % with a much lower rejection of building block around 65 %, equivalent to a separation factor of around 12 (Figure 99b). However, $\text{ThpO}-\text{Eg}_{24}-\text{OThp}$ (**71**) dimer rejection was very high at around 94 %, equivalent to a separation factor of only 2 with respect to the homostar product. Notably, the order of rejection for Hub^1 to Hub^3 was also reversed with these PBI membranes, with $\text{Hub}^1-\text{Eg}_{12}-\text{OThp}$ (**69**) exhibiting the highest rejection (c.f. Figure 84) which is indicative of a significant influence of polar interaction on selectivity.

The acetone-dried PEEK membranes shown in Figure 99c exhibited the expected trend of increasing rejection with increasing hub size in 1:4 v/v MeOH-THF. Compared to PBI18-DBX-(M-2005) in 1:1 v/v MeOH-MeCN, $\text{Hub}^3-\text{Eg}_{12}-\text{OThp}$ (**60**) exhibited similar rejection, while the other two hubs were rejected to a lesser extent. Rejection of $\text{ThpO}-\text{Eg}_{12}-\text{OTs}$ (**67**) was slightly higher, around 70 %, but at a low enough level to result in very similar selectivity. But similar to the PBI membranes, $\text{ThpO}-\text{Eg}_{24}-\text{OThp}$ (**71**) dimer rejection was high around 91 %, a selectivity slightly above 2 with respect to homostar.

(a) PBI18-DBX-(M-600), pure MeOH, 10 bar



(b) PBI18-DBX-(M-2005), 1:1 MeOH-MeCN, 10 bar



(c) PEEK Acetone-dried, 1:4 MeOH-THF, 20 bar

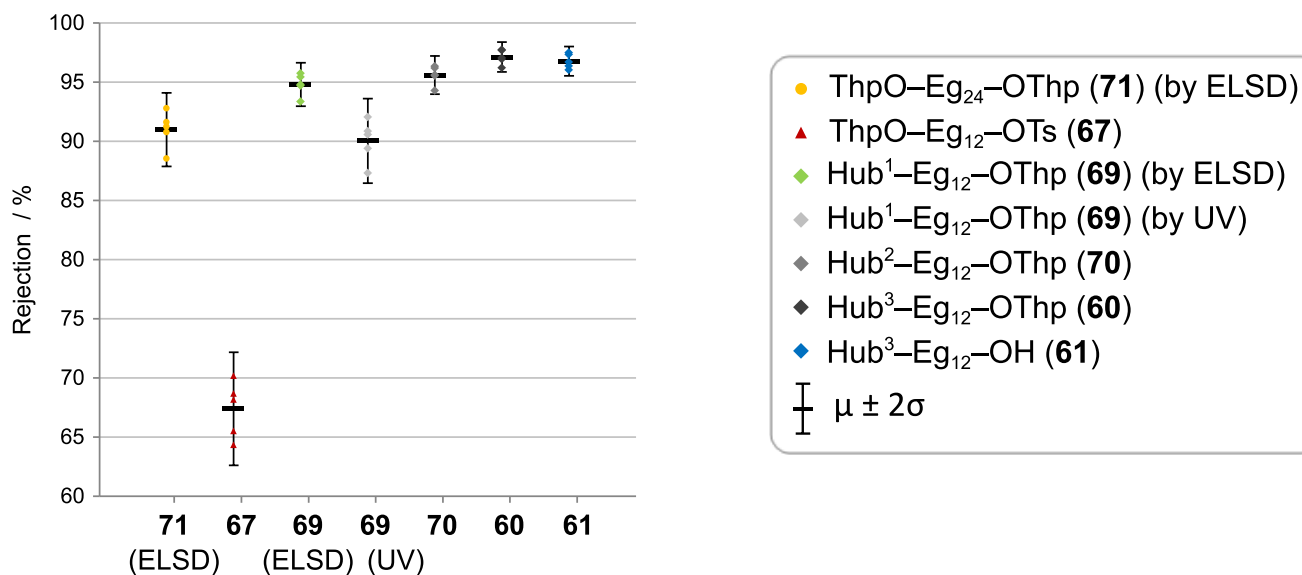


Figure 99. Rejections of ThpO-Eg₁₂-OTs (67) building block and ThpO-Eg₂₄-OThp (71) dimer alongside Eg₁₂ homostars of Hub¹, Hub² and Hub³ on (a) Jeffamine M-600 modified PBI in pure MeOH at 10 bar, (b) Jeffamine M-2005 modified PBI in 1:1 MeOH-MeCN at 10 bar and on (c) acetone-dried PEEK in 1:4 MeOH-THF at 20 bar. All species were measured by UV at 260 nm, except the dimer which was quantified with ELSD and Hub¹-Eg₁₂-OThp (69) which was quantified with both methods for comparison. (a) and (b) show different y scales.

It should be noted that quantification via an ELSD, a non-linear method requiring calibration, is fraught with some difficulty as exemplified by the difference in measured rejection by ELSD and UV for Hub¹–Eg₁₂–OThp. Either way, rejection of the dimer is high, and selectivity for its removal low when compared to the removal of building block. It is therefore critical that dimer formation is reduced to a minimum. Also, the concept of deprotection before or during diafiltration should be re-examined in further work, to determine whether the dimer exhibits lower rejection and thus better selectivity at the deprotected stage. A comparison between protected (**60**) and deprotected (**61**) Hub³–Eg₁₂ shows that rejection of the homostar should be similar. Lastly, selectivity should increase as the rejection of the homostar rises with increasing PEG chain length.

3.3.7. Synthesis of Eg₆₀ on Hub³ with ThpO–Eg₁₂–OTs building block

Detailed experimental information for this section is provided in the experimental chapter 5 on p. 214.

Several obstacles to the integration of nanofiltration into the iterative synthesis of uniform PEG oligomers had now been overcome to bring about an integrated process ready for trial. Selected for use were an Eg₁₂ building block with Thp as the acid labile protecting group and tosylate as leaving group, as well as Hub³ as the hydrogenolytically cleavable homostar core to improve homostar rejection and traceability. Purification was to involve diafiltration in a two-stage apparatus with separation carried out in the protected state using acetone-dried PEEK membranes with 1:4 v/v MeOH:THF as diafiltration solvent, followed by deprotection of the Thp acetal and extraction to remove deprotection debris. With all components in place, the trial synthesis of an Eg₆₀ oligomer could commence.

An Eg₁₂ building block was first constructed, with a tetrahydropyranyl (Thp) acetal protecting group in place of a dimethoxytrityl ether in order to reduce building block size, increase atom efficiency and improve membrane permeation of the building block. Excess tetragol (**1**) was desymmetrized by mono-protection with 3,4-dihydropyran, followed by two cycles of tosylation and unidirectional chain lengthening (Figure 100, i-iii). The resultant building block, ThpO–EG₁₂–OH (**66**), was then bound to the trivalent hub (**43d**) (Figure 100, iv). By tying three growing oligomers into a homostar, a branched, high molecular weight product is obtained which can be better distinguished from the building block by a membrane. The trivalent hub also improves traceability and protects one end of the growing PEG throughout subsequent chain extension cycles and permits heterobifunctionalization towards the end of the synthesis.

Each coupling cycle consists of chain extension by reaction of a ThpO–EG₁₂–OTs (**67**) building block with the unprotected chain termini of a PEG-homostar, followed by nanofiltration, and finally Thp deprotection (Figure 100, vi-vii, v).

Synthesis of the Eg₆₀ chain initiated via Williamson etherification of the first generation homostar, Hub³–Eg₁₂–OH (**61**) with 10 eq. ThpO–EG₁₂–OTs (**67**) (Figure 100, i). After quenching, the crude mixture contained second generation homostar, Hub³–Eg₂₄–OThp (**72**), alongside residual building block **67** as well as various salts (NaOTs, NH₄Cl, NaCl) and solvent (DMF, H₂O). In addition, building block dimer ThpO–Eg₂₄–OThp (**71**) had formed, due to the reaction of **67** with traces of hydroxide. Although present in relatively small amounts, this dimer is the largest species apart from homostar, presenting a significant separation challenge.

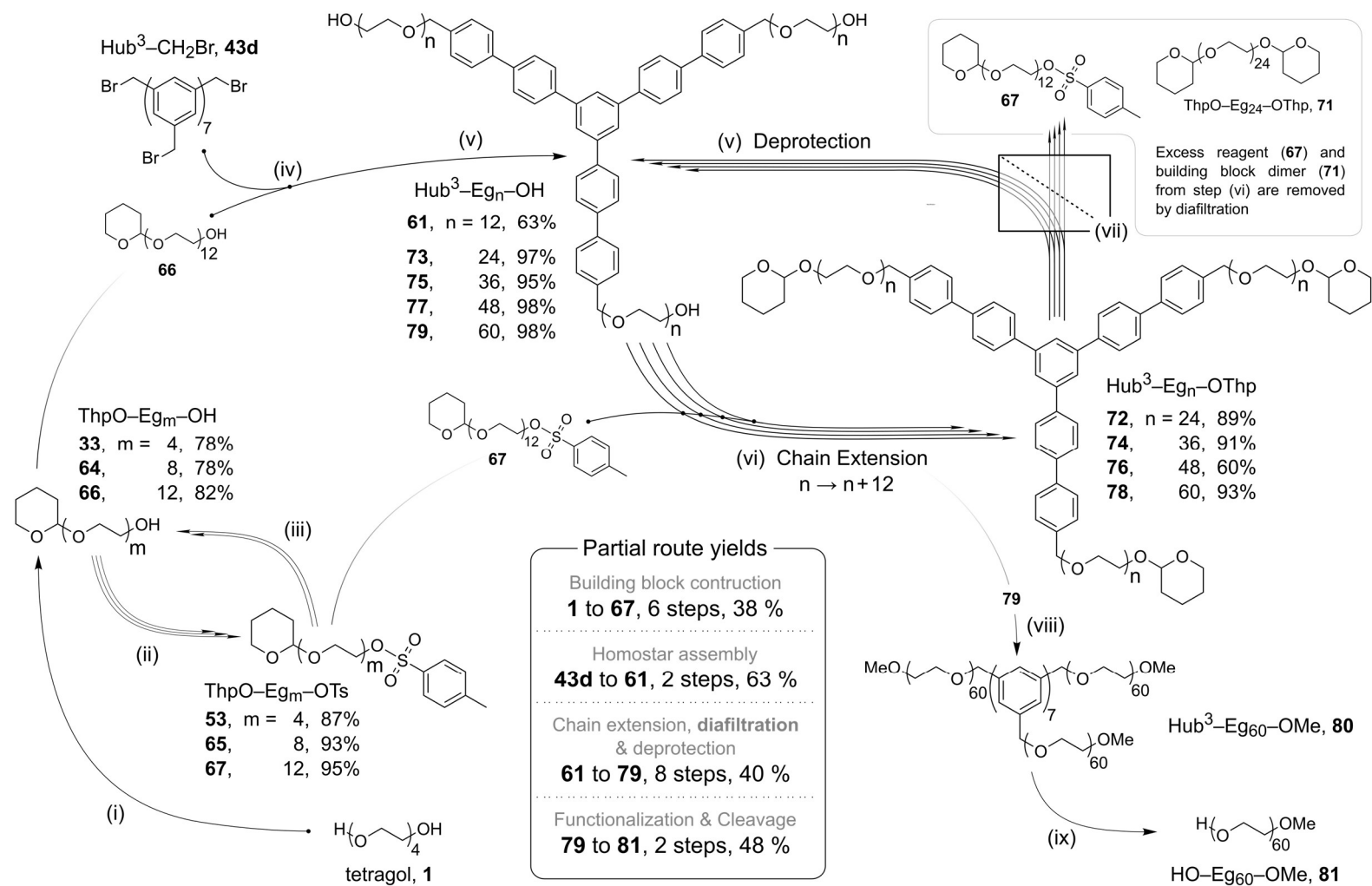


Figure 100. Membrane enabled synthesis of uniform HO-Eg₆₀-OMe (**81**) from Eg₄ starting material (**1**): (i) Desymmetrizing protection: 3,4-dihydropyran, 5 eq. **1**, MsOH, CH₂Cl₂ (ii) Leaving group activation (3 cycles): 1.3 eq. TsCl, 2 eq. Et₃N, CH₂Cl₂ (iii) Building block lengthening (2 cycles): 5 eq. **1**, 2 eq. NaH, THF (iv) Hub attachment: **43d**, 3.5 eq. **66**, 3.5 eq. KO^tBu, THF, 10 min, then (v) 80 mM MsOH, MeOH (vi) Chain extension (4 cycles): 10 eq. **67** (3.3 per arm), 6 eq. NaH, DMF (vii) Membrane purification of chain extension mixture, then (v); (viii) Functionalization: MeI, NaH, DMF (ix) Hub cleavage: Pd/C prepared in situ¹³⁸, H₂, MeOH, 1 atm.

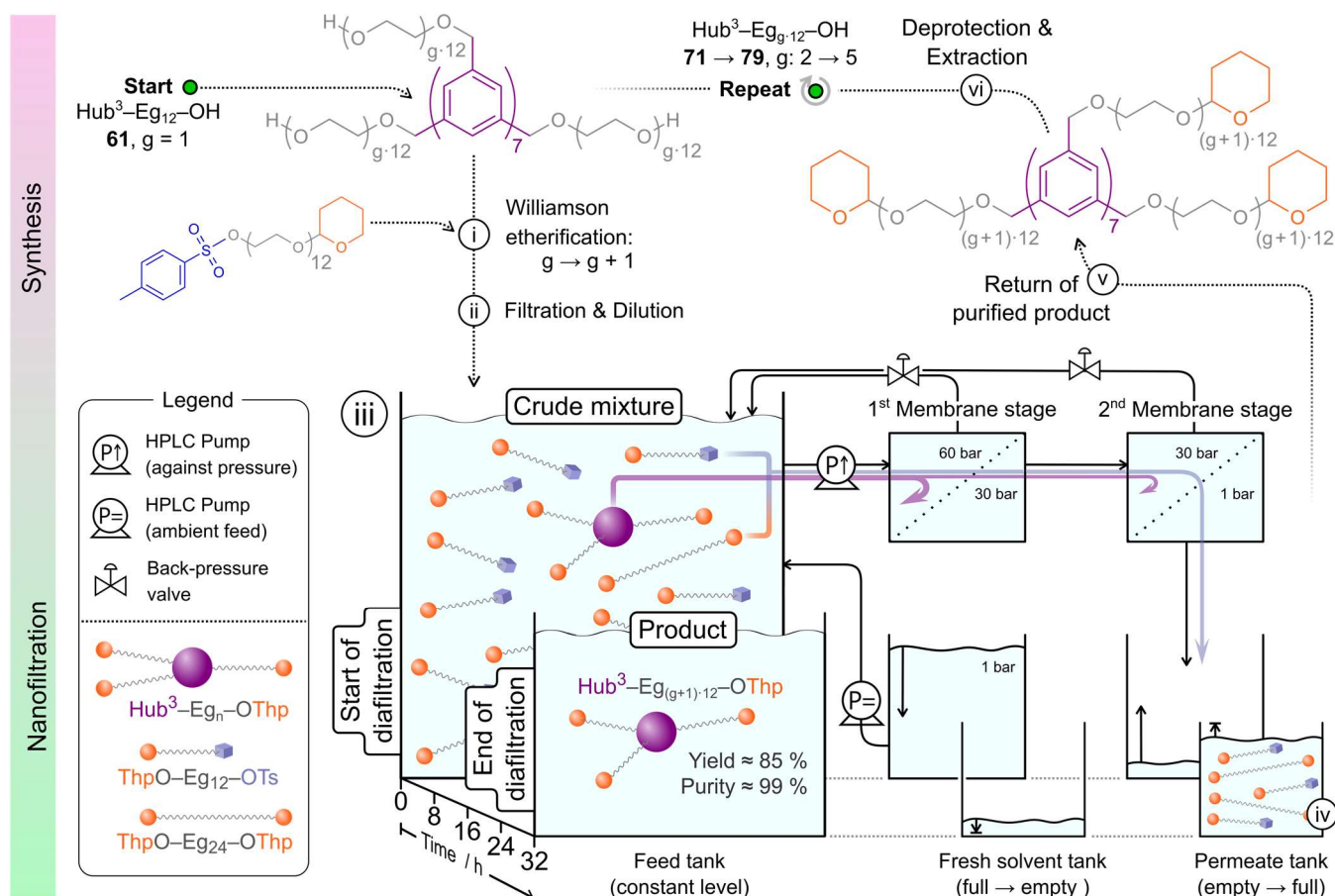


Figure 101. Iterative synthesis of consecutive homostar generations, $\text{Hub}^3\text{-Eg}_{g\cdot 12}\text{-OH}$ (**71** to **79**), starting from $\text{Hub}^3\text{-Eg}_{12}\text{-OH}$ (**61**) ($g = 1$) via nanofiltration. A chain extension cycle consists of (i) chain extension of deprotected homostar via Williamson etherification to yield the next generation homostar ($g \rightarrow g+1$), (ii) quenching of the reaction mixture, filtering to remove salts and dilution into 1:4 v/v MeOH-THF, (iii) diafiltration in a two-stage nanofiltration apparatus for 32 h, with (iv) excess building block (**67**) and dimer (**71**) removed as permeate, (v) washing of the purified, protected homostar from the apparatus and concentration (89-93 % isolated yield) and finally (vi) deprotection to yield the homostar triol ready for another cycle of chain extension.

Before commencing membrane purification of **72**, the crude mixture was first diluted with THF, then filtered to remove salts which had crystallized, and the mixture then made up to 1:4 v/v MeOH-THF, and transferred to the feed tank of the nanofiltration apparatus. The crude mixture was fed into the 1st stage of the diafiltration unit at elevated pressure to provide the driving force for filtration. Because homostar rejection is <100 % (Figure 97), two membrane stages were used in series to improve system selectivity and minimize yield loss of homostar to the permeate tank. In the two-stage apparatus, the permeate from the 1st membrane stage thus passes into a 2nd membrane stage for further purification and only the permeate from the 2nd stage flows into the permeate tank.¹¹¹ Throughout the diafiltration, fresh solvent is continuously fed into the feed tank, exactly balancing the volume of solvent lost through the 2nd membrane stage as permeate, to maintain the system volume constant.

As the impurities are washed from the system, their concentrations in each stage, as well as the overall system, follow an exponential decay (Figure 102). After 32 hours of diafiltration, the product mixture was drained from the feed tank and the retentate sides of both membrane units washed thoroughly and the resultant dilute mixture concentrated. PEG homostar was isolated with a yield of 89-93 % by dry weight and with over 99 % building block removal. The recovery of PEG homostar compared favourably with chromatographic purification and increased slightly with each subsequent cycle as the product homostar grew larger. In preparation for the next synthesis cycle, purified **72** was deprotected and the debris removed by extraction.

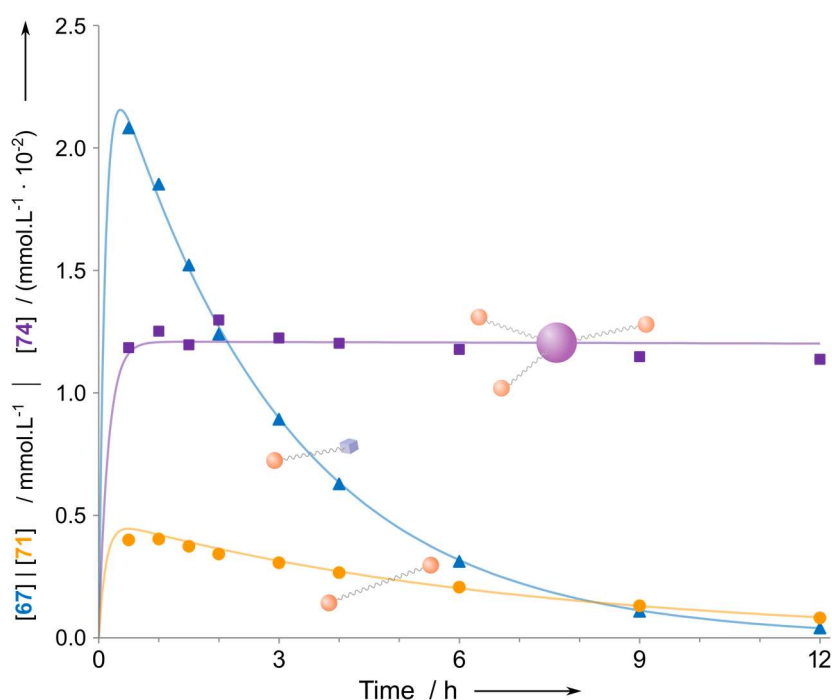


Figure 102. Concentrations during diafiltration on the retentate side of the 2nd membrane stage of Hub³-Eg₃₆-OThp product (**74**), ThpO-Eg₁₂-OTs building block (**67**) and ThpO-Eg₂₄-OThp dimer (**71**) over the first 12 hours of diafiltration.

Three further cycles of chain extension and membrane purification afforded Hub³-Eg₆₀-OH (**79**) in acceptable overall yield (40 % from **61**). Methylation of the chain termini gave Hub³-Eg₆₀-OMe (**80**) and was followed by hydrogenolytic cleavage of the three PEG chains from the central hub (Figure 100, viii-ix). Uniform HO-Eg₆₀-OMe (**81**) was obtained with excellent oligomer purity (97.1 %) and dispersity ($\mathcal{D} = 1.00057$) (Figure 103).

MALDI-ToF mass spectrometry was used to monitor the accumulation of chain errors with each successive generation of PEG homostar (Figure 103). The impurity profile was consistent with the defects expected from this synthesis and purification strategy. $[M - \text{Eg}_1]$ and $[M + \text{Eg}_1]$ were the most abundant impurities and derive from traces of trigol and pentagol in the tetragol (**1**) starting material, although depolymerization has also been suggested as a potential contributor to shortened oligomers.

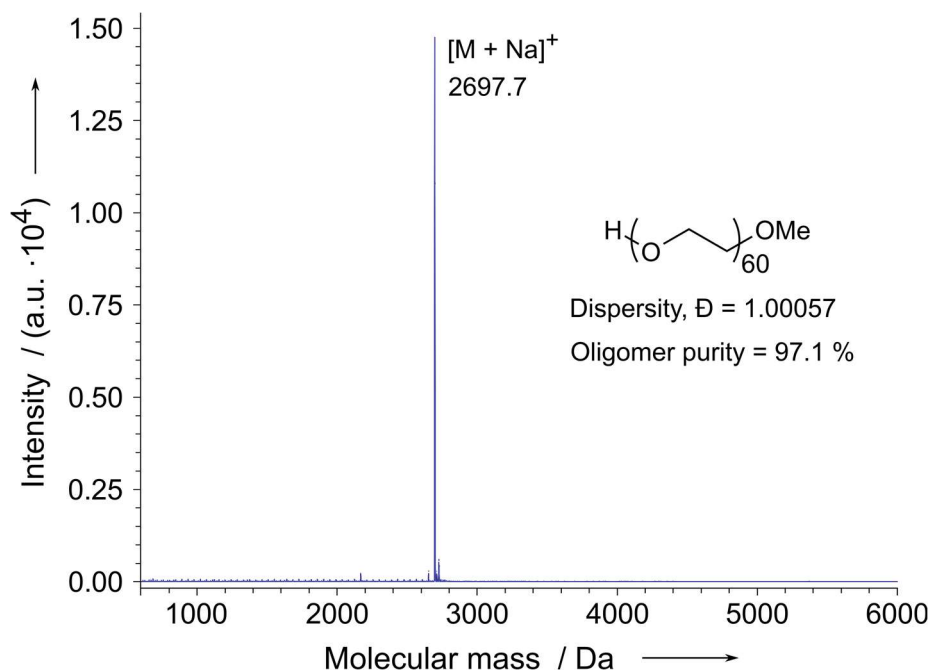


Figure 103. MALDI-ToF spectrum of mPEG-2700 (HO-Eg₆₀-OMe, **81**) with 97.1 % Eg₆₀, 1.5 % Eg₅₉ and 1.5 % Eg₄₈.

Apart from these, [M - Eg₁₂] is the main chain length impurity, but HPLC analysis suggests that the chain extension reactions were complete. Inspection of the ¹³C NMR of the deprotected homostars instead revealed a trace of incomplete Thp deprotection in some cases; chains bearing residual Thp acetals will not be available for chain extension during the next cycle. [M - Eg₂₄] and [M - Eg₃₆] could have arisen for similar reasons, but the higher intensity signal for the latter is inconsistent with this. Instead, it is most likely that [M - Eg₃₆] has arisen from incomplete washing of the diafiltration apparatus, leading to contamination of one generation of homostar with its predecessor. Lastly, the [M + Eg₁₂] is not thought to derive from premature deprotection of the building block during storage or handling, but rather because diafiltration is only continued up to around 99 % purity. Thus traces of residual **67** will be deprotected alongside the homostar to give HO-Eg₁₂-OTs (**68**), and this will then be available to react during the next cycle of Williamson etherification, leading to a small degree of double coupling.

The isotope distribution of the intermediate homostars (**72** to **80**) and the final HO-Eg₆₀-OMe (**81**) product was consistent with the expected theoretical isotope distribution.

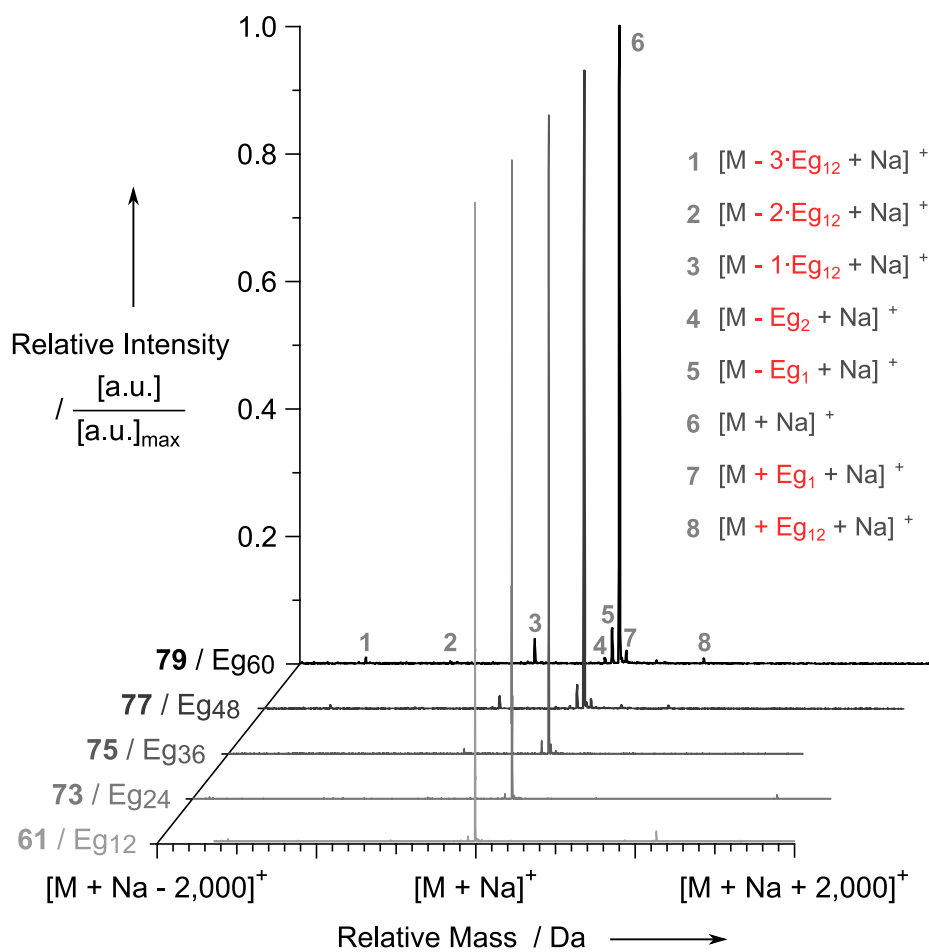


Figure 104. MALDI-ToF of consecutive homostar generations, **61 – 79**. Stack centred on molecular ion to highlight distribution of chain length impurities.

Table 22. Comparison of high oligomer purity PEGs.

n	R ¹ ≠ R ²	Oligomer Purity / %	D	Source
24	no	96 ^[a]	1.0001	Maranski et al. ³⁵
24	yes	100	1	Loiseau et al. ³²
28	no	100 ^[c,d]	1.000002	Polypure AS
48	yes	75 ^[c,d]	1.001	Quanta BioDesign, Ltd.
48	no	98	1.00002	French et al. ⁴²
56	yes	92	1.0003	Szekely et al. ³
60	yes	97 ^[c]	1.0006	This work (81)
64	yes	87 ^[b]	1.0004	Zhang et al. ²⁸

In several cases, oligomer purity could not be verified independently because mass spectrometry data were [a] not published or [b] not available over a sufficient range. [c] These samples were analyzed at the EPSRC UK National Mass Spectrometry Facility at Swansea University. [d] Commercial sample.

3.4. Conclusion

High purity uniform PEGs may be prepared on a three-arm hub support using nanofiltration, an efficient liquid phase purification technique. It was demonstrated that the selectivity of the separation can be improved by tailoring the building block from which the PEG chains are assembled, and the hub on which the oligomers are grown. Tetrahydropyranyl was confirmed to be a superior choice of protecting group in a nanofiltration set-up due to its smaller size and sufficient stability. In conjunction with an acid-compatible PEEK membrane, the Thp group may be deprotected inside the nanofiltration apparatus to provide a further process improvement and reduce all separations required during a chain extension cycle into a single diafiltration.

While sufficient separation of the homostars and building block species was demonstrated in multiple membranes systems, the formation of building block dimer was identified as a major concern due to its high rejection and low selectivity for removal. It is likely that an eventual optimized process would need to minimize dimer formation and improve its removal through the membrane, e.g. by using a membrane that can successfully permeate the diol at the deprotected stage.

Overall, the synthesis of uniform mono-methoxy PEG-2,700 (HO–Eg₆₀–OMe) with excellent quality (dispersity $\bar{D} = 1.00057$, oligomer purity = 97.1 %) was successfully accomplished in a two-stage diafiltration cascade. The results presented here suggest that this method can be driven to both greater oligomer lengths, and that it is scalable to manufacturing operations, both of which are key advantages. This membrane-enhanced iterative synthesis strategy may therefore potentially allow preparation of uniform PEG towards pharmaceutically relevant lengths above 5,000 Da which are not currently available and is compatible with the preparation of heterobifunctional PEGs bearing a range of functionalities at either end of the PEG chain, a much desired feature during PEGylation.

In principle, this homostar-based strategy should be extensible to other polymers where protecting group chemistry can be employed to add building blocks sequentially to provide high precision materials. One direction in which the diafiltration process can yet be improved is the use of further successive stages for separation and mitigating the high solvent consumption during diafiltration.

4. Chapter 4: Solvent recovery during diafiltration

The content of this chapter has been published in the form of a journal article⁹⁷ and the central narrative will be reproduced here. For the underlying experimental data and additional details, please also consult the relevant publication.

- Schaeperstoens, M.; Didaskalou, C.; Kim, J. F.; Livingston, A. G.; Szekeley, G., Solvent recycle with imperfect membranes: A semi-continuous workaround for diafiltration. *Journal of Membrane Science* **2016**, 514, 646-658.

The experimental set-up and acquisition of data including screening was performed by C. Didaskalou at the University of Manchester. All other work related to the manuscript was performed by the author.

The idea behind the manuscript stemmed from earlier work with Kim et al.¹²³

- Kim, J. F.; Szekeley, G.; Schaeperstoens, M.; Valtcheva, I. B.; Jimenez-Solomon, M. F.; Livingston, A. G., In Situ Solvent Recovery by Organic Solvent Nanofiltration. *ACS Sustainable Chemistry & Engineering* **2014**, 2 (10), 2371-2379.

4.1. Introduction

Diafiltration is an attractive batch technique for separating multi-component mixtures in the pharmaceutical industry because it can be carried out under mild conditions at ambient temperature. It relies on a pressure gradient as the driving force and requires no phase change. When compared to alternative separation techniques, such as distillation, diafiltration like most other membrane processes is less energy intensive. But, diafiltration processes consume large quantities of solvent. Because impurities are rinsed through the membrane with solvent as carrier, an equal volume of solvent needs to simultaneously be fed into the system. Diafiltrations therefore require replenishment of many multiples of the system volume with fresh solvent. As a result, the main operating cost of a diafiltration is usually attributed to solvent consumption and related disposal cost and recovery of said solvent is thus a target for optimization.

The high solvent consumption during diafiltration is one limitation of the aforementioned strategy towards uniform PEG not yet tackled and is a problem closely related to the selectivity of the membrane used. As previously described, the separation factor for a diafiltration (Equation 22) usually increases as the rejection of the product approaches 100 %, even if the impurity rejection increases at the same time. A diafiltration with high selectivity is therefore usually tighter and has higher overall rejection and correspondingly lower permeance. The combination of higher impurity rejection and lower solvent

permeance cause diafiltrations to take longer and require much more fresh solvent. The increase in diafiltration time can be compensated for by increasing the membrane area (provided the system volume remains similar). The higher solvent use on the other hand is a strict necessity for an impurity with higher rejection because more washing solvent is then needed to wash all impurity through the membrane (Equation 25). Overall, solvent recovery is therefore desirable, particularly for separations in which the product is valuable and highly selective membranes with correspondingly high impurity rejections are required to attain high yields. The practical implications of high yielding but solvent intensive membranes were previously clarified (Figure 63 and Figure 64).

The problem is directly applicable to the synthesis of Eg₆₀, where two PEEK membranes were potentially available, an acetone-dried membrane (Figure 97) with lower selectivity and an EtOH-dried version with higher selectivity (Figure 98). Ultimately, the lower selectivity membrane was chosen due to a lack of sufficient membrane area to carry out the separation in a reasonable timeframe, but also recognizing the need for far higher volumes of fresh solvent.

Common techniques for solvent recovery in the wider membrane field include non-selective adsorption of the impurities,^{100,115} hybrid distillation¹⁰⁴ or hybrid chromatography¹³⁹ processes, as well as recovery solely through a membrane.^{49,100,106,140–143} Where only membranes are used for solvent recovery, a common problem is the inability of most OSN membranes to fully retain an impurity. Particularly when impurities are very small, e.g. < 200 Da, their rejection is usually below 100 %, resulting in a “leaky” solvent recovery stage. In some hybrid applications this can be acceptable, e.g. where solvent is recycled to extraction, but for stand-alone diafiltration it is usually not. When solvent is recycled from a leaky solvent recovery stage back into the separation stages of a diafiltration in a closed-loop set-up, it carries impurity with it as a result (Figure 105). This can become limiting for a diafiltration when the impurity separated out by the separation is simultaneously reintroduced through the return flow from the recovery unit.

In order to enable solvent recovery with membranes that cannot always fully retain the impurity, a diafiltration set-up was developed in which the impure mixture of the solvent recovery stage is purged and replaced with fresh solvent when the leaky solvent recovery stage becomes limiting for the diafiltration. This set-up should also be a useful upgrade for the diafiltration-based synthesis of Eg₆₀ described in 3.3.7 and could also open up the possibility of using membranes that were described as high-yielding but solvent intensive in Figure 63 on page 140.

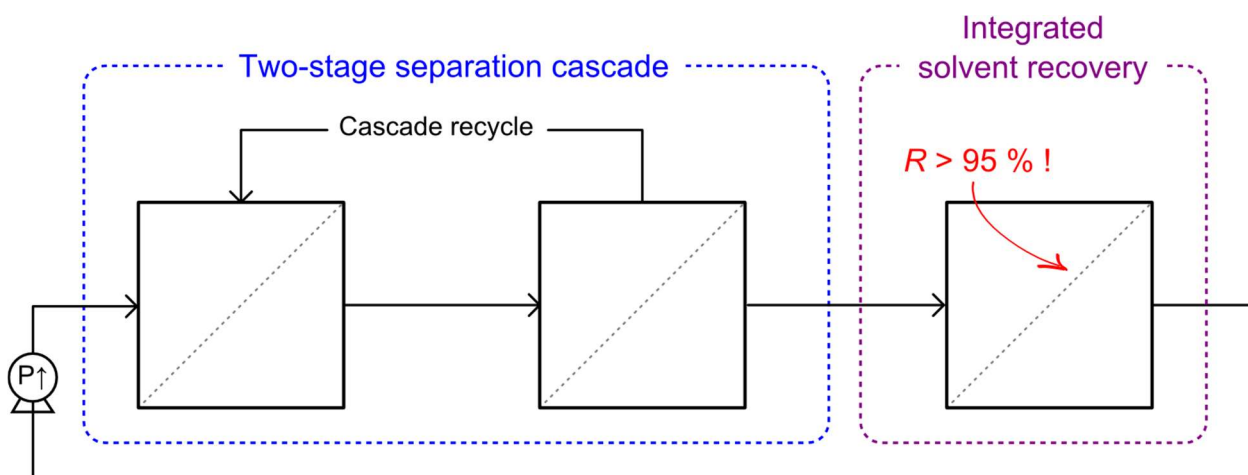


Figure 105. Closed-loop diafiltration set-up with a two-stage separation cascade and an integrated solvent recovery unit. Rejection of the impurity in the solvent recovery unit is high but not perfect (100 % > $R > 95\%$).

Model system

It was intended to demonstrate the viability of this work-around in general terms with a challenging, small impurity and the synthesis of dibenzo-18-crown-6 (**84**) from catechol (**82**) and bis(chloroethyl) ether (**83**) was therefore selected as a model system (Figure 106). For reasons of safety, bis(chloroethyl) ether (**83**), a chemical closely resembling mustard gas, was not investigated and the focus of the investigation thus lay on the separation of catechol (**82**) from dibenzo-18-crown-6 (**84**).

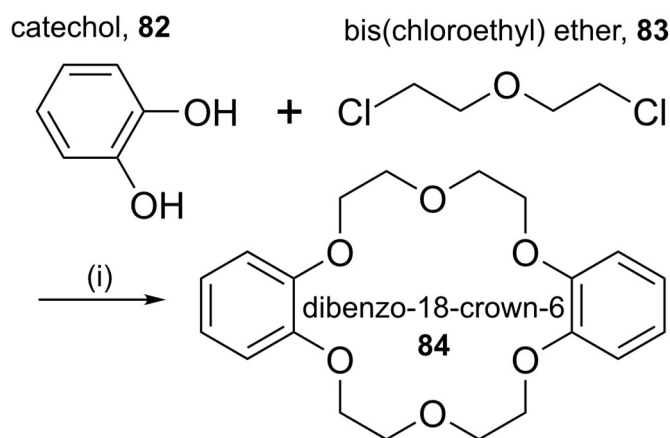


Figure 106. Synthesis of dibenzo-18-crown-6 from catechol and bis(chloroethyl) ether. (i) base, e.g. NaOH, NaH, solvent, e.g. THF, and elevated temperature. Reproduced from ¹¹⁴.

4.2. Materials and methods

4.2.1. Process set-up

A complete flow sheet for the set-up used for this study is shown in Figure 107. The set-up is conceptually very similar to the diafiltration apparatus described in Section 3.2.3, although the exact membrane areas and flowrates differ. The 1st separation stage is liquid-pressurized directly by the HPLC pump from the feed tank and the 2nd and 3rd stage are each pressurized indirectly by the permeate of the preceding stage. Unlike the two-stage diafiltration apparatus described previously, this apparatus includes a third stage as a solvent recovery stage which is fed with the permeate from the 2nd separation stage. The solvent recovery stage has no recycle flow and only one outlet in the permeate flow back to the feed tank.

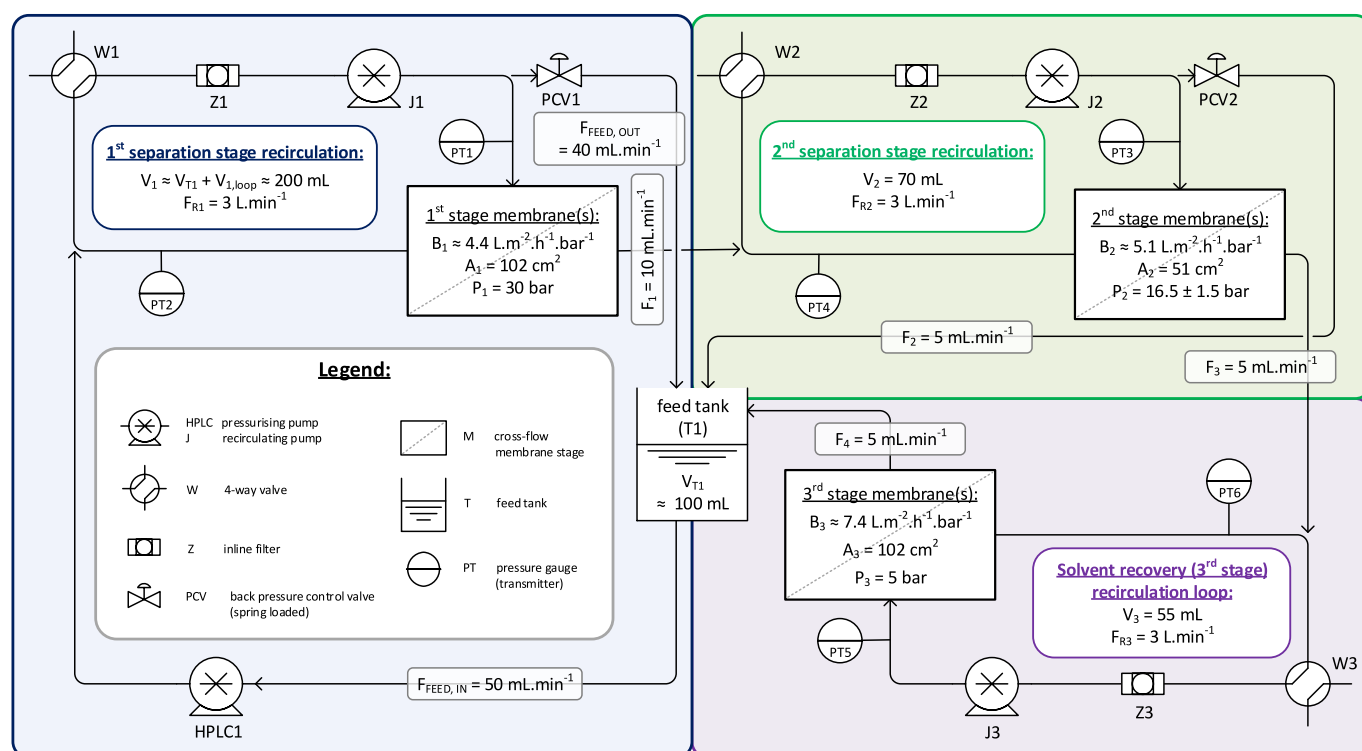


Figure 107. Process flow sheet of a two stage diafiltration cascade with integrated recovery. The 1st stage (blue), 2nd stage (green) and solvent recovery stage (purple) are all interconnected. Reproduced from ¹¹⁴.

Used in this solvent recovery study were transmembrane pressures of 15 bar, 13.5 bar and 4 bar in the 1st separation stage, 2nd separation stage and 3rd solvent recovery stage respectively. A recycle ratio (r_{21}) of 0.5 is used (Equation 30), corresponding to permeate flow rates of 10 mL·min⁻¹ and 5 mL·min⁻¹ in the 1st and 2nd stage respectively.

Lastly, the permeate flow from the 2nd separation stage is fed into stage 3, the solvent recovery unit. The solvent recovery stage pressure is not independently controlled by a relief valve but is directly determined by the 2nd stage permeate flowrate in relation to the 3rd stage membrane area. The membrane area in stage 3 needs to therefore be chosen to achieve a suitable pressure. The 3rd stage permeate is then returned to the feed tank to complete the closed-loop set-up.

Stage pressures are monitored upstream (PT1, PT3, PT5) and downstream (PT2, PT4, PT6) of the membrane units and the recirculation pumps (J1 – J3) are protected against particulates by inline filters (Z1 – Z3).

4.2.2. Mathematics

It follows from the set-up described in Section 4.2.1 and Figure 107 that the flows between the stages are interdependent as described in Equation 32.

$$\dot{V} = \frac{F_1}{\left(\frac{1}{1-r_{21}}\right)} = \frac{F_2}{\left(\frac{r_{21}}{1-r_{21}}\right)} = F_3 = F_4$$

Equation 32

With the assumption that the feed tank and 1st stage are well-mixed, they can be considered one volume with one concentration ($V_1 = V_{T1} + V_{1loop}$). By means of Equation 32, the mass balances of the complete process flow sheet (Figure 107) can therefore be condensed into the mathematical model in Figure 108.

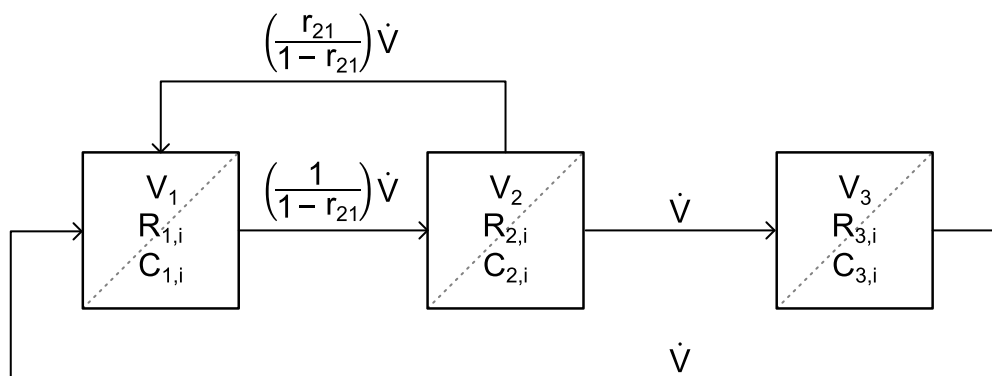


Figure 108. Simplification of the flowsheet to the minimum required for mathematical modelling. $C_{s,i}$ and $R_{s,i}$ denote the concentrations and rejections of component i in stage s and V_s denotes the volume of stage s . $s = 1,2,3$; $i =$ catechol, crown ether. \dot{V} denotes the volumetric flowrate through the system and r_{21} denotes the recycle ratio as defined in Equation 30. Reproduced from ¹¹⁴.

For a dilute system, where rejections are constant and not a function of concentration, the following set of equations applies:

$$\begin{aligned}
\text{Stage 1: } \frac{dC_{1,i}}{dt} &= \frac{\dot{V}}{V_1} \left(-\frac{1}{1-r_{21}} \cdot C_{1,i} \cdot (1-R_{1,i}) + \frac{r_{21}}{1-r_{21}} C_{2,i} + C_{3,i} \cdot (1-R_{3,i}) \right) \\
\text{Stage 2: } \frac{dC_{2,i}}{dt} &= \frac{\dot{V}}{V_2} \left(+\frac{1}{1-r_{21}} \cdot C_{1,i} \cdot (1-R_{1,i}) - \frac{r_{21}}{1-r_{21}} C_{2,i} - C_{2,i} \cdot (1-R_{2,i}) \right) \\
\text{Stage 3: } \frac{dC_{3,i}}{dt} &= \frac{\dot{V}}{V_3} \left(+ C_{2,i} \cdot (1-R_{2,i}) - C_{3,i} \cdot (1-R_{3,i}) \right)
\end{aligned}$$

Equation 33

4.2.3. Membranes

Nine different membranes from four different sources were used in this solvent recovery study. Seven membrane types were acquired: PEEK PI 300 (referred to as PI-PEEK) from Novamem LLC (Zürich, CH), GMT-NC-1, GMT-oNF-1 and GMT-oNF-2 from GMT Membrantechnik GmbH (Rheinfelden, DE) and SS010206, SS010306 and SS030306 from SolSep BV (Apeldoorn, NL).

Cross-linked and non-cross-linked polybenzimidazole (PBI) membranes (referred to as 20PBI and 20PBI.X respectively) were produced in-house. The PBI membranes described here were adapted from Valtcheva et al.^{123,124} by Szekely et al.^{144,145} and differ from the membranes used in prior chapters.

A set of 9 different membranes (Figure 109) was screened for rejection of catechol and the crown ether. While several membranes were suitable for the separation stages with separation factors varying between 10 and 50, only the PI-PEEK membrane (Novamem, CH) was very suitable with an impurity rejection of 98.4 %. The GMT-NC-1 had just sufficient impurity rejection of around 95 % but a prohibitively low flux in acetone ($< 0.2 \text{ L} \cdot \text{m}^{-2} \cdot \text{h}^{-1} \cdot \text{bar}^{-1}$) compared PI-PEEK ($\approx 7.4 \text{ L} \cdot \text{m}^{-2} \cdot \text{h}^{-1} \cdot \text{bar}^{-1}$). It should be noted that it is uncommon for a membrane to have both high permeance and excellent rejection as PI-PEEK does in this scenario. For the separation stage membranes, in-house manufactured 20PBI.X was selected but many of the other screened membranes would have been suitable for the separation.

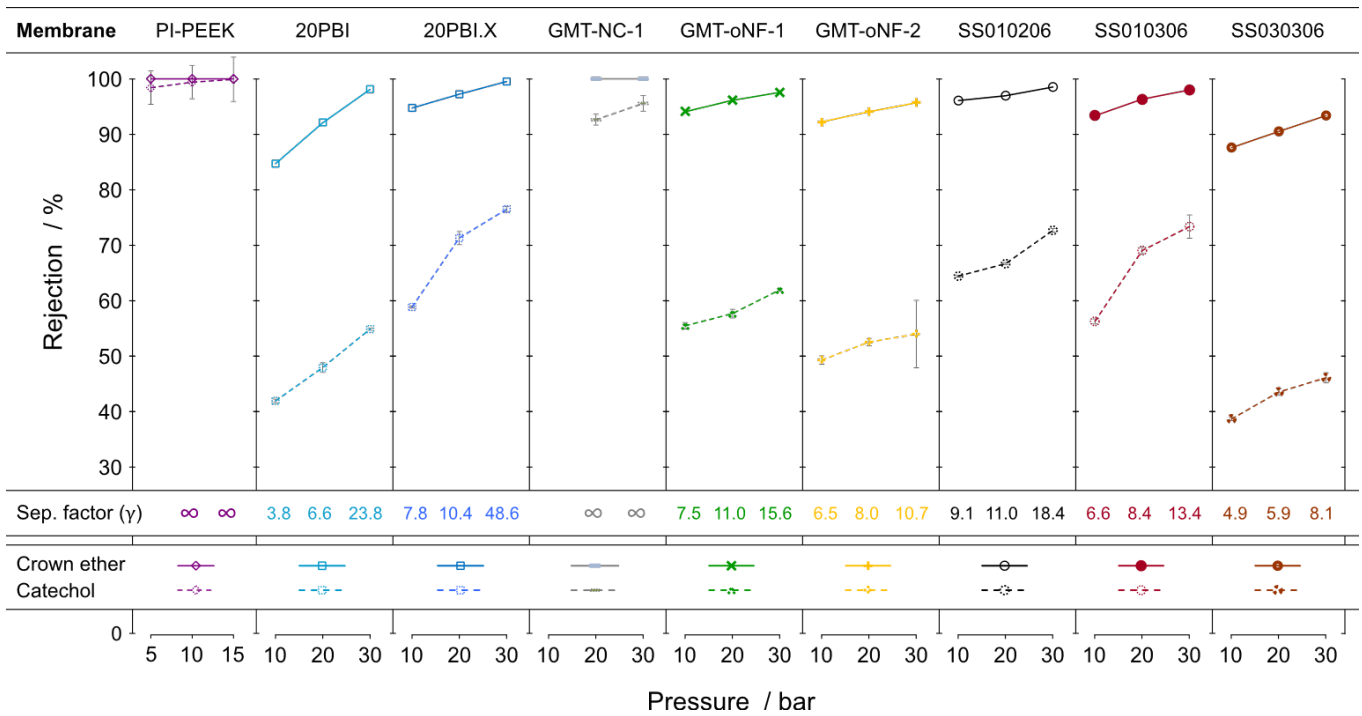


Figure 109. Rejection data for crown ether product (solid shapes, solid lines) with varying pressure for 9 different membrane types. Separation factors (γ) are shown for the corresponding rejection values and pressures. Reproduced from ¹¹⁴.

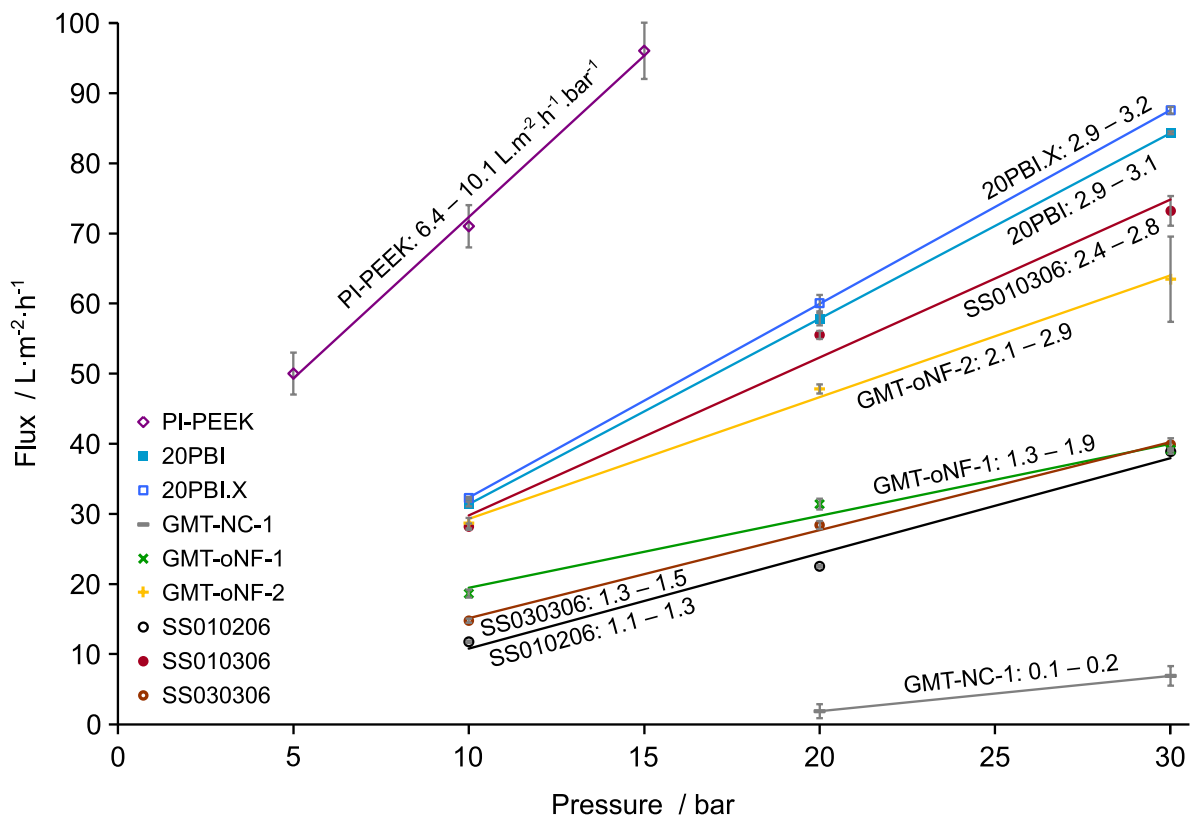


Figure 110. Flux data ($L \cdot m^{-2} \cdot h^{-1}$) in acetone with varying pressure (5 – 30 bar) for different membrane types. Written alongside the fitted linear trend lines are the corresponding minimum and maximum permeance values ($L \cdot m^{-2} \cdot h^{-1} \cdot bar^{-1}$) over the screened range. Reproduced from ¹¹⁴.

With suitable membranes chosen, all membrane and system parameters for the apparatus used in the study are set as given in Table 23. It should be noted that the combination of 3rd stage membrane area and transmembrane pressure is lower in this scenario than would usually be expected. In a typical scenario, the high rejection requirement of the solvent recovery membrane would go hand in hand with a lower permeance of the membrane, thus necessitating a higher 3rd stage transmembrane pressure, a larger membrane area, or both.

Table 23. Summary of the membrane and system parameters of the apparatus. Reproduced from ¹¹⁴.

Stage	Membrane	Stage volume	Absolute pressure		Membrane area	Permeance ^[a] (Permeate flowrate)	Rejection ^[b]	
			(Transmem. pressure)				Crown	Catechol
		mL	bar (bar)		cm ²	L·m ⁻² ·h ⁻¹ ·bar ⁻¹ (L·h ⁻¹)	%	%
1 (1 st Separation)	20PBI.X	200 ^[c]	30	(13.5 ± 1.5)	102	4.4 (0.6)	98.1	54.9
2 (2 nd Separation)	20PBI.X	70	16.5 ± 1.5 ^[d]	(11.5 ± 1.5)	51	5.1 (0.3)	98.1	54.9
3 (Solvent recovery)	PI-PEEK	55	5	(4)	102	7.4 (0.3)	99.5	98.4

[a] Permeance values are back-calculated from the experimentally measured flow-rates and corresponding membranes areas differ from the screened values.

[b] Rejection values are *screened* not fitted.

[c] The 1st separation stage comprises the feed tank and the 1st stage retentate loop and is assumed well-mixed.

[d] 2nd stage pressure was adjusted to keep the recycle ratio at 0.5.

4.3. Results and discussion

The feasibility of the separation was then tested in a diafiltration over 16 h with similar starting concentrations of catechol (**82**) and crown ether (**84**) ($1 \text{ g}\cdot\text{L}^{-1}$) in the 1st stage and clean solvent in the 2nd and 3rd stage. The experiment was run twice and the concentration profiles reflect the expected trend, with removal of catechol from the 1st and 2nd separation stages (Figure 111a and Figure 111b respectively) and accumulation of the impurity in the solvent recovery stage (Figure 111c).

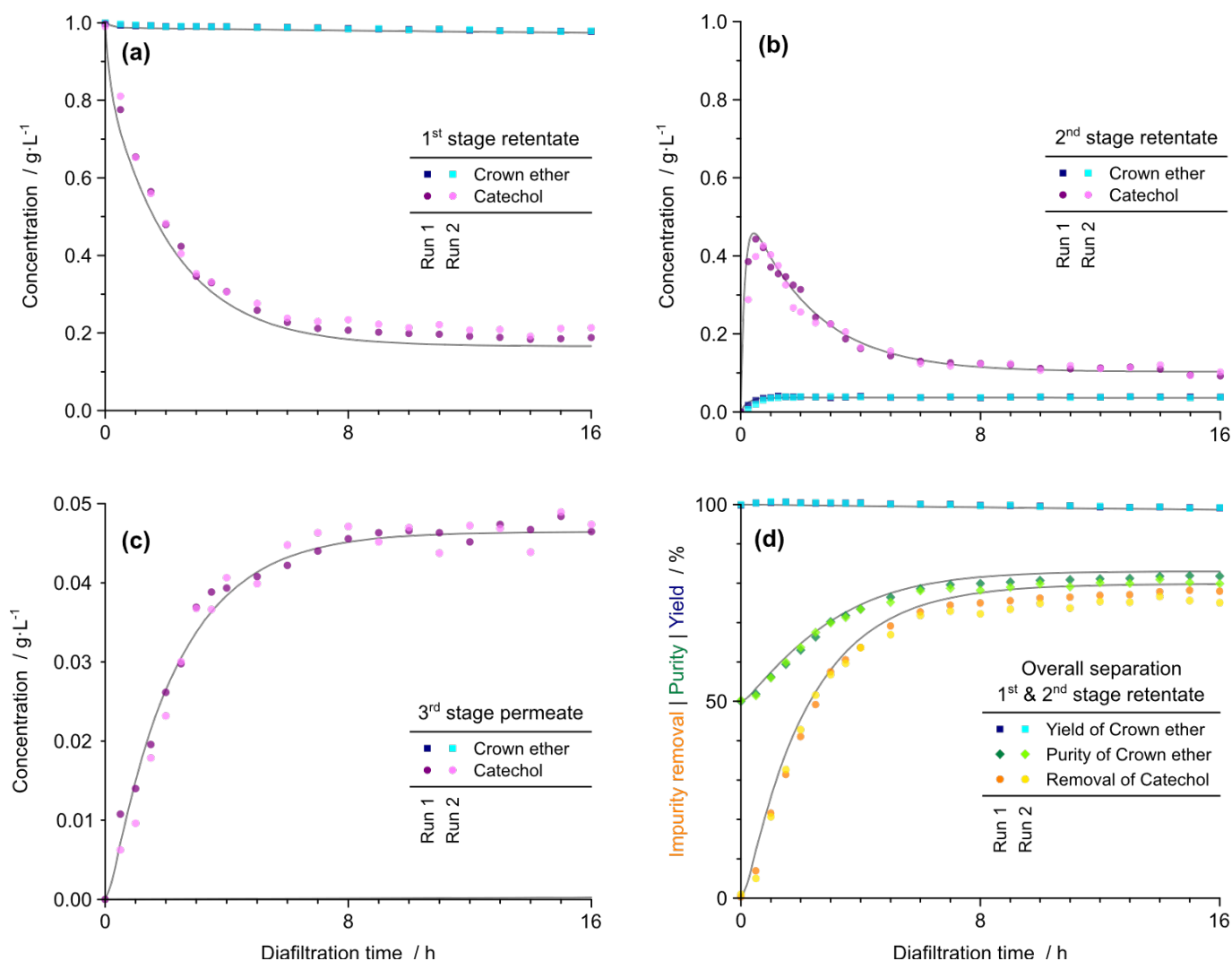


Figure 111. Concentration profiles of crown ether product (Run 1: ■ / Run 2: □) and catechol impurity (● / ○) in (a) 1st stage retentate, (b) 2nd stage retentate and (c) 3rd stage permeate for diafiltration over 16 h with solvent recovery. Two repeats were run. Panel (d) shows a summary of the diafiltration progress (1st and 2nd stage combined) in terms of the yield of crown ether (■ / □), purity of crown ether (◆ / ◇) and removal of catechol (● / ○). Concentration of the 3rd stage was only indirectly measured by sampling the 3rd stage permeate, as seen in panel (c). Underlying curves (solid grey) are not fitted but simulated based on the screened values and system parameters summarized in Table 23. Reproduced from ¹¹⁴.

The 3rd stage concentration was tracked indirectly by sampling the permeate exiting from the solvent recovery stage. Due to incomplete rejection of catechol in the SR stage ($R_{\text{cat}} = 98.4\%$) complete separation is not possible because the catechol removed from the separation stages is reintroduced via solvent recycled from the solvent recovery stage containing a small quantity of catechol.

When looking in more detail at the change of purity in the combined separation stages over time (Figure 112), we find that there is no significant increase in purity after around 12 h and purity actually decreases again after around 17.5 h. This is because at that point, the catechol impurity has reached a steady state across the three stages while the crown ether product is still being lost from the separation stages to the solvent recovery stage. (It is of course not intended for the crown ether to reach a steady state distribution across the stages as any loss from the separation stages to the solvent recovery unit is lost product.)

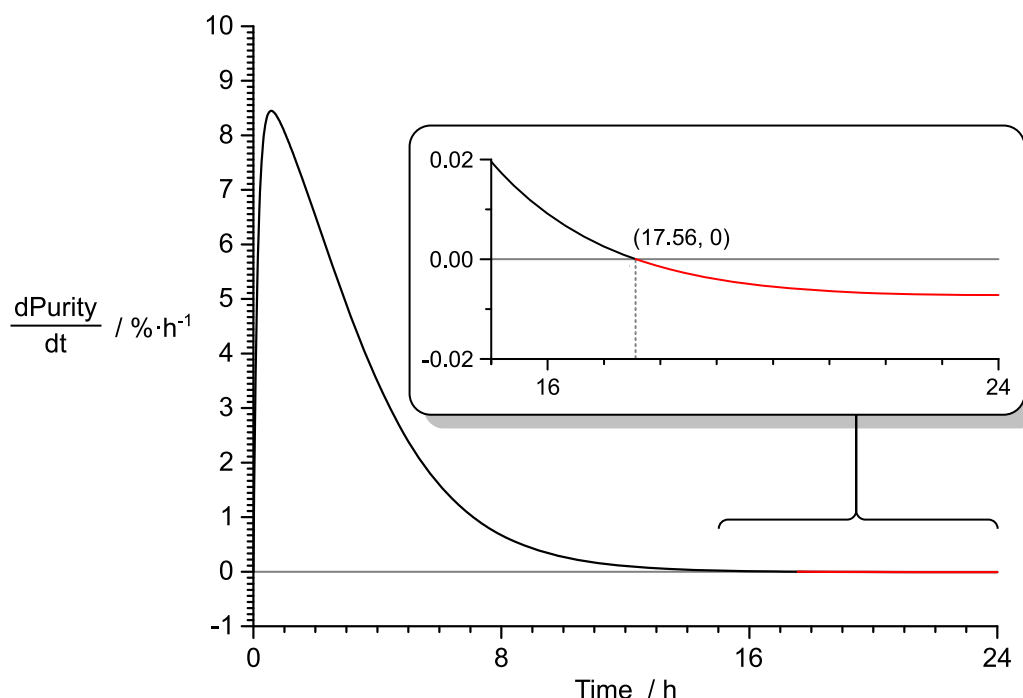


Figure 112. Change of purity for an overly long diafiltration highlighting the presence of a maximum attainable purity at around 17.56 h after which purity decreases again. Reproduced from ¹¹⁴.

In order to allow further purification, the concentration in the solvent recovery stage needs to be reset, so the solvent recovery stage needs to be washed out. By reducing the concentration in the solvent recovery stage close to zero and repeating this procedure at intervals, further diafiltration can be carried out at the expense of the solvent needed to wash the solvent recovery unit. Figure 113 shows the same diafiltration over 24 h but with washing of the SR stage carried out after 8 h and 16 h. The 3rd stage concentration therefore falls to zero at these intervals as visible in Figure 113 (c).

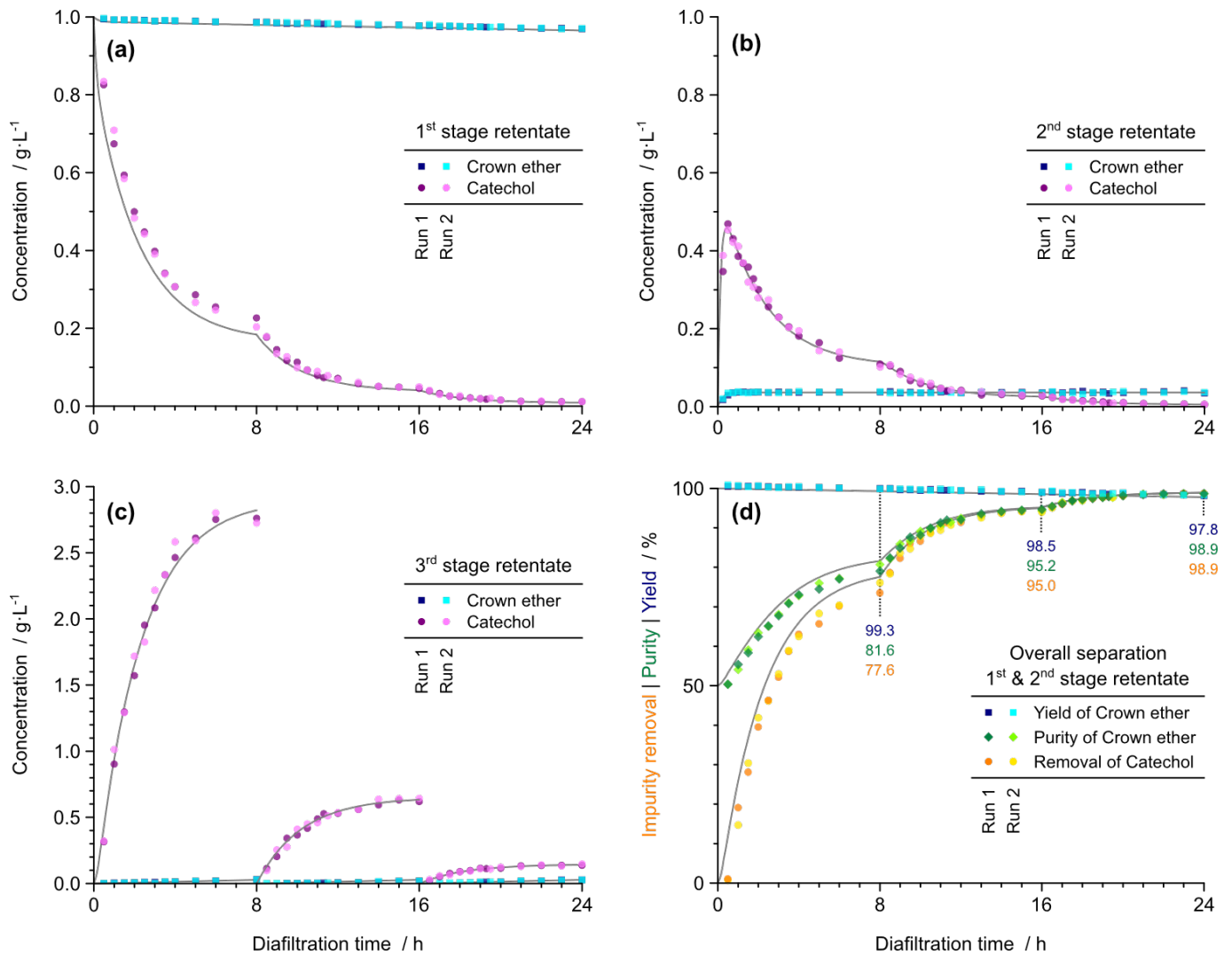


Figure 113. Concentration profiles of crown ether product (Run 1: ■ / Run 2: □) and catechol impurity (● / ○) in (a) 1st stage retentate, (b) 2nd stage ret. and (c) 3rd stage permeate for diafiltration over 24 h (3 x 8 h) with solvent recovery. Two repeats were run with washing of the solvent recovery stage at 8 h intervals. Panel (d) shows a summary of the diafiltration progress (1st and 2nd stage combined) in terms of the yield of crown ether (■ / □), purity of crown ether (◆ / ◇) and removal of catechol (● / ○). Concentration of the 3rd stage was only indirectly measured by sampling the 3rd stage permeate, as seen in panel (c). Underlying curves (solid grey) are not fitted, but simulated based on the screened values and system parameters summarized in Table 23. Reproduced from ¹¹⁴.

When a value is put on the quantity of solvent needed to wash the solvent recovery stage, this closed-loop system can be compared to a standard two-stage diafiltration without solvent recovery. Depending on the design and ease of draining, a reasonable estimate for the solvent consumption during washing is approximately three times the solvent recovery stage volume, V_3 . ($1 \times V_3$ is the minimum solvent consumption attained if it were possible to fully drain the solvent recovery stage without leaving any residual solute behind, and then refilling.)

Figure 114 shows the stark difference in solvent consumption, with 3.8 L used for a diafiltration apparatus without solvent recovery. In comparison, a diafiltration set-up with solvent recovery requires

only around 0.495 L of solvent attributable to three washes of the solvent recovery stage with $3 \times V_3$ each ($3 \times 3 \times 0.055$ L). This equates to a solvent saving of approximately 80 %.

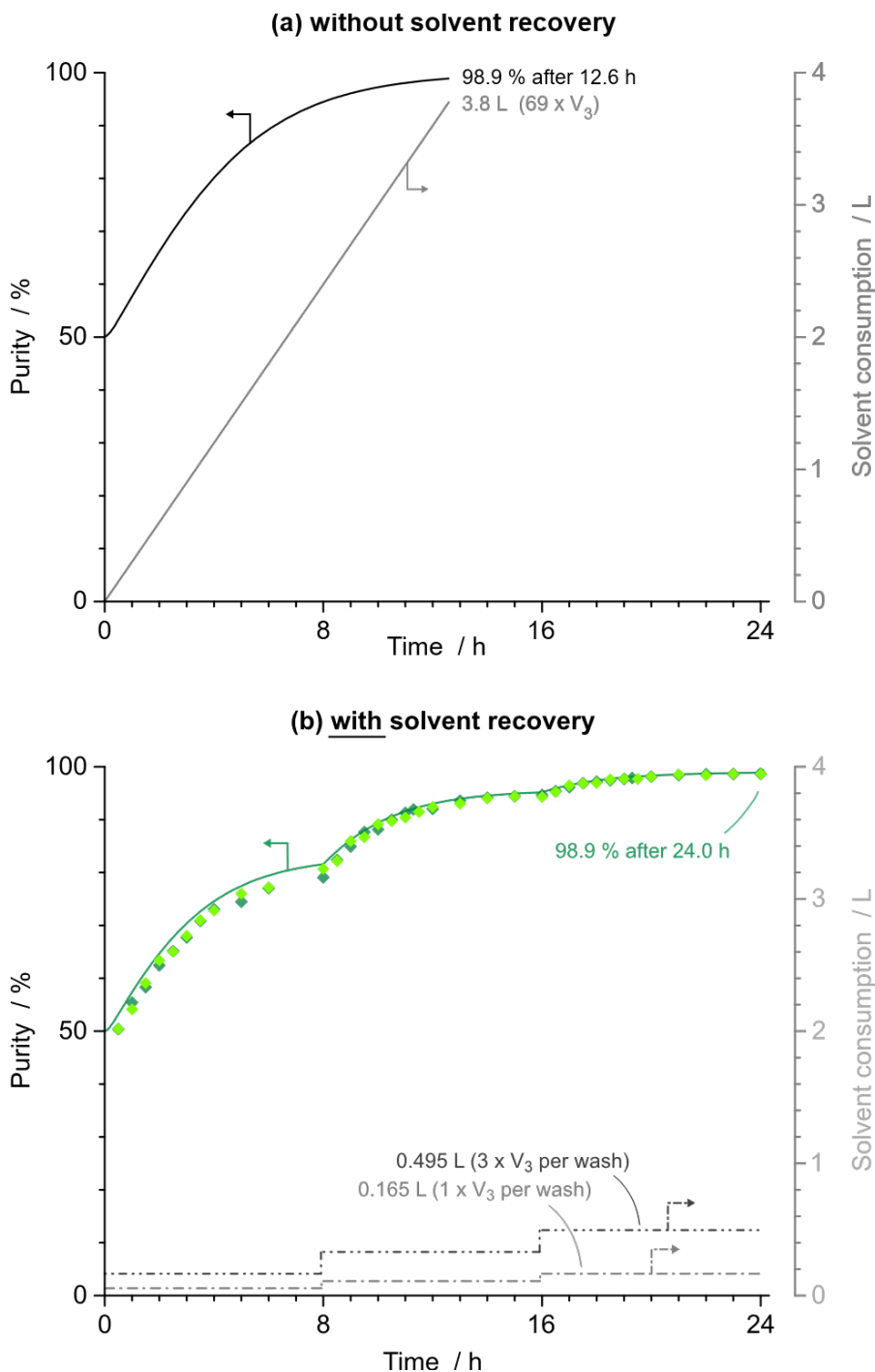


Figure 114. Comparison of solvent consumption between a two-stage diafiltration (a) without and (b) with integrated solvent recovery. A purity (solid, black) of 98.9 % is attained after 12.6 h with a solvent consumption (solid, grey) of 3.8 L for a system *without* solvent recovery. For a system *with* solvent recovery, a similar purity (◆ / ◆) of 98.9 % is attained after a longer diafiltration period of 24 h but with a significantly lower solvent consumption (dash dot dot, grey) of around 0.5 L. Purity curves are simulated based on the screening data analogous to Figure 113, not fitted.

4.4. Conclusion

It was demonstrated that high product purities can be attained in closed-loop diafiltration cascades with membrane-based integrated solvent recovery, even when the solvent recovery membranes do not exhibit total rejection of the impurity. The key to further purification is the washing of the solvent recovery stage at regular intervals before the impurity profile reaches a steady state. In this example, a solvent saving of around 80 % was demonstrated but further gains may be possible if the SR unit can be completely drained and the solvent consumption per wash reduced closer to the theoretical minimum.

Although solvent recovery was here demonstrated for a very small impurity for which only one membrane was available, the concept should hold for any diafiltration operation with solvent recovery. This system should therefore also be applicable to solvent recovery from the larger building block related impurities discussed in the prior chapters, if a solvent recovery membrane with close to absolute rejection of building block and dimer can be found.

This integrated nanofiltration-based solvent recovery concept should enable the use of very selective membranes with high rejection of impurity where many diafiltration volumes need to be put through in order to completely rinse out the impurity. Where ordinarily a large solvent consumption would have resulted, integrated solvent recovery will now conserve a large fraction of this solvent at the expense of a longer diafiltration time and the additional membrane area needed for solvent recovery.

Overall conclusion and outlook

The iterative synthesis of uniform oligomers is challenging because of the particularly high standards required to maintain high oligomer purity and obtain an acceptable final product yield over many extension cycles. The assembly of a molecule of PEG-10000 requires the addition of roughly 57 units of Eg₄, equivalent to 19 extension cycles when starting from an Eg₁₂ building block. It is clear, then, that a cycle yield of 90 %, ordinarily considered a good isolated yield, would here only result in a final product yield of around 14 % after 19 cycles. Similarly, purification up to a product purity of 99 % in each cycle would result in a final oligomer purity of only around 83 % at which point the product oligomer may no longer possess a clearly identifiable advantage over the disperse analogue.

This illustrates that, where reactant conversions in the high 90s would ordinarily suffice, the assembly of uniform oligomers over many iterative cycles requires the per cycle conversions to consistently and substantially exceed 99 % so that yield loss does not compound. Equally, purification of the growing oligomer from excess building block and reaction debris must be virtually complete to maintain high oligomeric purity up to the final product. This in turn has implications for all facets of the iterative strategy.

First, there is a need for sufficiently sensitive analysis. Looking back, Eg₆₀ was synthesized over four cycles with an oligomer purity of 97 %. The evidence shows that impurities had accumulated continuously and evenly over the four cycles and must therefore have arisen in the sub-percent range in each individual reaction step. For PEG oligomer synthesis up to pharmaceutically relevant length, optimization must therefore include the understanding of side reactions which are in the sub-percent range relative to the main reaction. The conjugated system of Hub³ was a successful step in this direction, providing UV absorbance over a broad range of wavelengths and providing absorption outside the spectrum occupied by the other UV-active functional groups. Hub³ thereby provides an opportunity to clearly identify all product-related homostar species during the synthesis and distinguish these from all building block related impurities which must be removed.

Turning towards reaction kinetics, the chain extension poses a challenge. Driving the chain extension reaction to completion will likely become more difficult with increasing chain length, although the present evidence suggests kinetic limitations may not be severe. In the kinetic study, it was demonstrated that the inherent reaction rate of Williamson etherification remains constant between extensions up to Eg₂₄ and up to Eg₅₆ which is promising. However, the continuously increasing molecular weight of the product homostar may eventually necessitate lowering reactant concentrations to overcome limits of viscosity, as the reaction mixture for extension to Eg₅₆, contains a combined 44 wt% of PEG reactants, was already becoming noticeably viscous. It is yet to be established whether inherent etherification reaction rates will

remain comparable towards higher chain lengths or if the solvent fraction in the reaction mixture was further lowered.

Related to the chain extension kinetics is the slow conversion of building block to dimer arising from the long reaction times required for complete conversion during chain extension. The mechanism has not been identified here but is important in two ways. First, in this system the dimer has been found to be the limiting separable component during diafiltration in the protected state. Depending on the exact overall chemistry and building block length, the dimer may also prove to be limiting in the unprotected state. This slows down the purification but also limits the potential for optimizing the diafiltration by tuning the building block chemistry. Mitigation of dimer formation is therefore significant for nanofiltration performance.

More generally, the formation of dimer from building block also ties into the question of how large an excess of building block should be used during chain extension reactions. This is an optimization question in multiple ways. Most directly, the excess of building block and its concentration will determine the rate of the chain extension reaction. But all excess building block and the dimer generated therefrom must be subsequently removed during diafiltration. Also, building block is unlikely to be recovered in this strategy given that this would probably require significant chromatographic effort. The use of a consistently lower building block excess would thus better the process economics by improving the building block input factor.

Another reaction requiring close attention is the deprotection of the Thp acetal which is reversible under acid catalysis. Despite the large excess of methanol used during deprotection, the mass spectrometry for the synthesis of Eg₆₀ shows the presence of shorter -Eg₁₂ oligomers which are likely to be at least partially the result of incomplete deprotection. To drive deprotection to completion, the reaction should thus ideally be carried out inside the nanofiltration apparatus during diafiltration (or be run twice consecutively with removal of the Thp deprotection debris in between). Combined nanofiltration and deprotection will in turn require the design of a diafiltration apparatus also withstanding the deprotection conditions without introducing impurities, e.g. through corrosion or leaching. Generally, apparatus design must be optimized in line with pharmaceutical standards to allow complete rinsing.

Regarding purification by nanofiltration, the successful diafiltration requires a membrane stable towards both organic solvent and towards acid, if deprotection is to be carried out inside the diafiltration apparatus. The membrane must further be sufficiently selective to allow a combination of high yield and high purity to be attained. It was demonstrated that two types of poly(ether ether ketone) membrane partially fulfilled these requirements with good stability and good selectivity for separation of building block ($\gamma > 8$), albeit with lesser selectivity for dimer removal ($\gamma \approx 2$). Polybenzimidazole was screened and found to be a promising material but was omitted in favour of PEEK to reduce acid interaction and

process complexity. As demonstrated by the very selective ethanol-dried PEEK sample ($\gamma > 20$), membranes with high selectivity often exhibit relatively high impurity rejections and the corresponding diafiltration processes will therefore consume large quantities of solvent. In turn, this makes an integrated solvent recovery via nanofiltration attractive and such a recovery process was demonstrated for a small impurity, with the potential to transfer the method to the synthesis of uniform PEG.

A last topic of concern is the oligomer purity of the starting material and the synthesis of building blocks. For building block precursors such as Eg_4 , bulk suppliers such as Sigma-Aldrich currently offer material with specified purities of 99 %, around 99.5 % oligomer purity in practice. Higher chain lengths and purity grades are available from specialist suppliers but not in bulk and at the expense expected for purpose-made uniform oligomers, e.g. Eg_{28} from Polypure. While the Eg_{12} building block used in the synthesis of Eg_{60} was shown to be virtually free of impurities derived from building block assembly, it showed the expected impurity from the starting material. The building block was also prepared using chromatography as the separation technique which would likely prove to be the limiting step in a scaled-up process. A successful integrated strategy thus requires a combination of affordable starting material procurement and scalable building block synthesis. It is conceivable that this requires the combination of different techniques such as crystallization using macrocyclic sulfates which hold promise to separate starting material impurities ($\pm Eg_1$) in combination with extraction as a replacement for chromatography to more economically prepare building blocks up to a length of Eg_{12} or Eg_{16} . Perhaps such a building block could even be chain doubled once and the resultant building block then used in conjunction with a nanofiltration-based homostar strategy from then on.

Overall, a comparison of the oligomer purity of the Eg_{60} synthesized here with the oligomers derived via more conventional techniques such as chromatography and extraction by other authors shows that purification via OSN yields comparable results up to Eg_{60} and holds potential for further optimization. Advantageously, a nanofiltration-based strategy allows to carry out the reaction and work-up of sequence-defined oligomers fully into the homogeneous liquid domain with the associated benefits in scalability, automation, quality control and potential economies of scale. More importantly, for higher PEG oligomer lengths, the combined homostar and nanofiltration strategy may allow the attainment of chain lengths currently inaccessible via chromatographic means.

From an economic viewpoint, the market for uniform poly(ethylene glycol) is currently still low volume. About 20 PEGylated drugs were approved since 1990 but, with the exception of a single drug, all used disperse grades of poly(ethylene glycol). The established technique for controlled PEG synthesis, living anionic polymerization, has become increasingly refined over the years, and routinely yields samples with dispersity ($\mathcal{D} < 1.05$) that appear to suffice in pharmaceutical applications for the time being. As a result, there appears to be little demand for a more uniform product, or a process for its preparation. However, the benefits in terms of analysability and traceability are stark with significantly cleaner spectra

in chromatographic and mass spectrometric techniques and when switching from a very low dispersity PEG to a uniform PEG, quality control may be improved. Also, there is a possibility that a PEGylation with a more uniform oligomer may in fact refine the in vivo characteristics of a drug, although that is yet to be proven.

The lack of large-scale demand for uniform PEGs to date may thus be attributed to the combination of a perceived lack of clear advantage and lack of availability of uniform PEGs at pharmaceutically relevant length. Notably, little fundamental change has until recently occurred in the synthetic strategies towards uniform PEG since the implementation of protecting group-based approaches over 20 years ago. It thus appears plausible that the problems of uniform PEG manufacture lie in the industrial implementation of large-scale manufacture towards pharmaceutically relevant lengths, at an affordable price.

To the author's knowledge, there have until recently only been two small companies, QuantaBioDesign Ltd. (US) and Polypure AS (NO), which specialize in supplying uniform PEGs, with a maximum length of Eg₄₈ available as a linear heterobifunctional product. Both manufacturers appear to rely on chromatographic separation. A third company, Exactmer Ltd. (UK), has recently started to commercialize the combined homostar and nanofiltration approach based on the work of the Livingston research group at Imperial College. The future may thus hold promise.

Overall, it was demonstrated that the iterative synthesis of uniform poly(ethylene glycol) via nanofiltration in harsh organic solvent environments is possible. The approach has the potential to supersede the established chromatographic purification methods and enable a step-change in scalability, automation, and attainable oligomer length. While these findings should partially translate to other oligomers that can be synthesized in an iterative fashion, the specific synthetic and purification challenges associated with each individual type of polymer are too specific to be generalized.

5. Chapter 5: Experimental

The experimental details for the preparation of all species in Chapter 1 (and Chapter 2) can be found in the main text and supporting information of Szekely et al.^{4,52}. This experimental section describes the synthesis of compounds in Chapter 3. (Chapter 4 does not feature any synthesis.)

5.1. General experimental

Tetra(ethylene glycol) (**1**) (110175, LOT: MKBS7714V) was purchased from Sigma-Aldrich. Hub²-COOH (**42a**) was purchased from Alfa Aesar (UK) (H60087, LOT: 81300934) and Hub³-COOH (**43a**) was purchased from Chemsoon Co., Ltd. (CN) (www.chemsoon.com, CAS: 911818-75-2, LOT: CS006080 and CS006112). Commercial PEG samples for comparison in Table 22 were purchased from Polypure AS (NO) (PEG-28, LOT: W28-3046) and Quanta BioDesign Ltd. (USA) (m-dPEG[®]48-OH, LOT: BD1-A4800-026-2). Solvents were purchased from VWR (UK); deionized water and organic solvents used for HPLC analysis were CHROMASOLV™ grade. All other reagents were purchased from Sigma-Aldrich (UK).

All solvents were dried over 4 Å molecular sieves prior to use with reactions conducted under an argon atmosphere. Thp deprotection may be run under air with standard methanol.

Drying to constant weight of PEG derivatives was carried out overnight under high vacuum (0.3 mbar). Slow stirring of the gummy materials, with intermittent gentle heating, particularly at the start of the process, assisted evaporation of entrained volatiles.

Compounds containing Hub³-CH₂OR are susceptible to oxidation of the benzylic methylene. Consequently, all THF was freshly distilled on a rotary evaporator, with Fe(II)SO₄·7H₂O in the bottoms immediately prior to use to provide THF free from peroxides, particularly for diafiltration where large quantities of solvent were used.

5.2. Hubs

Tetrakis(4-bromomethylphenyl)methane (**50**)¹³³ was synthesized according to the prior art.

NMR Annotation

For all hub precursors, the carbons are labelled from the innermost aromatic CH to the functional groups in one continuous sequence as shown in Figure 115 and Figure 116 below. All hydrogens are labelled according to the numbered carbon to which they are bonded, i.e. not in a continuous fashion, so that there is C¹H but no C²H or C³H because the next hydrogen resides on C⁴.

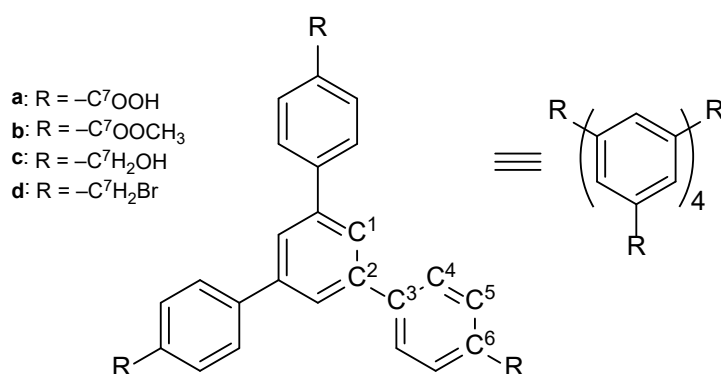


Figure 115. NMR annotation for Hub²-R (**42a-d**).

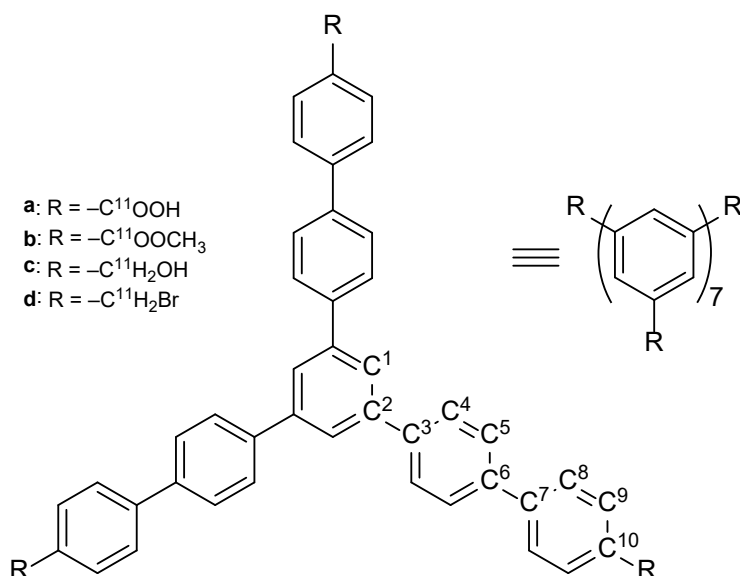
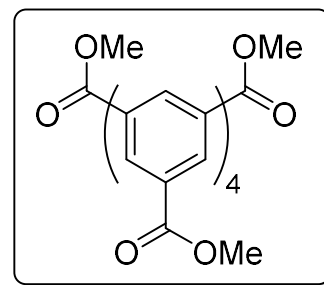


Figure 116. NMR annotation for Hub³-R (**43a-d**).

Hub²-COOMe (**42b**)¹⁴⁶

Into a 2 L Florentine flask were placed Hub²-COOH (5.19 g, 11.8 mmol) and methanol (360 mL). To the solution was slowly added 98 % H₂SO₄ (8 mL, 23.2 g). A condenser was fitted and the briskly stirred suspension was refluxed for 40 hr. Completion of the reaction was confirmed by TLC, and the stirred suspension was cooled in an ice bath for 30 minutes. The sulfuric acid was then quenched by slow addition of saturated aqueous NaHCO₃ (500



mL). Once gas evolution had subsided, the organic solvent was removed on a rotary evaporator. The residual aqueous suspension was transferred to a 2 L separatory funnel, diluted with deionized water (500 mL), and extracted with chloroform (3 x 500 mL). The solvent was removed on a rotary evaporator, and the final traces of solvent were removed under high vacuum (0.3 mbar). The crude Hub²-COOCH₃ (approx. 5.6 g) was used in the next step without further purification. If desired, crude Hub²-COOCH₃ may be crystallized from toluene.

*R*_f (CHCl₃-MeOH 9:1): 0.00 (Hub²-COOH), 0.84 (Hub²-COOCH₃)

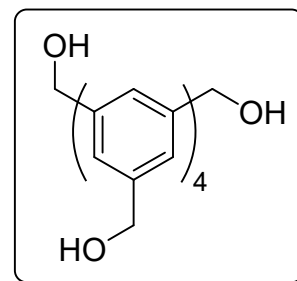
¹H NMR (400 MHz, CDCl₃): δ = 8.14 (d, *J* = 8.5 Hz, 6H; C⁵H), 7.82 (s, 3H; C¹H), 7.73 (d, *J* = 8.3 Hz, 6H; C⁴H), 3.95 (s, 9H; C⁷OOCH₃).

¹³C NMR (101 MHz, CDCl₃): δ = 166.9 (C⁷OOCH₃), 145.0 (C³), 141.6 (C²), 130.3 (C⁵H), 129.6 (C⁶), 127.3 (C⁴H), 126.1 (C¹H), 52.3 (C⁷OOCH₃).

MALDI-ToF (LD-): *m/z* (%): 479.15 (40) [*M* - H]⁻; Calc.: [*M* - H]⁻ 479.15. MALDI-ToF (LD+): *m/z* (%): 481.16 (30) [*M* + H]⁺; Calc.: [*M* - H]⁺ 481.16.

Hub²-CH₂OH (**42c**)¹⁴⁶

Into a 500 mL round-bottomed flask were placed the crude Hub²-COOCH₃ (approx. 5.6 g) from the previous step and anhydrous THF (120 mL). The stirred milky white suspension was cooled in an ice bath for 20 minutes. Separately 4 M HCl (100 mL) and deionized water (500 mL) were also cooled in an ice bath. To the chilled suspension of starting material was slowly added 1.0 M LiEt₃BH in THF (35 mL, 35 mmol, 3.0 eq.), followed by addition of LiAlH₄ in small aliquots (0.6 g, 16 mmol, 1.3 eq.), and the resulting suspension was stirred for 2 h. Further 1.0 M LiEt₃BH in THF (5 mL, 5 mmol, 0.4 eq.) was then added. TLC then confirmed that the reaction was complete.



Under a brisk stream of argon, the reaction was quenched by the dropwise addition of water. Care should be taken as vigorous evolution of hydrogen occurs. After the effervescence ceased, cold deionized water (500 mL) and 4.0 M HCl (100 mL) were added to give a milky white suspension; acidification was confirmed using an indicator strip. The remaining triethylborane-related species must then be quenched with extreme caution due to the fire hazard. With vigorous stirring, air was gently bubbled into the ice cold solution through a Pasteur pipette for 5 minutes, when the reaction mixture became noticeably warm. Once the initial reaction had subsided, air was then vigorously bubbled through the solution for a further 10 minutes.

Once the reaction had been safely quenched, the organic solvent was removed on a rotary evaporator and the crude product was separated from the aqueous suspension by filtration. The filter cake was rinsed with deionized water (500 mL), 1.0 M HCl (500 mL), and once again deionized water (500 mL). After air drying in the sinter funnel, thorough drying in vacuo (0.3 bar) overnight provided the crude Hub²-CH₂OH which was used without further purification. If desired, this material may be crystallized from either ethyl acetate:ethanol or *n*-butanol.

R_f (CHCl₃-MeOH 9:1): 0.39 (Hub²-CH₂OH), 0.84 (Hub²-COOCH₃)

¹H NMR (500 MHz, [D₈]THF): δ = 7.84 (s, 3H; C¹H), 7.73 (d, *J* = 8.4 Hz, 6H; C⁴H), 7.45 (d, *J* = 8.5 Hz, 6H; C⁵H), 4.64 (d, *J* = 5.8 Hz, 6H; C⁷H₂OH), 4.30 (t, *J* = 5.8 Hz, 3H; C⁷H₂OH).

¹³C NMR (126 MHz, [D₈]THF): δ = 143.37 (C⁶), 143.23 (C²), 140.7 (C³H), 127.86 (C⁴H), 127.80 (C⁵H), 125.4 (C¹H), 64.7 (C⁷H₂OH).

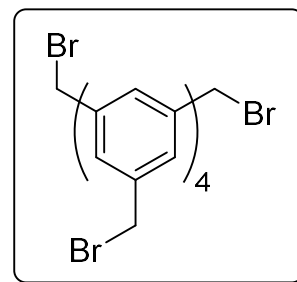
¹H NMR (500 MHz, [D₆]DMSO): δ = 7.86 (s, 3H; C¹H), 7.82 (d, *J* = 8.3 Hz, 6H; C⁴H), 7.46 (d, *J* = 8.5 Hz, 6H; C⁵H), 5.28 (t, *J* = 5.8 Hz, 3H; C⁷H₂OH), 4.58 (d, *J* = 5.7 Hz, 6H; C⁷H₂OH).

¹³C NMR (126 MHz, [D₆]DMSO): δ = 142.1 (C⁶), 141.5 (C²), 138.6 (C³), 127.03 (C⁵H), 126.86 (C⁴H), 123.9 (C¹H), 62.7 (C⁷H₂OH).

MALDI-ToF: *m/z* (%):396.4 (30) [M + H]⁺; Calc.: [M + H]⁺ 397.2.

Hub²-CH₂Br (**42d**)¹⁴⁶⁻¹⁴⁸

Into a 500 mL round-bottomed flask were placed crude Hub²-CH₂OH and CH₂Cl₂ (150 mL) and *n*-heptane (350 mL). A four-way Claisen adaptor was fitted to the flask: one socket was connected to an argon line; one to a



Dreschel bottle bubbler containing 1.0 M aqueous KOH (800 mL) to scavenge HBr fumes; the remaining vertical socket was fitted with a rubber stopper having a circular hole. With a continuous flow of argon sweeping through the equipment, thionyl bromide (5.5 mL, 71 mmol, 6.0 eq.) was measured into the reaction flask using a graduated pipette that fitted firmly into the rubber stopper. Once vigorous HBr evolution had abated, the empty pipette and rubber stopper were replaced by a glass stopper. The reaction mixture turned dark-red to brown upon addition of SOBr₂, and all solids dissolved.

After 30 minutes, TLC confirmed that the reaction was complete. The solvent and excess reagent was then removed on a rotary evaporator and subsequently under high vacuum. The crude product was crystallized from boiling anhydrous toluene and *n*-heptane, without hot filtering. After 20 h, the crystals were collected by filtration, and washed with *n*-heptane. After thorough drying overnight in vacuo (0.3 mbar), Hub³-CH₂Br (4.97 g, 72 % yield from Hub²-COOH over 3 steps) was obtained as a brownish-orange solid, containing traces of toluene and *n*-heptane. The crystal morphology was unsuitable for X-ray crystallography.

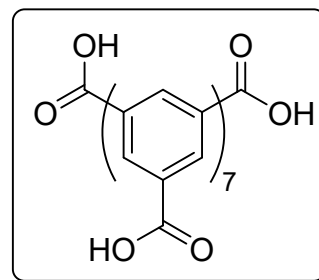
R_f (CH₂Cl₂): 0.81 (Hub²-CH₂Br)

¹H NMR (400 MHz, CDCl₃): δ = 7.76 (s, 3H; C¹H), 7.70 (d, J = 8.3 Hz, 6H; C⁴H), 7.52 (d, J = 8.3 Hz, 6H; C⁵H), 4.58 (s, 6H; C⁷H₂OH).

¹³C NMR (101 MHz, CDCl₃): δ = 141.9 (C²), 141.1 (C³), 137.4 (C⁶), 129.8, 127.9, 125.4 (C¹H), 33.4 (C⁷H₂Br).

Information on Hub³-COOH (**43a**) reagent

Hub³-COOH (**43a**), a pale yellow powder, was used as received. According to the supplier, the methyl ester of Hub³-COOH was synthesized via Suzuki coupling from 1,3,5-tris(4-bromophenyl)benzene ($\geq 99\%$ purity) and 4-methoxycarbonylphenylboronic acid ($\geq 99.5\%$), followed by recrystallization from 1,4-dioxane.¹⁴⁹ The free carboxylic acid was then obtained by hydrolysis of the esters, followed by crystallization from 1,4-dioxane/H₂O.



Since the hydrolysis is reversed here in an esterification step, it would be more efficient to obtain the intermediate methyl ester directly, saving a reaction step and increasing the overall yield. It should be noted that the ¹H NMR peaks of Hub³-COOH are well resolved in THF-d₈ but overlap significantly in

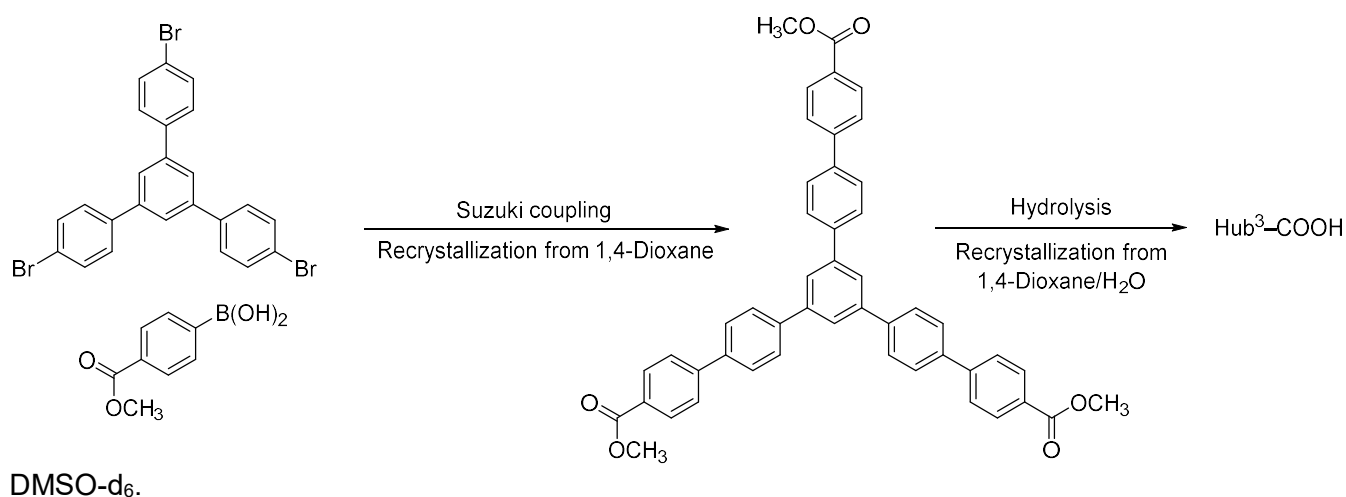
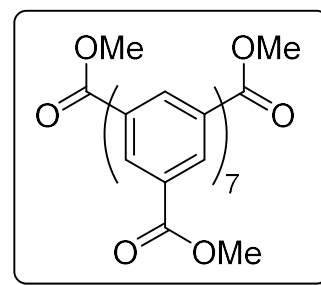


Figure 117. Hub³-COOH (**43a**) synthesis via Suzuki coupling as described by the supplier, Chemsoon Ltd. (CN).

Hub³-COOMe (**43b**)^{149–151}

Into a 2 L Florentine flask were placed Hub³-COOH (10.0 g, 15.0 mmol) and methanol (550 mL). The suspension was sonicated for several minutes to give a hazy, yellow solution. To the solution was slowly added 98 % H₂SO₄ (16 mL, 29.4 g). A reflux condenser was fitted and the briskly stirred suspension was refluxed for 40 hr. Completion of the reaction was confirmed by TLC, and the stirred suspension was cooled in an ice bath for 30 minutes.



The sulfuric acid was then quenched by slow addition of saturated aqueous NaHCO₃ (1 L). Once gas evolution had subsided, the organic solvent was removed on a rotary evaporator. The residual aqueous suspension was transferred to a 5 L separatory funnel, diluted with deionized water (1 L), and extracted with chloroform (4 x 700 mL). The solvent was removed on a rotary evaporator, and the final traces of solvent were removed under high vacuum (0.3 mbar). The crude Hub³-COOCH₃ was crystallized from toluene and *n*-heptane with hot filtration. After 20 h, the crystals were collected by filtration and washed with 3:1 v/v toluene:*n*-heptane, then rinsed with *n*-heptane. After air drying in the sinter funnel and drying in vacuo (0.3 mbar), crystalline 77 wt% Hub³-COOCH₃ plus toluene and *n*-heptane (11.6 g, 85 %) was obtained.

Note: In an earlier iteration of this reaction, tetrahydrofuran was used as a co-solvent because it was suspected that the intermediate partially esterified products would not be sufficiently soluble in pure methanol. While the main reaction was successful, and the refluxing solution passes through a solubility minimum where the suspension turns clear, THF undergoes acid-catalyzed ring opening to give high boiling 4-methoxybutan-1-ol which is difficult to remove.

*R*_f (CHCl₃-MeOH 9:1): 0.00 (Hub³-COOH), 0.86 (Hub³-COOCH₃)

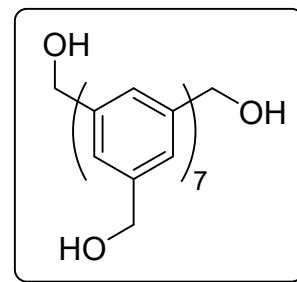
¹H NMR (500 MHz, CDCl₃): δ = 8.14 (d, *J* = 8.6 Hz, 6H; C⁹H), 7.87 (s, 3H; C¹H), 7.80 (d, *J* = 8.4 Hz, 6H; C⁴H), 7.74 (d, *J* = 11.9 Hz, 6H; C⁵H), 7.73 (d, *J* = 12.4 Hz, 6H; C⁸H), 3.96 (s, 9H; C¹¹OOCH₃).

¹³C NMR (126 MHz, CDCl₃): δ = 167.1 (C¹¹OOCH₃), 145.0 (C⁷), 141.9 (C²), 140.8 (C³), 139.4 (C⁶), 130.3 (C⁹H), 129.2 (C¹⁰), 127.96 (C⁴H), 127.89 (C⁵H), 127.0 (C⁸H), 125.3 (C¹H), 52.3 (C¹¹OOCH₃).

MALDI-ToF: *m/z* (%): 709.0 (100) [*M* + H]⁺; Calc.: [*M* + H]⁺ 709.3.

Hub³-CH₂OH (**43c**)

Into a 1 L round-bottomed flask were placed 77 wt% Hub³-COOCH₃ (11.6 g, 12.7 mmol) and anhydrous THF (100 mL). The stirred milky white suspension was cooled in an ice bath for 20 minutes. Separately 4 M HCl (100 mL) and deionized water (500 mL) were also cooled in an ice bath. To the chilled suspension of starting material was slowly added 1.0 M LiEt₃BH^{25,62,152} in THF (84 mL, 84 mmol, 6.6 eq.); once approximately 2/3 of the reducing agent had been added all solids were completely dissolved. The cold mixture was stirred for several minutes, after which TLC confirmed that the reaction was complete.



Under a brisk stream of argon, the reaction was quenched by the dropwise addition of water. Care should be taken as vigorous evolution of hydrogen occurs. After the effervescence ceased, cold deionized water (500 mL) and 4.0 M HCl (100 mL) were added to give a milky white suspension; acidification was confirmed using an indicator strip. The remaining triethylborane-related species must then be quenched with extreme caution due to the fire hazard. With vigorous stirring, air was gently bubbled into the ice cold solution through a Pasteur pipette for 5 minutes, when the reaction mixture becomes noticeably warm. Once the initial reaction had subsided, air was then vigorously bubbled through the solution for a further 10 minutes. Note: Hydrogen peroxide was deliberately not used for triethylborane oxidation because the benzylic methylenes of the product are prone to re-oxidation. In earlier studies employing THF as a superior solvent, it was observed that traces of THF-hydroperoxide (that forms spontaneously in THF in air) were sufficient to cause such re-oxidation.

Once the reaction had been safely quenched, the organic solvent was removed on a rotary evaporator and the crude product was separated from the aqueous suspension by filtration. The filter cake was rinsed with deionized water (500 mL), 1.0 M HCl (500 mL), and once again deionized water (500 mL). After air drying in the sinter funnel, thorough drying in vacuo (0.3 bar) overnight provided the crude Hub³-CH₂OH (8.64 g). This material was crystallized, with hot filtration, from *n*-butanol (approx. 500 mL). After 20 h, the crystals were collected by filtration and washed with *n*-butanol, followed by *n*-heptane. After air drying in the sinter funnel, the crystals were dried in vacuo (0.3 mbar) to give 6.4 g of crystalline material. A second crop of product was obtained from the mother liquor and filter washings, again crystallizing from *n*-butanol (approx. 100 mL) to yield 1.28 g of crystalline material. Both batches were of similar purity yielding 82 wt% Hub³-CH₂OH plus *n*-butanol (7.70 g, 79 %). Crystallization may also be performed from EtOAc:EtOH.

Note: Attempted reduction of Hub³-COOH with LiAlH₄ over 7 days at reflux in THF proceeded to only around 50 % functional group conversion, with a very low yield of the final triply reduced species; the reaction failure is ascribed to solubility issues. Furthermore, some over-reduction to the toluyl derivative

was observed. On the other hand, reduction of Hub³-COOCH₃ with LiEt₃BH is rapid and selective, but LiEt₃BH does not readily reduce carboxylic acids, necessitating the initial esterification step.

Consequently, any residual carboxylic acid groups from incomplete esterification will not be reduced under these conditions. (There reportedly is a possibility of using Et₃B only catalytically with a separate hydride source.¹⁵³)

R_f (CHCl₃-MeOH 9:1): 0.44 (Hub³-CH₂OH), 0.86 (Hub³-COOCH₃)

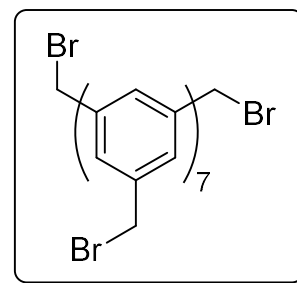
¹H NMR (500 MHz, [D₆]DMSO) δ = 7.99 (s, 3H; C¹H), 7.98 (d, J = 8.3 Hz, 6H), 7.81 (d, J = 8.3 Hz, 6H), 7.71 (d, J = 8.1 Hz, 6H; C⁸H), 7.44 (d, J = 8.1 Hz, 6H; C⁹H), 5.29 (t, J = 5.7 Hz, 3H; C¹¹H₂OH), 4.57 (d, J = 5.7 Hz, 6H; C¹¹H₂OH).

¹³C NMR (126 MHz, [D₆]DMSO): δ = 142.0 (C¹⁰), 141.2 (C²), 139.4 (C⁶), 138.9 (C³), 138.0 (C⁷), 127.7 (C⁴H), 127.11 (C⁹H), 127.05 (C⁵H), 126.3 (C⁸H), 124.2 (C¹H), 62.6 (C¹¹H₂OH).

MALDI-ToF: m/z (%): 624.9 (30) [$M + H$]⁺, 607.9 (100) [$M + H - H_2O$]⁺; Calc.: [$M + H$]⁺ 625.3, [$M + H - H_2O$]⁺ 608.3.

Hub³-CH₂Br (**43d**)¹⁵⁴

In a 500 mL round-bottomed flask were placed 82 wt% Hub³-CH₂OH (7.65 g, 10.1 mmol) and CH₂Cl₂ (300 mL). A four-way Claisen adaptor was fitted to the flask: one socket was connected to an argon line; one to a Dreschel bottle bubbler containing 1.0 M aqueous KOH (800 mL) to scavenge HBr fumes; the remaining vertical socket was fitted with a rubber stopper having a circular hole. With a continuous flow of argon sweeping through the equipment, thionyl bromide (6.2 mL, 80 mmol, 7.9 eq.) was measured into the reaction flask using a graduated pipette that fitted firmly into the rubber stopper. Once vigorous HBr evolution had abated, the empty pipette and rubber stopper were replaced by a glass stopper. The reaction mixture turned dark-red to brown upon addition of SOBr₂, and all solids dissolved.



After 30 minutes, TLC confirmed that the reaction was complete. The solution was then cooled in an ice bath and stirred for another 10 minutes. Ice-cold deionized water (200 mL) was added and the suspension was transferred to a 2 L separatory funnel. Further ice-cold water (800 mL) was added and the mixture was quickly extracted with CH₂Cl₂ (3 x 500 mL), immediately drying each fraction over Na₂SO₄; three faint lower R_f impurities observed by TLC are assumed to derive from hydrolysis of the -CH₂Br moieties. The solvent from the combined organic phases was removed on a rotary evaporator, followed by drying in vacuo (0.3 mbar) overnight to yield the crude Hub³-CH₂Br (8.64 g). The product

was crystallized from boiling anhydrous toluene (300 mL) and *n*-heptane (200 mL), without hot filtering. After 20 h, the crystals were collected by filtration, washing with 3:1 v/v toluene:*n*-heptane. After thorough drying overnight in vacuo (0.3 mbar), crystalline 94 wt% Hub³-CH₂Br (8.02 g, 92 %) was obtained containing toluene and *n*-heptane.

R_f (CH₂Cl₂): 0.82 (Hub³-CH₂Br)

¹H NMR (500 MHz, CDCl₃): δ = 7.88 (s, 3H; C¹H), 7.81 (d, *J* = 8.5 Hz, 6H; C⁴H), 7.73 (d, *J* = 8.5 Hz, 6H; C⁵H), 7.65 (d, *J* = 8.3 Hz, 6H; C⁸H), 7.51 (d, *J* = 8.3 Hz, 6H; C⁹H), 4.58 (s, 6H; C¹¹H₂Br).

¹³C NMR (126 MHz, CDCl₃): δ = 142.1 (C²), 140.9 (C⁷), 140.4 (C³), 139.9 (C⁶), 137.1 (C¹⁰), 129.8 (C⁹H), 127.94 (C⁴H), 127.73 (C⁵H), 127.61 (C⁸H), 125.2 (C¹H), 33.5 (C¹¹H₂Br).

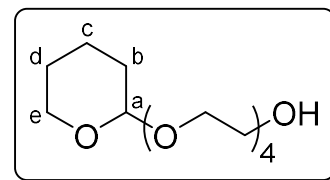
MALDI-ToF: *m/z* (%): 813.7 (10) [M + H]⁺, 733.7 (80) [M + H - HBr]⁺, 654.8 (60) [M + H - 2·HBr]⁺, 573.7 (100) [M + H - 3·HBr]⁺; Calc.: [M + H]⁺ 813.0, [M + H - HBr]⁺ 733.1, [M + H - 2·HBr]⁺ 654.2, [M + H - 3·HBr]⁺ 573.3.

5.3. Building blocks

Most linear building block precursors including HO–Eg₄–OTs (**36**),^{38,155,156} HO–Eg₄–OMs (**40**),^{157–159} HO–Eg₄–Br (**41**)^{160,161} were synthesized previously.

ThpO–Eg₄–OH (**33**)^{38,162–164}

Into a 3 L Florentine flask equipped with a magnetic stirrer were placed 3,4-dihydropyran (24.5 g), followed by CH₂Cl₂ (930 mL) and **1** (280 g, 5 eq.). Under stirring, MsOH (0.2 mL, 0.01 eq.) was added and the solution was stirred for 16 h. The reaction was quenched with Et₃N (1 mL), and after 5 minutes the solution was transferred to a 5 L separatory funnel. The mixture was partitioned once with deionized water (2 L), followed by repeated extraction of the aqueous phase with CH₂Cl₂ (4 x 250 mL). Because HO–Eg₄–OH also extracts into CH₂Cl₂ to a low degree, the fractions were kept separate. The ratio of ThpO–Eg₄–OH product to tetra(ethylene glycol) in each fraction was monitored by TLC, and those fractions containing mainly product were combined. The solvent was removed on a rotary evaporator, followed by azeotropic drying with MeCN (2 x 100 mL). Removal of residual solvent in vacuo (0.3 mbar) for several hours gave a colourless, low viscosity oil (80 g).



A large sinter funnel (D = 14 cm) packed with Geduran® Si 60 (750 g, 10.5 cm depth) was prepared. *n*-Heptane (200 mL) was added to the crude product and the mixture diluted with CH₂Cl₂ until a single phase was obtained. From this point a trace of Et₃N was added to all solvents to prevent acid-catalyzed degradation of the tetrahydropyranyl protecting group. After loading the crude solution onto the column, this was eluted firstly with 8:2 *n*-heptane:CH₂Cl₂ (2 L), followed by a gradient up to 100 % CH₂Cl₂ (4 L total), until the higher *R_f* ThpO–Eg₄–OThp impurity had fully eluted. The solvent was then switched to 100 % MeCN, followed by a gradient of MeOH (2.5 % steps per 500 mL) until the ThpO–Eg₄–OH had fully eluted; the lower *R_f* HO–Eg₄–OH impurity is almost immobile in this system. The appropriate fractions were combined and the solvent removed on a rotary evaporator. Drying to constant weight in vacuo (0.3 mbar) gave the product, ThpO–Eg₄–OH (63.5 g, 78 %), as a colourless, low viscosity oil.

R_f (CHCl₃-MeOH 9:1, KMnO₄): 0.36 (HO–Eg₄–OH), 0.53 (ThpO–Eg₄–OH), 0.70 (ThpO–Eg₄–OThp).

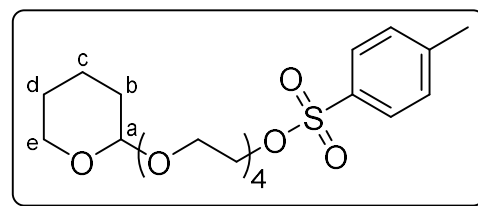
¹H NMR (400 MHz, CDCl₃): δ = 4.57 (dd, *J* = 4.3, 2.9 Hz, 1H; OC^aHO), 3.85 – 3.75 (m, 2H; C^eHHO + ThpOCH^hHCH₂O), 3.69 – 3.63 (m br, 2H; OCH₂CH₂OH), 3.63 – 3.58 (m, 10H; OCH₂CH₂O), 3.58 – 3.49 (m, 3H; ThpOCH^hHCH₂O + OCH₂CH₂OH), 3.48 – 3.39 (m, 1H; C^eHHO), 2.99 (s br; OCH₂CH₂OH), 1.83 – 1.70 (m, 1H; C^cHH), 1.70 – 1.59 (m, 1H; C^bHH), 1.59 – 1.39 (m, 4H; C^bHH + C^dH₂ + C^cHH).

^{13}C NMR (101 MHz, CDCl_3): δ = 98.9 ($\text{OC}^{\text{a}}\text{HO}$), 72.60 ($\text{OCH}_2\text{CH}_2\text{OH}$), 70.62, 70.59, 70.56, 70.52, 70.34 (all $\text{OCH}_2\text{CH}_2\text{O}$ + $\text{ThpOCH}_2\text{CH}_2\text{O}$), 66.6 ($\text{ThpOCH}_2\text{CH}_2\text{O}$), 62.2 ($\text{C}^{\text{e}}\text{H}_2\text{O}$), 61.7 ($\text{OCH}_2\text{CH}_2\text{OH}$), 30.5 ($\text{C}^{\text{b}}\text{H}_2$), 25.4 ($\text{C}^{\text{d}}\text{H}_2$), 19.4 ($\text{C}^{\text{c}}\text{H}_2$).

ES-ToF: m/z (%): 301.2 (100) [$M + \text{Na}$] $^+$; Calc.: [$M + \text{Na}$] $^+$ 301.2.

ThpO–Eg₄–OTs (**53**)^{38,162–164}

In a 1 L round-bottomed flask equipped with a magnetic stirrer, ThpO–Eg₄–OH (60.8 g) was dissolved in CH_2Cl_2 (140 mL), followed by addition of Et_3N (46 mL, 1.5 eq.), *p*-toluenesulfonyl chloride (54.1 g, 1.3 eq.) and 1-methylimidazole (0.18 mL, 0.01 eq.). After 2 h, the reaction mixture was diluted with *n*-heptane



(250 mL) to give a biphasic mixture, and then diluted with CHCl_3 until a single liquid phase, plus undissolved salts, was obtained. A large sinter funnel (D = 14 cm) was packed with Geduran[®] Si 60 (750 g, 10.5 cm depth), and the crude suspension loaded; from this point onward Et_3N (2 mL per 500 mL CHCl_3) was added to all solvent to prevent acid-catalyzed degradation of the tetrahydropyranyl protecting group caused by TsCl hydrolysis. The column was eluted first with 8:2 *n*-heptane: CHCl_3 (2 L), followed by a gradient up to 100 % CHCl_3 (4 L total); during this phase all higher R_f TsCl impurity eluted, and all the salts on the top of the column gradually dissolved. The column was then washed with isocratic CHCl_3 until the high R_f ThpO–Eg₄–OTs product had fully eluted. The appropriate fractions were combined and the solvent was removed on a rotary evaporator. Drying to constant weight under high vacuum (0.3 mbar) gave the product, ThpO–Eg₄–OTs (82.5 g, 87 %), as a pale yellow oil.

R_f (CHCl_3 -MeOH 9:1, KMnO_4): 0.53 (ThpO–Eg₄–OH), 0.74 (ThpO–Eg₄–OTs).

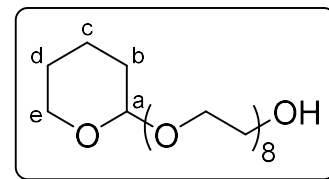
^1H NMR (400 MHz, CDCl_3): δ = 7.74 (d, J = 8.3 Hz, 2H; Ar SO_3CCH), 7.29 (d, J = 8.0 Hz, 2H; Ar CHCCH_3), 4.57 (dd, J = 4.4, 2.9 Hz, 1H; $\text{OC}^{\text{a}}\text{HO}$), 4.14 – 4.07 (m, 2H; CH_2OTs), 3.85 – 3.76 (m, 2H; $\text{C}^{\text{e}}\text{HHO}$ + $\text{ThpOCHHCH}_2\text{O}$), 3.67 – 3.50 (m, 13H; $\text{ThpOCHHCH}_2\text{O}$ + $\text{OCH}_2\text{CH}_2\text{O}$), 3.48 – 3.40 (m, 1H; $\text{C}^{\text{e}}\text{HHO}$), 2.39 (s, 3H; Ar CCH_3), 1.85 – 1.71 (m, 1H; $\text{C}^{\text{c}}\text{HH}$), 1.70 – 1.60 (m, 1H; $\text{C}^{\text{b}}\text{HH}$), 1.60 – 1.39 (m, 4H; $\text{C}^{\text{b}}\text{HH}$ + $\text{C}^{\text{d}}\text{H}_2$ + $\text{C}^{\text{c}}\text{HH}$).

^{13}C NMR (101 MHz, CDCl_3): δ = 144.8 (Ar CCH_3), 133.1 (Ar SO_3C), 129.9 (2C; Ar CHCCH_3), 128.0 (2C; Ar SO_3CCH), 99.0 ($\text{OC}^{\text{a}}\text{HO}$), 70.81 (1C), 70.71 (1C), 70.65 (1C), 70.60 (2C) (all $\text{OCH}_2\text{CH}_2\text{O}$ + $\text{ThpOCH}_2\text{CH}_2\text{O}$), 69.3 (CH_2OTs), 68.7 ($\text{OCH}_2\text{CH}_2\text{OTs}$), 66.7 ($\text{ThpOCH}_2\text{CH}_2\text{O}$), 62.3 ($\text{C}^{\text{e}}\text{H}_2\text{O}$), 30.6 ($\text{C}^{\text{b}}\text{H}_2$), 25.5 ($\text{C}^{\text{d}}\text{H}_2$), 21.7 (Ar CCH_3), 19.6 ($\text{C}^{\text{c}}\text{H}_2$).

ES-ToF: m/z (%): 455.2 (100) [$M + \text{Na}$] $^+$; Calc.: [$M + \text{Na}$] $^+$ 455.2.

ThpO–Eg₈–OH (**64**)^{38,163,165}

A mixture of HO–Eg₄–OH (520 g, 460 mL) and THF (230 mL) was dried over 4 Å molecular sieves. A fraction of this dry solution of tetragol (250 mL, equivalent to 5.0 eq.) was placed in a 2 L Florentine flask equipped with a magnetic stirrer. The well stirred solution was cooled in an ice bath prior to careful batch-wise addition of a 60 % suspension of NaH in mineral oil (15.3 g, 2 eq.). ThpO–Eg₄–OTs (82.5 g) dissolved in THF (80 mL) was then added to the reaction mixture. The ice bath was removed and the solution was allowed to warm to room temperature over 1 h. The reaction was then heated to 50 °C overnight.



After 16 h, the reaction was quenched with sat. aqueous NH₄Cl (100 mL, 4 eq.), and diluted with deionized water (500 mL). After removing the organic solvent on a rotary evaporator, the remaining aqueous mixture was transferred to a 5 L extraction funnel. The aqueous solution was diluted with water to about 2 L, and extracted with CHCl₃ (1 x 1000 mL, then 4 x 250 mL), keeping the fractions separate. The ratio of ThpO–Eg₈–OH product to tetra(ethylene glycol) in each fraction was monitored by TLC, and those fractions containing mainly product were combined. The solvent was removed on a rotary evaporator, followed by azeotropic drying with MeCN (2 x 100 mL). Removal of residual solvent in vacuo (0.3 mbar) for several hours gave the crude product as a pale yellow oil.

A large sintered funnel (D = 14 cm) packed with Geduran[®] Si 60 (750 g, 10.5 cm depth) was then prepared, and the crude mixture was loaded in CHCl₃; from this point onward Et₃N (2 mL per 500 mL CHCl₃) was added to all solvent to prevent acid-catalyzed degradation of the tetrahydropyranyl protecting group. The column was eluted first with CHCl₃ (2 L), followed by a slow gradient of MeOH:CHCl₃ until all the higher *R_f* ThpO–Eg₁₂–OThp had eluted, then more rapidly up to 20 % MeOH until all until all the ThpO–Eg₈–OH product had eluted, but before low *R_f* HO–Eg₄–OH emerged. The appropriate fractions were combined and the solvent removed on a rotary evaporator. Drying to constant weight under high vacuum (0.3 mbar) gave the product, ThpO–Eg₈–OH (67.8 g, 78 %), as a pale yellow oil.

R_f (CHCl₃-MeOH 9:1, KMnO₄): 0.48 (ThpO–Eg₈–OH), 0.57 (ThpO–Eg₁₂–OThp), 0.74 (ThpO–Eg₄–OTs), 0.86 (Mineral oil).

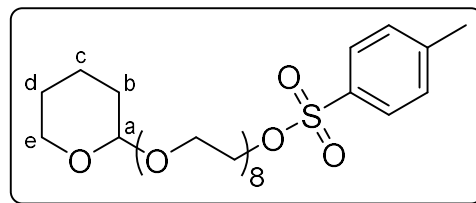
¹H NMR (400 MHz, CDCl₃): δ = 4.56 (dd, *J* = 4.3, 2.9 Hz, 1H; OC^aHO), 3.84 – 3.72 (m, 2H; C^eHHO + ThpOCH^hHCH₂O), 3.68 – 3.62 (m br, 2H; OCH₂CH₂OH), 3.62 – 3.48 (m, 29H; OCH₂CH₂O + ThpOCH^hHCH₂O + OCH₂CH₂OH), 3.48 – 3.38 (m, 1H; C^eHHO), 2.87 (s br; OCH₂CH₂OH), 1.83 – 1.70 (m, 1H; C^cHH), 1.70 – 1.58 (m, 1H; C^bHH), 1.58 – 1.37 (m, 4H; C^bHH + C^dH₂ + C^cHH).

^{13}C NMR (101 MHz, CDCl_3): δ = 98.9 ($\text{OC}^{\text{a}}\text{HO}$), 72.6 ($\text{OCH}_2\text{CH}_2\text{OH}$), 70.57-70.49 (12C), 70.32 (1C) (all $\text{OCH}_2\text{CH}_2\text{O} + \text{ThpOCH}_2\text{CH}_2\text{O}$), 66.6 ($\text{ThpOCH}_2\text{CH}_2\text{O}$), 62.1 ($\text{C}^{\text{e}}\text{H}_2\text{O}$), 61.6 ($\text{OCH}_2\text{CH}_2\text{OH}$), 30.5 ($\text{C}^{\text{b}}\text{H}_2$), 25.4 ($\text{C}^{\text{d}}\text{H}_2$), 19.4 ($\text{C}^{\text{c}}\text{H}_2$).

ES-ToF: m/z (%): 477.3 (100) [$M + \text{Na}$] $^+$; Calc.: [$M + \text{Na}$] $^+$ 477.3.

ThpO–Eg₈–OTs (**65**)^{38,163,165}

ThpO–Eg₈–OTs was synthesized according to the protocol for the smaller analogue, ThpO–Eg₄–OTs (**2b**). ThpO–Eg₈–OH (67.8 g), in CH_2Cl_2 (95 mL) plus 1-methylimidazole (0.119 mL), was reacted with TsCl (37.0 g, 1.3 eq.) to give the product, ThpO–Eg₈–OTs (84.3 g, 93 %), as a pale yellow oil.



R_f (CHCl_3 -MeOH 9:1, KMnO_4): 0.48 (ThpO–Eg₈–OH), 0.64 (ThpO–Eg₈–OTs).

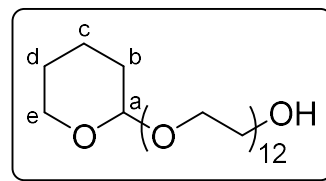
^1H NMR (400 MHz, CDCl_3): δ = 7.74 (d, J = 8.2 Hz, 2H; Ar SO_3CCH), 7.29 (d, J = 7.9 Hz, 2H; Ar CHCCH_3), 4.57 (dd, J = 4.4, 2.9 Hz, 1H; $\text{OC}^{\text{a}}\text{HO}$), 4.14 – 4.05 (m, 2H; CH_2OTs), 3.86 – 3.75 (m, 2H; $\text{C}^{\text{e}}\text{HHO} + \text{ThpOCHHCH}_2\text{O}$), 3.68 – 3.48 (m, 29H; $\text{ThpOCHHCH}_2\text{O} + \text{OCH}_2\text{CH}_2\text{O}$), 3.48 – 3.40 (m, 1H; $\text{C}^{\text{e}}\text{HHO}$), 2.39 (s, 3H; Ar CCH_3), 1.84 – 1.71 (m, 1H; $\text{C}^{\text{c}}\text{HH}$), 1.71 – 1.59 (m, 1H; $\text{C}^{\text{b}}\text{HH}$), 1.59 – 1.38 (m, 4H; $\text{C}^{\text{b}}\text{HH} + \text{C}^{\text{d}}\text{H}_2 + \text{C}^{\text{c}}\text{HH}$).

^{13}C NMR (101 MHz, CDCl_3): δ = 144.8 (Ar CCH_3), 133.0 (Ar SO_3C), 129.8 (2C; Ar CHCCH_3), 127.9 (2C; Ar SO_3CCH), 98.9 ($\text{OC}^{\text{a}}\text{HO}$), 70.71 (1C), 70.58-70.49 (12C) (all $\text{OCH}_2\text{CH}_2\text{O} + \text{ThpOCH}_2\text{CH}_2\text{O}$), 69.2 (CH_2OTs), 68.6 ($\text{OCH}_2\text{CH}_2\text{OTs}$), 66.6 ($\text{ThpOCH}_2\text{CH}_2\text{O}$), 62.2 ($\text{C}^{\text{e}}\text{H}_2\text{O}$), 30.6 ($\text{C}^{\text{b}}\text{H}_2$), 25.4 ($\text{C}^{\text{d}}\text{H}_2$), 21.6 (Ar CCH_3), 19.5 ($\text{C}^{\text{c}}\text{H}_2$).

ES-ToF: m/z (%): 631.3 (100) [$M + \text{Na}$] $^+$; Calc.: [$M + \text{Na}$] $^+$ 631.3.

ThpO–Eg₁₂–OH (**66**)³⁸

The crude product of ThpO–Eg₁₂–OH was obtained according to the protocol for the smaller analogue, ThpO–Eg₈–OH (**3a**). ThpO–Eg₈–OTs (77.5 g), in THF (103 mL) plus tetragol (110 mL, 5 eq.), was reacted with a 60 % suspension of NaH in mineral oil (10.2 g, 2 eq.). Extraction with CHCl₃ needed fewer partitions (1 x 1 L, 2 x 250 mL). Fractionation, as above, through a large sinter funnel packed with flash silica separated high *R_f* contaminants and low *R_f* HO–Eg₄–OH from the product. The majority of the product (49.8 g, 62 %) was successfully purified in this fashion, but the remainder was contaminated with ThpO–Eg₂₀–OThp dimer due to their similar *R_f* values. For this reason the mixed fraction was separated by reverse phase chromatography.



The mixed fraction (28.4 g) was dissolved in MeCN (100 mL) and silanized silica gel 60 (200 mL) was added. From this point all solvents contained a trace of aqueous ammonia to prevent acid-catalyzed acetal cleavage. The slurry was slowly diluted with water (300 mL) under continuous gentle swirling, and the MeCN was then removed on a rotary evaporator. A large sintered funnel (D = 8.5 cm) packed with silanized silica 60 (500 mL dry volume, 8.5 cm deep) was then prepared. The now aqueous slurry of pre-absorbed crude product was carefully poured onto the top of the packed column, which was then eluted with a gradient of MeCN:water. Pure ThpO–Eg₁₂–OH eluted from 5 % up to 30 % MeCN, after which a mixed fraction containing ThpO–Eg₂₀–OThp dimer impurity came off up to 95:5 MeCN:H₂O. After removal of the organic solvent, the residue was partitioned into CHCl₃ with a trace Et₃N. The solution was dried over Na₂SO₄, followed by removal of solvent and drying in vacuo (0.3 mbar) to give a colourless oil (16.2 g, 20 %).

R_f (CHCl₃-MeOH 9:1, KMnO₄): 0.44 (ThpO–Eg₁₂–OH), 0.52 (ThpO–Eg₂₀–OThp), 0.64 (ThpO–Eg₈–OTs), 0.86 (Mineral oil)

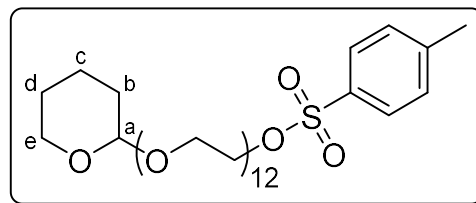
¹H NMR (400 MHz, CDCl₃): δ = 4.53 (dd, *J* = 4.3, 2.9 Hz, 1H; OC^aHO), 3.82 – 3.69 (m, 2H; C^eHHO + ThpOCH^hHCH₂O), 3.67 – 3.43 (m, 47H; OCH₂CH₂OH + OCH₂CH₂O + ThpOCH^hHCH₂O + OCH₂CH₂OH), 3.43 – 3.34 (m, 1H; C^eHHO), 2.96 (s br; OCH₂CH₂OH), 1.80 – 1.66 (m, 1H; C^cHH), 1.66 – 1.55 (m, 1H; C^bHH), 1.55 – 1.34 (m, 4H; C^bHH + C^dH₂ + C^cHH).

¹³C NMR (126 MHz, CDCl₃): δ = 98.7 (OC^aHO), 72.5 (OCH₂CH₂OH), 70.45-70.38 (20C), 70.17 (1C) (all OCH₂CH₂O + ThpOCH₂CH₂O), 66.5 (ThpOCH₂CH₂O), 62.0 (C^eH₂O), 61.5 (OCH₂CH₂OH), 30.4 (C^bH₂), 25.3 (C^dH₂), 19.3 (C^cH₂).

NSI: *m/z* (%): 648.4150 (100) [*M* + NH₄]⁺; Calc.: [*M* + NH₄]⁺ 648.4165. MALD-ToF: *m/z* (%): 653.4 (100) [*M* + Na]⁺; Calc.: [*M* + Na]⁺ 653.4.

ThpO–Eg₁₂–OTs (**67**)³⁸

ThpO–Eg₁₂–OTs was synthesized according to the protocol for the smaller analogue, ThpO–Eg₄–OTs (**2b**). ThpO–Eg₁₂–OH (30.0 g), in CH₂Cl₂ (40 mL) plus 1-methylimidazole (0.038 mL), was reacted with TsCl (11.8 g, 1.3 eq.) to give the product, ThpO–Eg₁₂–OTs (37.3 g, 95 %), as a pale yellow oil.



R_f (CHCl₃-MeOH 9:1, KMnO₄): 0.44 (ThpO–Eg₁₂–OH), 0.60 (ThpO–Eg₁₂–OTs)

¹H NMR (400 MHz, CDCl₃; ref. (CH₃CH₂)₃N = 0.975): δ = 7.74 (d, J = 8.3 Hz, 2H; Ar SO₃CCH), 7.30 (d, J = 8.1 Hz, 2H; Ar CHCCH₃), 4.58 (dd, J = 4.3, 2.9 Hz, 1H; OC^aHO), 4.14 – 4.06 (m, 2H; CH₂OTs), 3.86 – 3.74 (m, 2H; C^eHHO + ThpOCHHCH₂O), 3.68 – 3.49 (m, 45H; ThpOCHHCH₂O + OCH₂CH₂O), 3.48 – 3.38 (m, 1H; C^eHHO), 2.40 (s, 3H; Ar CCH₃), 1.84 – 1.71 (m, 1H; C^cHH), 1.71 – 1.60 (m, 1H; C^bHH), 1.60 – 1.40 (m, 4H; C^bHH + C^dH₂ + C^cHH).

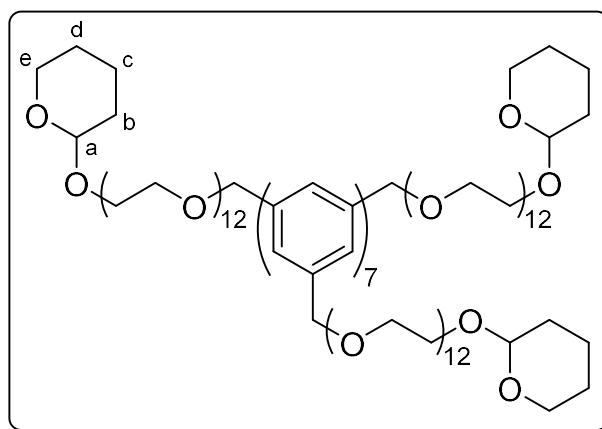
¹³C NMR (126 MHz, CDCl₃): δ = 144.7 (Ar CCH₃), 132.9 (Ar SO₃C), 129.7 (2C; Ar CHCCH₃), 127.9 (2C; Ar SO₃CCH), 98.8 (OC^aHO), 70.61 (1C), 70.49-70.38 (20C) (all OCH₂CH₂O + ThpOCH₂CH₂O), 69.2 (CH₂OTs), 68.5 (OCH₂CH₂OTs), 66.5 (ThpOCH₂CH₂O), 62.1 (C^eH₂O), 30.5 (C^bH₂), 25.3 (C^dH₂), 21.5 (Ar CCH₃), 19.4 (C^cH₂).

NSI: m/z (%): 802.4234 (100) [$M + \text{NH}_4$]⁺; Calc.: [$M + \text{NH}_4$]⁺ 802.4253. MALD-ToF: m/z (%): 807.4 (100) [$M + \text{Na}$]⁺; Calc.: [$M + \text{Na}$]⁺ 807.4.

5.4. Eg₁₂ homostars

Hub³-Eg₁₂-OThp (**60**) (via **66** with **43d**, not **59**)

In a 100 mL round-bottomed flask equipped with a magnetic stirrer was placed ThpO-Eg₁₂-OH (7.68 g, 3.3 eq.). This was evaporated from MeCN (3 x 10 mL), and then dissolved in THF (30 mL). To the stirred solution was added fresh sublimed grade KO^tBu (1.45 g, 3.5 eq.), and after 5 minutes when all the KO^tBu had dissolved, 94 wt% Hub³-CH₂Br (3.2 g) was also added. After 10 minutes, the reaction was quenched with sat. aqueous NH₄Cl (0.3 mL, 0.6 eq.), and the



organic solvent removed on a rotary evaporator. The mixture was then transferred to a 2 L separatory funnel, diluted with water (500 mL), and extracted with CHCl₃ (400 mL then 200 mL). The combined organic fractions were dried over anhydrous Na₂SO₄, and the solvent was removed on a rotary evaporator, followed by drying under high vacuum (0.3 mbar).

A sinter funnel (D = 6 cm) was then packed with silanized silica (4 cm depth). To the crude mixture dissolved in MeCN was added a small amount of silanized silica. An equal volume of H₂O was slowly added and the slurry was carefully poured onto the packed column. The column was eluted with a gradient of MeCN:water from 50 % to 95 % MeCN. ThpO-Eg₁₂-OH eluted 50 – 70 % MeCN and the product homostar 80 – 95 % MeCN. The appropriate fractions were combined, the organic solvent was evaporated, and residual water was removed by co-evaporated from further MeCN. The residue was then re-dissolved in CHCl₃, filtered and the solvent once again removed on a rotary evaporator, followed by drying under high vacuum (0.3 mbar) to give Hub³-Eg₁₂-OThp (7.5 g, 83 %) which was used in the next step without further purification. The building block containing fractions were worked up similarly to return pure ThpO-Eg₁₂-OH (0.86 g, 0.37 eq.).

Note: The 3-armed Hub³-Eg₁₂-OThp product contains traces of 2-armed homostar arising from the side reaction of the benzylic bromomethyl moiety with traces of hydroxide. This two-armed species is difficult to remove chromatographically. Beyond thorough drying to minimize residual adventitious water, a high grade of sublimed KO^tBu should be used to minimize the introduction of KOH that is present in lower grades. The reaction of Hub³-CH₂OH with ThpO-Eg₄-OTs was also attempted as a strategy to avoid generation of the two-armed byproduct, but was very slow.

R_f (CHCl₃-MeOH 9:1, KMnO₄/UV): 0.46 (ThpO-Eg₁₂-OH), 0.56 [Hub³-(CH₂O-Eg₁₂-OThp)₃], 0.58 [Hub³-(CH₂O-Eg₁₂-OThp)₂(CH₂OH)] The two higher R_f species almost fully overlap. Notably the two-arm by-

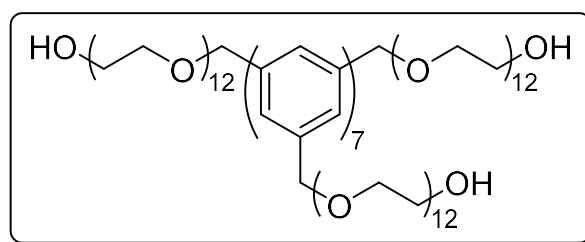
product appears as a distinctly blueish spot on fluorescent TLC plates under UV (254 nm) as opposed to the darker spot for the main three-arm product.

^1H NMR (400 MHz, CDCl_3): δ = 7.81 (s, 3H; C^1H), 7.73 (d, J = 8.0 Hz, 6H; C^4H), 7.66 (d, J = 8.1 Hz, 6H; C^5H), 7.58 (d, J = 7.9 Hz, 6H; C^8H), 7.38 (d, J = 7.8 Hz, 6H; C^9H), 4.59 – 4.52 (m, 9H; $\text{C}^{11}\text{H}_2\text{O}$ + OC^aHO), 3.84 – 3.73 (m, 6H; C^eHHO + $\text{ThpOCHHCH}_2\text{O}$), 3.70 – 3.48 (br m, 141H; $\text{OCH}_2\text{CH}_2\text{O}$ + $\text{ThpOCHHCH}_2\text{O}$), 3.47 – 3.37 (m, 3H; C^eHHO), 1.83 – 1.69 (m, 3H; C^eHH), 1.69 – 1.58 (m, 3H; C^bHH), 1.58 – 1.38 (m, 12H; C^bHH + C^dH_2 + C^eHH).

^{13}C NMR (101 MHz, CDCl_3): δ = 141.7 (C^2), 139.86 (C^6), 139.64 + 139.57 (C^3 + C^7), 137.4 (C^{10}), 128.0 (2C; C^9H), 127.46 (2C; C^4H), 127.25 (2C; C^5H), 126.74 (2C; C^8H), 124.6 (C^1H), 98.6 (OC^aHO), 72.7 ($\text{C}^{11}\text{H}_2\text{O}$), 70.42, 70.32 (22C; all $\text{OCH}_2\text{CH}_2\text{O}$), 69.3 ($\text{C}^{11}\text{H}_2\text{OCH}_2\text{CH}_2\text{O}$), 66.4 ($\text{ThpOCH}_2\text{CH}_2\text{O}$), 61.9 ($\text{C}^e\text{H}_2\text{O}$), 30.3 (C^bH_2), 25.2 (C^dH_2), 19.2 (C^eH_2).

Hub³–Eg₁₂–OH (**61**) (via **60**)

In a 100 mL round-bottomed flask were placed Hub³–Eg₁₂–OThp (**61**) (5.8 g, 2.36 mmol) and MeOH (20 mL). To the stirred solution was added MsOH (60 μL). After 1 h the reaction was quenched with sat. aqueous NaHCO_3 (1.7 mL), and the organic solvent was removed on a rotary evaporator. The residue was diluted with 10 %



brine (300 mL) and extracted into chloroform (2 x 300 mL). The combined fractions were dried over Na_2SO_4 , filtered and the solvent removed on a rotary evaporator, followed by drying under high vacuum (0.3 mbar) to give the crude product (5.2 g). A sinter funnel (D = 6.5 cm) was packed with flash silica (depth 12 cm), and the crude material loaded in chloroform. The mixture was eluted with a gradient up to 20 % MeOH in CHCl_3 . A higher R_f contaminant eluted first, and was found to be two-arm homostar (50 mg) derived from traces of water in the preceding reaction. A mixed fraction followed containing mostly the main product (1.34 g). Pure Hub³–Eg₁₂–OH was then isolated in acceptable yield (3.61 g, 69 %) as the lower R_f species.

R_f (CHCl_3 -MeOH 9:1, KMnO_4 /UV): 0.34 [Hub^3 –(CH_2O –Eg₁₂–OH)₃], 0.41 [Hub^3 –(CH_2O –Eg₁₂–OH)₂(CH_2O)₁]. Notably the two-arm byproduct appears as a distinctly blueish spot on fluorescent TLC plates under UV (254 nm) as opposed to the darker spot for the main product.

^1H NMR (400 MHz, CDCl_3): δ = 7.863 (s, 3H; C^1H), 7.786 (d, J = 8.3 Hz, 6H; C^4H), 7.706 (d, J = 8.5 Hz, 6H; C^5H), 7.629 (d, J = 8.2 Hz, 6H; C^8H), 7.433 (d, J = 8.3 Hz, 6H; C^9H), 4.609 (s, 6H; $\text{C}^{11}\text{H}_2\text{O}$), 3.71 – 3.59 (m, 138H; $\text{OCH}_2\text{CH}_2\text{O}$), 3.59 – 3.55 (m, 6H; $\text{CH}_2\text{CH}_2\text{OH}$).

^{13}C NMR (101 MHz, CDCl_3): δ = 142.0 (C^2), 140.18 (C^6), 139.97 + 139.92 ($\text{C}^3 + \text{C}^7$), 137.6 (C^{10}), 128.3 (C^9H), 127.74 (C^4H), 127.55 (C^5H), 127.06 (C^8H), 125.0 (C^1H), 72.97 ($\text{C}^{11}\text{H}_2\text{O}$), 72.62 ($\text{OCH}_2\text{CH}_2\text{OH}$), 70.69, 70.68, 70.61, 70.57 (all $\text{OCH}_2\text{CH}_2\text{O}$, main peak at 70.57 ± 0.15), 70.30 ($\text{C}^{11}\text{H}_2\text{OCH}_2\text{CH}_2$), 69.6 ($\text{C}^{11}\text{H}_2\text{OCH}_2\text{CH}_2$), 61.7 ($\text{OCH}_2\text{CH}_2\text{OH}$).

5.5. Chain extension, diafiltration and deprotection

General etherification procedure: $\text{Hub}^3\text{-Eg}_n\text{-OH}$ with **67** to $\text{Hub}^3\text{-Eg}_{n+12}\text{-OThp}$ (**72**, **74**, **76**, **78**)

In separate 100 mL round-bottomed flasks, both equipped with magnetic stirrers, were placed $\text{Hub}^3\text{-Eg}_n\text{-OH}$ (see Table 24) and $\text{ThpO-Eg}_{12}\text{-OTs}$ (10 eq., see Table 24). Each was evaporated from MeCN ($3 \times 3 \text{ mL}\cdot\text{g}^{-1}$), the latter with a trace of Et_3N added prior to the first round of drying.

$\text{Hub}^3\text{-Eg}_n\text{-OH}$ was re-dissolved in a fraction of the total DMF volume (see Table 24), followed by the addition of a 60 % dispersion of NaH in mineral oil (6 eq., see Table 24). The $\text{ThpO-Eg}_{12}\text{-OTs}$ (10 eq., see Table 24) was then re-dissolved in the remaining volume of DMF (see Table 24), and transferred into the reaction mixture using a glass syringe. The mixture was stirred at room temperature for 1 h. Thereafter, the shorter oligomer reactions (Eg_{24} , Eg_{36}) were stirred at room temperature overnight, while the longer oligomers (Eg_{48} , Eg_{60}) were run at 40°C overnight; the latter were less concentrated due to the addition of extra solvent needed to permit free stirring of the otherwise viscous mixtures. Note: It is possible that anionic depolymerization of unprotected chain termini might compete with slow Williamson etherification, causing PEG chain-length dispersity, but this cannot occur on the arms that have already been extended. For this reason, reactions were not heated initially to obtain significant conversion under milder conditions, before using more forcing conditions.

After 24 h, the reaction was quenched with sat. aqueous NH_4Cl , diluted with THF, and after a few minutes the solids were removed by filtration. The filtrate was further diluted with methanol to achieve a ratio of 1:4 v/v MeOH-THF; solvent amounts were selected to achieve a final volume of 60-80 mL that could be accommodated in the 100 mL feed tank for nanofiltration. The general nanofiltration procedure is described in a later section with any deviations listed here.

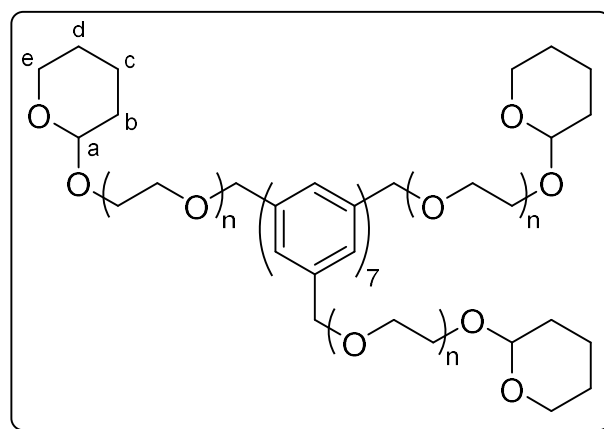


Table 24. Reagent summary for etherification to Hub³-Eg_{n+12}-OThp (**72**, **74**, **76**, **78**).

n	Hub ³ -Eg _n -OH			67	NaH ^[a]	DMF	Hub ³ -Eg _{n+12} -OThp			Yield
	g	g·mol ⁻¹	μmol				g	g·mol ⁻¹	μmol	
12	1.500	2210.7	679	5.326	163	10.5	2.477	4049.0	604	89
24	1.967	3796.6	518	4.067	124	8.0	2.660	5634.9	472	91
36	2.177	5382.5	404	3.174	97	8.0	1.765	7220.8	244	60
48	1.075	6968.4	154	1.211	37	6.7	1.264	8806.7	144	93

[a] 60 wt% suspension in mineral oil

Hub³-Eg₂₄-OThp (**72**)

Diafiltration was first run for 29.2 hours with EtOH-dried PEEK membranes. The gradual decrease in 2nd stage homostar concentration was greater than the expected decrease over the time interval. The behaviour was suggestive of a small leak which could not be located. It was then clear that the leak would diminish the selectivity of the EtOH-dried PEEK membranes. The diafiltration was therefore stopped after 29.2 hours and the membranes exchanged for acetone-dried PEEK membranes. The apparatus was washed according to the standard protocol, the solvent evaporated, and the residue dried under high vacuum (0.3 mbar) to yield a thick pale yellow oil (4.25 g). The permeate over the 29.2 hours was concentrated and dried in a similar fashion to yield an orange-brown oil containing solids (1.91 g).

The recovered crude product was once again diluted into THF-MeOH 1:4 (v/v) and diafiltration resumed for 24 hours with acetone-dried PEEK membranes, according to the standard protocol. After diafiltration, the apparatus was washed, and the solvent evaporated to yield a thick pale yellow oil which solidified upon drying under high vacuum (0.3 mbar), Hub³(-Eg₂₄-OThp)₃ (2.45 g, 89 %).

¹H NMR (500 MHz, CDCl₃) δ 7.85(s, 3H; C¹H), 7.77 (d, *J* = 8.2 Hz, 6H; C⁴H), 7.69 (d, *J* = 8.3Hz, 6H; C⁵H), 7.62 (d, *J* = 8.1 Hz, 6H; C⁸H), 7.42 (d, *J* = 8.3 Hz, 6H; C⁹H), 4.61 – 4.57 (m, 9H; C¹¹H₂O + OC^aHO), 3.86 – 3.79 (m, 6H; C^eHHO + ThpOCH₂CH₂O), 3.72 – 3.51 (br m, 285H; OCH₂CH₂O + ThpOCH₂CH₂O), 3.49 – 3.42 (m, 3H; C^eHHO), 1.84 – 1.74 (m, 3H; C^cHH), 1.72 – 1.63 (m, 3H; C^bHH), 1.61 – 1.42 (m, 12H; C^bHH + C^dH₂ + C^cHH).

¹³C NMR (126 MHz, CDCl₃): δ = 141.96 (C²), 140.18 (C⁶), 139.97 + 139.92 (C³ + C⁷), 137.58 (C¹⁰), 128.30 (C⁹H), 127.74 (C⁴H), 127.54 (C⁵H), 127.05 (C⁸H), 124.97 (C¹H), 98.92 (OC^aHO), 72.97 (C¹¹H₂O), 70.89, 70.69, 70.68 (all OCH₂CH₂O), 70.57 (br, OCH₂CH₂O main peak), 69.56 (C¹¹H₂OCH₂CH₂O), 66.65 (ThpOCH₂CH₂O), 62.20 (C^eH₂O), 30.58 (C^bH₂), 25.45 (C^dH₂), 19.49 (C^cH₂).

Hub³-Eg₃₆-OThp (74)

The quenched crude reaction mixture was diluted into THF-MeOH 1:4 (v/v) and diafiltration run for 32 hours with acetone-dried PEEK membranes, according to the standard protocol. A 1st stage recirculation pump failure approximately 1 hour long, detected after 13.8 h, caused a large spike in the 2nd stage concentrations of all solutes. The recirculation pump was restarted and the concentrations stabilized back to their steady state value by 18.0 h. After diafiltration, the apparatus was washed, the solvent evaporated, and the product dried under high vacuum (0.3 mbar) to yield a brownish yellow solid, Hub³(-Eg₃₆-OThp)₃ (2.66 g, 91 %). The combined permeate fractions from 0.0-15.0 h gave a yellowish oil containing solids (2.88 g).

¹H NMR (500 MHz, CDCl₃) δ 7.83 (s, 3H; C¹H), 7.75 (d, *J* = 7.9 Hz, 6H; C⁴H), 7.67 (d, *J* = 7.8 Hz, 6H; C⁵H), 7.59 (d, *J* = 7.8 Hz, 6H; C⁸H), 7.40 (d, *J* = 7.8 Hz, 6H; C⁹H), 4.62 – 4.52 (m, 9H; C¹¹H₂O + OC^aHO), 3.84 – 3.76 (m, 6H; C^eH₂O + ThpOCH₂CH₂O), 3.70 – 3.47 (br m, 429H; OCH₂CH₂O + ThpOCH₂CH₂O), 3.46 – 3.41 (m, 3H; C^eH₂O), 1.83 – 1.70 (m, 3H; C^bHH), 1.70 – 1.59 (m, 3H; C^bHH), 1.59 – 1.39 (m, 12H; C^bHH + C^dH₂ + C^cHH).

¹³C NMR (126 MHz, CDCl₃): δ = 141.87 (C²), 140.08 (C⁶), 139.87 + 139.82 (C³ + C⁷), 137.49 (C¹⁰), 128.22 (C⁹H), 127.65 (C⁴H), 127.45 (C⁵H), 126.96 (C⁸H), 124.87 (C¹H), 98.83 (OC^aHO), 72.87 (C¹¹H₂O), 70.80, 70.61, 70.59 (all OCH₂CH₂O), 70.49 (br, OCH₂CH₂O main peak), 69.46 (C¹¹H₂OCH₂CH₂O), 66.56 (ThpOCH₂CH₂O), 62.11 (C^eH₂O), 30.49 (C^bH₂), 25.36 (C^dH₂), 19.41 (C^cH₂).

Hub³-Eg₄₈-OThp (76)

The quenched crude reaction mixture was diluted into THF-MeOH 1:4 (v/v) and diafiltration was started with acetone-dried PEEK membranes, according to the standard protocol. A weld failure in the 1st stage retentate loop membrane cell caused sustained leakage at a low level, with significant loss of product over a period of 5.5 h. The diafiltration was stopped, the remaining mixture washed from the apparatus, according to standard protocol, and concentrated. The faulty cell was exchanged, re-using the original membrane in another cell. The diafiltration was restarted and run for 32 h. The apparatus was then washed, the solvent evaporated, and the product dried under high vacuum (0.3 mbar) to yield a pale brown solid, Hub³(-Eg₄₈-OThp)₃ (1.77 g, 60 %). The low yield is attributed to the leak; a yield around 85 – 90 % would otherwise have been expected, similar to the other diafiltrations.

¹H NMR (500 MHz, CDCl₃) δ 7.83 (s, 3H; C¹H), 7.75 (d, *J* = 7.6 Hz, 6H; C⁴H), 7.67 (d, *J* = 7.7 Hz, 6H; C⁵H), 7.60 (d, *J* = 8.1 Hz, 6H; C⁸H), 7.40 (d, *J* = 7.6 Hz, 6H; C⁹H), 4.61 – 4.54 (m, 9H; C¹¹H₂O + OC^aHO), 3.85 – 3.77 (m, 6H; C^eH₂O + ThpOCH₂CH₂O), 3.70 – 3.47 (br m, 573H; OCH₂CH₂O

+ThpOCHHCH₂O), 3.47 – 3.41 (m, 3H; C^eHHO), 1.83 – 1.71 (m, 3H; C^cHH), 1.71 – 1.60 (m, 3H; C^bHH), 1.60 – 1.40 (m, 12H; C^bHH + C^dH₂ + C^eHH).

¹³C NMR (126 MHz, CDCl₃): δ = 141.89 (C²), 140.11 (C⁶), 139.89 + 139.85 (C³ + C⁷), 137.51 (C¹⁰), 128.24 (C⁹H), 127.67 (C⁴H), 127.48 (C⁵H), 126.99 (C⁸H), 124.90 (C¹H), 98.86 (OC^aHO), 72.90 (C¹¹H₂O), 70.83, 70.63, 70.61 (all OCH₂CH₂O), 70.51 (br, OCH₂CH₂O main peak), 69.49 (C¹¹H₂OCH₂CH₂O), 66.59 (ThpOCH₂CH₂O), 62.14 (C^eH₂O), 30.52 (C^bH₂), 25.39 (C^dH₂), 19.43 (C^cH₂).

Hub³-Eg₆₀-OThp (**78**)

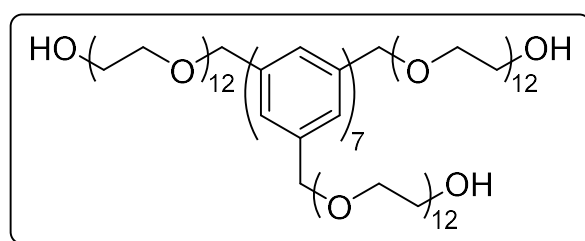
The quenched crude reaction mixture was diluted into THF-MeOH 1:4 (v/v) and diafiltration run for 32 h with acetone-dried PEEK membranes, according to the standard protocol. A 1st stage recirculation pump failure at 6.92 h was quickly detected and only caused a small temporary spike in the 2nd stage concentration. The recirculation pump was restarted, and the concentrations stabilized back to their steady state values by 9.00 h. After diafiltration, the apparatus was washed, the solvent evaporated, and the product dried under high vacuum (0.3 mbar) to yield a pale brown solid, Hub³(-Eg₆₀-OThp)₃ (1.26 g, 93 %).

¹H NMR (500 MHz, CDCl₃) δ 7.88 (s, 3H; C¹H), 7.80 (d, *J* = 8.4 Hz, 6H; C⁴H), 7.72 (d, *J* = 8.3 Hz, 6H; C⁵H), 7.65 (d, *J* = 8.2 Hz, 6H; C⁸H), 7.45 (d, *J* = 7.9 Hz, 6H; C⁹H), 4.65 – 4.60 (m, 9H; C¹¹H₂O + OC^aHO), 3.89 – 3.83 (m, 6H; C^eHHO + ThpOCHHCH₂O), 3.75 – 3.55 (br m, 717H; OCH₂CH₂O + ThpOCHHCH₂O), 3.53 – 3.46 (m, 3H; C^eHHO), 1.87 – 1.78 (m, 3H; C^cHH), 1.75 – 1.67 (m, 3H; C^bHH), 1.64 – 1.46 (m, 12H; C^bHH + C^dH₂ + C^eHH).

¹³C NMR (126 MHz, CDCl₃): δ = 141.86 (C²), 140.08 (C⁶), 139.86 + 139.80 (C³ + C⁷), 137.49 (C¹⁰), 128.21 (C⁹H), 127.64 (C⁴H), 127.44 (C⁵H), 126.95 (C⁸H), 124.87 (C¹H), 98.82 (OC^aHO), 72.86 (C¹¹H₂O), 70.80, 70.60, 70.59 (all OCH₂CH₂O), 70.48 (br, OCH₂CH₂O main peak), 69.46 (C¹¹H₂OCH₂CH₂O), 66.55 (ThpOCH₂CH₂O), 62.10 (C^eH₂O), 30.49 (C^bH₂), 25.36 (C^dH₂), 19.40 (C^cH₂).

General deprotection procedure: Hub³-Eg_n-OThp to Hub³-Eg_n-OH (**73**, **75**, **77**, **79**)

Similar to the deprotection of Hub³-Eg₁₂-OThp, homostar Hub³-Eg₁₂-OThp was dissolved in methanol (10 mg·L⁻¹), followed by addition of methanesulfonic acid (100 mM).



After 1 hour, the reaction was quenched with sat. aqueous NaHCO₃ (2 eq.), the organic solvent was removed on a rotary evaporator. The residue was diluted with 10 vol% brine in water (300 mL) and extracted into chloroform (2 x 300 mL). The combined fractions were dried over Na₂SO₄, filtered and solvent removed on a rotary evaporator, followed by drying under high vacuum (0.3 mbar) to give the pure product, Hub³-Eg_{n-12}-OH (95-98 %, see Table 25), ready for the next cycle of chain extension.

Table 25. Reagent summary for deprotection to Hub³-Eg_n-OH (**73**, **75**, **77**, **79**).

n	Hub ³ -Eg _n -OH			MsOH	MeOH	Hub ³ -Eg _{n+12} -OThp			Yield
	g	g·mol ⁻¹	μmol	μL	mL	g	g·mol ⁻¹	μmol	%
24	2.273	4049.0	561	148	22.7	2.073	3796.6	546	97
36	2.577	5634.9	457	168	25.8	2.338	5382.5	434	95
48	1.577	7220.8	218	103	15.8	1.487	6968.4	213	98
60	1.046	8806.7	119	68	10.5	0.993	8554.3	116	98

Hub³-Eg₂₄-OH (**73**)

¹H NMR (500 MHz, CDCl₃): δ = 7.84 (s, 3H; C¹H), 7.76 (d, *J* = 8.5 Hz, 6H; C⁴H), 7.68 (d, *J* = 8.3 Hz, 6H; C⁵H), 7.61 (d, *J* = 8.2 Hz, 6H; C⁸H), 7.42 (d, *J* = 7.9 Hz, 6H; C⁹H), 4.59 (s, 6H), 3.70 – 3.50 (m, 288H; OCH₂CH₂O).

¹³C NMR (126 MHz, CDCl₃): δ = 141.90 (C²), 140.12 (C⁶), 139.90 + 139.85 (C³ + C⁷), 137.53 (C¹⁰), 128.24 (C⁹H), 127.68 (C⁴H), 127.48 (C⁵H), 126.99 (C⁸H), 124.90 (C¹H), 72.90 (C¹¹H₂O), 72.52 (OCH₂CH₂OH), 70.84, 70.64, 70.62, 70.57 (all OCH₂CH₂O), 70.52 (br, OCH₂CH₂O main peak), 70.29 (C¹¹H₂OCH₂CH₂), 69.50 (C¹¹H₂OCH₂CH₂), 61.63 (OCH₂CH₂OH).

Hub³-Eg₃₆-OH (**75**)

¹H NMR (500 MHz, CDCl₃): δ = 7.83 (s, 3H; C¹H), 7.75 (d, *J* = 8.4 Hz, 6H; C⁴H), 7.67 (d, *J* = 8.4 Hz, 6H; C⁵H), 7.59 (d, *J* = 8.1 Hz, 6H; C⁸H), 7.39 (d, *J* = 8.0 Hz, 6H; C⁹H), 4.57 (s, 6H), 3.69 – 3.47 (m, 432H; OCH₂CH₂O).

¹³C NMR (126 MHz, CDCl₃): δ = 141.84 (C²), 140.06 (C⁶), 139.84 + 139.79 (C³ + C⁷), 137.48 (C¹⁰), 128.20 (C⁹H), 127.63 (C⁴H), 127.43 (C⁵H), 126.94 (C⁸H), 124.85 (C¹H), 72.85 (C¹¹H₂O), 72.49 (OCH₂CH₂OH), 70.78, 70.59, 70.57 (all OCH₂CH₂O), 70.47 (br, OCH₂CH₂O main peak), 70.23 (C¹¹H₂OCH₂CH₂), 69.45 (C¹¹H₂OCH₂CH₂), 61.56 (OCH₂CH₂OH).

Hub³-Eg₄₈-OH (**77**)

^1H NMR (500 MHz, CDCl_3): δ = 7.82 (s, 3H; C^1H), 7.76 (d, J = 8.6 Hz, 6H; C^4H), 7.67 (d, J = 8.4 Hz, 6H; C^5H), 7.59 (d, J = 7.8 Hz, 6H; C^8H), 7.39 (d, J = 7.7 Hz, 6H; C^9H), 4.57 (s, 6H), 3.69 – 3.45 (m, 576H; $\text{OCH}_2\text{CH}_2\text{O}$).

^{13}C NMR (126 MHz, CDCl_3): δ = 141.86 (C^2), 140.08 (C^6), 139.86 + 139.80 (C^3 + C^7), 137.49 (C^{10}), 128.21 (C^9H), 127.64 (C^4H), 127.44 (C^5H), 126.95 (C^8H), 124.86 (C^1H), 72.86 ($\text{C}^{11}\text{H}_2\text{O}$), 72.49 ($\text{OCH}_2\text{CH}_2\text{OH}$), 70.80, 70.60, 70.58 (all $\text{OCH}_2\text{CH}_2\text{O}$), 70.48 (br, $\text{OCH}_2\text{CH}_2\text{O}$ main peak), 70.25 ($\text{C}^{11}\text{H}_2\text{OCH}_2\text{CH}_2$), 69.46 ($\text{C}^{11}\text{H}_2\text{OCH}_2\text{CH}_2$), 61.56 ($\text{OCH}_2\text{CH}_2\text{OH}$).

Hub³-Eg₆₀-OH (79)

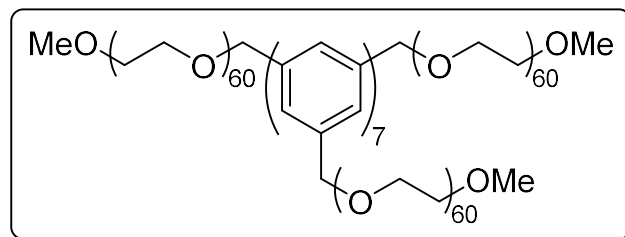
^1H NMR (500 MHz, CDCl_3): δ = 7.88 (s, 3H; C^1H), 7.81 (d, J = 8.4 Hz, 6H; C^4H), 7.73 (d, J = 8.3 Hz, 6H; C^5H), 7.65 (d, J = 8.2 Hz, 6H; C^8H), 7.45 (d, J = 8.3 Hz, 6H; C^9H), 4.63 (s, 6H), 3.75 – 3.54 (m, 720H; $\text{OCH}_2\text{CH}_2\text{O}$).

^{13}C NMR (126 MHz, CDCl_3): δ = 141.66 (C^2), 139.88 (C^6), 139.64 + 139.58 (C^3 + C^7), 137.34 (C^{10}), 128.03 (C^9H), 127.47 (C^4H), 127.26 (C^5H), 126.75 (C^8H), 124.65 (C^1H), 72.66 ($\text{C}^{11}\text{H}_2\text{O}$), 72.34 ($\text{OCH}_2\text{CH}_2\text{OH}$), 70.62, 70.43, 70.41 (all $\text{OCH}_2\text{CH}_2\text{O}$), 70.31 (br, $\text{OCH}_2\text{CH}_2\text{O}$ main peak), 70.07 ($\text{C}^{11}\text{H}_2\text{OCH}_2\text{CH}_2$), 69.29 ($\text{C}^{11}\text{H}_2\text{OCH}_2\text{CH}_2$), 61.35 ($\text{OCH}_2\text{CH}_2\text{OH}$).

5.6. Functionalization and hub cleavage

Hub³-Eg₆₀-OMe (**80**)

In a 100 mL round-bottomed flask equipped with a magnetic stirrer was placed Hub³-Eg₆₀-OH (0.461 g, 0.054 mmol). This was evaporated from MeCN (3 x 3 mL), and then dissolved in THF (8 mL). To the stirred solution cooled in an ice bath was added a 60 % suspension of NaH in mineral oil (45 mg, 20 eq.), and



after 5 minutes methyl iodide (180 μ L, 50 eq.) was also added. Within a few minutes a white precipitate had formed. After 10 minutes, the solution was lifted out of the ice bath and stirred at room temperature overnight.

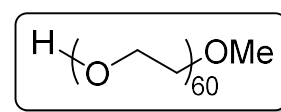
After 12 h, some brown solids were visible in solution. Methyl iodide was removed under vacuum, the reaction was quenched with sat. aqueous NH₄Cl (0.5 mL), and the remaining organic solvent also removed under high vacuum. The mixture was then transferred to a 500 mL separatory funnel, diluted with 0.1 M sodium thiosulfate (300 mL), and extracted with CHCl₃ (2 x 150 mL). The combined fractions were dried over anhydrous Na₂SO₄, and the solvent was removed on a rotary evaporator, followed by drying under high vacuum (0.3 mbar) to yield Hub³-Eg₆₀-OMe (0.472 g, 102 %) containing traces of mineral oil which was used without further purification.

¹H NMR (500 MHz, CDCl₃): δ = 7.88 (s, 3H; C¹H), 7.81 (d, J = 8.4 Hz, 6H; C⁴H), 7.73 (d, J = 8.4 Hz, 6H; C⁵H), 7.65 (d, J = 8.2 Hz, 6H; C⁸H), 7.45 (d, J = 8.4 Hz, 6H; C⁹H), 4.63 (s, 6H; C¹¹H₂O), 3.73 – 3.56 (m, 714H; OCH₂CH₂O, main peak centred at 3.64), 3.56 – 3.53 (m, 6H; OCH₂CH₂OCH₃ or OCH₂CH₂OCH₃), 3.38 (s, 9H; OCH₂CH₂OCH₃).

¹³C NMR (126 MHz, CDCl₃): δ = 141.7 (C²), 139.95 (C⁶), 139.7 (2C; C³ + C⁷), 137.4 (C¹⁰), 128.1 (C⁹H), 127.52 (C⁴H), 127.32 (C⁵H), 126.8 (C⁸H), 124.7 (C¹H), 72.7 (C¹¹H₂O), 71.7 (OCH₂CH₂OCH₃), 70.7 (OCH₂CH₂O), 70.37 \pm 1 (117C; broad, main peak centred at 70.37; OCH₂CH₂O), 69.4 (C¹¹H₂OCH₂CH₂O), 58.8 (OCH₂CH₂OCH₃).

HO-Eg₆₀-OMe (**81**)

Pd(OAc)₂ (8.3 mg) was dissolved in THF (0.60 mL) and briefly sonicated. A 10 mL round-bottomed, two neck flask equipped with a magnetic stirrer was fitted with a Young's tap and a thick rubber septum. In this was placed Hub³-Eg₆₀-OH



(123 mg, 143 μmol) and methanol (3.4 mL). To the stirred mixture was added activated charcoal (56 mg), followed by $\text{Pd}(\text{OAc})_2$ in THF (0.55 mL). The suspension was evacuated until vigorous boiling was observed, and then let down to argon, repeating the process four times. After a final evacuation, the suspension was connected to a double walled balloon via the Young's tap and let down to hydrogen. The suspension was stirred vigorously overnight and after 20 h, another smaller batch of $\text{Pd}(\text{OAc})_2$ in THF (0.35 mL) was added via a syringe through the rubber septum. The suspension was then stirred for another 20 h, after which the hydrogen balloon was removed. The suspension repeatedly evacuated and let down to argon to remove all hydrogen, as above, followed by the addition of 9:1 MeOH:H₂O (5 mL).

The suspension was filtered through filter paper and liberally washed with 9:1 MeOH:H₂O. The filtrate was evaporated and the residue co-evaporated from MeCN to remove residual water, then redissolved in 8:2 CHCl_3 :MeOH and filtered through a plug of Na_2SO_4 to remove solids, followed by evaporation of solvent to give crude HO-Eg₆₀-OMe (95 mg, 78 %); this contained traces of presumed Hub³ with one PEG arm still attached, plus traces of mineral oil. Washing the remaining palladized charcoal with 9:1 CHCl_3 :MeOH gave a white solid, containing largely Hub³-CH₃ (17 mg), plus traces of PEG. The crude HO-Eg₆₀-OMe was adsorbed onto normal phase silica which was rinsed with 1:49 MeOH: CHCl_3 . Once contaminants had washed off, the product was then eluted with 1:4 MeOH: CHCl_3 . Removal of organic solvent gave the pure product, HO-Eg₆₀-OMe (55 mg, 48 %), as a colourless solid. **Note:** Care should be taken to use a sufficiently small amount of normal phase silica to prevent loss of product.

¹H NMR (500 MHz, CDCl_3): δ = 3.73 – 3.56 (s, 239H; $\text{OCH}_2\text{CH}_2\text{O}$, main peak centred at 3.633), 3.55 – 3.52 (m, 2H; $\text{OCH}_2\text{CH}_2\text{OCH}_3$ or $\text{OCH}_2\text{CH}_2\text{OCH}_3$), 3.368 (s, 3H; $\text{OCH}_2\text{CH}_2\text{OCH}_3$).

¹³C NMR (126 MHz, CDCl_3): δ = 72.7 ($\text{OCH}_2\text{CH}_2\text{OH}$), 72.1 ($\text{OCH}_2\text{CH}_2\text{OCH}_3$), 70.7 (117C; broad, main peak centred at 70.7; $\text{OCH}_2\text{CH}_2\text{O}$ and $\text{OCH}_2\text{CH}_2\text{OCH}_3$), 61.8 ($\text{OCH}_2\text{CH}_2\text{OH}$), 59.2 ($\text{OCH}_2\text{CH}_2\text{OCH}_3$).

5.7. Other compounds

Hub¹-Eg₄-OH (**45**), Hub²-Eg₄-OH (**47**) and Hub³-Eg₄-OH (**49**)

For rejection testing, the Eg₄ homostars Hub¹-Eg₄-OH (**45**), Hub²-Eg₄-OH (**47**) and Hub³-Eg₄-OH (**49**) were synthesized similarly to the protocol for Hub³-Eg₁₂-OH (**60**) via Hub³-Eg₁₂-OThp (**61**), but with ThpO-Eg₄-OH (**33**) as the building block.

HO-Eg₁₂-OTs (**68**)

For rejection testing, ThpO-Eg₁₂-OTs (**67**) (1.23 g, 1.57 mmol) was deprotected using the general deprotection conditions to yield HO-Eg₁₂-OTs (**68**) (1.09 g, 99 %).

Appendix A – Historical methods towards uniform PEG

Synthesis of uniform oligo(ethylene glycol) from 1936 to 1970

There is a wealth of published literature on the synthesis of ethylene glycol oligomers, starting in 1936 with work by H. Hibbert et al., initially towards Eg₁₀, and later supposedly to Eg₁₈₆^{166,167} Hibbert and co-workers performed their syntheses before chromatography techniques became standard tools, and so had difficulty identifying the need for protecting group chemistry to prevent the formation of undesired side products.

The first attempts at synthesizing uniform ethylene glycol oligomers were made by Perry & Hibbert in 1936 by reacting 2 eq. of a PEG oligomer sodium alkoxide salt with 1 eq. of a dichloride derivative of another oligomer.¹⁶⁶ Their understanding of the reaction is summarized in Figure 118 below. Their initial publication reveals the synthesis of several oligomers (Eg₄, Eg₆, Eg₈) up to decaethylene glycol (Eg₁₀) and their respective dichloride derivatives. However, this early method suffers from shortfalls as discussed in detail by Rauterkus et al. in 1961 where several requirements for a clean reaction are listed.¹⁶⁸

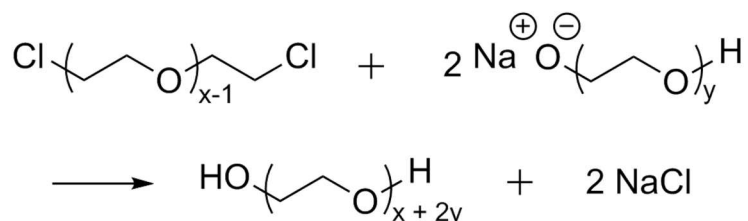


Figure 118. Synthesis of oligo(ethylene glycol) according to Perry & Hibbert (1936)¹⁶⁶. The representation is an idealized depiction of the reaction as higher oligomers are likely formed due to a lack of protecting groups being utilized.

During reaction with sodium or sodium methylate to generate the sodium alkoxide from the respective glycol, only the monoalkoxide must be generated, because longer homologues may be generated through reactions of the dialkoxides with the dichlorides. Perry et. al appear to have appreciated the problem noting on their use of a 3:1 molar excess of glycol to sodium that “the large excess of the glycol prevents the formation of the disodium salt”¹⁶⁶. The assumption may also be true to the extent that the formation of a divalent salt for such a short chain is probably much less favourable.

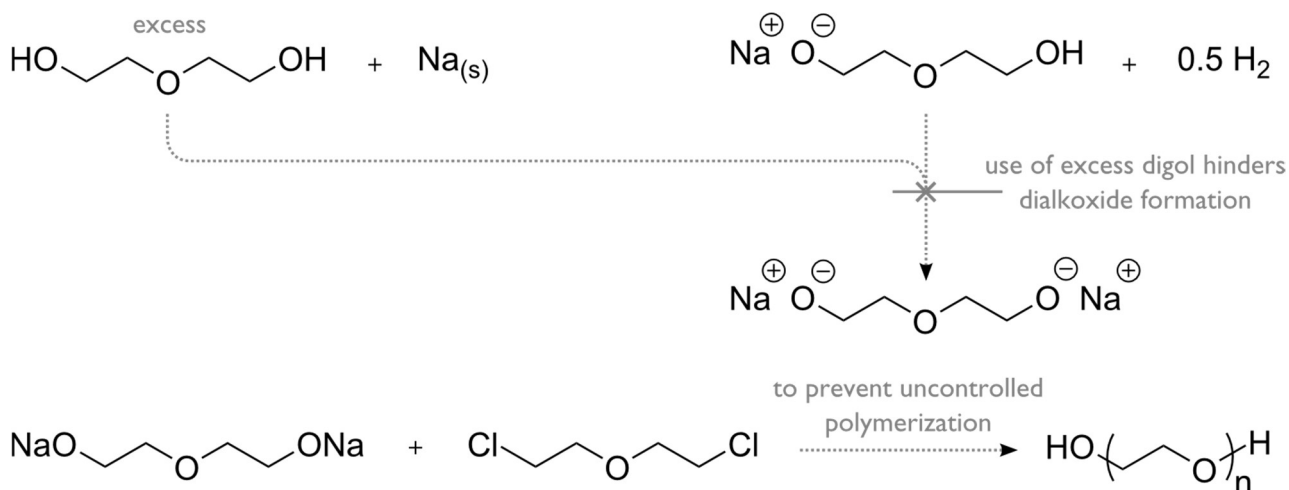


Figure 119. Synthesis of oligo(ethylene glycol) according to Perry & Hibbert (1936)¹⁶⁶. An excess of the diol is meant to hinder dialkoxide formation to prevent uncontrolled polymerization.

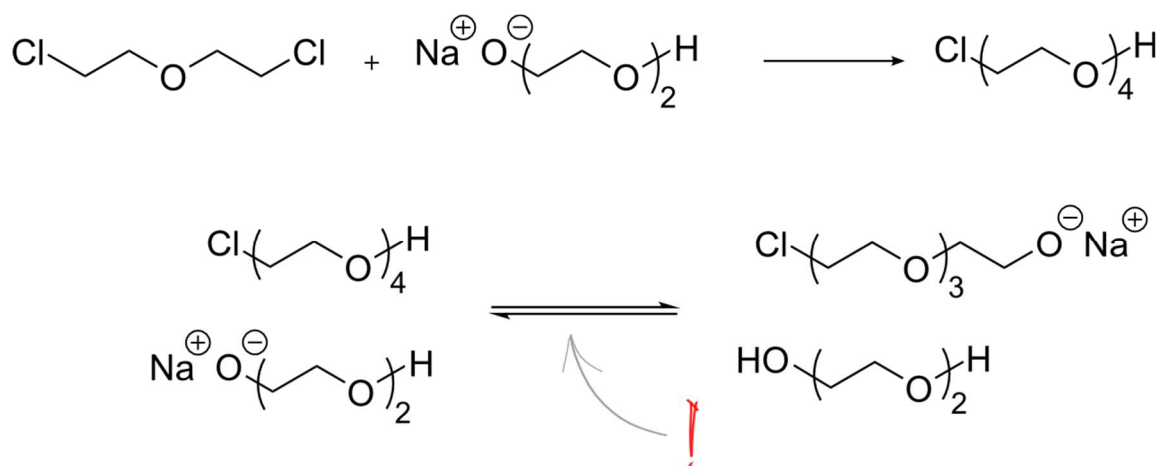


Figure 120. Synthesis of oligo(ethylene glycol) according to Perry & Hibbert (1936)⁵¹. Despite an excess of the diol and probably unfavourable formation of the dialkoxide as shown in Figure 119, an uncontrolled oligomerization can also occur due to equilibration. After the first extension step on one side of the dichloride, the product may be deprotonated by any other alkoxide.

But further, no equilibration must occur between the partially extended intermediate products and yet unreacted monoalkoxide as shown in Figure 120.

In at least one reaction, their synthesis of hexaethylene glycol, Perry et al. isolate the sodium alkoxide salt of diethylene glycol ($\text{NaO-Eg}_2\text{-OH}$) from the mixture by filtration upon cooling and then react it with the theoretical amount of Bis(2-chloroethyl) ether ($\text{Cl-Eg}_2\text{-Cl}$) which suggests that they may not have appreciated the possibility of equilibration at the time. The use of protecting group chemistry can help to eliminate both above problems.

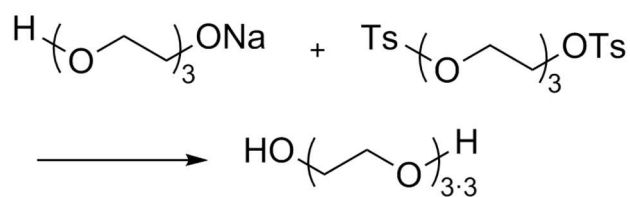
When repeating the synthesis of hexaethylene glycol in similar fashion and purifying by fractional distillation as described by Perry et al., Rauterkus et al. obtain three main fractions: as first distillate a

fraction containing largely unreacted excess Eg_2 , as second distillate a fraction largely hexaethylene glycol product and as bottom residue the longer homologues (Eg_{10} , etc.). All fractions tested positive on Baeyer's reagent/ KMnO_4 and bromine addition (Br_2) confirming the presence of unsaturation, i.e. vinyl ethers. Further, both distillate fractions also tested positive for chloride residue (presumably using AgNO_3). The reactions under the conditions described by Perry et al. therefore also do not proceed to completion and suffer from significant elimination which is consistent with the use of chloride as a relatively weak nucleofuge. The use of bromide, tosylate and other stronger leaving groups preferred in more modern syntheses helps to rectify these problems and allows for more complete reactions with a lower degree of competing elimination. Rauterkus et al. report that constant boiling hexaethylene glycol testing negative for unsaturation and chloride residue can be obtained by repeated fractional distillation, but with difficulty. They conclude that the synthesis of longer homologues such as Eg_{18} , and up to Eg_{90} and Eg_{186} as reported separately¹⁶⁷, had been extremely unlikely to have succeeded under the conditions used, as the method of repeated fractional crystallization apparently does not yield products completely free of vinyl and chloride residue. Further, fractional distillation of these longer homologues, even under high vacuum, is not possible.

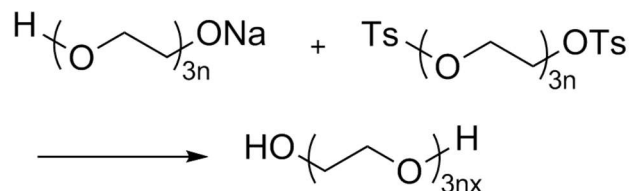
Synthesis of uniform oligo(ethylene glycol) from 1970 onwards

In 1970, with gel permeation chromatography (GPC) then available as an established separation technique, Bömer et al. revisited the problem.¹⁶⁹ They proceed via a 'triplication' route similar to Hibbert et al.'s, but using 4-toluenesulfonate ester (tosylate) as a more potent leaving group than chloride and thus improve selectivity by increasing the rate of the desired $\text{S}_{\text{N}}2$ substitution relative to the competing $\text{E}2$ elimination. Bömer et al. also highlight the importance of the starting material purity (in their case of Eg_3) which is true for all syntheses of ethylene glycol oligomers. Their Eg_3 was found to contain no more than 0.1 % of the neighbouring oligomers (Eg_2 and Eg_4) by analysis of the bis(trimethylsilyl) ethers by gas chromatography.

Their route proceeds via reaction of $\text{HO-Eg}_3\text{-ONa}$ with $\text{TsO-Eg}_3\text{-OTs}$ in an excess of tri(ethylene glycol) for 50 days at room temperature yielding over 90 % conversion, followed by separation of NaOTs by ion-exchange chromatography and removal of excess Eg_3 by vacuum distillation. From the remaining mixture of polymer homologues, Eg_9 and Eg_{15} are isolated by repeated molecular distillation, and shown to be pure by gel chromatography. Based on $\text{TsO-Eg}_3\text{-OTs}$, the limiting reagent, a 74 % yield is reported.



Generalized:



$x = 1, 2, 3, 4, 5 \dots$

Figure 121. Synthesis of oligo(ethylene glycol) according to Bömer et al. (1970)¹⁶⁹ The use of tosylate as a leaving group improves upon conversion and reduces the formation of vinyl side products.

Another triplication step is carried out from Eg₉ starting materials, in toluene as solvent, with 90 % conversion after 8 days. Here, in contrast to Hibbert et al.'s original method of using a slight excess of dichloride towards the end of the reaction to consume all remaining alkoxide, Bömer et al. instead hydrolyze unreacted tosylate groups with water under reflux, to obtain a mixture of homologues containing only hydroxyl end groups (as well as potentially some vinyl end groups from undesired elimination). This is advantageous as it will avoid crosslinking of desired product oligomer into higher homologues. Excess Eg₉ is again separated by molecular distillation but the resultant mixture of higher homologues (Eg₁₈ and higher) then needs to be separated by gel chromatography. The need to use some form of chromatography to separate desired higher oligomers from its reaction side products is a recurring theme in syntheses of uniform ethylene glycol oligomers to the present day. The authors highlight that separation becomes increasingly difficult with increasing oligomer length, and in their work use columns of aspect ratio around 40:1.

The authors make a meaningful observation with regard to impurity formation noting that “[...] only the products which are formed by linking an even number of units can include side products, formed by elimination or cyclization in appreciable amounts.” As exemplified in their synthesis, an uneven multiple of starting material oligomers in the product oligomer (product oligomer length = 3n, 5n, 7n, etc. where n is the length of starting oligomer) implies successful coupling via Williamson etherification of all tosylate groups in the constituent starting material oligomers. An E₂ type elimination of a tosylate group leading to a vinyl terminated side product prevents attachment of an alkoxide group at that same position, leading to a side product with one less multiple of starting oligomer, and thus an even number of starting oligomers in the side product (2n, 4n, 6n, etc.).

The presence of impurities in those fractions is highlighted by the lower melting points (**Table 26**) of the products with even multiples of starting oligomer, which is consistent with the lower interaction forces in molecules with hydroxyl groups replaced by other end groups^{170,171}, such as vinyl groups or ether groups in cyclized crown ethers.

Importantly, they mention this possibility for cyclization which would be particularly relevant for short oligomers (e.g. HO–Eg_n–Lg for n = 4, 5, 6) where templating around a cation favours intramolecular reaction to form the crown ether¹⁷², but also occurs with longer oligomers with higher prevalence in dilute reactions.

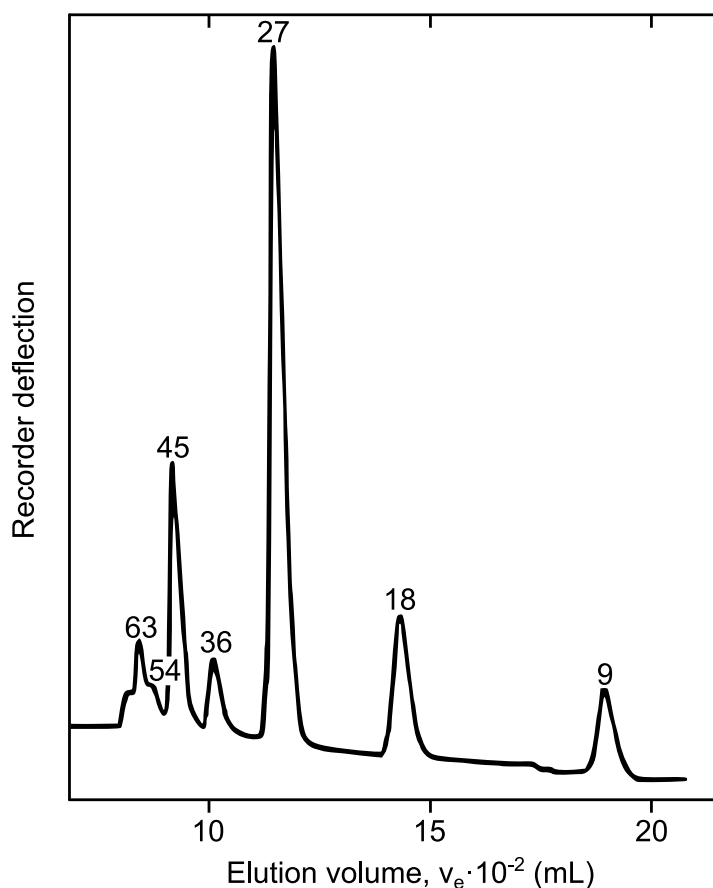


Figure 122. Analytical gel chromatogram of a discontinuous polymer homologous series of oligoethylene glycols. HO–Eg_n–OH (n = 9x; x = 1,2,3...) as synthesized by Bömer et al. The numbers above the peaks correspond to the degree of polymerization n. Reproduced from ¹⁶⁹ with permission from Elsevier.

In a useful reproduction of the work, Marshall et al. in 1980 significantly expand upon the sparse synthetic protocols of Bömer et al., give a succinct summary of the problems of ethylene glycol oligomer synthesis hitherto, and visualize the progress in oligomer purity (reflected in higher T_m) achieved through chromatographic methods, as well as the superiority of uniform samples in chromatographic resolution.¹⁷³

n	T _m / °C (Bömer et al.)	T _m / °C (lit. values)
9	29.8 – 30.0	only b.p.
14	-	29.5
15	38.6 – 38.8	-
18	32.0 – 32.4	24, 35
27	44.6 – 44.8	-
30	-	38.6
36	43.0 – 43.4	-
42	-	33.8
45	49.9 – 50.1	-
90	-	40.6
186	-	44.1

Table 26. Melting points of oligoethylene glycols, HO–Eg_n–OH. Reproduced from ¹⁶⁹ with permission from Elsevier.

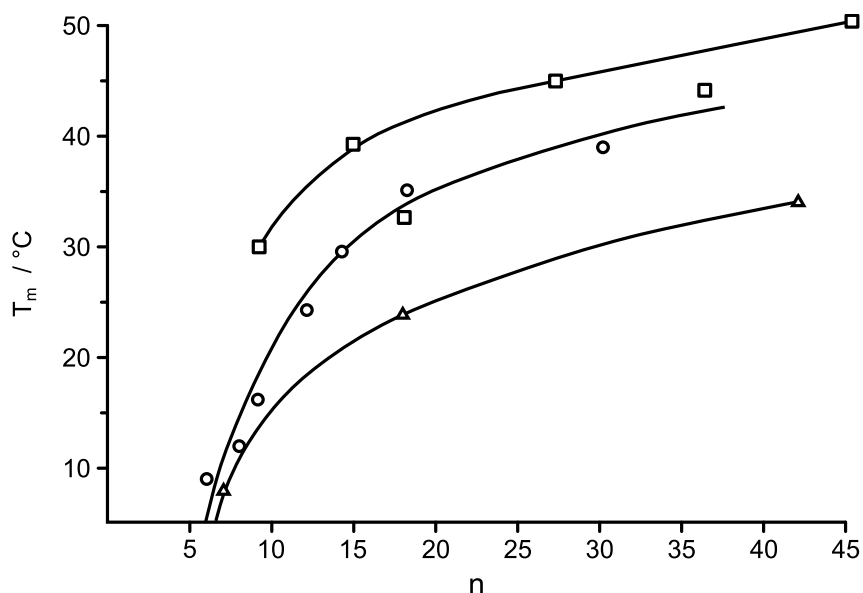


Figure 123. Melting point (T_m) vs oligomer length (n) for ethylene glycol oligomers synthesized by (□) Bömer et al.¹⁶⁹, (o) other workers ^{171,174,175} via the method of Hibbert et al. and (Δ) Hibbert et al.^{166,167,176} Reproduced from ¹⁷³ with permission from Elsevier.

As is evident from a comparison between the melting points obtained by Bömer et al. in Figure 123 and commercial samples of polydisperse PEG (DOW CARBOWAX™) in Figure 124, there is good agreement at higher molecular weights. At lower molecular weights, the commercial polydisperse PEG shows better agreement with earlier work, i.e. actually slightly lower T_m than reported by Hibbert et al. Similarly to commercial polydisperse PEG, these earlier PEG samples contained circular crown ethers alongside other contaminants resulting in lower melting points.

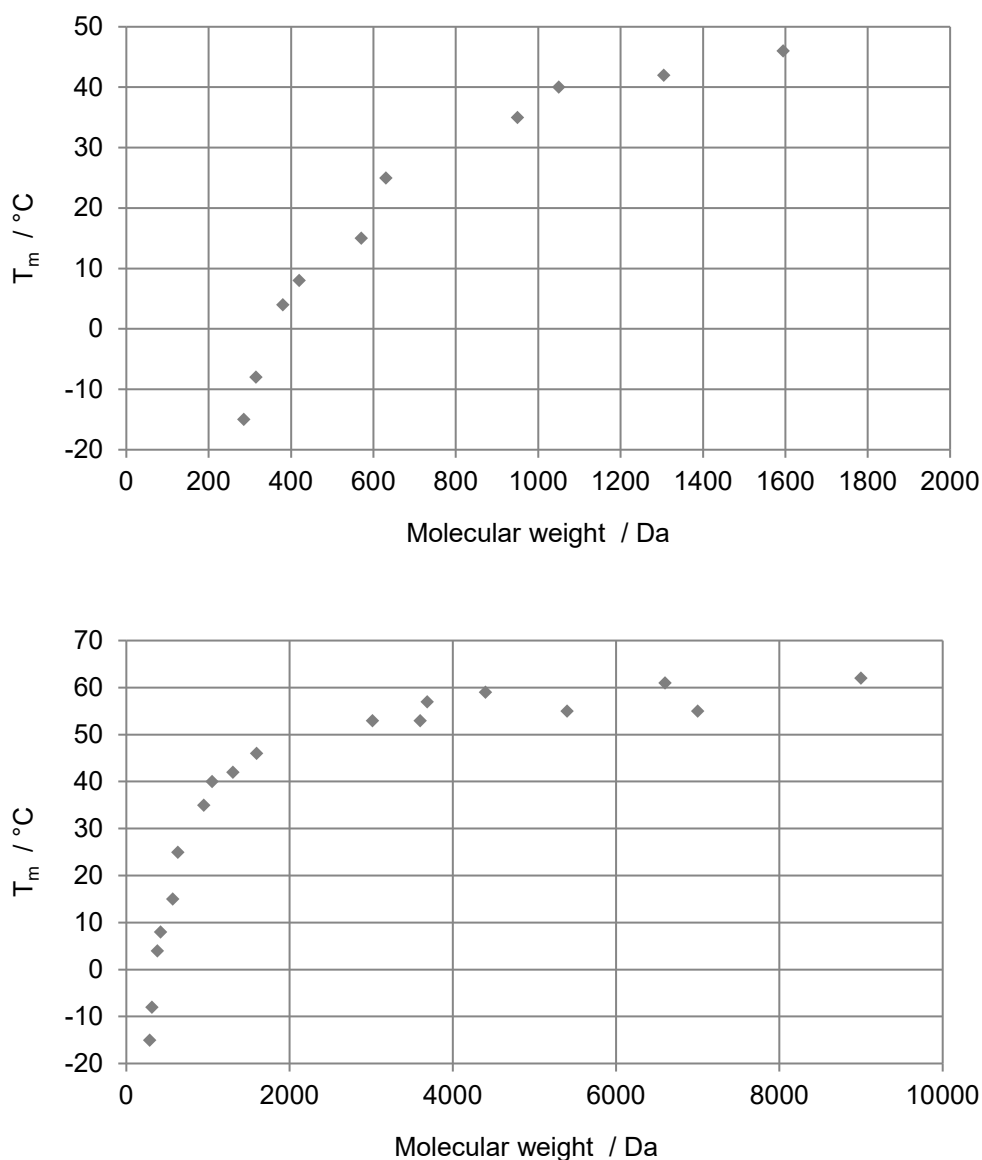


Figure 124: DOW Carbowax™ polydisperse PEG melting points over a range of molecular weights. For each individual product, a molecular weight range and corresponding melting point range were given. Each data points correspond to the start and end point of a range. For example, for the product PEG400, a M_w range of 380-420 Da and a T_m range of 4-8 °C are given so (380,4) and (420,8) are plotted.¹⁷⁷

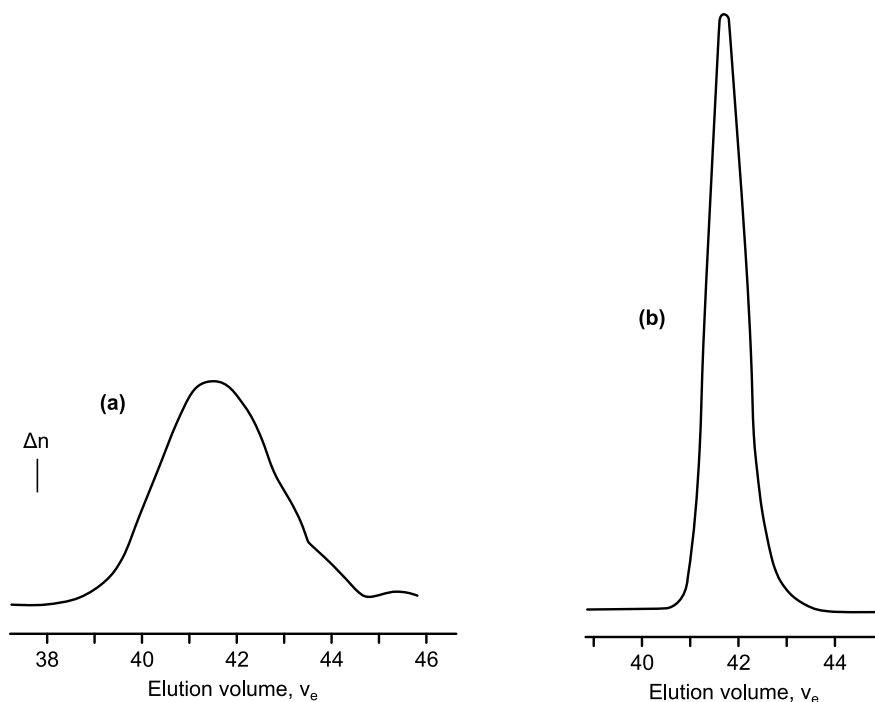


Figure 125. Differential refractive index (Δn , arbitrary scale) against elution volume (v_e) for GPC of (a) PEG-400 ($x_n \sim 9$; 2 cm^3 injection of $1.7 \text{ g}\cdot\text{gm}^{-3}$ solution) and (b) pure nonaethylene glycol (2 cm^3 injection of $1.5 \text{ g}\cdot\text{dm}^{-3}$ solution). Reproduced from ¹⁷³ with permission from Elsevier.

Finally, Marshall et al. demonstrated the superior traceability of uniform PEG over the polydisperse versions in chromatographic techniques as shown in Figure 125. In the context of uniform polymer synthesis, the development of chromatographic separation techniques was key to understanding and quantifying the dispersity of samples. Only with chromatography was a detailed assessment of the composition of higher boiling, i.e. non-distillable, mixtures feasible. To the author's knowledge, the work of Marshall et al. is one of the last routes not yet using protecting group chemistry to further improve upon uniformity. Hereafter, synthesis of uniform PEG continued with the different strategies utilizing protecting group chemistry as previously described in Section 1.1.1. With the need for protecting groups established, the targeted synthesis of ethylene glycol oligomers has not changed significantly since.

Appendix B – Functionalization and hub disassembly for Eg₅₆

The functionalization described here was performed by Piers R.J. Gaffney and is included for completion.

The fourth and last part of the strategy concerns itself with the functionalization of the oligomer and cleavage from the hub at the homostar centre. Once chain extensions have been carried out up to the desired chain length, the PEG can be functionalized at the terminus. Similar to the chain extension reactions, the functionalization conditions need to be chosen to avoid concomitant hub cleavage. PEGs were functionalized with TsCl to yield the toluenesulfonate ester as well as with tert-butylbromoacetate to yield the *t*Bu protected carboxylic acid. After functionalization, the monofunctionalized chains were cleaved off the hub via hydrogenolysis over Pd/C (prepared in situ¹³⁸) under H₂ atmosphere at room temperature and pressure. The high activity of the freshly prepared catalyst system allows for the hydrogenolysis to be carried out at low temperatures thus serving to protect the functional group from side reaction and degradation, e.g. against ester exchange at elevated temperature. Via the tosylate moiety, a variety of other functional groups can be accessed after cleavage from the hub. Notably, the azide functionality needs to be accessed in this indirect manner, as the azide group is reduced to the amine under hydrogenolytic conditions. The functionalization of PEGs is also abundantly discussed in the literature and can be directly applied at the end of the homostar strategy, with the caveat that the functional group introduction must leave the hub linkage intact, and that the functional group itself needs to be stable towards the hub cleavage in the subsequent step.

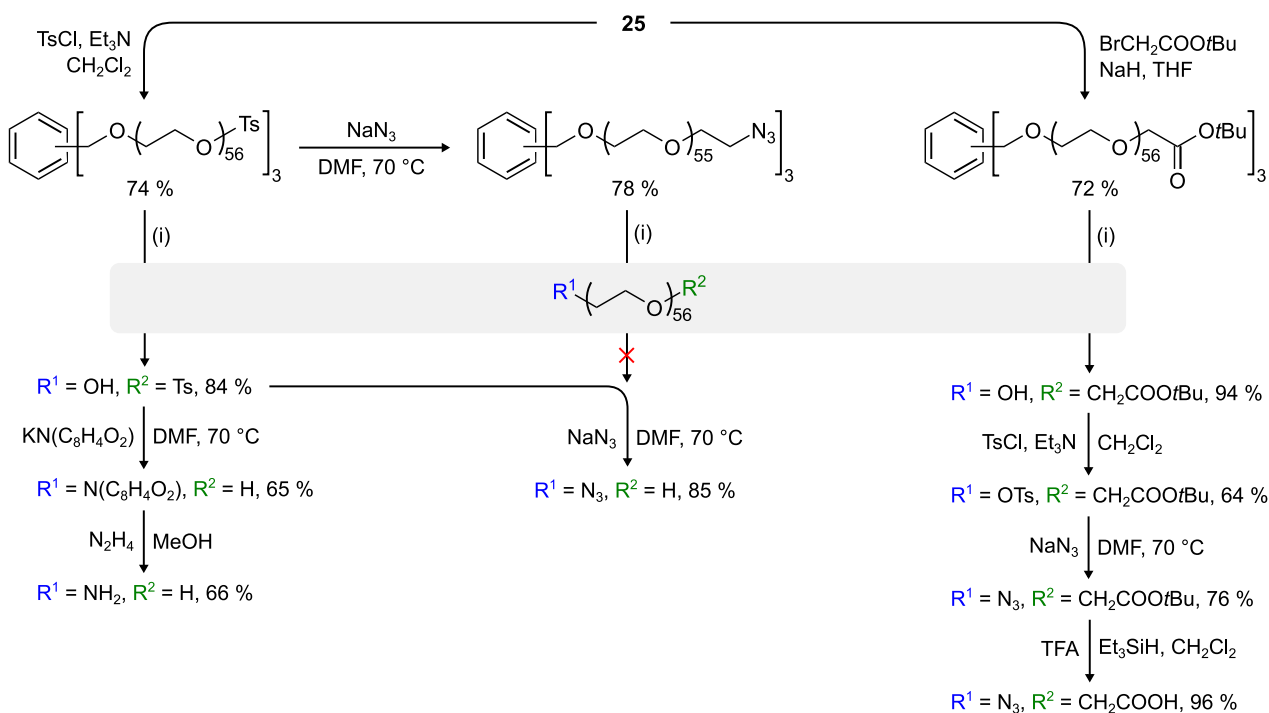


Figure 126. Homostar disassembly and functionalization yielding uniform, heterobifunctional PEG2500. Adapted from ⁴ with permission of John Wiley & Sons.

Appendix C – Industrial synthesis of Eg₁ – Eg₄

The higher oligo(ethylene glycol)s are by-products of the industrial synthesis of ethylene glycol. Until the mid-2000s, ethylene glycol was produced largely by direct hydrolysis of ethylene oxide with a large excess of water. As described in the literature, “[t]he formation of [...] higher homologues is inevitable because ethylene oxide reacts with ethylene glycols more quickly than with water; their yields can, however, be minimized if an excess of water is used – a 20-fold molar excess is usually employed., which in turn is produced by direct oxidation of ethylene with air or oxygen.”¹⁷⁸

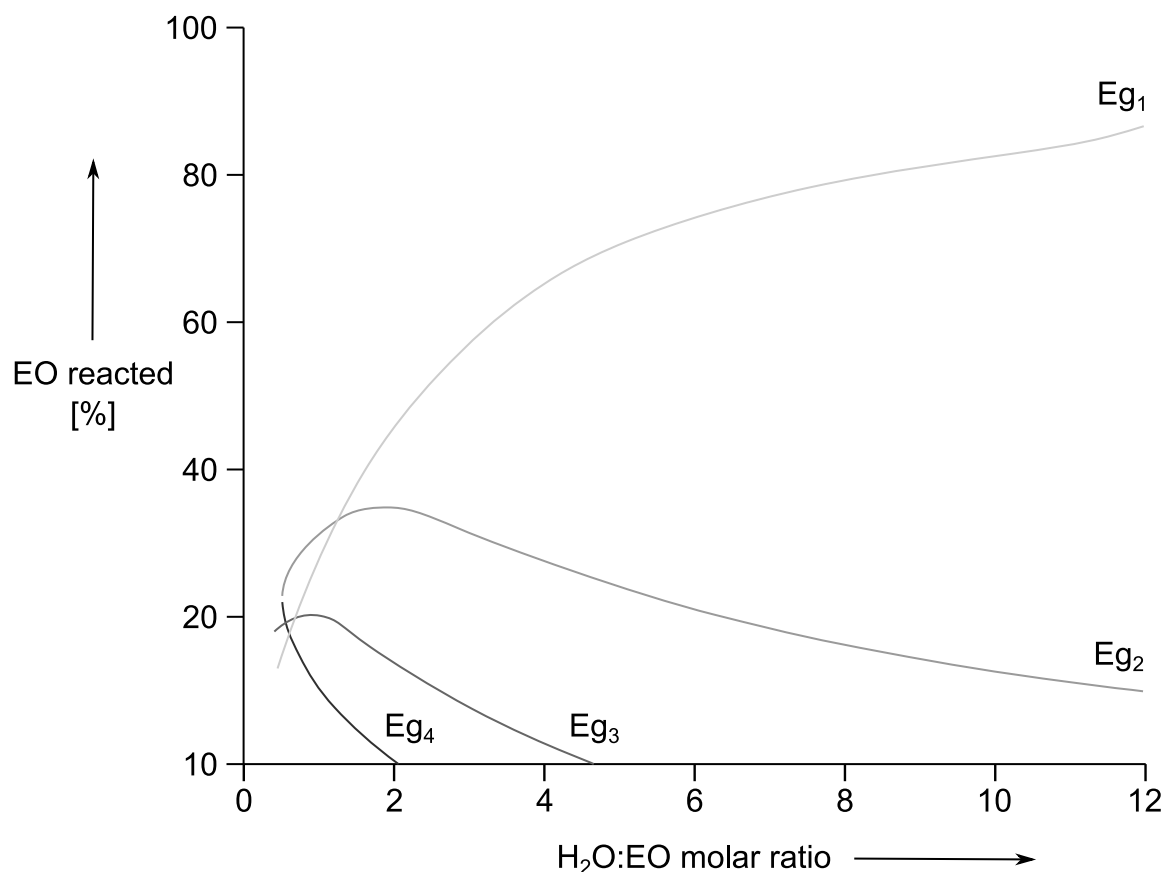


Figure 127. Composition of the product obtained on hydrolysis of ethylene oxide (EO) as a function of the water to ethylene oxide ratio. a) Monoethylene glycol; b) Diethylene glycol; c) Triethylene glycol; d) Higher poly(ethylene glycols). Adapted from ¹⁷⁸ with permission from John Wiley & Sons.

The higher homologues of ethylene glycol (Eg₂ – Eg_n) are therefore produced as by-products with respectively decreasing yields and are separated from the main product by vacuum distillation (Figure 128) as homologues beyond Eg₃ would otherwise decompose upon heating.¹⁷⁸ While the higher homologues are undesired side products, and manufacturers attempt to minimize their yields, the world production of ethylene glycol (> 6.7 Million t) is so large that sub-percentage levels of side product suffice to supply appreciable quantities.

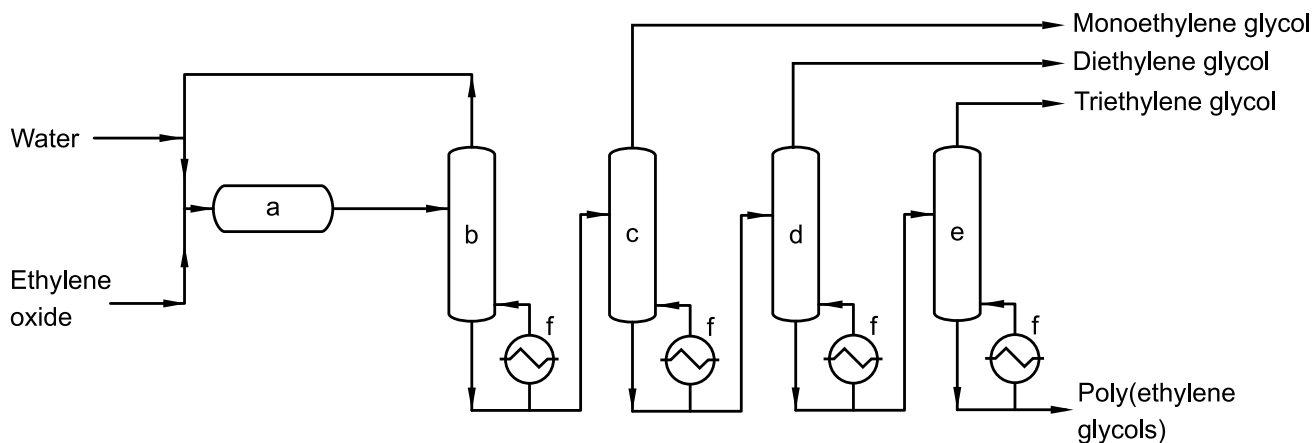


Figure 128: Flow diagram for a glycol plant. a) Reactor; b) Drying column; c) Monoethylene glycol column; d) Diethylene glycol column; e) Triethylene glycol column; f) Heat exchanger. Columns not drawn to scale ($b \gg c \gg d > e$). Reproduced from ¹⁷⁸ with permission from John Wiley & Sons.

(The requirement to use a large molar excess of water in the region of 20:1 which needs to be separated by distillation downstream is unfavourable, despite heat integration with the reactor. This has led to the development of the OMEGA catalytic Process by Shell Global Solutions, also from ethylene oxide, but with prior reaction with CO_2 to ethylene carbonate as an intermediate.)

Appendix D – Kinetics from Eg₁₆ to Eg₅₆

Analysis for each of the chain extensions between Eg₁₆ and Eg₄₈ was carried out according to the same protocol as used for the chain extension from Eg₈ to Eg₁₆ discussed in the main text (Section 2.2.3 on p. 95).

Extension from Eg₁₆ to Eg₂₄

During analysis of the HPLC UV traces for the chain extension from Eg₁₆ to Eg₂₄, integration of the Hub¹(–Eg₁₆–OH)₃ (**15**) triol peaks was unreliable due to peak overlap with species close to the solvent front (Figure 132, 3.5–4.2 min). The resultant scattered data set could nevertheless be used to gain a first estimate of the reaction rate coefficient. The pseudo first-order rate coefficient ($k' \approx 0.14 \text{ min}^{-1}$) obtained from an exponential fit of the data (Figure 129) was comparable to the coefficient previously obtained for the extension from Eg₈ to Eg₁₆. An estimated rate constant of $0.4 \text{ M}^{-1} \cdot \text{min}^{-1}$ is deduced for the extension of the first homostar arm when accounting for the average building block concentration of 0.33 M over the time period.

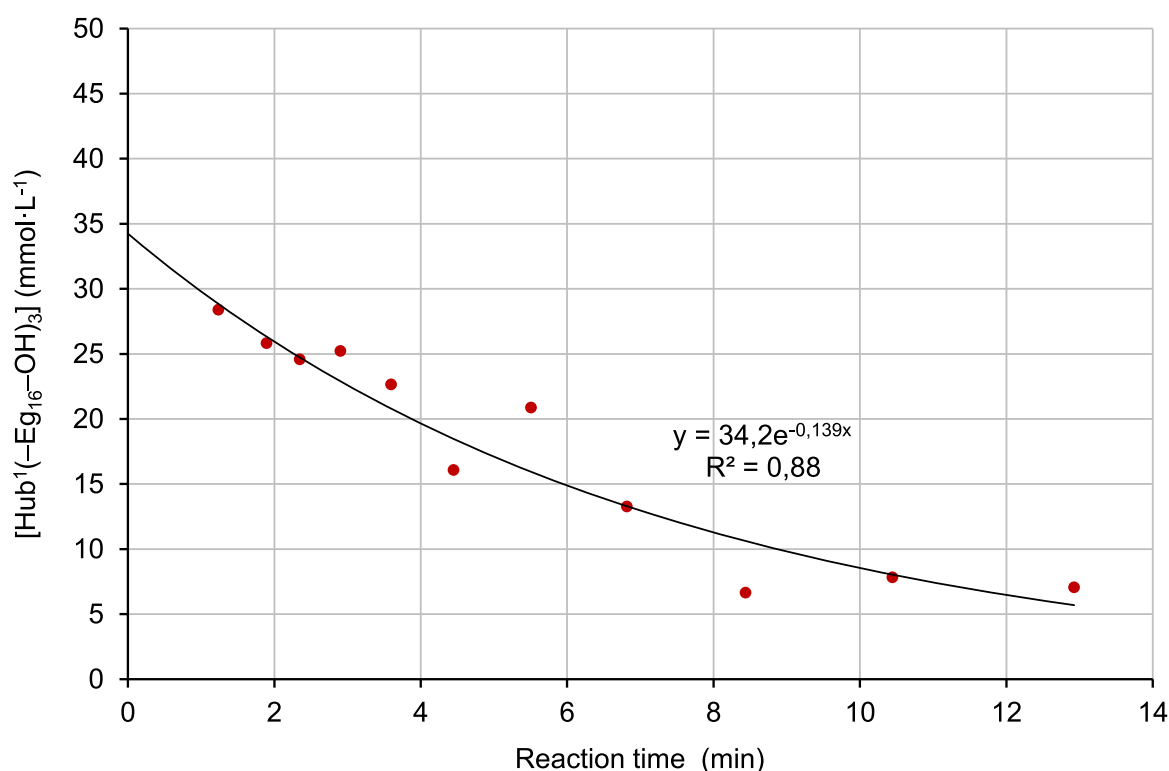


Figure 129. Concentration profile of Hub¹(–Eg₁₆–OH)₃ (**15**) homostar triol at the start of the chain extension from Eg₁₆ to Eg₂₄. Peak overlap with solvent front led to unreliable integration.

Further analysis of the traces showed that the peaks of the doubly extended homostar, Hub¹(–Eg₁₆–OH)₁(–Eg₂₄–ODmtr)₂ (**15c**), overlapped with the main DmtrO–Eg₈–OTs (**8**) building block peak. As a

result, the concentrations of these two species could only be tracked jointly. In the full simulation of the chain extension (Figure 130), a joint concentration profile (**8** + **15c**) was therefore simulated alongside the concentration profiles of the individual species and individual concentration data for **8** or **15c** was not available. As described in the method (Section 2.2.5), precedence was given to a good fit of the concentration profiles of the Dmtr containing species as these could be more reliably integrated, and this resulted in a poor fit of the homostar triol concentration in this instance (Figure 130). The HPLC raw data with ELSD and UV (260 nm) detection is shown in Figure 131 to Figure 133.

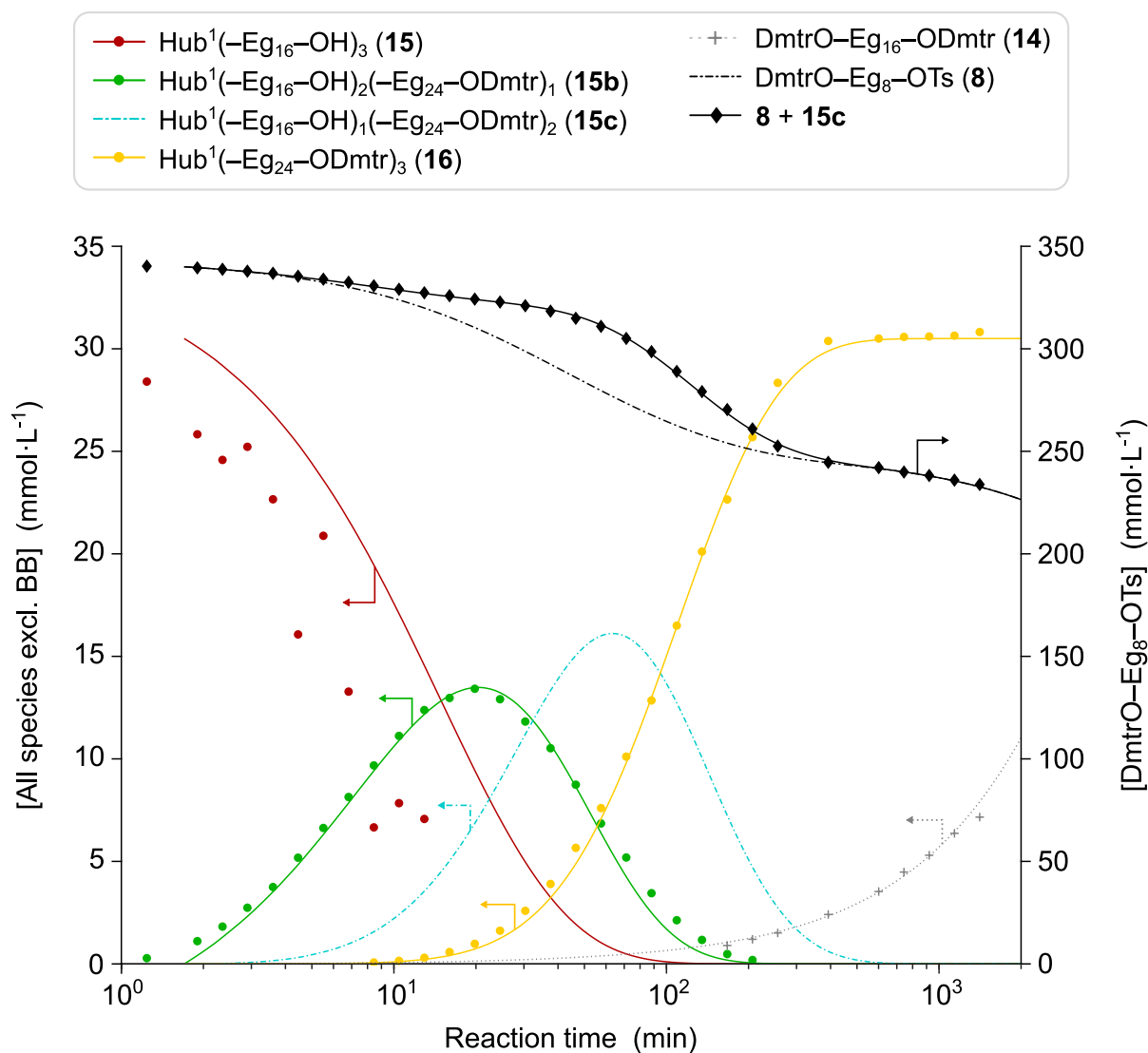


Figure 130. Simulated concentration profiles for chain extension from Eg_{16} to Eg_{24} over 1,140 min (19 h). $T = 30\text{ }^{\circ}\text{C}$, $t_{\text{ind}} = 1.7\text{ min}$, $k_1 = 0.20\text{ M}^{-1}\cdot\text{min}^{-1}$, $k_2 = 0.135\text{ M}^{-1}\cdot\text{min}^{-1}$, $k_3 = 0.045\text{ M}^{-1}\cdot\text{min}^{-1}$, $k_4 = 2.3 \cdot 10^{-4}\text{ min}^{-1}$, $c_{\text{HS-triol}}^{i=0} = 30.5\text{ mmol}\cdot\text{L}^{-1}$, $c_{\text{BB}}^{i=0} = 340\text{ mmol}\cdot\text{L}^{-1}$. Peaks for **8** and **15c** overlapped during integration of the HPLC UV traces (Figure 131, 13 min).

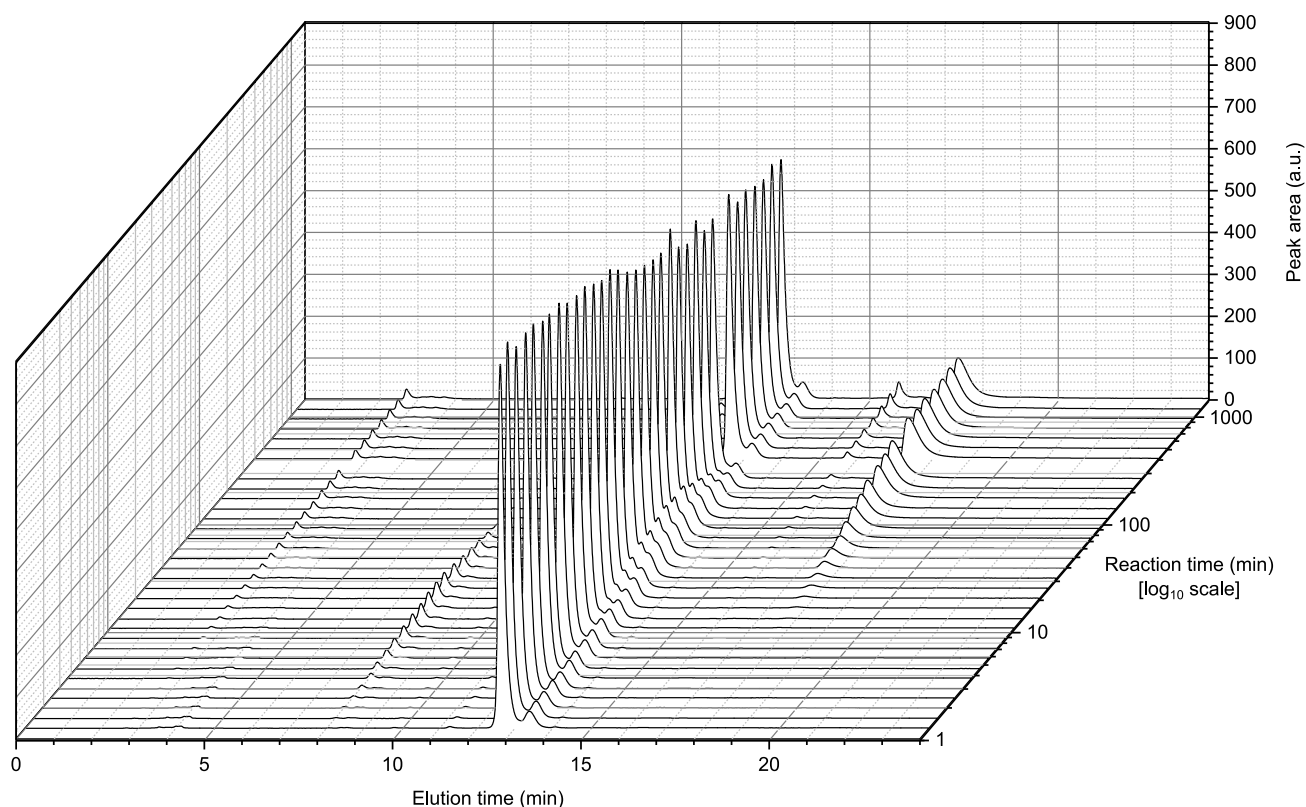
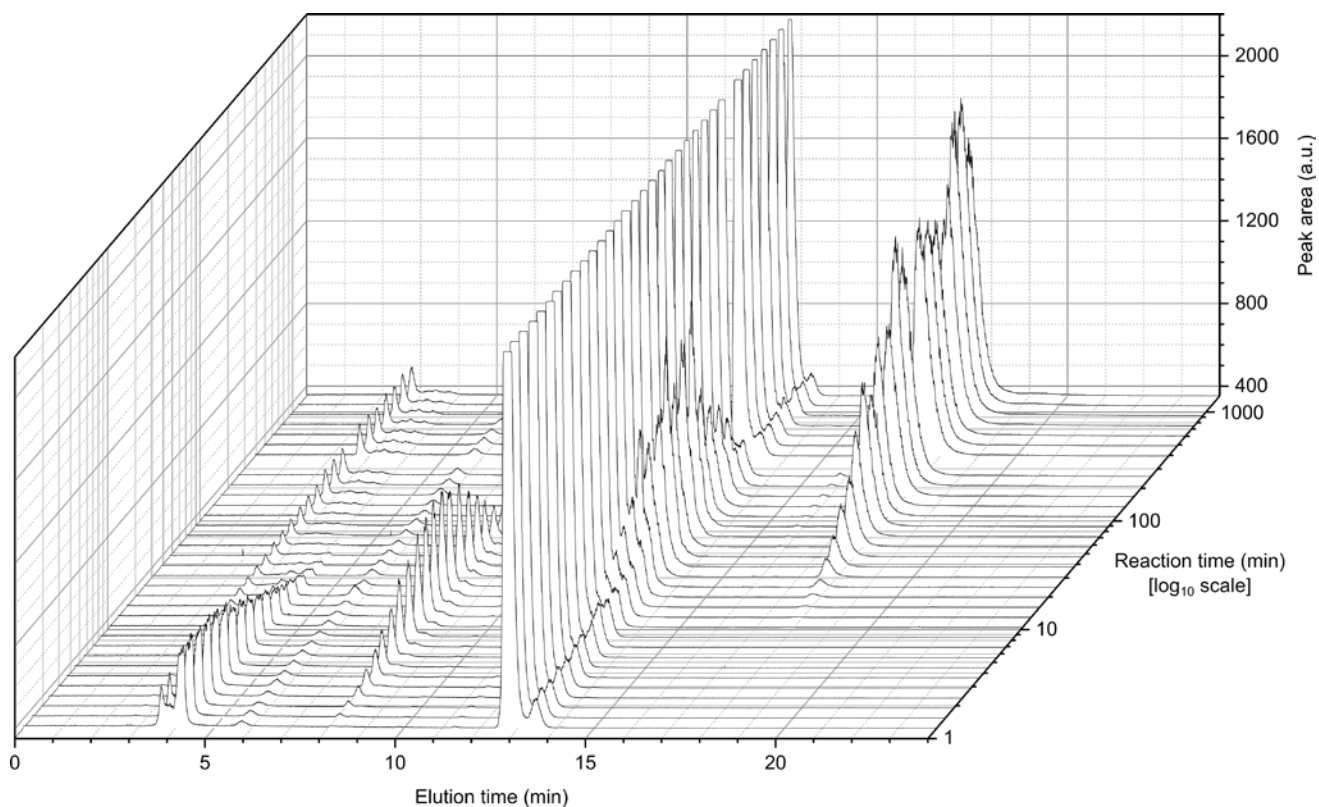


Figure 131. Waterfall plot of HPLC traces with (top) ELSD and (bottom) UV (260 nm) detection for the chain extension from Eg_{16} to Eg_{24} . NaOTs (2.8 min), $\text{Hub}^1(-\text{Eg}_{16}-\text{OH})_3$ (**15**) (3.5-4.2 min), $\text{Hub}^1(-\text{Eg}_{16}-\text{OH})_2(-\text{Eg}_{24}-\text{ODmtr})_1$ (**15b**) (8.0 min), $\text{DmtrO}-\text{Eg}_8-\text{OTs}$ (**8**) (12.5-13.5 min), $\text{Hub}^1(-\text{Eg}_{16}-\text{OH})_1(-\text{Eg}_{24}-\text{ODmtr})_2$ (**15c**) (approx. 13 min, overlapping with the building block peak) $\text{DmtrO}-\text{Eg}_{16}-\text{ODmtr}$ (**14**) (16 min), $\text{Hub}^1(-\text{Eg}_{24}-\text{ODmtr})_3$ (**16**) (18 min).

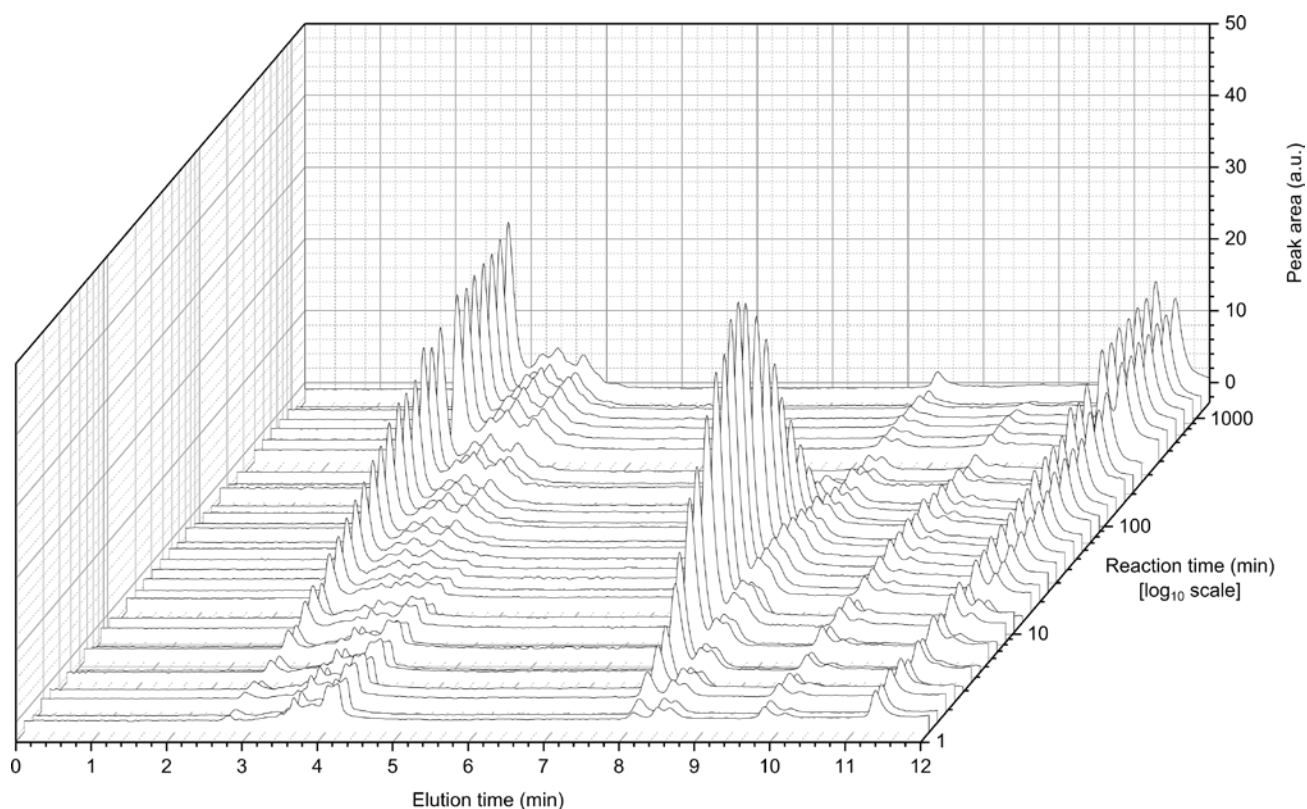
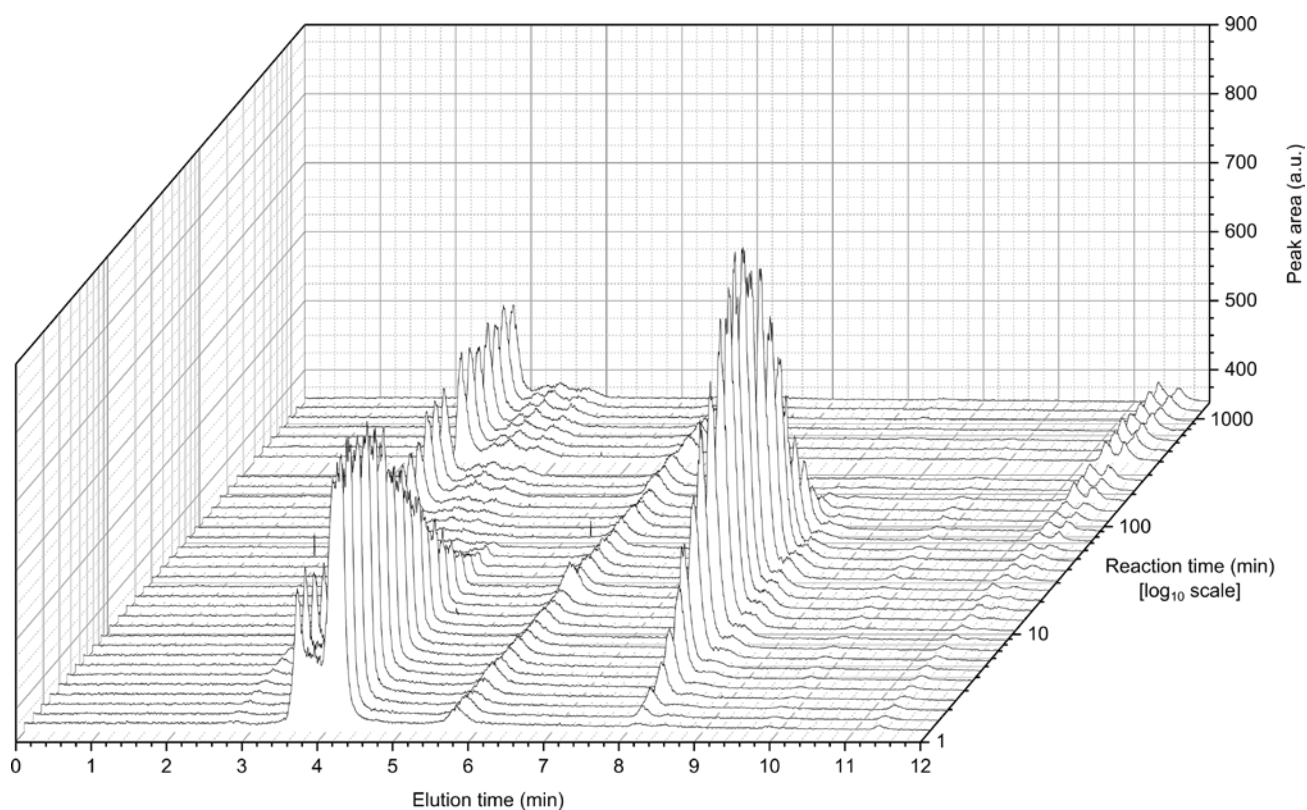


Figure 132. Expansion of Figure 131. HPLC traces with (top) ELSD and (bottom) UV (260 nm) detection for the chain extension from Eg_{16} to Eg_{24} . $\text{Hub}^1(-\text{Eg}_{16}-\text{OH})_3$ (**15**) is visible between 3.5-4.2 min. When comparing ELSD and UV traces, integration of the homostar triol from the ELSD trace could have been an alternative in this instance but would have required calibration.

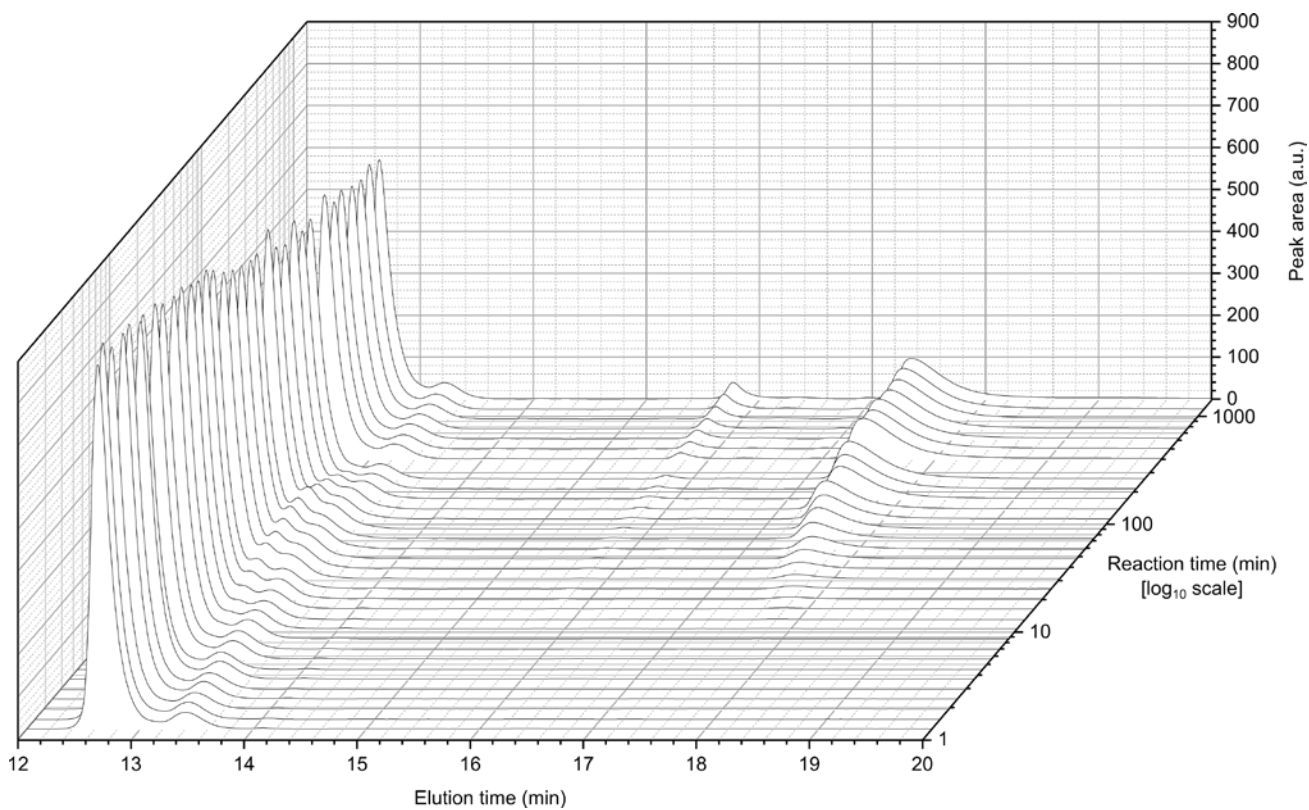
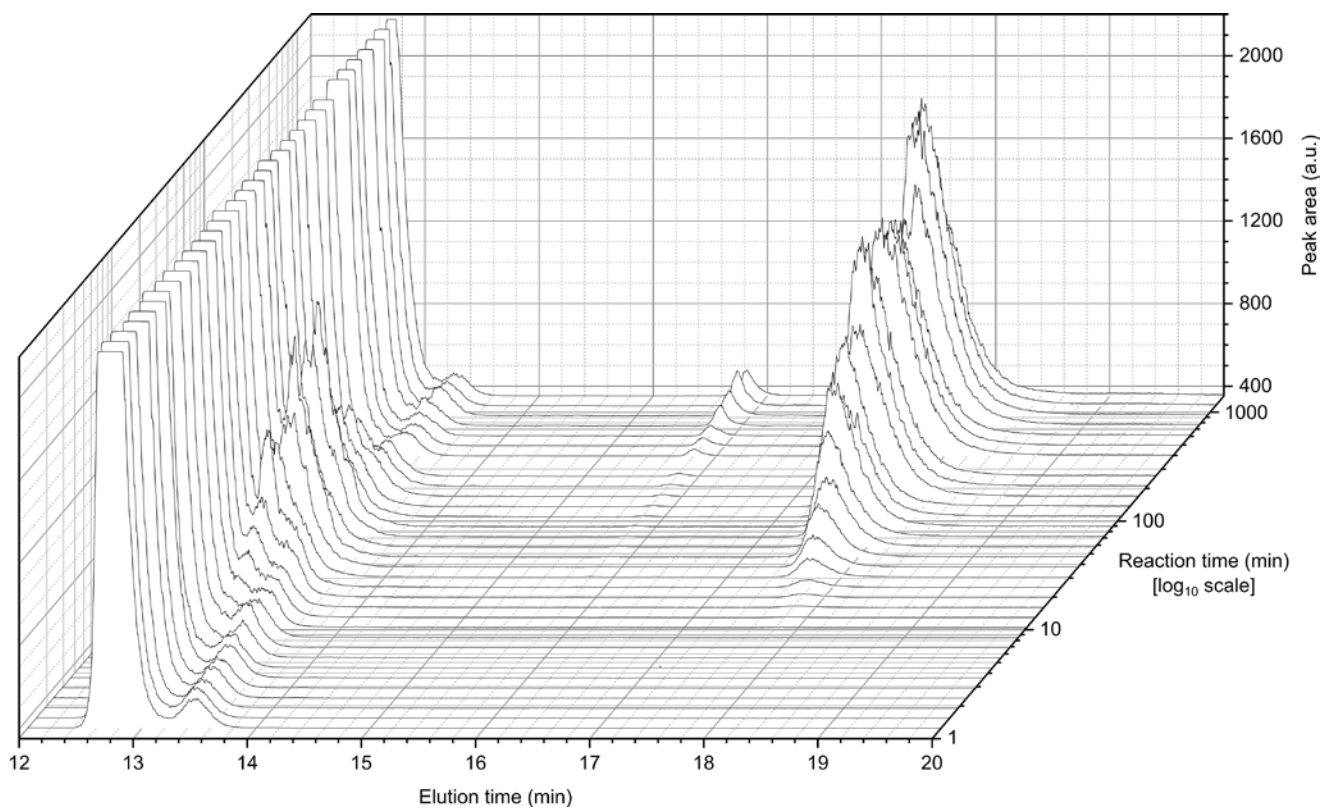


Figure 133. Expansion of Figure 131. HPLC traces with (top) ELSD and (bottom) UV (260 nm) detection for the chain extension from Eg_{16} to Eg_{24} .

Extension from Eg₂₄ to Eg₃₂

For analysis of the chain extension from Eg₂₄ to Eg₃₂ and onwards, a different type of reverse phase column was used (Phenomenex Aeris Widepore 3.6 mm XB-C18 150 mm x 4.6 mm), resulting in sharper peaks and altered retention times.

The consumption of Hub¹(-Eg₂₄-OH)₃ (**17**) triol appeared to follow a slower trend during the first 10 minutes of reaction (Figure 134), suggesting formation of the alkoxide had occurred slower than expected as induction times of under 2 minutes had been observed for the first two extensions. The longer induction period may have been the result of incomplete washing of the NaH suspension prior to addition to the reaction mixture. The hypothesis appears to be supported by the presence of a species, likely mineral oil, with good retention by reverse phase HPLC, eluting around 18.2 min (Figure 138), and with an ELSD signal but no UV response. The species also appears not to be present in any of the HPLC traces of other chain extension where induction times were typically shorter. After minute 10, the speed of reaction then appears to pick up and follow the expected exponential trend (Figure 134). The Hub¹(-Eg₂₄-OH)₃ (**17**) peak (Figure 137, 9.1 min) was preceded by an artefact or low level impurity peak (Figure 137, 8.8 min) but was sufficiently separate to allow for reliable integration which is reflected in the good agreement between the trendlines and the integral data set (see Figure 134).

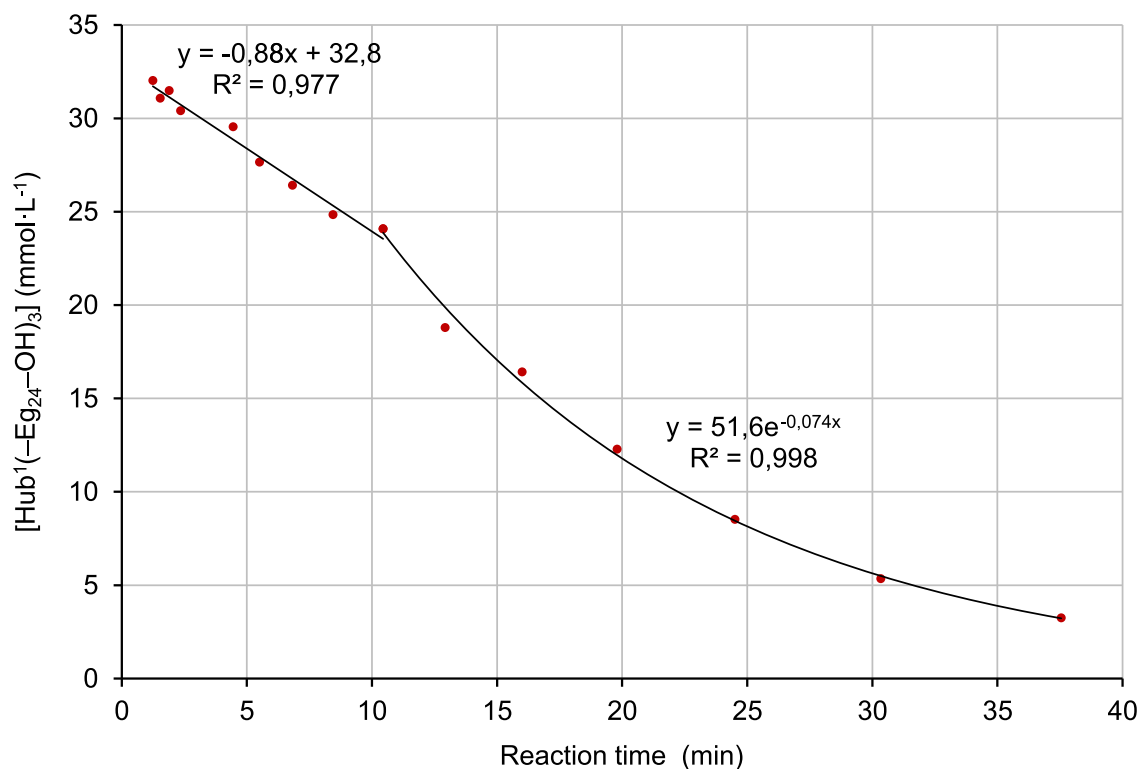


Figure 134. Concentration profile of Hub¹(-Eg₂₄-OH)₃ (**17**) homostar triol at the start of the chain extension from Eg₂₄ to Eg₃₂

Like during analysis of the previous chain extension, two peaks of Dmtr containing species overlapped. This time, the peaks of the singly extended homostar, $\text{Hub}^1(-\text{Eg}_{24}-\text{OH})_2(-\text{Eg}_{32}-\text{ODmtr})_1$ (**17b**) and the main $\text{DmtrO}-\text{Eg}_8-\text{OTs}$ (**8**) building block peak were fully superimposed (Figure 136, 14 min). As a result, the concentrations of the two species could only be tracked jointly and a combined concentration profile (**8 + 17b**) was simulated alongside the concentration profiles of the individual species (Figure 135). The reaction rate coefficients derived from the overall simulation (Figure 135) are comparable to the coefficients of the prior extension when accounting for the higher reaction temperature, 40 °C instead of 30 °C, by making the simplistic assumption that reaction rates approximately double every 10 °C around room temperature.

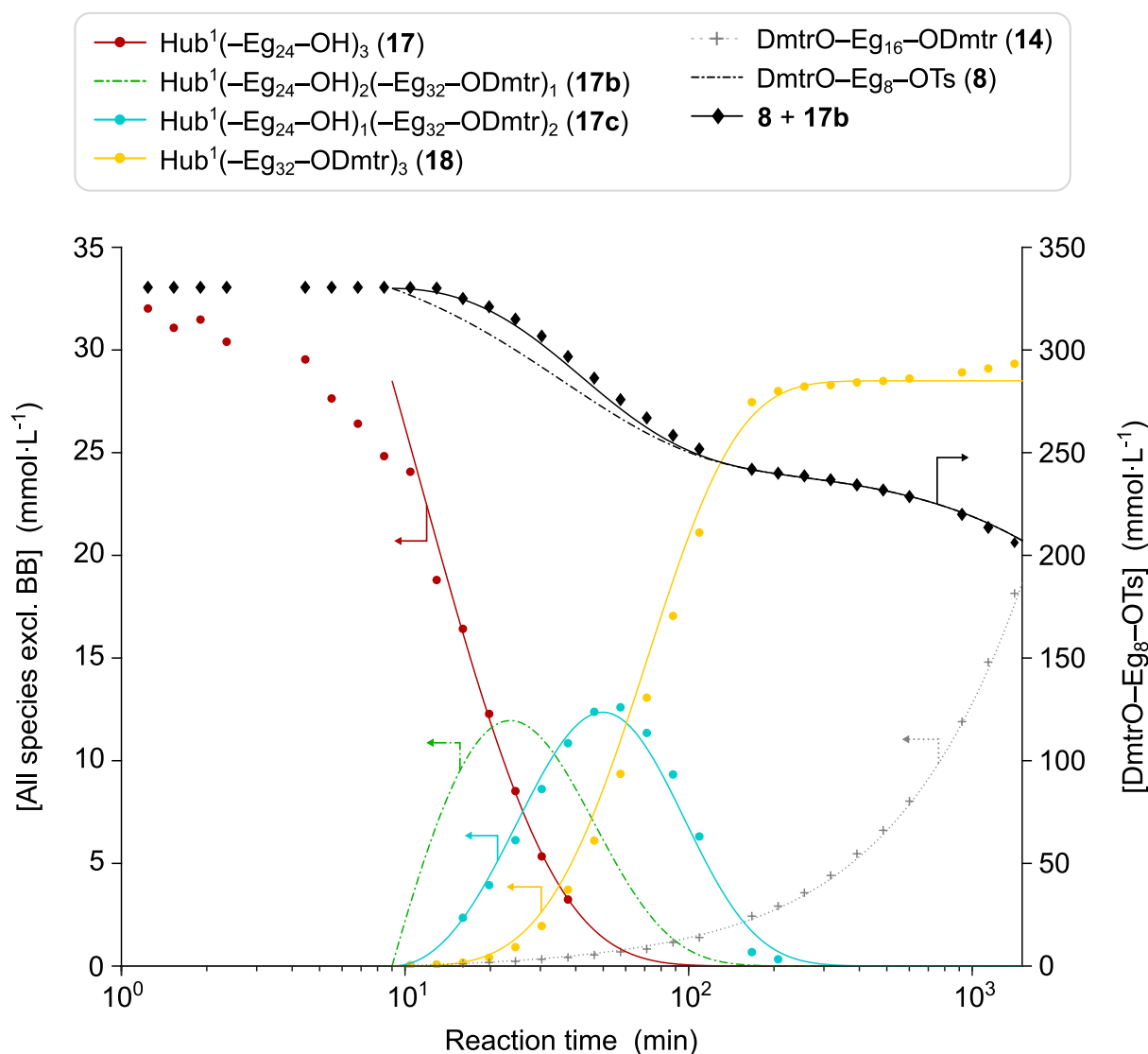


Figure 135. Simulated concentration profiles for chain extension from Eg_{24} to Eg_{32} over 1,410 min (23.5 h). $T = 40\text{ }^\circ\text{C}$, $t_{\text{ind}} = 9.0\text{ min}$, $k_1 = 0.25\text{ M}^{-1}\cdot\text{min}^{-1}$, $k_2 = 0.19\text{ M}^{-1}\cdot\text{min}^{-1}$, $k_3 = 0.095\text{ M}^{-1}\cdot\text{min}^{-1}$, $k_4 = 0.55 \cdot 10^{-4}\text{ min}^{-1}$, $c_{\text{HS-triol}}^{t=0} = 28.5\text{ mmol}\cdot\text{L}^{-1}$, $c_{\text{BB}}^{t=0} = 330\text{ mmol}\cdot\text{L}^{-1}$. Peaks for **8** and **17b** overlapped during integration of the HPLC UV traces (Figure 136, 14.0 min).

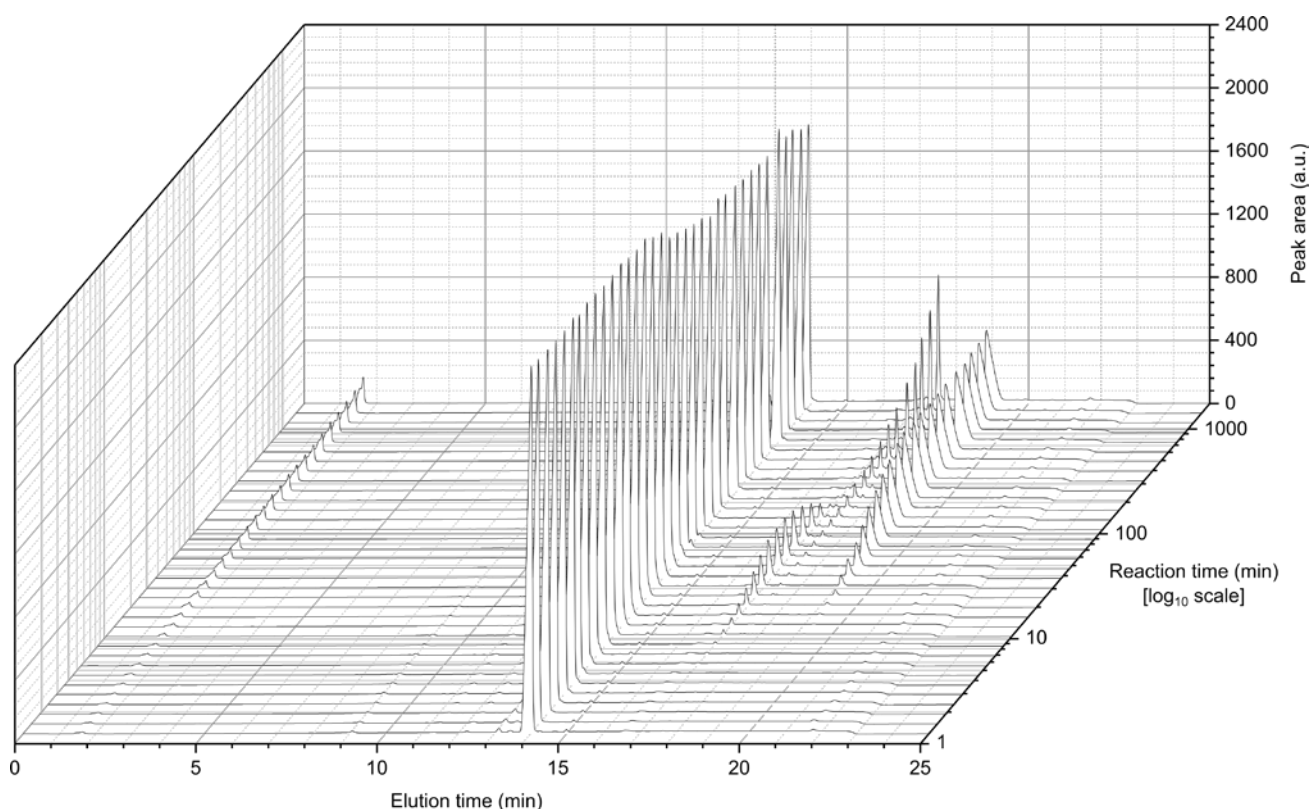
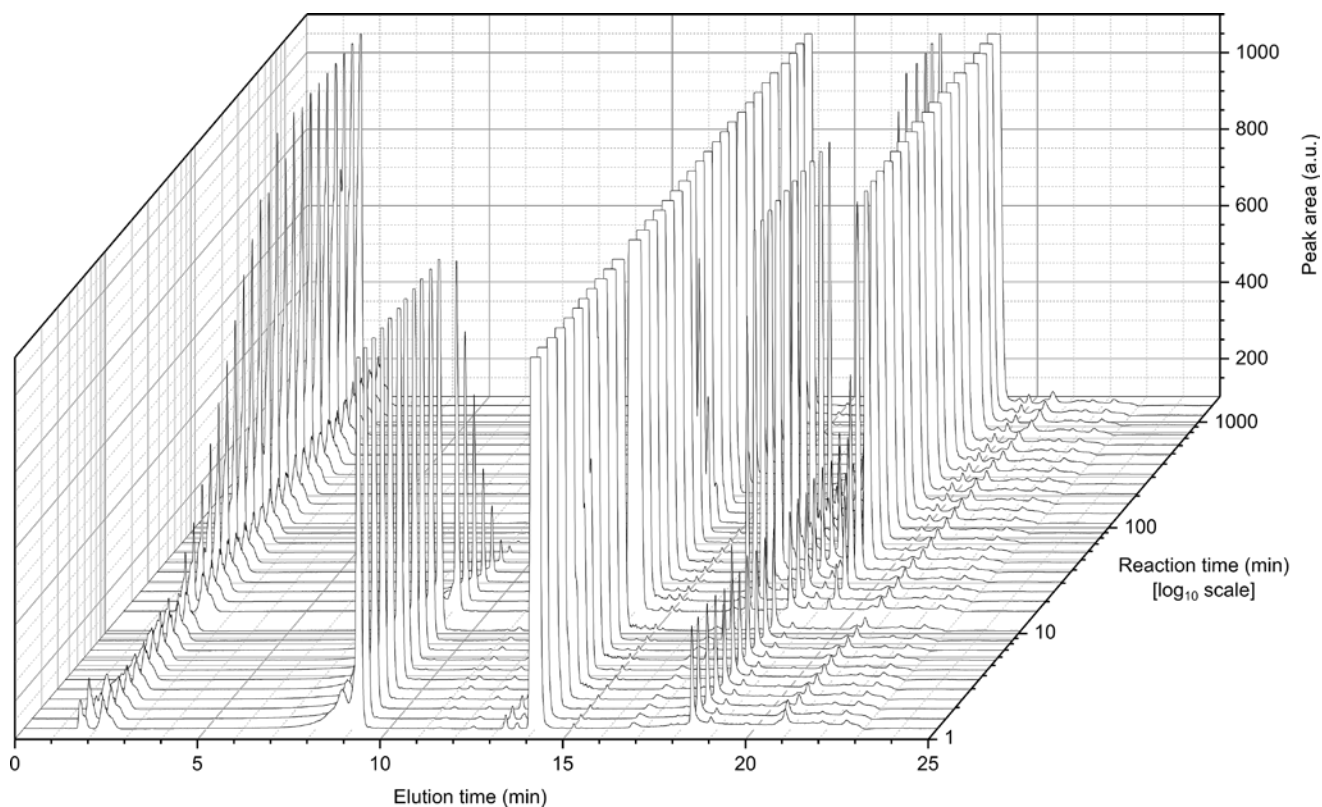


Figure 136. Waterfall plot of HPLC traces with (top) ELSD and (bottom) UV (260 nm) detection for the chain extension from Eg₂₄ to Eg₃₂. NaOTs (1.5 min), Hub¹(-Eg₂₄-OH)₃ (**17**) (9.1 min), Hub¹(-Eg₂₄-OH)₂(-Eg₃₂-ODmtr)₁ (**17b**) (14.0 min, overlapping with the building block peak), DmtrO-Eg₈-OTs (**8**) (14.0 min), Hub¹(-Eg₂₄-OH)₁(-Eg₃₂-ODmtr)₂ (**17c**) (17.0 min), DmtrO-Eg₁₆-ODmtr (**14**) (17.5 min), Hub¹(-Eg₃₂-ODmtr)₃ (**18**) (19.2 min).

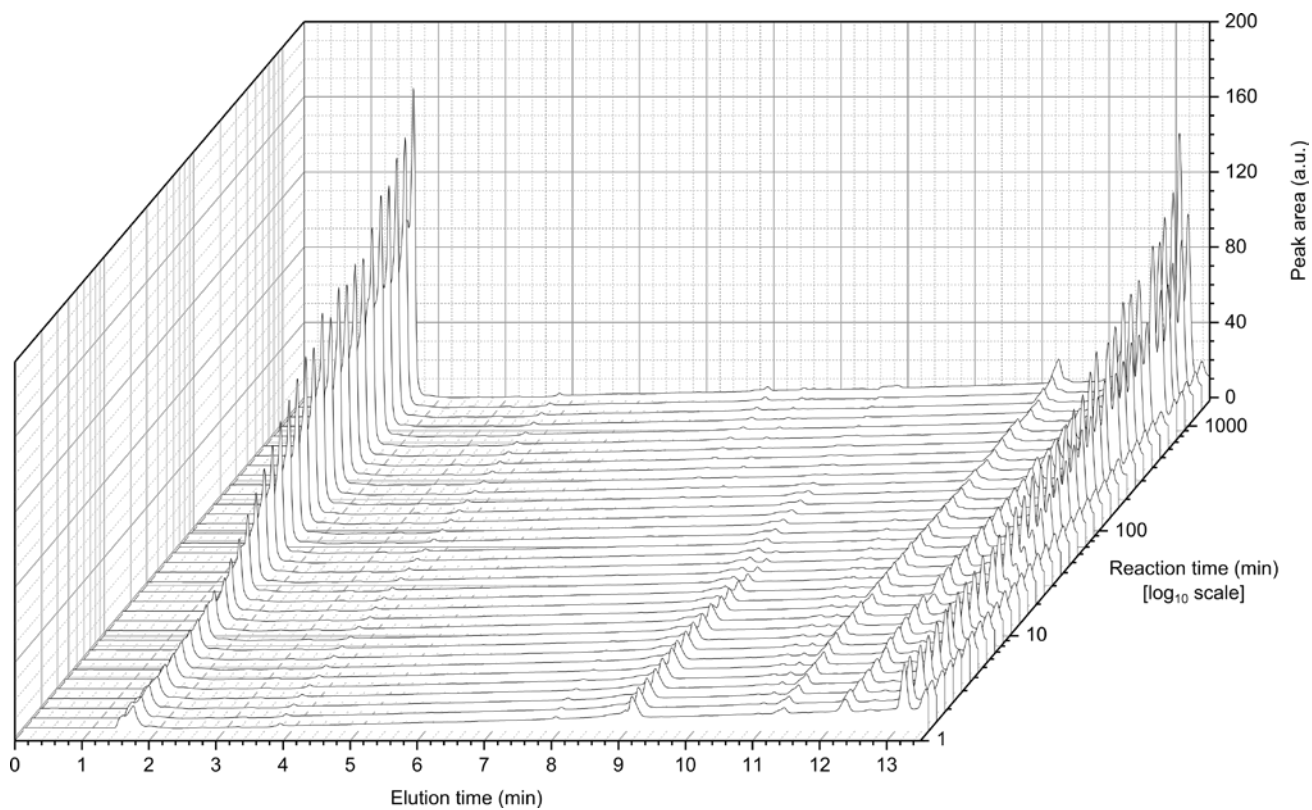
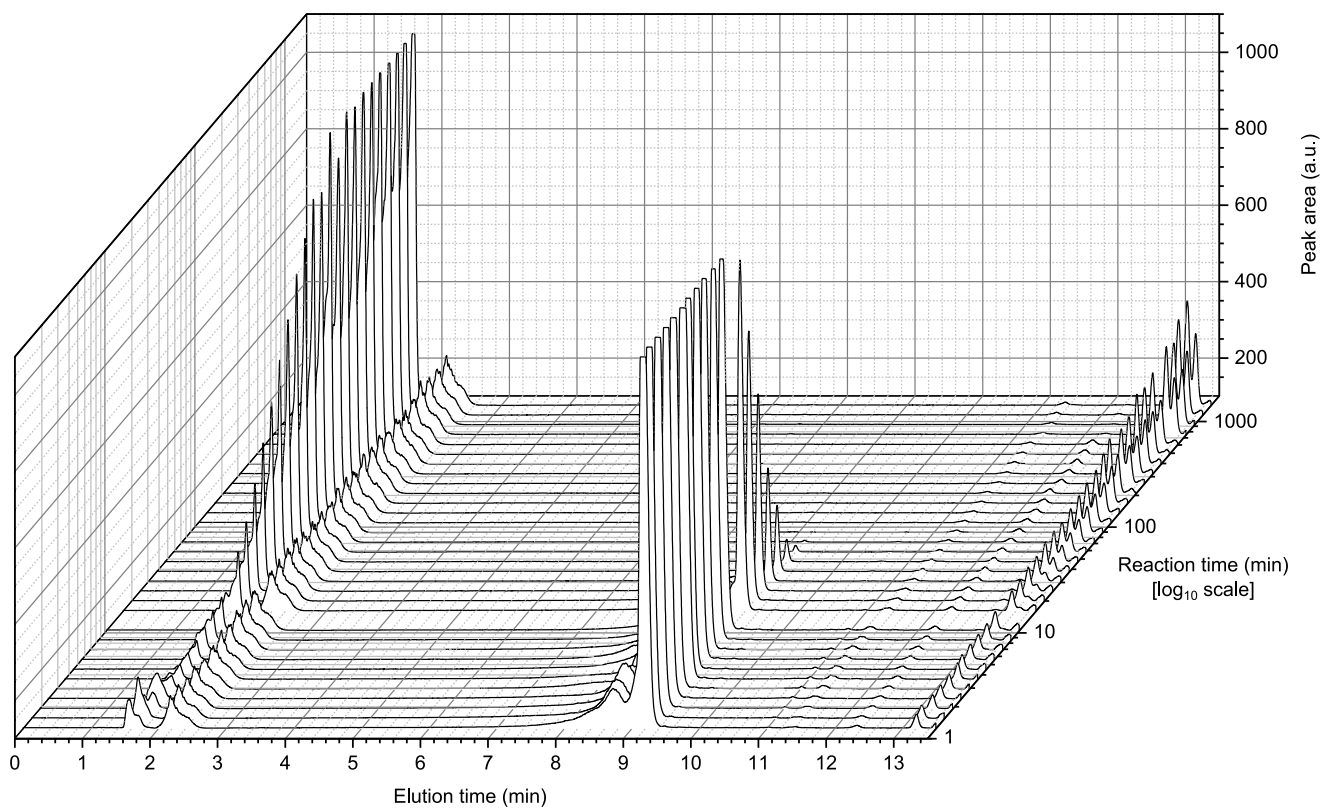


Figure 137. Enlarged from Figure 136. HPLC traces with (top) ELSD and (bottom) UV (260 nm) detection for the chain extension from Eg₂₄ to Eg₃₂.

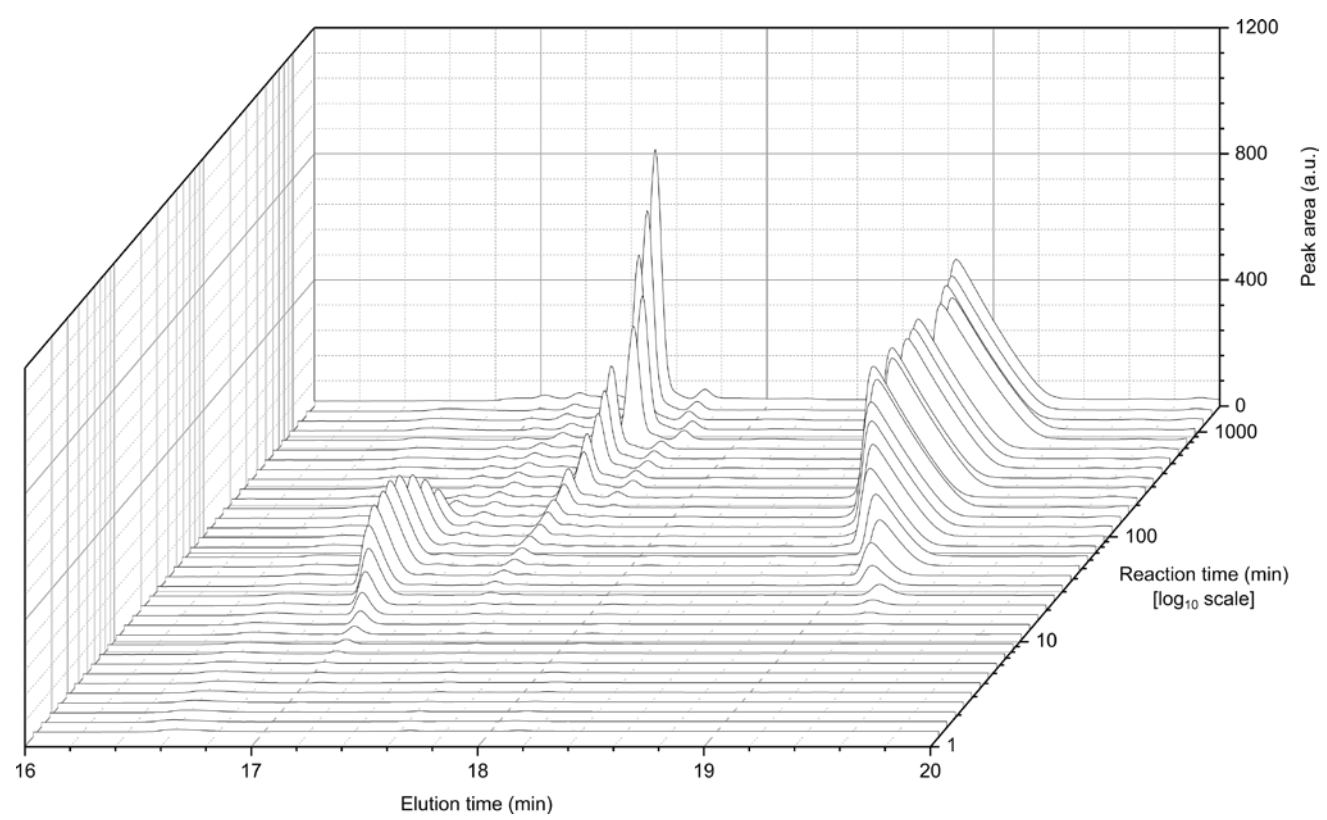
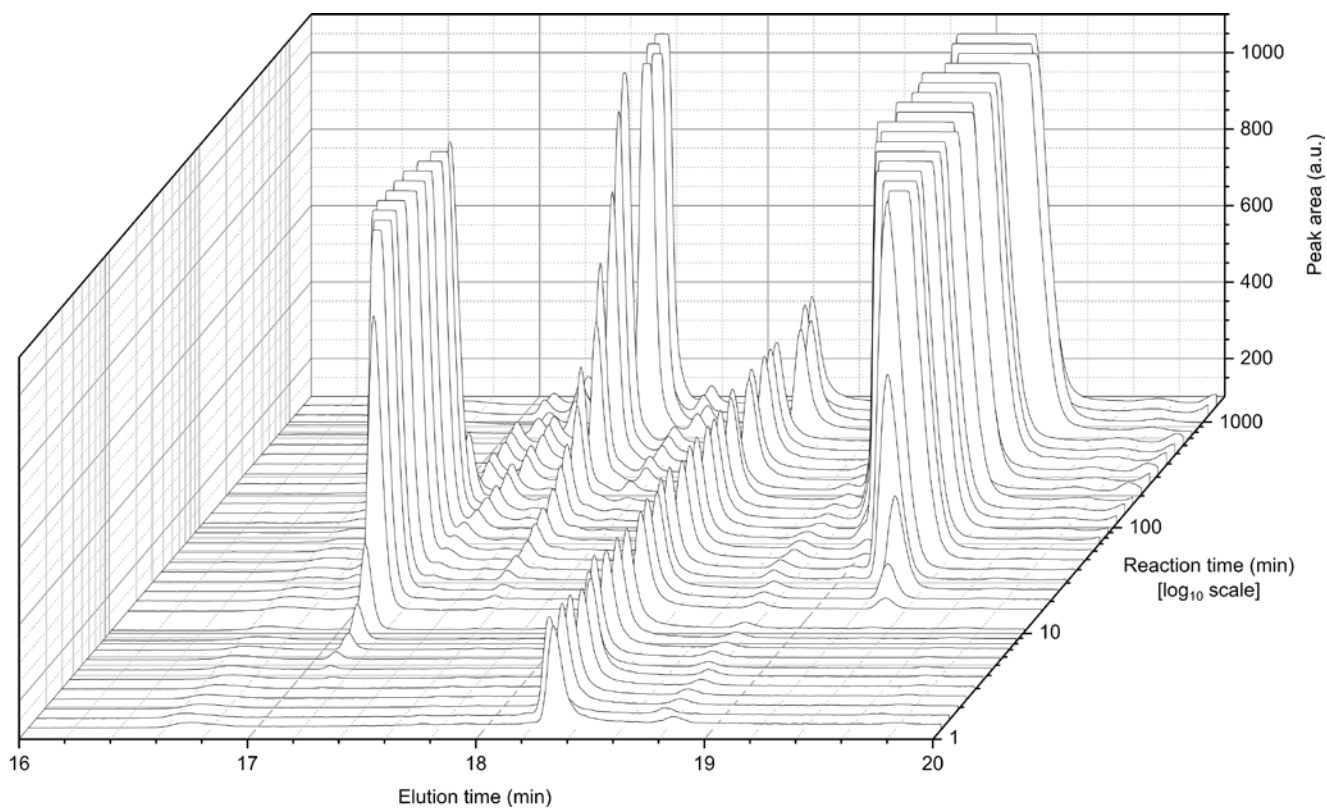


Figure 138. Enlarged from Figure 136. HPLC traces with (top) ELSD and (bottom) UV (260 nm) detection for the chain extension from Eg₂₄ to Eg₃₂.

Extension from Eg₃₂ to Eg₄₀

For the extension from Eg₃₂ to Eg₄₀, the peaks of all species were cleanly separated during HPLC analysis and could be integrated accurately (Figure 141). Analysis of the disappearance of the Hub¹(–Eg₃₂–OH)₃ (**19**) triol revealed an induction period of around 1.5 min in line with the earlier extensions between Eg₈ and Eg₂₄ (Figure 139). Notably, the homostar triol slightly overlapped with another species causing the peak to look as if it were fronting (Figure 142, 9.9 min) but reliable integration could be achieved.

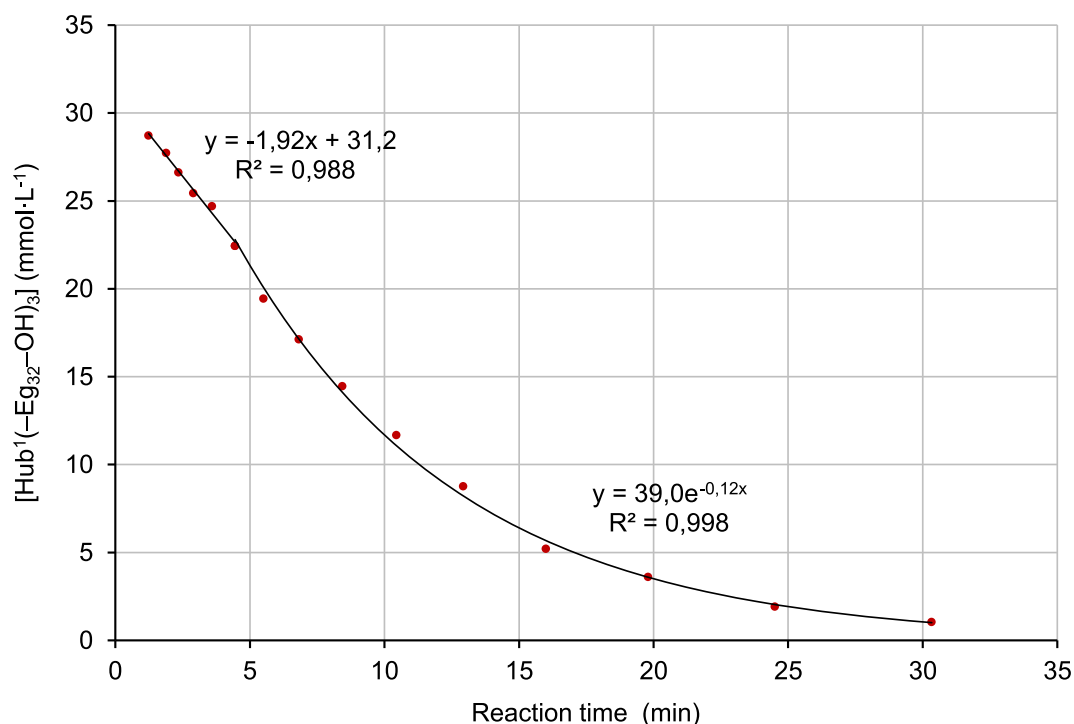


Figure 139. Concentration profile of Hub¹(–Eg₃₂–OH)₃ (**19**) homostar triol at the start of the chain extension from Eg₃₂ to Eg₄₀.

A full simulation of the chain extension (Figure 140) then revealed comparable albeit slightly higher reaction rate coefficients at a similar reaction temperature of 40 °C.

During integration of the HPLC UV traces, it was noticed that the peak of the doubly extended Hub¹(–Eg₃₂–OH)₁(–Eg₄₀–ODmtr)₂ (**19c**) homostar seen at an HPLC elution time of around 17.1–17.2 min did not fully disappear after 150 min of reaction time (Figure 143). Instead, the peak declined to a constant residual area after 150 min. It was unclear whether the residual peaks were artefacts stemming from the HPLC apparatus, e.g. by trace **19c** having contaminated the injector needle and being continuously rinsed out therefrom, or if an unrelated impurity had formed during the reaction, or worse still, whether chain extension was incomplete. Because a large quantity of building block was still present and dimer was still being formed after 150 min, the reaction must have still been active with enough base present.

This suggests that the peaks are artefacts or stem from an unrelated impurity rather than incomplete reaction at that point.

For the last two analyzed samples at 1,410 and 1,740 min, the traces appear to have inadvertently shifted with most peaks eluting slightly earlier.

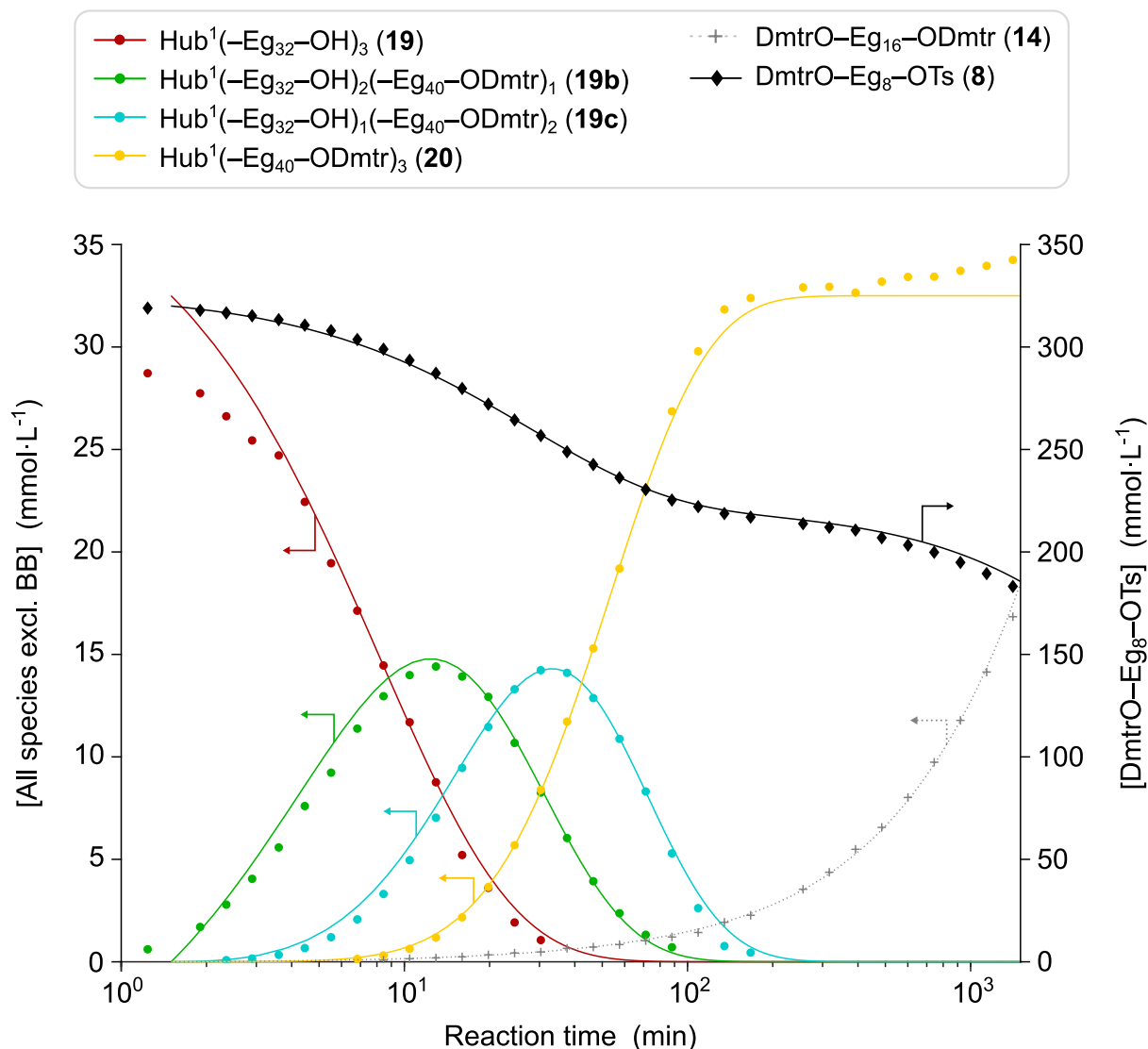


Figure 140. Simulated concentration profiles for chain extension from Eg₃₂ to Eg₄₀ over 1,740 min (29 h). T = 40 °C, t_{ind} = 1.5 min, k₁ = 0.38 M⁻¹·min⁻¹, k₂ = 0.24 M⁻¹·min⁻¹, k₃ = 0.125 M⁻¹·min⁻¹, k₄ = 0.6 · 10⁻⁴ min⁻¹, c_{HS-triol}^{t=0} = 32.5 mmol·L⁻¹, c_{BB}^{t=0} = 320 mmol·L⁻¹.

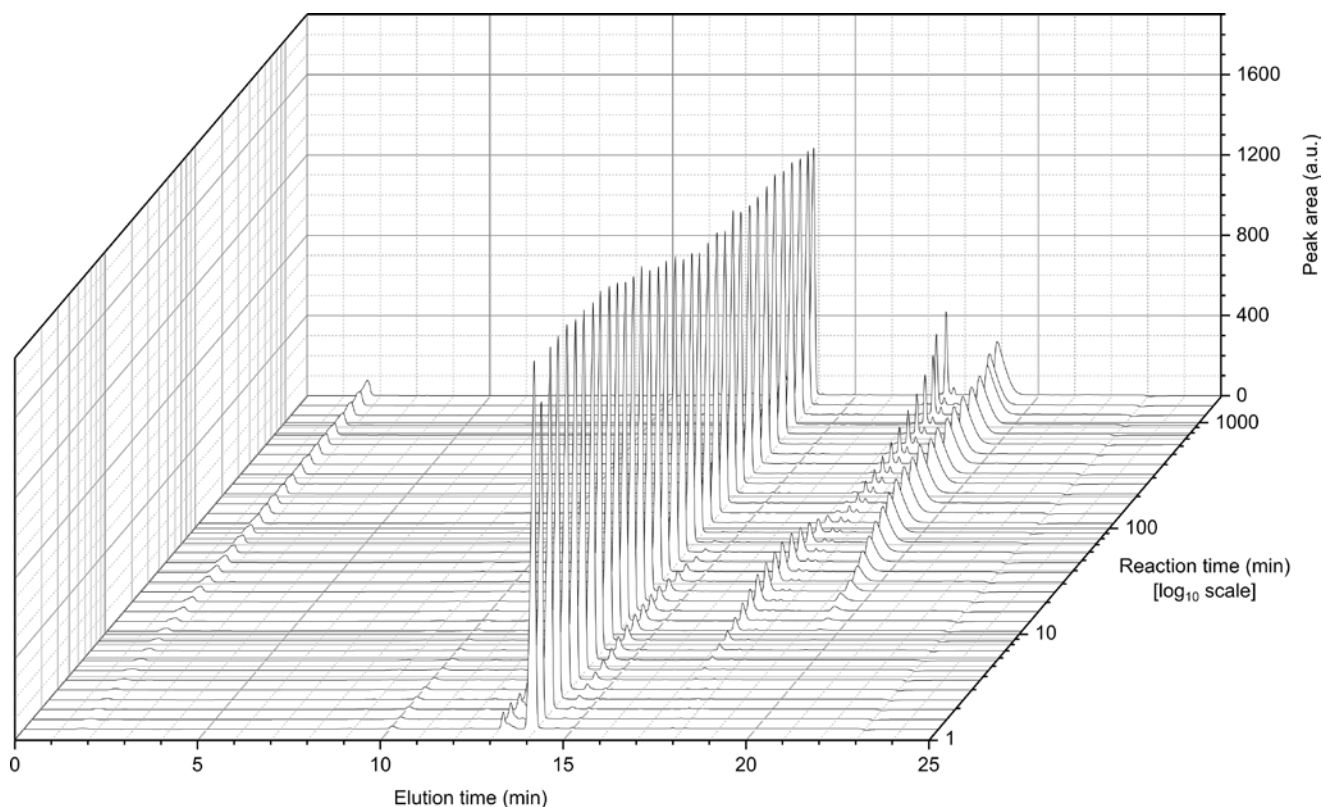
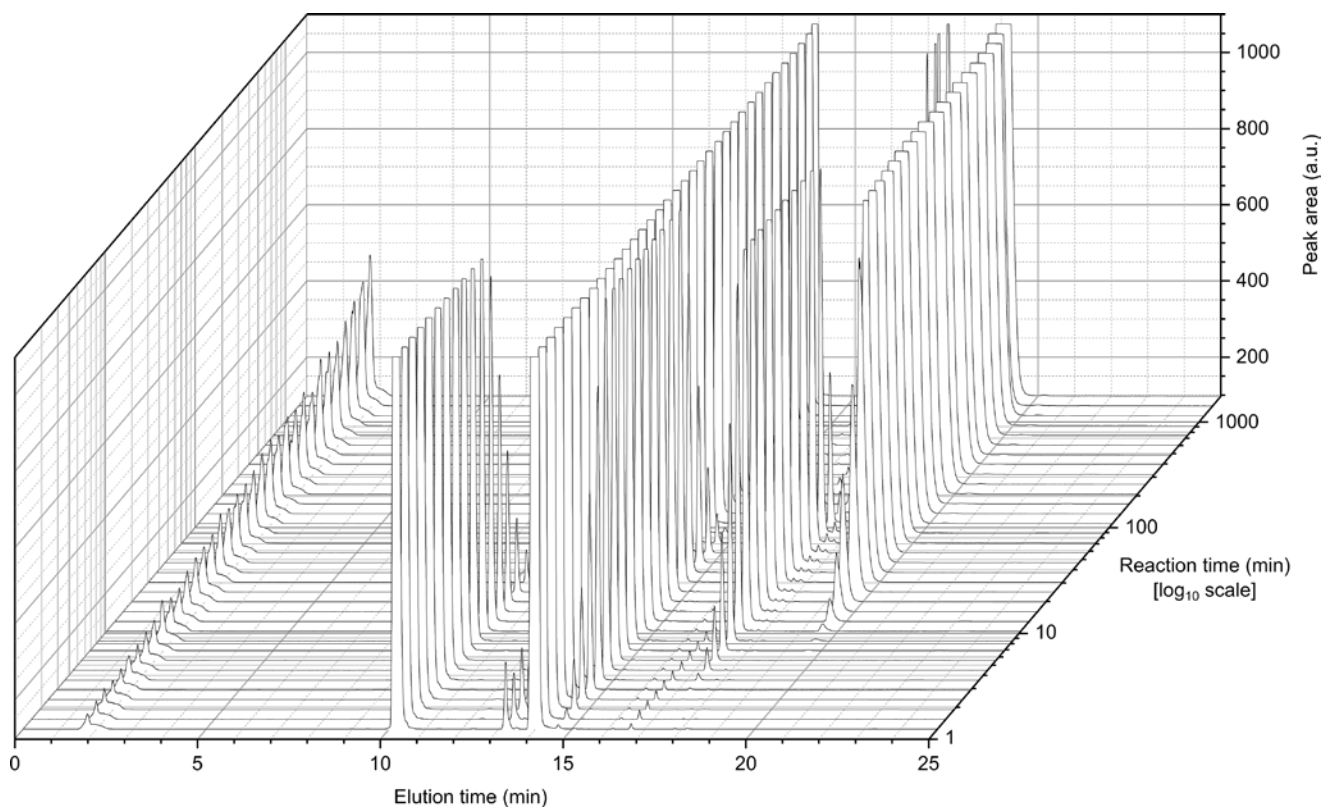


Figure 141. Waterfall plot of HPLC traces with (top) ELSD and (bottom) UV (260 nm) detection for the chain extension from Eg₃₂ to Eg₄₀. NaOTs (1.7 min), Hub¹(-Eg₃₂-OH)₃ (**19**) (10.2 min), DmtrO-Eg₈-OTs (**8**) (14.0 min), Hub¹(-Eg₃₂-OH)₂(-Eg₄₀-ODmtr)₁ (**19b**) (14.6 min), Hub¹(-Eg₃₂-OH)₁(-Eg₄₀-ODmtr)₂ (**19c**) (17.4 min), DmtrO-Eg₁₆-ODmtr (**14**) (17.6 min), Hub¹(-Eg₄₀-ODmtr)₃ (**20**) (19.5 min).

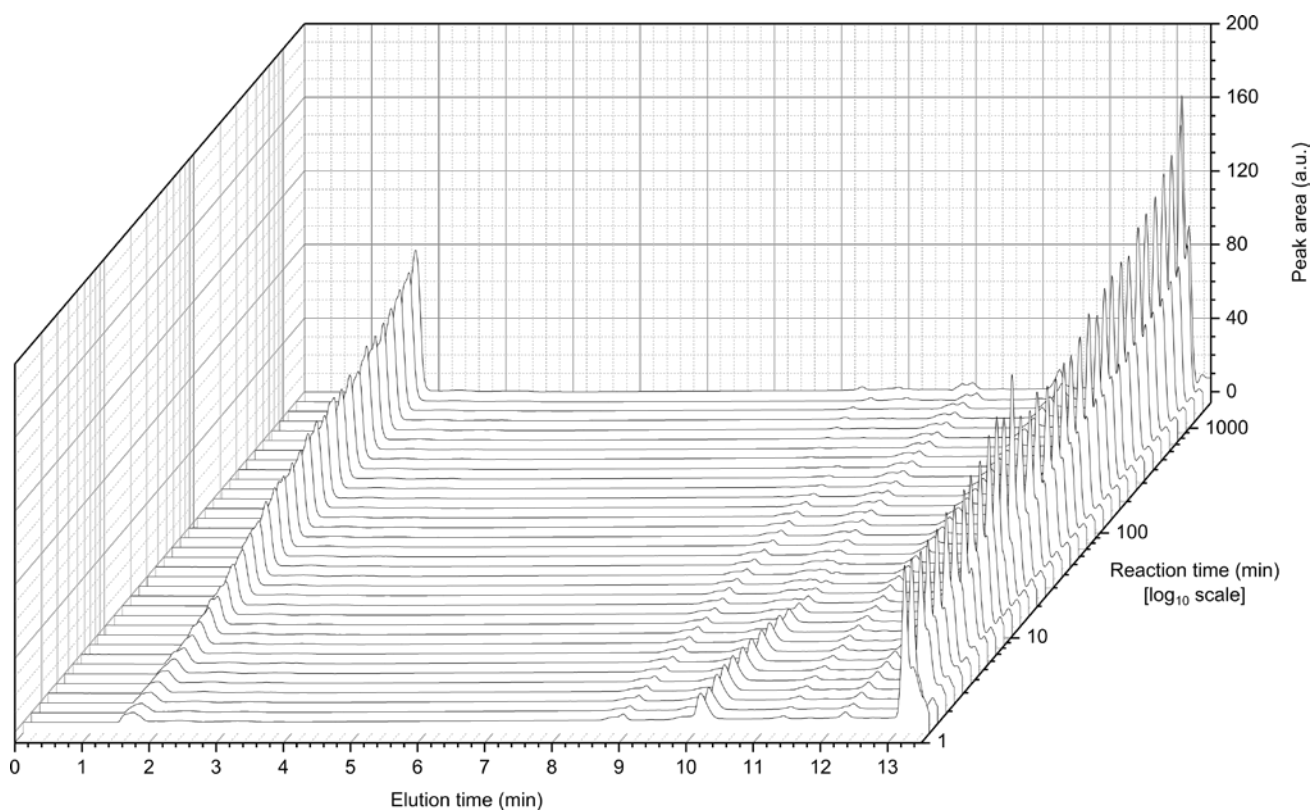
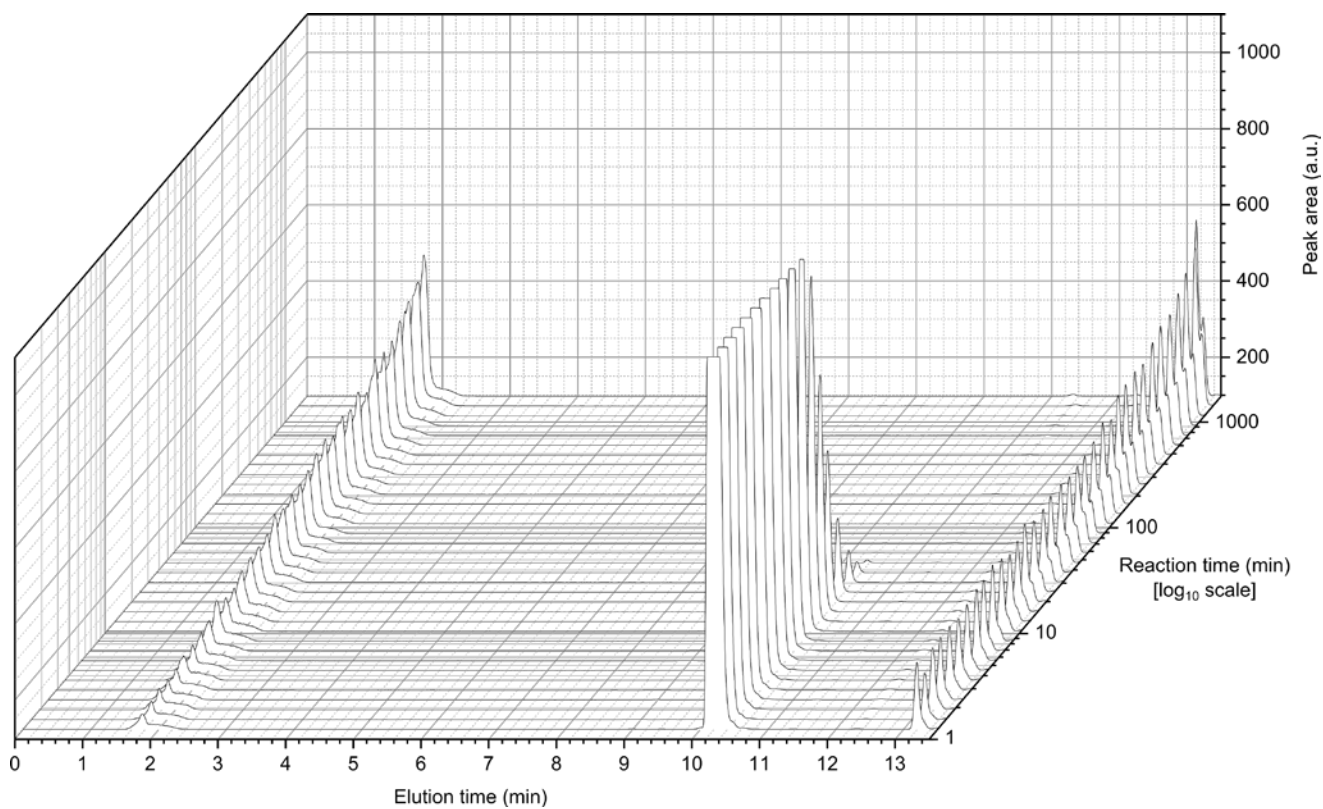


Figure 142. Enlarged from Figure 141. HPLC traces with (top) ELSD and (bottom) UV (260 nm) detection for the chain extension from Eg₃₂ to Eg₄₀.

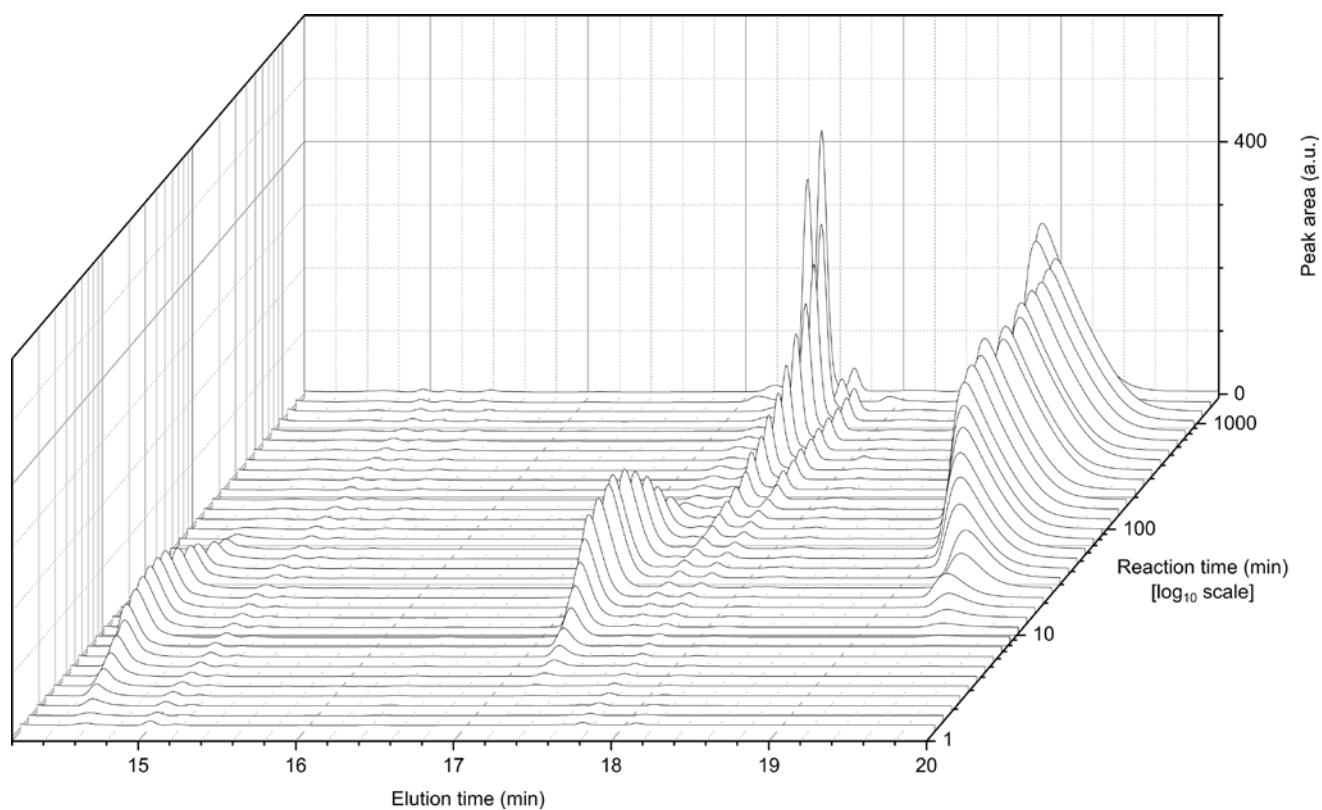
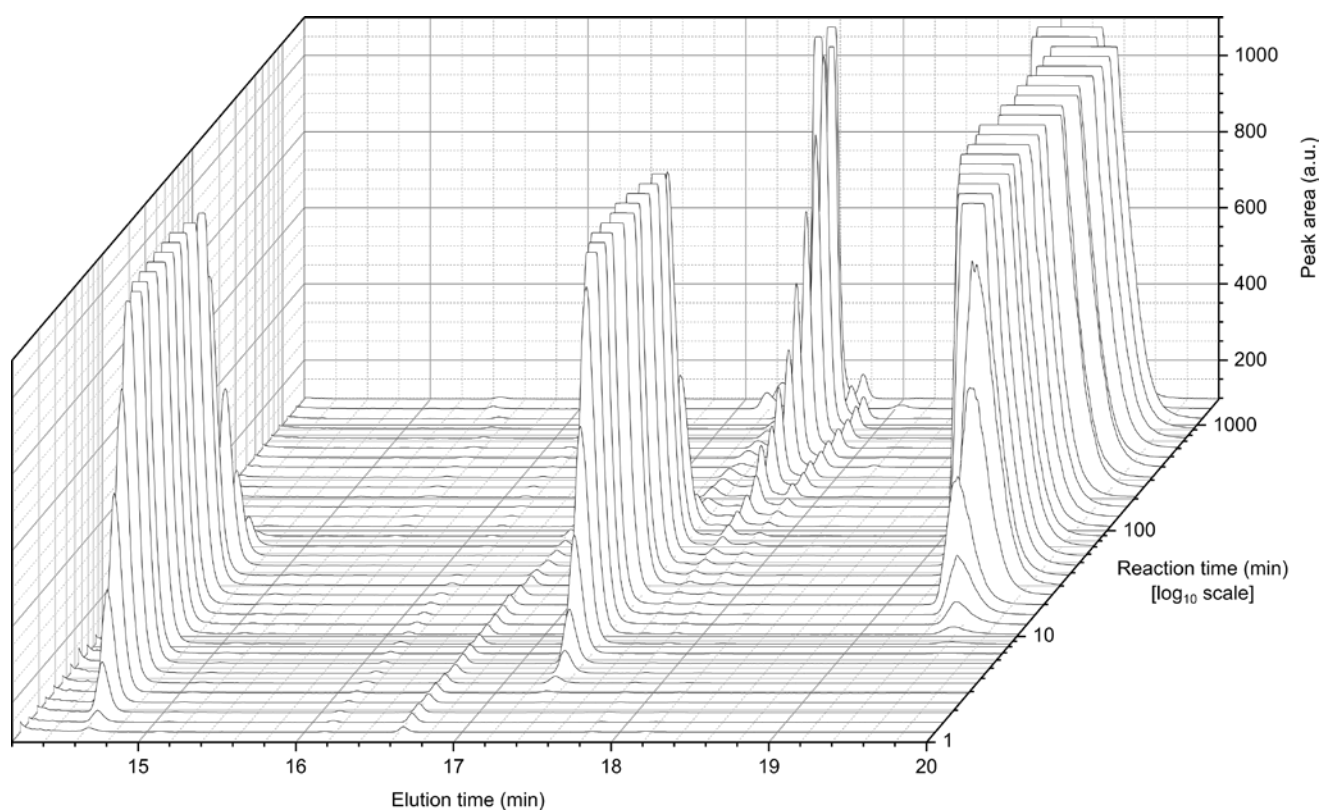


Figure 143. Enlarged from Figure 141. HPLC traces with (top) ELSD and (bottom) UV (260 nm) detection for the chain extension from Eg_{32} to Eg_{40} .

Extension from Eg₄₀ to Eg₄₈

For the extension from Eg₃₂ to Eg₄₀, the peaks of all species were separated during HPLC analysis and could be integrated reliably (Figure 146). However, while the Hub¹(-Eg₄₀-OH)₃ (**21**) homostar triol at 11 min is currently still sufficiently separated (Figure 147), there occurs a consistent shift towards higher elution time with increasing chain length as observed over the previous chain extensions. This means that the triol likely cannot be analyzed reliably by UV under these conditions within a few generations of further chain extension.

Further, the gap between the doubly extended Hub¹(-Eg₄₀-OH)₁(-Eg₄₈-ODmtr)₂ (**21c**) homostar and DmtrO-Eg₁₆-ODmtr (**14**) dimer is narrowing (Figure 148, peaks at 17.4 min and 17.6 min respectively) and the region around the elution time between 17-18 minutes is becoming crowded. There appear to be artefacts or unrelated impurity peaks on either side of the building block dimer peak (Figure 148, 17.6 min). Also, like in the previous extension, a residual peak of doubly extended homostar remains after 90 min of reaction time giving the appearance of incomplete reaction, despite continual generation of dimer indicating that the reaction is active.

Analysis of the concentration profile of Hub¹(-Eg₄₀-OH)₃ (**21**) homostar triol (Figure 144) and full simulation of the concentration profiles for all species (Figure 145) then yielded reaction rate coefficients approximately twice as high as for the prior extension, consistent with the higher reaction temperature, 50 °C instead of 40 °C.

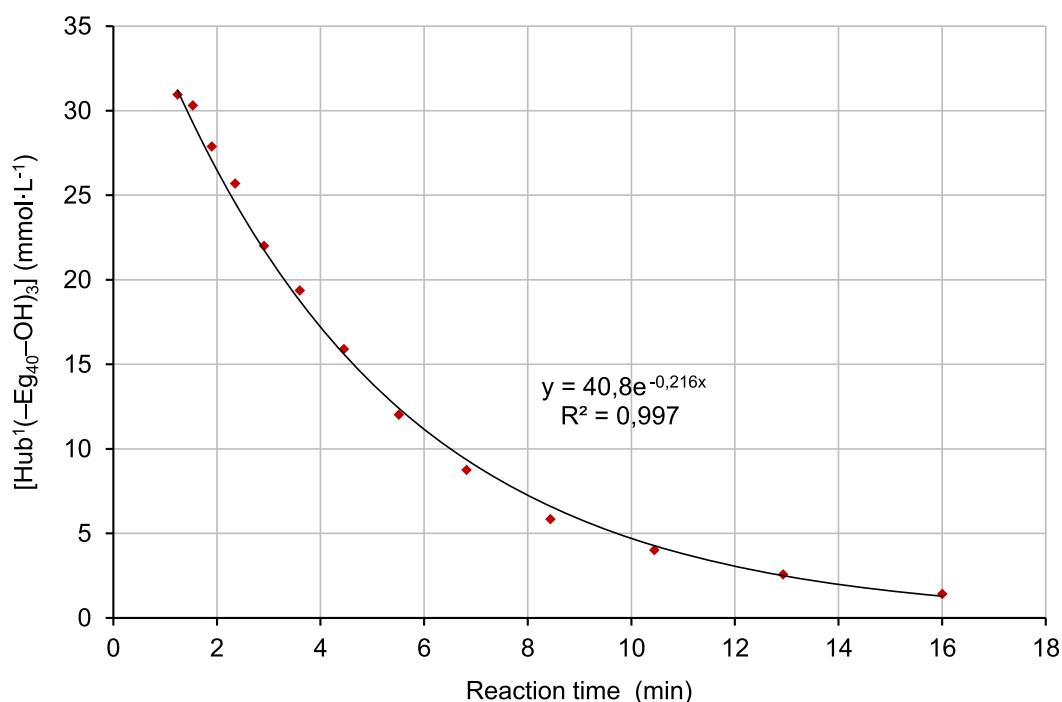


Figure 144. Concentration profile of Hub¹(-Eg₄₀-OH)₃ (**21**) homostar triol at the start of the chain extension from Eg₄₀ to Eg₄₈.

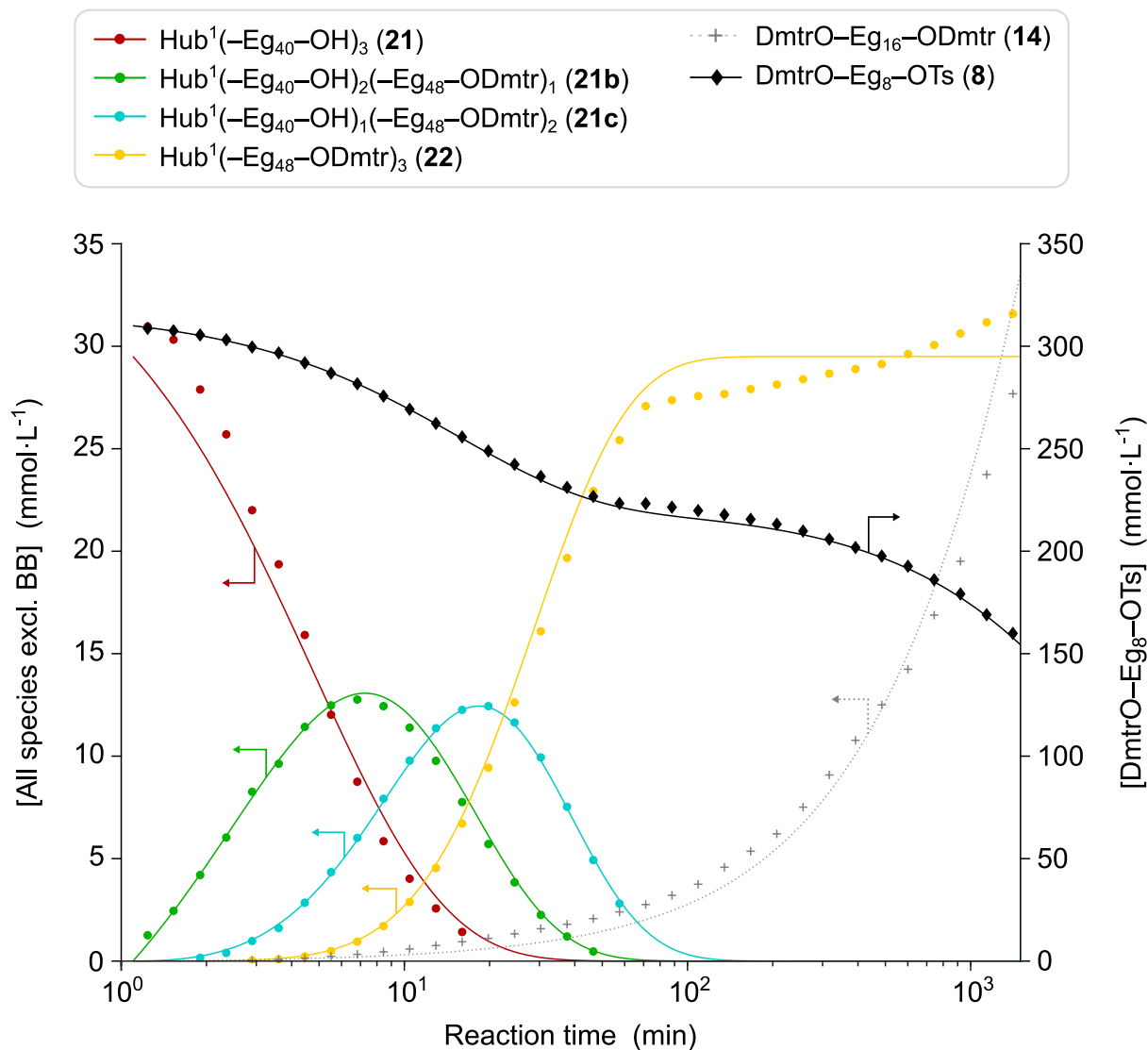


Figure 145. Simulated concentration profiles for chain extension from Eg_{40} to Eg_{48} over 1,740 min (29 h). $T = 50\text{ }^{\circ}\text{C}$, $t_{ind} = 1.1\text{ min}$, $k_1 = 0.67\text{ M}^{-1}\cdot\text{min}^{-1}$, $k_2 = 0.45\text{ M}^{-1}\cdot\text{min}^{-1}$, $k_3 = 0.25\text{ M}^{-1}\cdot\text{min}^{-1}$, $k_4 = 1.2 \cdot 10^{-4}\text{ min}^{-1}$, $c_{HS-triol}^{t=0} = 29.5\text{ mmol}\cdot\text{L}^{-1}$, $c_{BB}^{t=0} = 310\text{ mmol}\cdot\text{L}^{-1}$.

Notably, the generation of $DmtrO-Eg_{16}-ODmtr$ (**14**) dimer from building block could not be accurately fitted with a first order reaction in this case in contrast to all previous chain extensions.

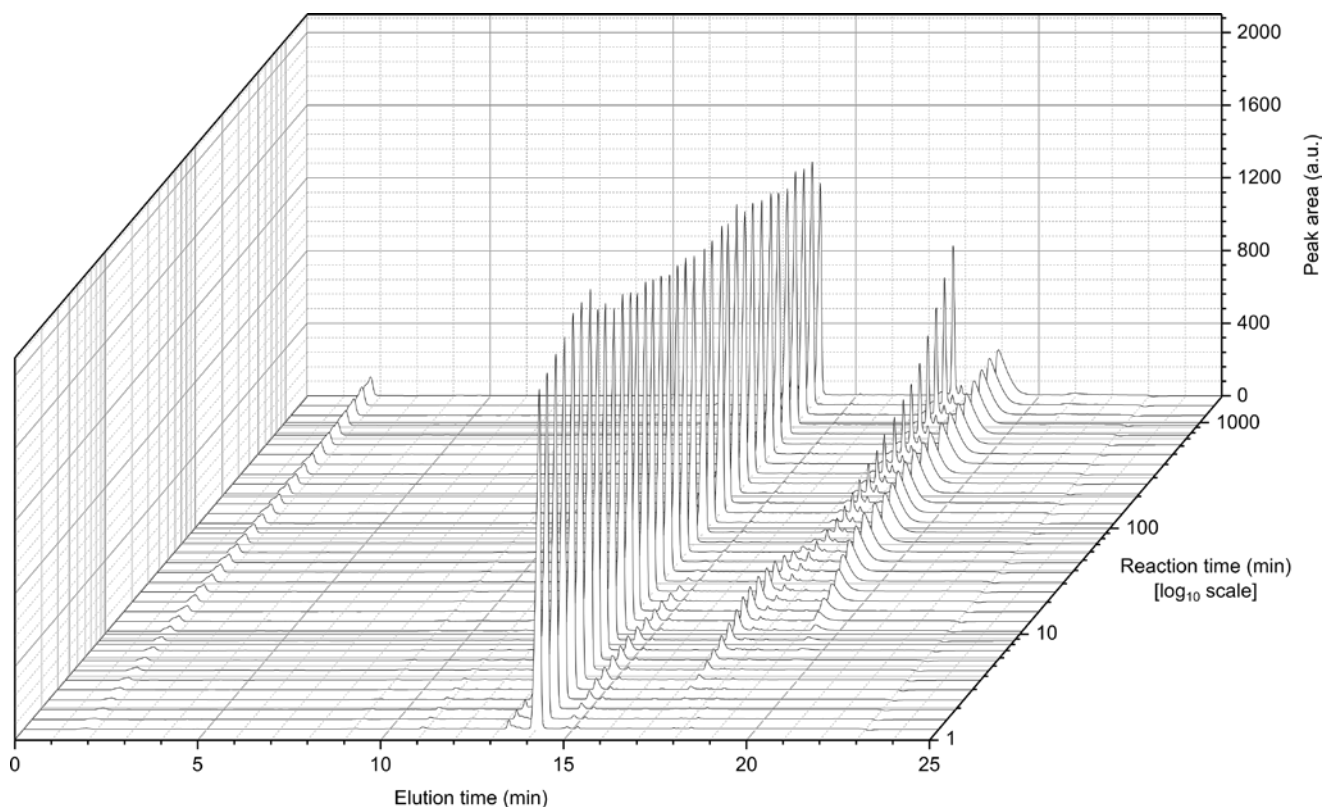
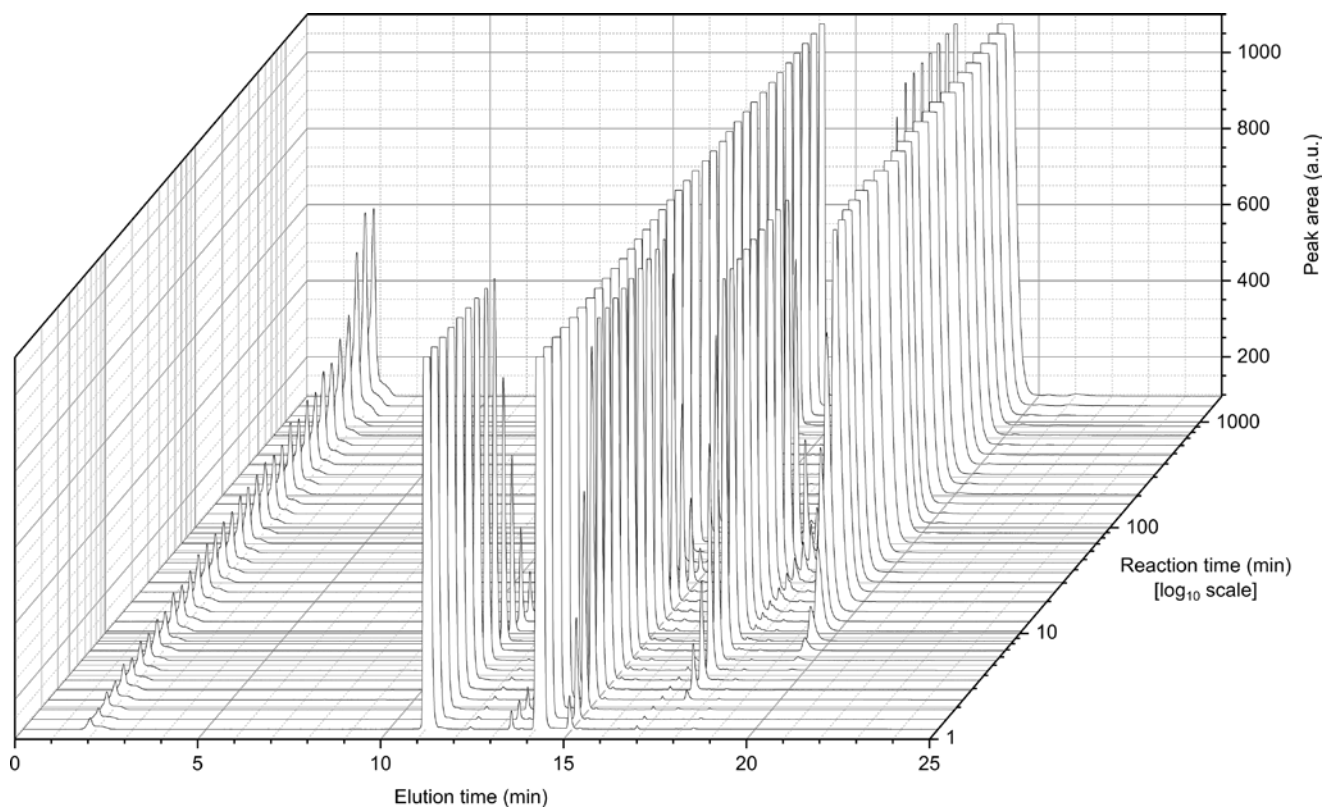


Figure 146. Waterfall plot of HPLC traces with (top) ELSD and (bottom) UV (260 nm) detection for the chain extension from Eg₄₀ to Eg₄₈. NaOTs (1.7 min), Hub¹(-Eg₄₀-OH)₃ (**21**) (10.9 min), DmtrO-Eg₈-OTs (**14**) (14.1 min), Hub¹(-Eg₄₀-OH)₂(-Eg₄₈-ODmtr)₁ (**21b**) (14.8 min), Hub¹(-Eg₄₀-OH)₁(-Eg₄₈-ODmtr)₂ (**21c**) (17.4 min), DmtrO-Eg₁₆-ODmtr (**14**) (17.6 min), Hub¹(-Eg₄₈-ODmtr)₃ (**22**) (19.6 min).

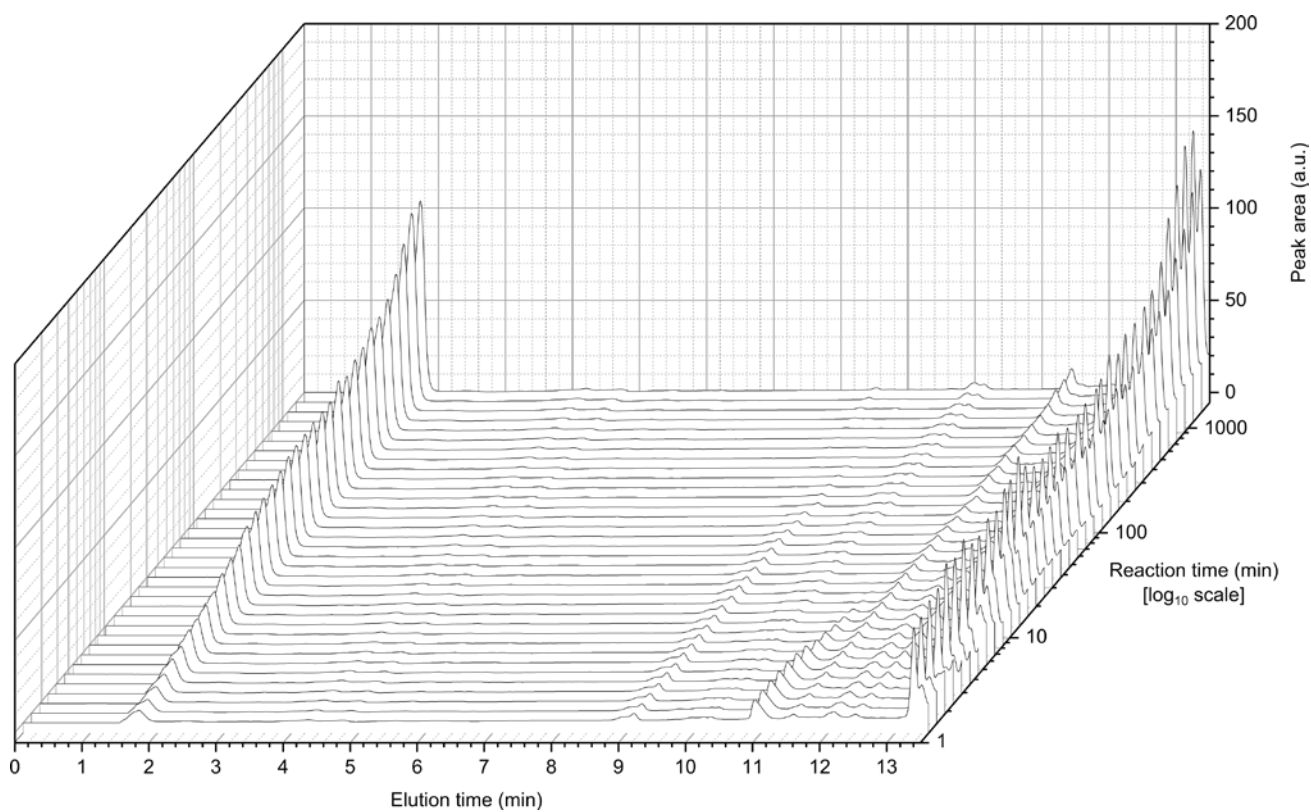
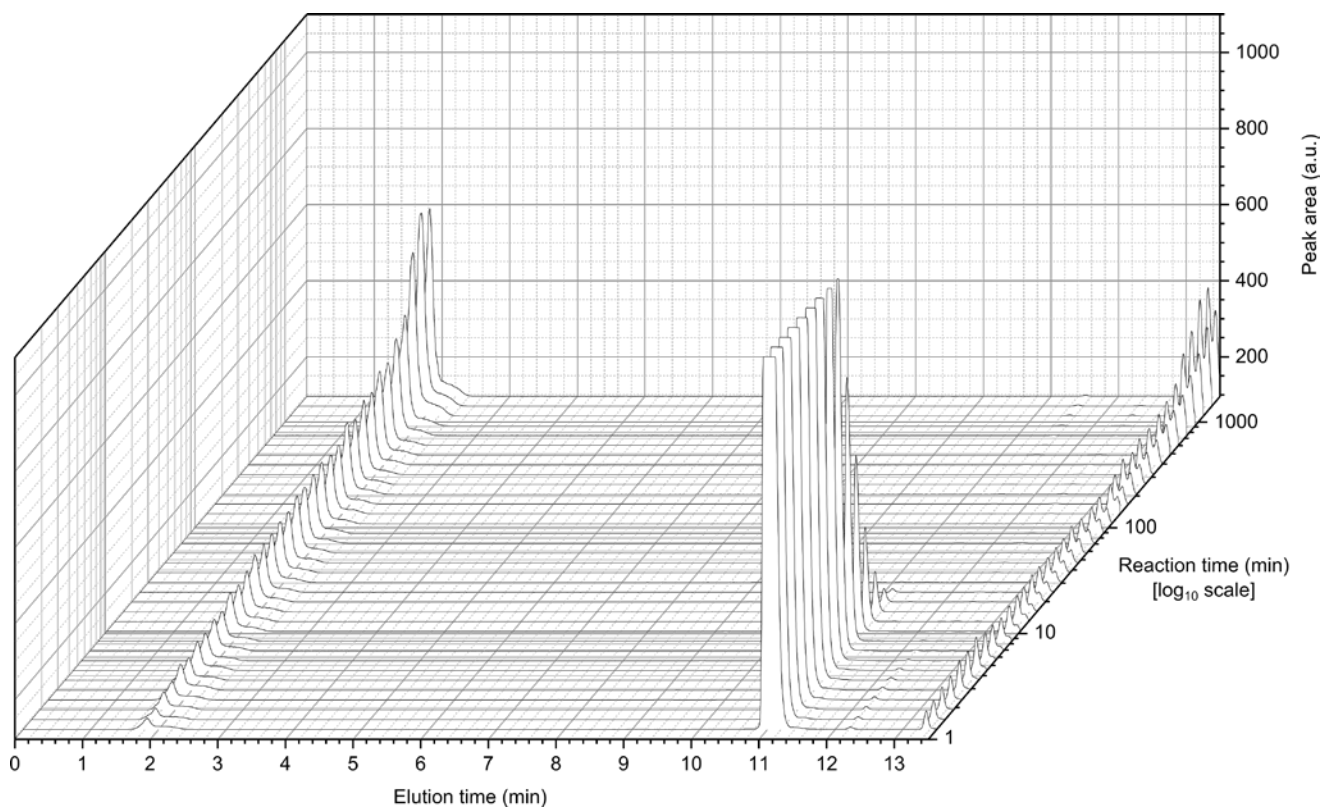


Figure 147. Enlarged from Figure 146. HPLC traces with (top) ELSD and (bottom) UV (260 nm) detection for the chain extension from Eg_{40} to Eg_{48} .

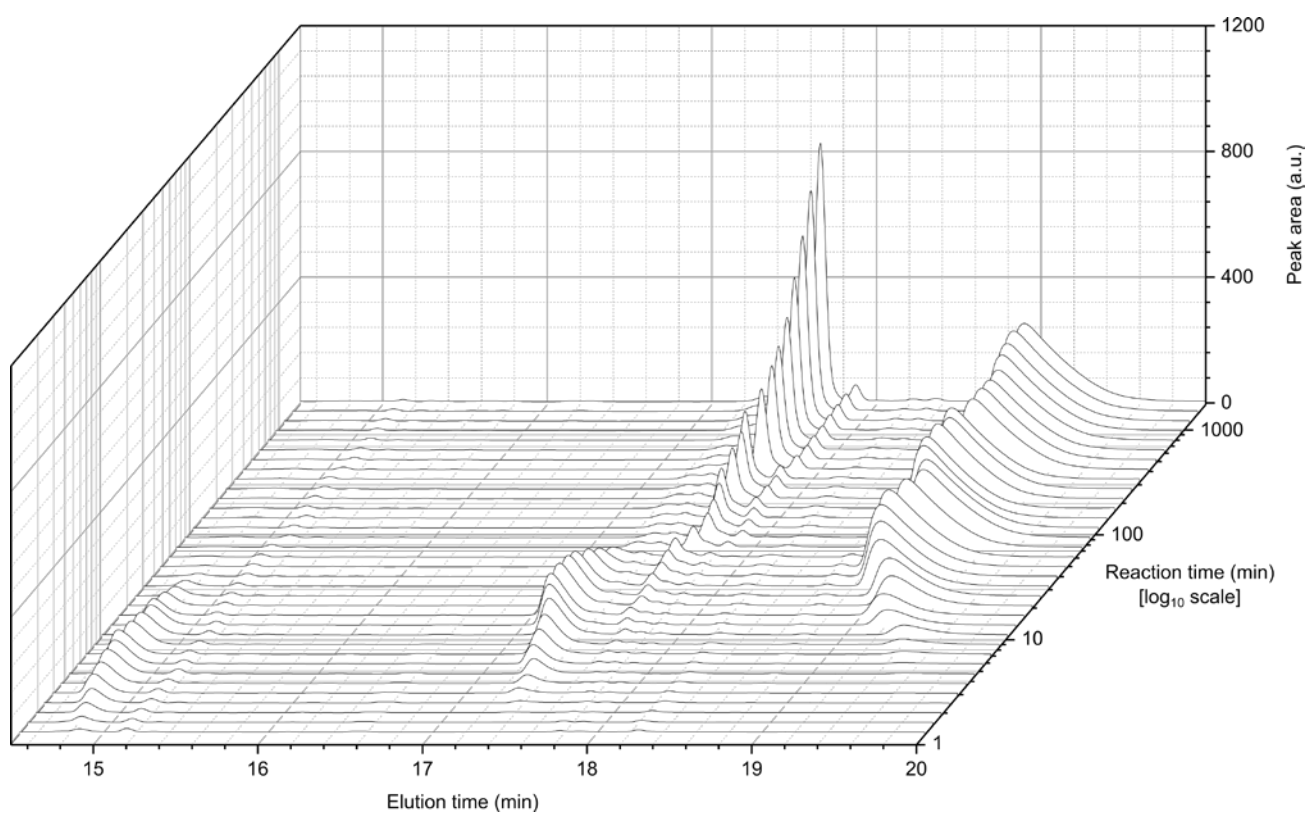
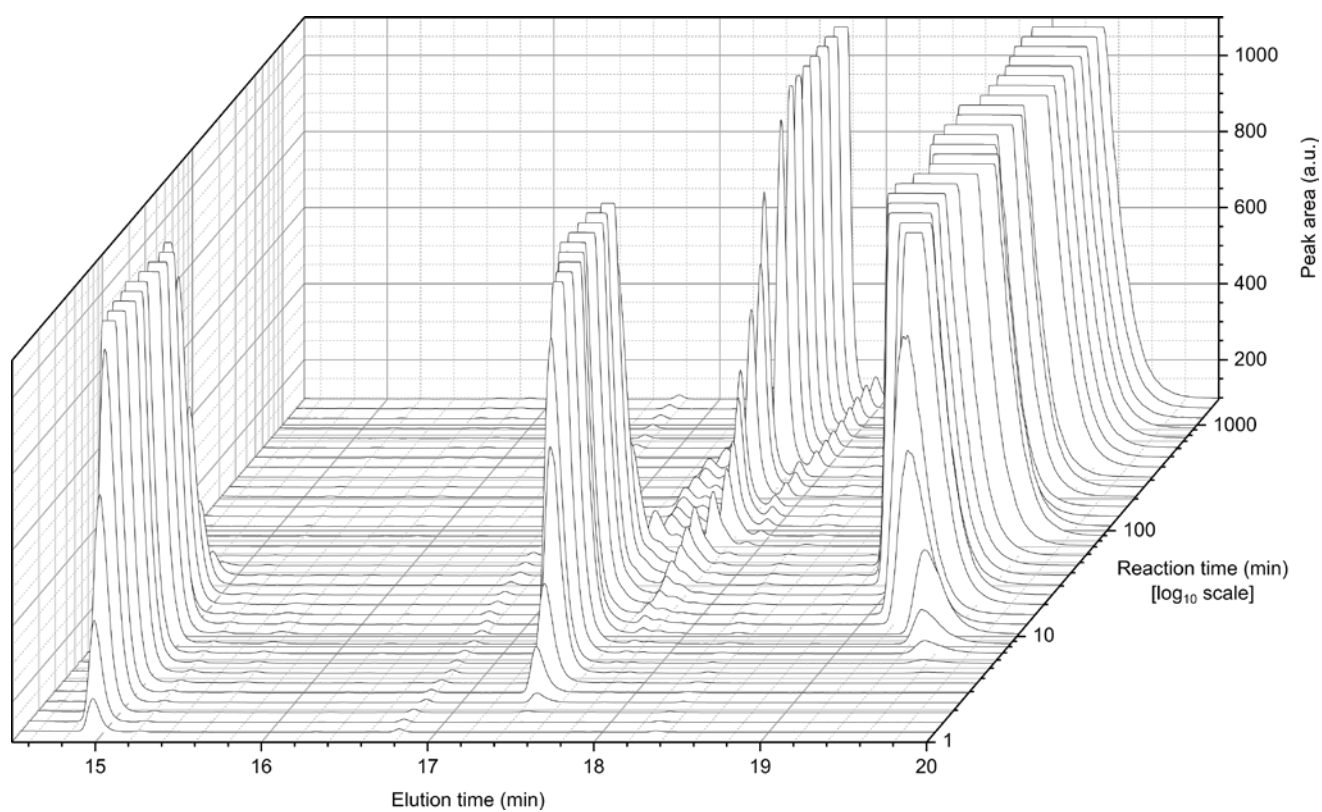


Figure 148. Enlarged from Figure 146. HPLC traces with (top) ELSD and (bottom) UV (260 nm) detection for the chain extension from Eg_{40} to Eg_{48} .

Extension from Eg₄₈ to Eg₅₆

For the last chain extension reaction from Eg₄₈ to Eg₅₆, a different reaction vessel was chosen. Due to the small overall reaction volume (8 mL), no sufficiently small two-necked round bottomed flask was available which could be properly stirred and sampled with a micropipette. Instead, a narrow test tube fitted with a two-way adapter stopped closed at the straight connection and connected to a Schlenk line at the side arm was used. A micropipette could be inserted through the straight connection into the test tube for sampling.

However, after starting the reaction by adding sodium hydride, a foam layer several centimetres thick formed and did not readily dissipate. This prevented regular sample taking from the beginning of the reaction. Samples were therefore taken at longer intervals and as a result, no reliable quantification could be performed. Nevertheless, the ELSD and UV traces give an idea of the approximate time of completion.

The elution times are comparable to the chain extension from Eg₄₀ to Eg₄₈ and similar challenges were encountered during peak integration. The Hub¹(-Eg₄₈-OH)₃ (**23**) homostar triol peak is visible around 11.5 min, seen overlapping with an impurity peak in the first UV trace (Figure 150, 3.6 min reaction time). It is also apparent that two impurity peaks appear on either side of the DmtrO-Eg₁₆-ODmtr (**14**) dimer peak (Figure 151, 17.6 min) and increase in size with increasing reaction time. The peak at around 17.4 min elutes at a similar time as the the doubly extended homostar. This would likely have complicated accurate quantification towards the end of the reaction.

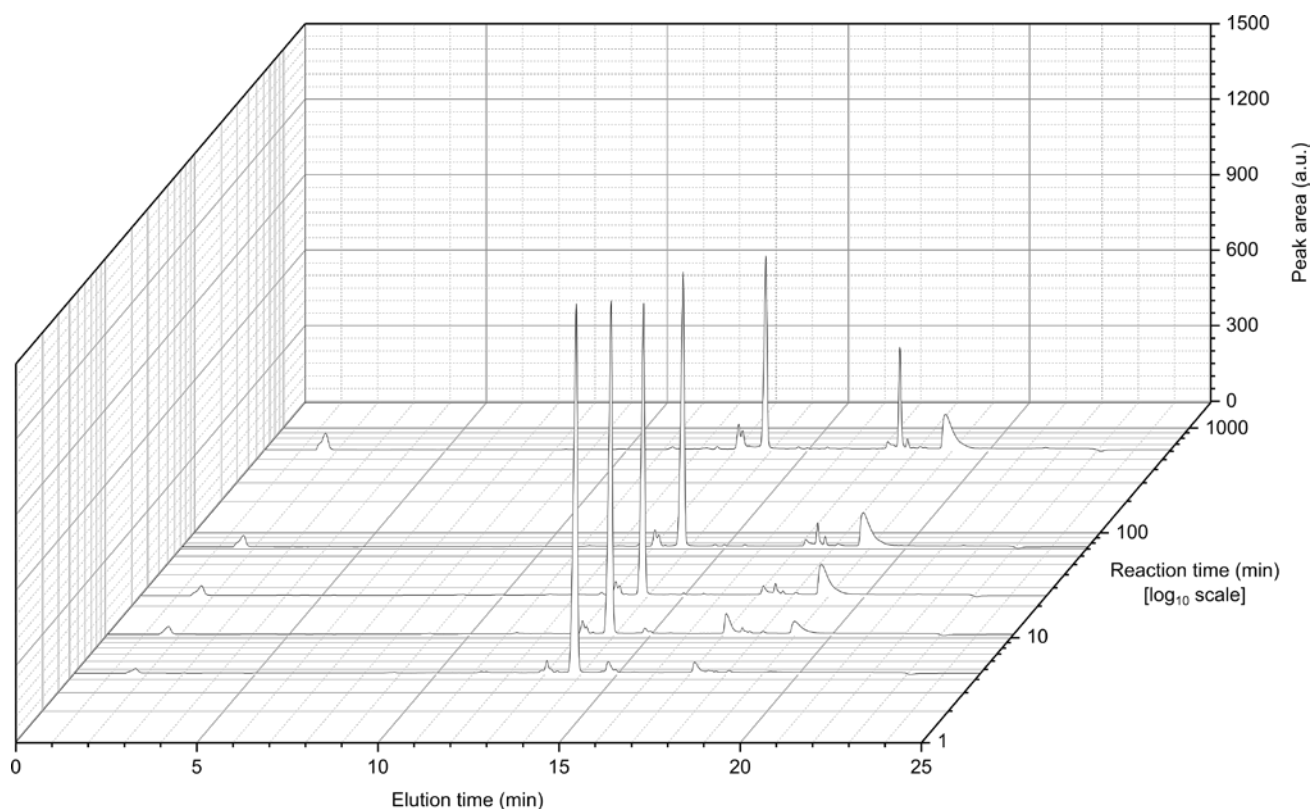
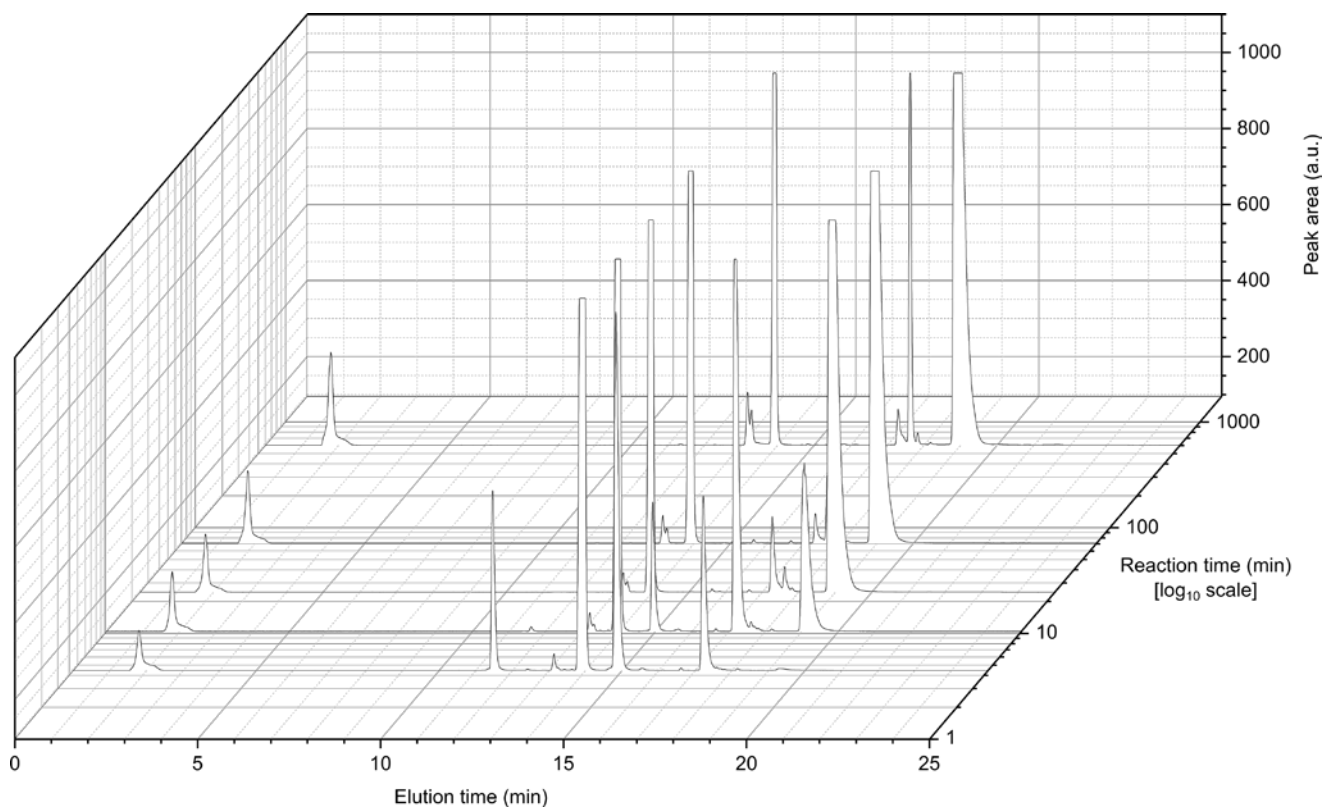


Figure 149. Waterfall plot of HPLC traces with (top) ELSD and (bottom) UV (260 nm) detection for the chain extension from Eg₄₈ to Eg₅₆. NaOTs (2 min), Hub¹(-Eg₄₈-OH)₃ (**23**) (11.5 min), DmtrO-Eg₈-OTs (**8**) (14 min), Hub¹(-Eg₄₈-OH)₂(-Eg₅₆-ODmtr)₁ (**23b**) (15 min), Hub¹(-Eg₄₈-OH)₁(-Eg₅₆-ODmtr)₂ (**23c**) (17.2 min), DmtrO-Eg₁₆-ODmtr (**14**) (17.7 min), Hub¹(-Eg₄₈-ODmtr)₃ (**24**) (19.2 min).

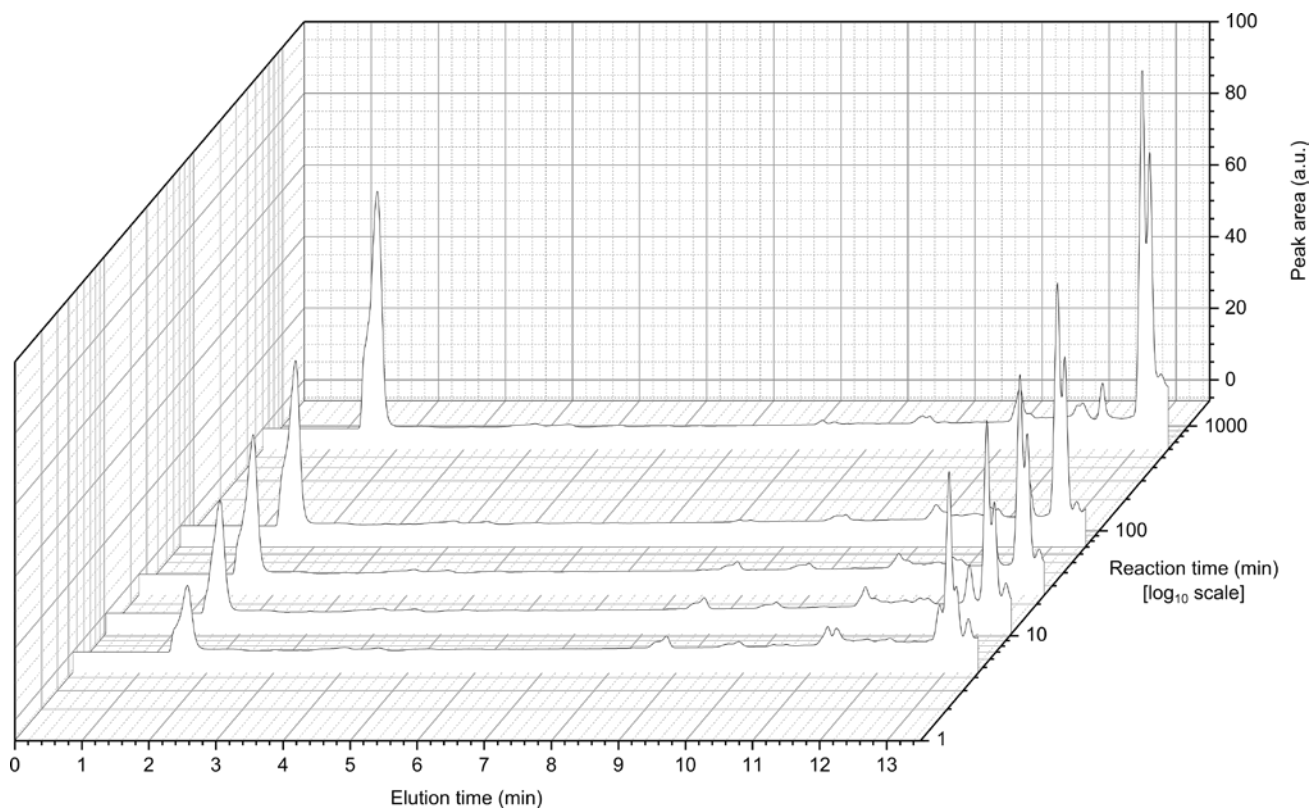
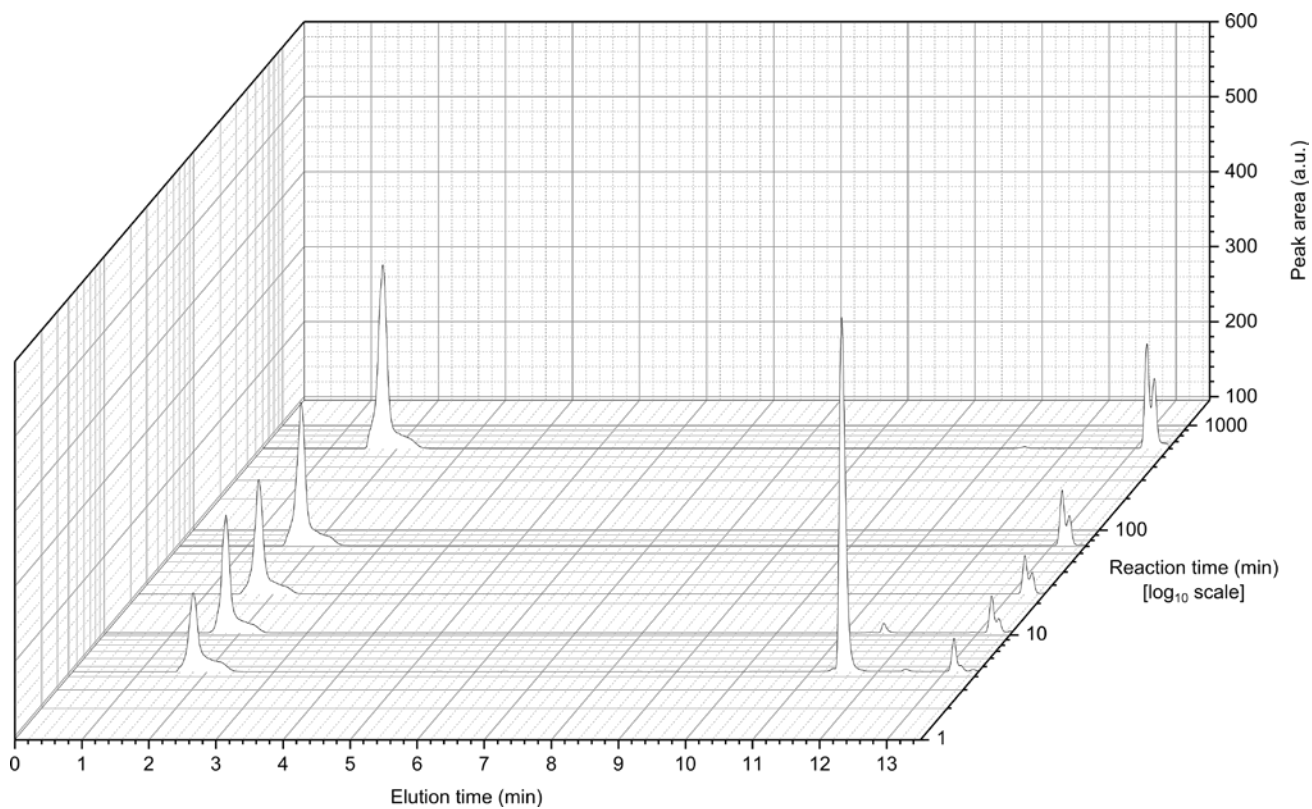


Figure 150. Enlarged from Figure 149. HPLC traces with (top) ELSD and (bottom) UV (260 nm) detection for the chain extension from Eg₄₈ to Eg₅₆.

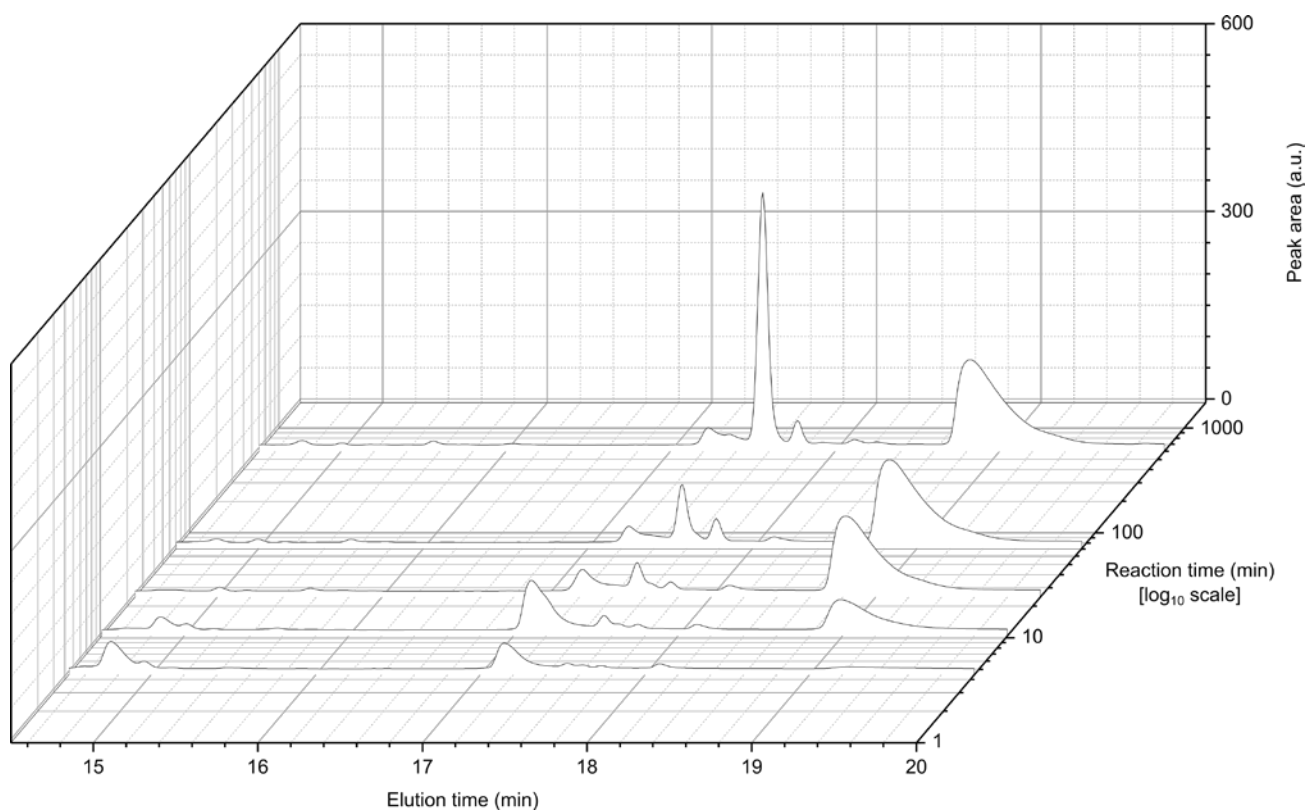
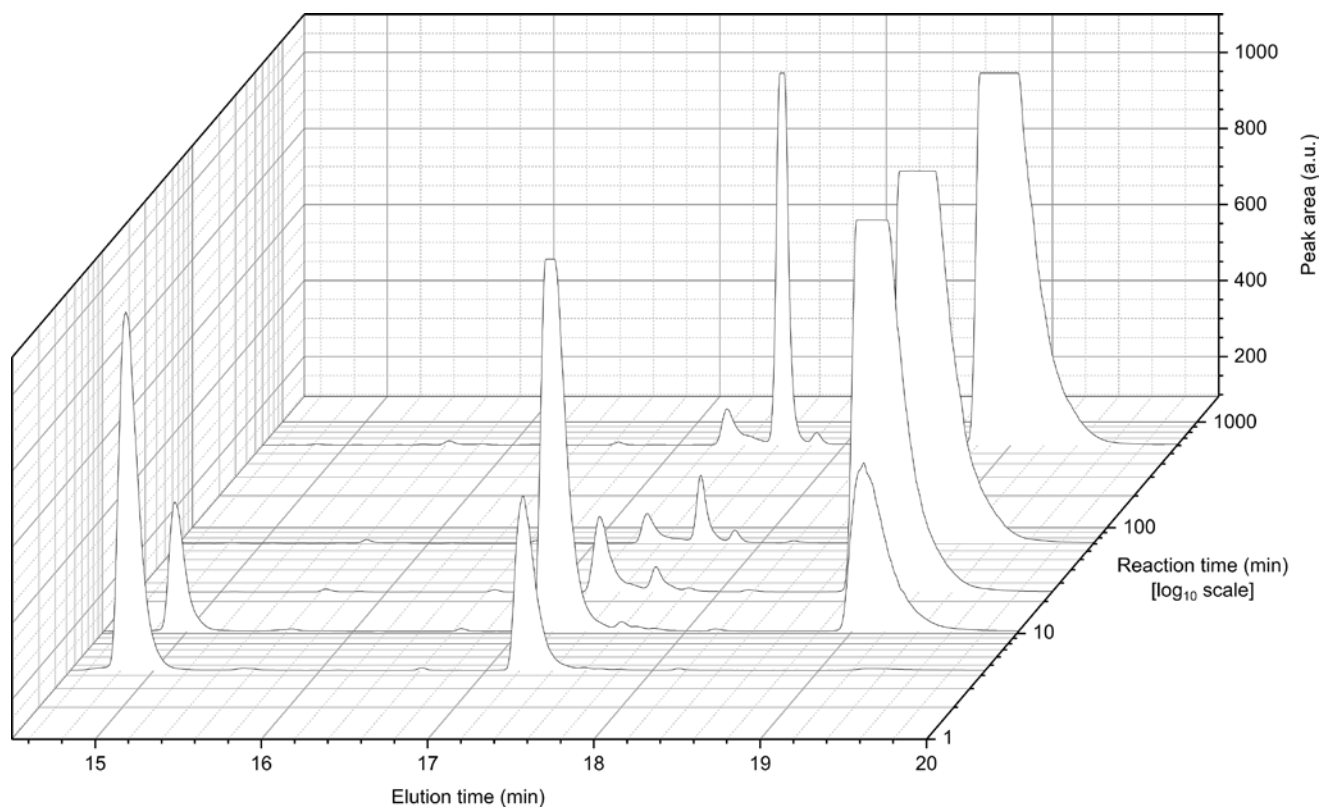


Figure 151. Enlarged from Figure 149. HPLC traces with (top) ELSD and (bottom) UV (260 nm) detection for the chain extension from Eg_{48} to Eg_{56} .

Appendix E – HPLC spectra for the synthesis of Eg₆₀

HPLC spectra gathered for the isolated dry product after each chain extension and each deprotection en route from Eg₁₂ to the final HO–Eg₆₀–OMe product (Section 3.3.7) are shown below (Figure 152 to Figure 154). It is apparent that unless the sample is oversaturated (Figure 152, **76**), impurities can hardly be detected by ELSD. On the other hand, the UV spectra typically show smaller impurity peaks on either side of the main peak and a comparison between the relative peak intensities at different wavelengths (260 and 300 nm) confirms when these peaks are hub related, i.e. product related. Preparative chromatographic separation, followed by mass spectrometry, or in situ analysis via HPLC-MS is the next logical step in identifying these minor contaminants.

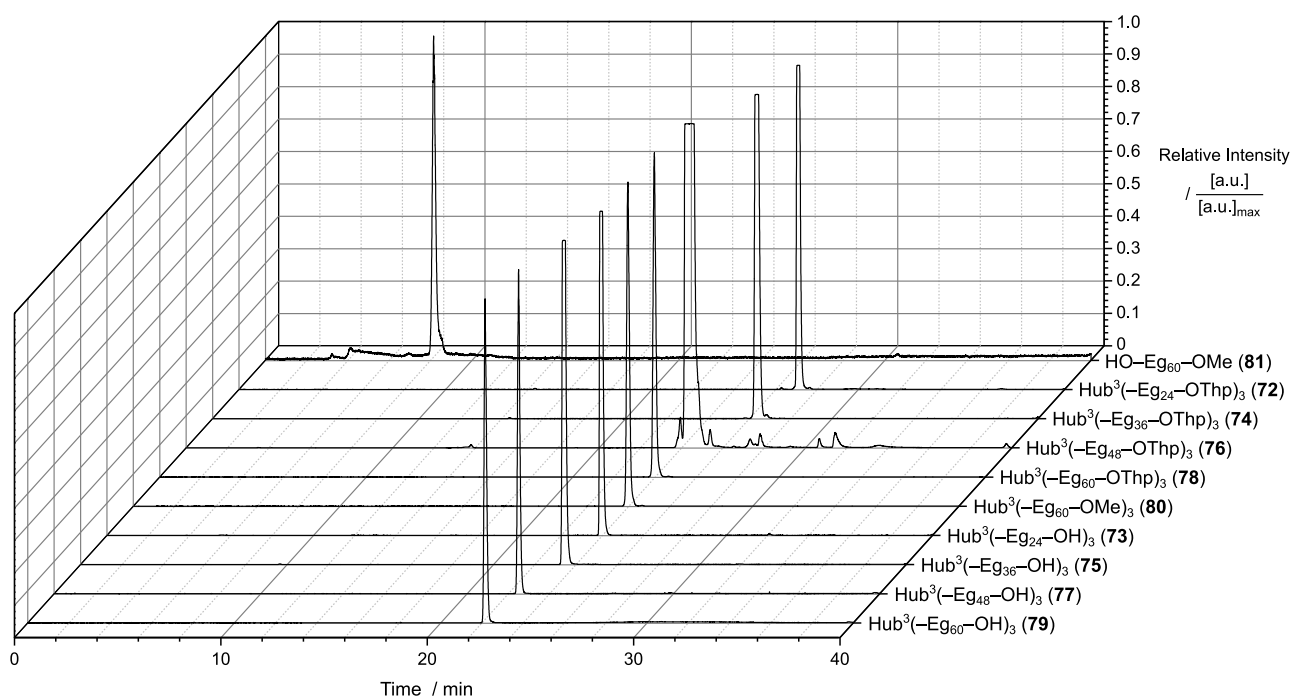


Figure 152. Summary of the product analysis by ELSD for the synthesis of HO–Eg₆₀–OMe (**81**).

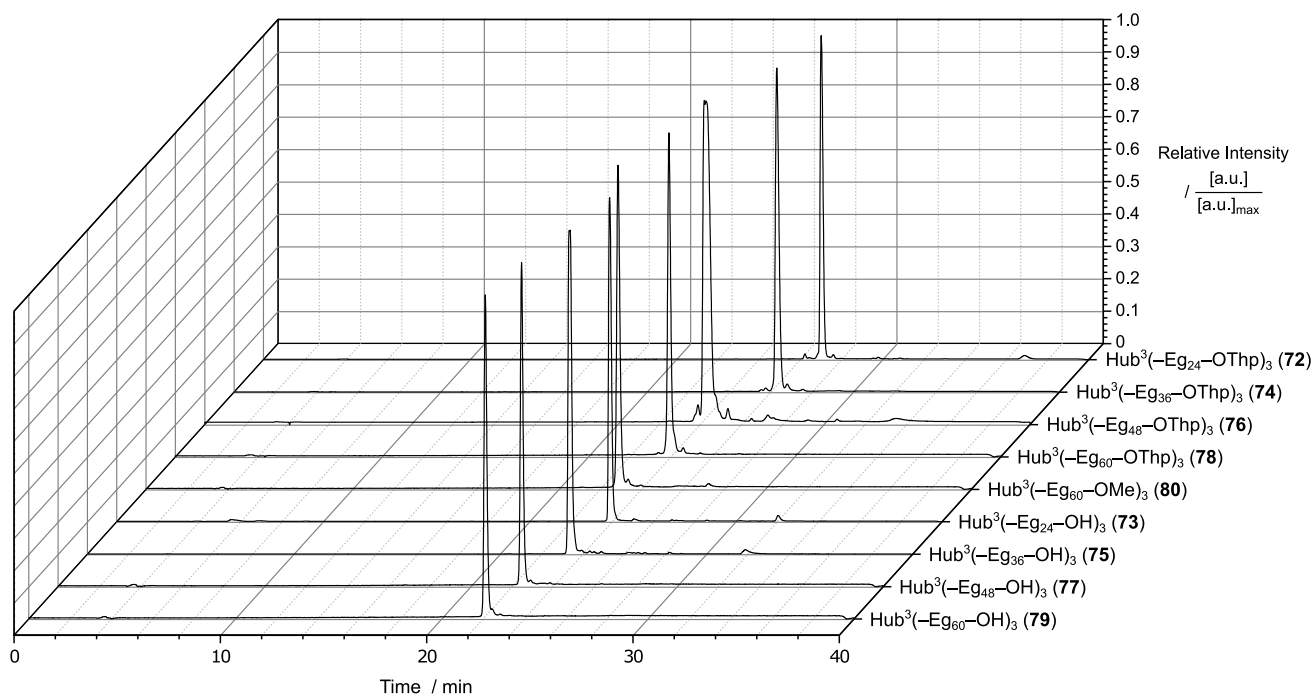


Figure 153. Summary of the product analysis by UV (260 nm) for the synthesis of HO-Eg₆₀-OMe (**81**).

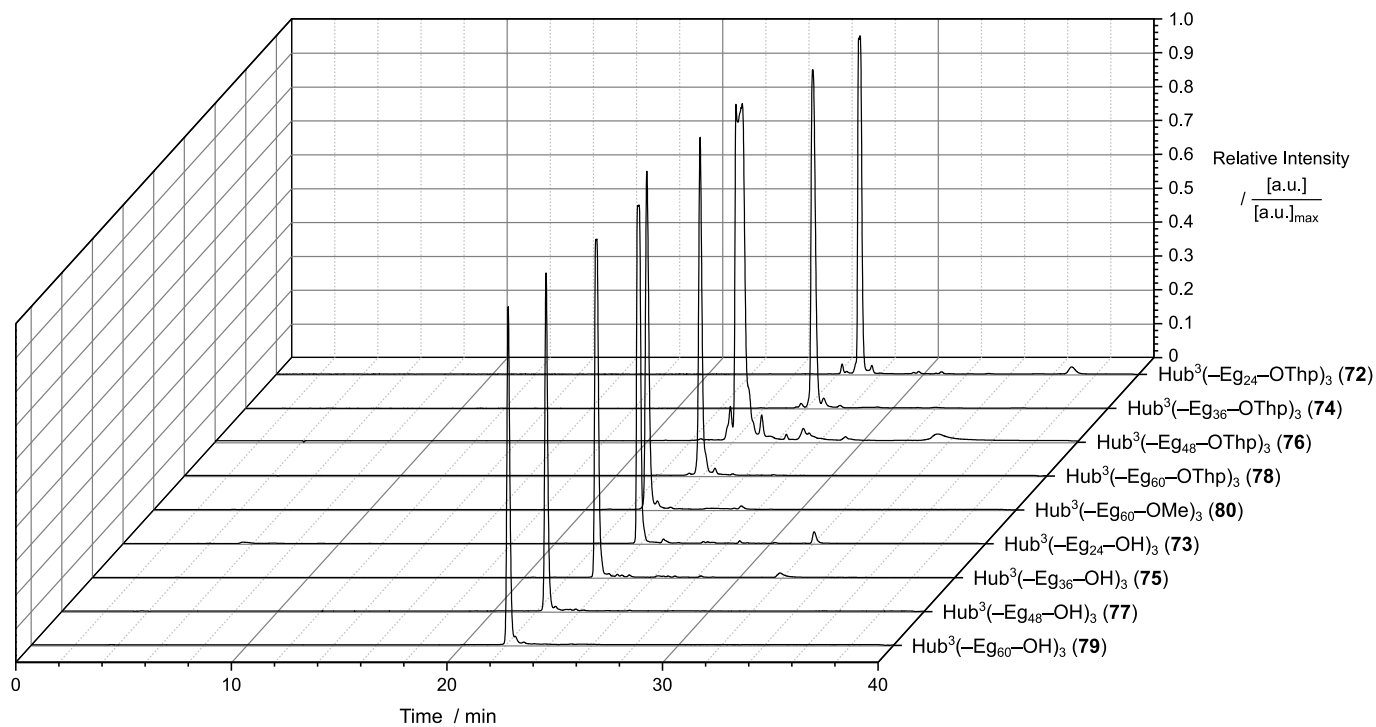


Figure 154. Summary of the product analysis by UV (300 nm) for the synthesis of HO-Eg₆₀-OMe (**81**).

Appendix F – Membrane cell assembly

The nanofiltration membranes are housed inside stainless steel cells suitable for operation at elevated pressure. Details of the membrane cell design is shown in Figure 155, Figure 156 and Figure 157 below and membrane insertion and cell assembly is shown in Figure 158 and Figure 159.



Figure 155. Membrane housing cell upper half outside (see Figure 156 for the inside). (a) Overview with (b) angled feed inlet, (c) permeate outlet and (i) retentate outlet as well as (ii) optional threads for attachment to a frame. (d) The angled feed inlet is drilled from the outside and the gap between feed tube and outside subsequent welded closed. (e) Fittings are inserted into the topside via 1/8" NPT threads.



Figure 156. Upside-down view of the membrane housing cell upper half inside (see Figure 155 for the outside). (a) Overview with (b) angled feed inlet, (c) permeate outlet and (i) retentate outlet. (d) Overview with inner and outer O-rings inside their respective grooves. The inner O-ring seals the feed/retentate compartment against the permeate compartment, i.e. it separates the compartments on either side of the membrane. The outer O-ring seals the permeate compartment from the atmosphere outside the cell.

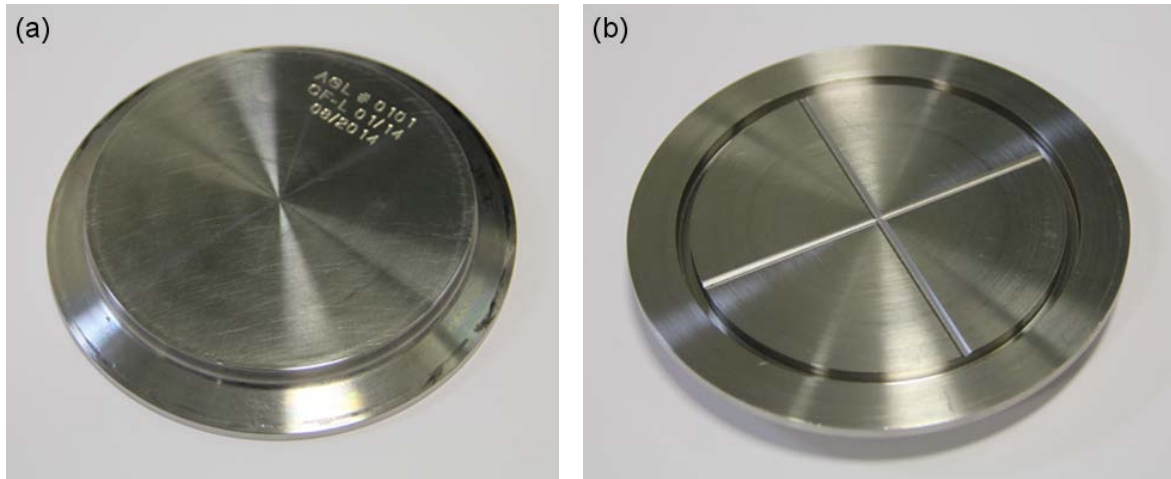


Figure 157. Membrane housing cell bottom half (a) outer and (b) inner side. As seen in (b), the grooves along the inside as well as the porosity of the sintered steel disc (see Figure 158) facilitate the flow of permeate fluid into the outer ring from where it passes through the permeate tube (shown in Figure 156c) back to the other side of the cell. It is convenient to have all connections on one side of the cell so that it can be rested on a flat surface and more easily disassembled.



Figure 158. Step 1 - 6 (a – f) of membrane cell assembly in upside-down position. The flat white sheet of polymeric material visible in Step 1 - 3 is a PEEK membrane coupon; the PEEK active layer is facing towards the feed and retentate side (towards the O-ring) and the polypropylene backing is facing towards the permeate side (towards the sintered steel disc).



Figure 159. The (a) loaded membrane cell is (c) clamped with a (b) 4.0" high pressure clamp to give the (d) fully assembled membrane cell.

Appendix G – Diafiltration apparatus

Equipment list

As pressurizing feed pump and fresh solvent replenishment pump were used Gilson 305 and Gilson 307 Series HPLC pumps, equipped with 100SC pump heads.

As recirculation pumps in both stages were used Micropump GD Series magnetically coupled gear pumps (GD-M35/J/F5/S/6/N1 ATEX with SmCo Hub P/N 83554 driving magnet magnetically coupled to 0.55 kW, 2 pole, 400 volt, three phase, 25 to 70 Hertz, ATEX II 2 G Eex-d IIB T4 inverter rated motor with thermistors). Each pump was controlled via a mounted IP54 Lenze SMV Panel (0.75 kW, 230 volt, single phase input vector, integral mains filter, isolator and membrane control pad with thermistor relay; suitable for 0 to 10 volt DC or 4-20 mA input signals) assembled by Michael Smith Engineers, Ltd. (Surrey, UK).

1st and 2nd stage pressure was measured both upstream and downstream of the membrane cells using WIKA Bourdon tube pressure gauges (Model 232.50, 100 mm, Class 1.0) ranging from 0 – 60 bar in the 1st stage and 0 – 40 bar in the second stage. (0 – 80 bar gauges in the 1st stage would be more appropriate). The Bourdon tubes were directly connected to the system via ¼" NPT process connections; an instrument with a diaphragm seal to separate gauge and process fluid would have been more appropriate here, as it minimizes dead-end process volume, and thus cross-contamination between diafiltrations.

R3A Series externally adjustable proportional relief valves with Kalrez O-rings and yellow spring kit (24.1 to 51.7 bar), 8F Series in-line particulate filters with 40 µm pore size elements, and all other tubing connections and adapters were supplied by Swagelok, UK.

Membrane housing cells were custom made by the Department of Chemical Engineering Workshop at Imperial College London. The membrane cells were clamped with 4.0" diameter pressure clamps from Dairy Pipelines Ltd (Essex, UK).

The membranes were supported by 1000 Series pressed discs [OD = 3.593" (90 mm), OD machined to size, Thickness = 0.078" (2 mm), Media Grade = 20, Material = 316 LSS] (Mott Corporation, USA) and sealed inside the membrane housing using 99 mm x 3 mm (Diameter x Thickness) outer and 80 mm x 4 mm inner O-rings (Eriks, UK).

1/8" (Gauge 22), 1/4" (Gauge 20) and 3/8" (Gauge 20) 316 stainless steel fixed tubing and 1/8" (ID 1/16"), 1/4" (ID 1/8") and 3/8" (ID 1/4") PTFE flexible tubing were supplied by NCE Solutions (Rochester,

UK). Flexible tubing needs to be fully solvent resistant; Materials such as polyamide should not be used as the plasticizer leaches when in contact with strong solvent such as THF.

Diafiltration set-up

The pressurized section of the diafiltration set-up is shown Figure 160a with equipment in stream order as follows: (i) 4-way valve for washing and product recovery, (ii) inline filter to protect the (iii) recirculation pump, (iv) pressure gauge upstream of the membrane cells, connections (v) upstream and (vi) downstream of the (vii) membrane cells and (viii) pressure gauge downstream of the membrane cells. For flow which does not pass through the 1st stage membranes, the 1st recirculation stage has an overflow through the (ix) 1st stage proportional relief valve which recycles back to the feed tank any excess flow coming through the (x) feed port from the feed pressurization pump. If the feed flow through (x) and (ix), from and to the feed tank respectively, are sufficiently large compared to the 1st stage permeate flowrate, the feed tank and 1st stage recirculation interchange is fast and the two compartments can be considered one well-mixed compartment. The (xi) 1st stage permeate is under pressure and provides the feed to the 2nd stage. The (xii) 2nd stage proportional relief valve is adjusted to give a recycle ratio of 0.5 as described in Section 3.2. The remaining equipment in the 2nd recirculation stage is similar and in similar stream order to the 1st stage and therefore not labelled.

Figure 160b shows the recirculating loops: the 1st stage (green), the 1st stage permeate to the 2nd stage (yellow) and the 2nd stage (teal) are highlighted. The 1st and 2nd stage flows are recirculating while the 1st to 2nd stage permeate flow is unidirectional.

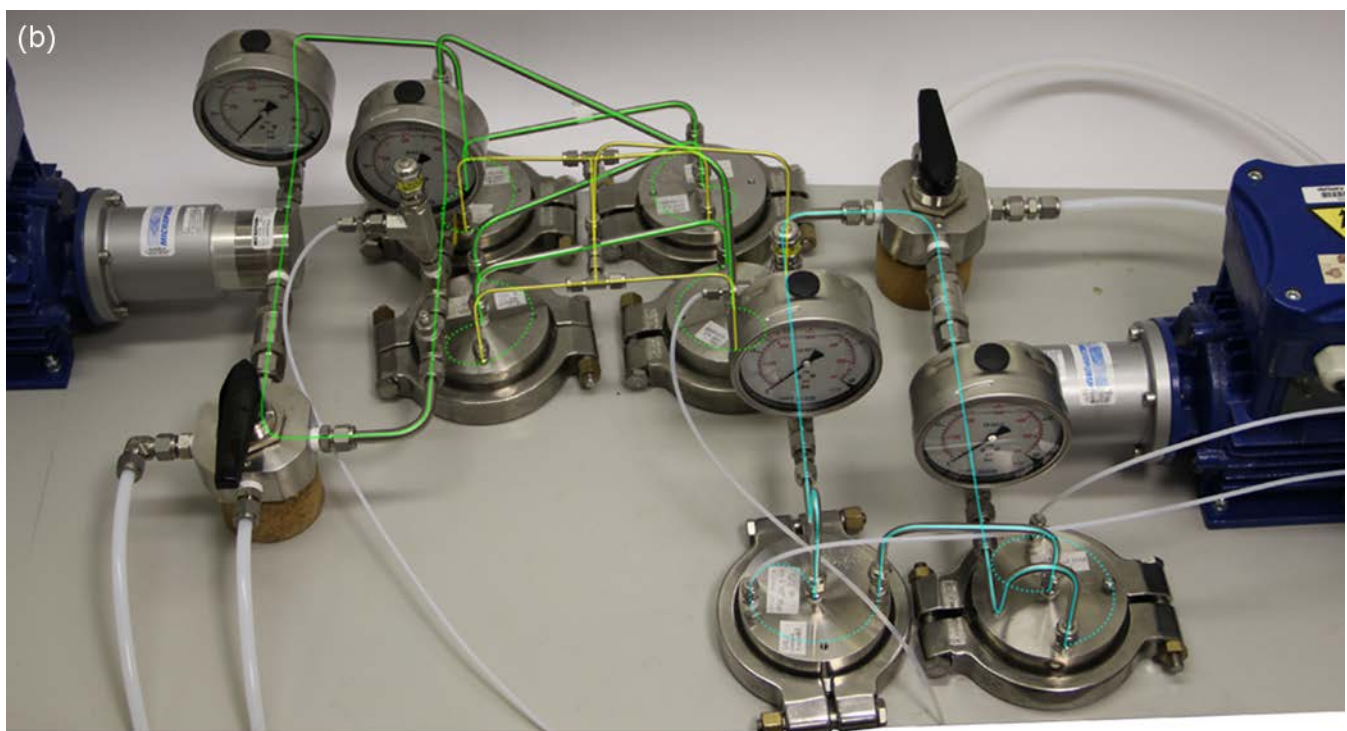
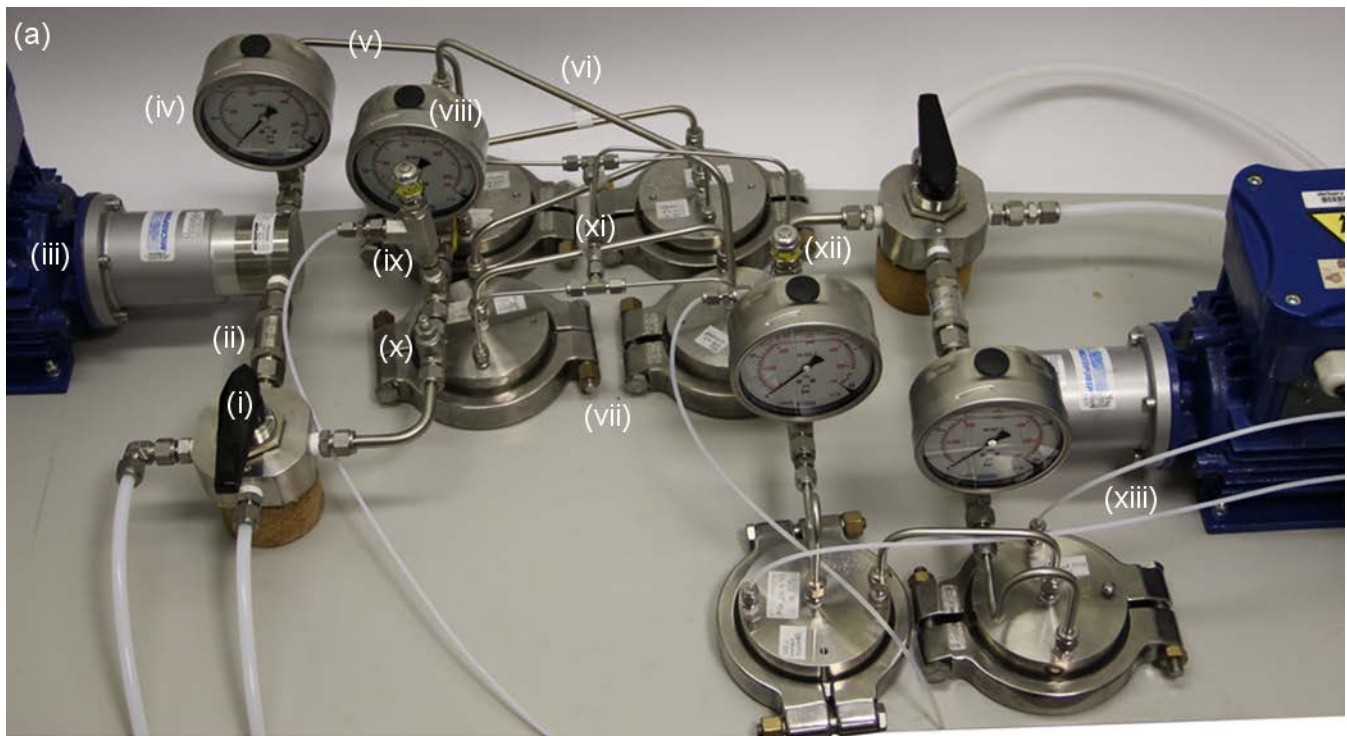


Figure 160. Overview of the 1st and 2nd membrane stage of the diafiltration apparatus with (a) equipment and (b) recirculation loops highlighted. For clarity, only the two main recirculation loops, i.e. the stages that are pressurized (30-60 bar) during operation, are shown. Also visible in opaque white are the PTFE connections exiting the stages at atmospheric pressure. The overview of the fully assembled apparatus with all equipment is shown in Figure 161 below.

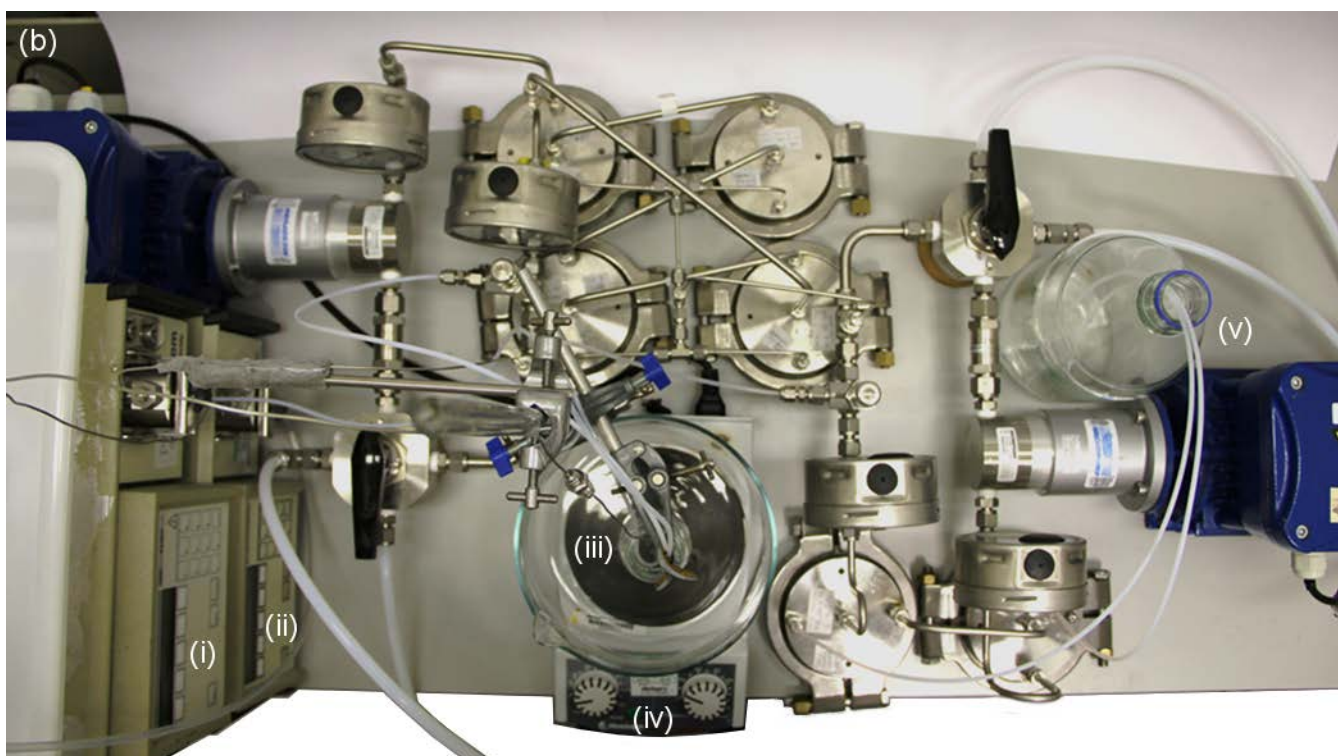
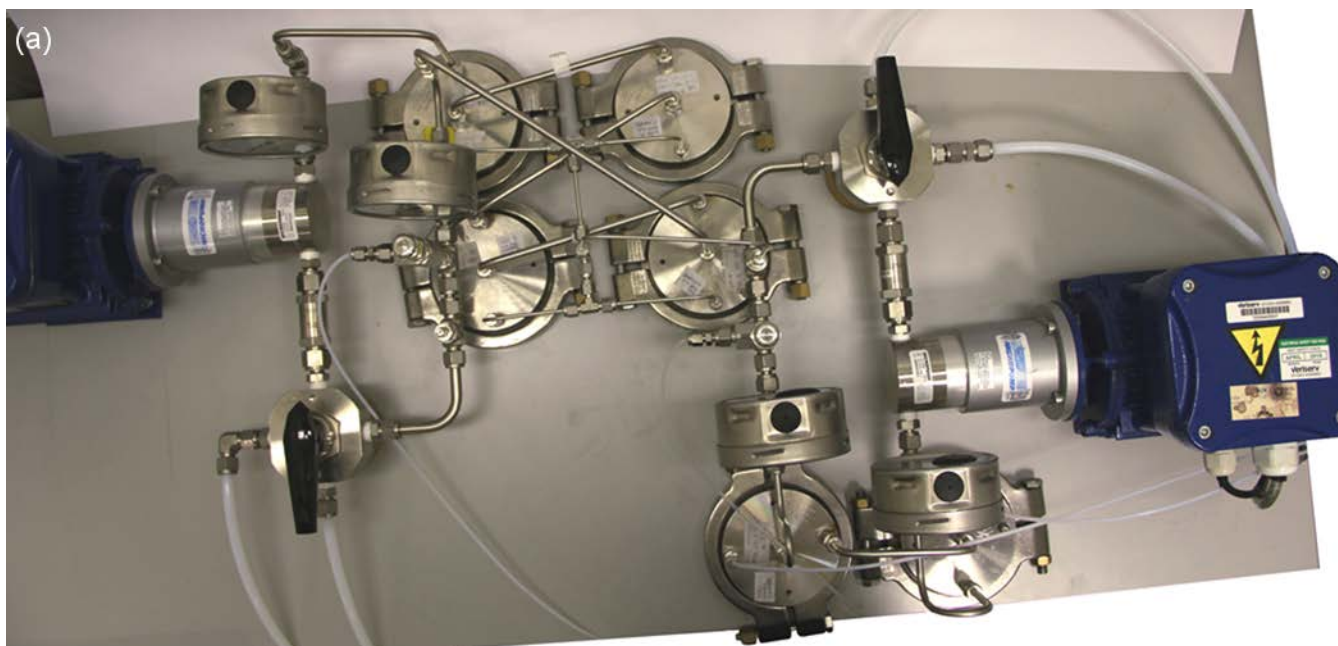


Figure 161. Top-down overview of the (a) 1st and 2nd membrane stage and the (b) fully assembled nanofiltration apparatus. The recirculation loop equipment is described in Figure 160 and any further equipment is described here. (i) Feed pressurization HPLC pump feeding and pressurizing solvent from the feed tank into the 1st stage recirculation loop, (ii) solvent replenishment HPLC pump feeding fresh solvent from the solvent reservoir into the feed tank, (iii) the feed tank inside a clean glass containment to protect against overflow, (iv) magnetic stirring plate to provide feed tank mixing and (v) permeate tank receiving the 2nd stage permeate flow.

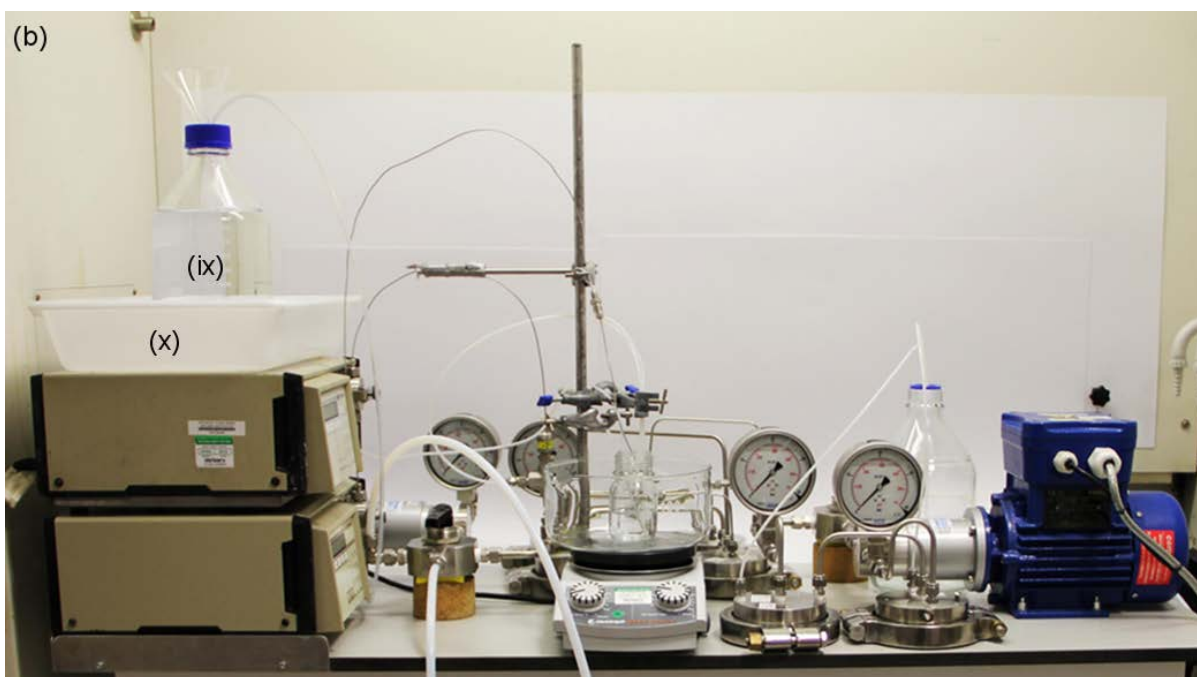
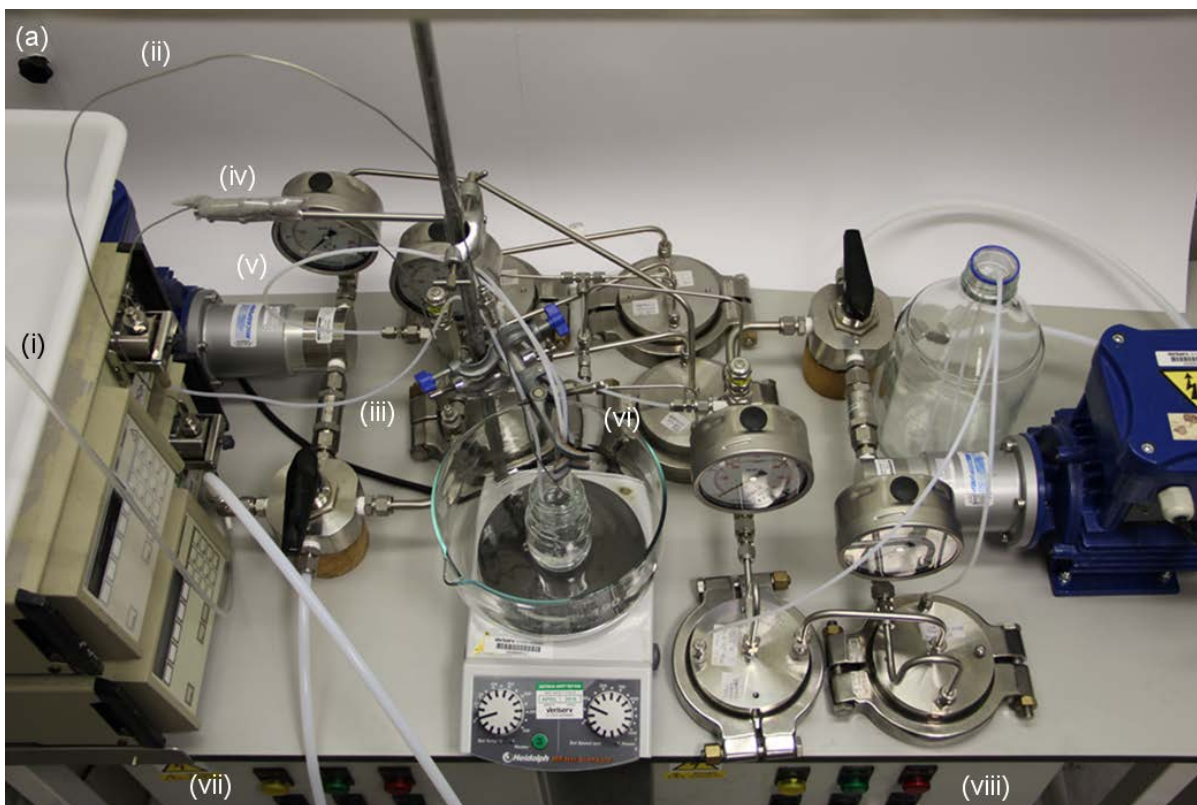


Figure 162. Frontal overview of the fully assembled nanofiltration apparatus with (a) highlighting of all the flows from and to the feed tank. Flows (i) from the fresh solvent tank through the solvent replenishment HPLC pump (ii) to the feed tank, (iii) from the feed tank through the feed pressurization HPLC pump (iv) into the 1st stage recirculation loop. (The grey wrapping around the tube is used to dampen vibration from the HPLC piston motion.) (v) The excess feed return flow from the 1st stage recirculation loop, and the (vi) 2nd stage return flow, both recycle back into the feed tank. (vii) and (viii) are the pump inverter controllers for the 1st and 2nd stage respectively. In (b), the (ix) fresh solvent feed tank is positioned within a (x) solvent tray to protect the HPLC pumps.

Appendix H – X-ray crystallography

X-ray crystallography was performed by Dr. Andrew J P White (Department of Chemistry, Imperial College London) and the following analysis was performed and set down by him.

X-ray crystal structure of Hub²-CH₂OH (**42c**)

Crystal data for **42c**: C₂₇H₂₄O₃, *M* = 396.46, monoclinic, *P*2₁/*c* (no. 14), *a* = 13.3311(10), *b* = 21.882(2), *c* = 7.1954(5) Å, β = 97.694(7)°, *V* = 2080.0(3) Å³, *Z* = 4, *D*_c = 1.266 g cm⁻³, μ(Mo-Kα) = 0.081 mm⁻¹, *T* = 173 K, colourless needles, Agilent Xcalibur 3 E diffractometer; 5585 independent measured reflections (*R*_{int} = 0.064), *F*² refinement,^[X1,X2] *R*₁(obs) = 0.0742, *wR*₂(all) = 0.1969, 3050 independent observed absorption-corrected reflections [|*F*_o| > 4σ(|*F*_o|)], 2θ_{max} = 57°, 278 parameters. CCDC 1550924.

The crystal of **42c** that was studied was found to be a two component twin in a ca. 51:49 ratio, with the two lattices related by the approximate twin law [−1.01 0.00 0.00 0.01 −1.00 −0.01 0.48 0.00 1.00]. The three O–H hydrogen atoms could not be reliably located from Δ*F* maps and so were added in idealised positions with an O–H separation of 0.90 Å and allowed to rotate about the C–O vector to find the best fit with the observed electron density (the SHELXL HFIX/AFIX 147 command).

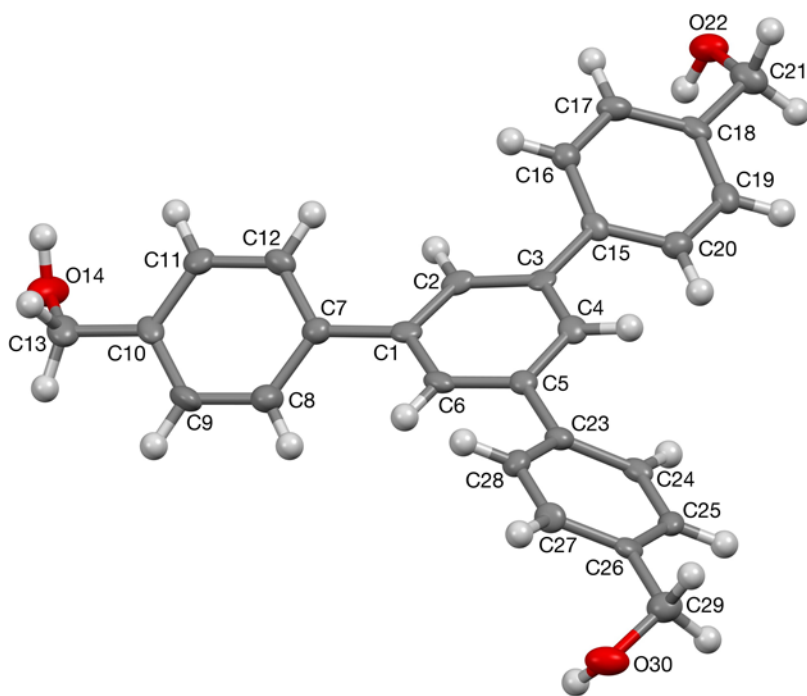


Figure X1. The crystal structure of **42c** (50% probability ellipsoids).

X-ray crystal structure of Hub³-CH₂OH (**43c**)

Crystal data for 43c: C₄₅H₃₆O₃·EtOAc·1.5EtOH, *M* = 781.94, triclinic, *P*-1 (no. 2), *a* = 9.7306(4), *b* = 18.7567(10), *c* = 24.2549(11) Å, α = 82.240(4), β = 85.575(4), γ = 86.911(4)°, *V* = 4369.0(4) Å³, *Z* = 4 [2 independent molecules], *D*_c = 1.189 g cm⁻³, μ (Cu-K α) = 0.612 mm⁻¹, *T* = 173 K, colourless tabular needles, Agilent Xcalibur PX Ultra A diffractometer; 16622 independent measured reflections (*R*_{int} = 0.0406), *F*² refinement,^[X1,X2] *R*₁(obs) = 0.0884, *wR*₂(all) = 0.2822, 10965 independent observed absorption-corrected reflections [$|F_o| > 4\sigma(|F_o|)$], $2\theta_{\max}$ = 148°, 871 parameters. CCDC 1550925.

The six unique O–H hydrogen atoms in the structure of **43c** could not be reliably located from ΔF maps and so were added in idealised positions with an O–H separation of 0.90 Å and allowed to rotate about the C–O vector to find the best fit with the observed electron density (the SHELXL HFIX/AFIX 147 command).

The included solvent was found to be highly disordered, and the best approach to handling this diffuse electron density was found to be the SQUEEZE routine of PLATON.^[X3] This suggested a total of 335 electrons per unit cell, equivalent to *ca.* 83.8 electrons per asymmetric unit. Before the use of SQUEEZE the solvent resembled a mixture of ethyl acetate (C₄H₈O₂, 48 electrons) and ethanol (C₂H₆O, 26 electrons). A mixture of one ethyl acetate molecule with 1.5 ethanol molecules corresponds to 87 electrons, so this was used as the solvent present. As a result, the atom list for the asymmetric unit is low by 2 × [C₄H₈O₂ + 1.5(C₂H₆O)] = C₁₄H₃₄O₇ (and that for the unit cell low by C₂₈H₆₈O₁₄) compared to what is actually presumed to be present.

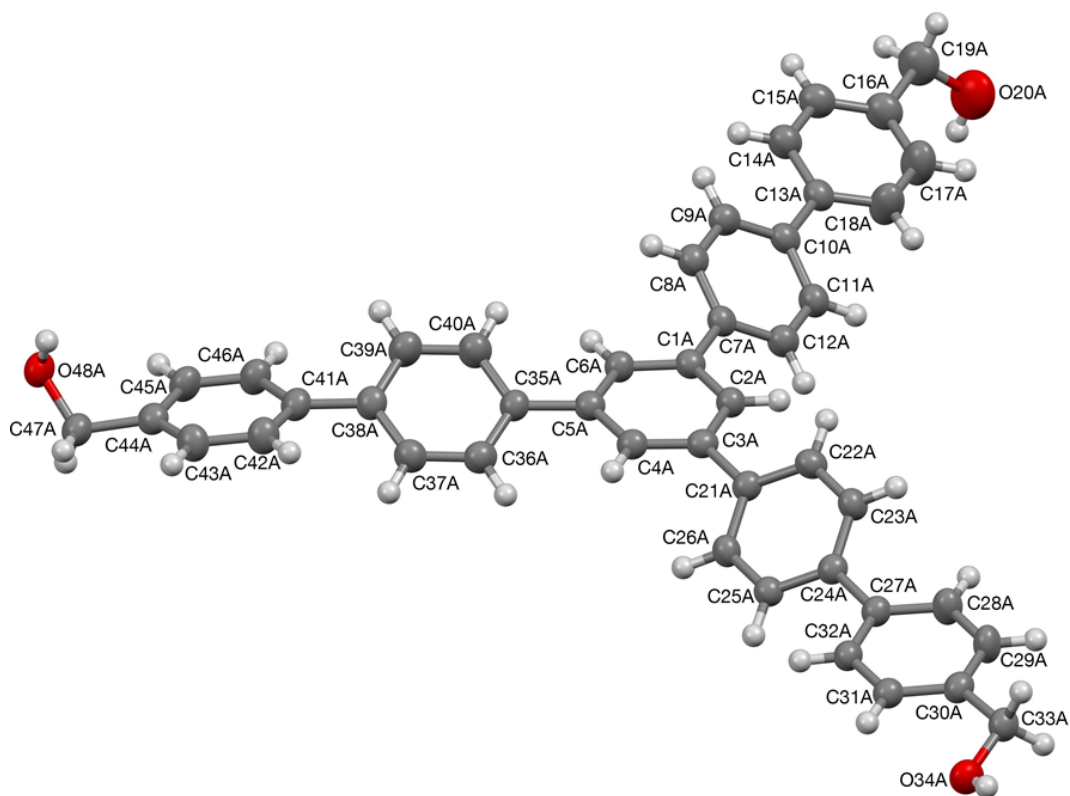


Figure X2. The structure of one (**43c-A**) of the two independent molecules present in the crystal of **43c** (50% probability ellipsoids).

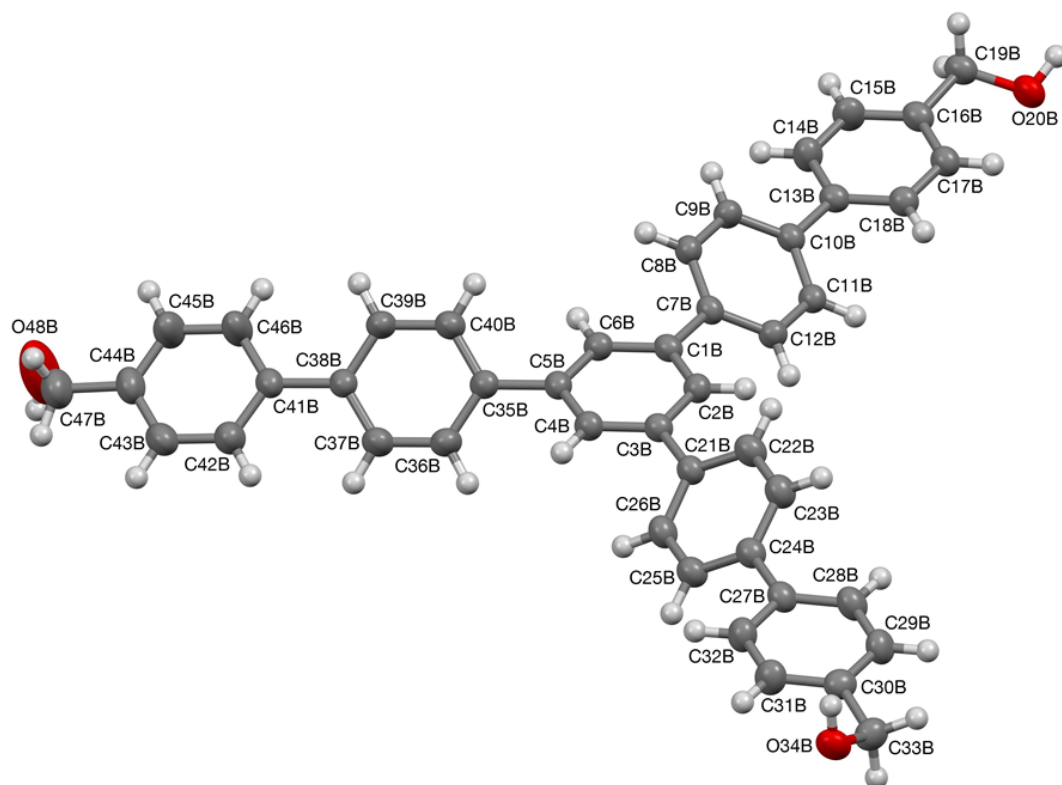


Figure X3. The structure of one (**43c-B**) of the two independent molecules present in the crystal of **43c** (50% probability ellipsoids).

X-ray crystal structure of Hub³-CH₂Br (**43d**)

Crystal data for 43d: C₄₅H₃₃Br₃·1.25(C₇H₈), *M* = 928.61, monoclinic, *P*2₁/*c* (no. 14), *a* = 14.8204(6), *b* = 29.866(2), *c* = 9.8134(5) Å, β = 90.027(4)°, *V* = 4343.6(4) Å³, *Z* = 4, *D*_c = 1.420 g cm⁻³, μ(Cu-Kα) = 3.708 mm⁻¹, *T* = 173 K, colourless platy needles, Agilent Xcalibur PX Ultra A diffractometer; 8310 independent measured reflections (*R*_{int} = 0.0535), *F*² refinement,^[X1,X2] *R*₁(obs) = 0.1078, *wR*₂(all) = 0.3453, 4917 independent observed absorption-corrected reflections [*|F*_o| > 4σ(*|F*_o)], 2θ_{max} = 147°, 433 parameters. CCDC 1550926.

The included solvent in the structure of **43d** was found to be highly disordered, and the best approach to handling this diffuse electron density was found to be the SQUEEZE routine of PLATON.^[X3] This suggested a total of 263 electrons per unit cell, equivalent to *ca.* 65.8 electrons per asymmetric unit. Before the use of SQUEEZE the solvent most resembled toluene (C₇H₈, 50 electrons), and 1.25 toluene molecules corresponds to 62.5 electrons, so this was used as the solvent present. As a result, the atom list for the asymmetric unit is low by 1.25(C₇H₈) = C_{8.75}H₁₀ (and that for the unit cell low by C₃₅H₄₀) compared to what is actually presumed to be present.

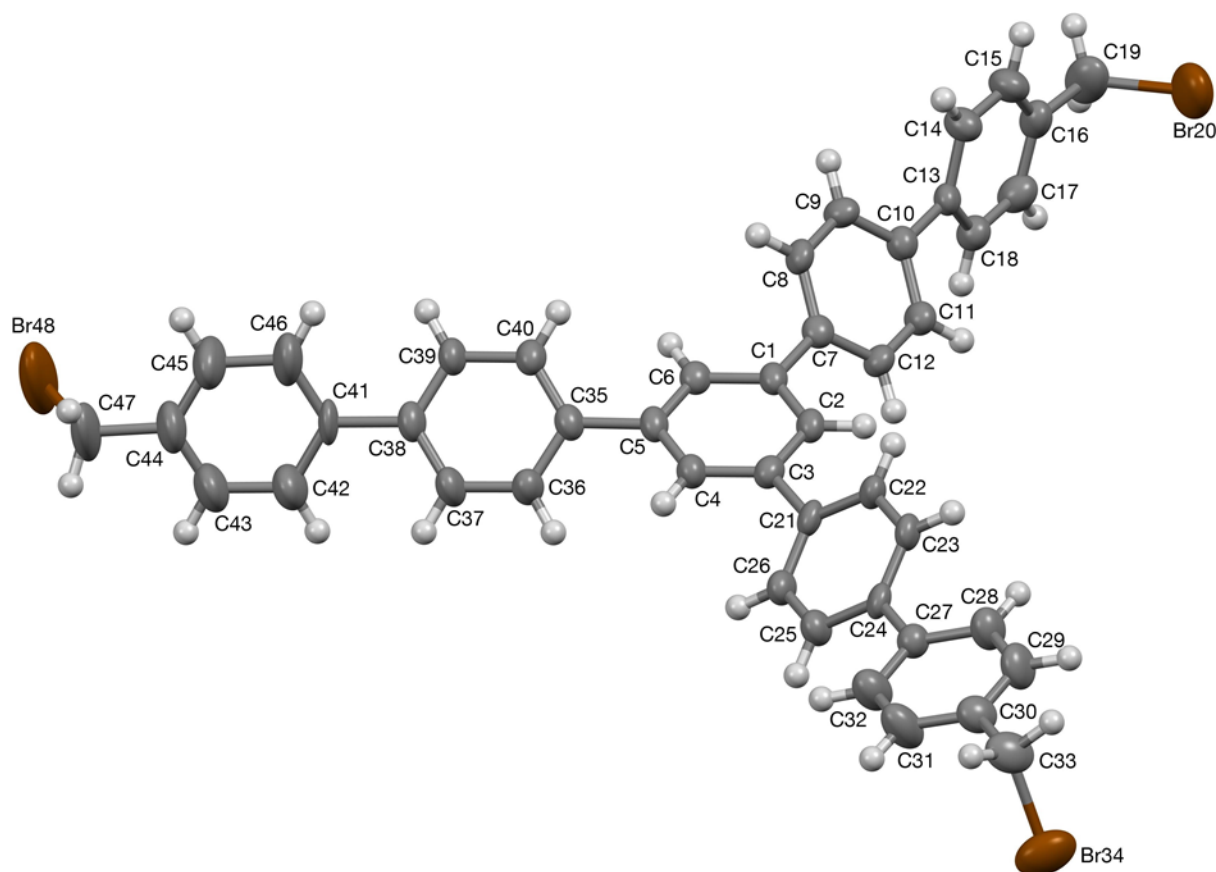


Figure X4. The crystal structure of **43d** (50% probability ellipsoids).

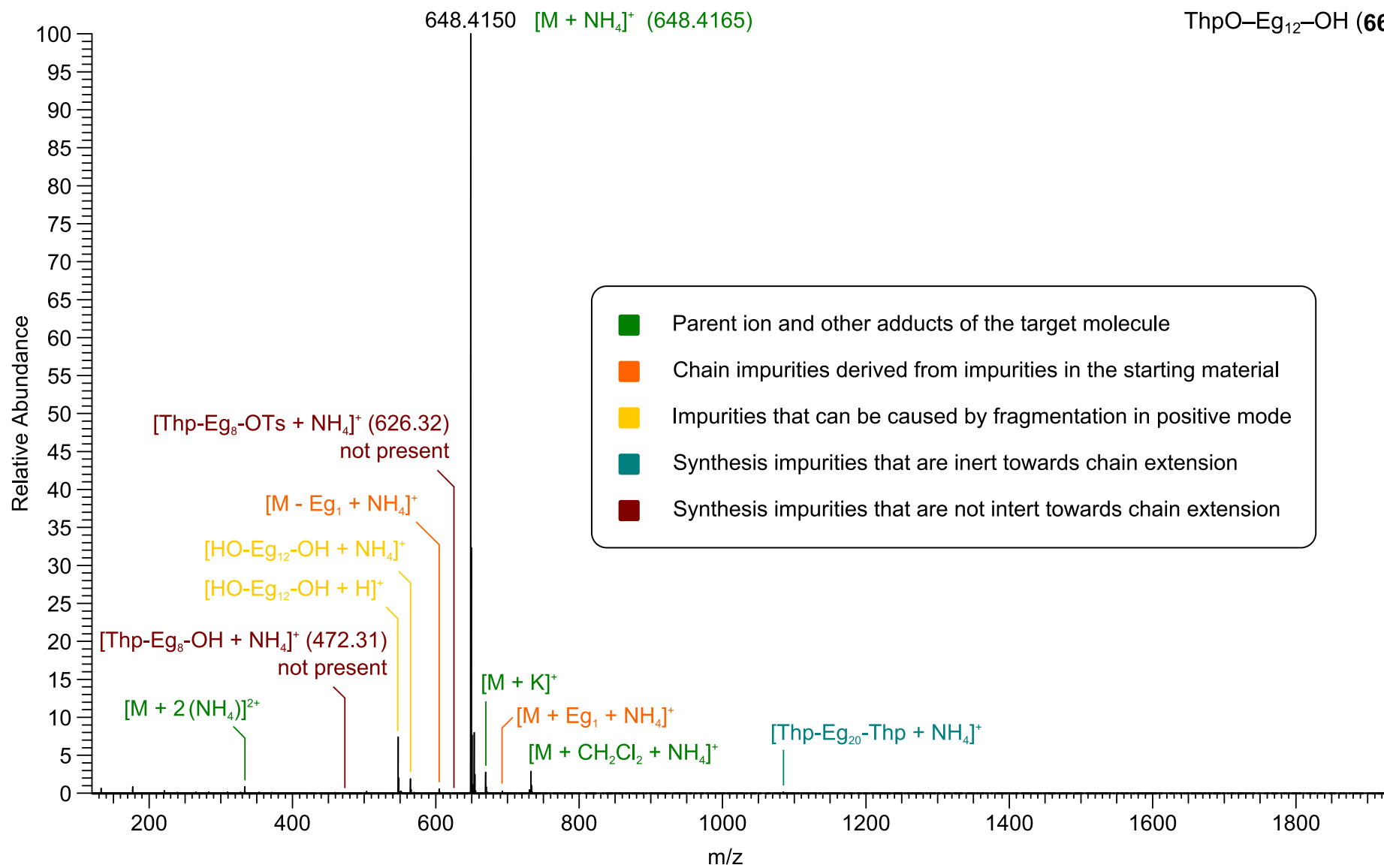
Appendix I – Mass spectra for the synthesis of Eg₆₀

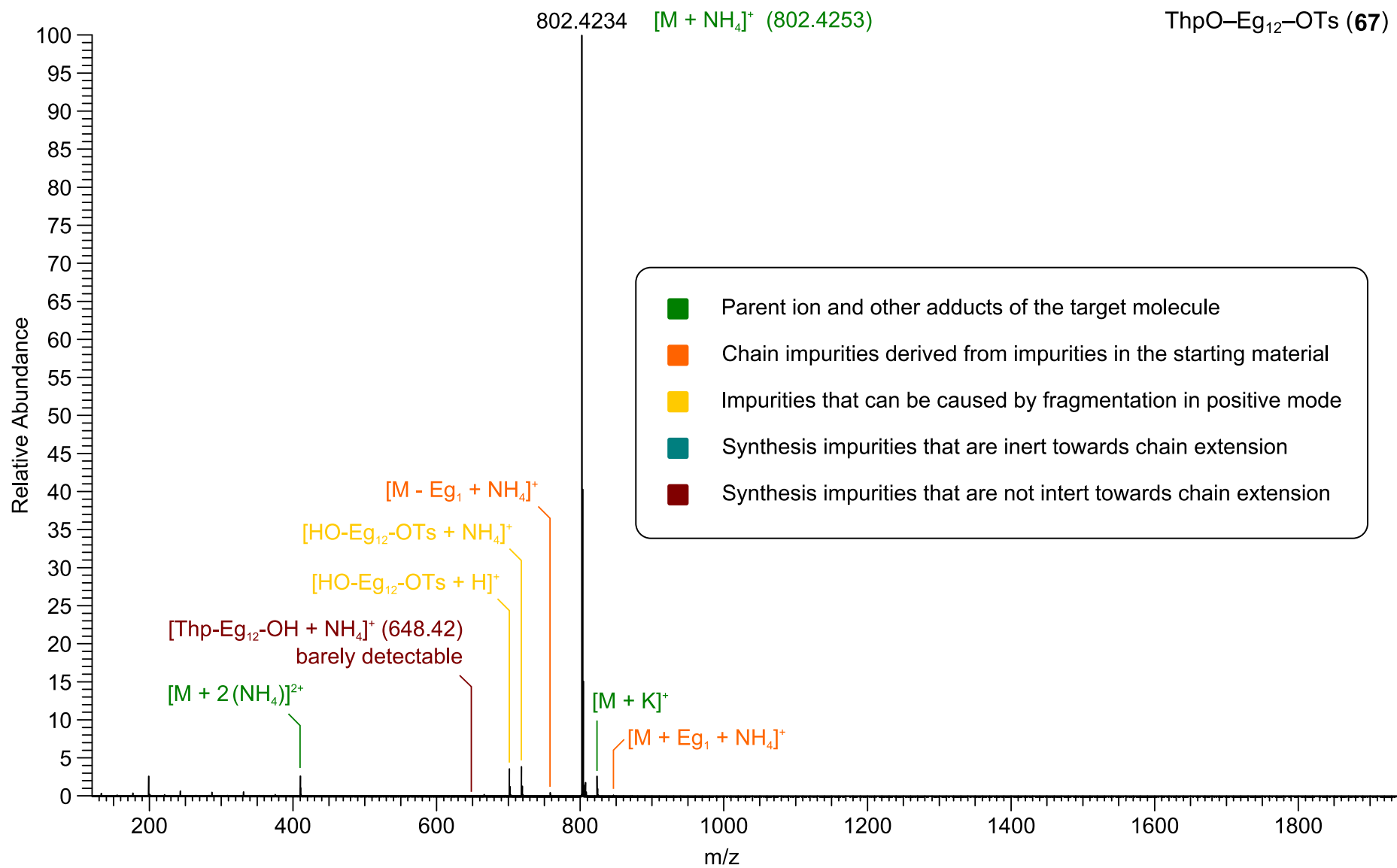
High resolution mass spectrometry was performed at the EPSRC UK National Mass Spectrometry Facility (NMSF) at Swansea University. The following text was set down by Dr. Mark F. Wyatt.

MALDI: MALDI-TOF mass spectra were acquired using an UltrafleXtreme mass spectrometer (Bruker Daltonics, Germany), which is equipped with a Nd:YAG laser ($\lambda = 355$ nm). Data was acquired using FlexControl software v3.4, while post-acquisition processing of data was performed by FlexAnalysis software v3.4. The sample was dissolved in tetrahydrofuran (THF; Sigma-Aldrich, UK) at approximately 10 mg/mL. Dithranol (Dith; Sigma-Aldrich, UK) was prepared at 20 mg/mL in THF, and aliquots of the two solutions were mixed in a 1:49 (μ L) sample-to-matrix ratio. 0.5 μ L of sodium acetate (NaOAc; Sigma-Aldrich, UK) was added to the mixture, vortex-mixed, and 0.5 μ L was deposited on to the MALDI target plate and allowed to air dry. The plate was inserted into the instrument and data acquired in both positive-linear and -reflectron modes.

nESI: nESI mass spectra were acquired via direct infusion using an LTQ Orbitrap XL mass spectrometer (Thermo Fisher Scientific, USA) in positive mode. Data was processed using vendor Xcalibur software. The sample was dissolved in dichloromethane (DCM; HPLC grade, Fisher Scientific, UK) at 1 mg/mL, then diluted approximately 1000-fold in ammonium acetate (NH₄OAc; Sigma-Aldrich, UK) solution in methanol (MeOH; HPLC grade, Fisher Scientific, UK). An aliquot was loaded into the NanoMate microtiter plate well and infused into the Orbitrap instrument for acquisition. The Orbitrap source temperature was 200 °C, capillary voltage was +1.4kV, and tube lens voltage was +150V in positive mode.

A summary of the sample information and experimental conditions are in the spectra header information.



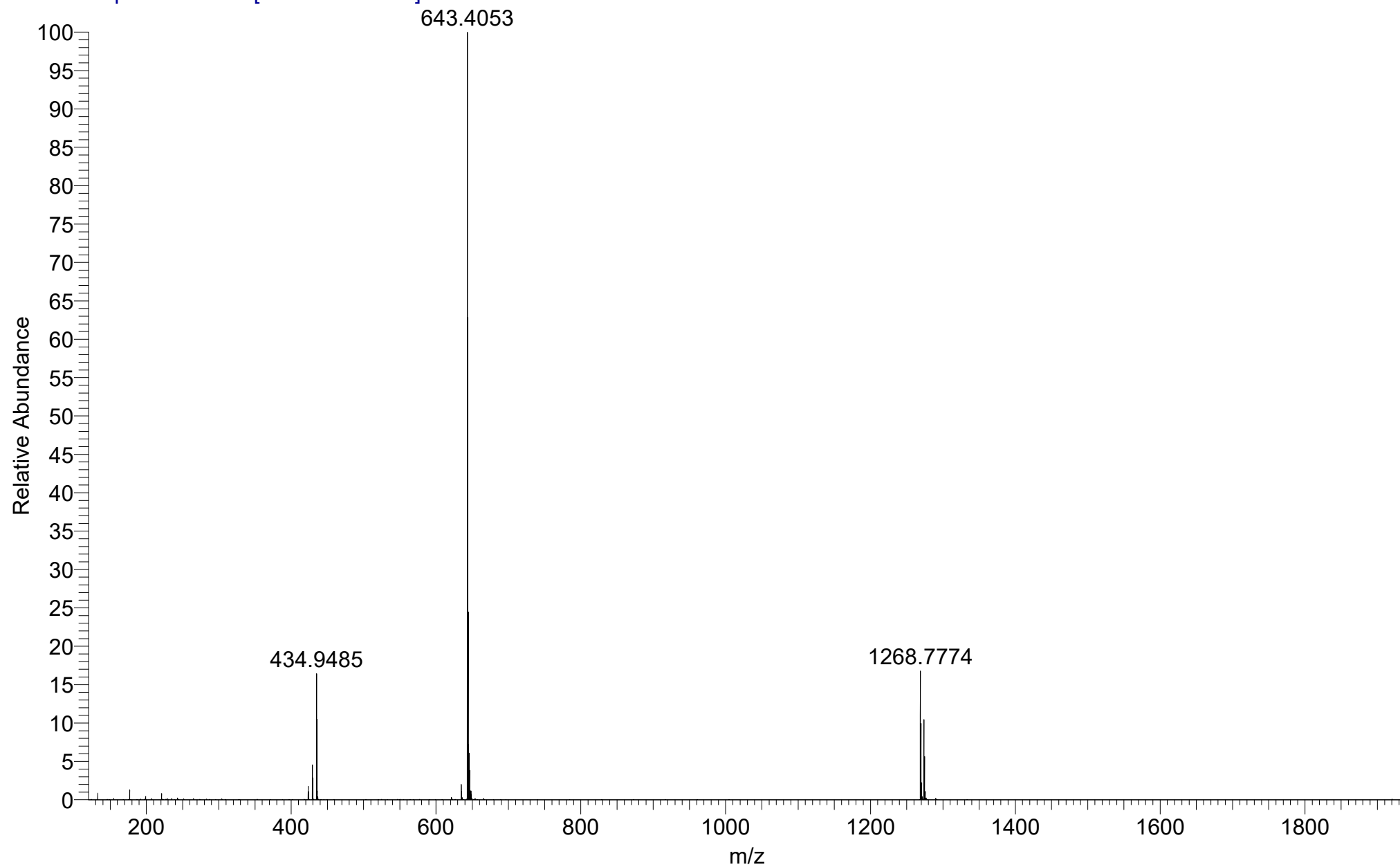


Polypure HO-Eg₂₈-OH
(DCM)/MeOH + NH₄OAc
C₅₆H₁₁₄O₂₉

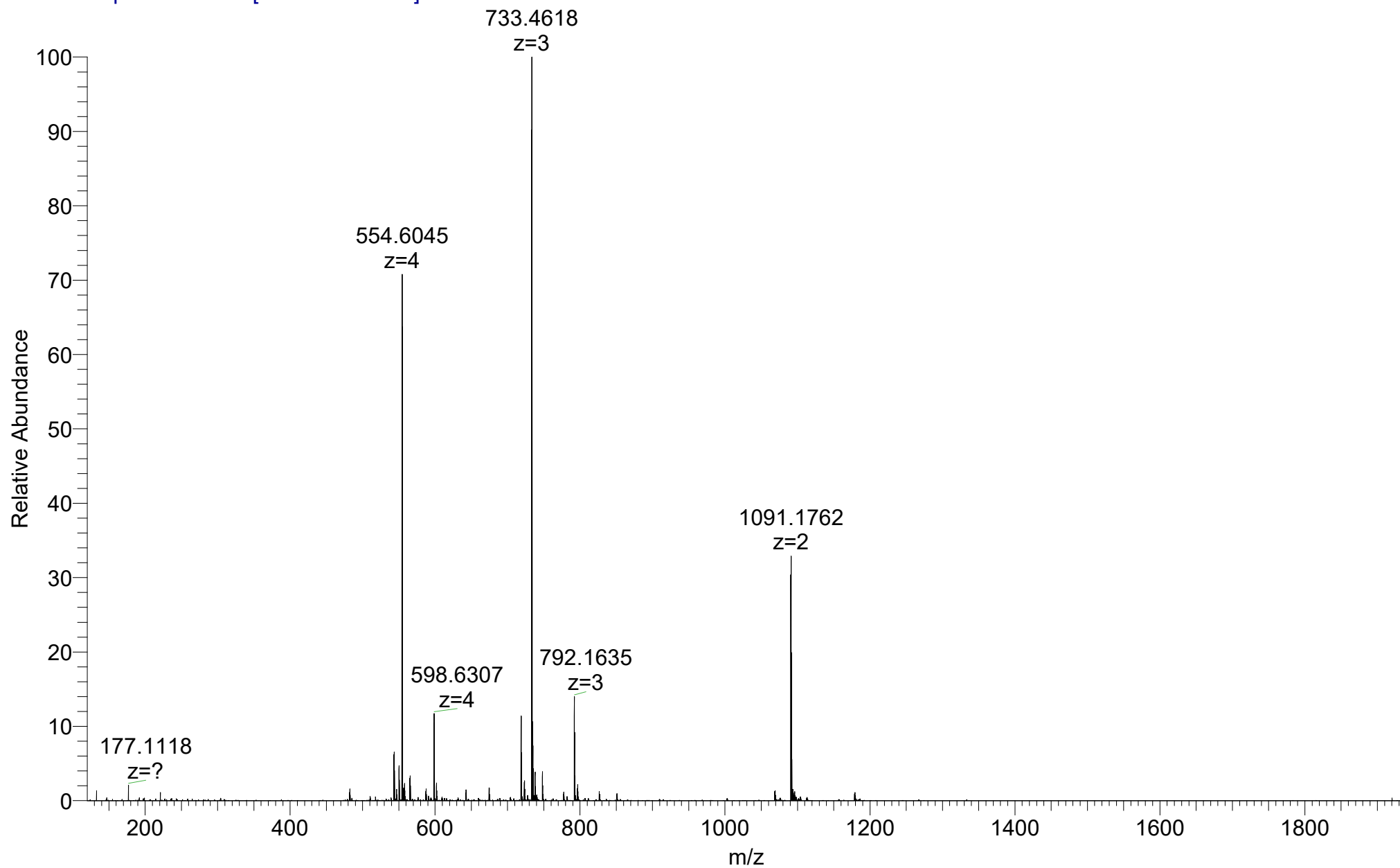
EPSRC National Facility Swansea
LTQ Orbitrap XL

RT: 0.74-1.04 AV: 12 SM: 7G NL: 8.65E7

T: FTMS + p NSI Full ms [120.00-1935.00]



RT: 0.74-1.04 AV: 12 SM: 7G NL: 2.91E7
T: FTMS + p NSI Full ms [120.00-1935.00]

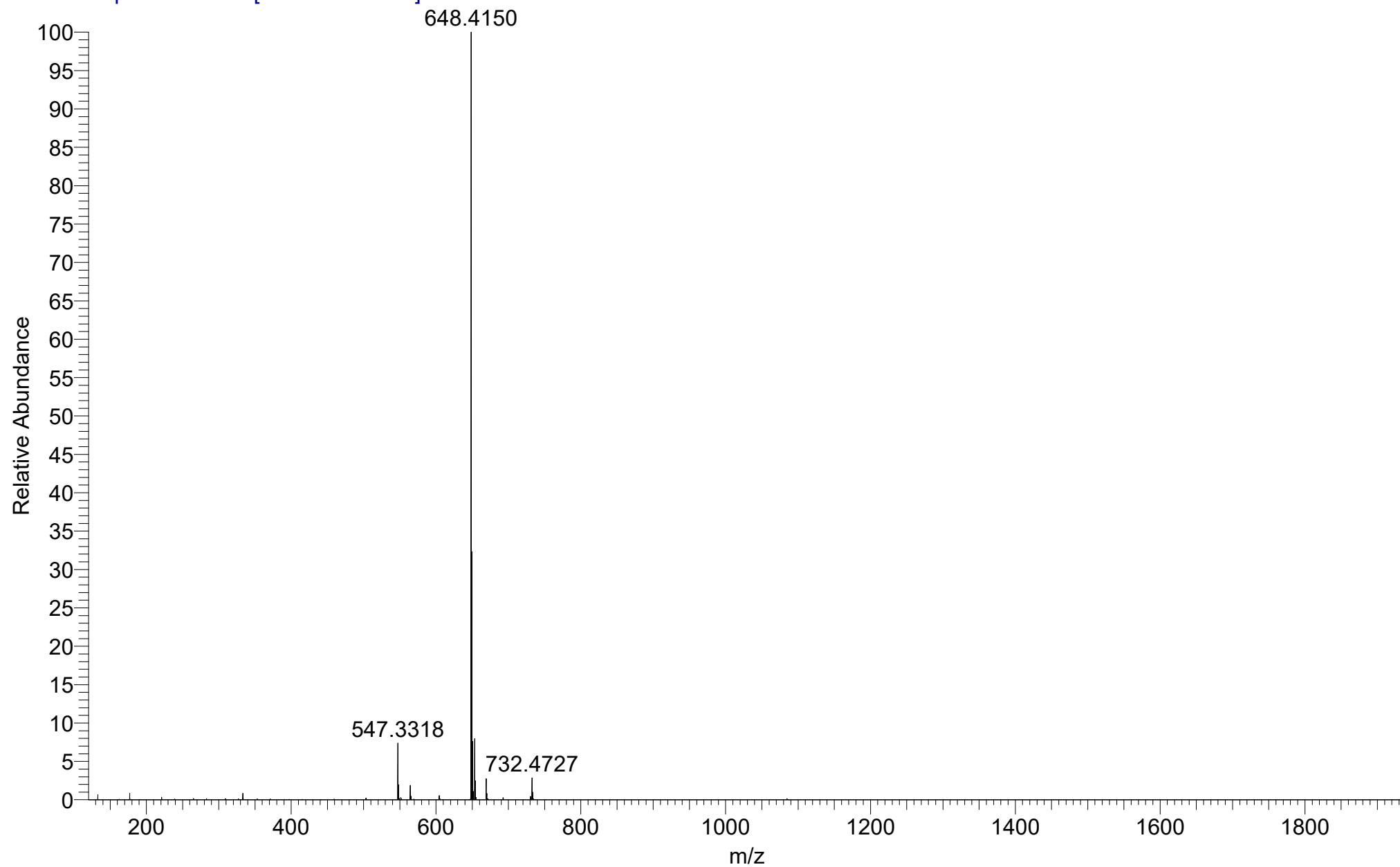


ThpO-Eg₁₂-OH (66)
(DCM)/MeOH + NH₄OAc
C₂₉H₅₈O₁₄

EPSRC National Facility Swansea
LTQ Orbitrap XL

RT: 0.74-1.04 AV: 12 SM: 7G NL: 3.02E8

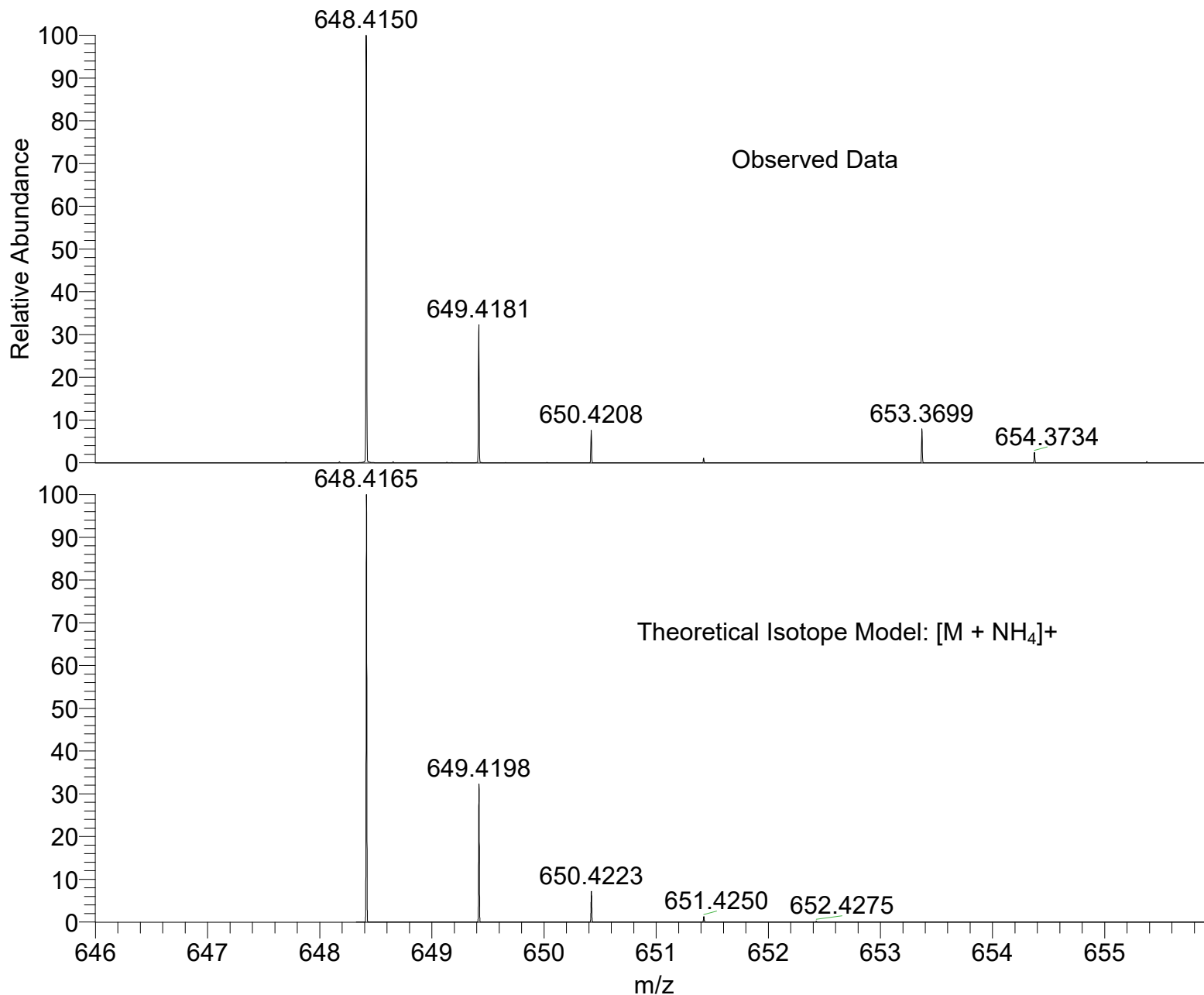
T: FTMS + p NSI Full ms [120.00-1935.00]



ThpO-Eg₁₂-OH (66)
(DCM)/MeOH + NH₄OAc
C₂₉H₅₈O₁₄

EPSRC National Facility Swansea
LTQ Orbitrap XL

SM: 7G



NL:
3.02E8
RT: 0.74-1.04 AV: 12
T: FTMS + p NSI Full ms
[120.00-1935.00]

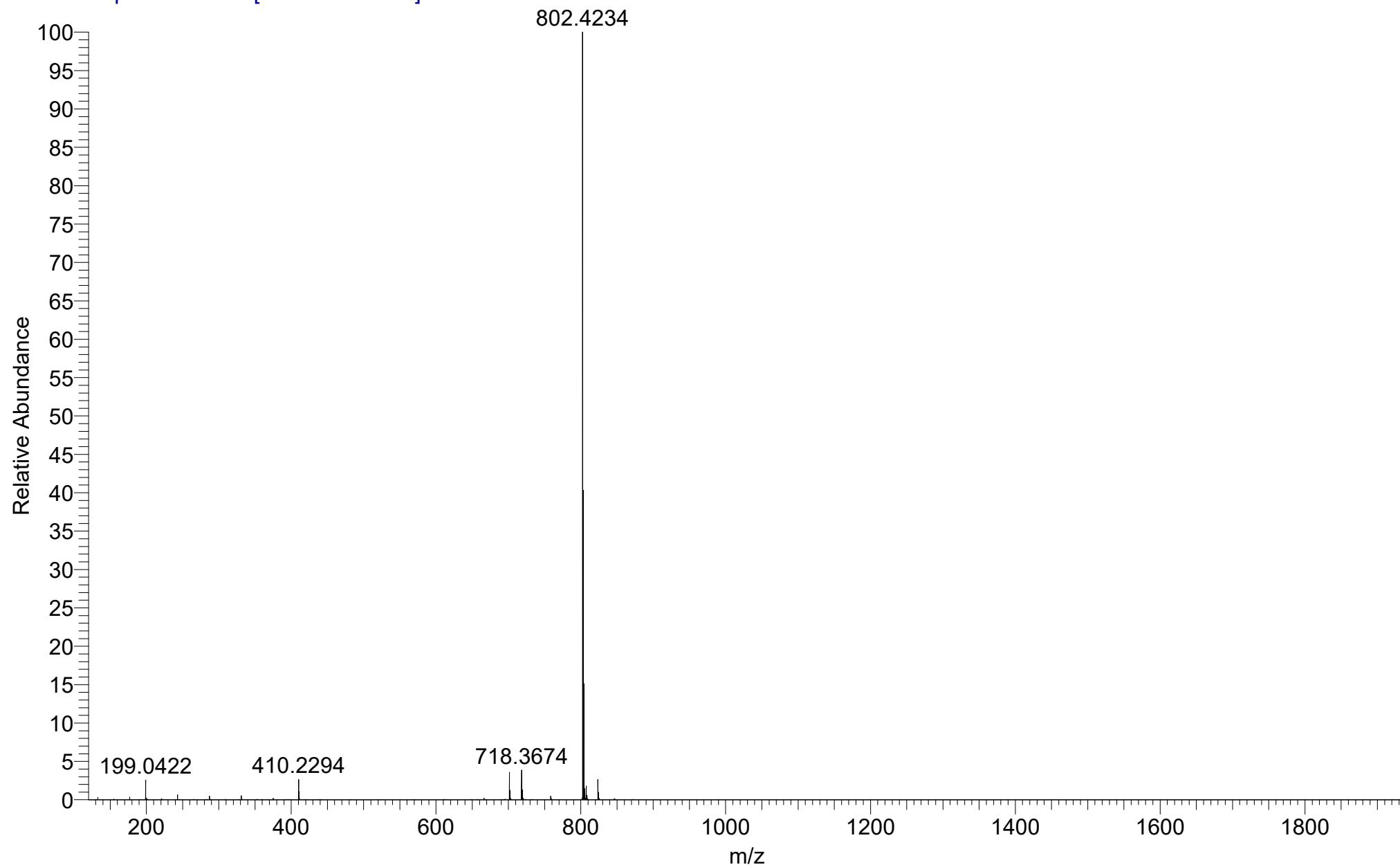
NL:
1.64E4
C₂₉ H₅₈ O₁₄ NH₄:
C₂₉ H₆₂ O₁₄ N₁
p (gss, s /p:40) Chrg 1
R: 100000 Res .Pwr . @FWHM

ThpO-Eg₁₂-OTs (**67**)
(DCM)/MeOH + NH₄OAc
C₃₆H₆₄O₁₆S

EPSRC National Facility Swansea
LTQ Orbitrap XL

RT: 0.74-1.04 AV: 12 SM: 7G NL: 3.00E8

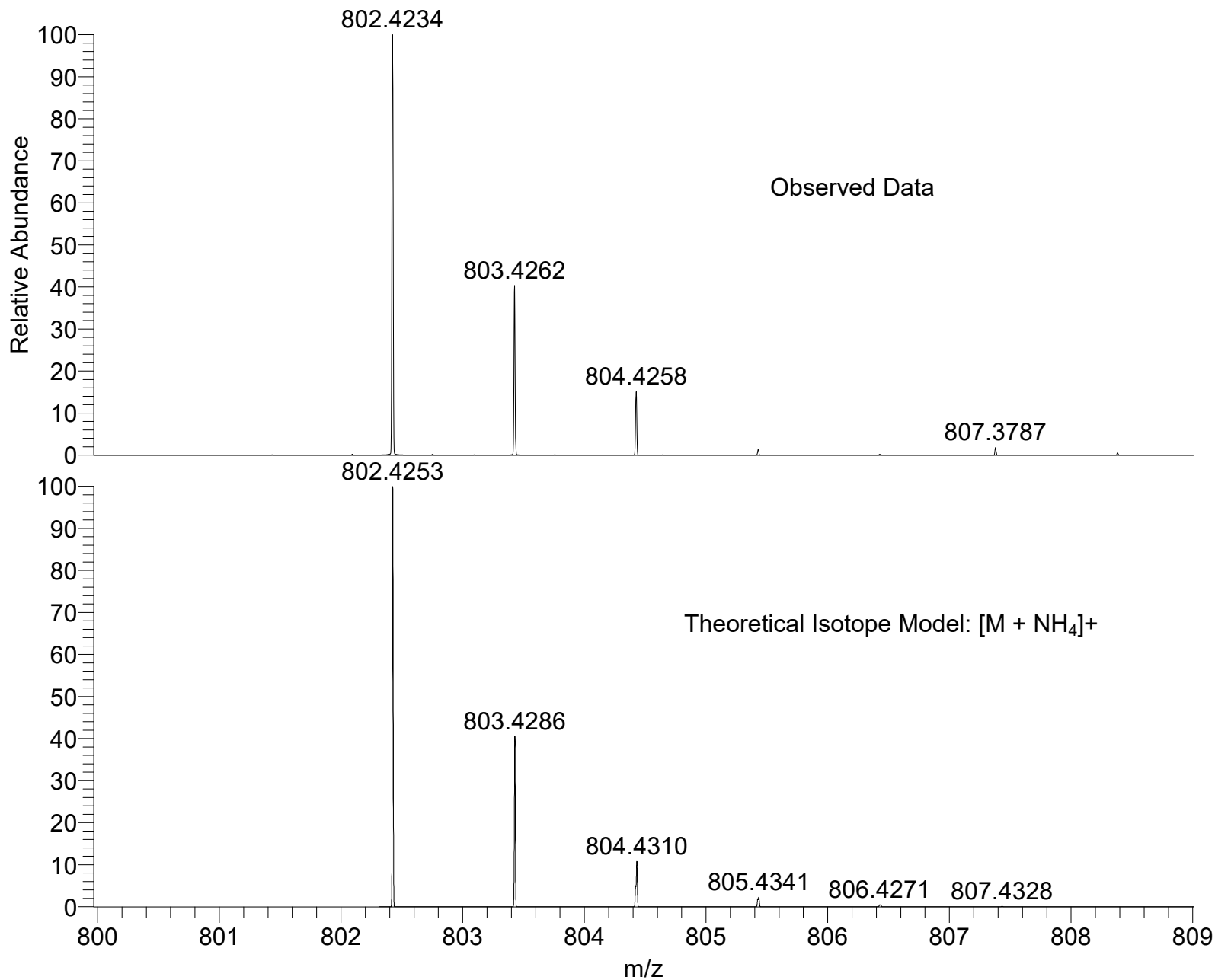
T: FTMS + p NSI Full ms [120.00-1935.00]



ThpO-Eg₁₂-OTs (67)
(DCM)/MeOH + NH₄OAc
C₃₆H₆₄O₁₆S

EPSRC National Facility Swansea
LTQ Orbitrap XL

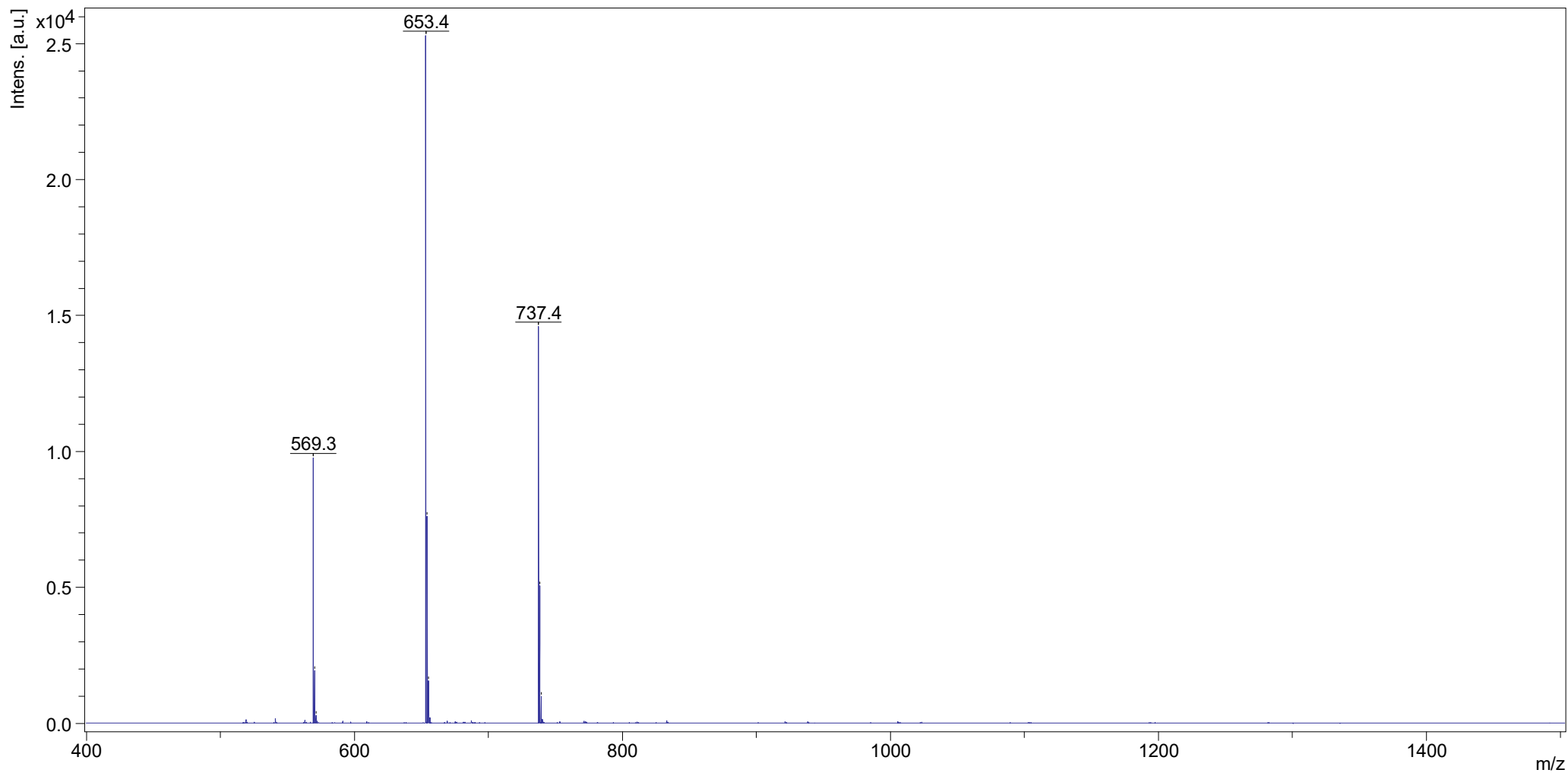
SM: 7G



NL:
3.00E8
RT: 0.74-1.04 AV: 12
T: FTMS + p NSI Full ms
[120.00-1935.00]

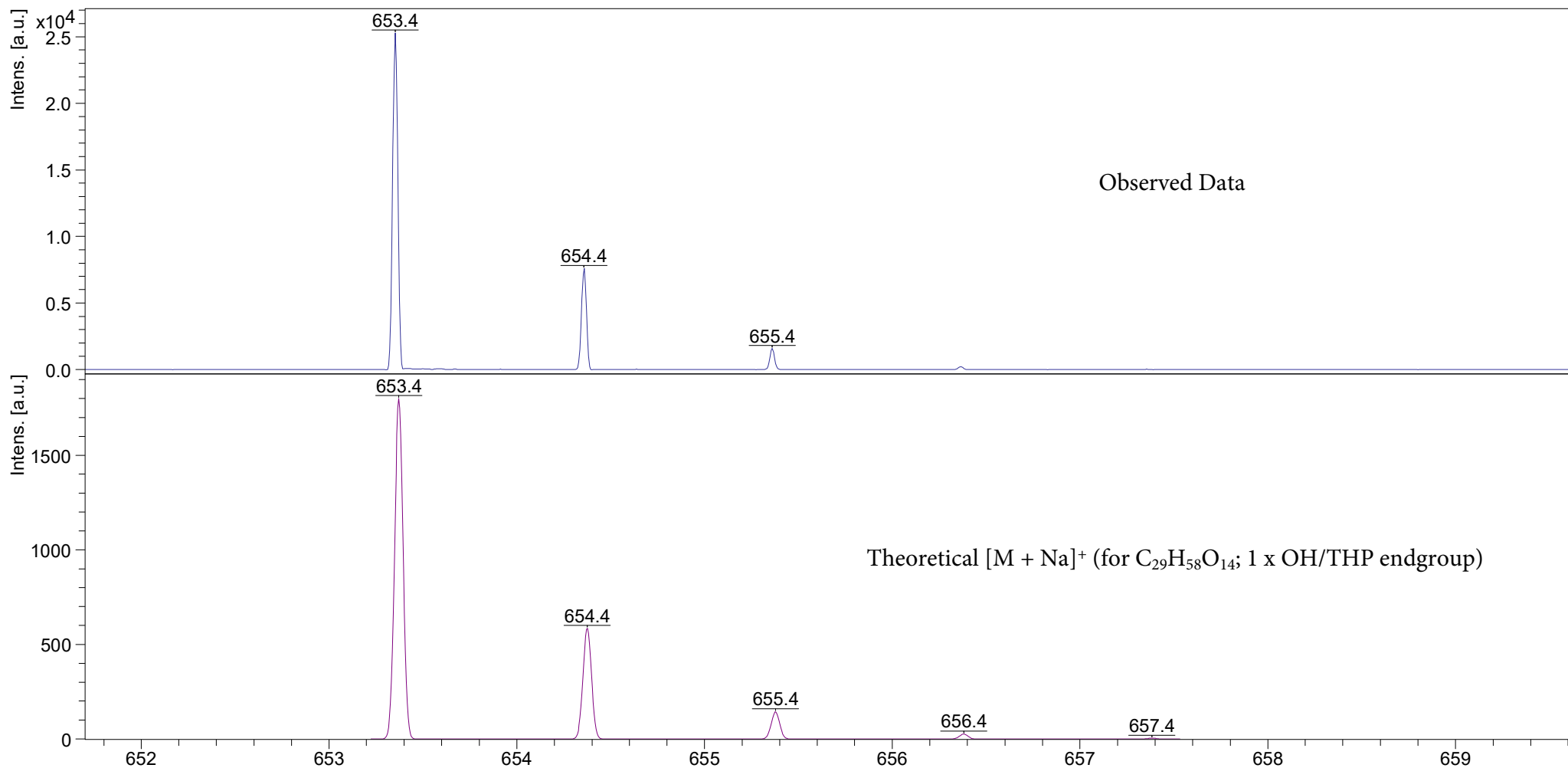
NL:
1.44E4
C₃₆ H₆₄ O₁₆ SNH₄:
C₃₆ H₆₈ O₁₆ S₁ N₁
p (gss, s /p:40) Chrg 1
R: 100000 Res .Pwr . @FWHM

ThpO-Eg₁₂-OH (66) PosRef DCM [1:49] (Dith;THF) +NaOAc



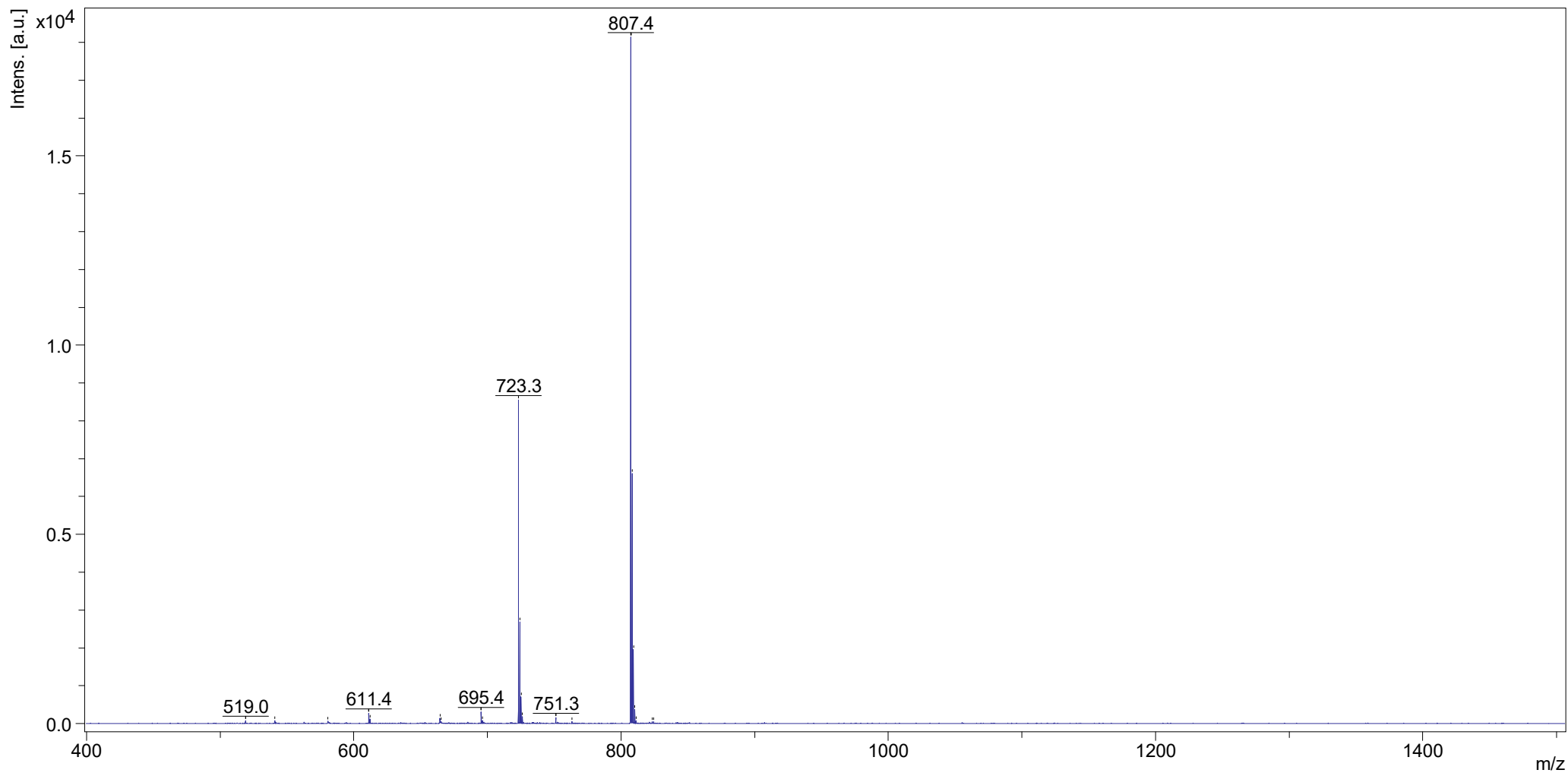
ultrafleXtreme MALDI

ThpO-Eg₁₂-OH (**66**) PosRef DCM [1:49] (Dith;THF) +NaOAc



ultrafleXtreme MALDI

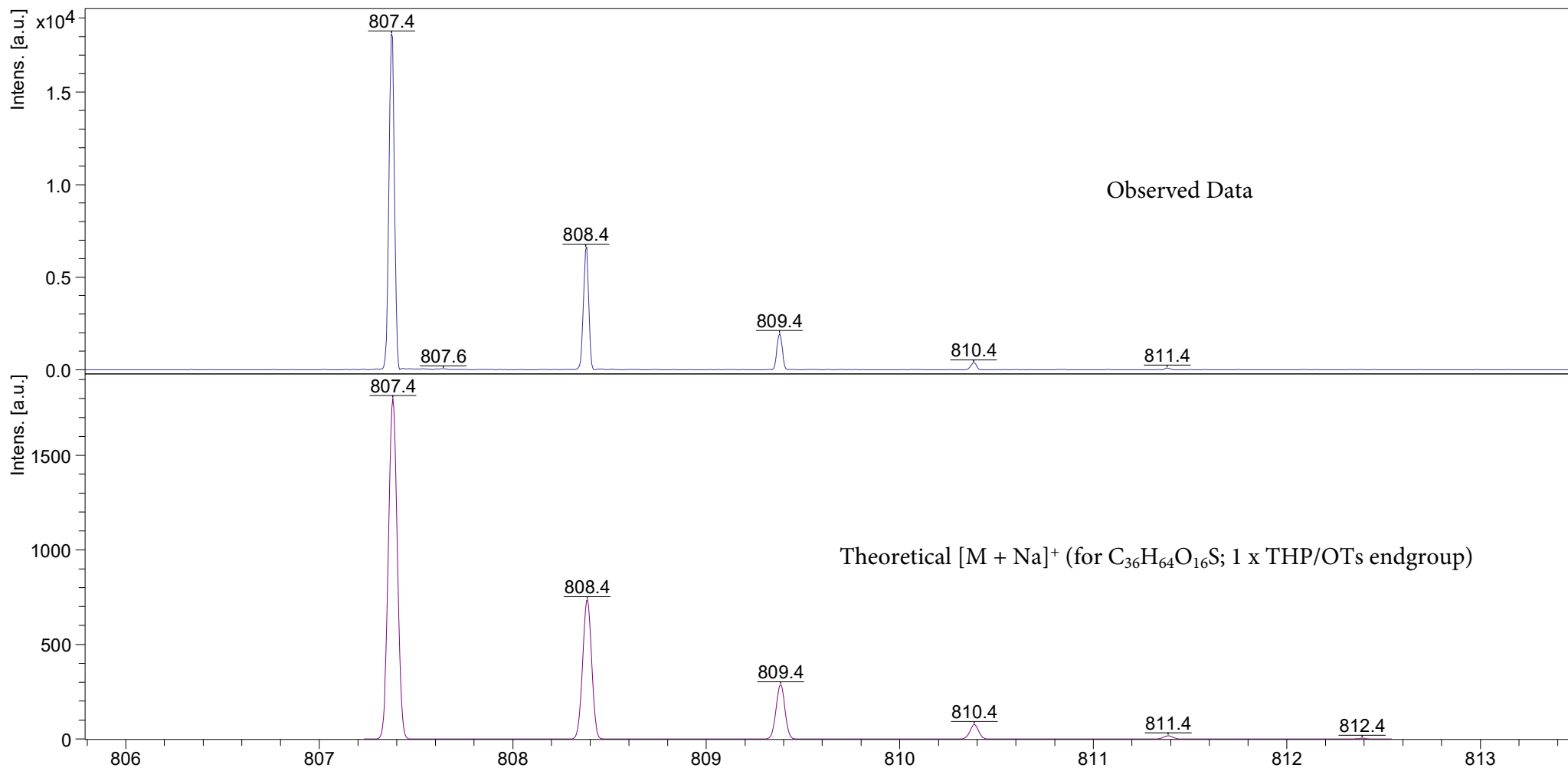
ThpO-Eg₁₂-OTs (**67**) PosRef DCM [1:49] (Dith;THF) +NaOAc



ultrafleXtreme MALDI

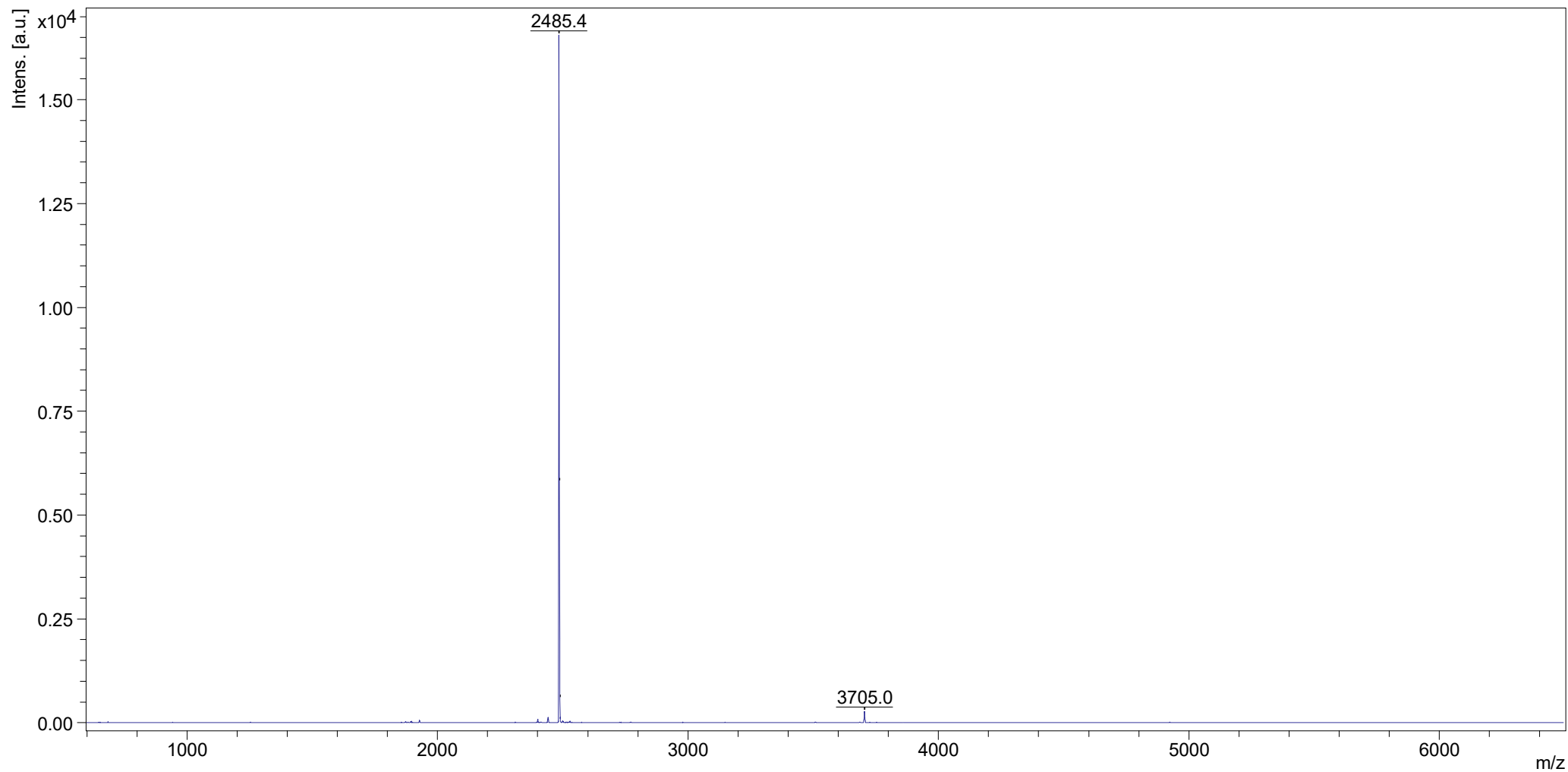
EPSRC UK National Mass Spectrometry Facility (NMSF), Swansea

ThpO-Eg₁₂-OTs (**67**) PosRef DCM [1:49] (Dith;THF) +NaOAc



ultrafleXtreme MALDI

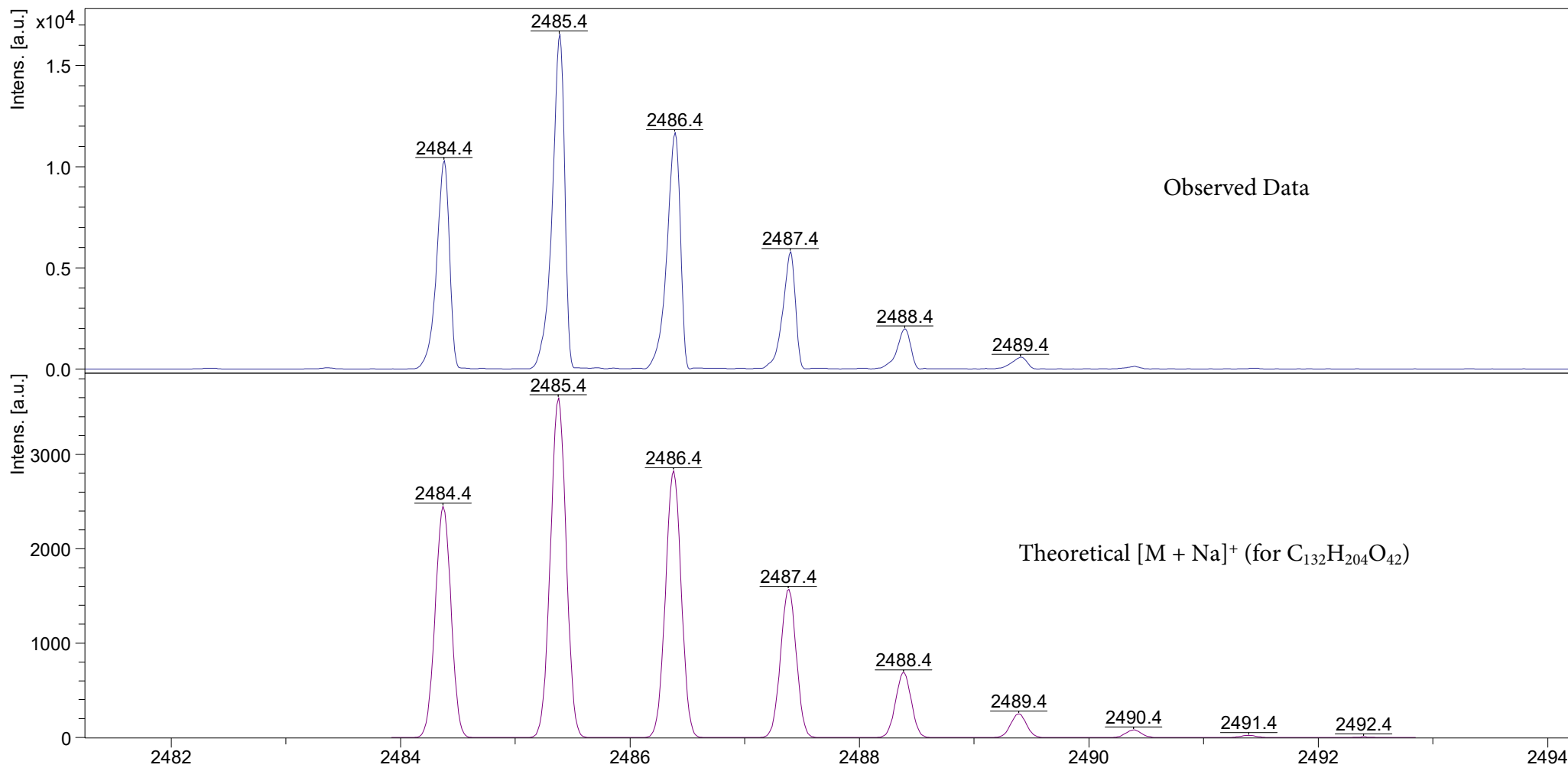
Hub³-Eg₁₂-OThp (**60**) PosRef THF [1:5] (Dith;THF) +NaOAc



ultrafleXtreme MALDI

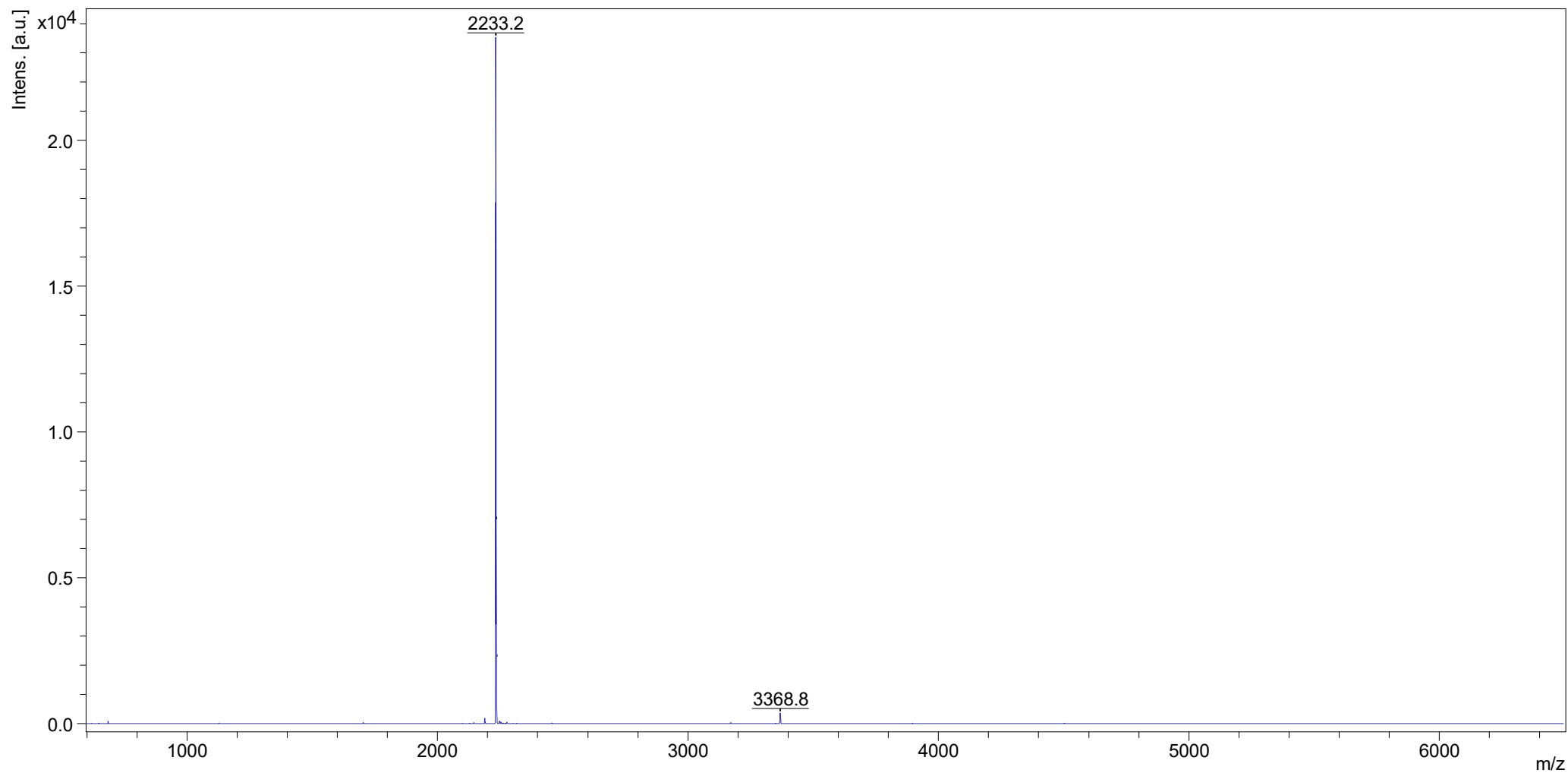
EPSRC UK National Mass Spectrometry Facility (NMSF), Swansea

Hub³-Eg₁₂-OThp (60) PosRef THF [1:5] (Dith;THF) +NaOAc



ultrafleXtreme MALDI

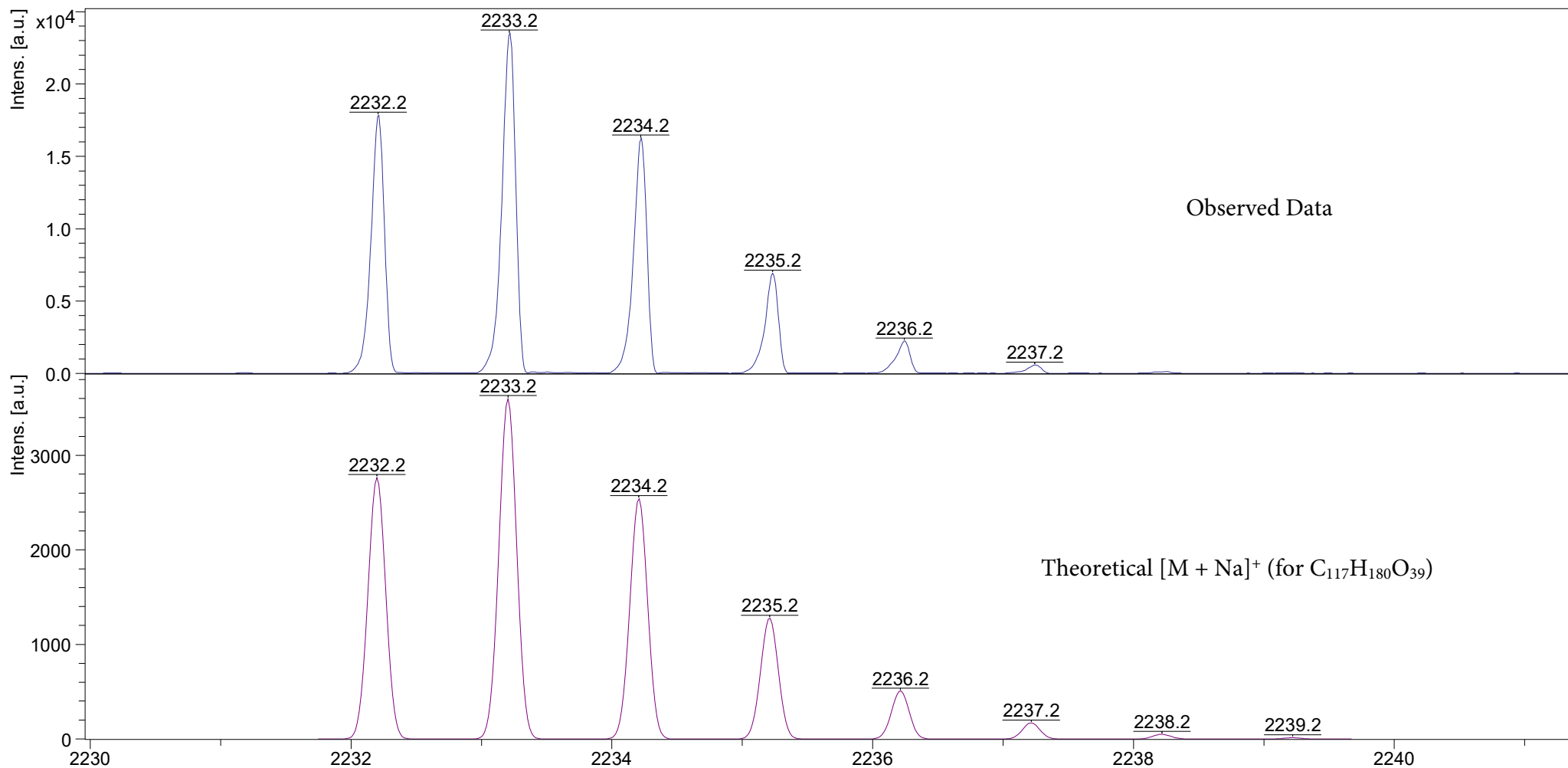
Hub³-Eg₁₂-OH (61) PosRef THF [1:5] (Dith;THF) +NaOAc



ultrafleXtreme MALDI

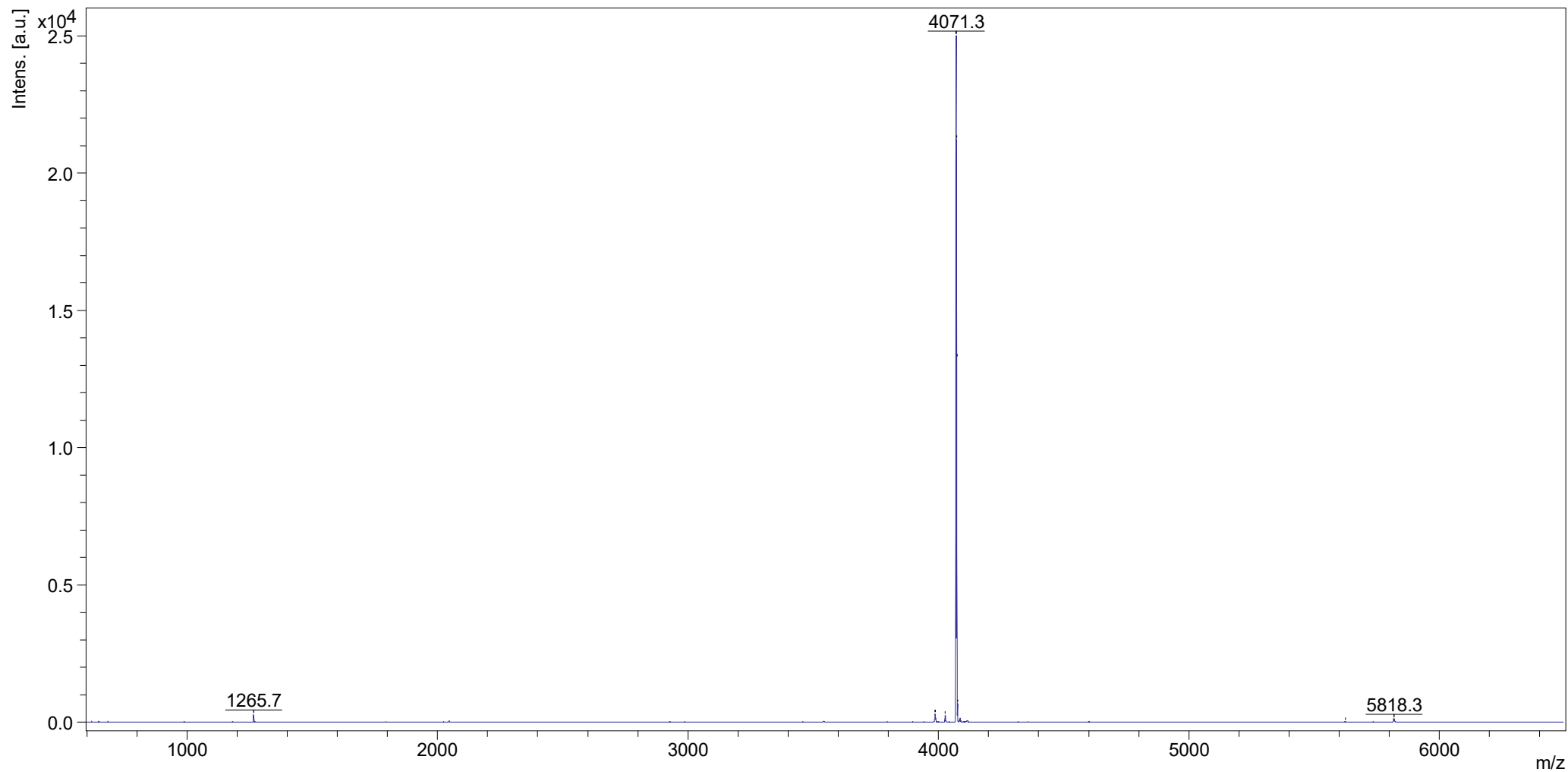
EPSRC UK National Mass Spectrometry Facility (NMSF), Swansea

Hub³-Eg₁₂-OH (61) PosRef THF [1:5] (Dith;THF) +NaOAc



ultrafleXtreme MALDI

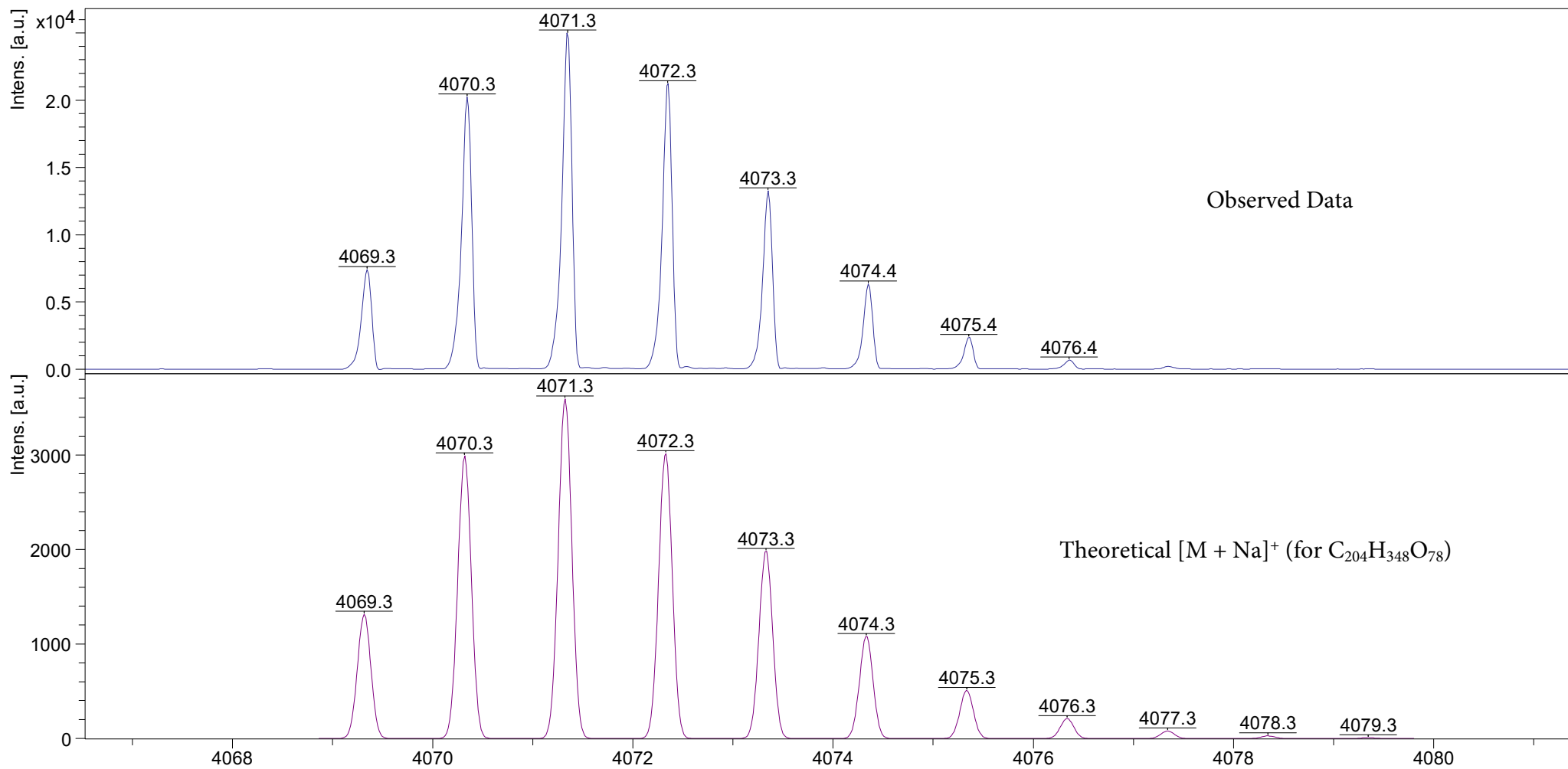
Hub³-Eg₂₄-OThp (**72**) PosRef THF [1:5] (Dith;THF) +NaOAc



ultrafleXtreme MALDI

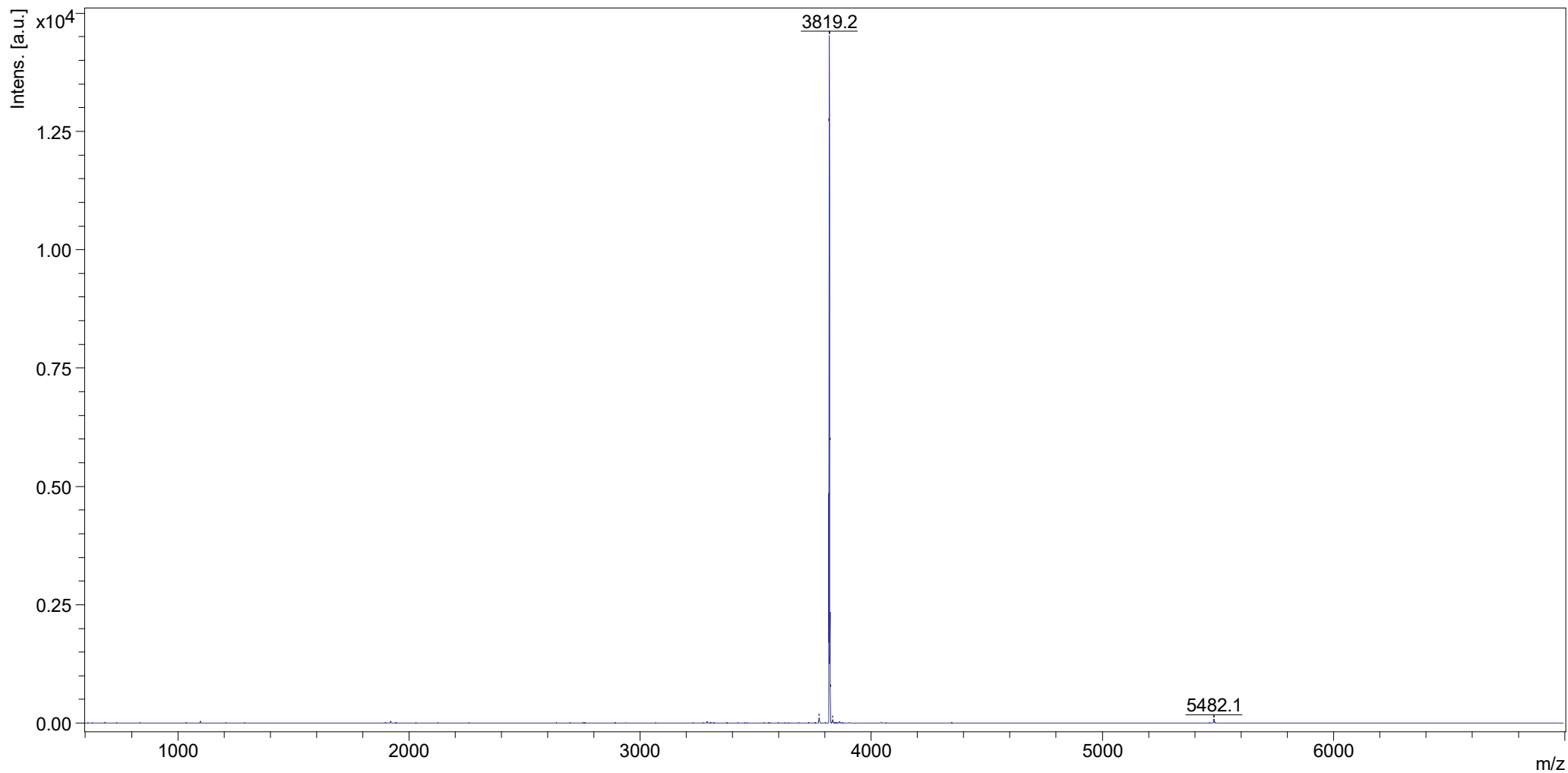
EPSRC UK National Mass Spectrometry Facility (NMSF), Swansea

Hub³-Eg₂₄-OThp (72) PosRef THF [1:5] (Dith;THF) +NaOAc



ultrafleXtreme MALDI

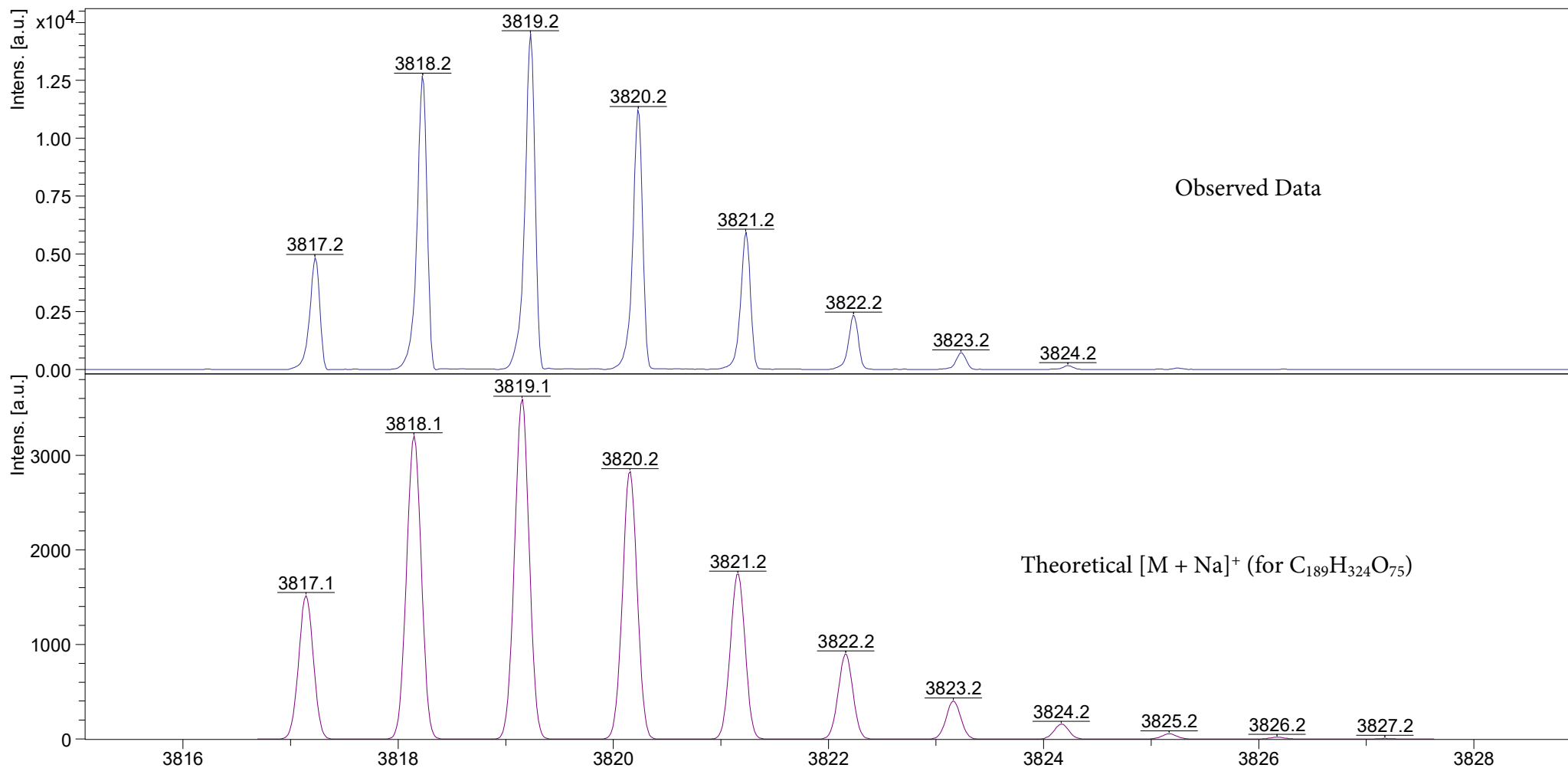
Hub³-Eg₂₄-OH (73) PosRef THF [1:49] (Dith;THF) +NaOAc



ultrafleXtreme MALDI

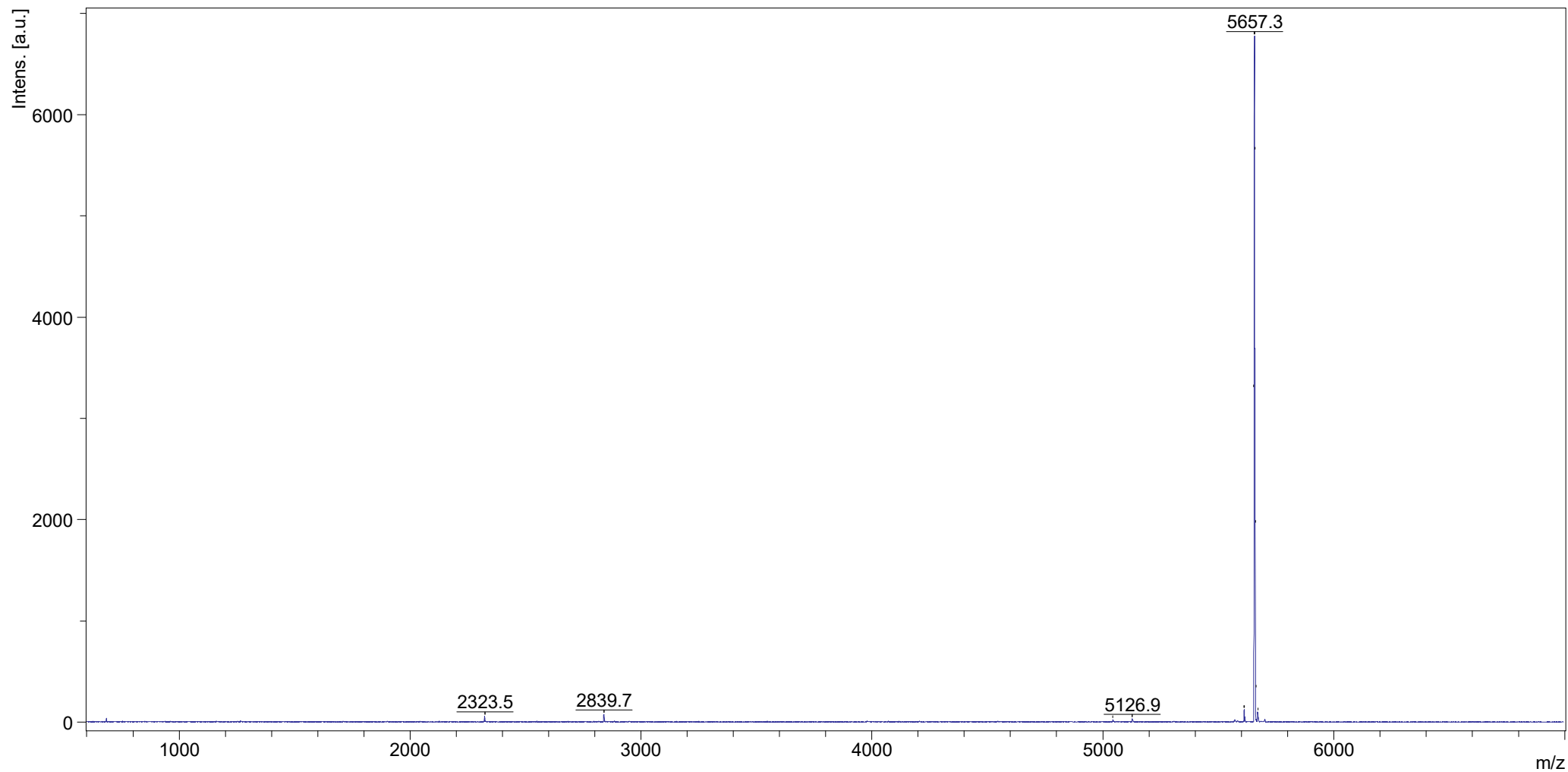
EPSRC UK National Mass Spectrometry Facility (NMSF), Swansea

Hub³-Eg₂₄-OH (73) PosRef THF [1:49] (Dith;THF) +NaOAc



ultrafleXtreme MALDI

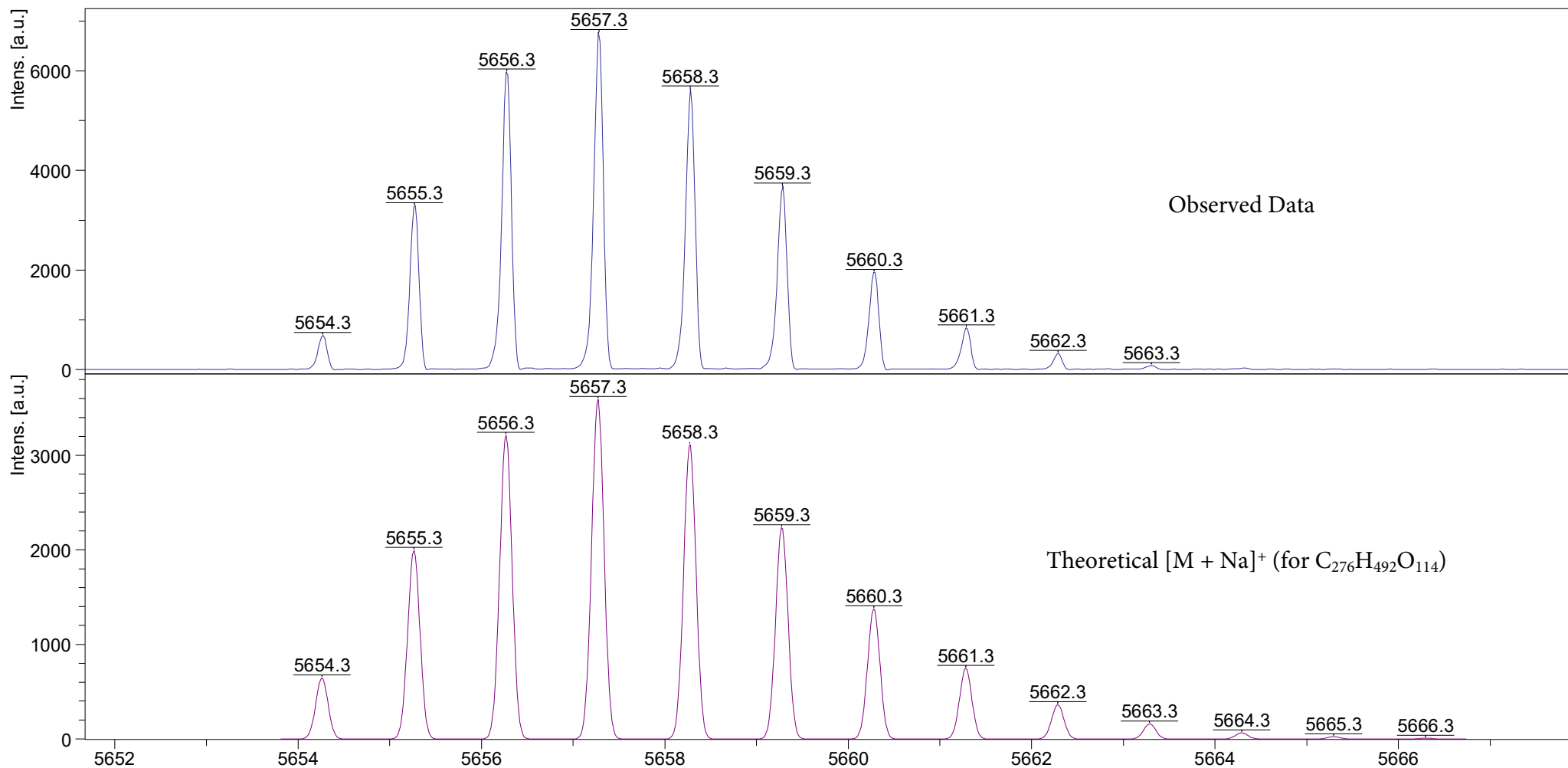
Hub³-Eg₃₆-OThp (74) PosRef THF [1:49] (Dith;THF) +NaOAc



ultrafleXtreme MALDI

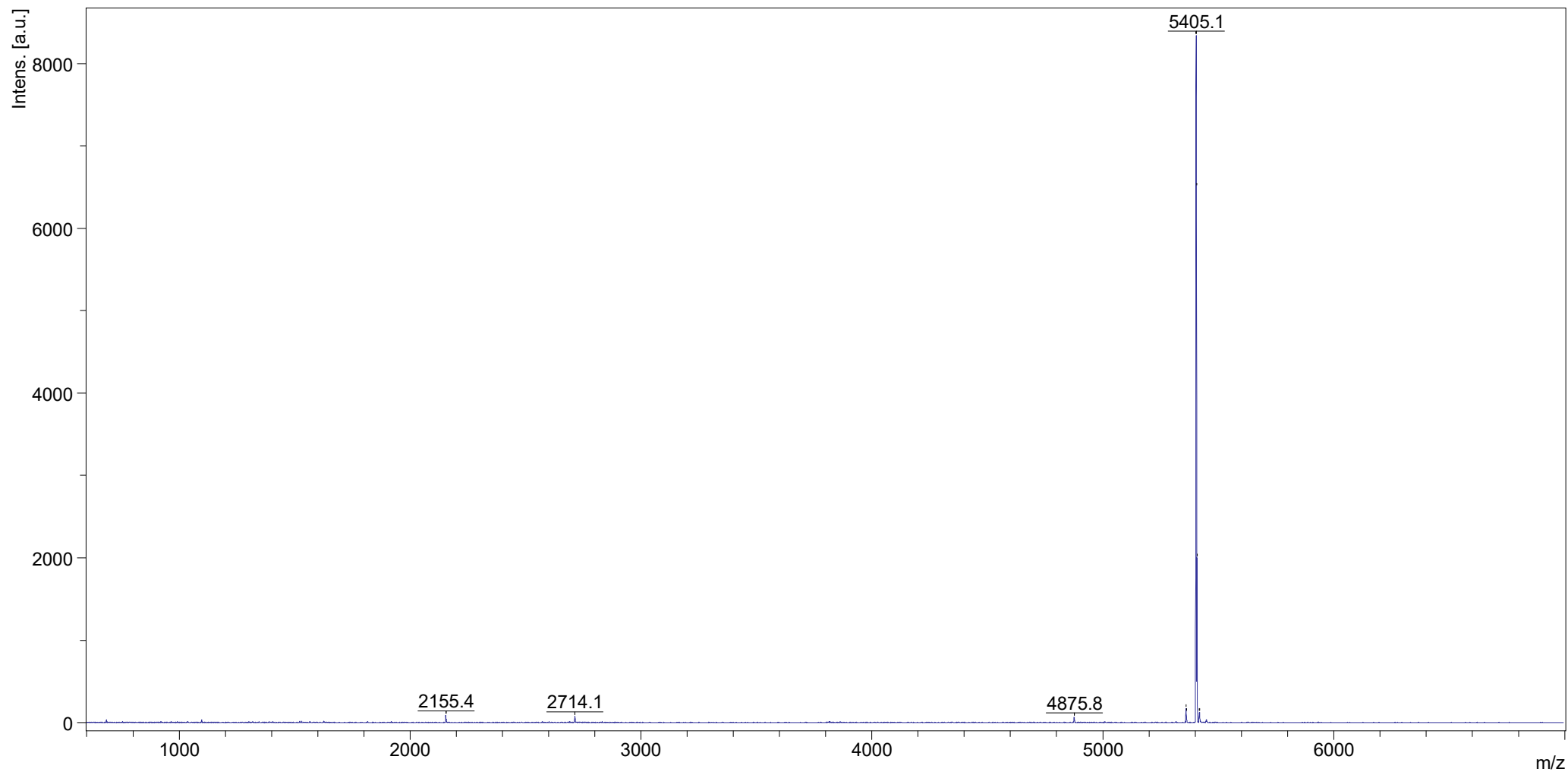
EPSRC UK National Mass Spectrometry Facility (NMSF), Swansea

Hub³-Eg₃₆-OThp (74) PosRef THF [1:49] (Dith;THF) +NaOAc



ultrafleXtreme MALDI

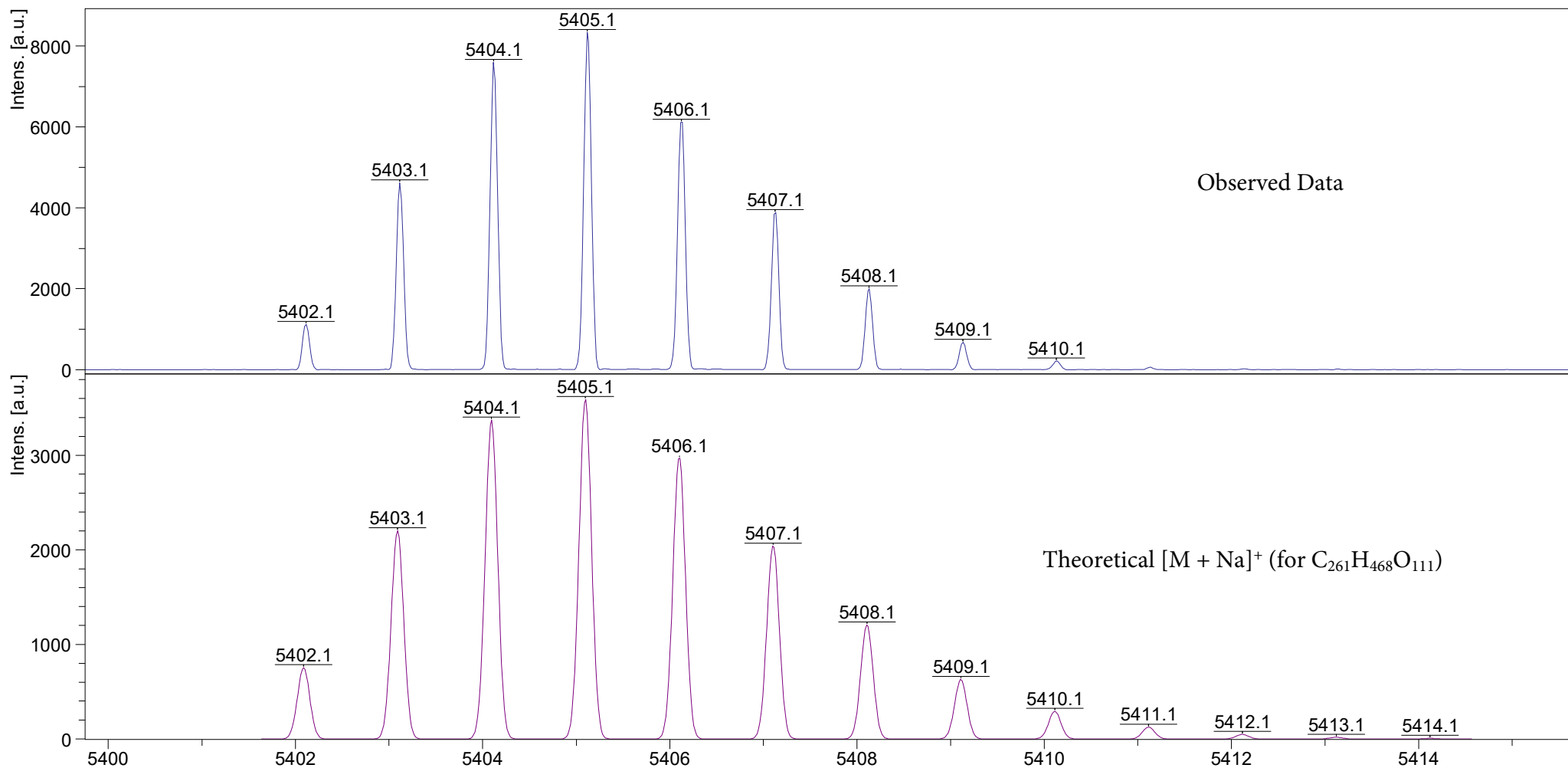
Hub³-Eg₃₆-OH (75) PosRef THF [1:49] (Dith;THF) +NaOAc



ultrafleXtreme MALDI

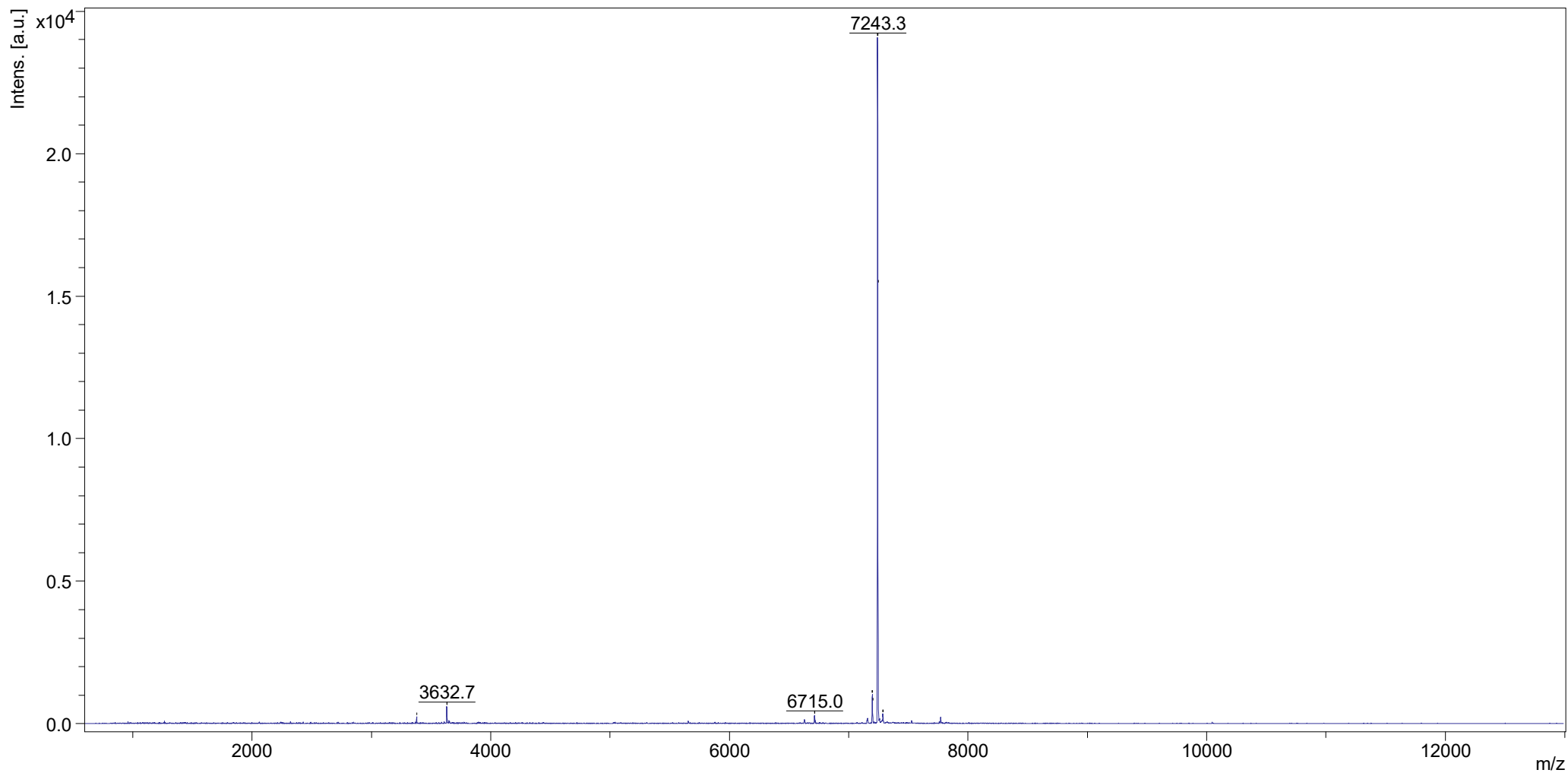
EPSRC UK National Mass Spectrometry Facility (NMSF), Swansea

Hub³-Eg₃₆-OH (75) PosRef THF [1:49] (Dith;THF) +NaOAc



ultrafleXtreme MALDI

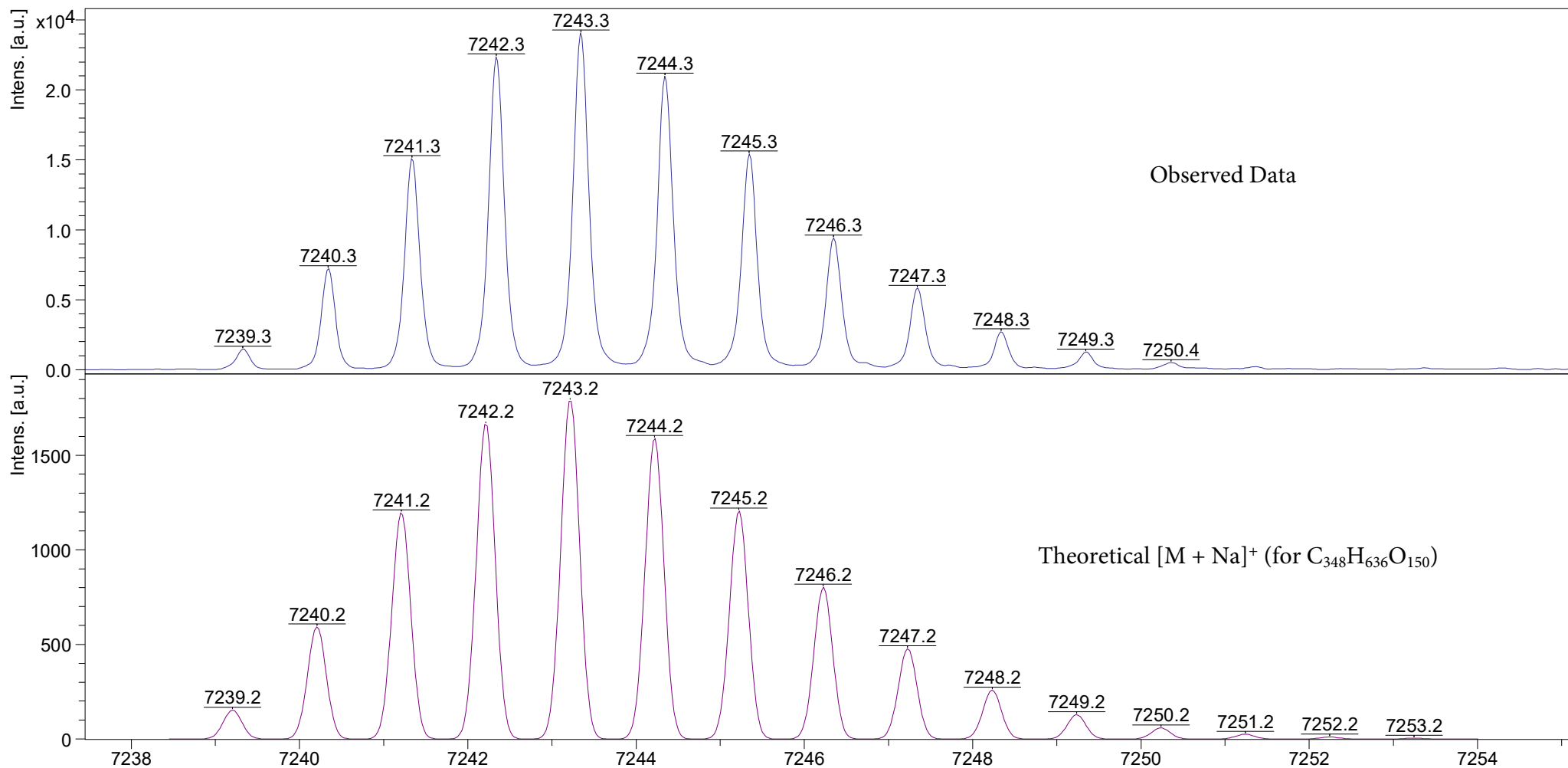
Hub³-Eg₄₈-OThp (**76**) PosRef THF [1:49] (Dith;THF) +NaOAc



ultrafleXtreme MALDI

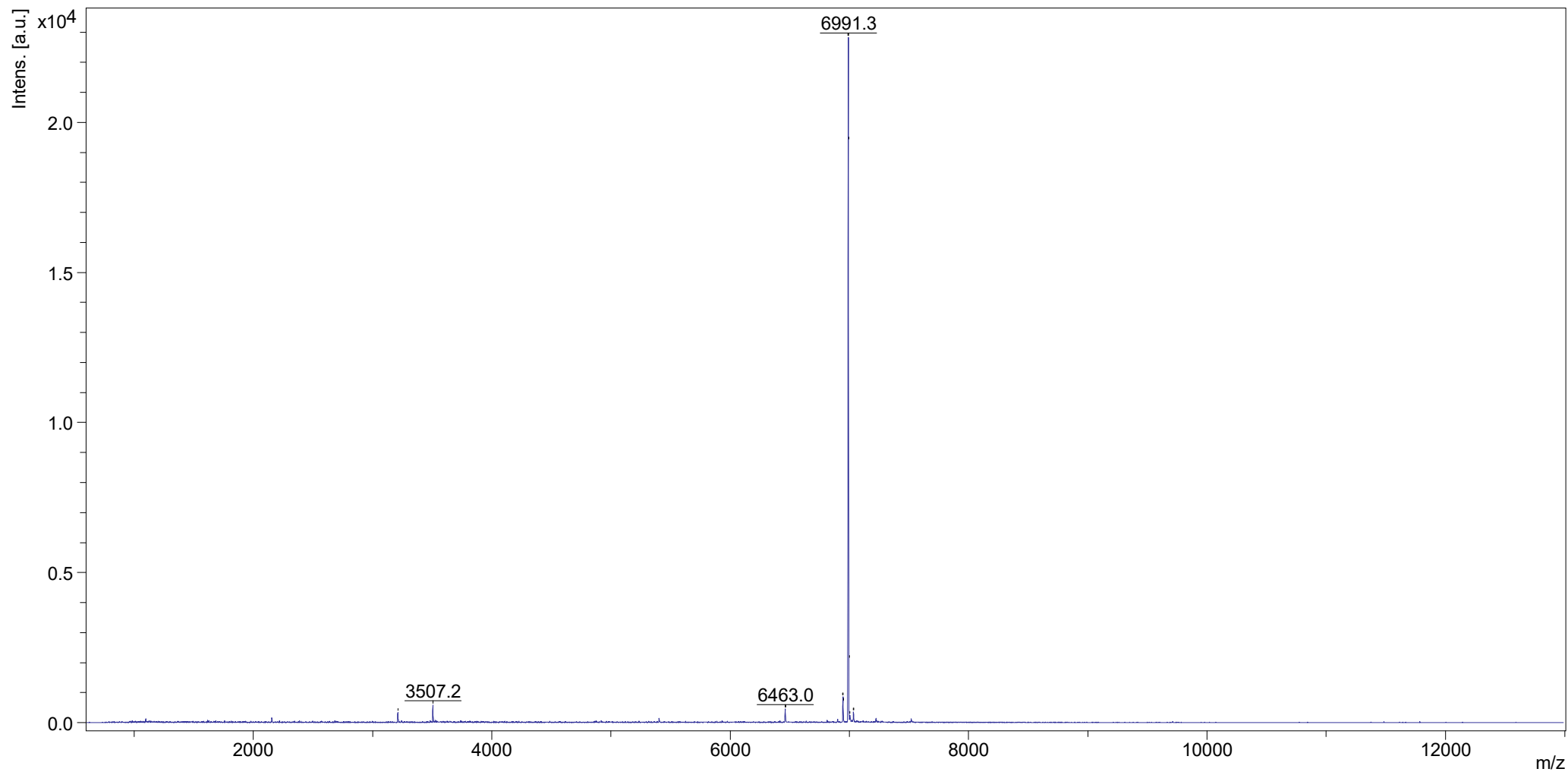
EPSRC UK National Mass Spectrometry Facility (NMSF), Swansea

Hub³-Eg₄₈-OThp (76) PosRef THF [1:49] (Dith;THF) +NaOAc



ultrafleXtreme MALDI

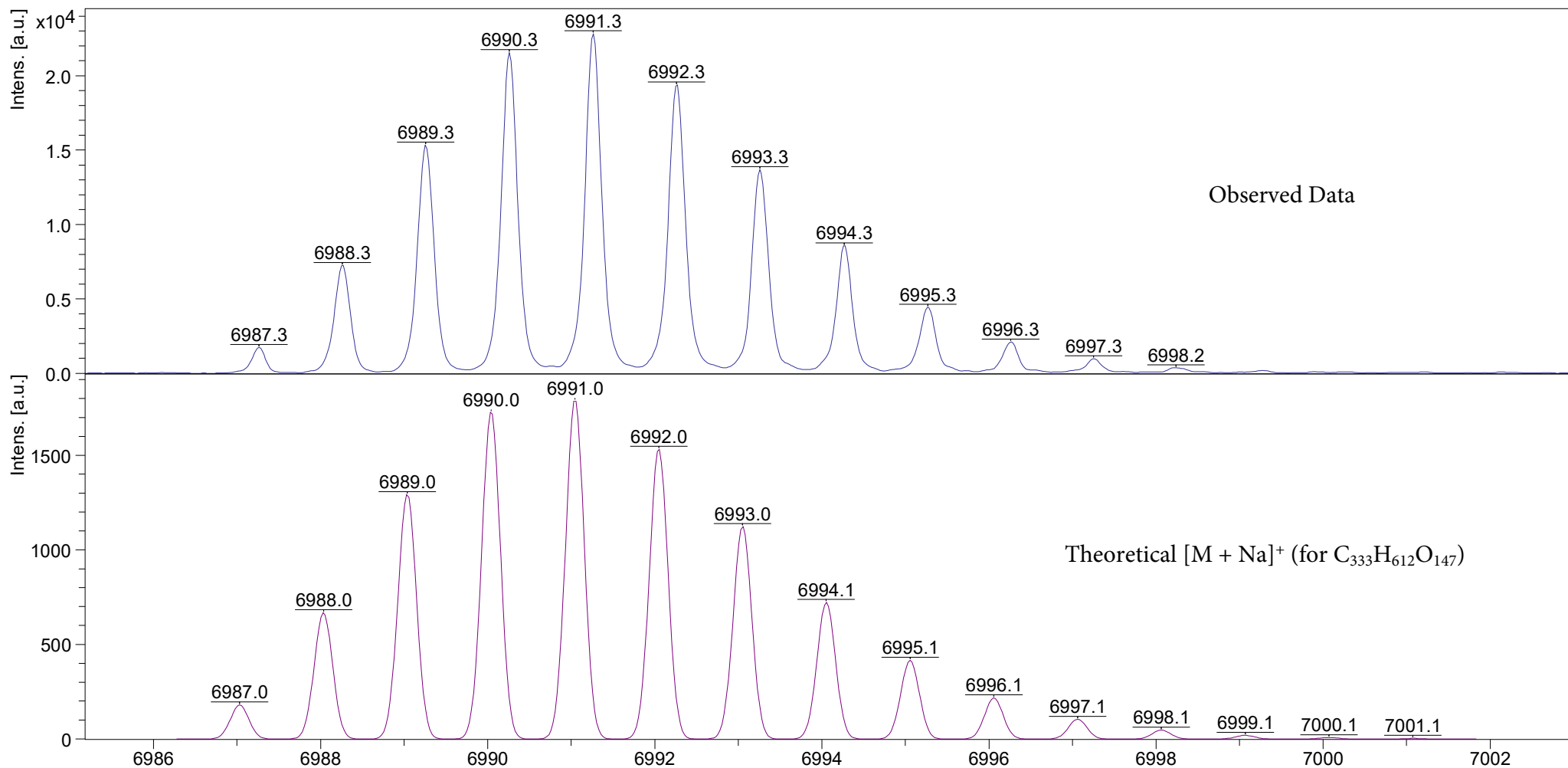
Hub³-Eg₄₈-OH (77) PosRef THF [1:49] (Dith;THF) +NaOAc



ultrafleXtreme MALDI

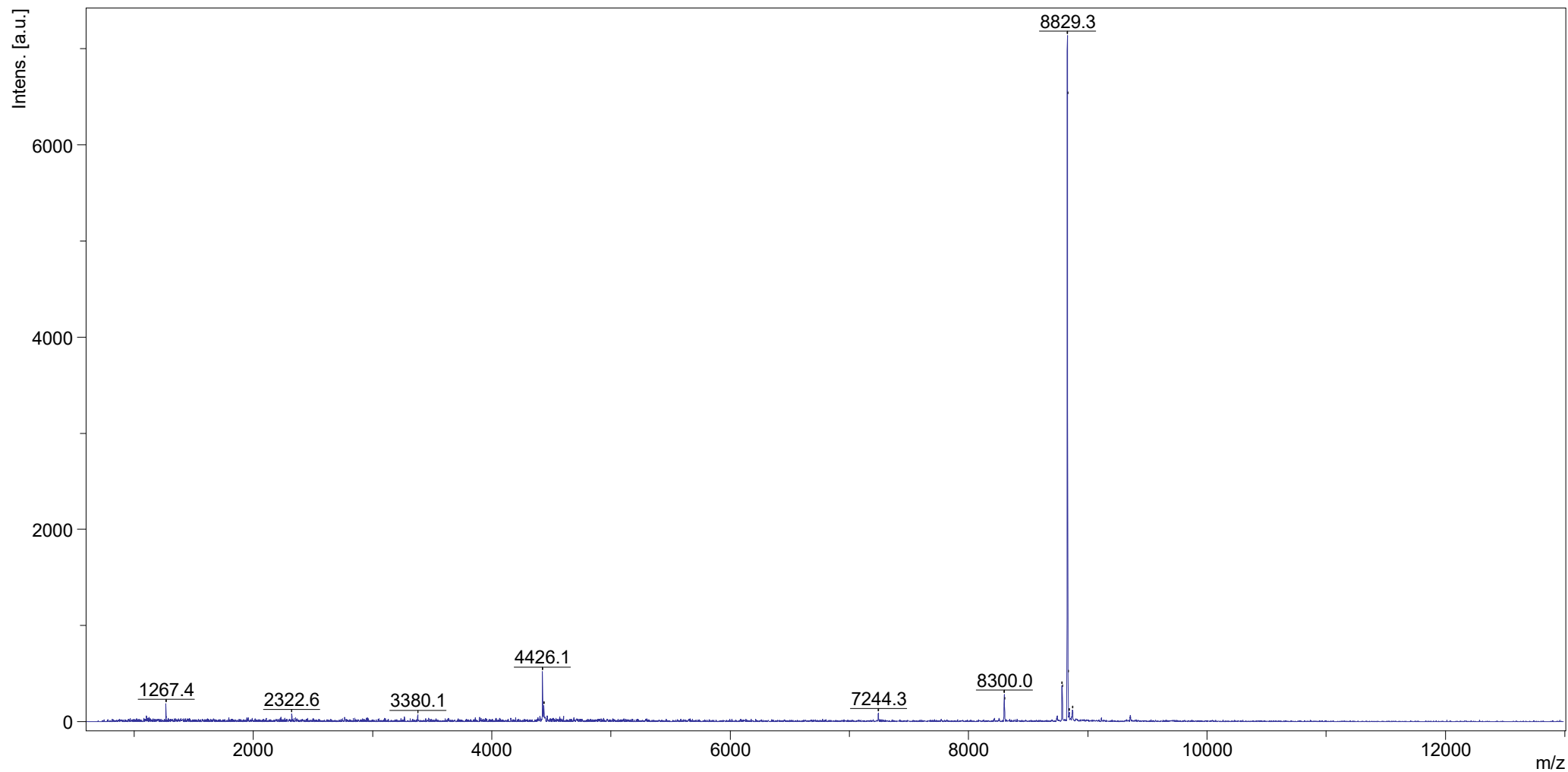
EPSRC UK National Mass Spectrometry Facility (NMSF), Swansea

Hub³-Eg₄₈-OH (77) PosRef THF [1:49] (Dith;THF) +NaOAc



ultrafleXtreme MALDI

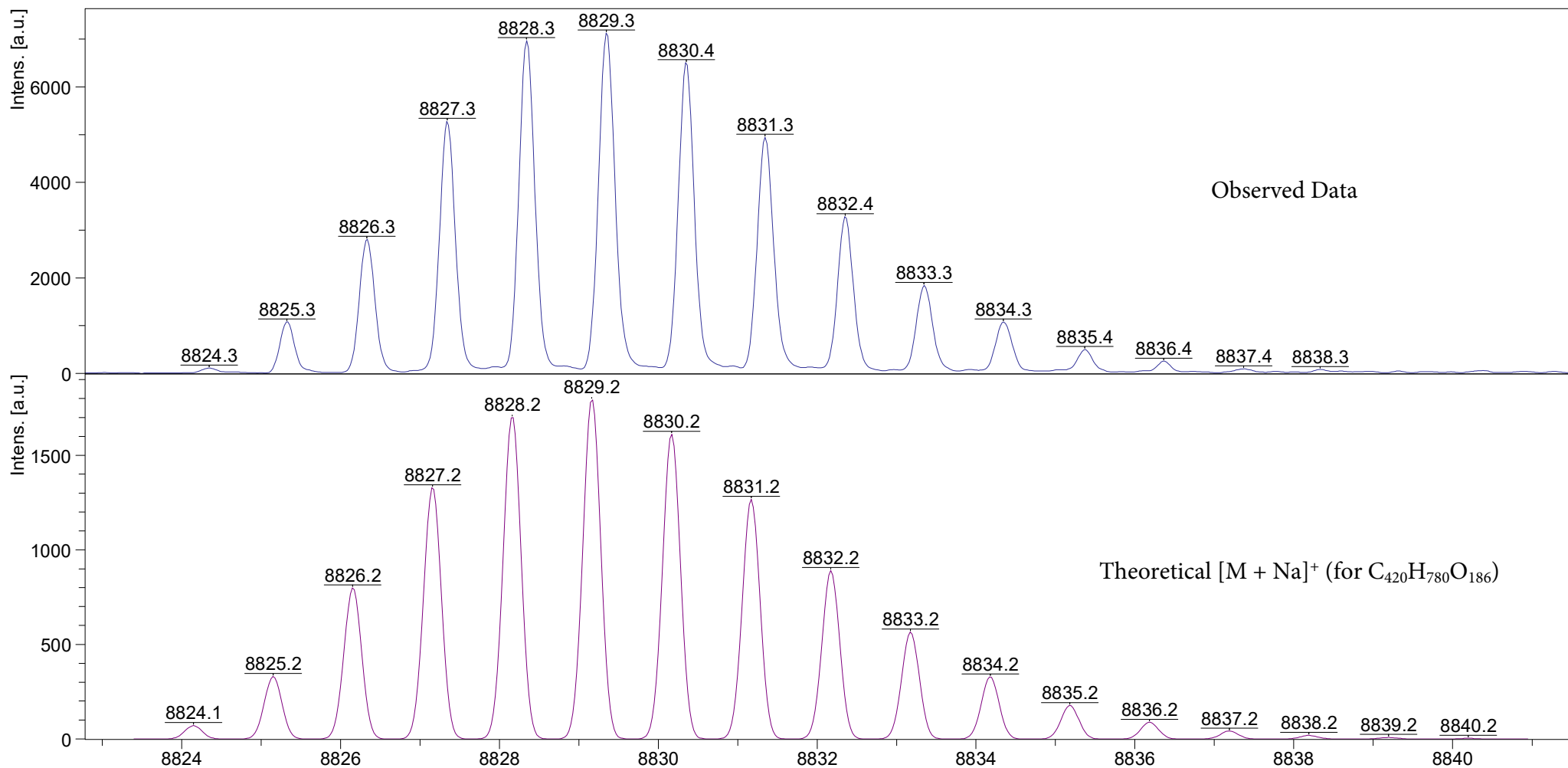
Hub³-Eg₆₀-OThp (**78**) PosRef THF [1:49] (Dith;THF) +NaOAc



ultrafleXtreme MALDI

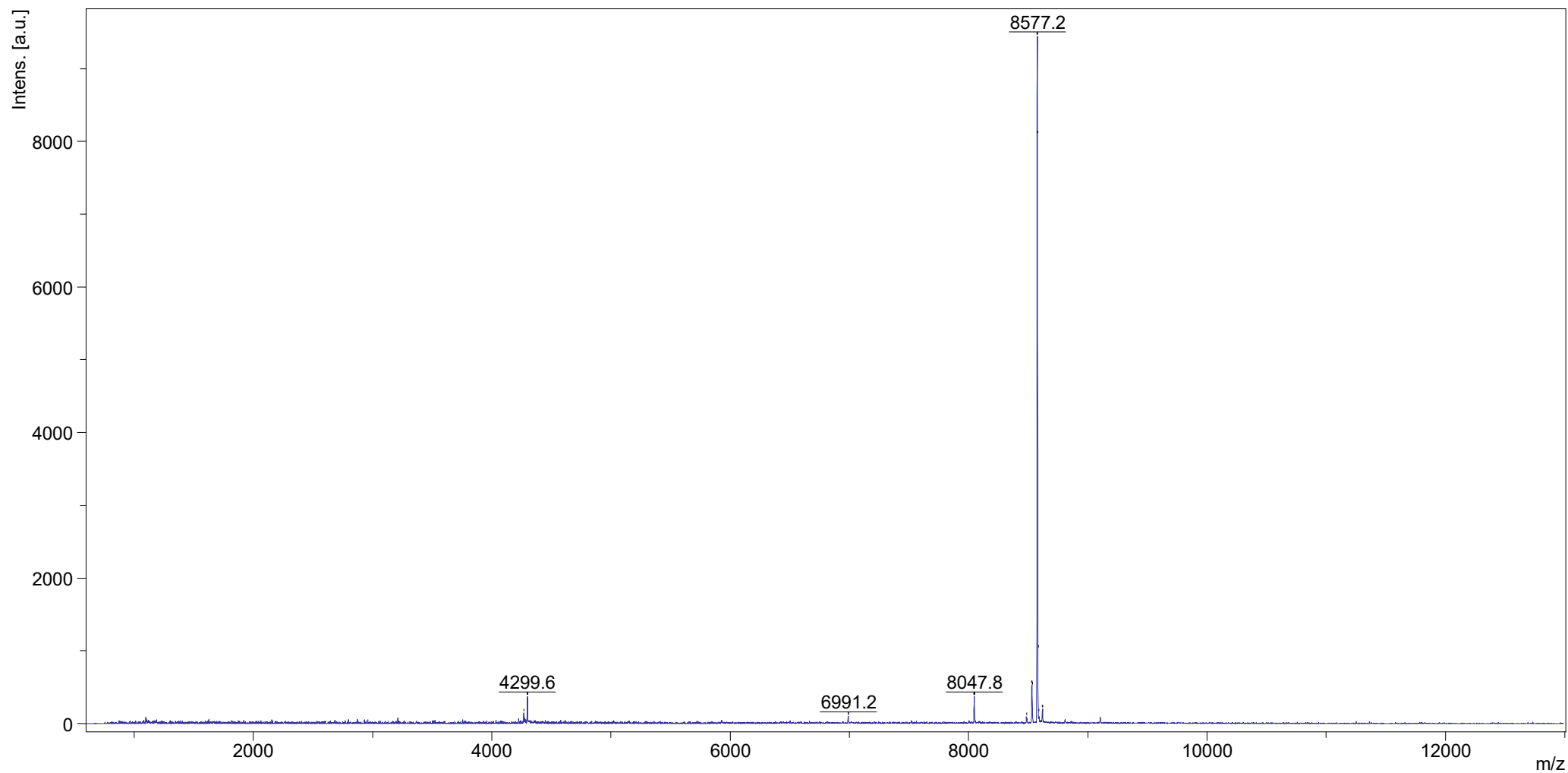
EPSRC UK National Mass Spectrometry Facility (NMSF), Swansea

Hub³-Eg₆₀-OThp (78) PosRef THF [1:49] (Dith;THF) +NaOAc



ultrafleXtreme MALDI

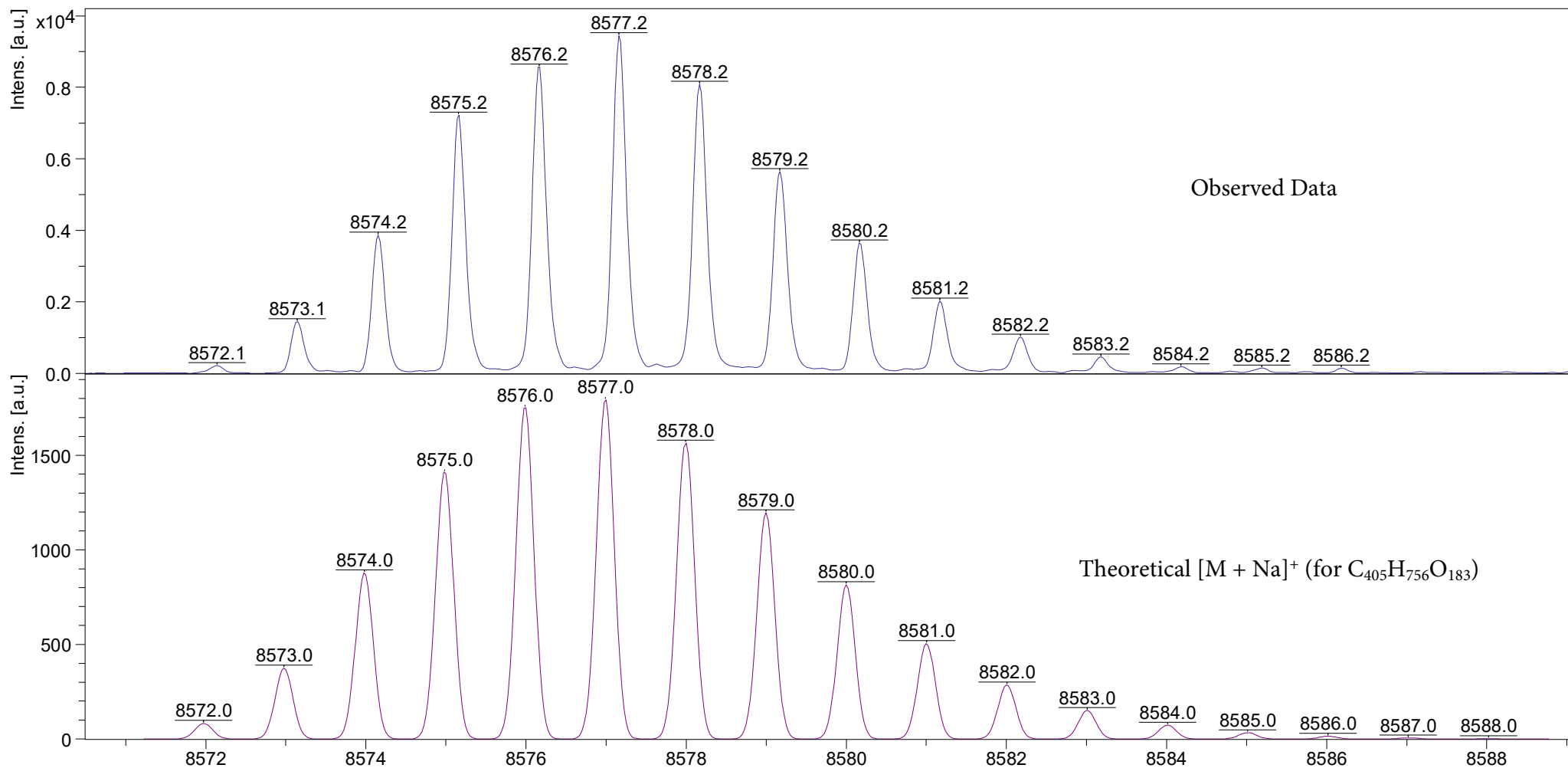
Hub³-Eg₆₀-OH (79) PosRef THF [1:49] (Dith;THF) +NaOAc



ultrafleXtreme MALDI

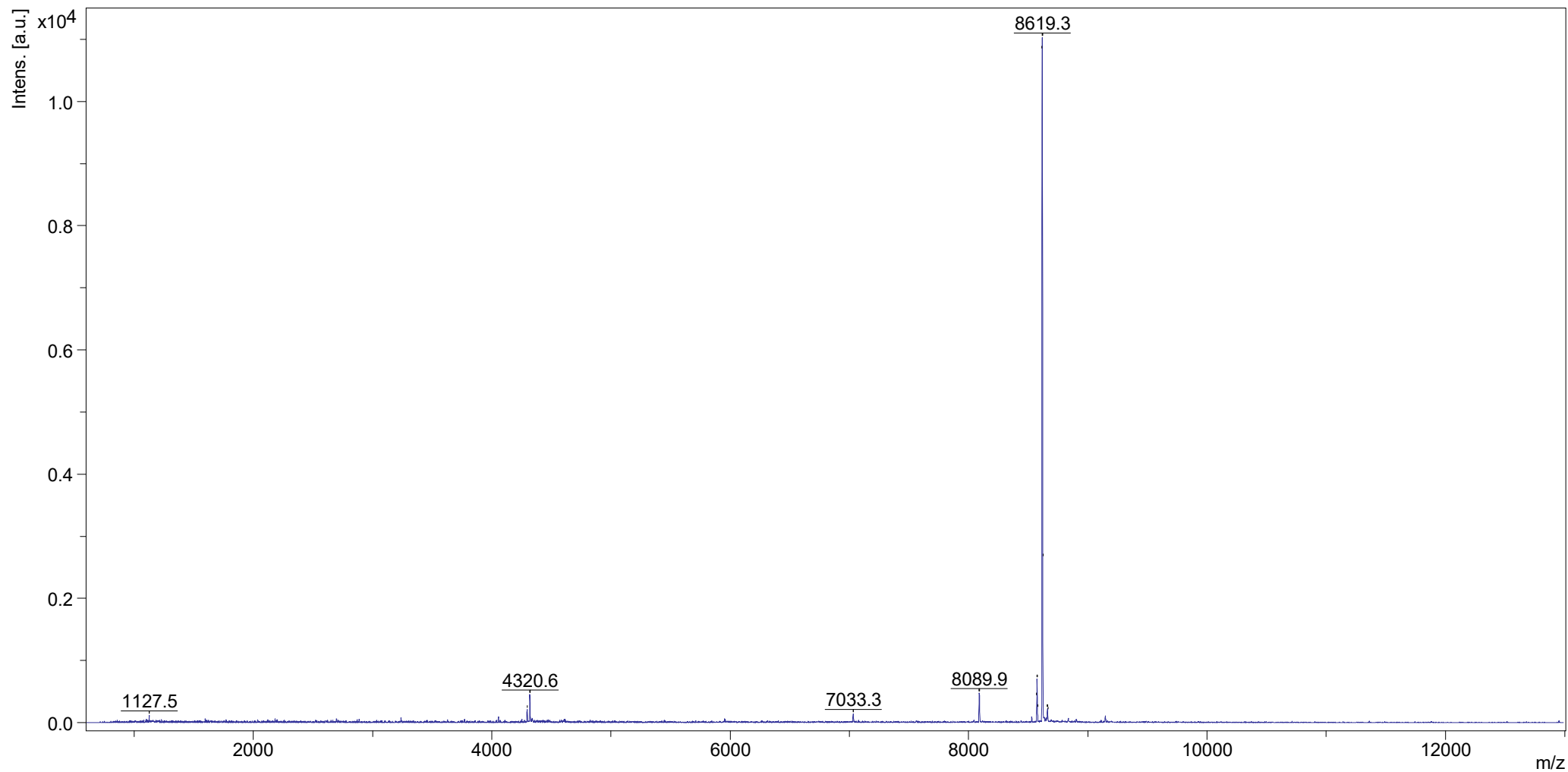
EPSRC UK National Mass Spectrometry Facility (NMSF), Swansea

Hub³-Eg₆₀-OH (79) PosRef THF [1:49] (Dith;THF) +NaOAc



ultrafleXtreme MALDI

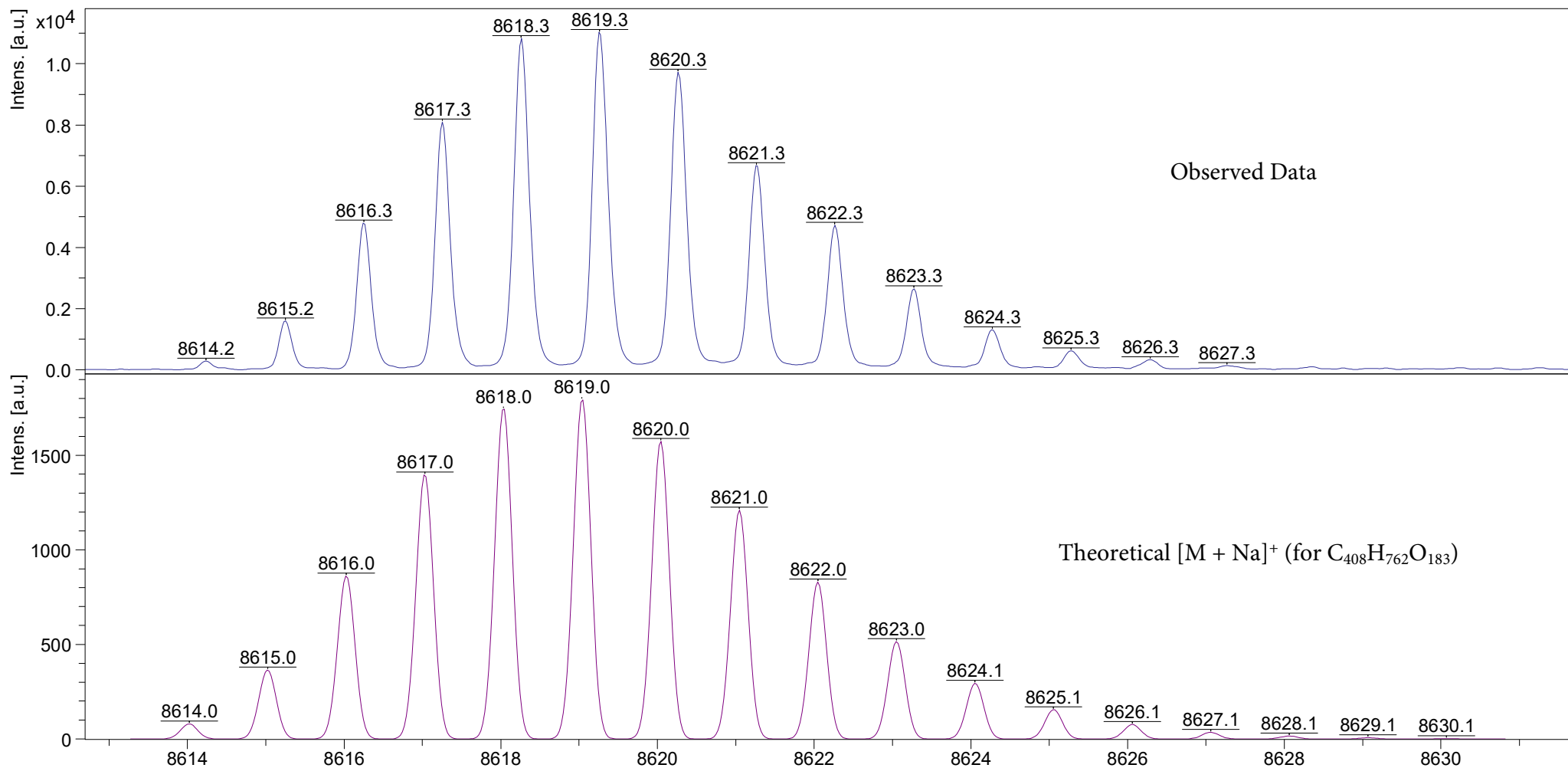
Hub³-Eg₆₀-OMe (**80**) PosRef THF [1:49] (Dith;THF) +NaOAc



ultrafleXtreme MALDI

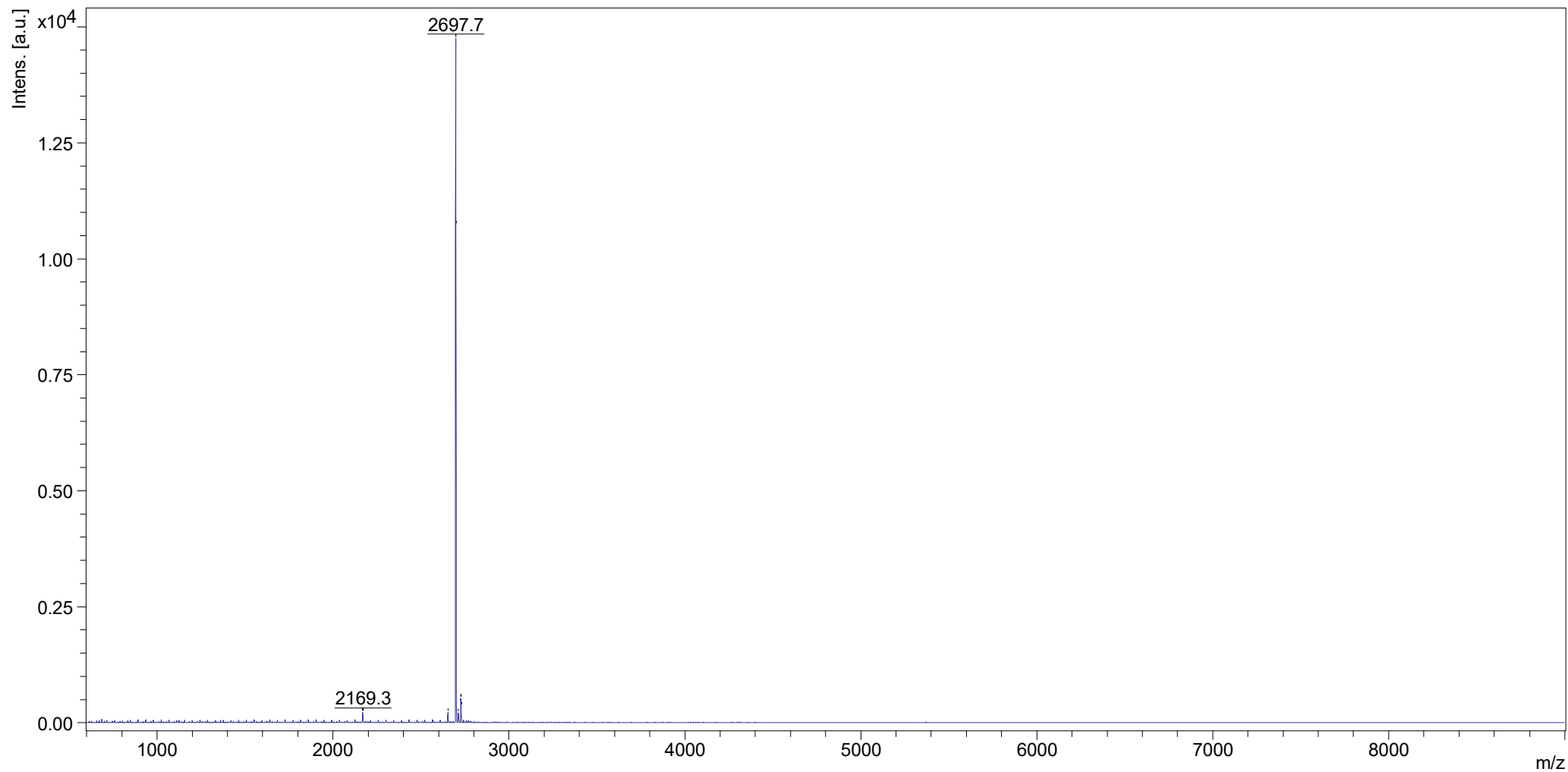
EPSRC UK National Mass Spectrometry Facility (NMSF), Swansea

Hub³-Eg₆₀-OMe (80) PosRef THF [1:49] (Dith;THF) +NaOAc



ultrafleXtreme MALDI

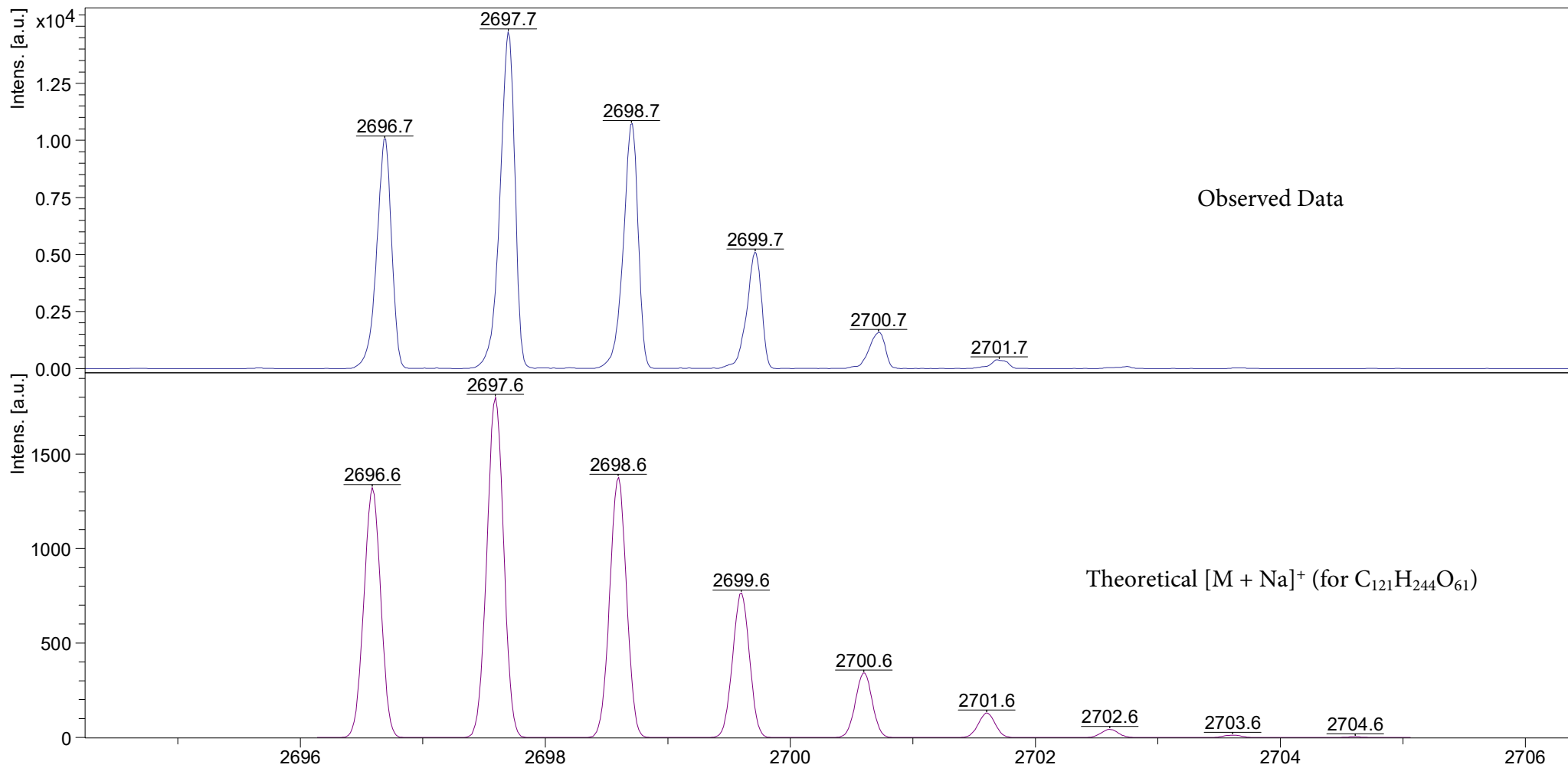
HO-Eg₆₀-OMe (81) PosRef THF [1:49] (Dith;THF) +NaOAc



ultrafleXtreme MALDI

EPSRC UK National Mass Spectrometry Facility (NMSF), Swansea

HO-Eg₆₀-OMe (81) PosRef THF [1:49] (Dith;THF) +NaOAc



ultrafleXtreme MALDI

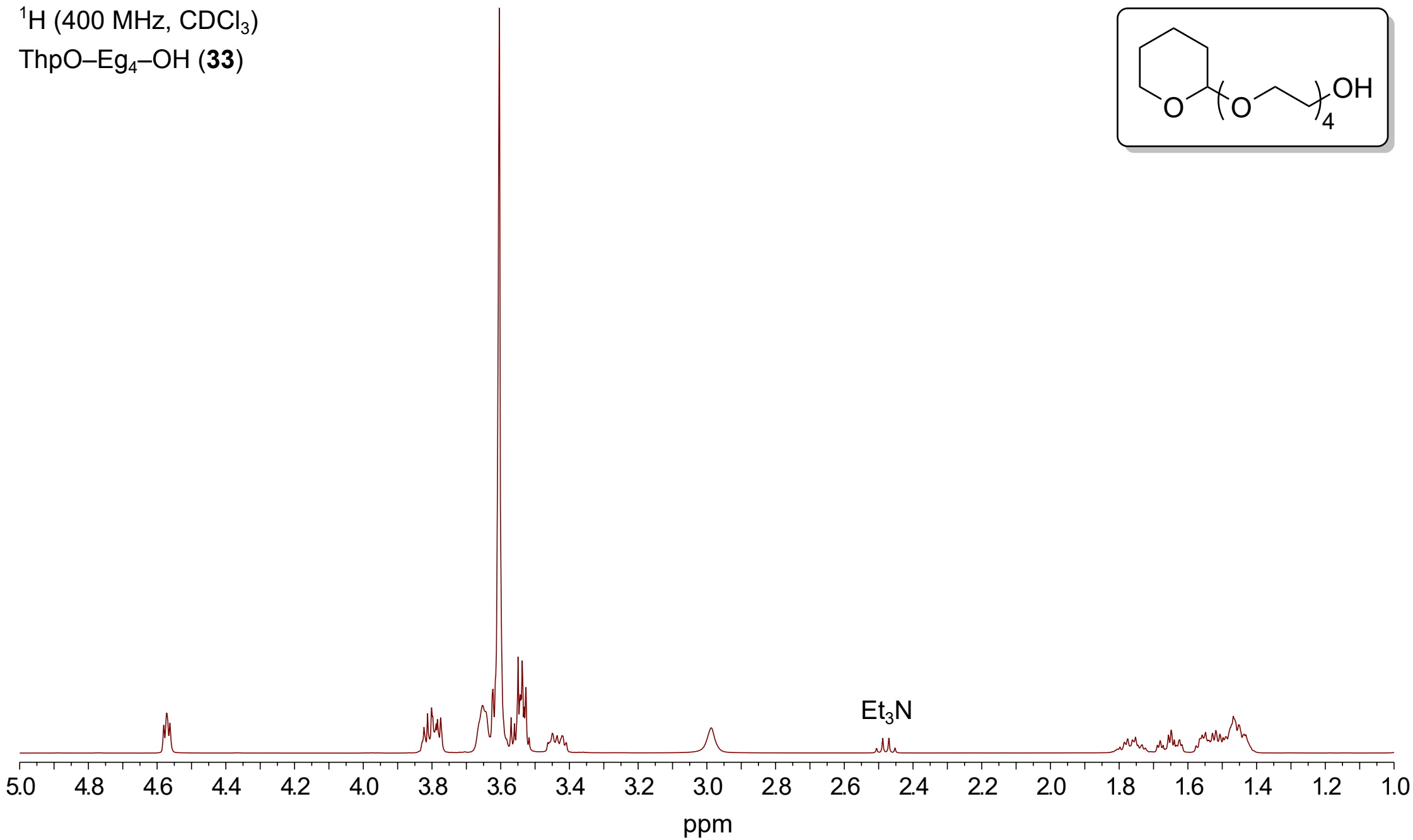
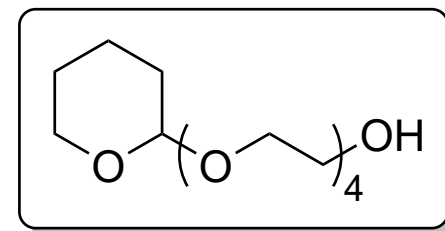
Appendix J – NMR spectra for the synthesis of Eg₆₀

NMR samples were prepared by filtering a solution of the compound in a suitable deuterated solvent through a thin plug of anhydrous Na₂SO₄ over cotton wool. PEG-containing samples and the hubs with a benzylic bromomethyl moiety were analyzed in CDCl₃ (7.260, 77.16) and the other hubs were analyzed in either DMSO-d₆ (2.500, 39.52) or THF-d₈ (3.580, 67.57). A trace of Et₃N was added to NMR samples in CDCl₃ when Thp ethers were present.

Compounds containing Hub³-CH₂OR are susceptible to oxidation of the benzylic methylene. Aerobic oxidation can apparently occur as resonances characteristic of oxidation appeared in NMR samples dissolved in CDCl₃ and stored at room temperature. Therefore Hub³-CH₂OR compounds should be stored in the dark under argon at 4 °C or below, and the diafiltration product should be concentrated and dried immediately after diafiltration.

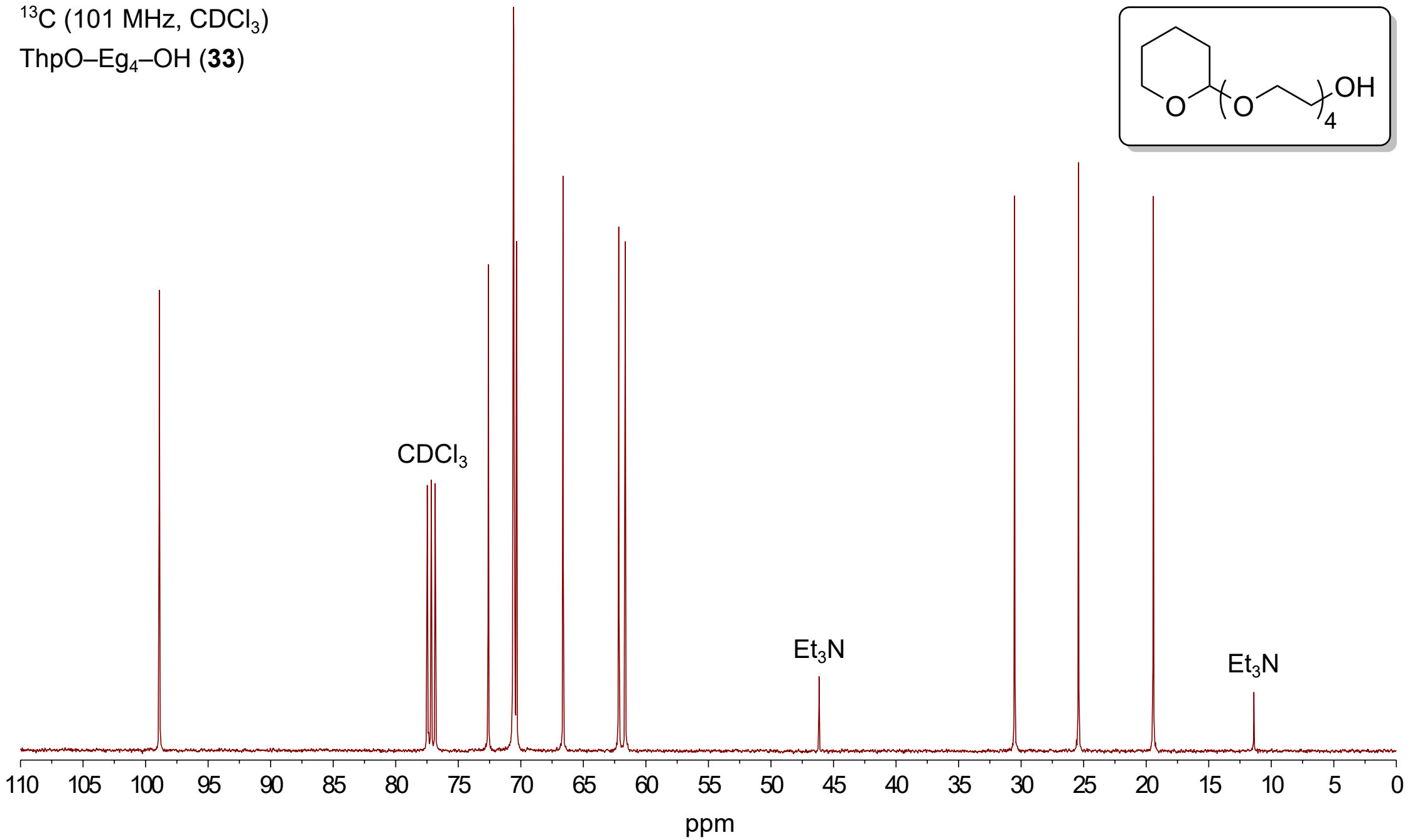
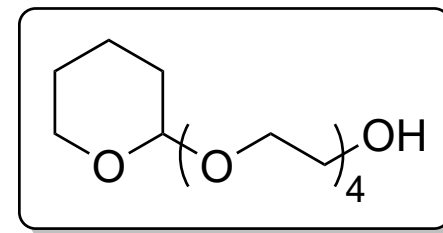
^1H (400 MHz, CDCl_3)

ThpO-Eg₄-OH (**33**)



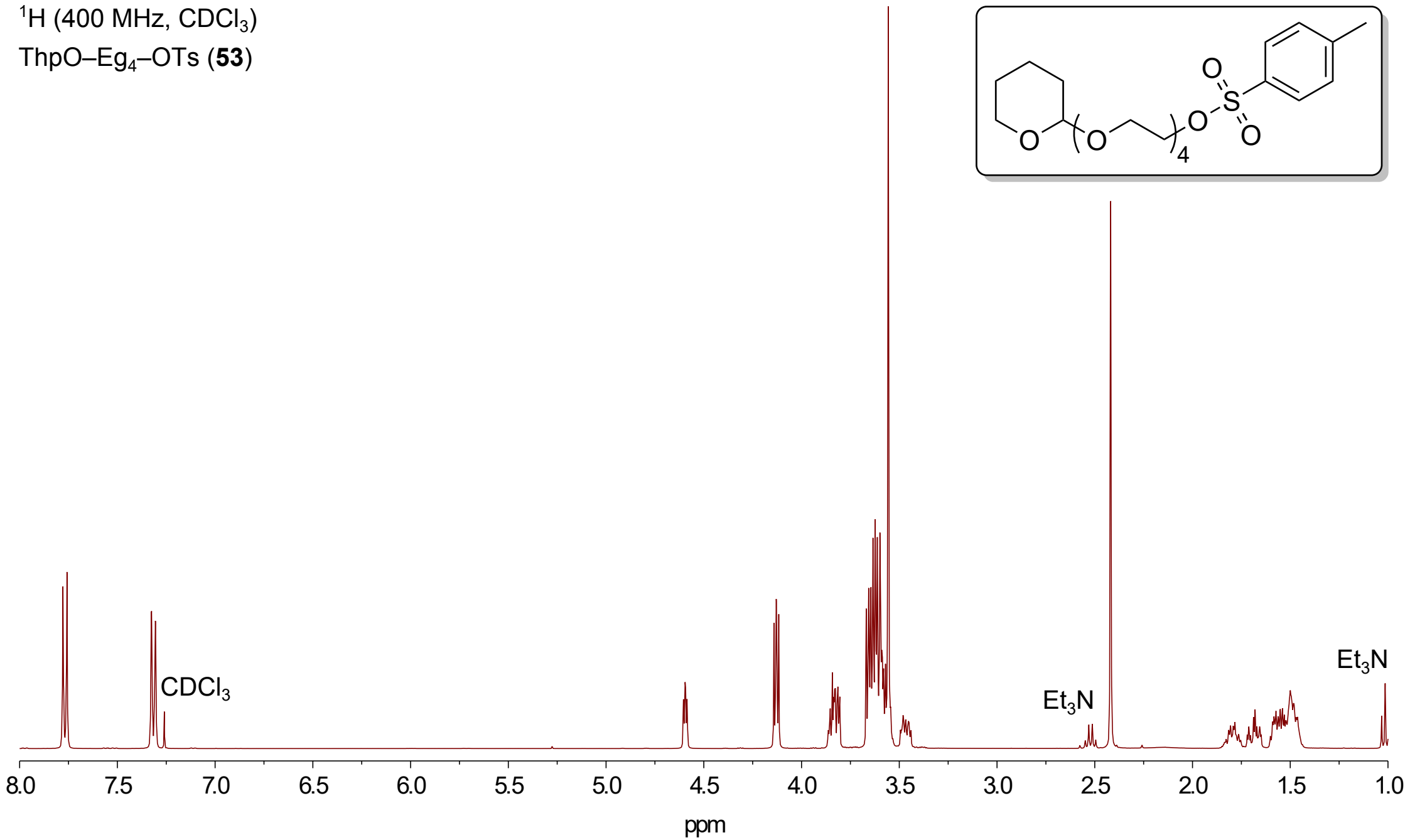
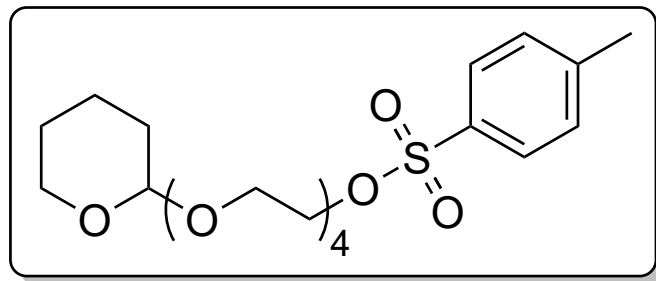
^{13}C (101 MHz, CDCl_3)

ThpO-Eg₄-OH (**33**)

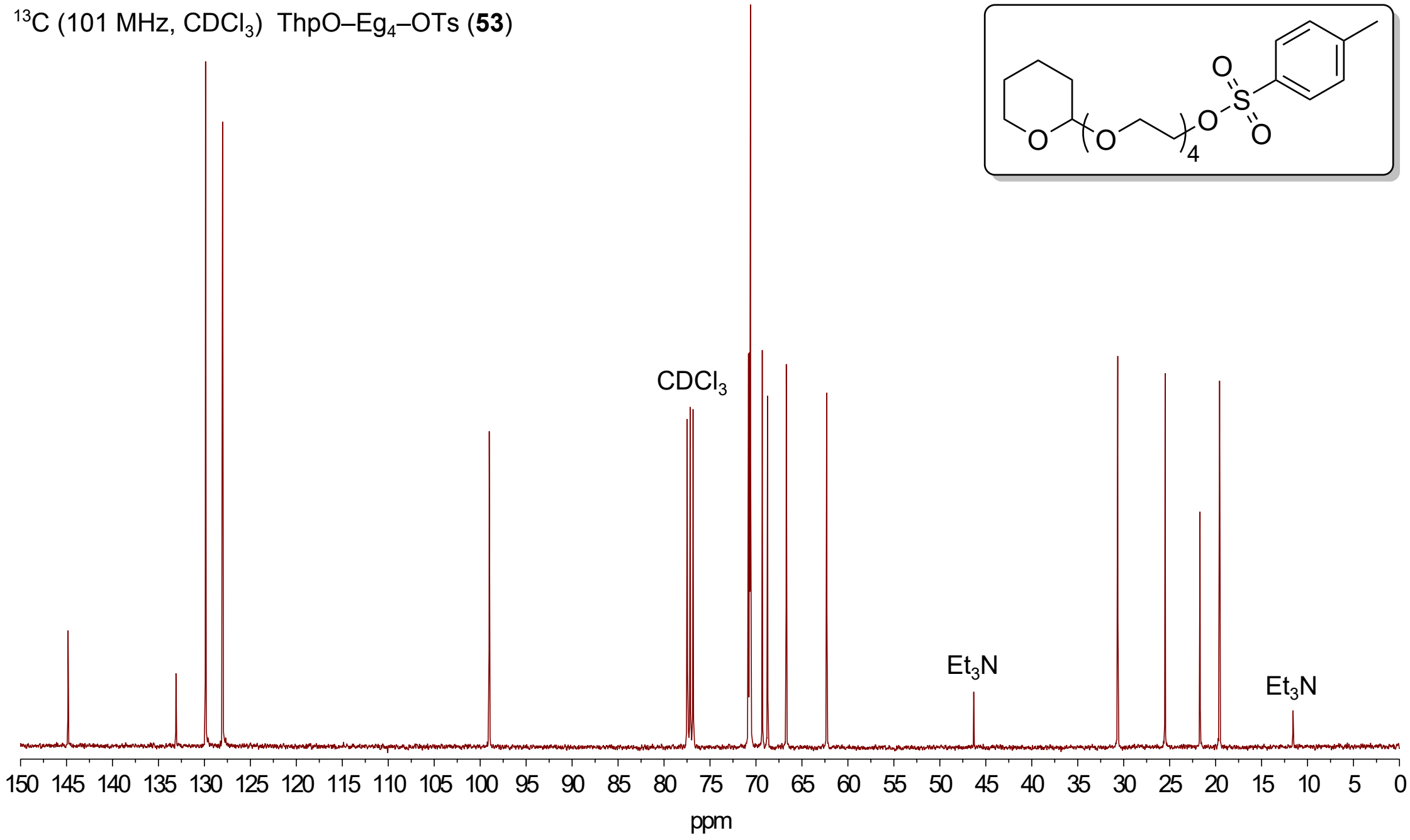
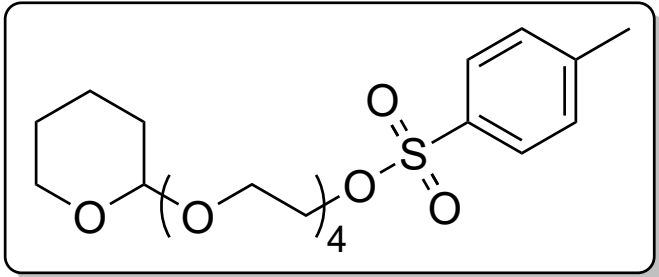


^1H (400 MHz, CDCl_3)

ThpO-Eg₄-OTs (**53**)

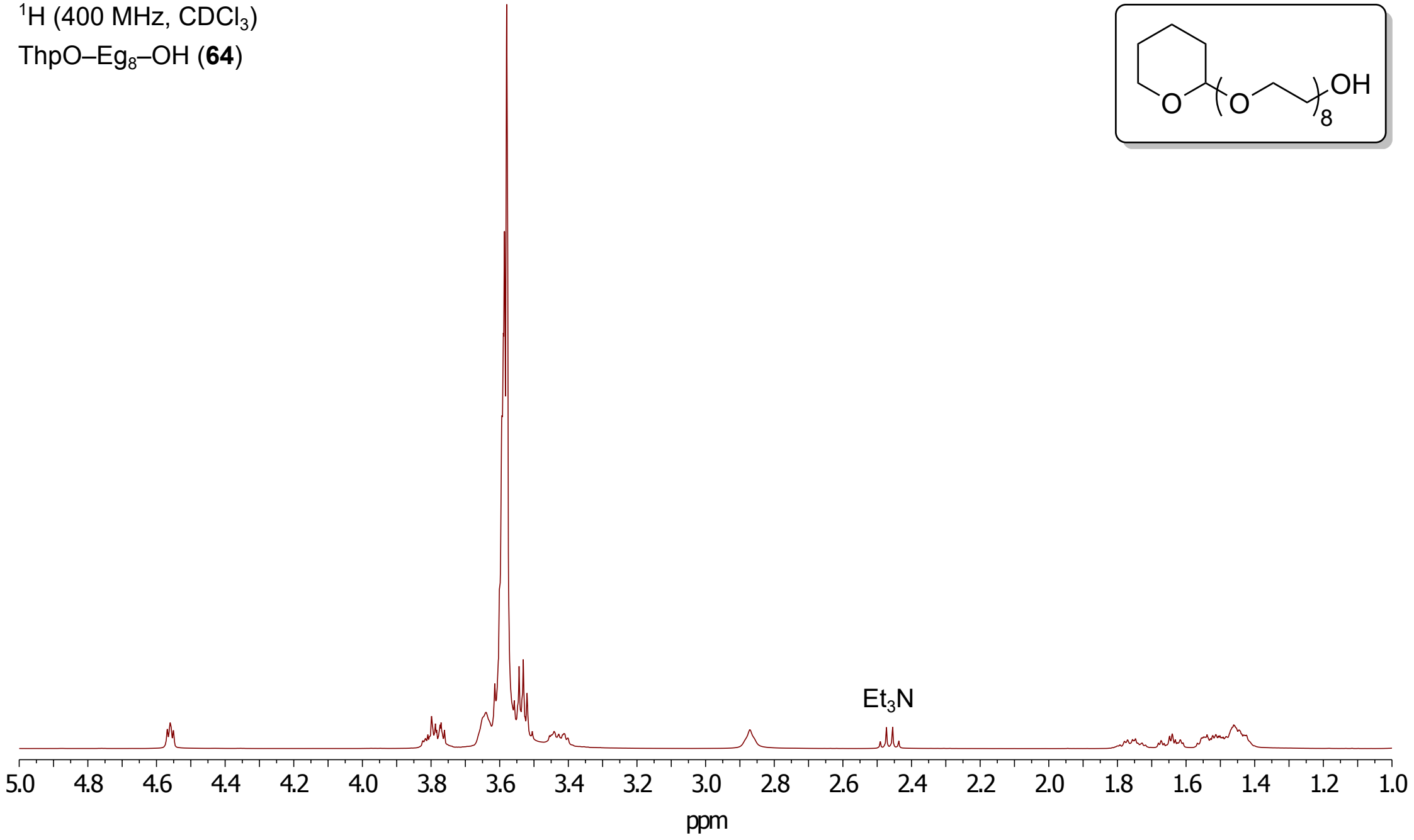
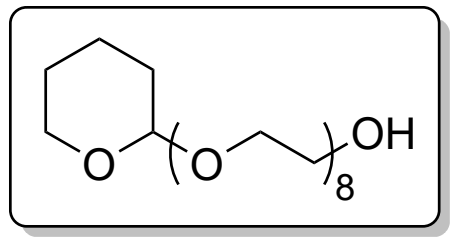


¹³C (101 MHz, CDCl₃) ThpO–Eg₄–OTs (**53**)



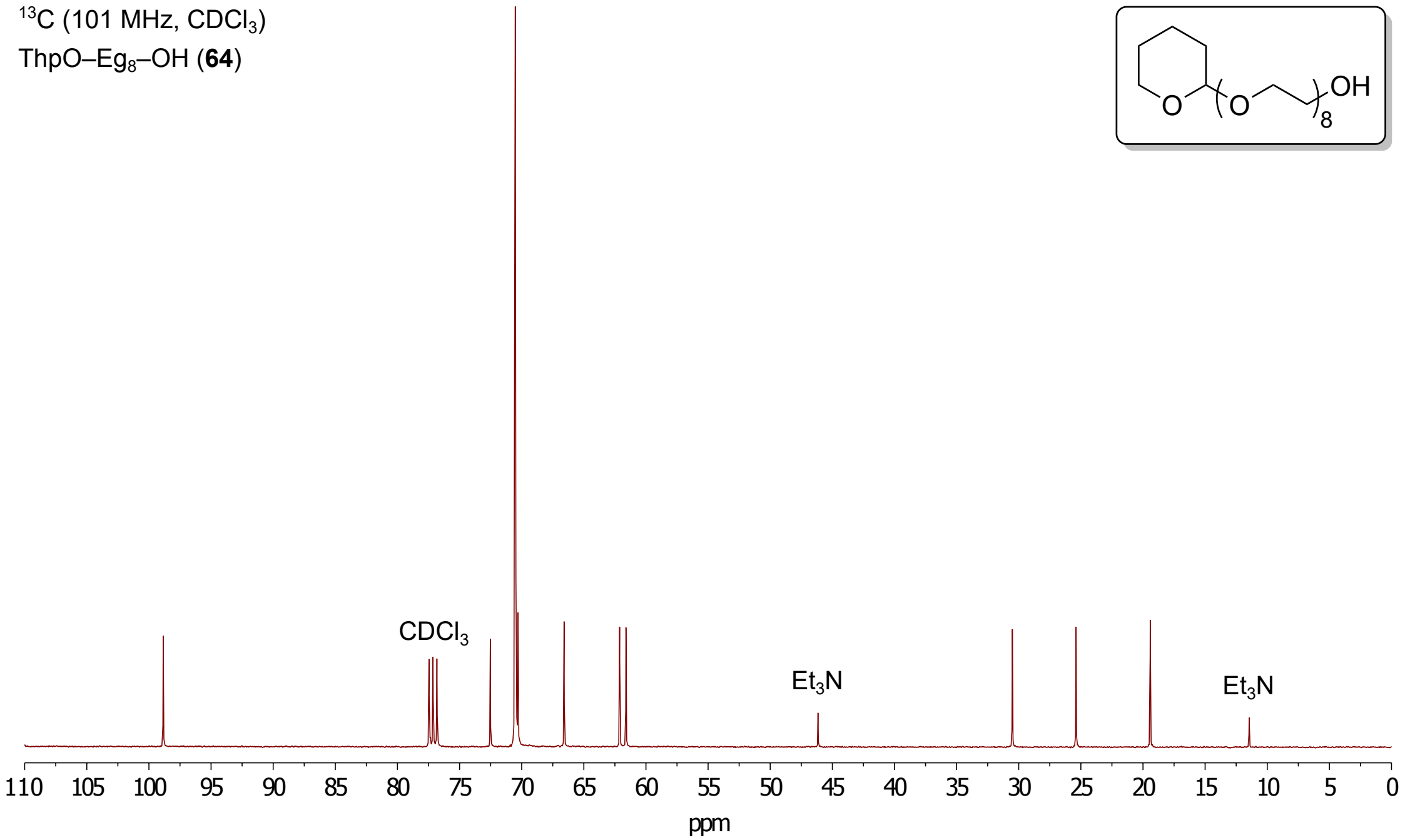
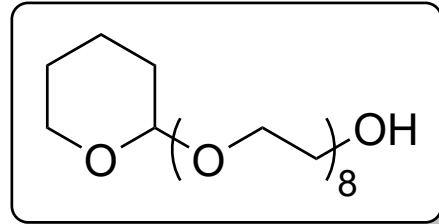
^1H (400 MHz, CDCl_3)

ThpO-Eg₈-OH (**64**)



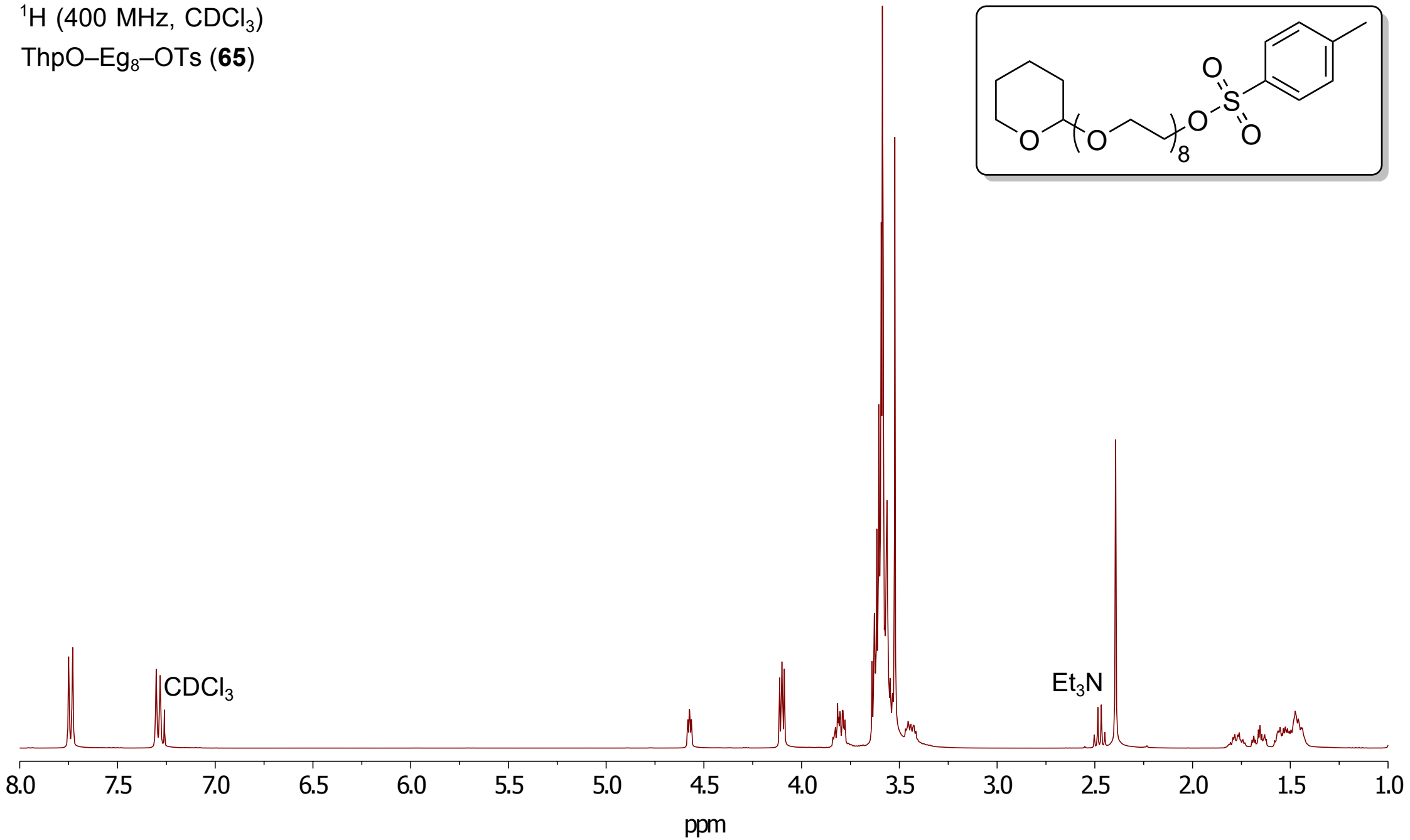
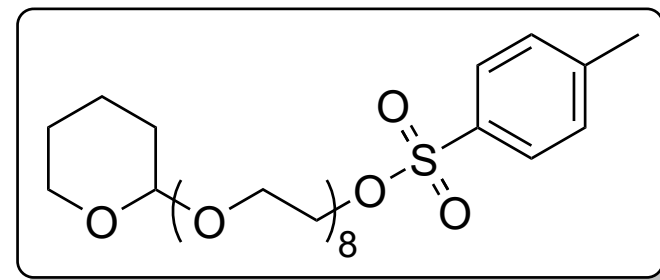
^{13}C (101 MHz, CDCl_3)

ThpO-Eg₈-OH (**64**)



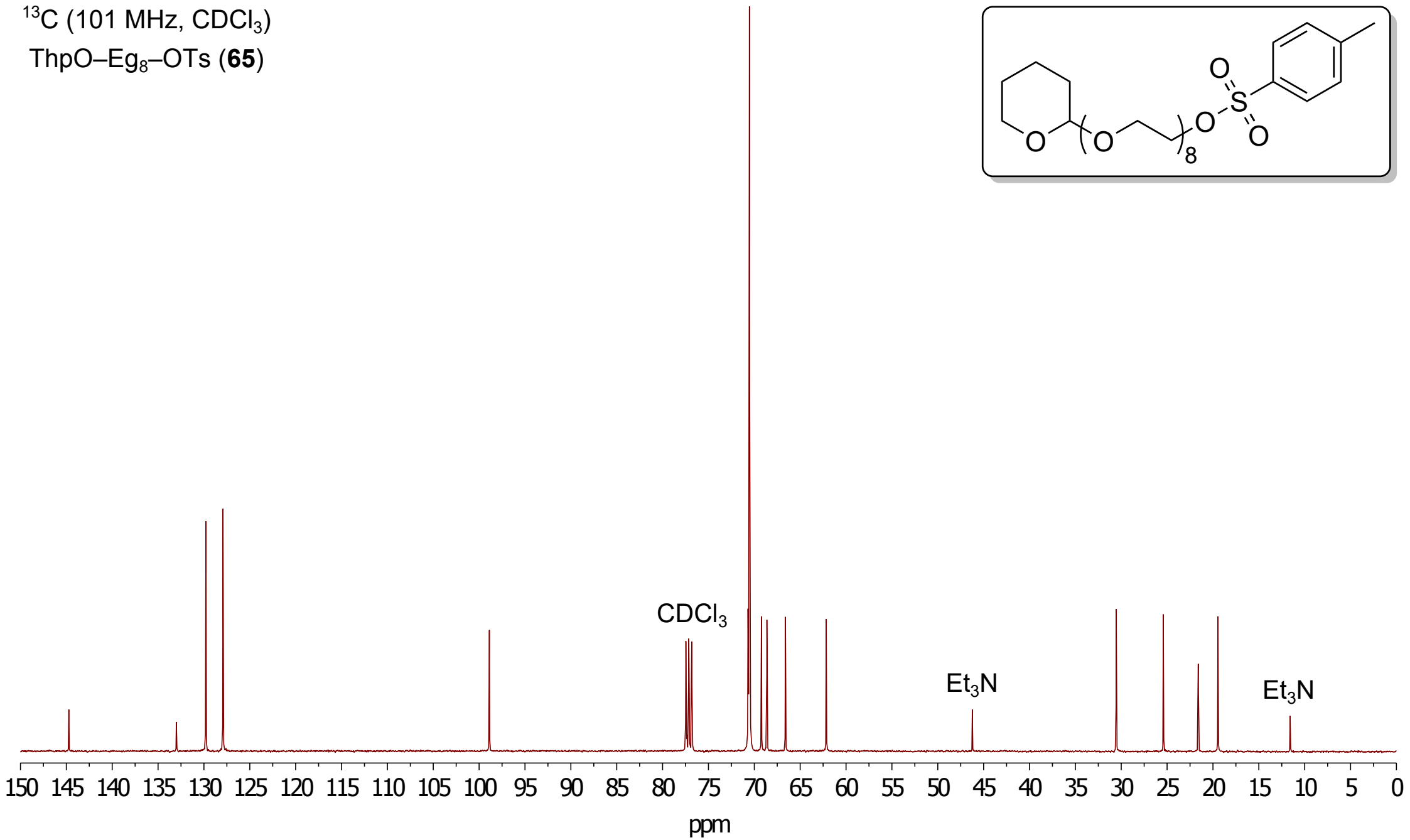
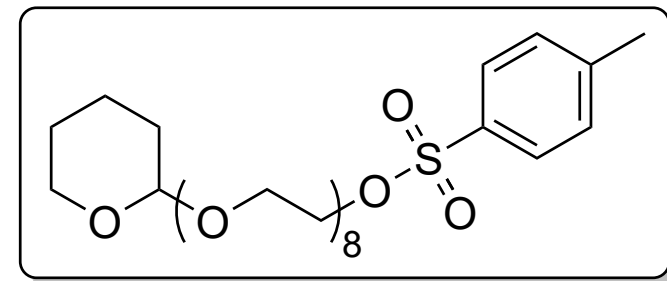
^1H (400 MHz, CDCl_3)

ThpO-Eg₈-OTs (**65**)



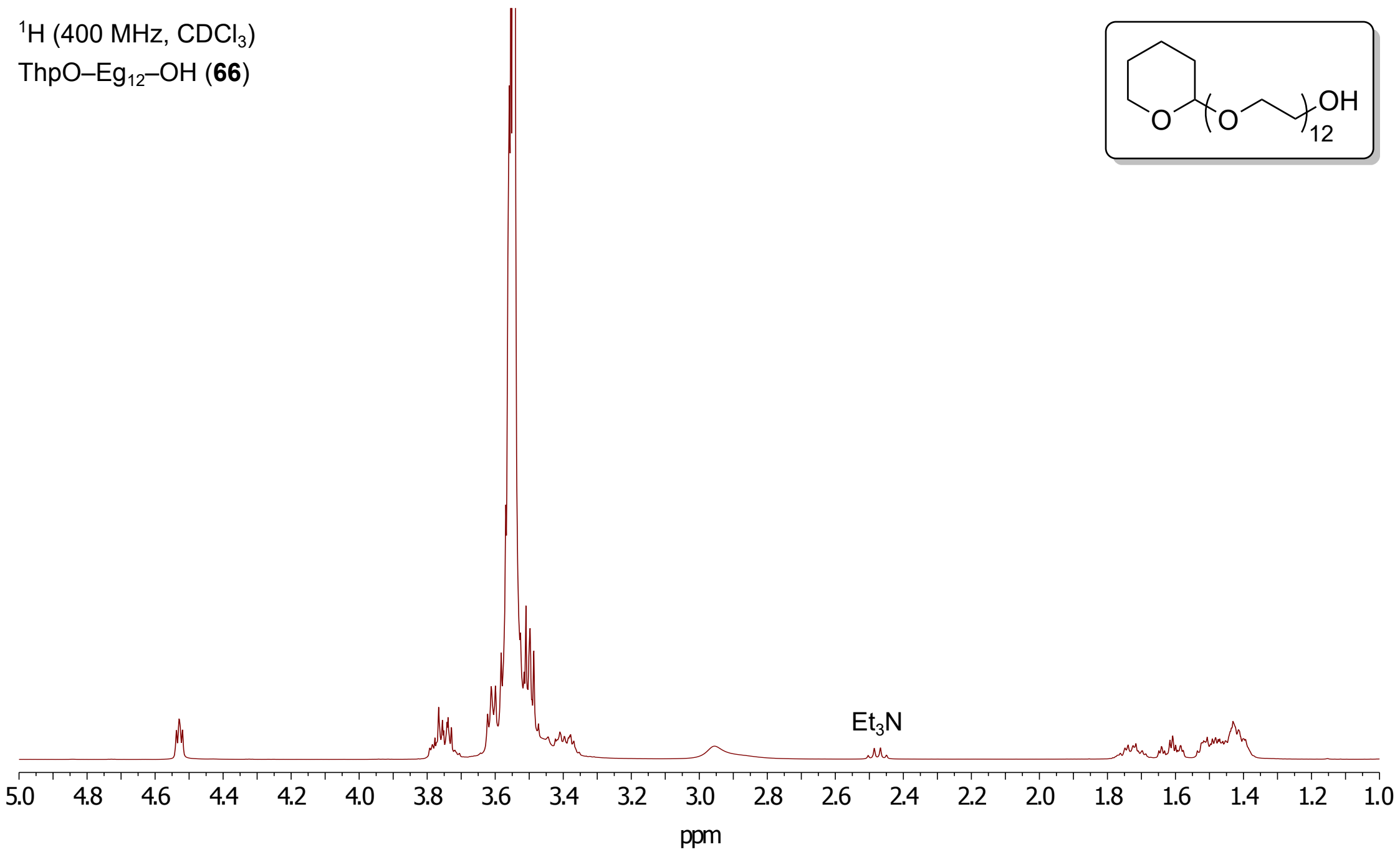
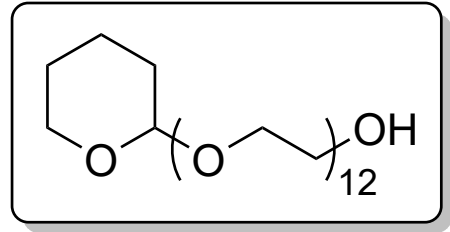
^{13}C (101 MHz, CDCl_3)

ThpO-Eg₈-OTs (**65**)



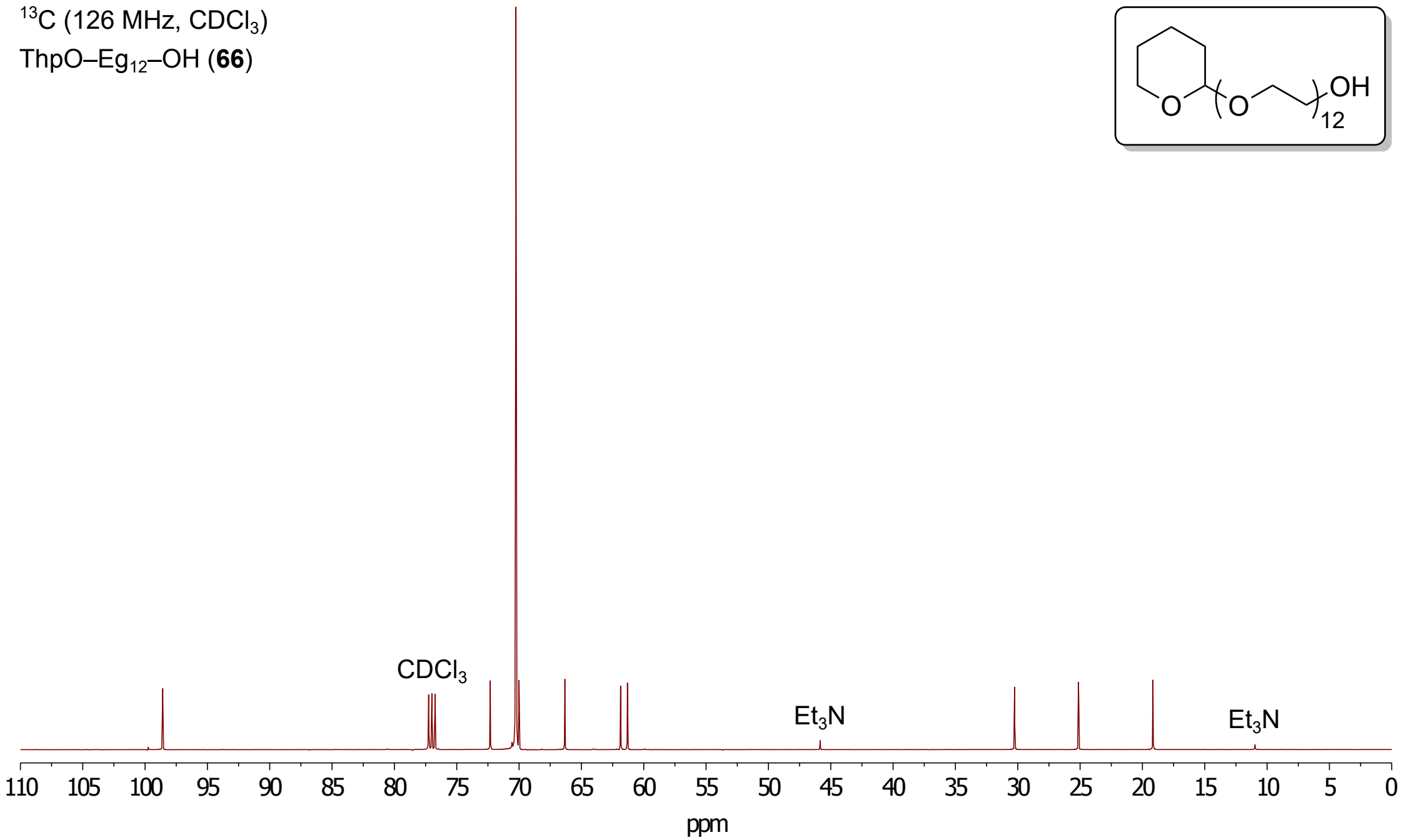
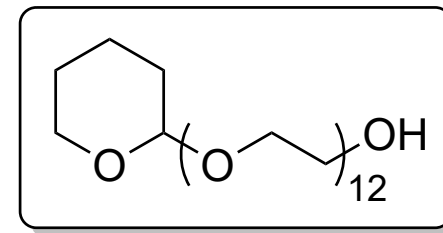
^1H (400 MHz, CDCl_3)

ThpO-Eg₁₂-OH (**66**)

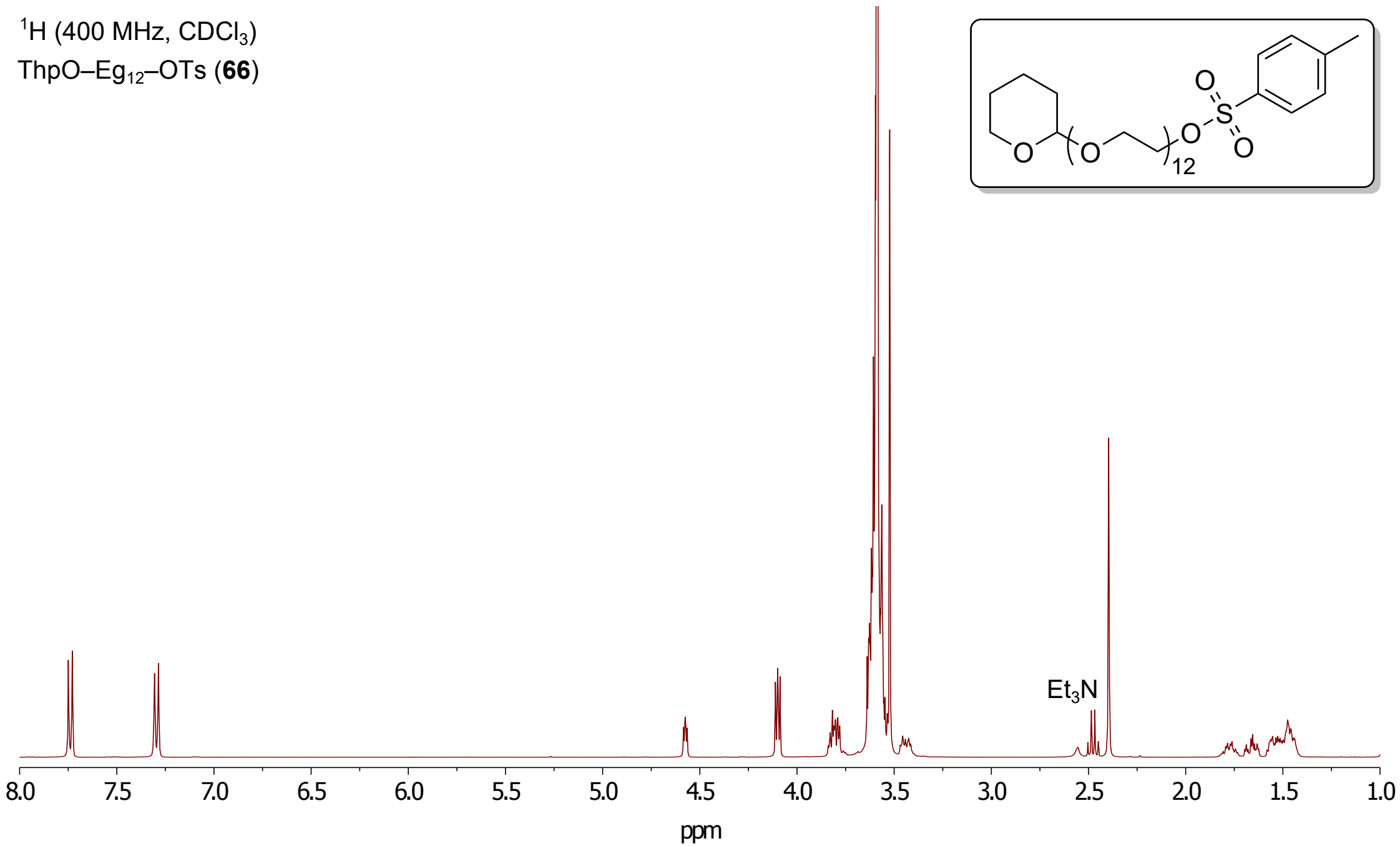
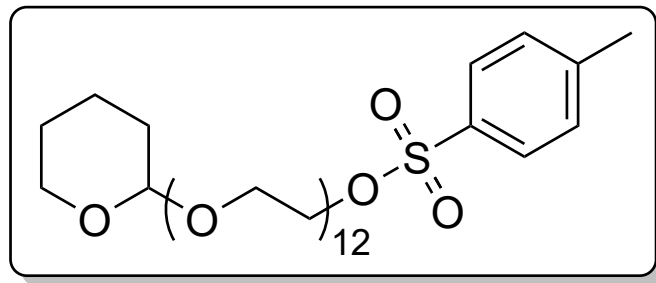


^{13}C (126 MHz, CDCl_3)

ThpO-Eg₁₂-OH (**66**)

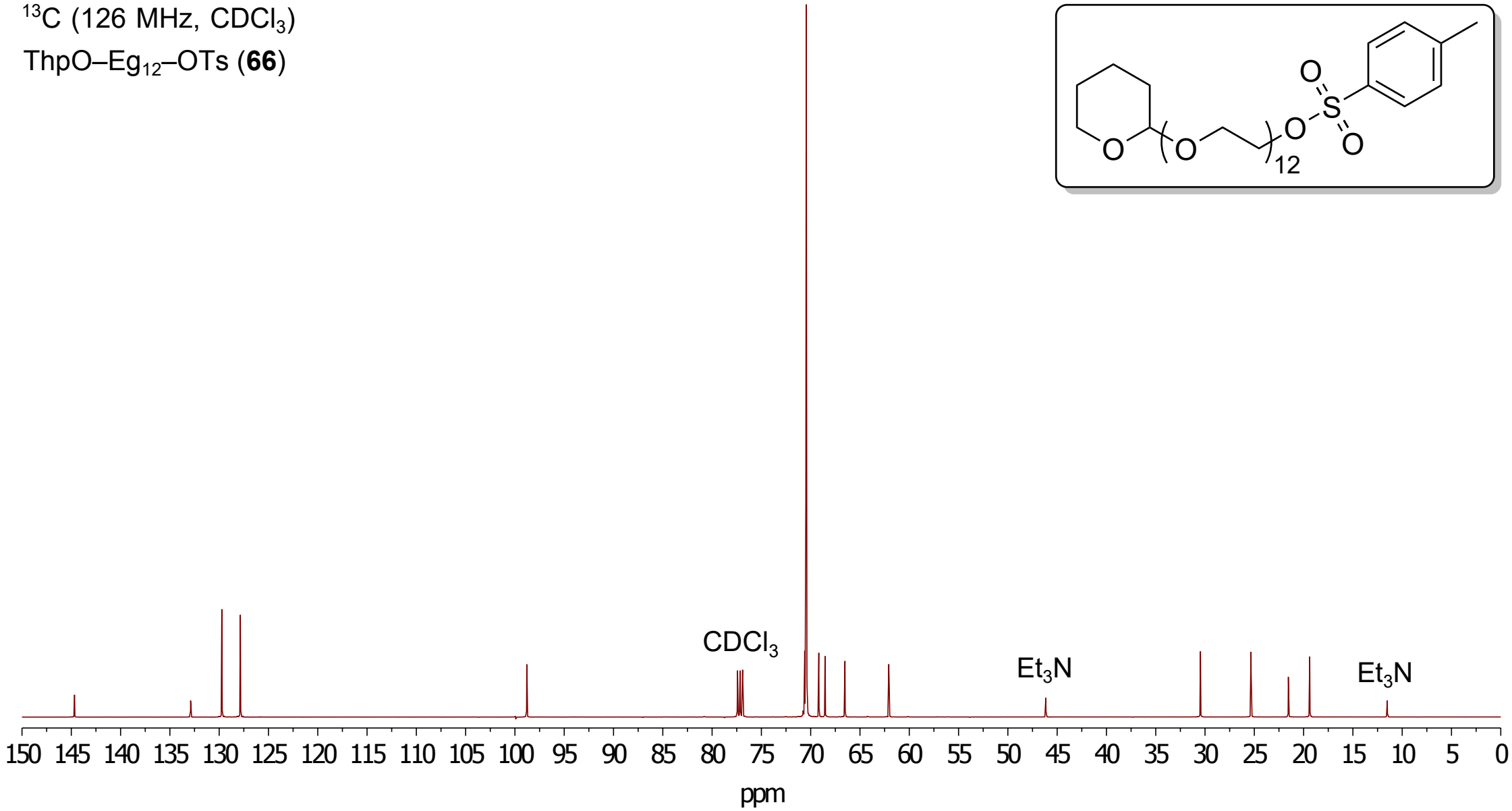
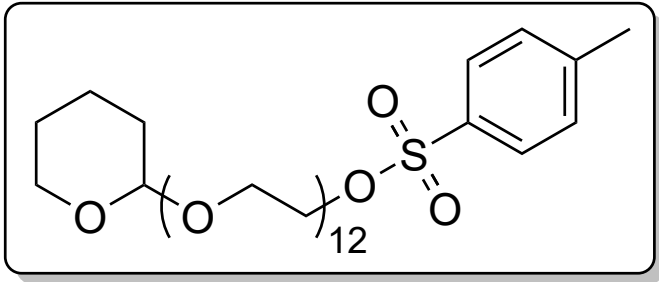


^1H (400 MHz, CDCl_3)
ThpO–Eg₁₂–OTs (**66**)

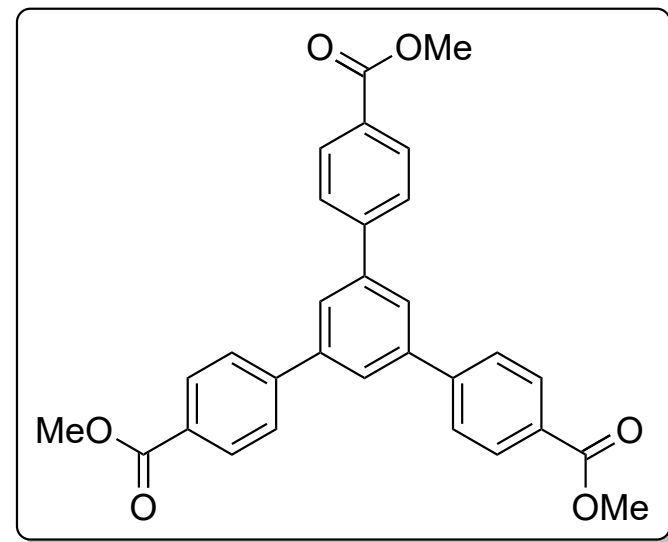
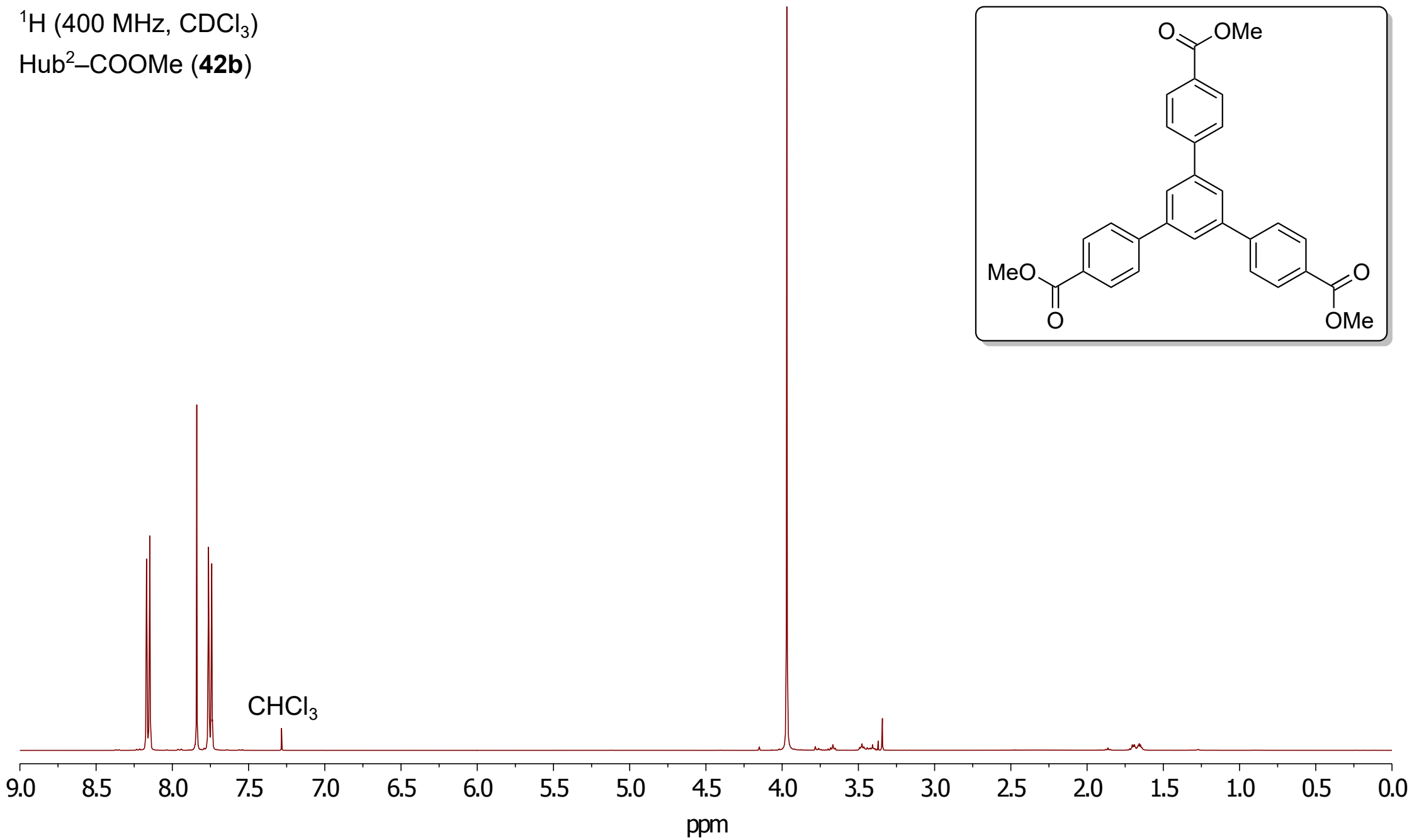


^{13}C (126 MHz, CDCl_3)

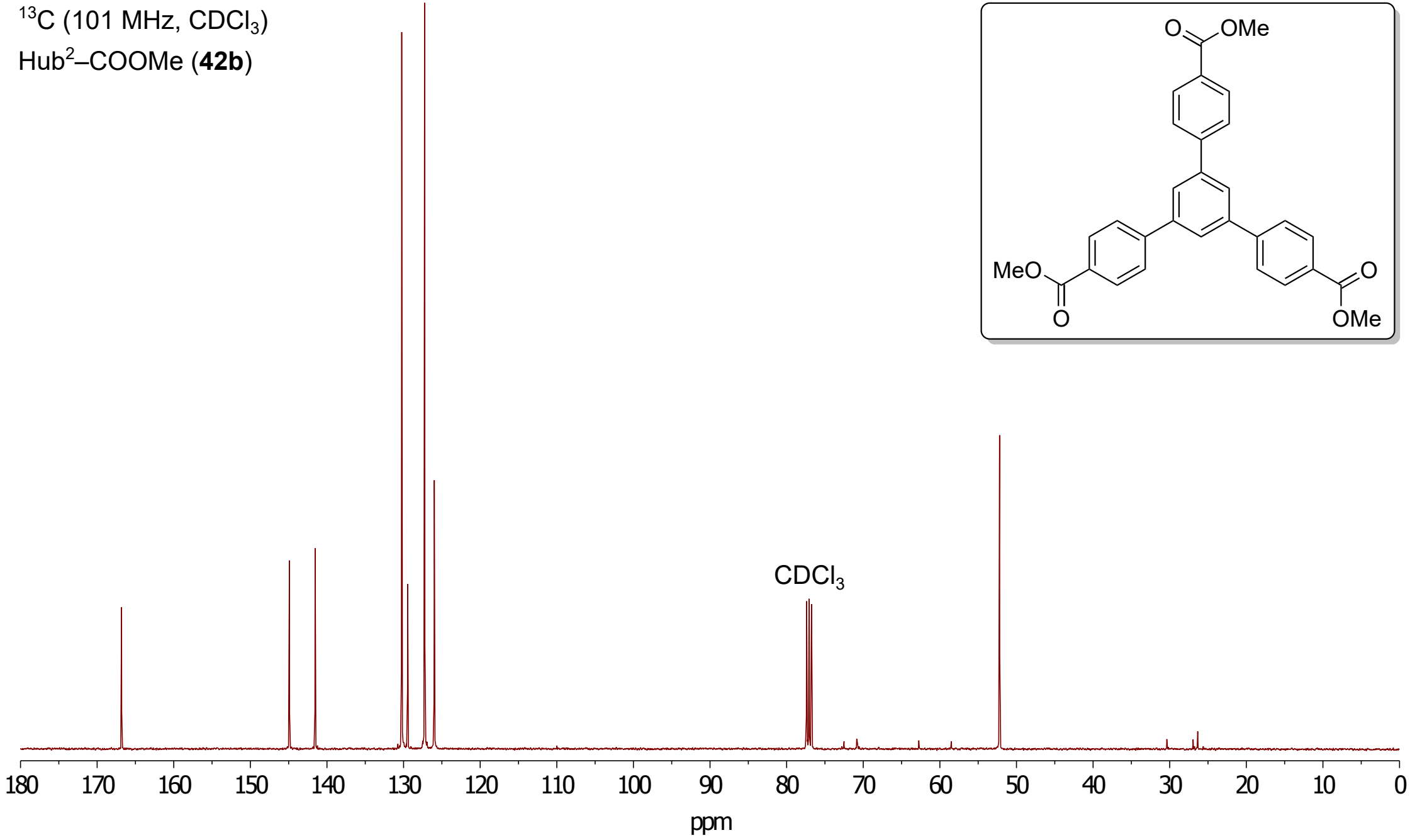
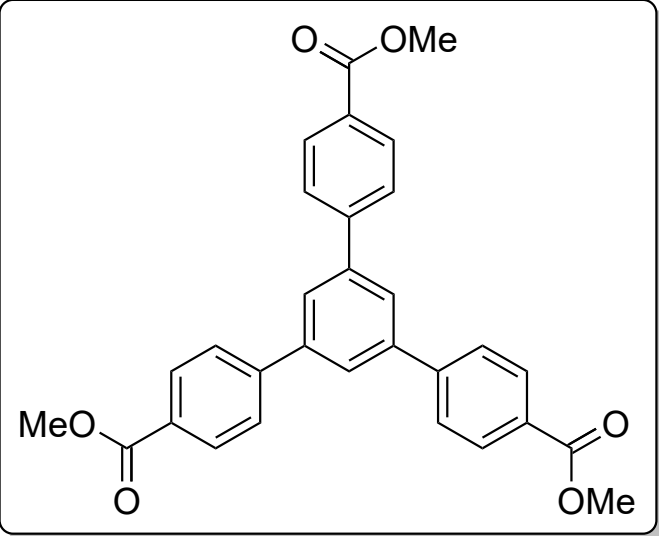
ThpO-Eg₁₂-OTs (**66**)



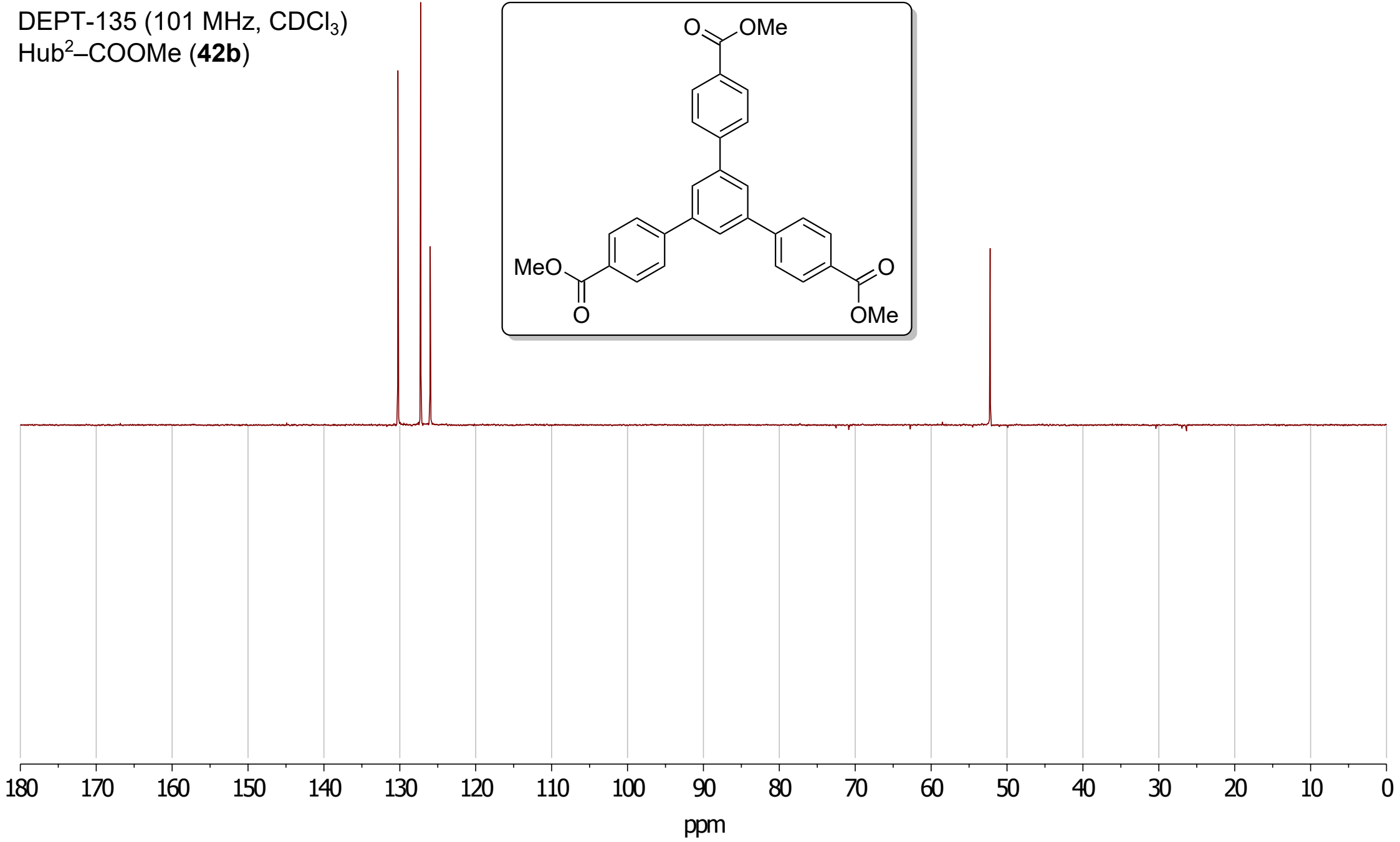
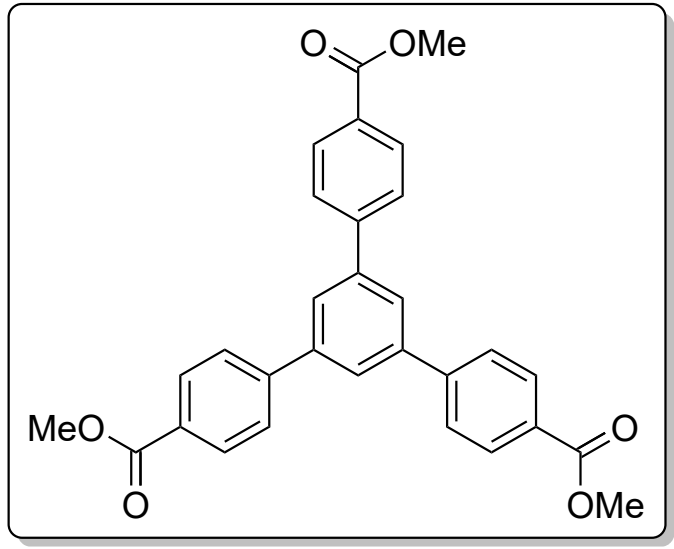
^1H (400 MHz, CDCl_3)
Hub²-COOMe (**42b**)



^{13}C (101 MHz, CDCl_3)
Hub²-COOMe (**42b**)

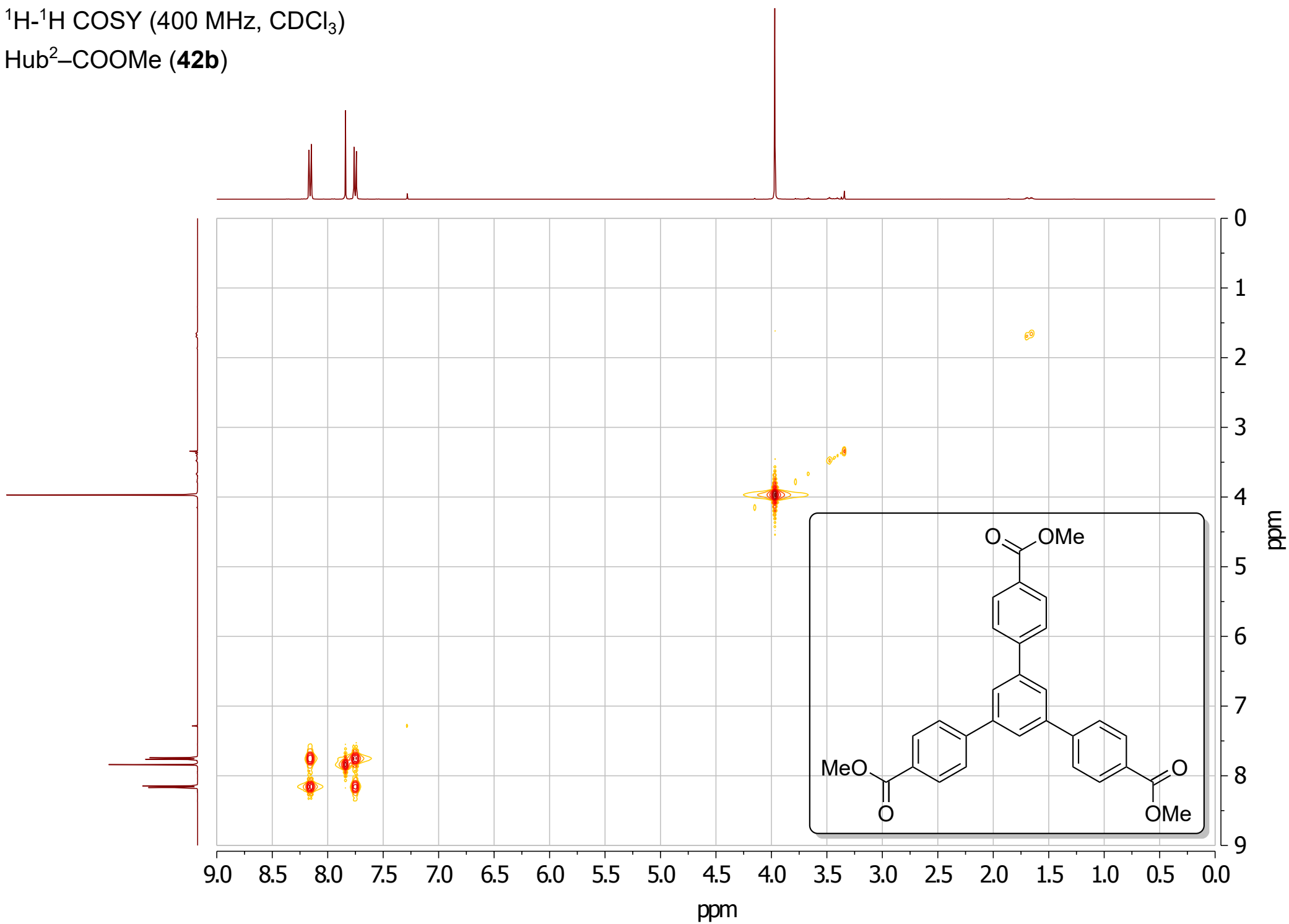


DEPT-135 (101 MHz, CDCl₃)
Hub²-COOMe (**42b**)



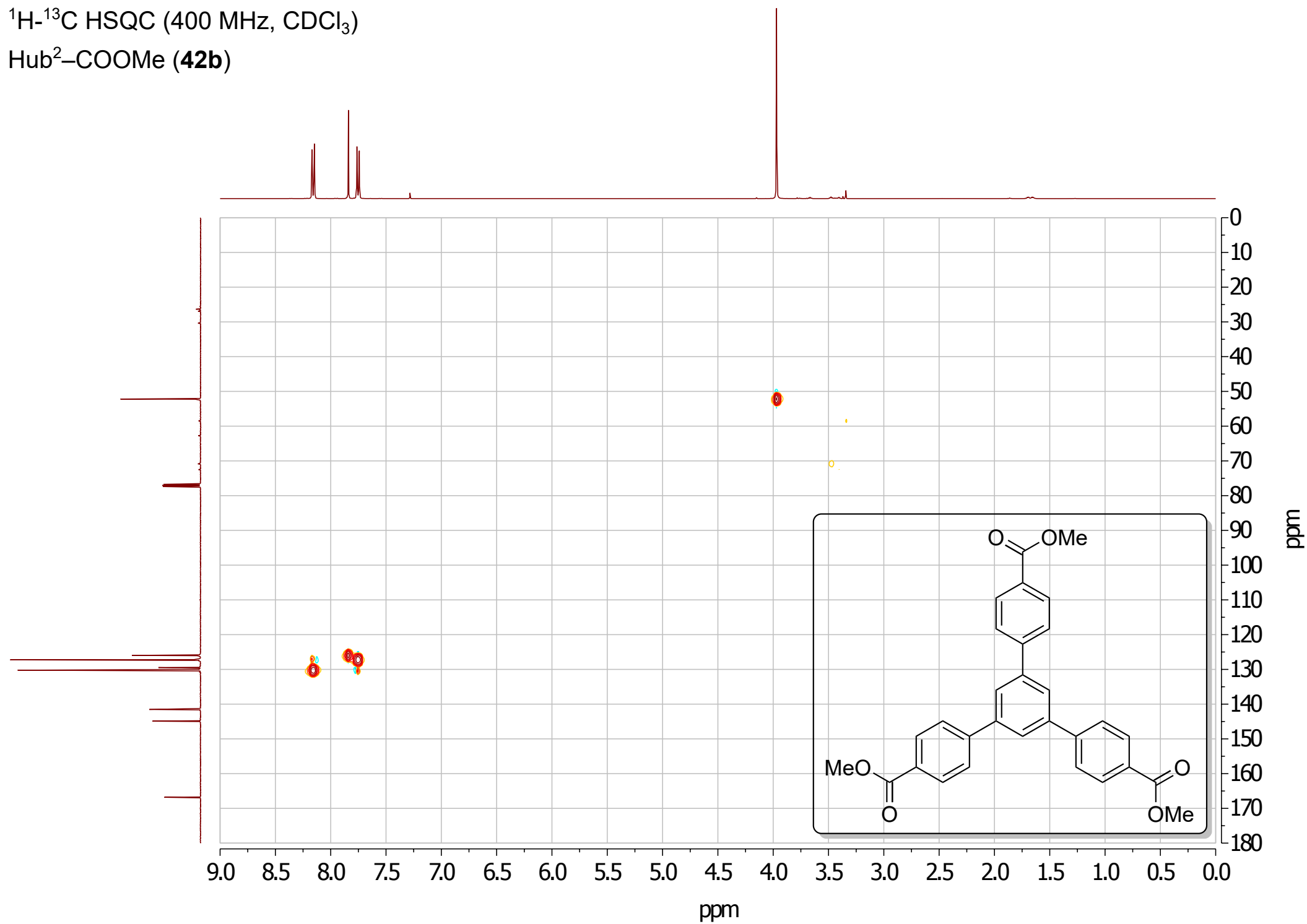
^1H - ^1H COSY (400 MHz, CDCl_3)

Hub²-COOMe (**42b**)



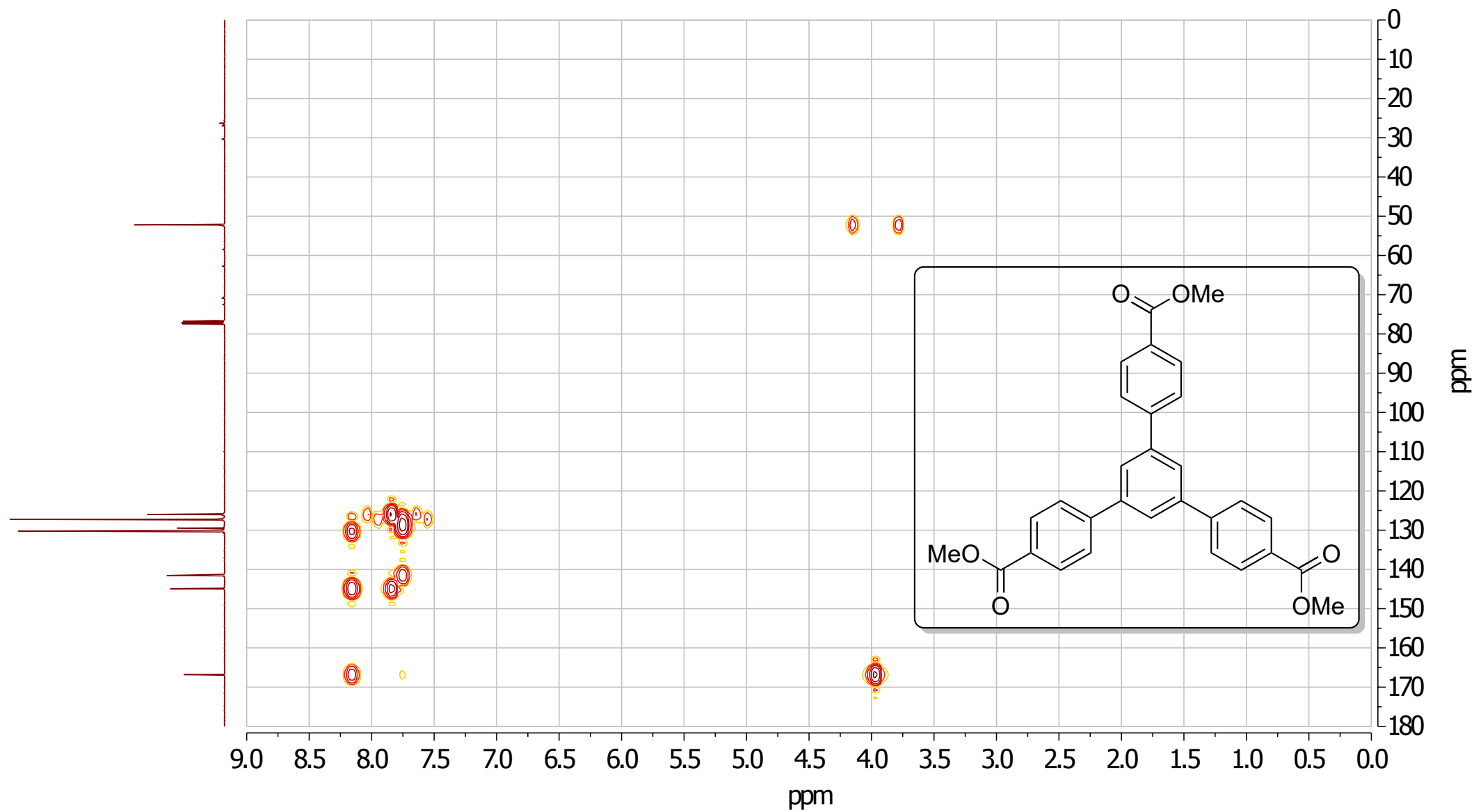
^1H - ^{13}C HSQC (400 MHz, CDCl_3)

Hub²-COOMe (**42b**)

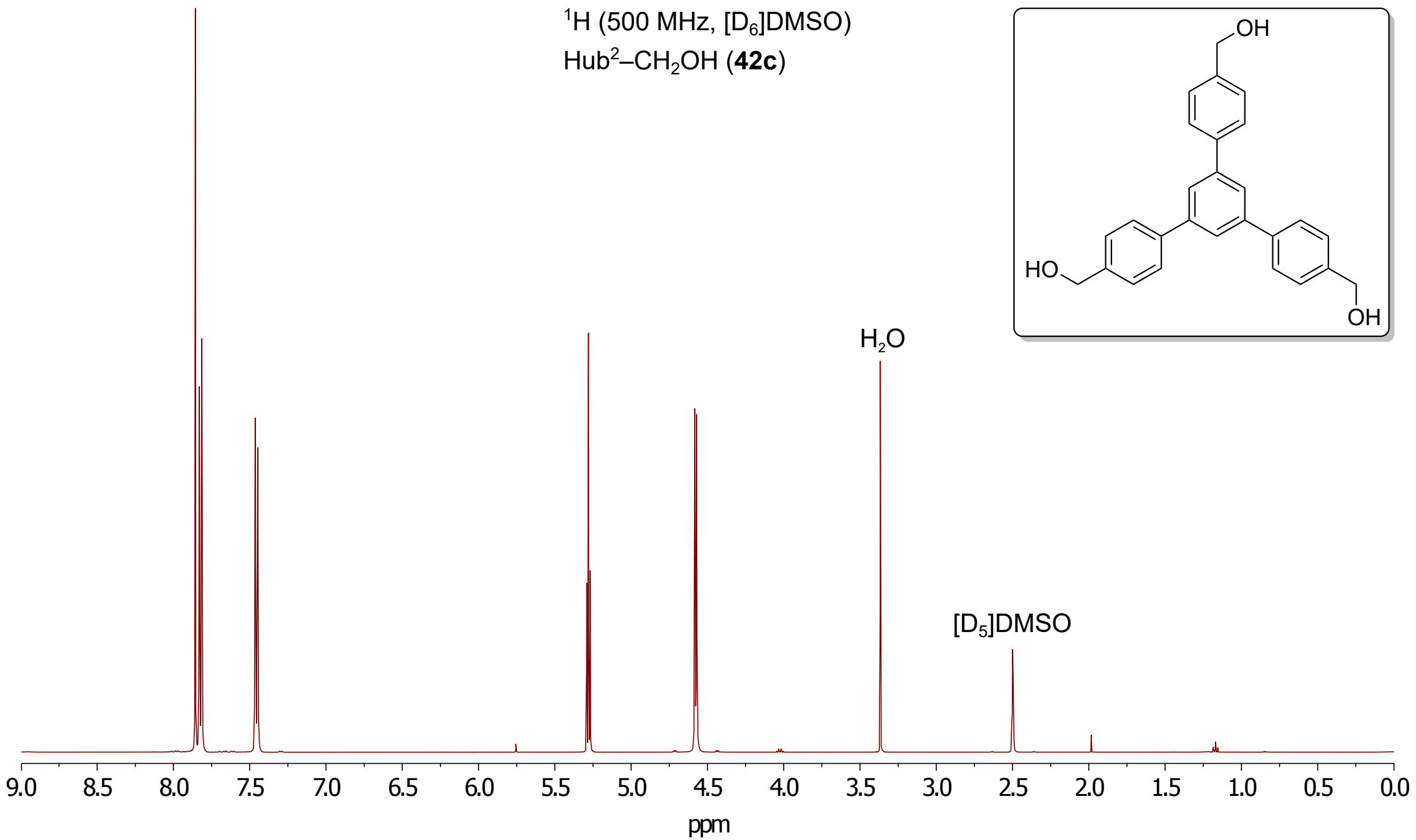
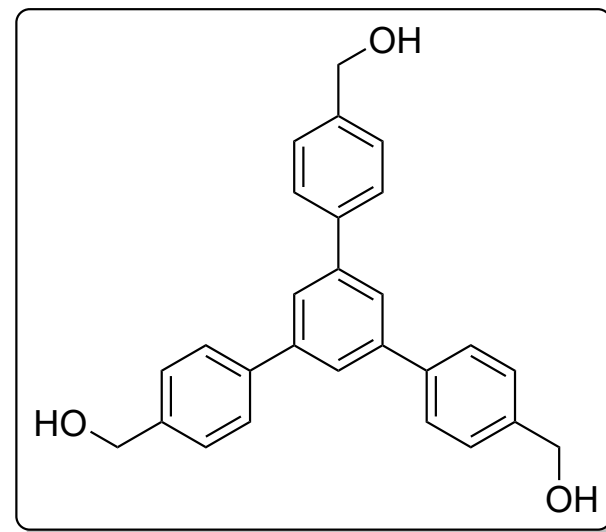


^1H - ^{13}C HMBC (400 MHz, CDCl_3)

Hub²-COOMe (**42b**)

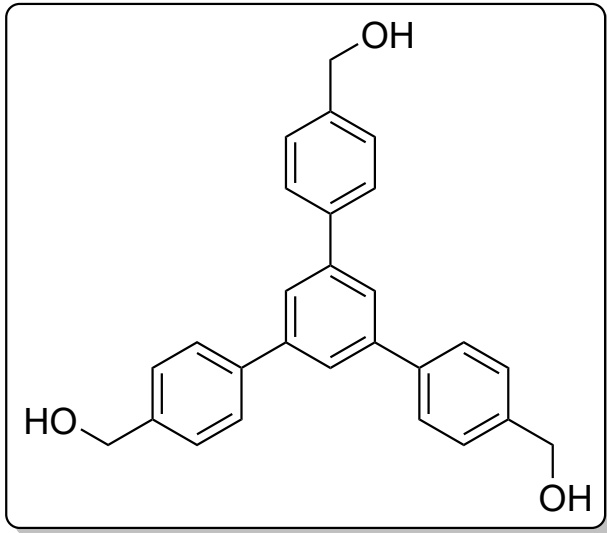


^1H (500 MHz, $[\text{D}_6]\text{DMSO}$)
Hub²-CH₂OH (**42c**)

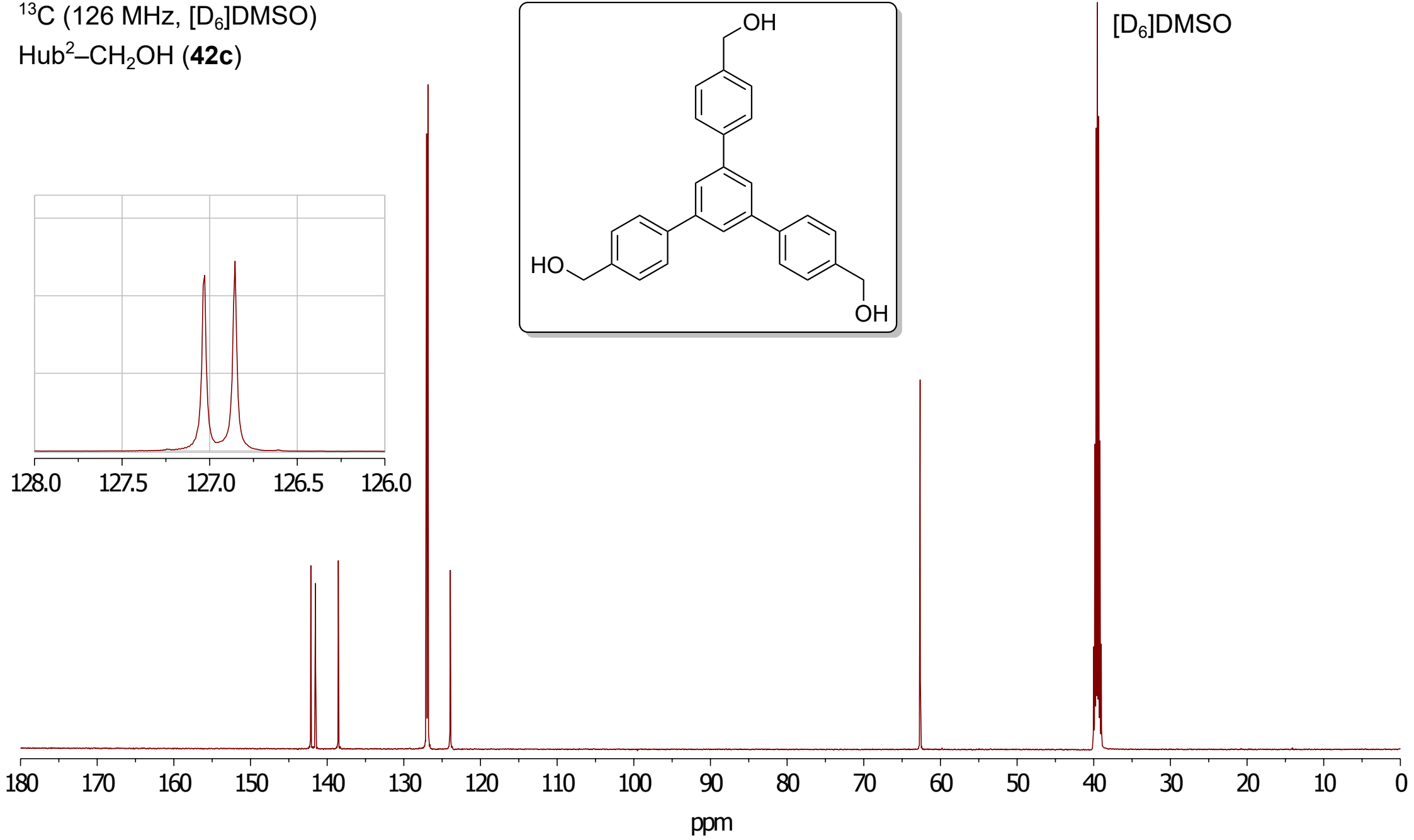
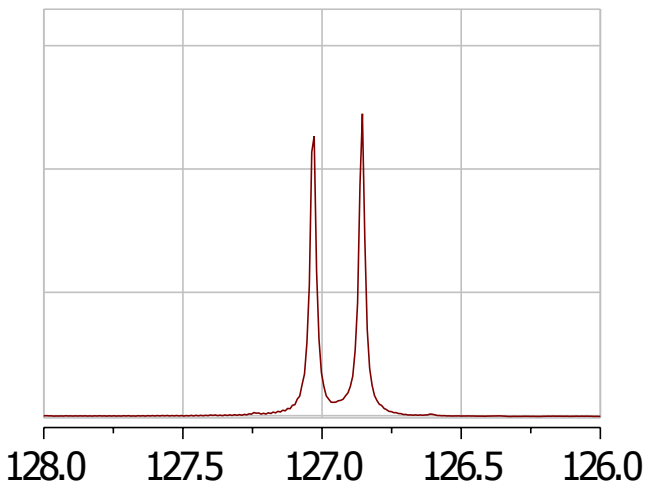


^{13}C (126 MHz, $[\text{D}_6]\text{DMSO}$)

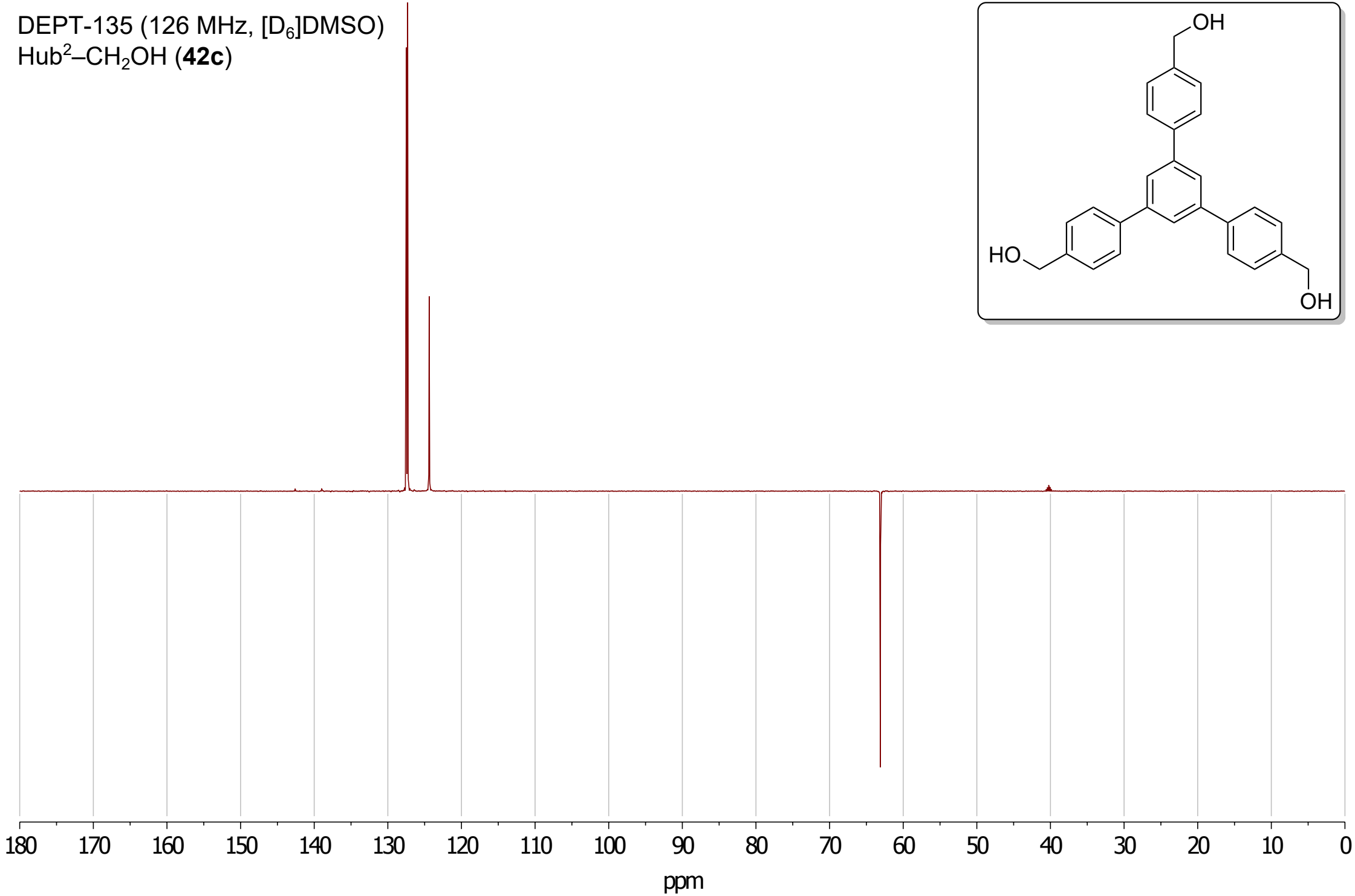
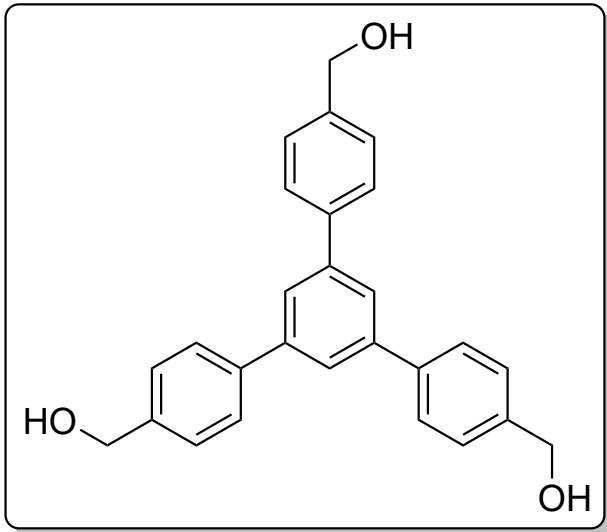
Hub²-CH₂OH (**42c**)



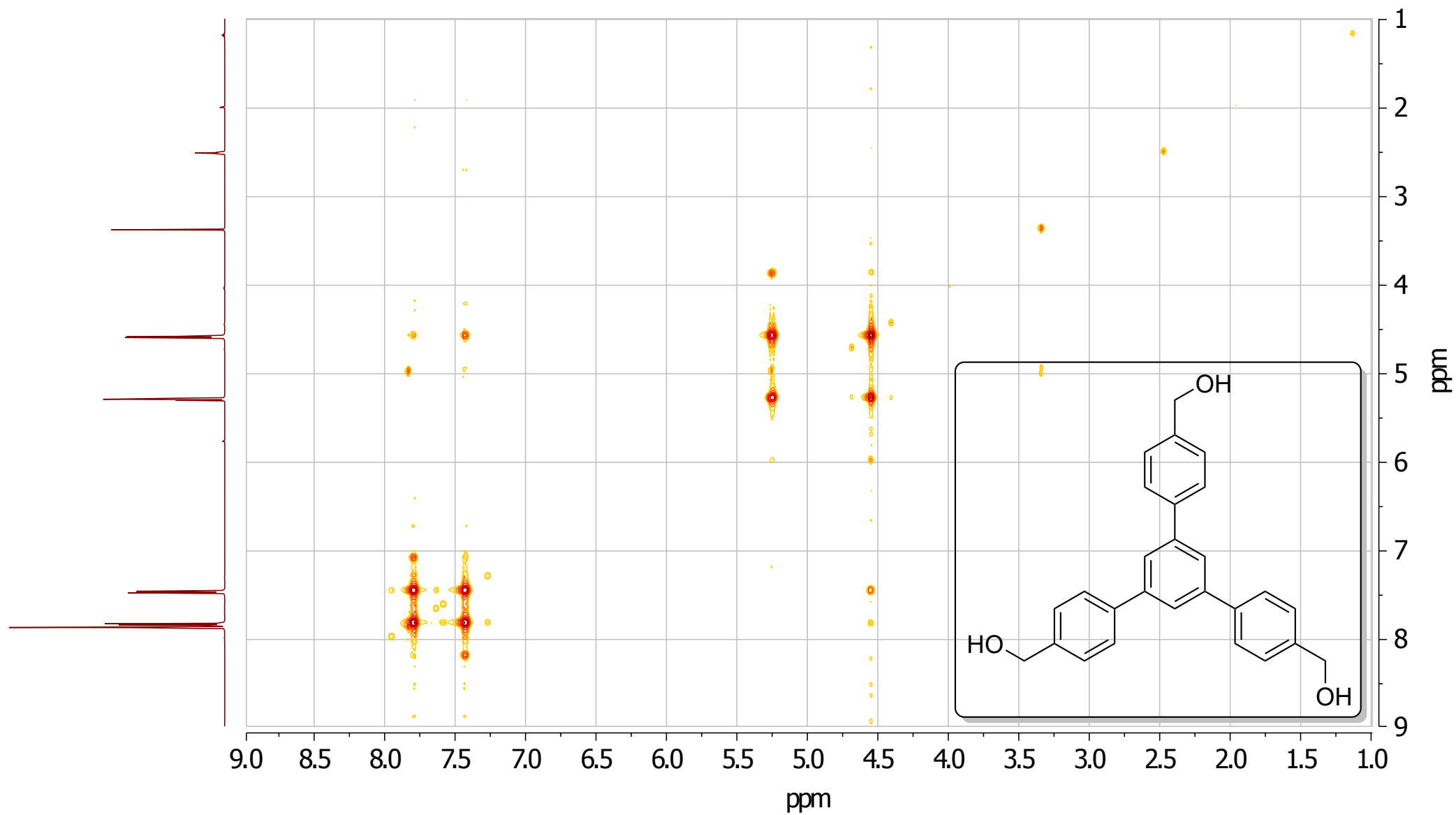
$[\text{D}_6]\text{DMSO}$



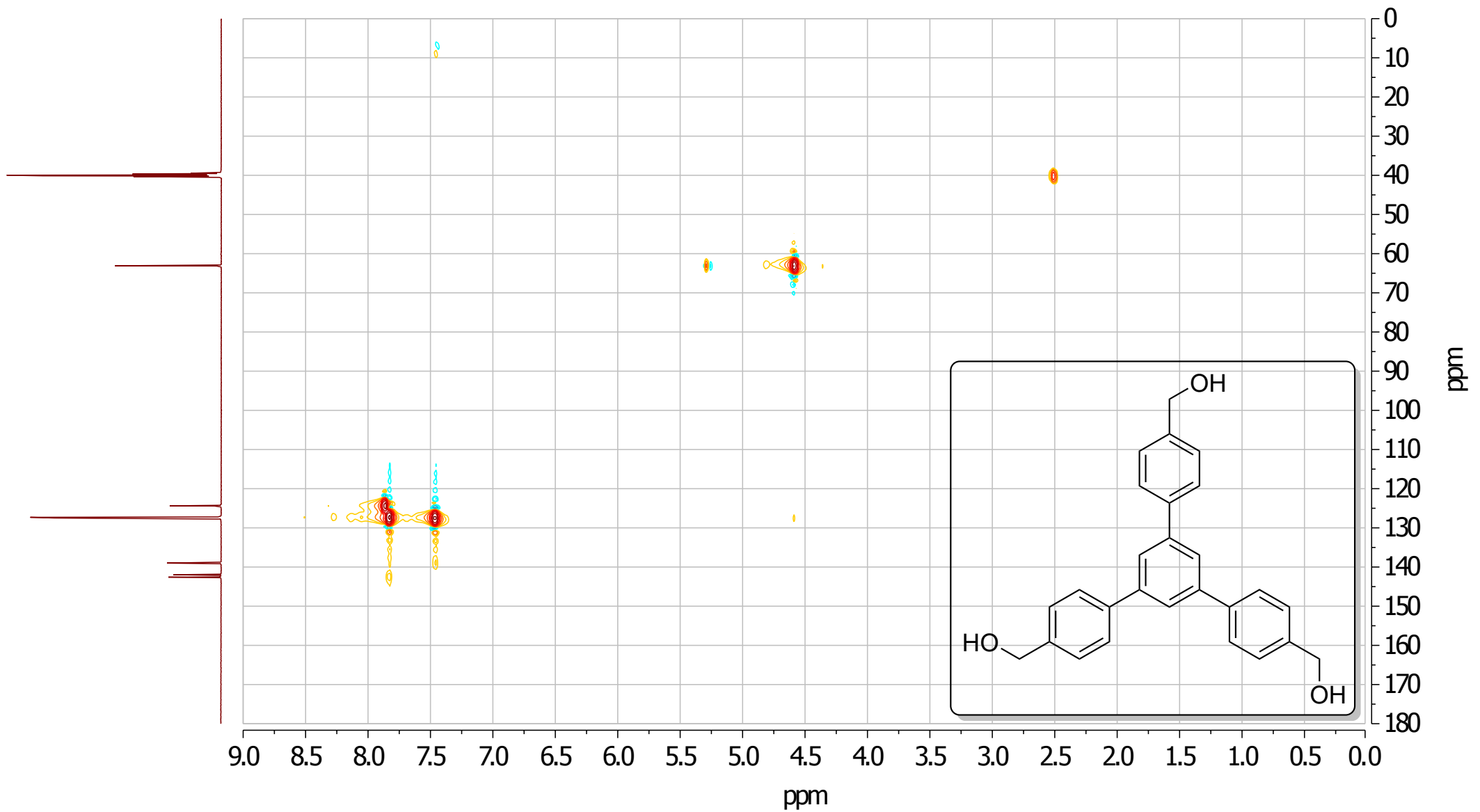
DEPT-135 (126 MHz, [D₆]DMSO)
Hub²-CH₂OH (**42c**)



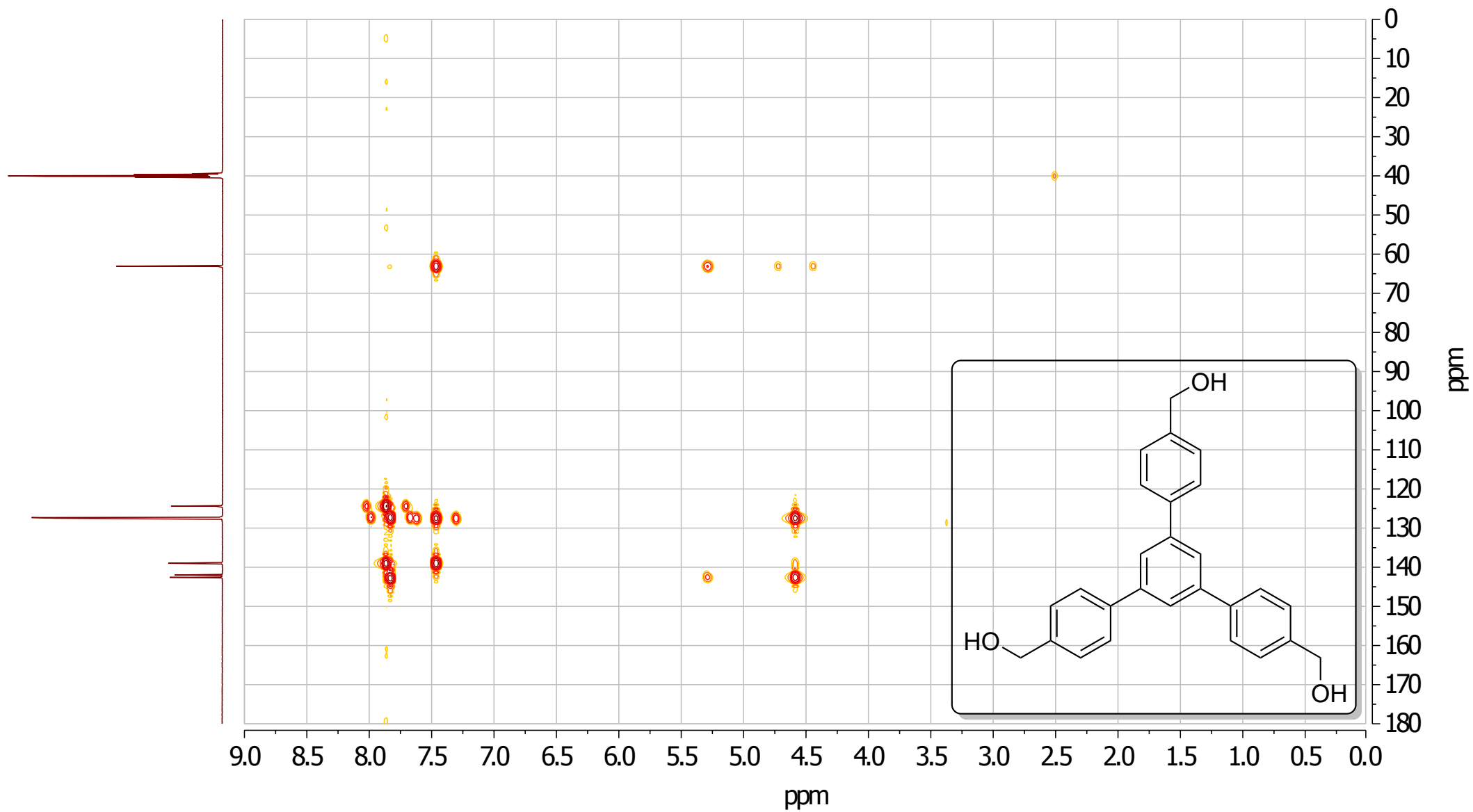
^1H - ^1H COSY (500 MHz, $[\text{D}_6]$ DMSO)
Hub²-CH₂OH (**42c**)



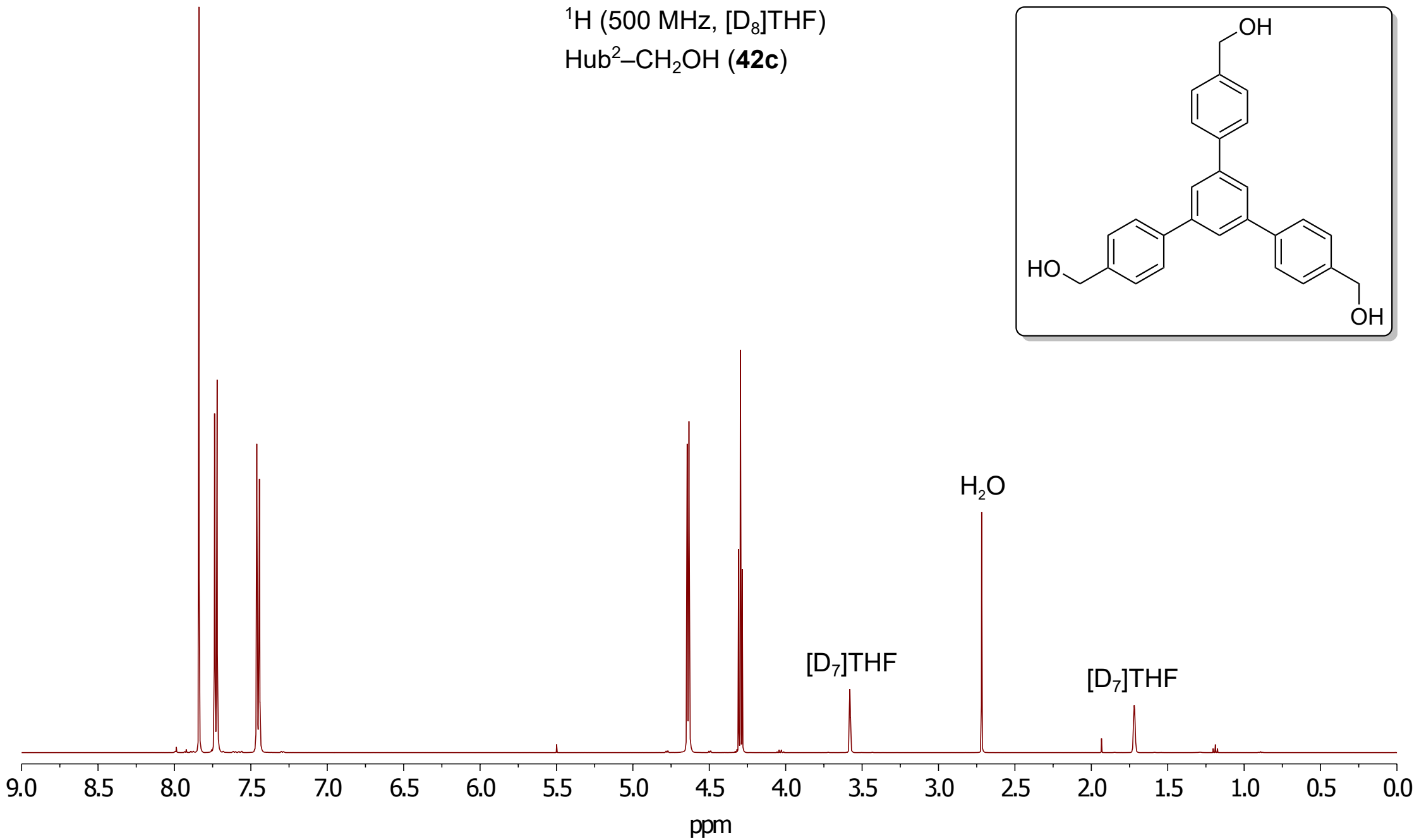
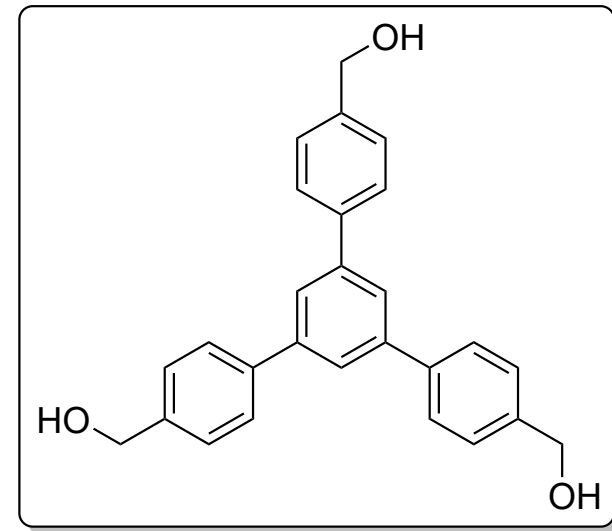
^1H - ^{13}C HSQC (500 MHz, $[\text{D}_6]\text{DMSO}$)
Hub²-CH₂OH (**42c**)



^1H - ^{13}C HMBC (500 MHz, $[\text{D}_6]$ DMSO)
Hub²-CH₂OH (**42c**)

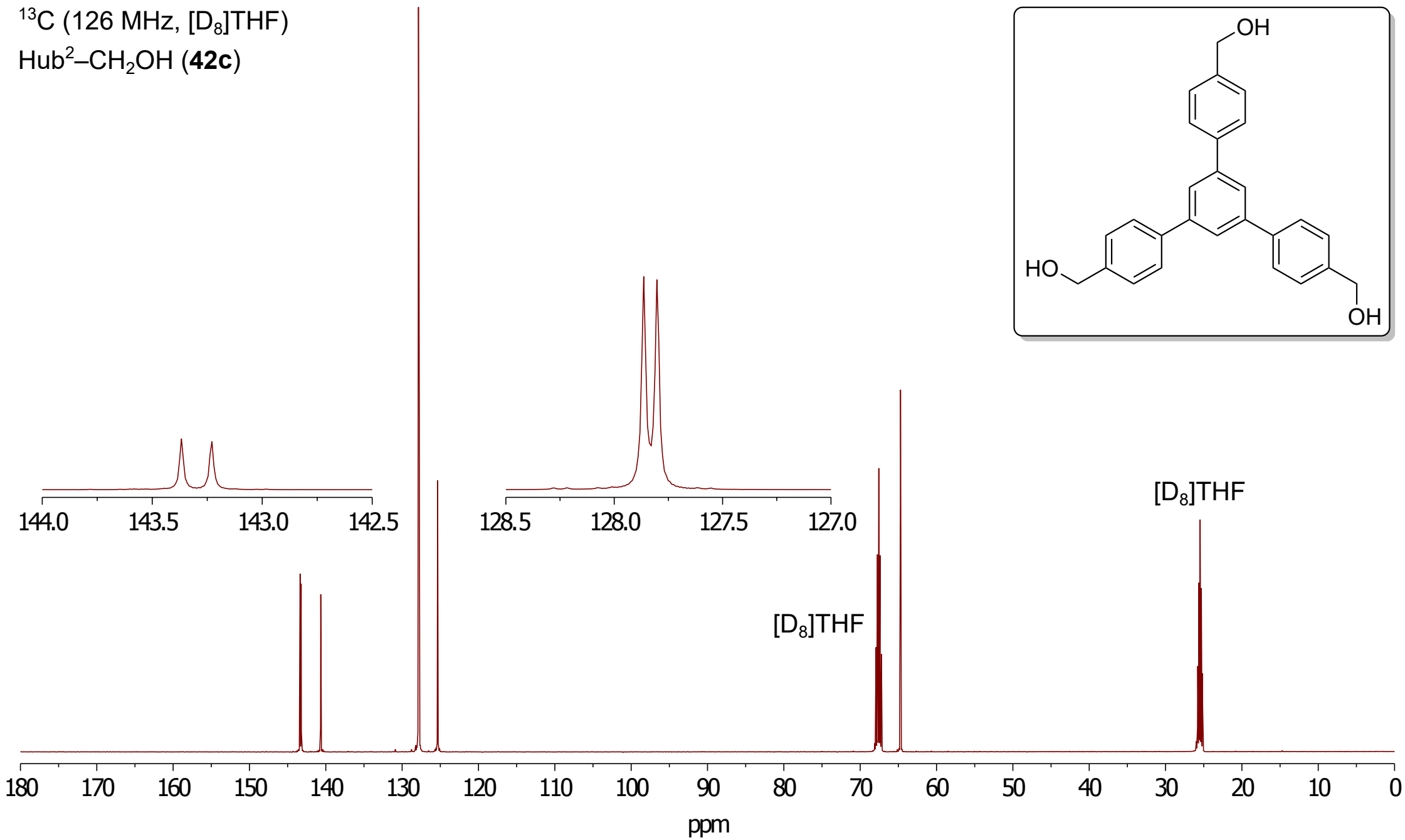
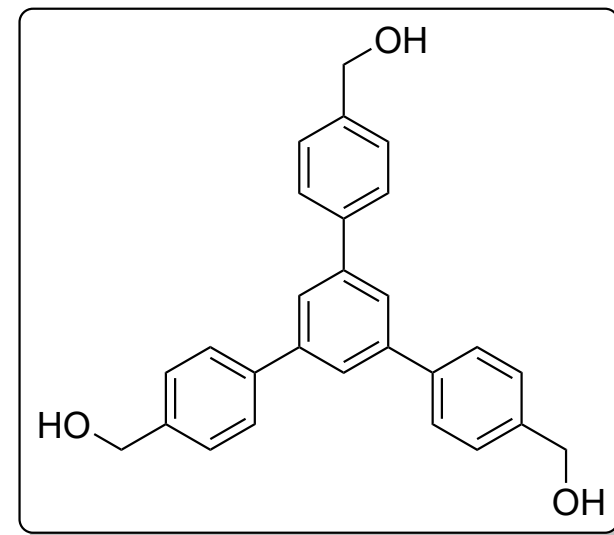


^1H (500 MHz, $[\text{D}_8]\text{THF}$)
Hub²-CH₂OH (**42c**)

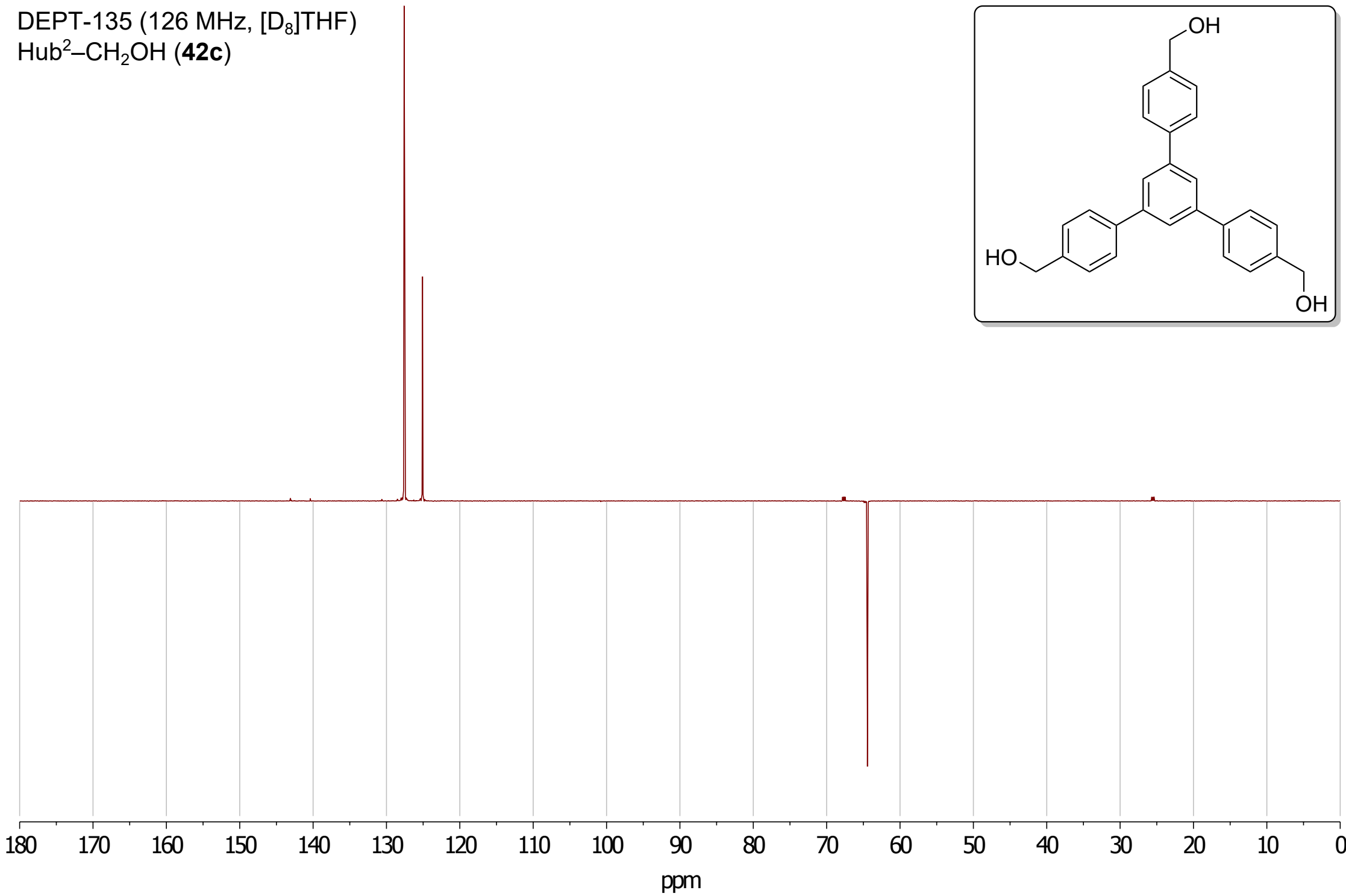
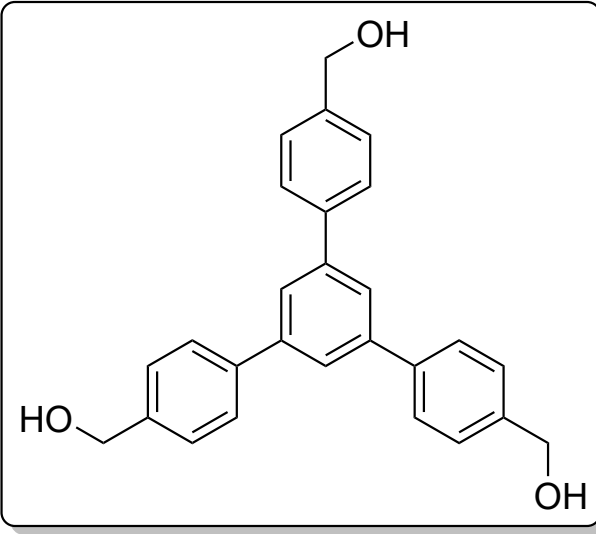


^{13}C (126 MHz, $[\text{D}_8]\text{THF}$)

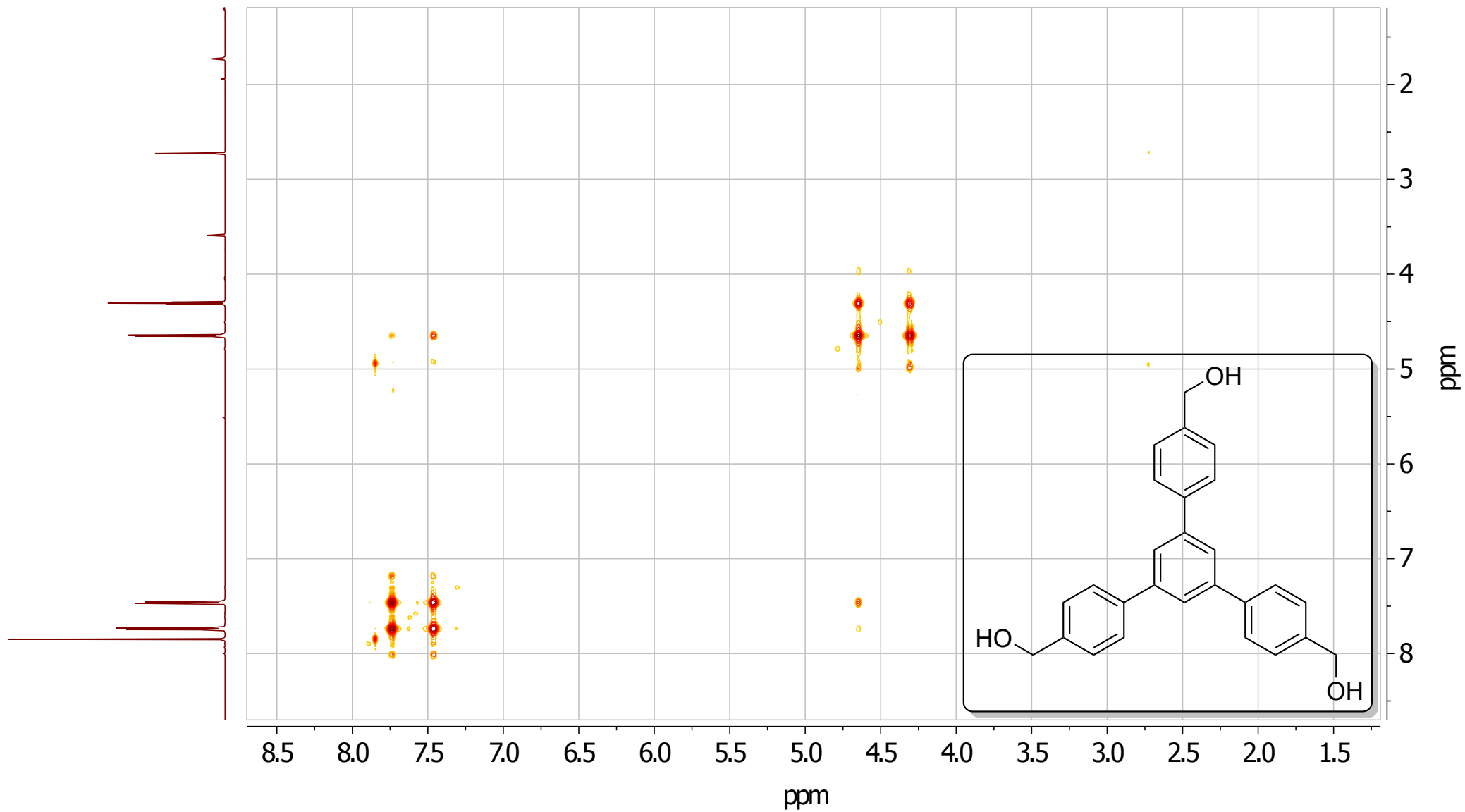
Hub²-CH₂OH (**42c**)



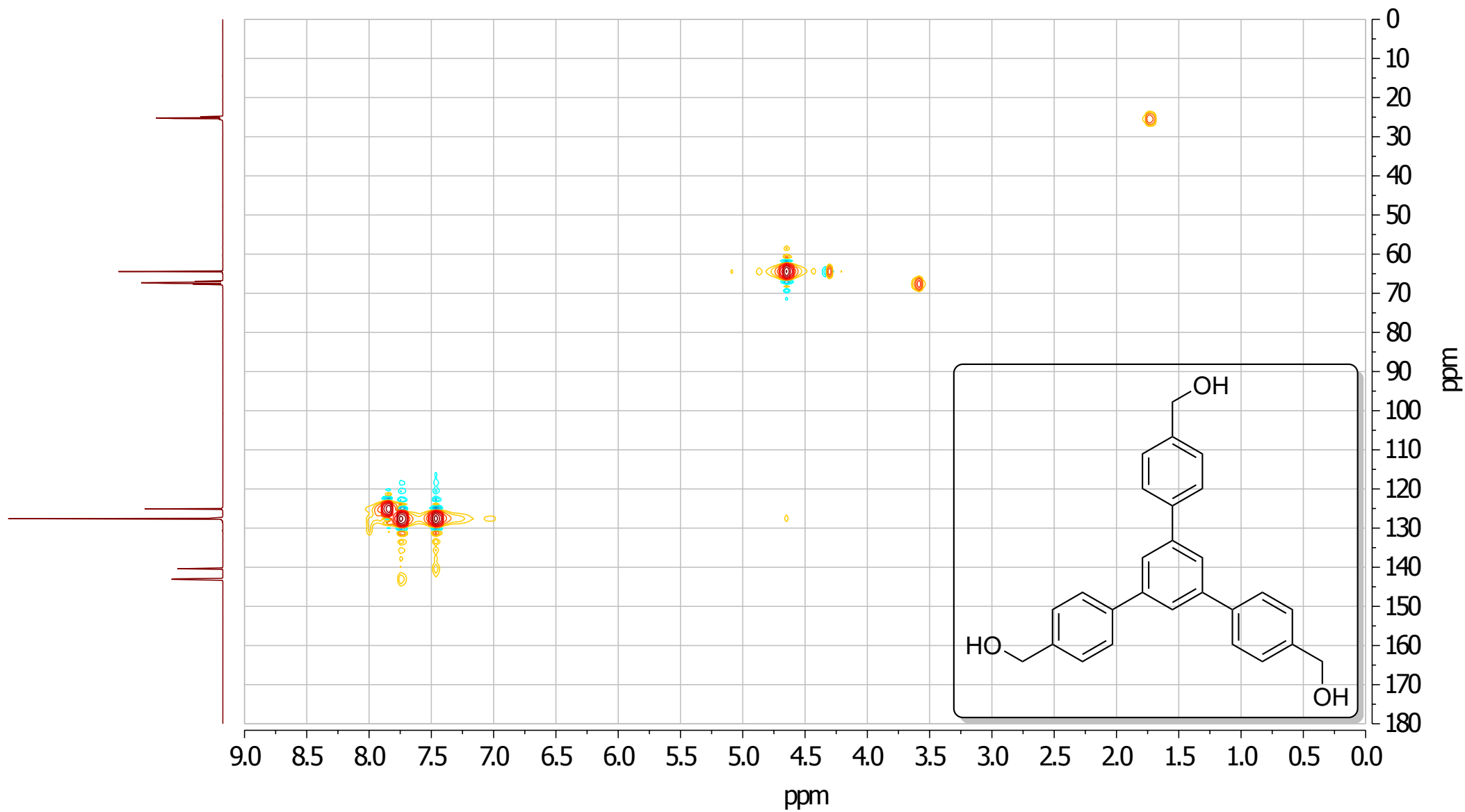
DEPT-135 (126 MHz, [D₈]THF)
Hub²-CH₂OH (**42c**)



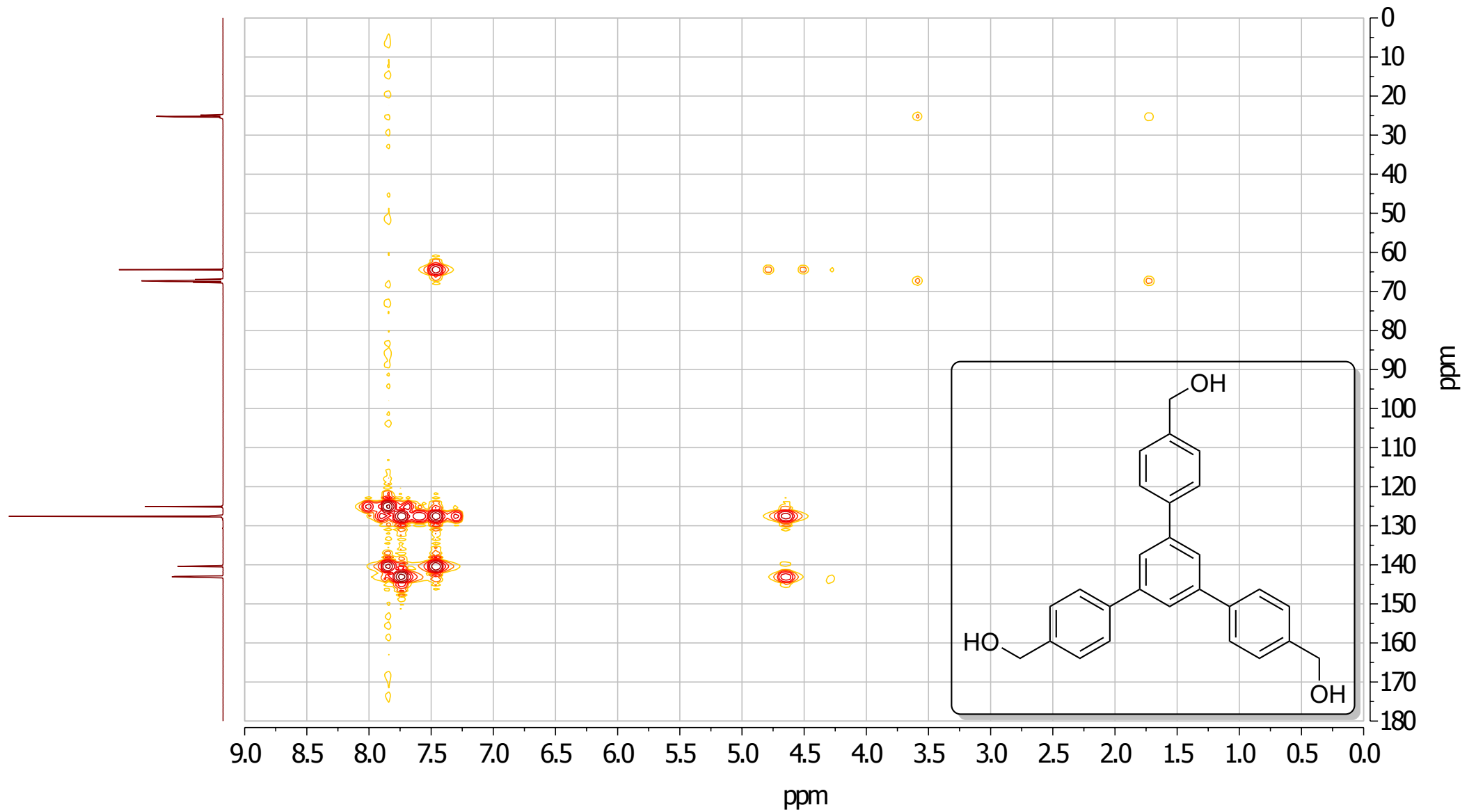
^1H - ^1H COSY (500 MHz, $[\text{D}_8]$ THF)
Hub²-CH₂OH (**42c**)



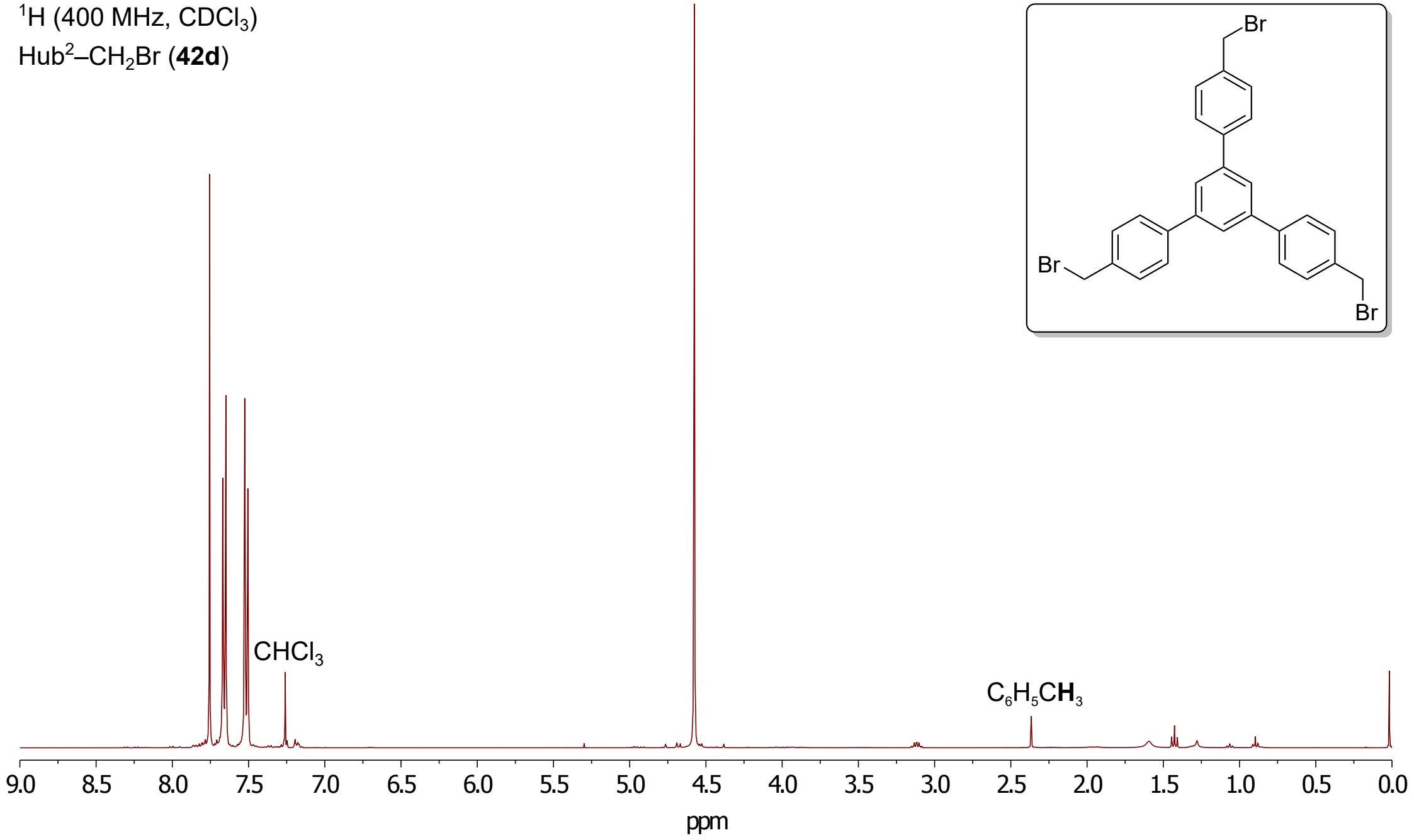
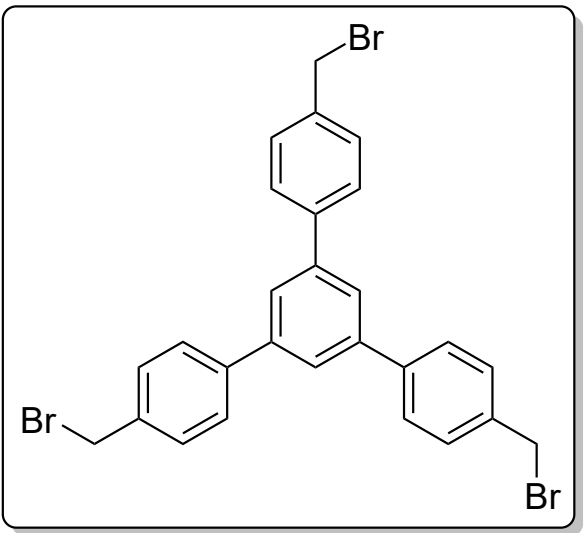
^1H - ^{13}C HSQC (500 MHz, $[\text{D}_8]$ THF)
Hub²-CH₂OH (**42c**)



^1H - ^{13}C HMBC (500 MHz, $[\text{D}_8]\text{THF}$)
Hub²-CH₂OH (42c)

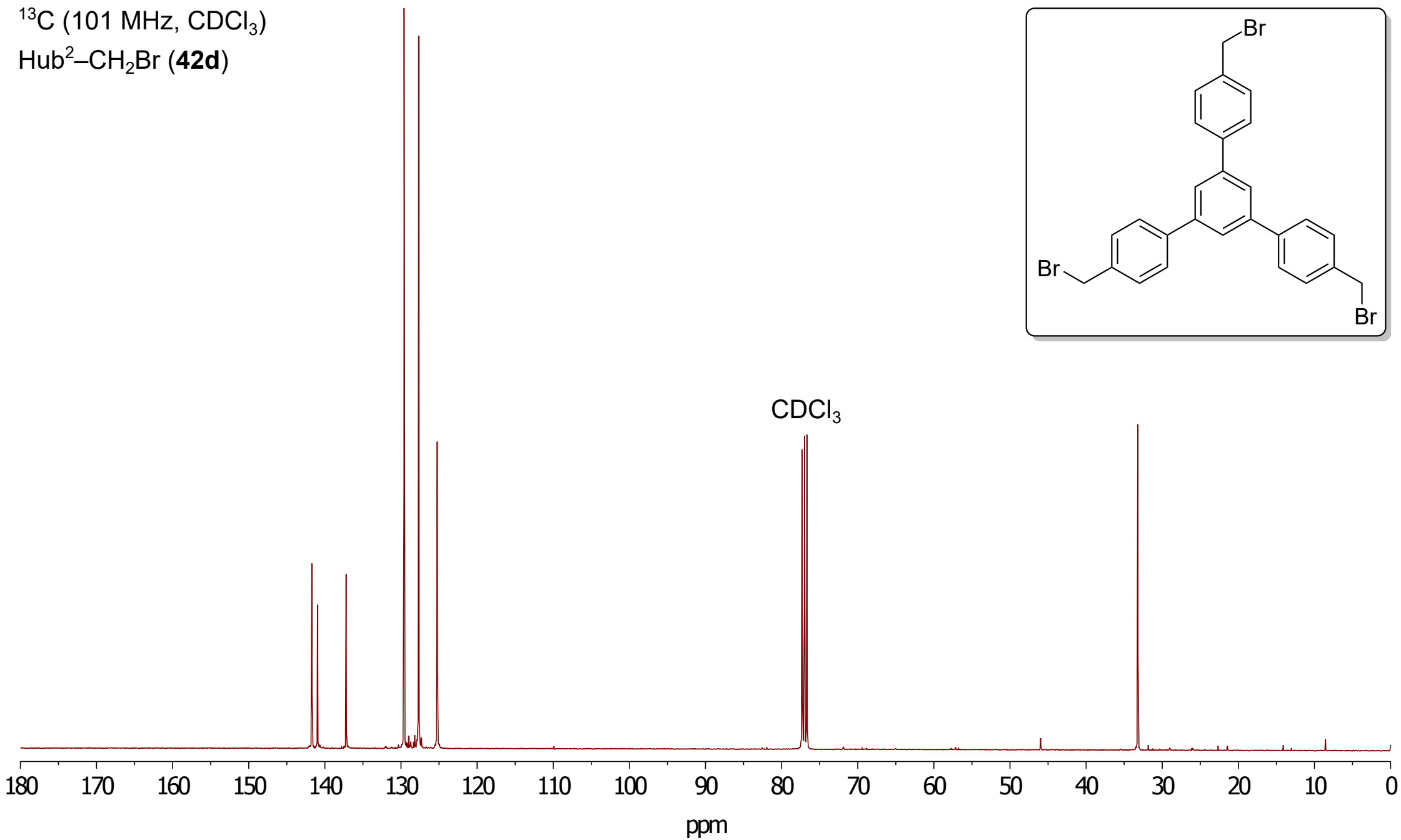
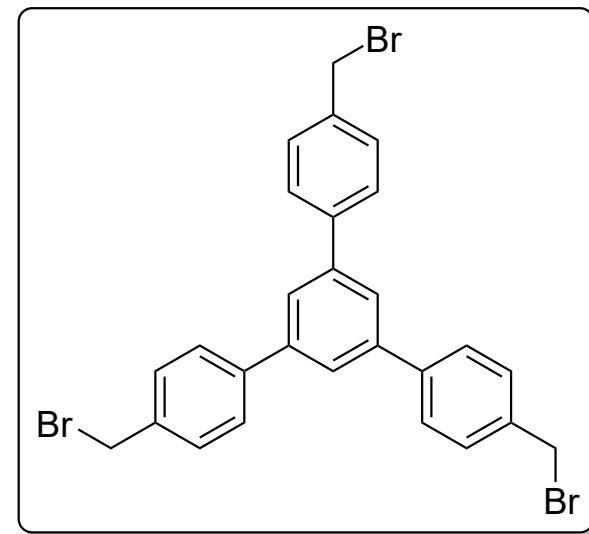


^1H (400 MHz, CDCl_3)
Hub²-CH₂Br (**42d**)

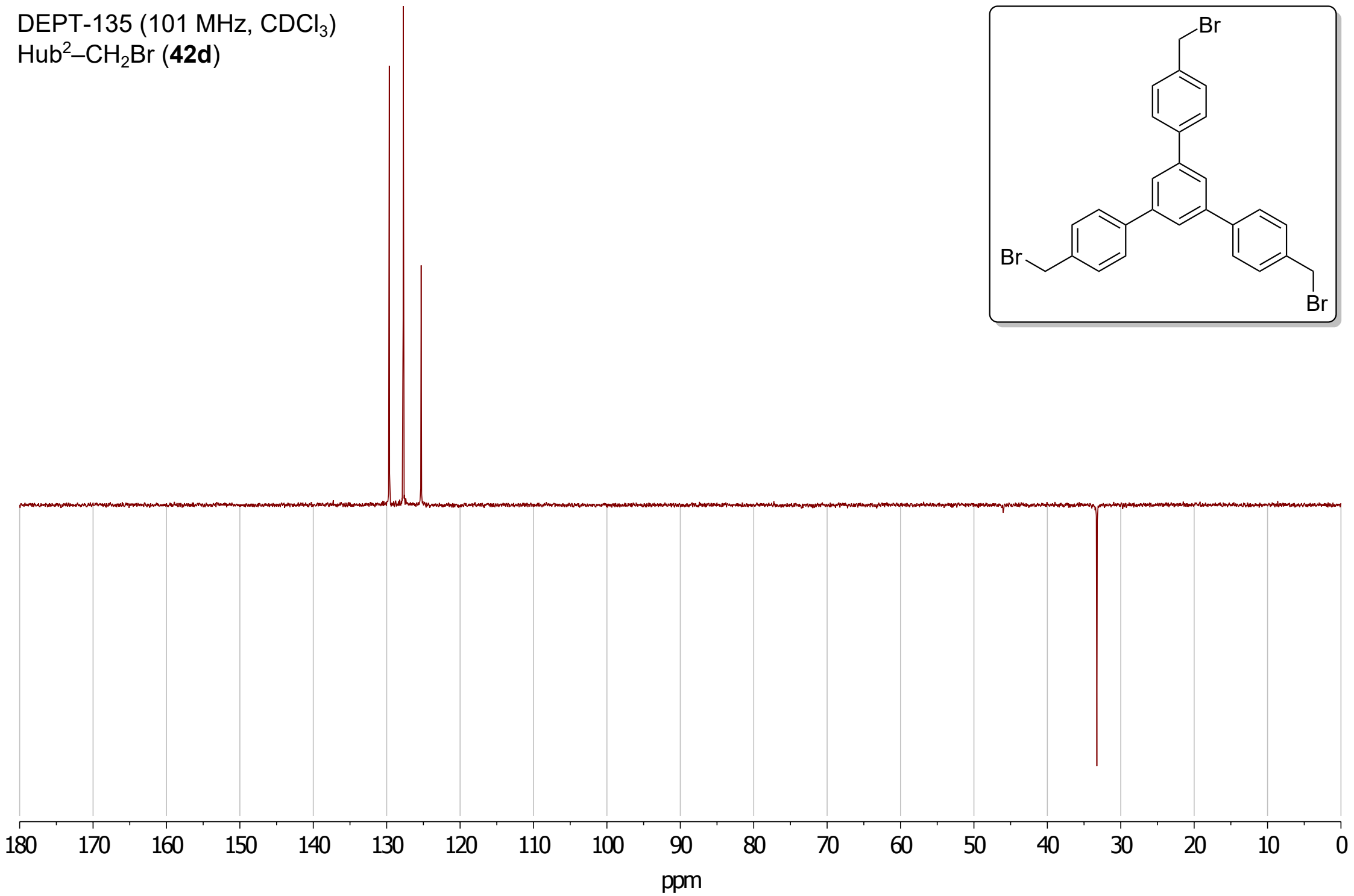
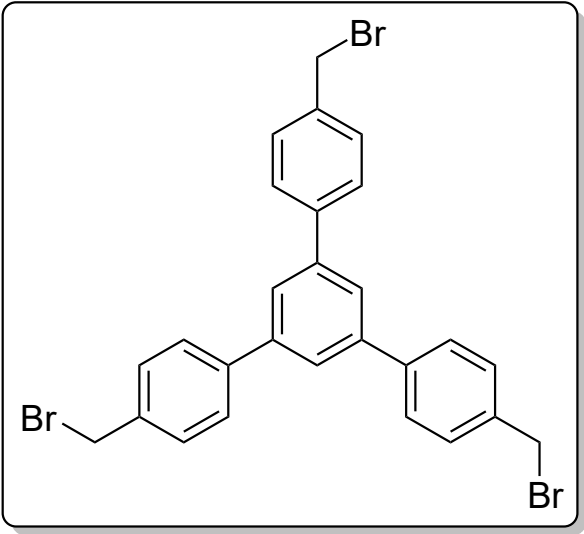


^{13}C (101 MHz, CDCl_3)

Hub²-CH₂Br (**42d**)

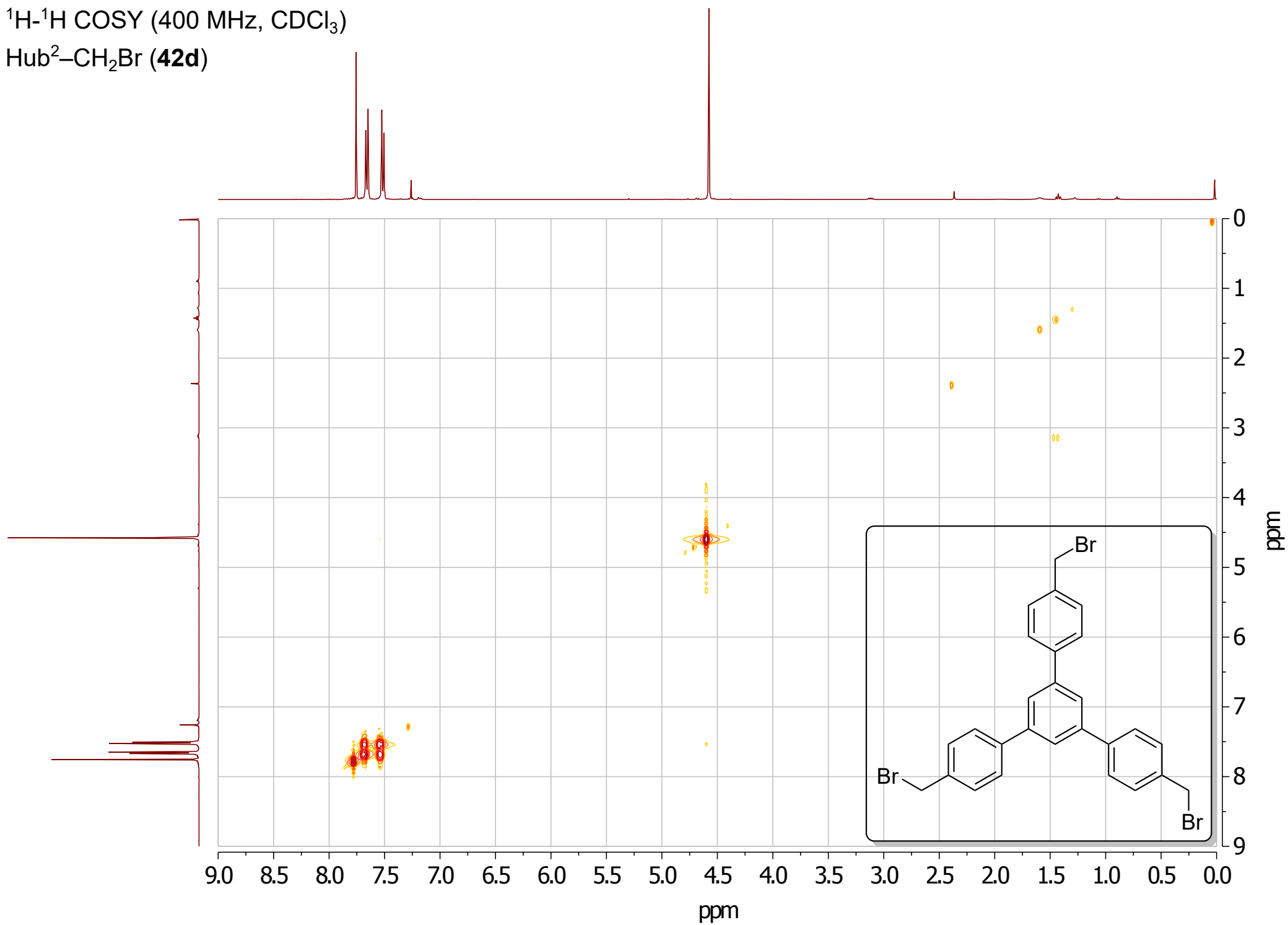


DEPT-135 (101 MHz, CDCl₃)
Hub²-CH₂Br (**42d**)



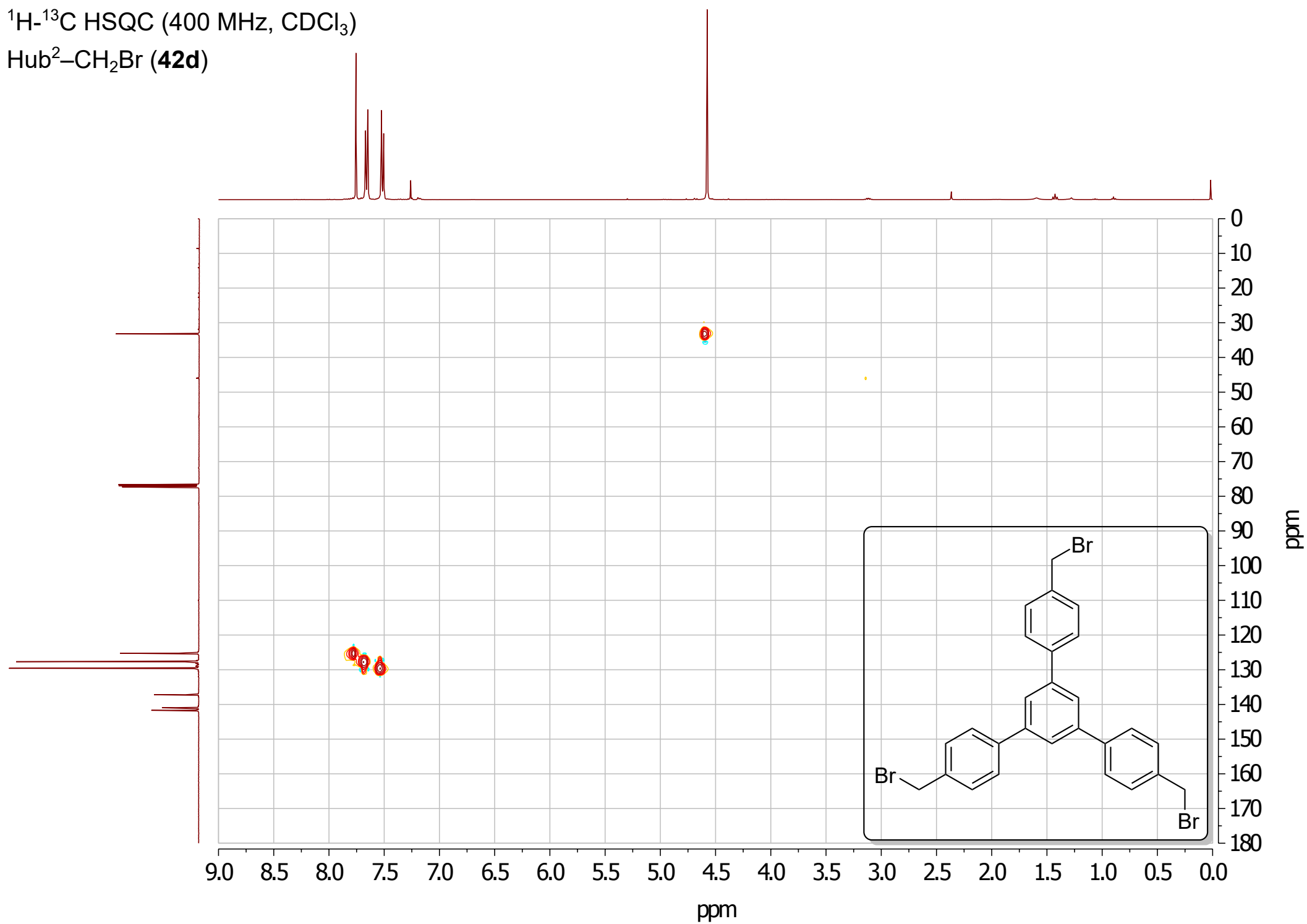
^1H - ^1H COSY (400 MHz, CDCl_3)

Hub²-CH₂Br (**42d**)



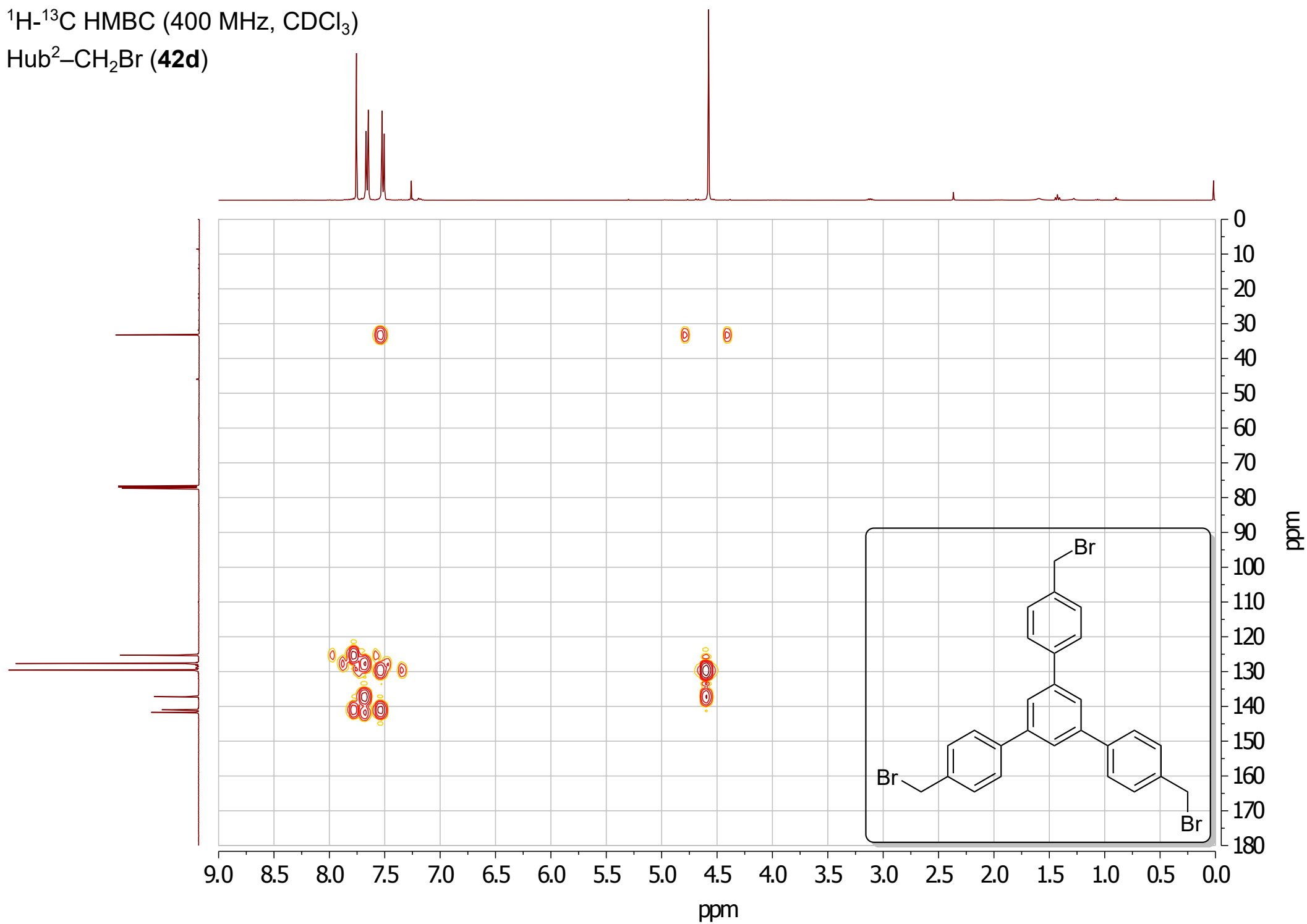
^1H - ^{13}C HSQC (400 MHz, CDCl_3)

Hub²-CH₂Br (**42d**)

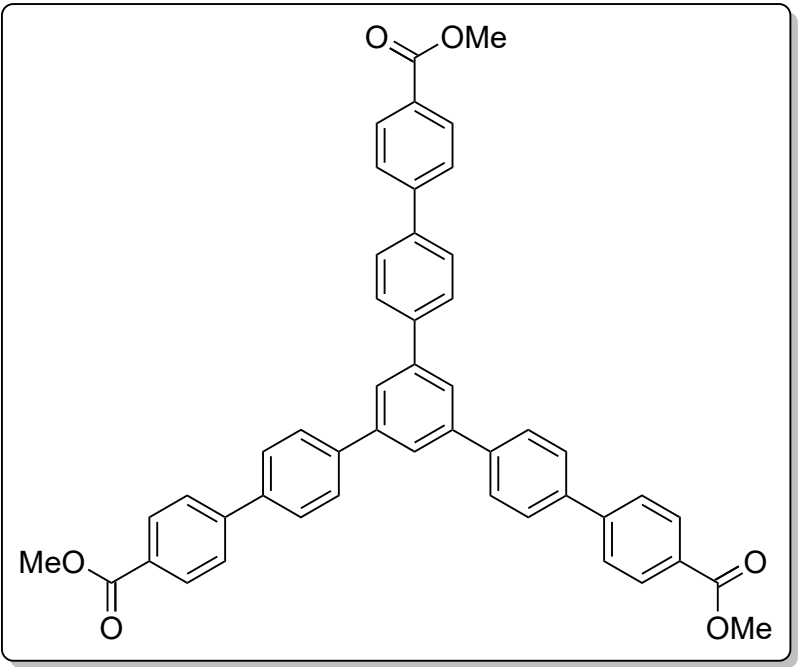
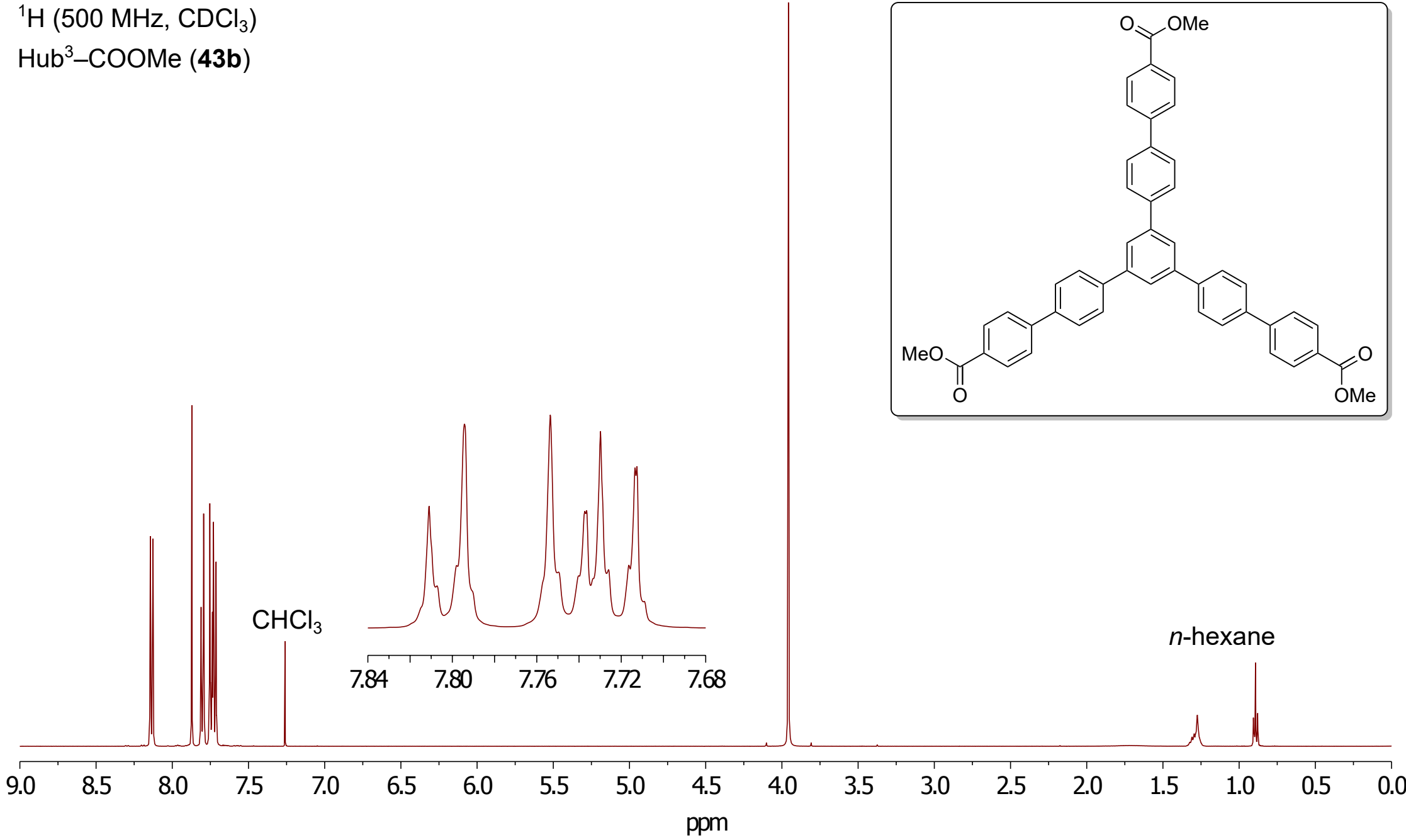


^1H - ^{13}C HMBC (400 MHz, CDCl_3)

Hub²-CH₂Br (**42d**)

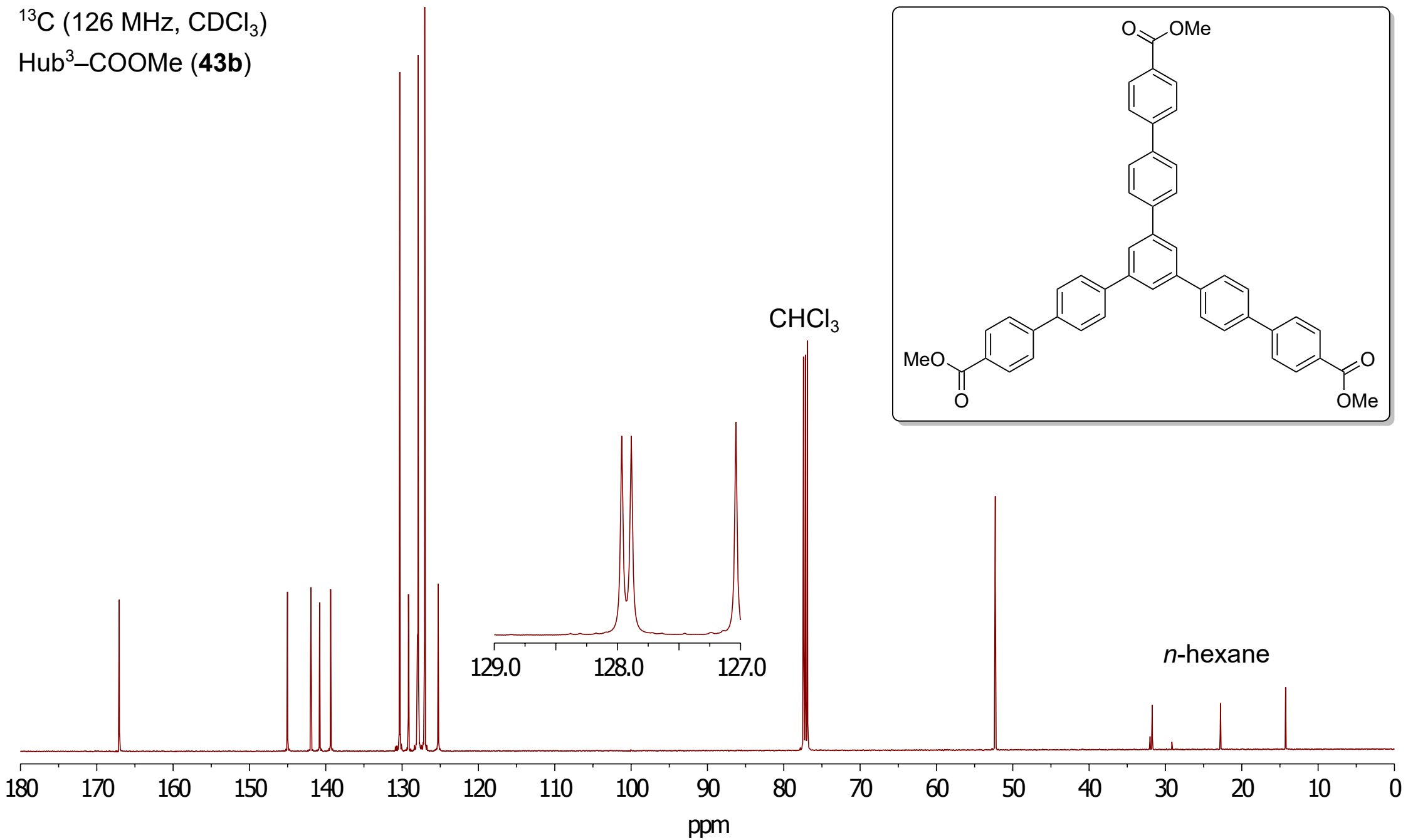


^1H (500 MHz, CDCl_3)
Hub³-COOMe (**43b**)

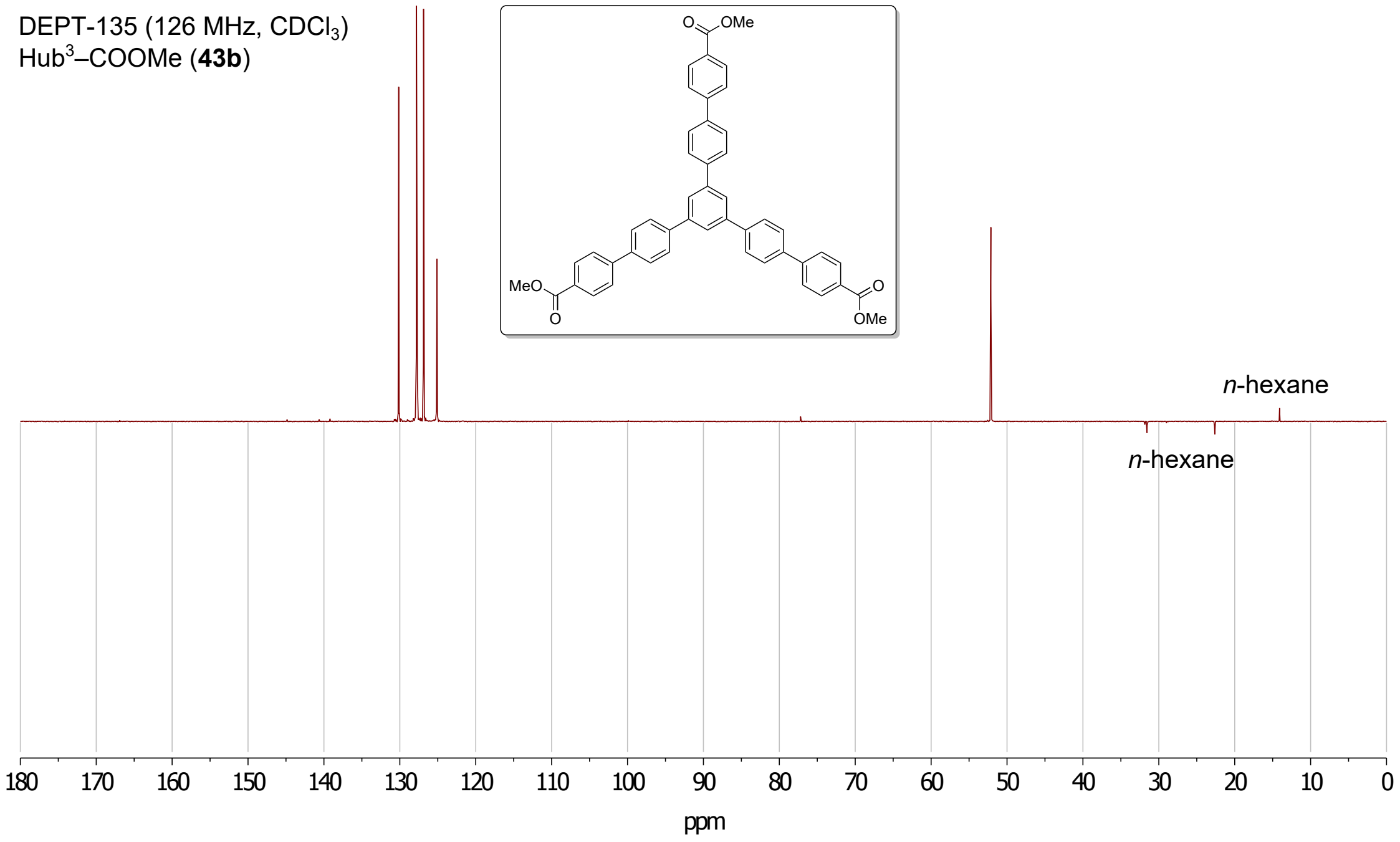
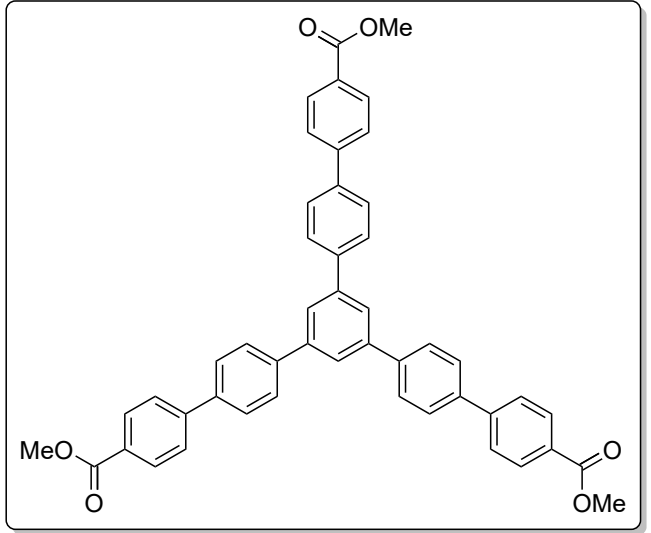


^{13}C (126 MHz, CDCl_3)

Hub³-COOMe (**43b**)

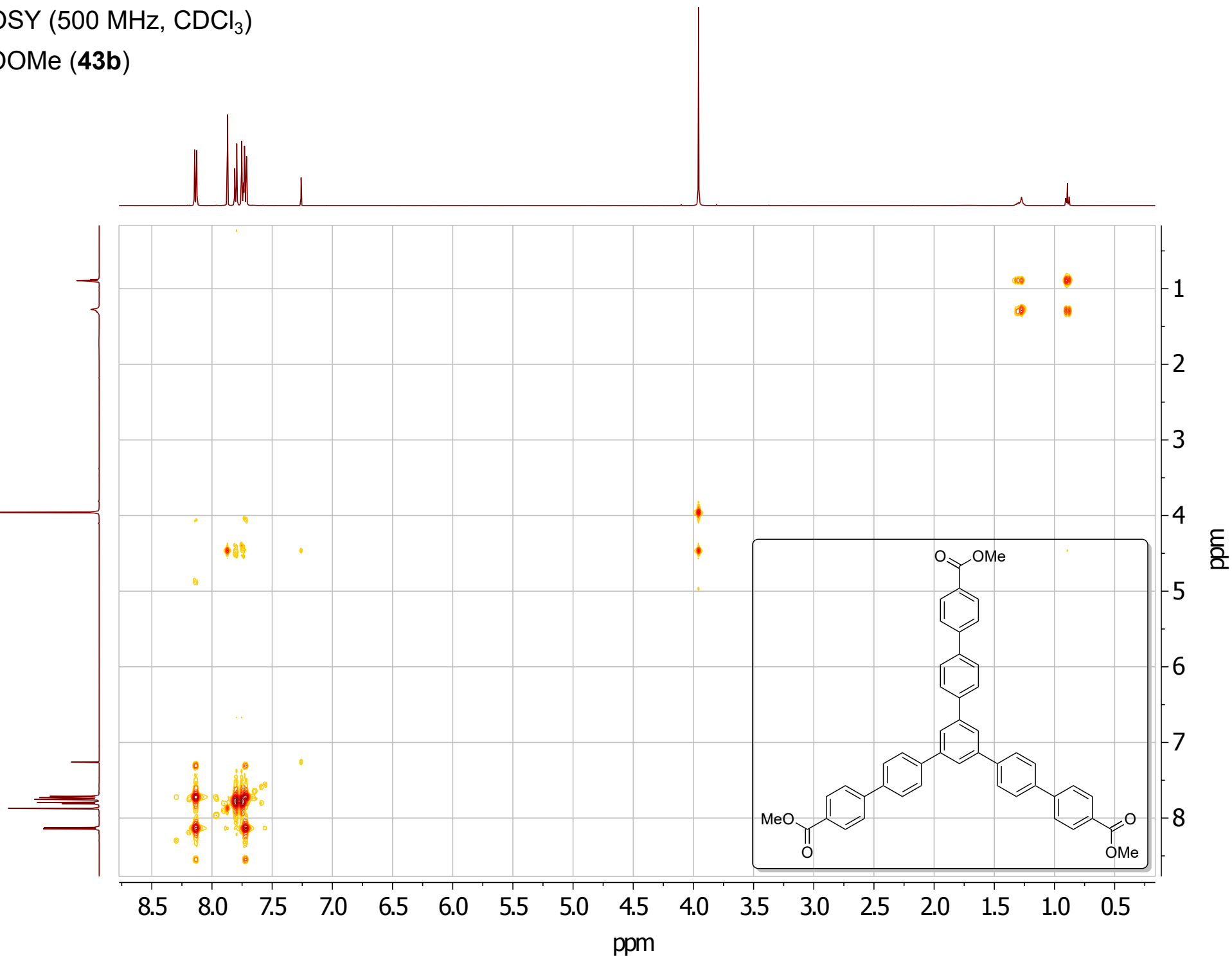


DEPT-135 (126 MHz, CDCl₃)
Hub³-COOMe (**43b**)



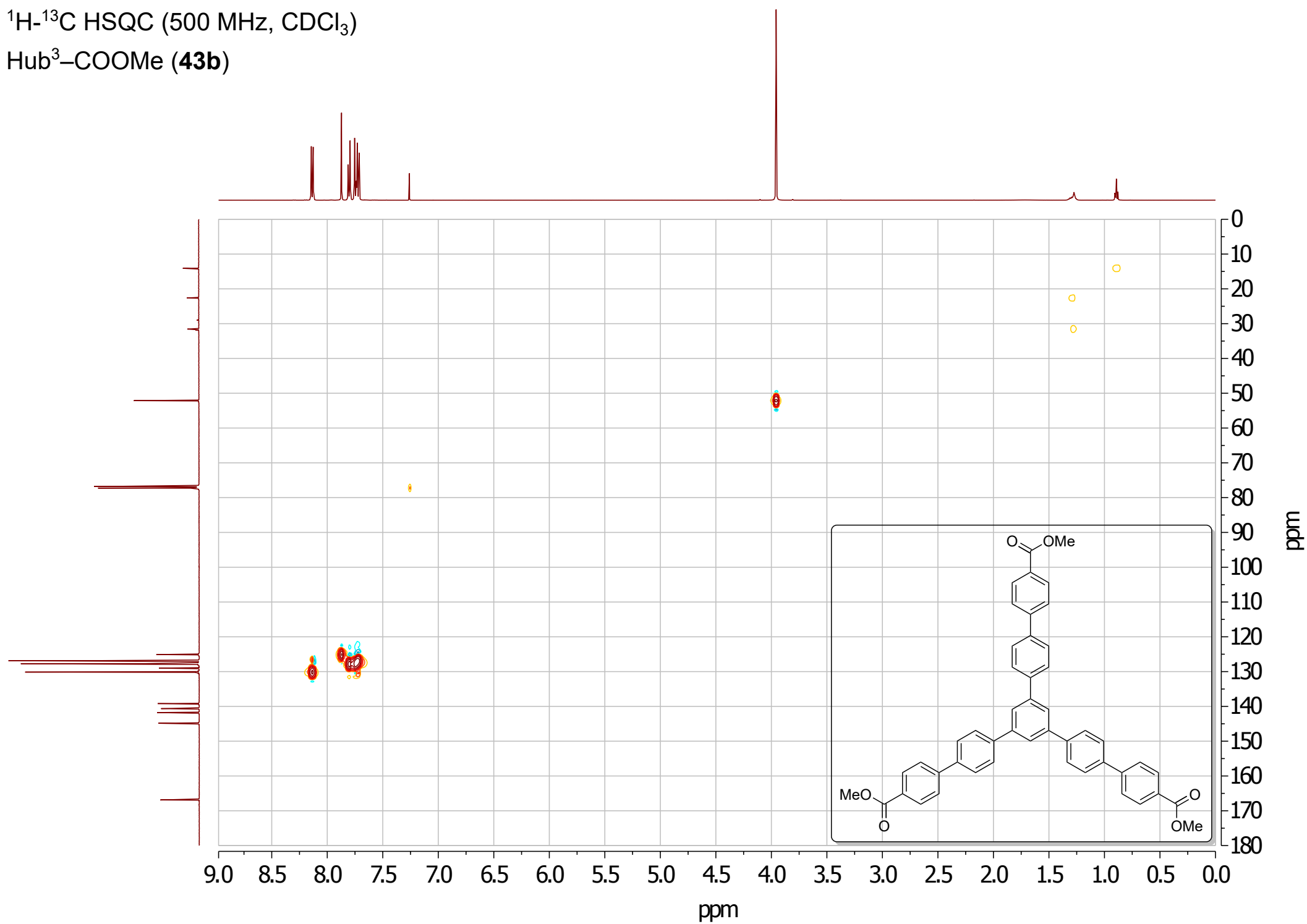
^1H - ^1H COSY (500 MHz, CDCl_3)

Hub³-COOMe (**43b**)



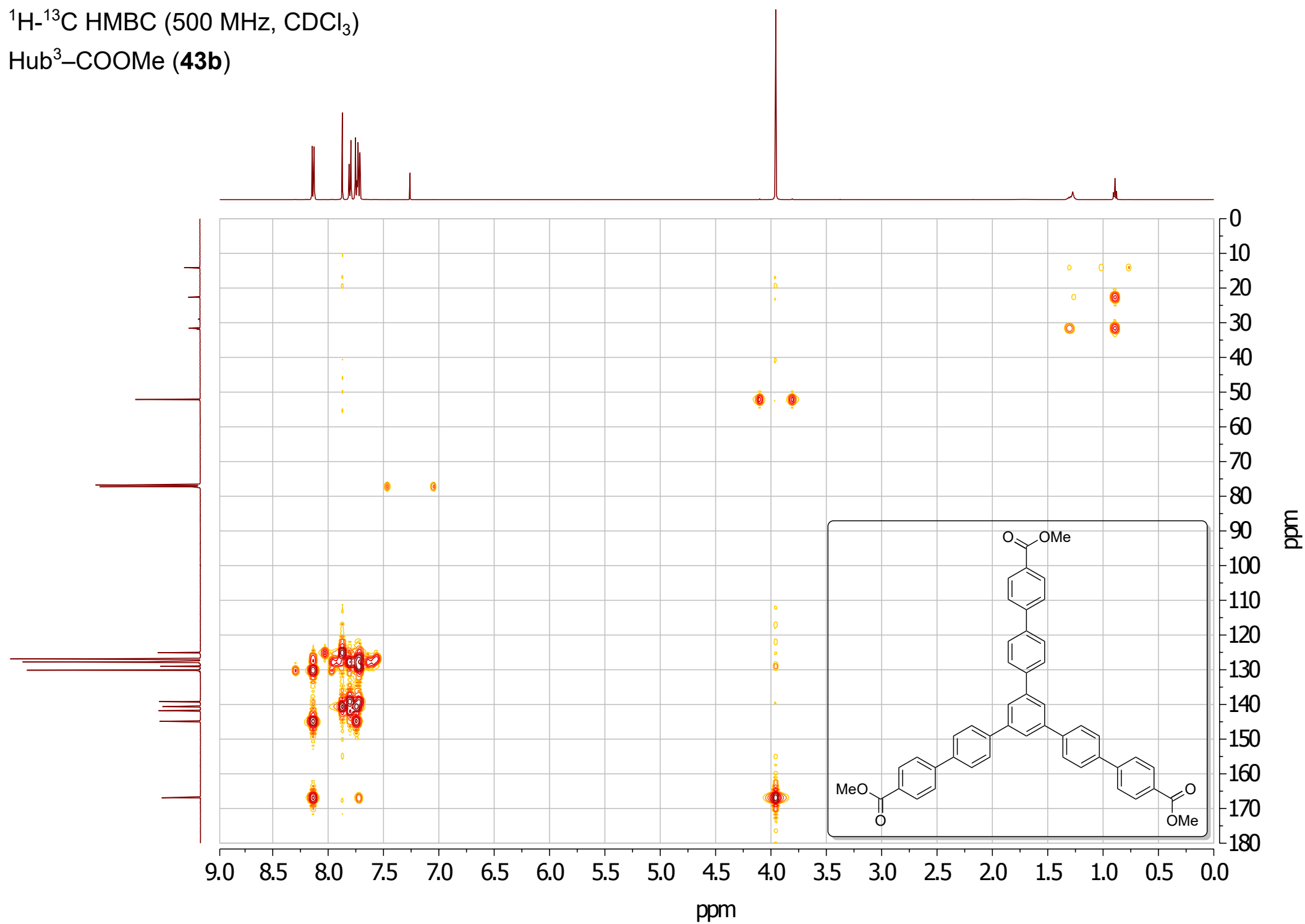
^1H - ^{13}C HSQC (500 MHz, CDCl_3)

Hub³-COOMe (**43b**)



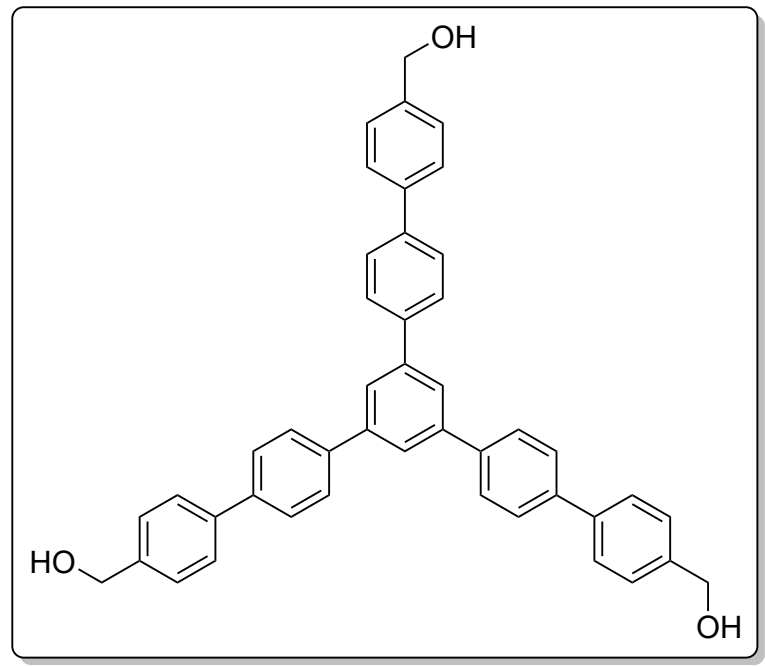
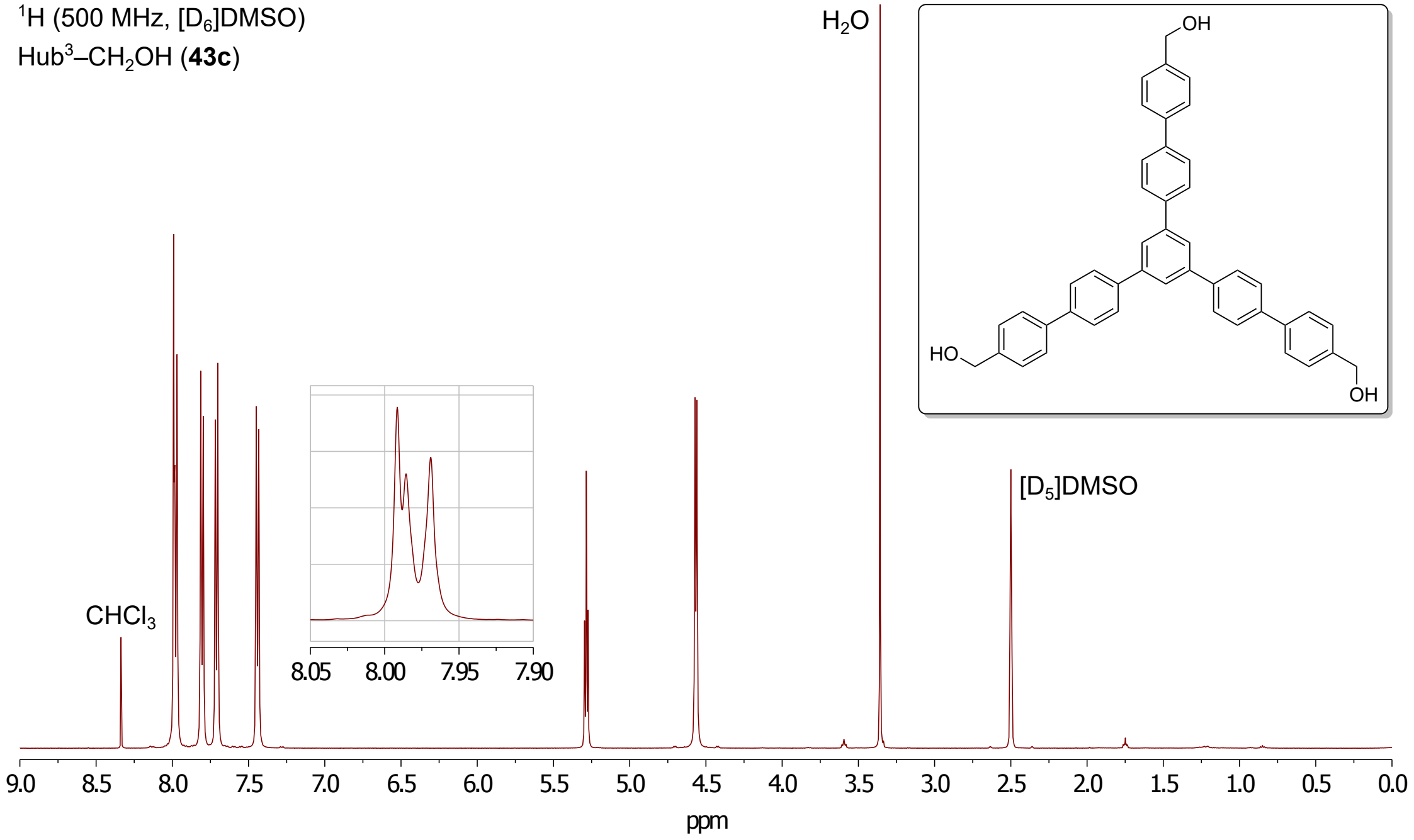
^1H - ^{13}C HMBC (500 MHz, CDCl_3)

Hub³-COOMe (**43b**)

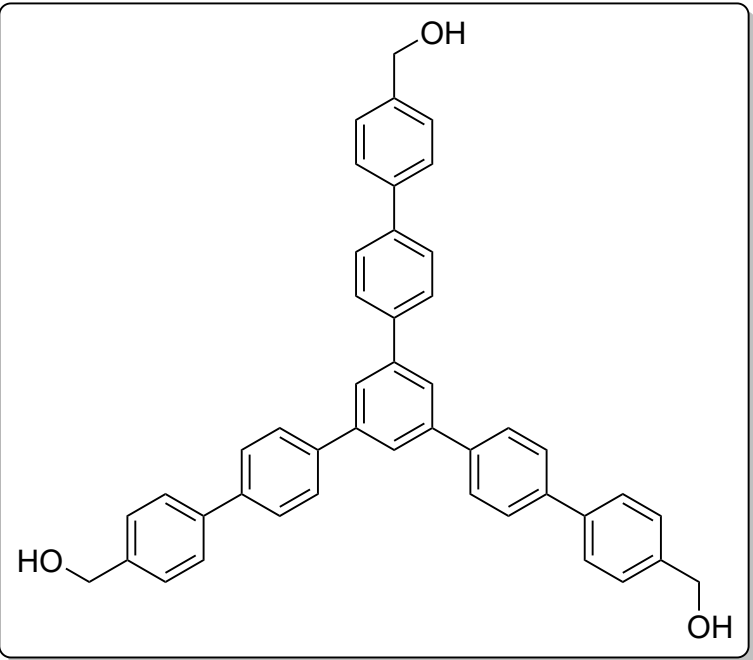


^1H (500 MHz, $[\text{D}_6]\text{DMSO}$)

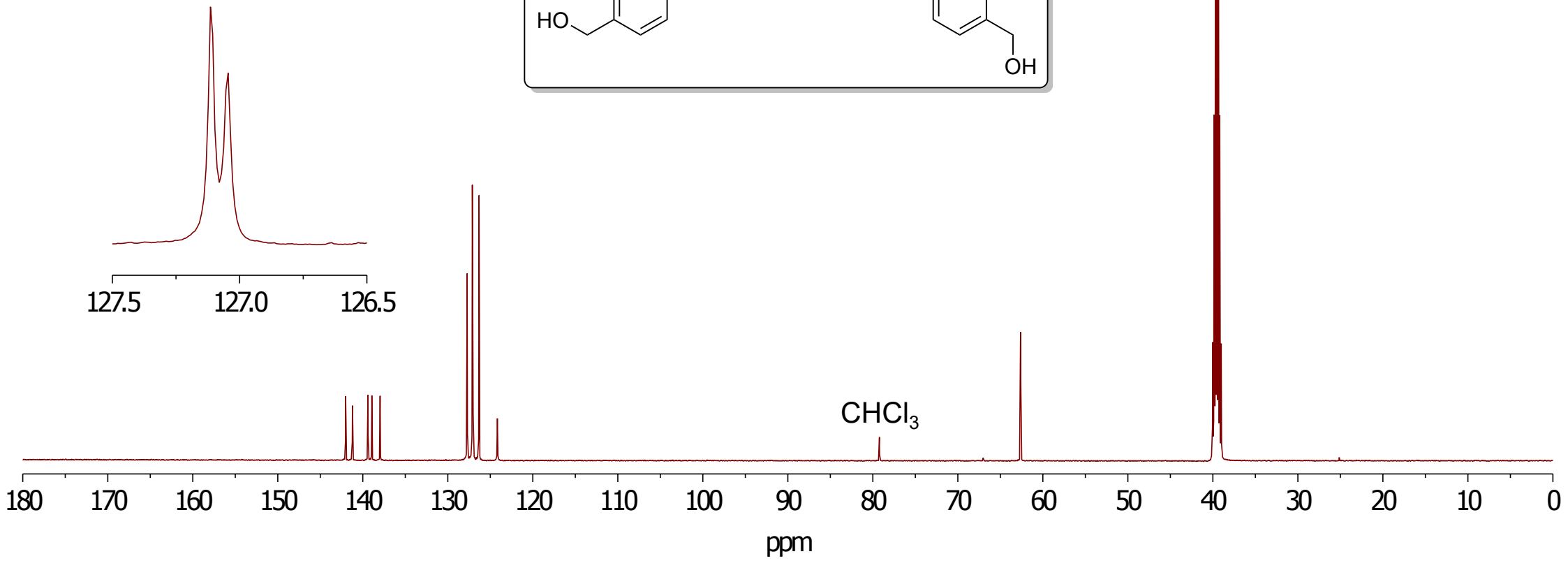
Hub³-CH₂OH (**43c**)



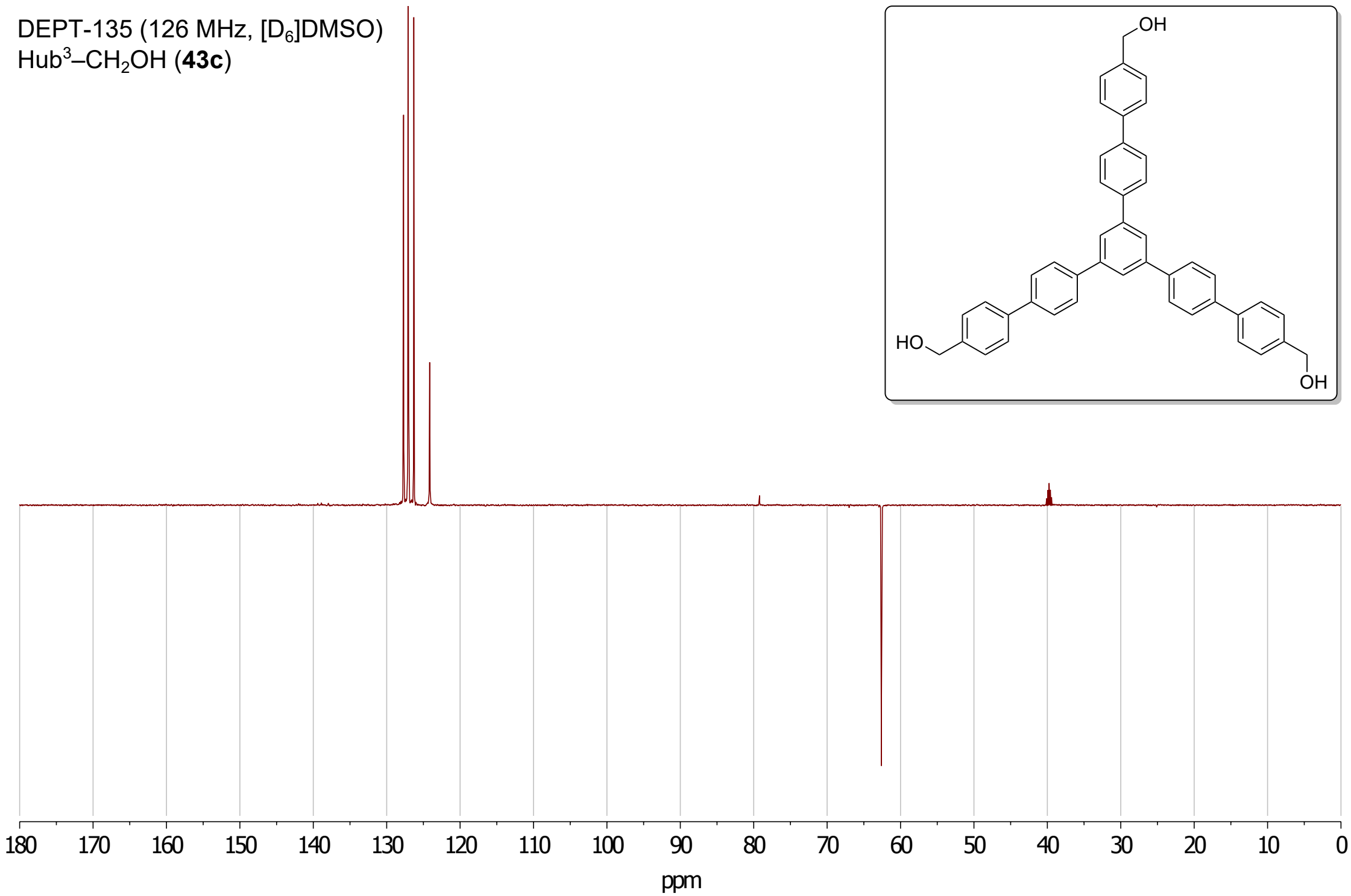
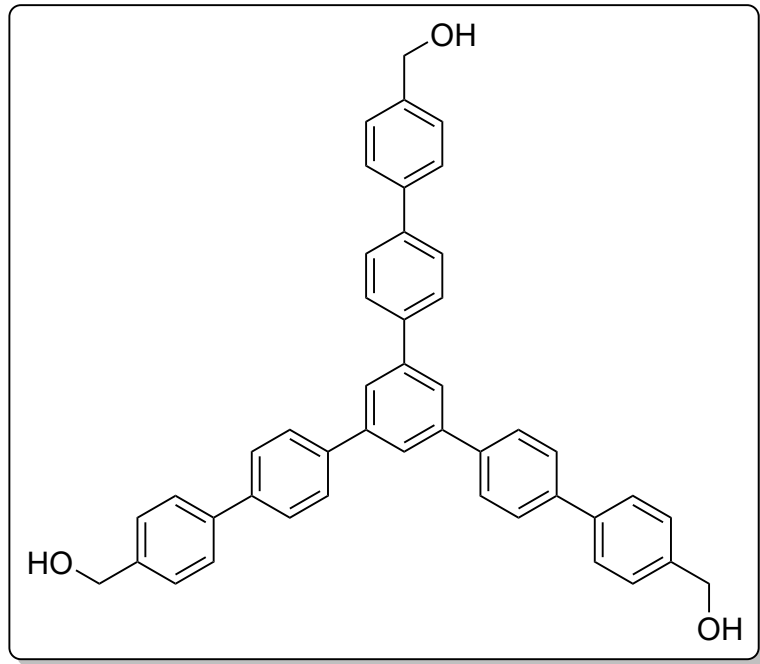
^{13}C (126 MHz, $[\text{D}_6]\text{DMSO}$)
Hub³-CH₂OH (**43c**)



$[\text{D}_5]\text{DMSO}$

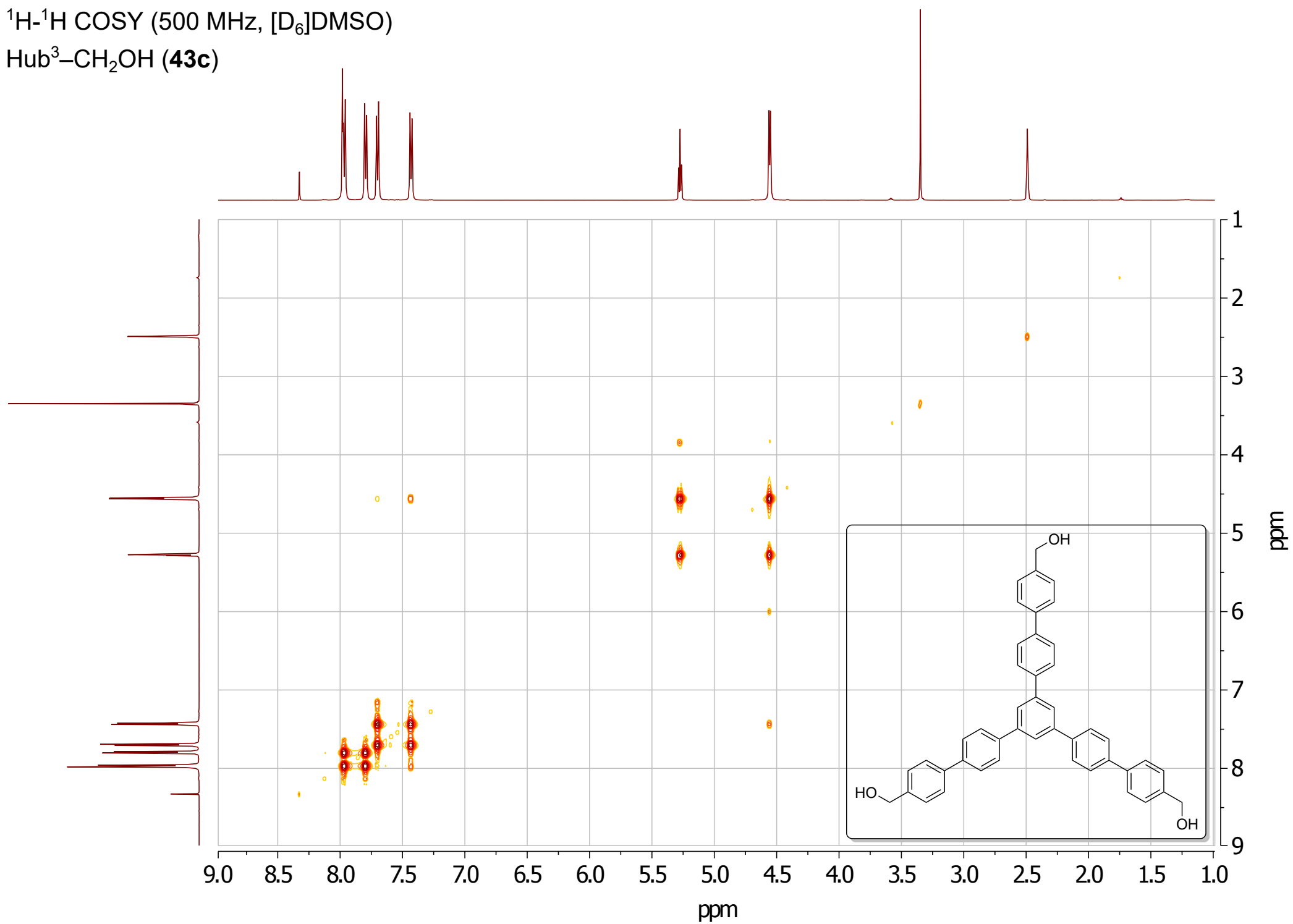


DEPT-135 (126 MHz, [D₆]DMSO)
Hub³-CH₂OH (**43c**)



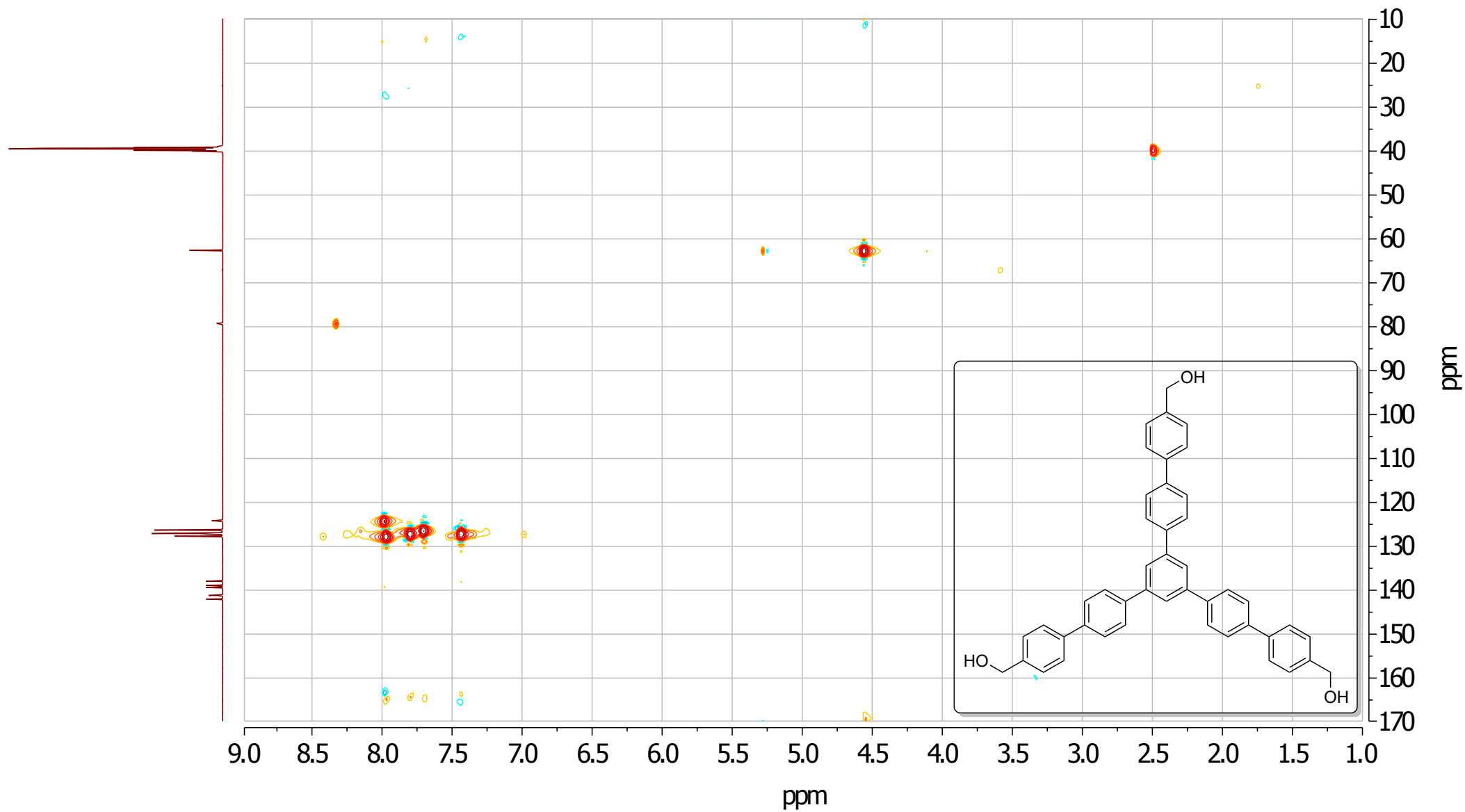
^1H - ^1H COSY (500 MHz, $[\text{D}_6]$ DMSO)

Hub³-CH₂OH (**43c**)



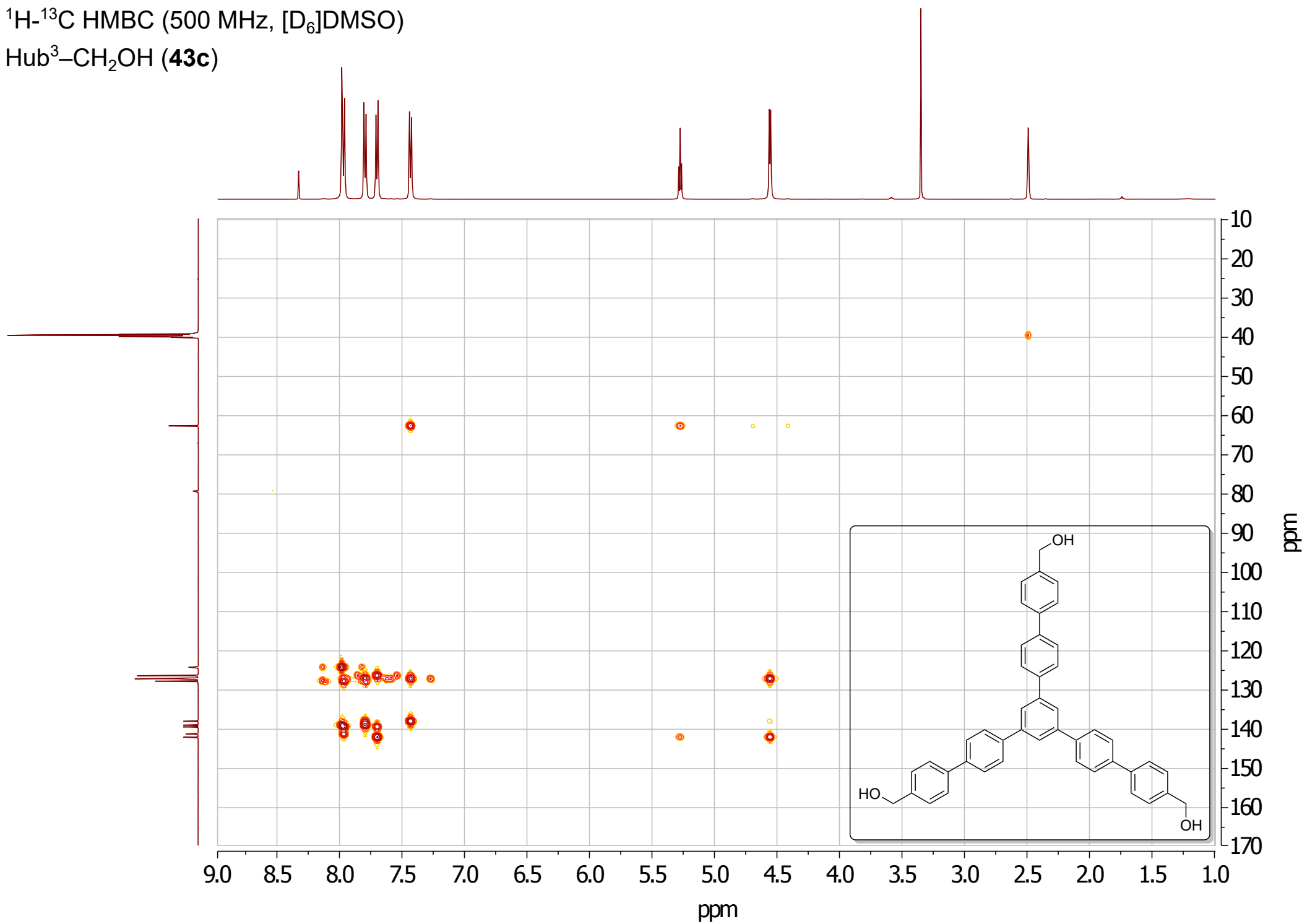
^1H - ^{13}C HSQC (500 MHz, $[\text{D}_6]$ DMSO)

Hub³-CH₂OH (**43c**)

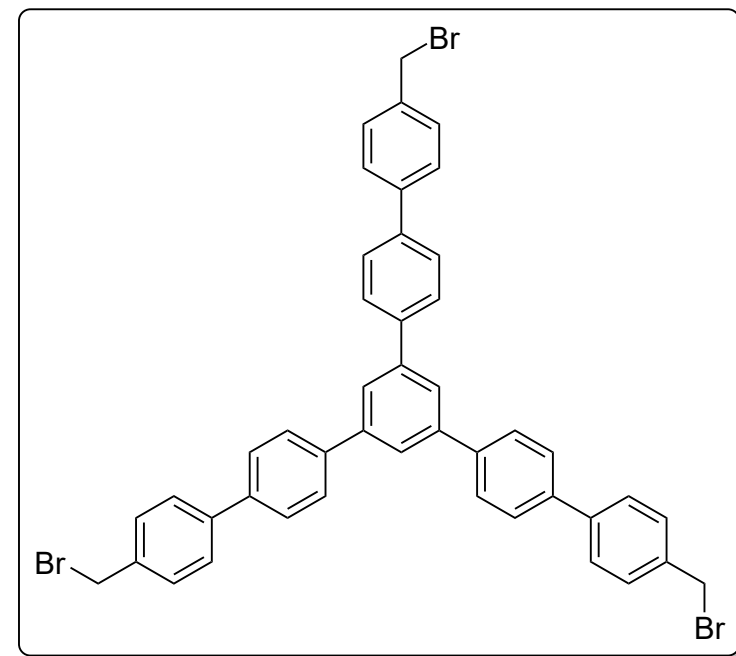
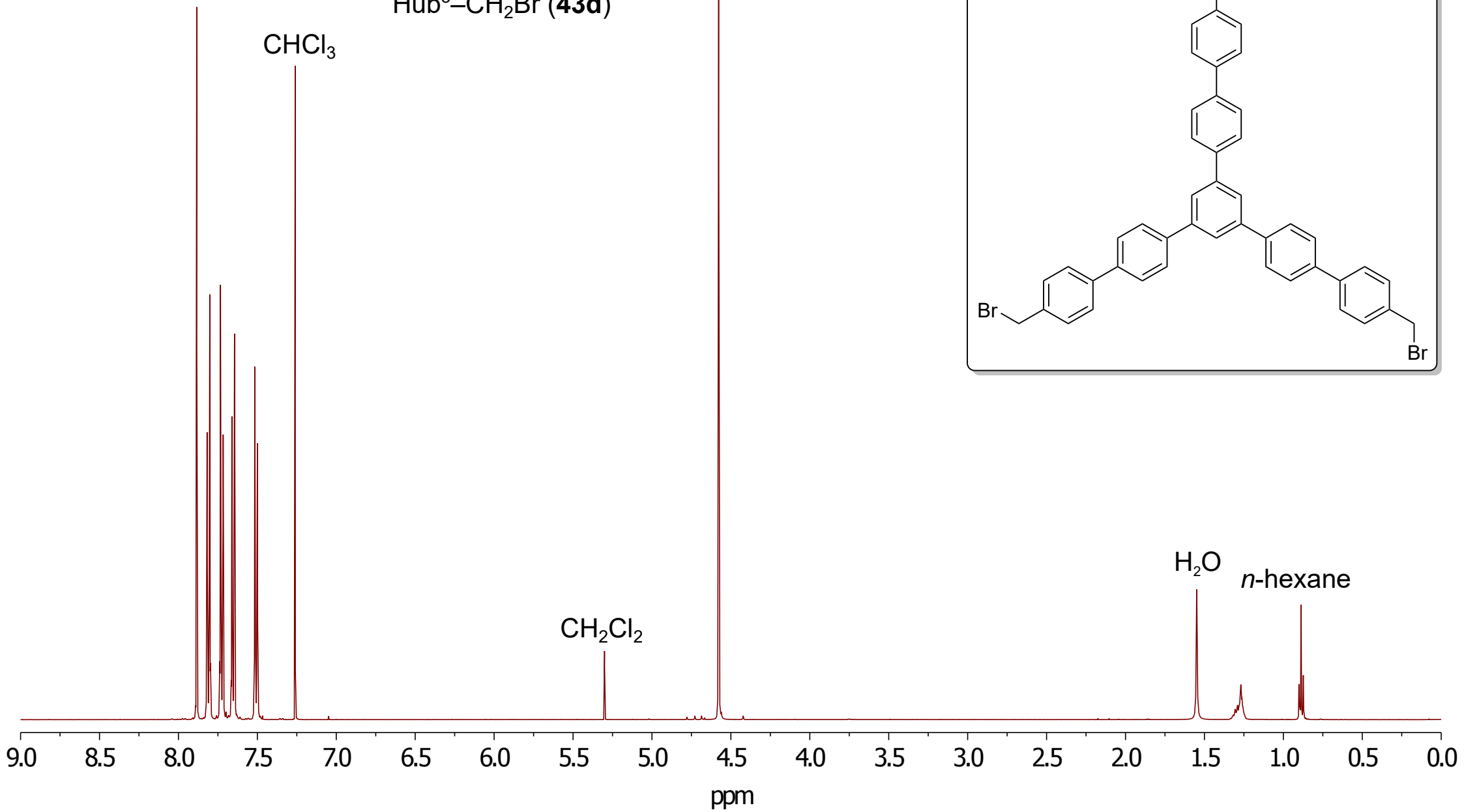


^1H - ^{13}C HMBC (500 MHz, $[\text{D}_6]$ DMSO)

Hub³-CH₂OH (**43c**)



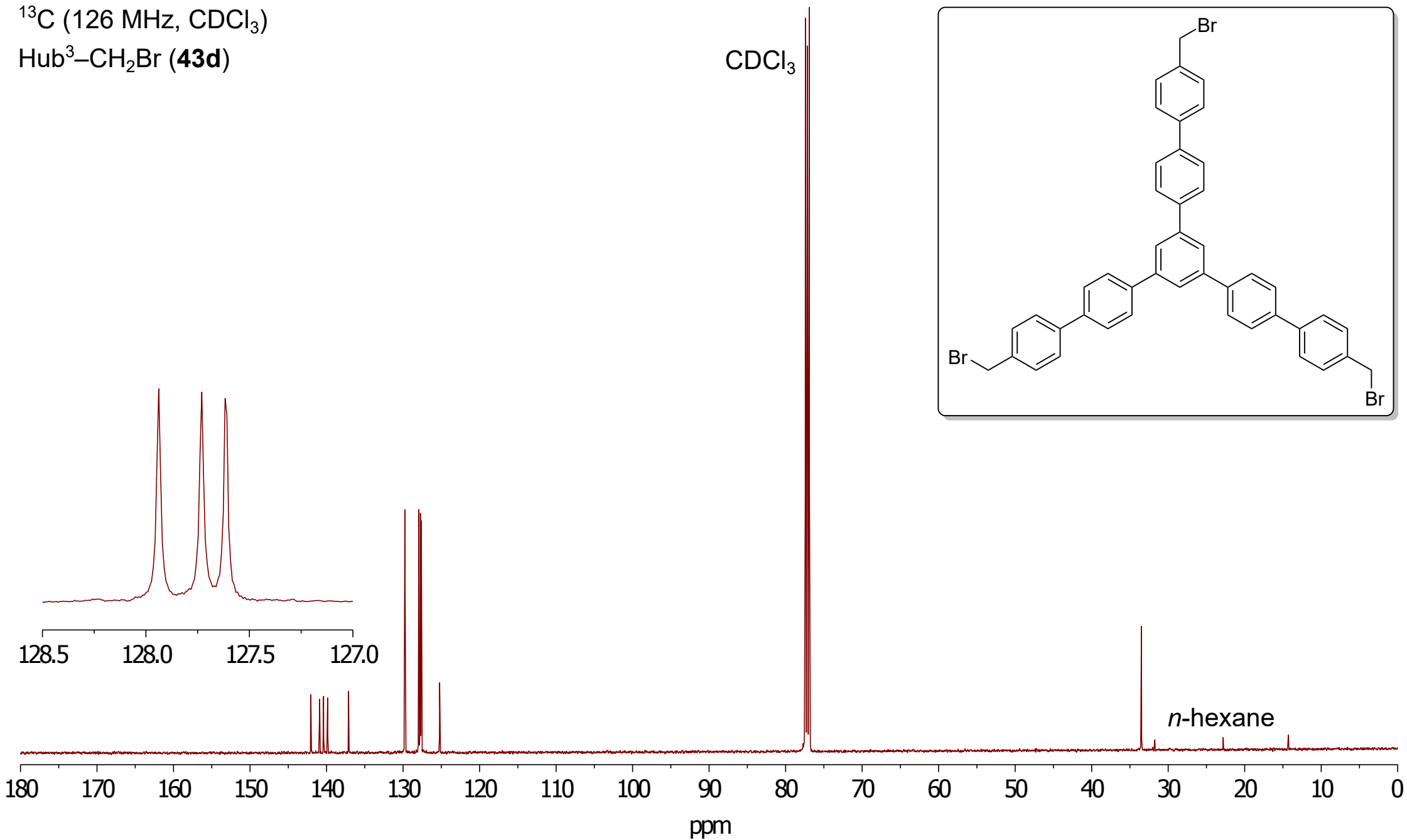
^1H (500 MHz, CDCl_3)
Hub³-CH₂Br (**43d**)



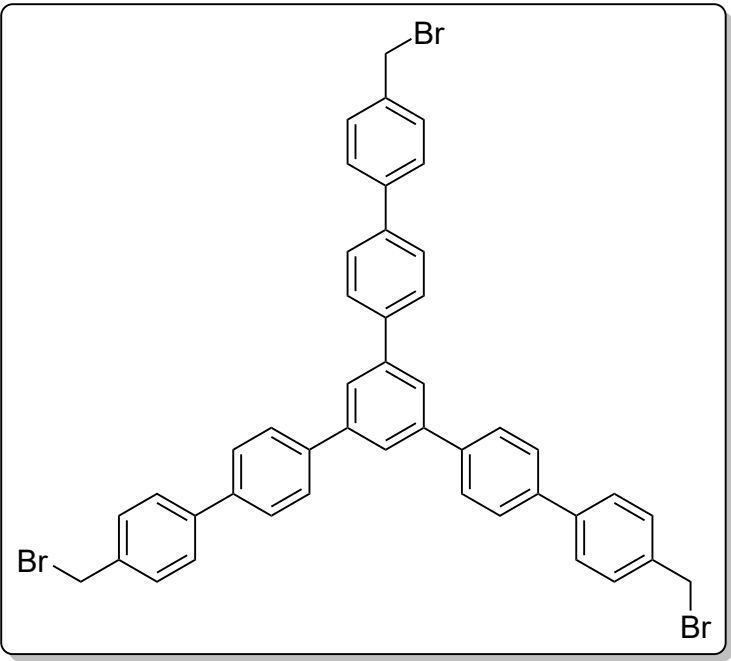
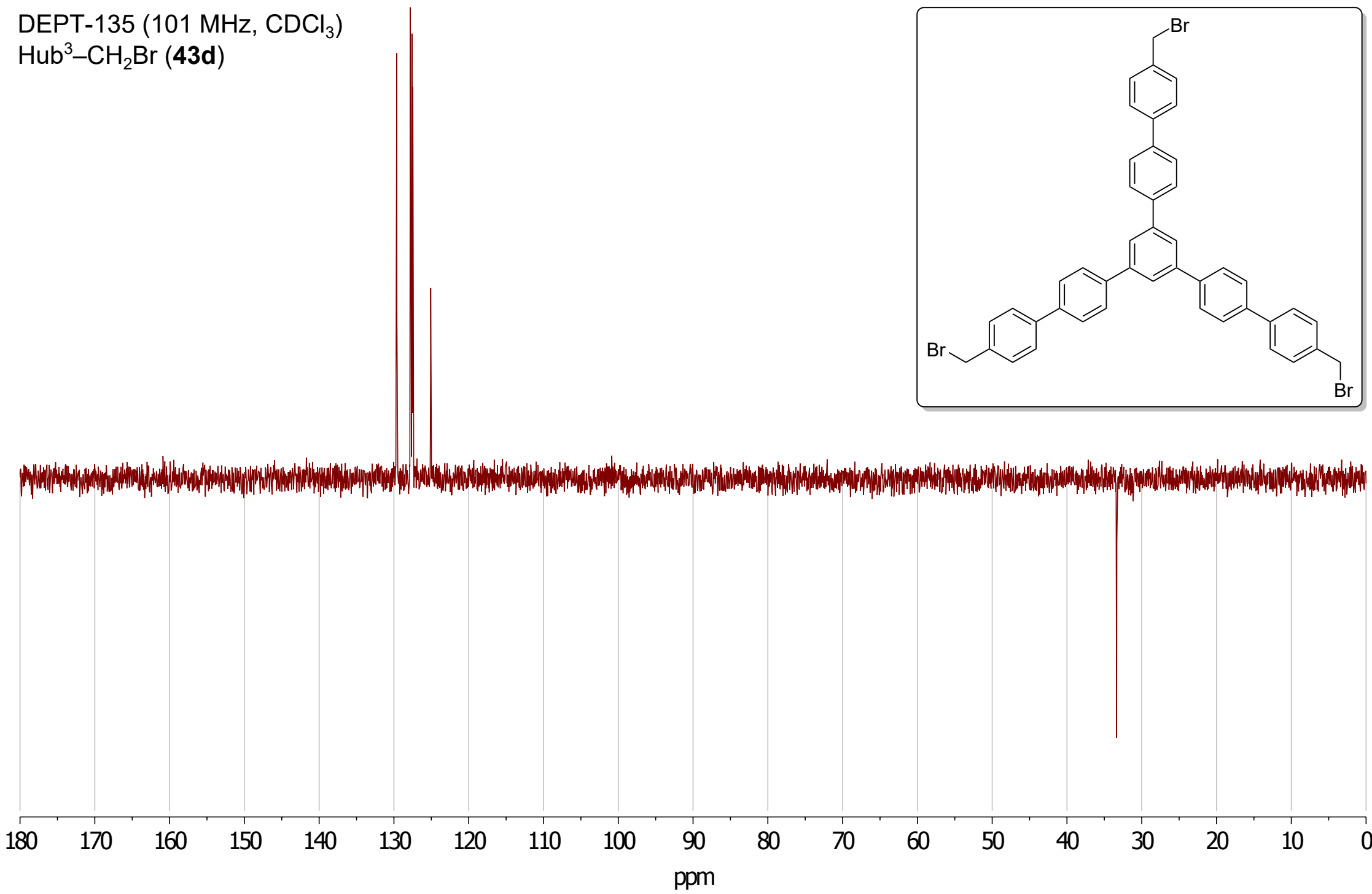
^{13}C (126 MHz, CDCl_3)

Hub³-CH₂Br (**43d**)

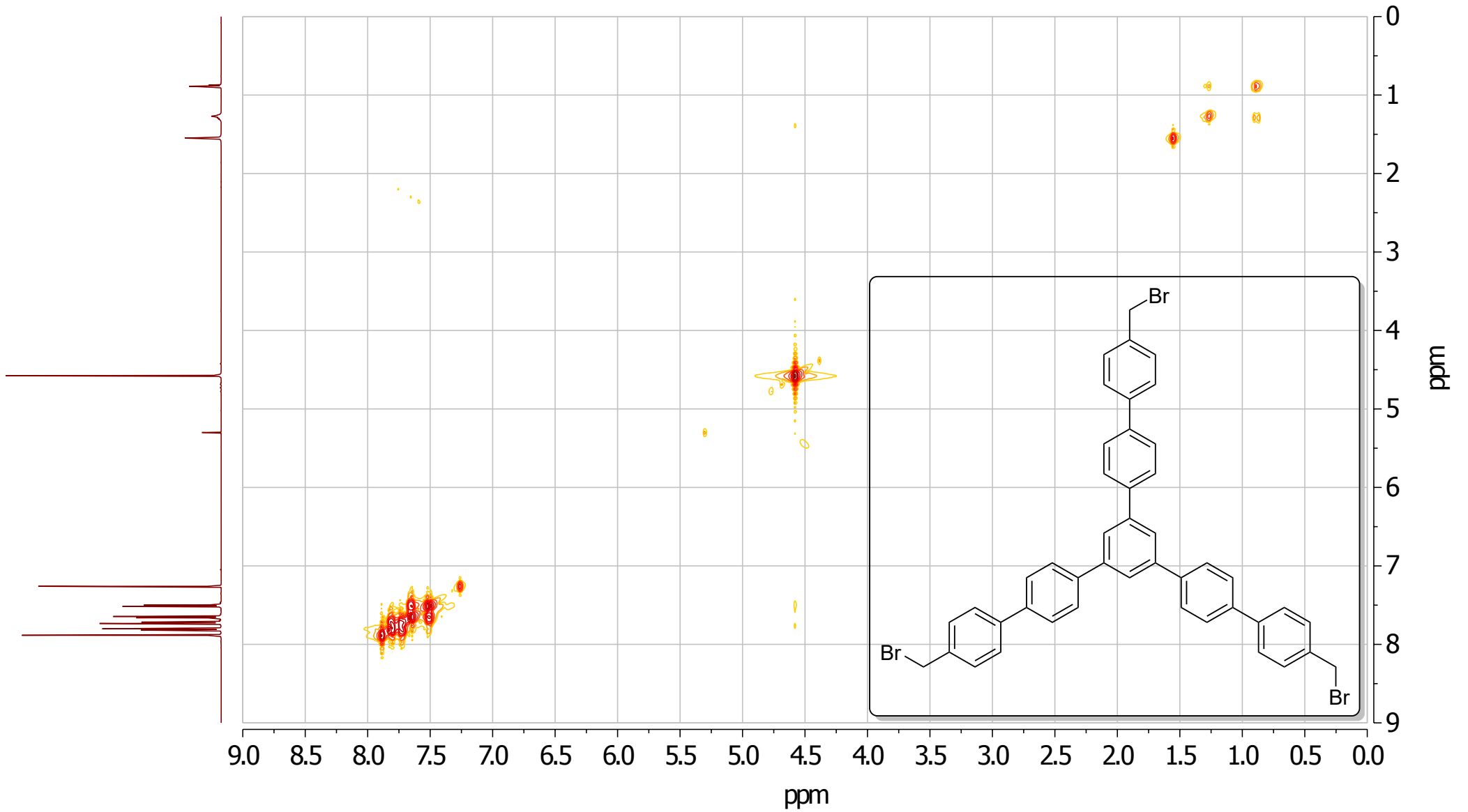
CDCl_3



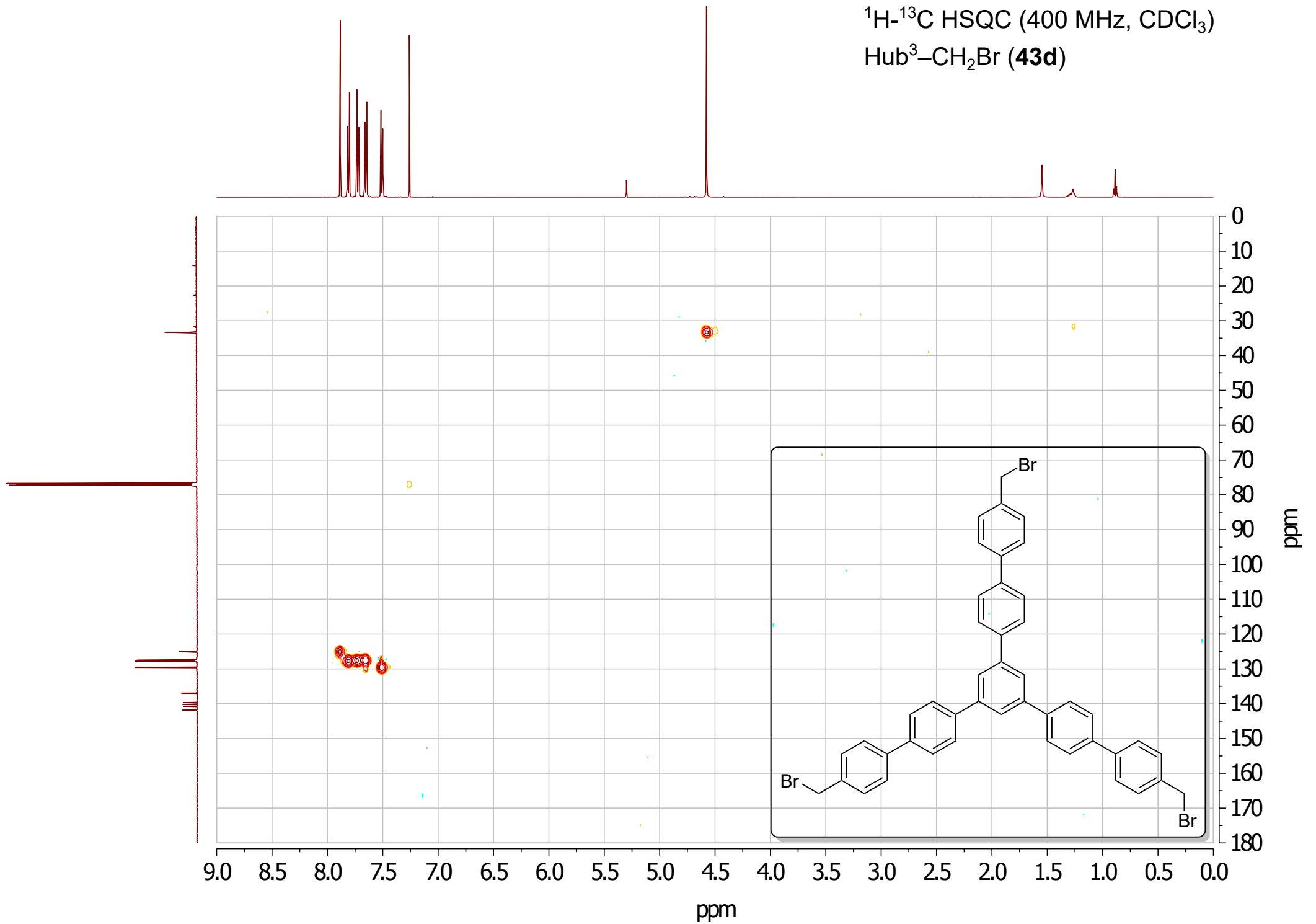
DEPT-135 (101 MHz, CDCl₃)
Hub³-CH₂Br (**43d**)



^1H - ^1H COSY (400 MHz, CDCl_3)
Hub³-CH₂Br (**43d**)

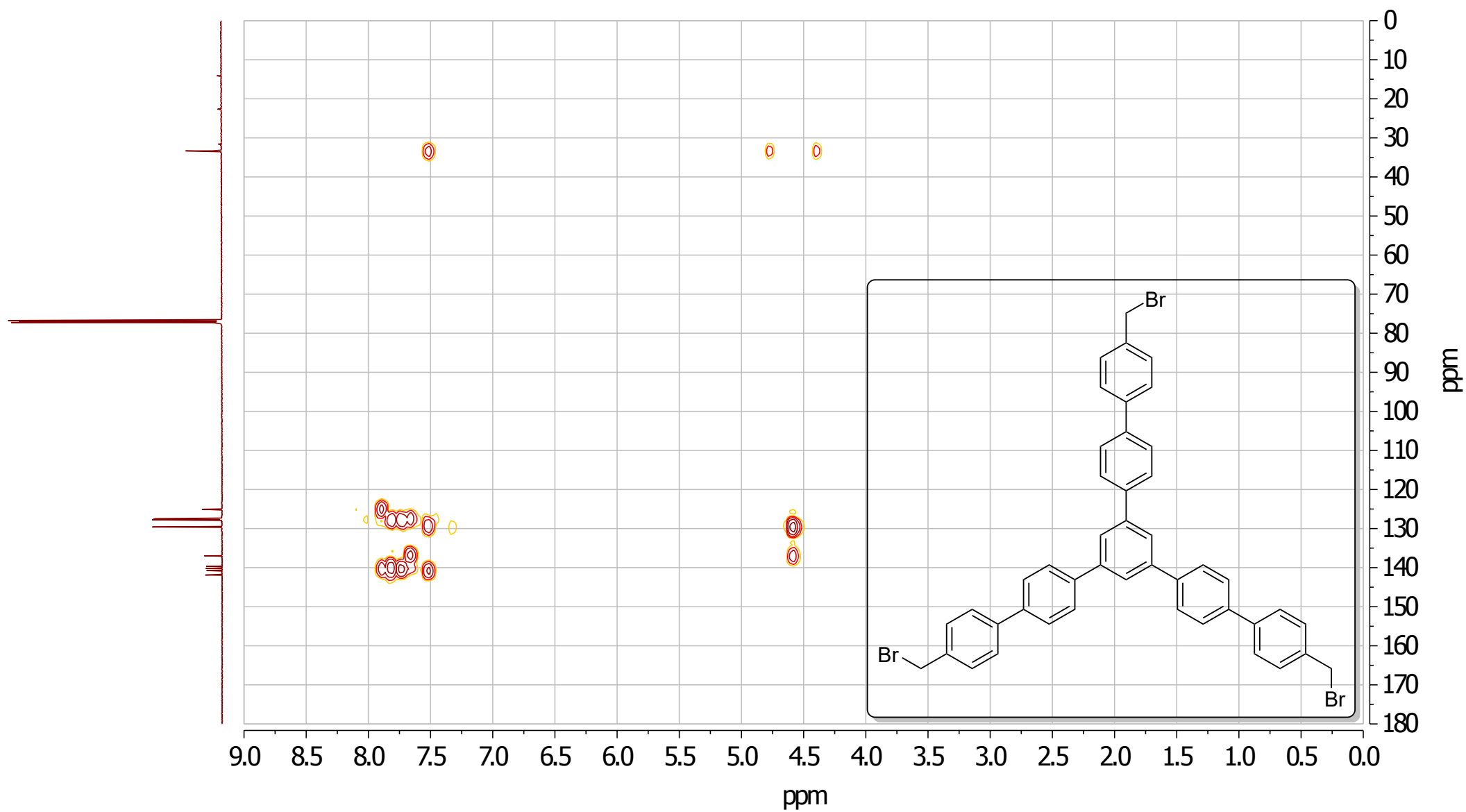


^1H - ^{13}C HSQC (400 MHz, CDCl_3)
Hub³-CH₂Br (**43d**)



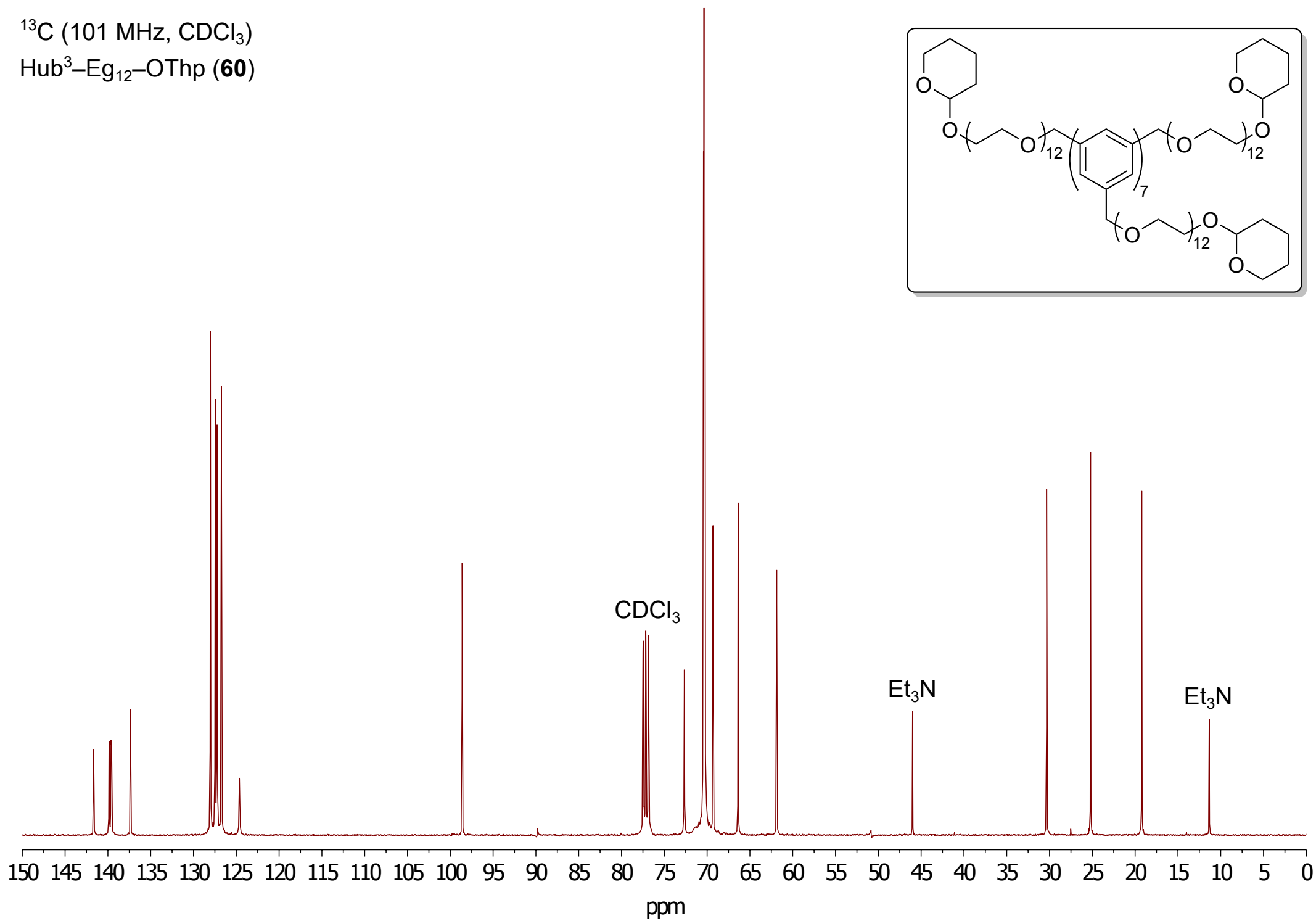
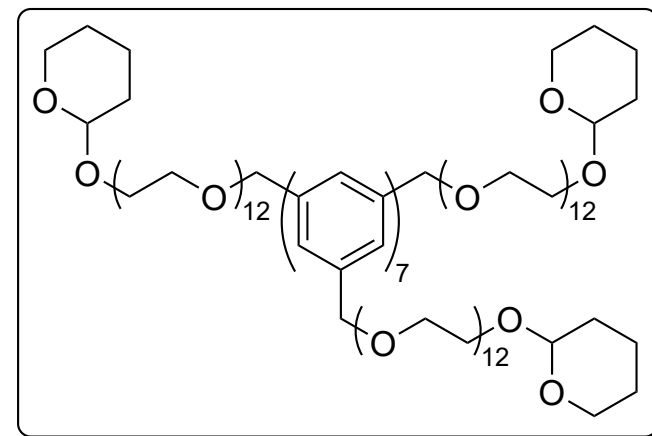
^1H - ^{13}C HMBC (400 MHz, CDCl_3)

Hub³-CH₂Br (**43d**)

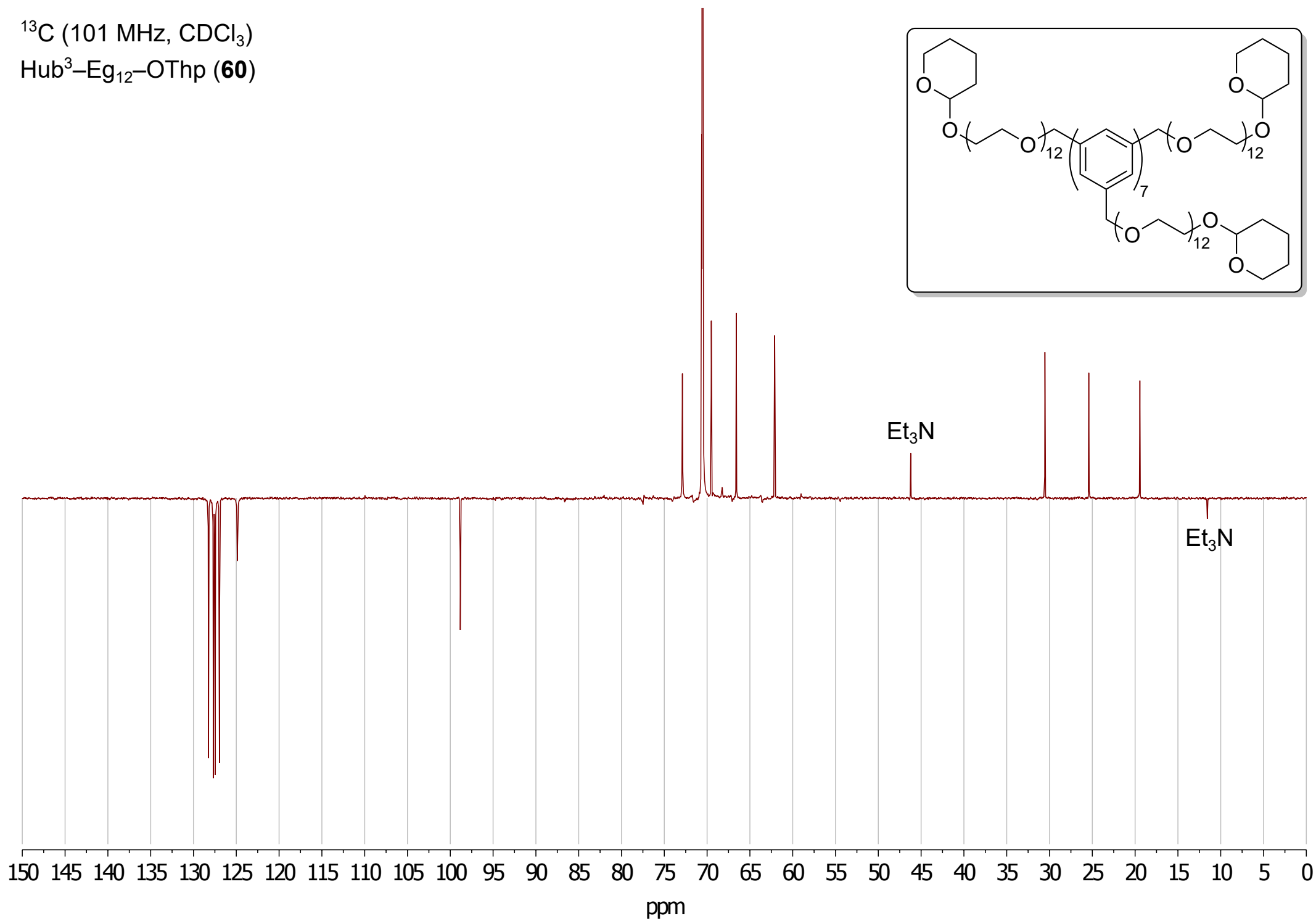
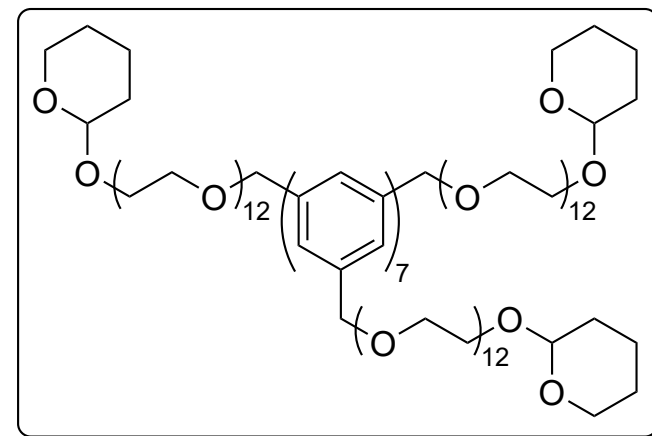


^{13}C (101 MHz, CDCl_3)

Hub³-Eg₁₂-OThp (**60**)

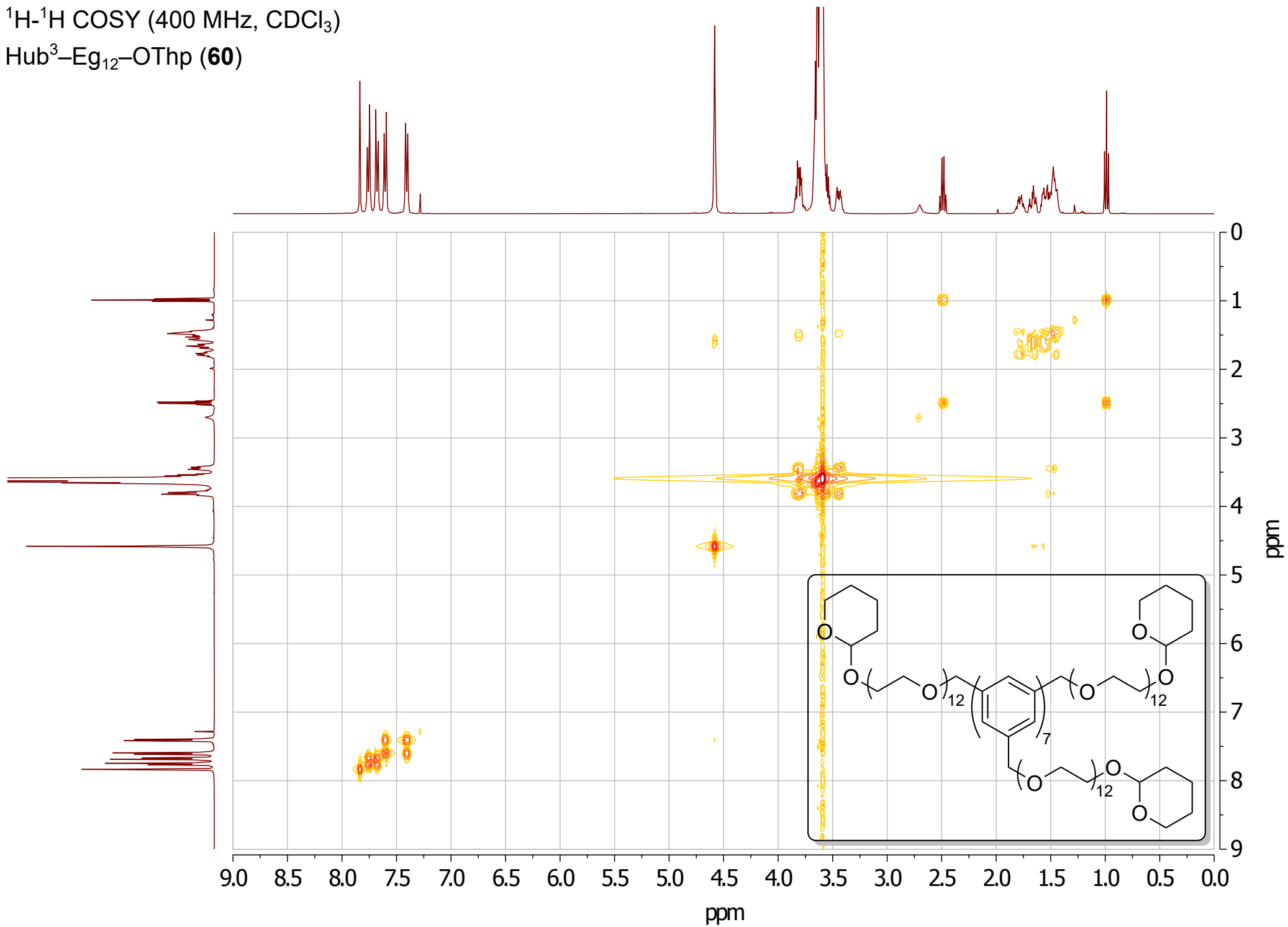


^{13}C (101 MHz, CDCl_3)
Hub³-Eg₁₂-OThp (**60**)



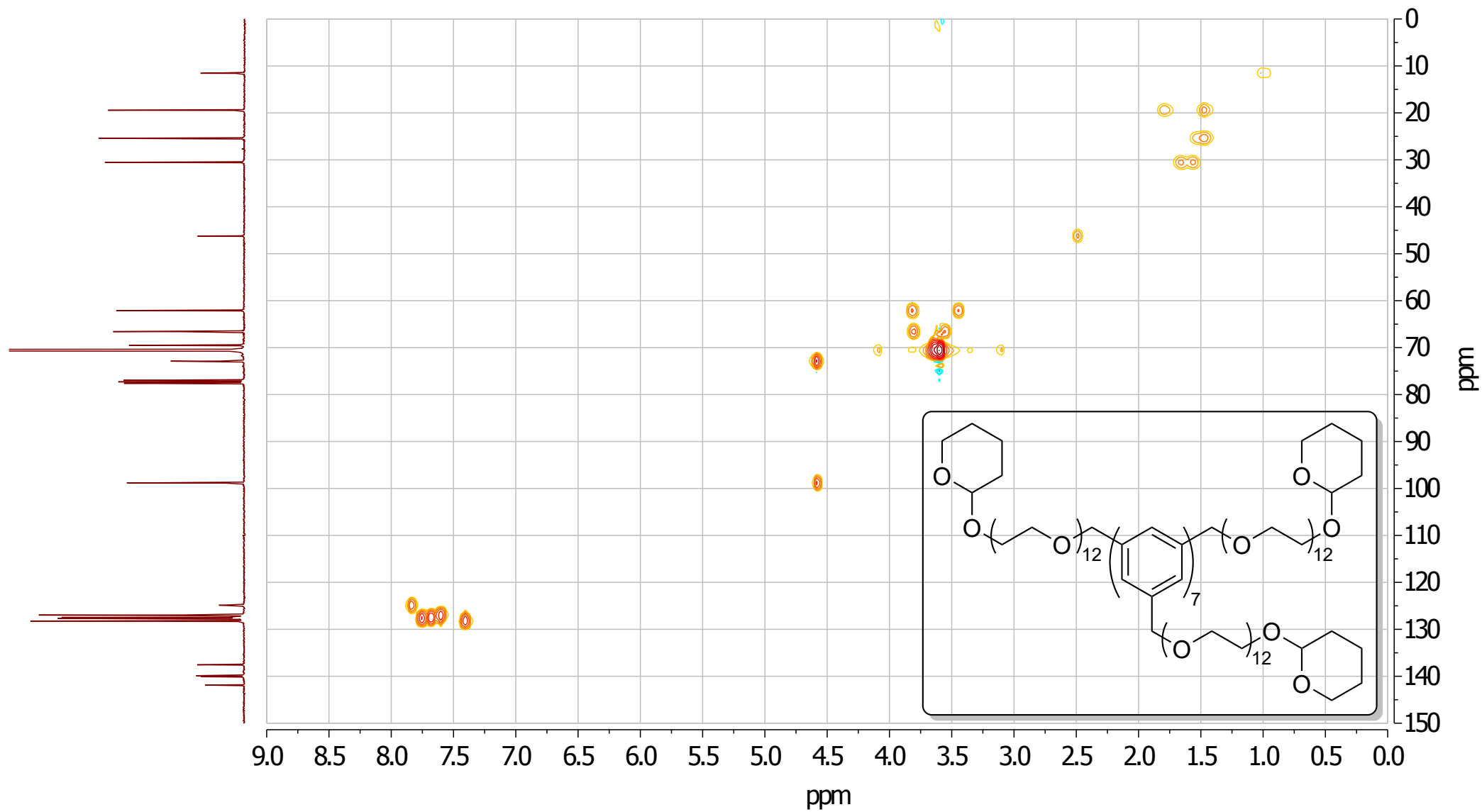
^1H - ^1H COSY (400 MHz, CDCl_3)

Hub³-Eg₁₂-OThp (**60**)



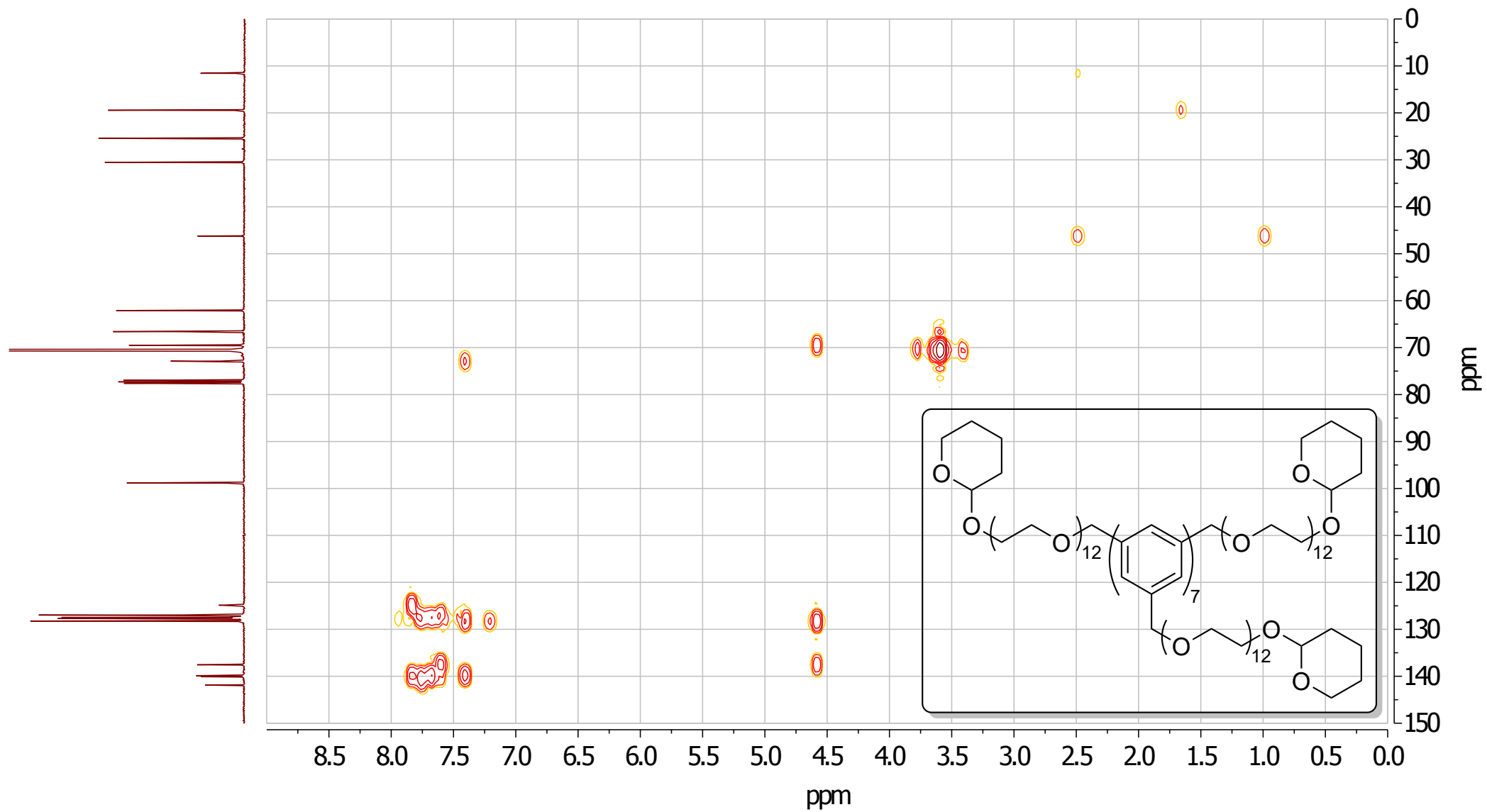
^1H - ^{13}C HSQC (400 MHz, CDCl_3)

Hub³-Eg₁₂-OThp (**60**)

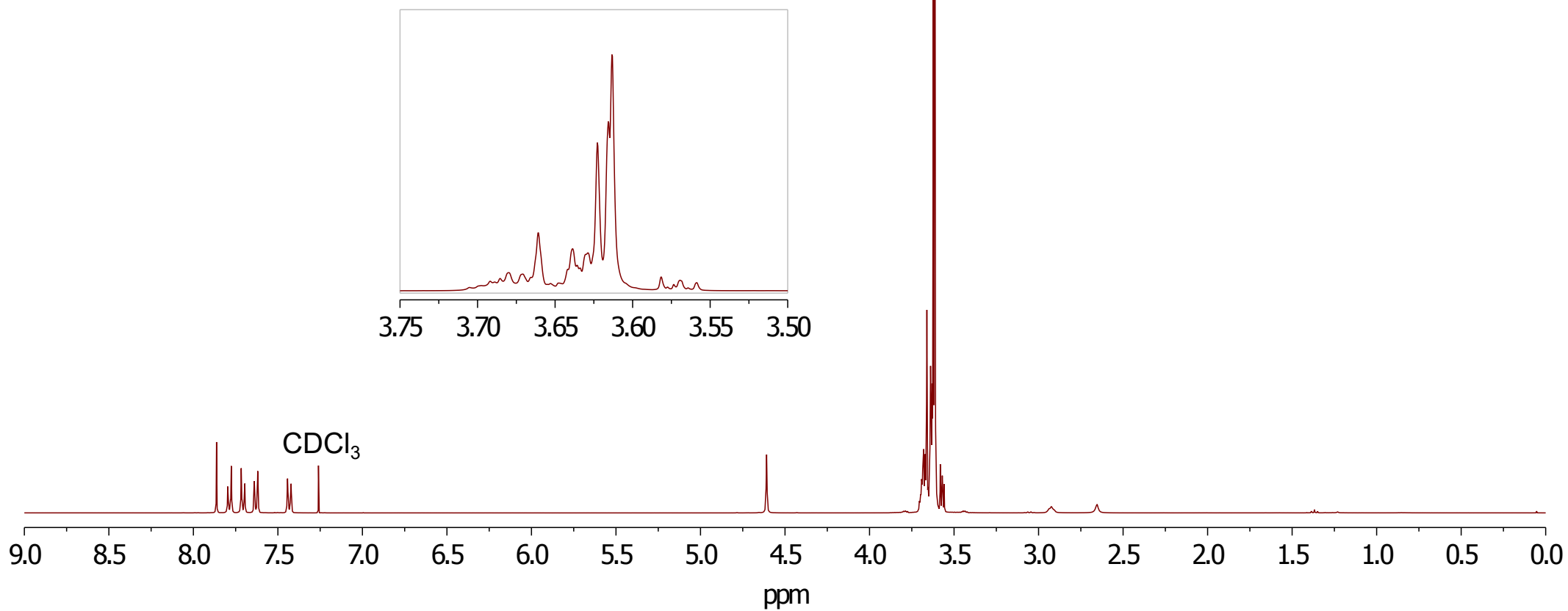
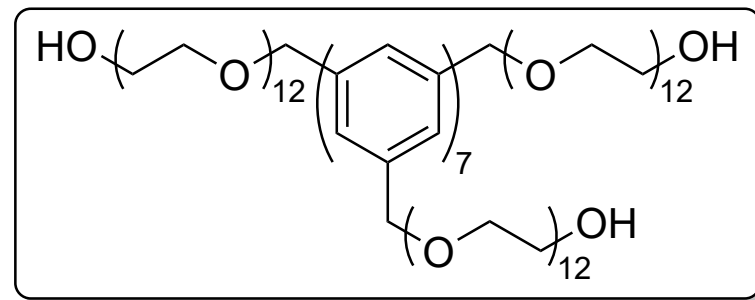


^1H - ^{13}C HMBC (400 MHz, CDCl_3)

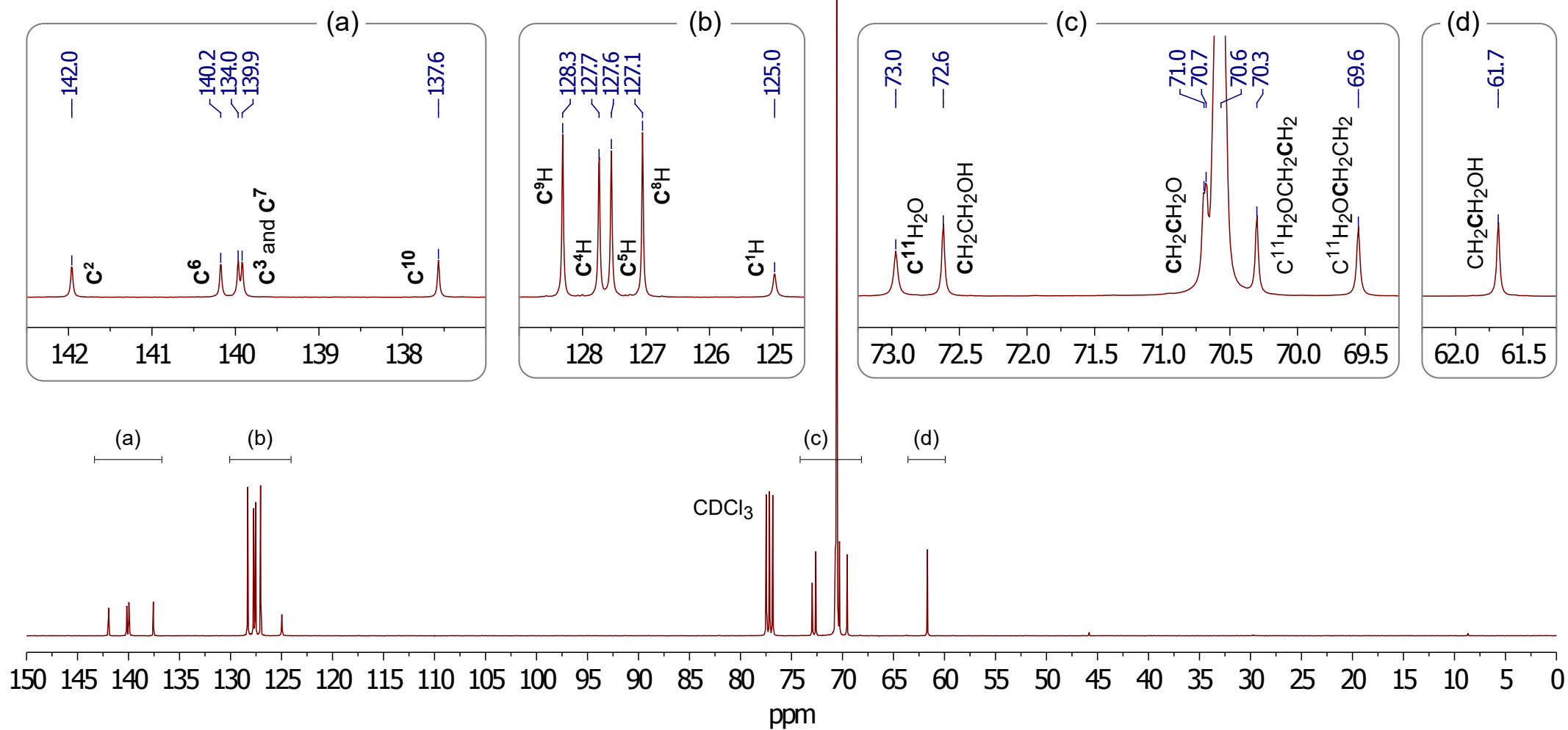
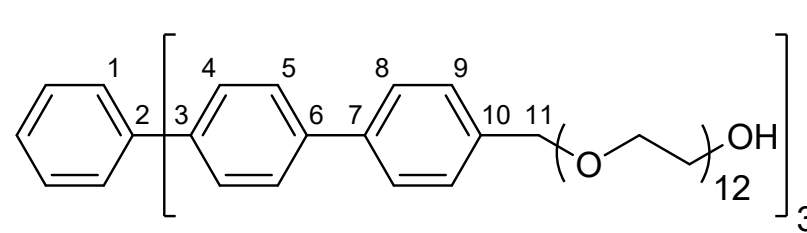
Hub³-Eg₁₂-OThp (**60**)



^1H (400 MHz, CDCl_3)
Hub³-Eg₁₂-OH (**61**)



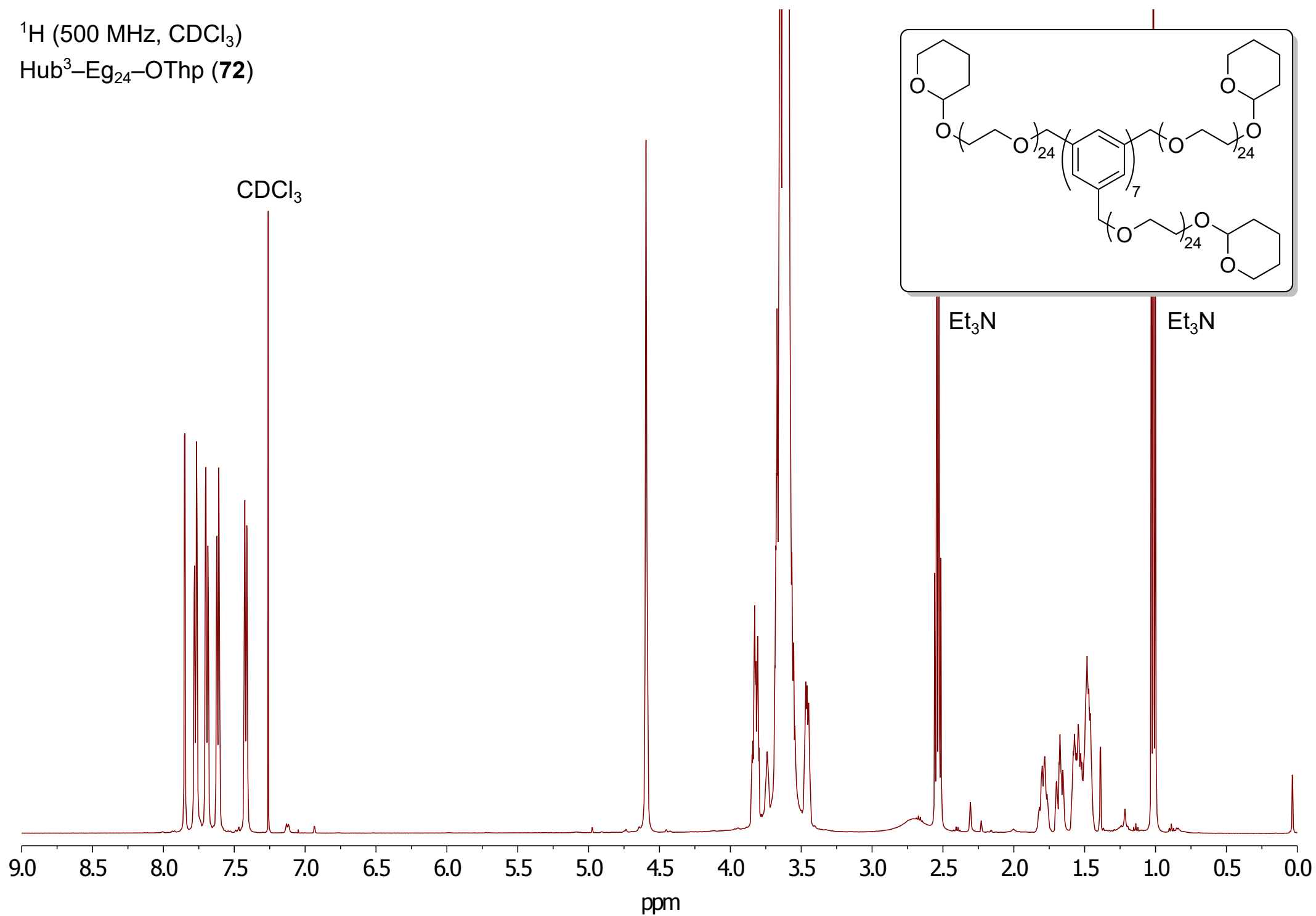
^{13}C (101 MHz, CDCl_3)
Hub³-Eg₁₂-OH (**61**)



^1H (500 MHz, CDCl_3)

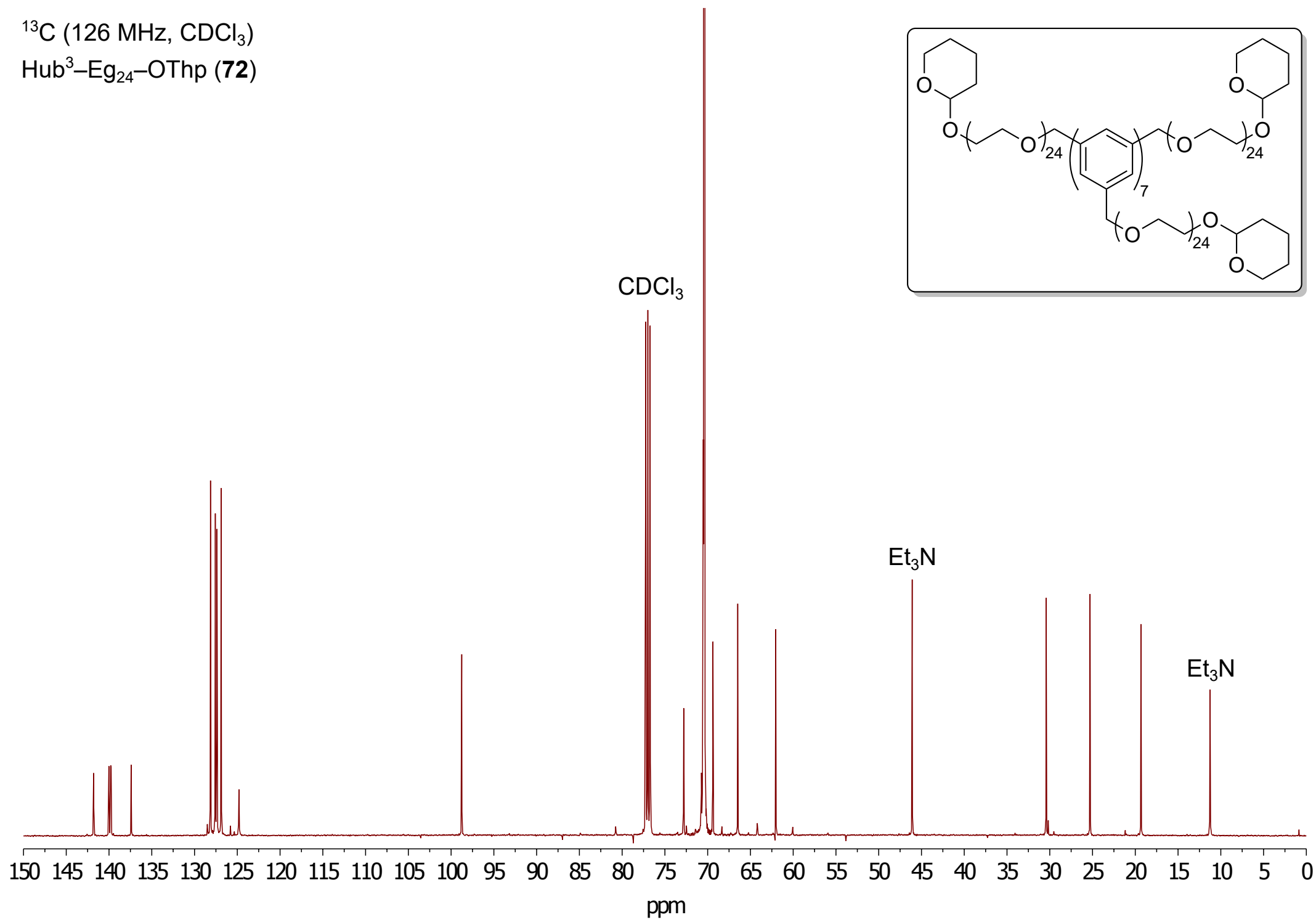
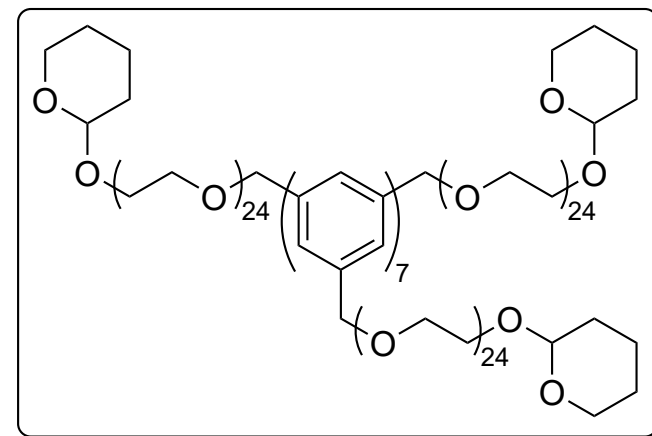
Hub³-Eg₂₄-OThp (**72**)

CDCl_3



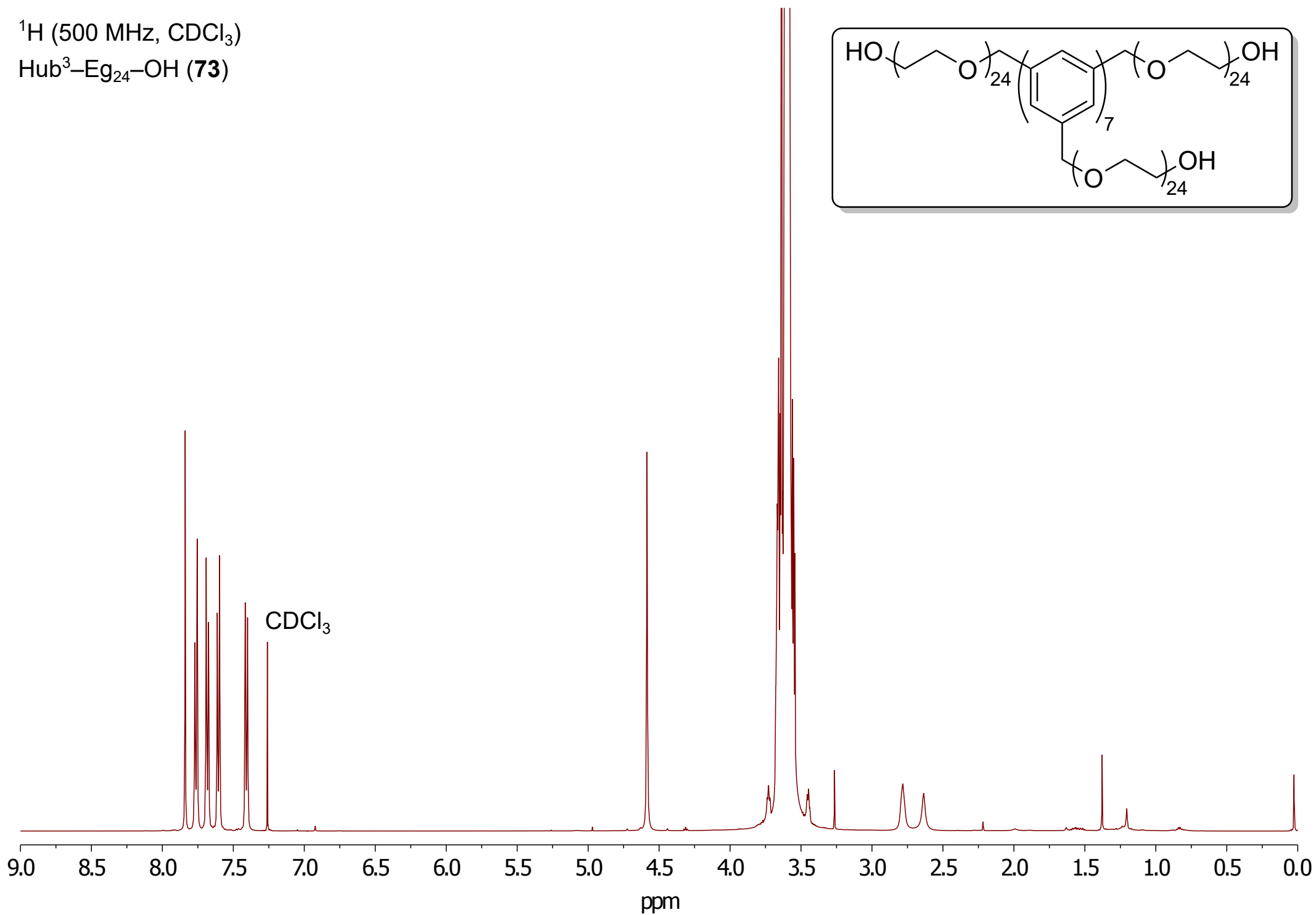
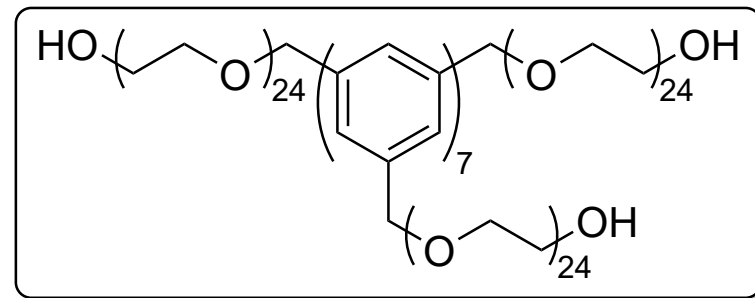
^{13}C (126 MHz, CDCl_3)

Hub³-Eg₂₄-OThp (**72**)



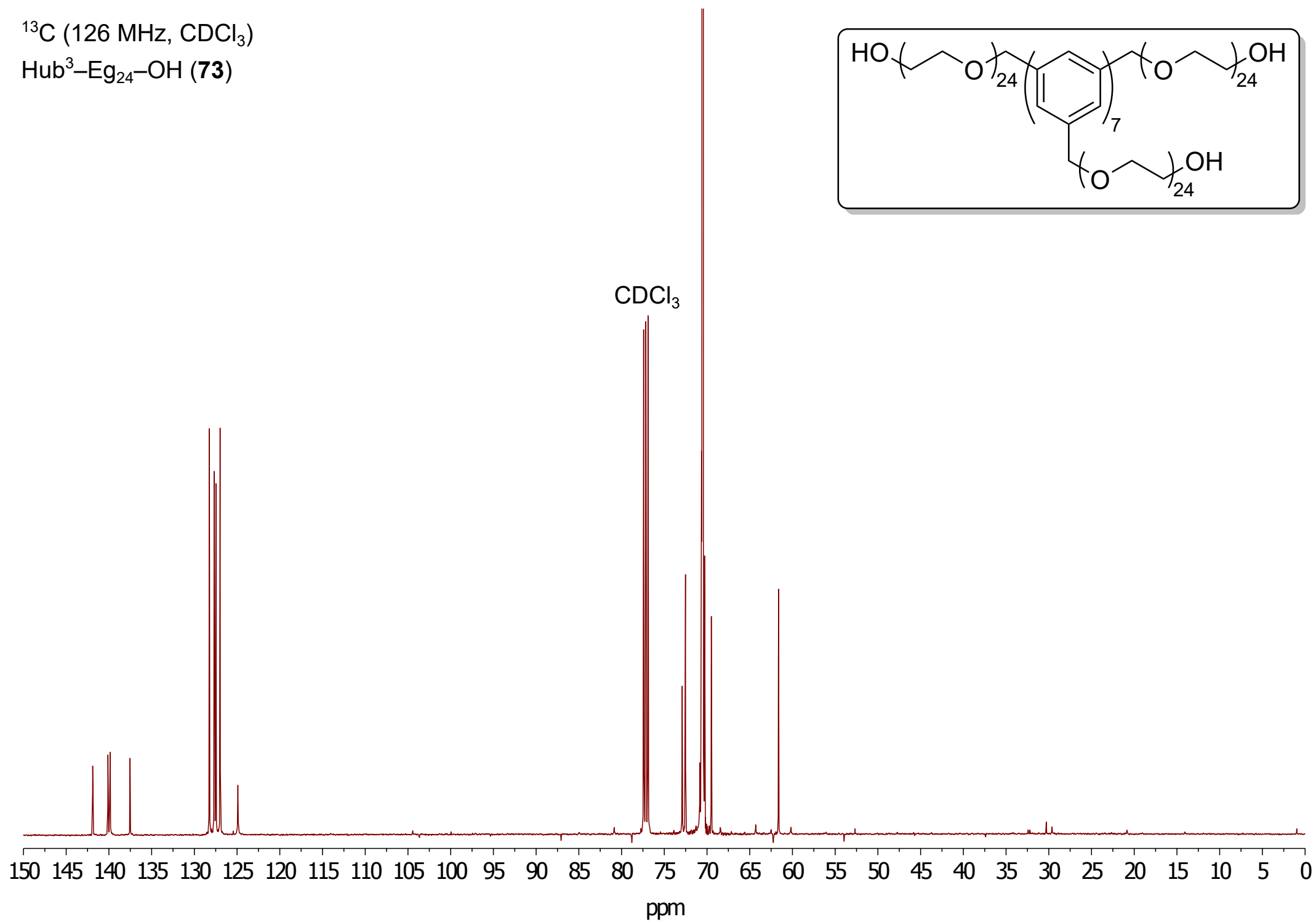
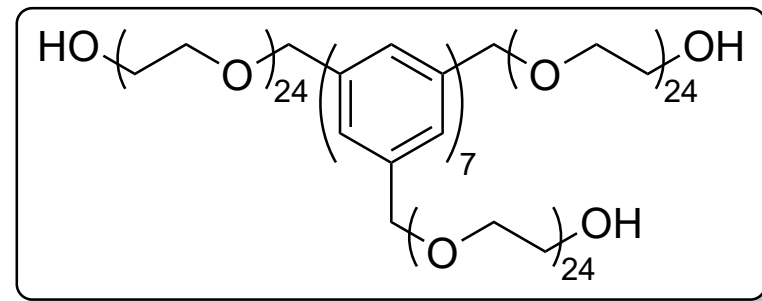
^1H (500 MHz, CDCl_3)

Hub³-Eg₂₄-OH (73)



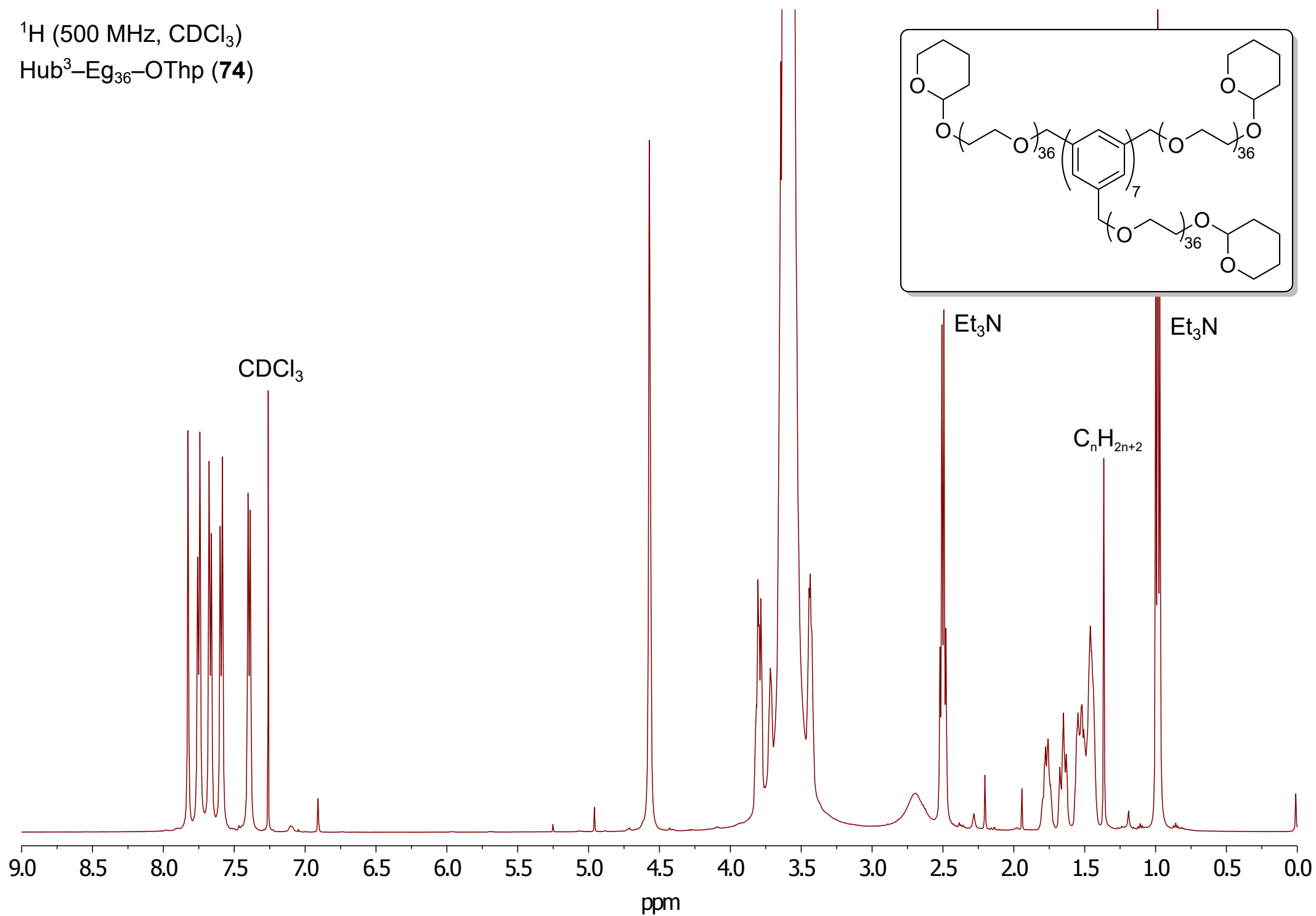
^{13}C (126 MHz, CDCl_3)

Hub³-Eg₂₄-OH (**73**)



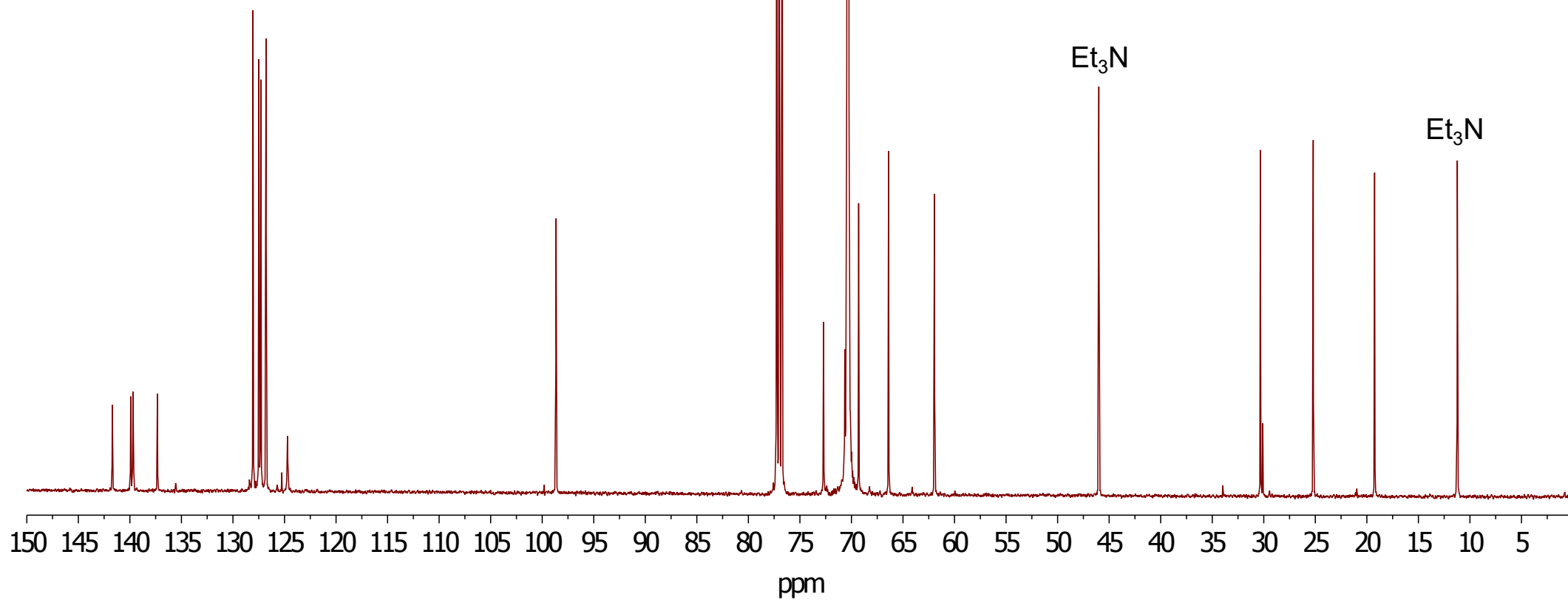
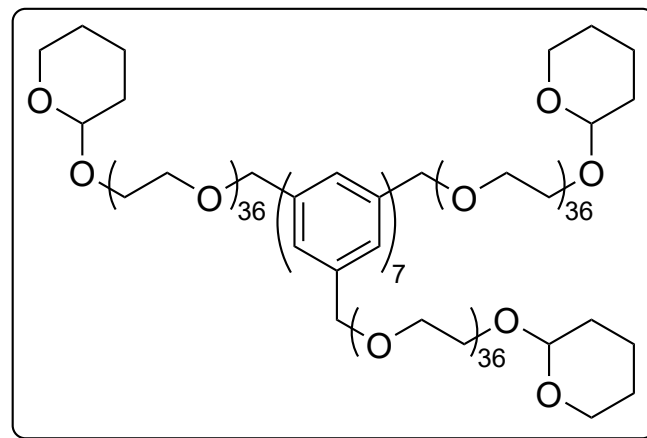
^1H (500 MHz, CDCl_3)

Hub³-Eg₃₆-OThp (**74**)



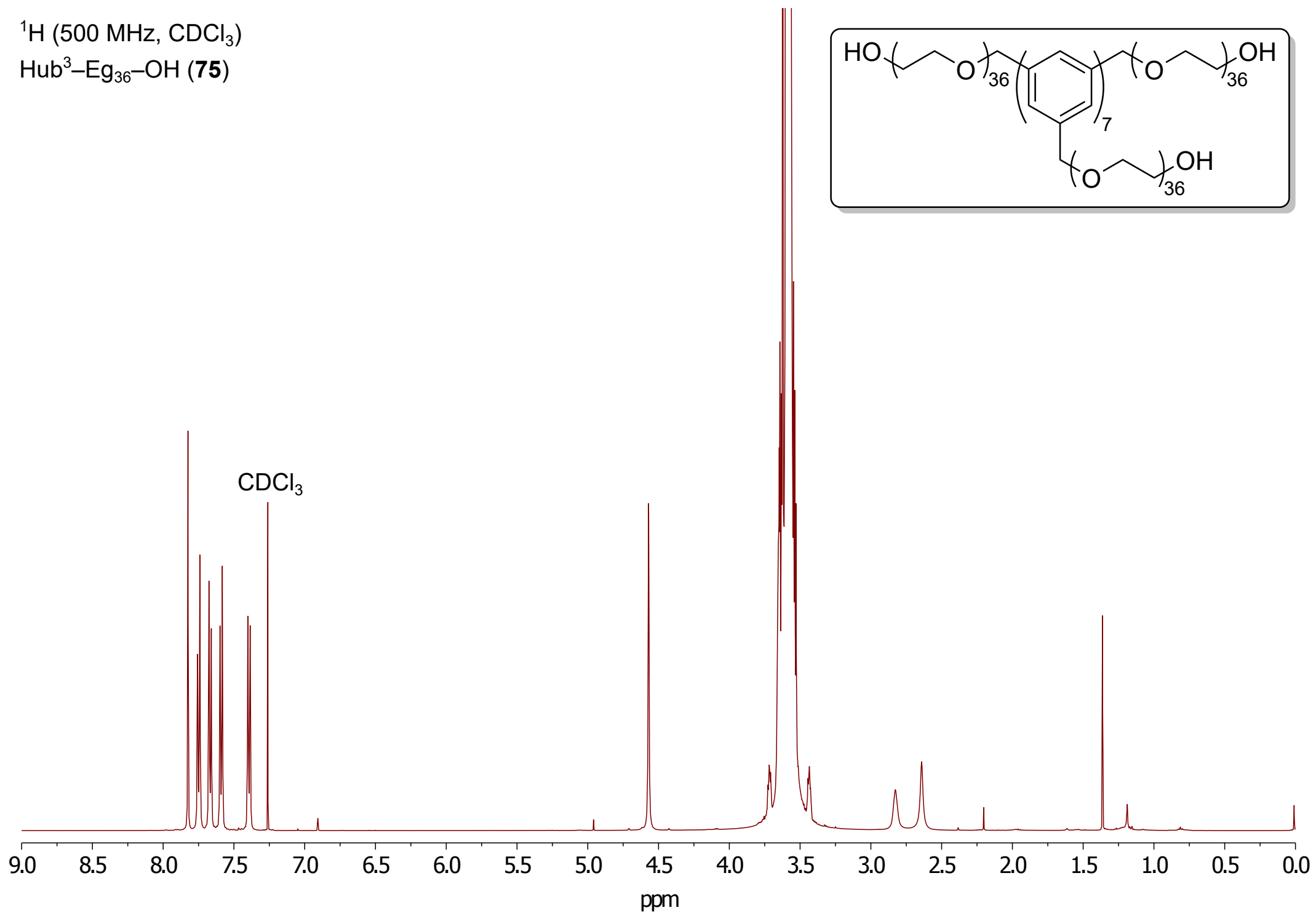
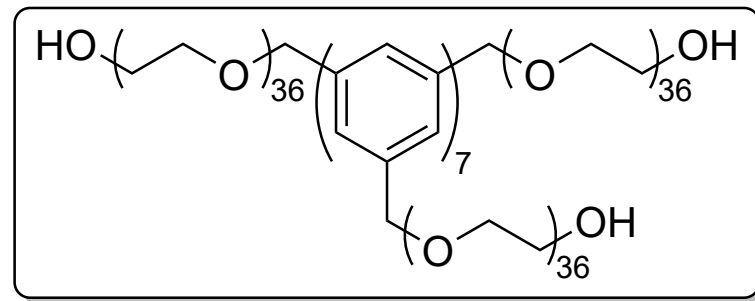
^{13}C (126 MHz, CDCl_3)
Hub³-Eg₃₆-OThp (**74**)

CDCl_3



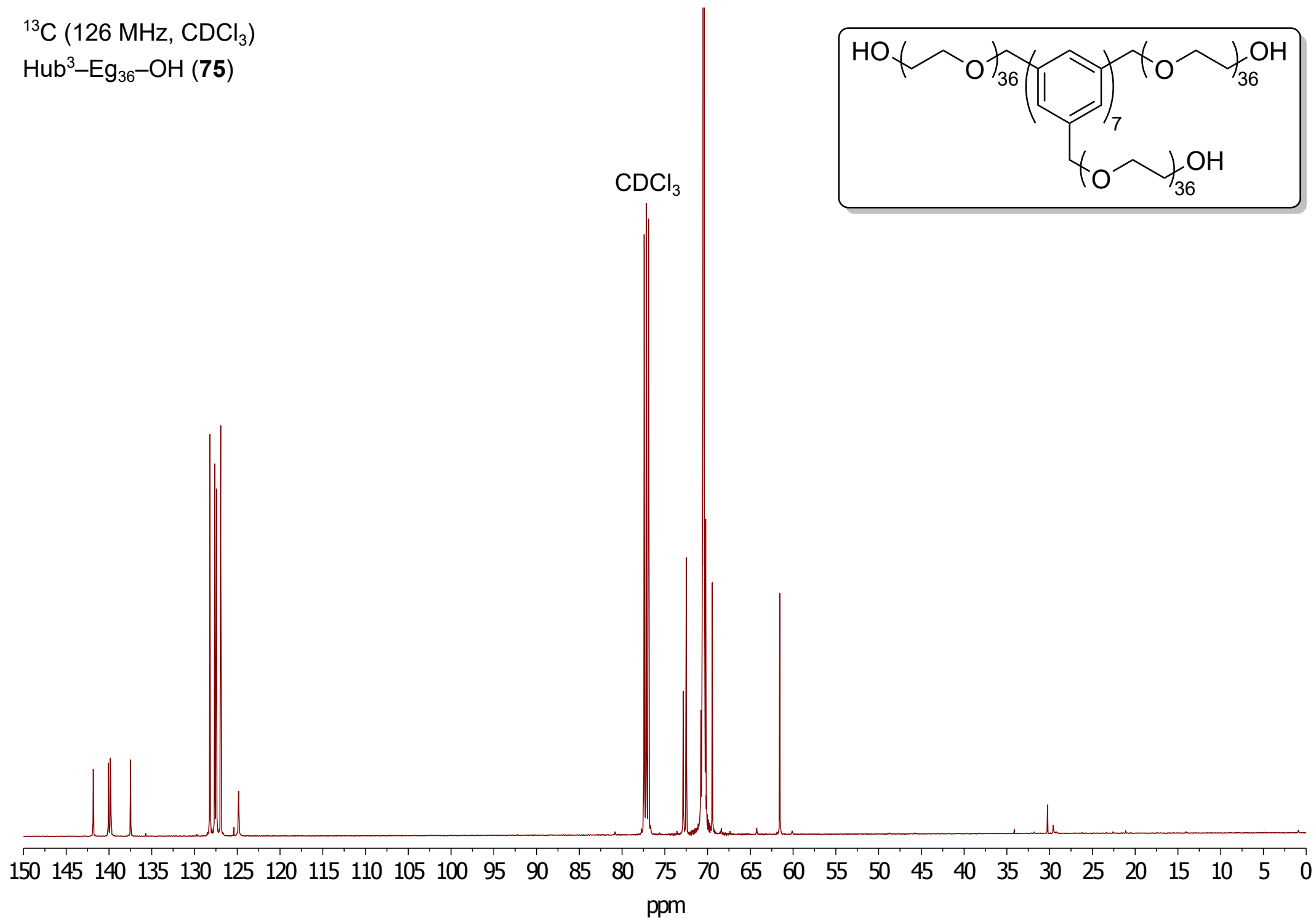
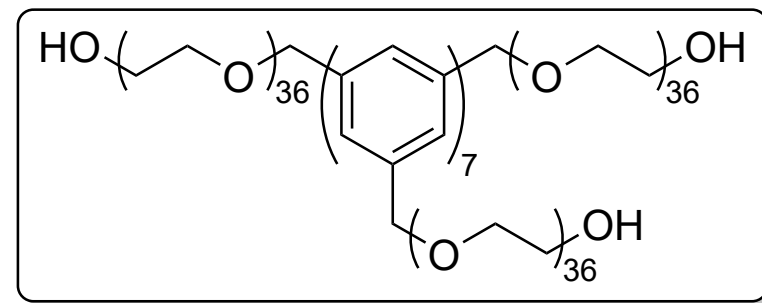
^1H (500 MHz, CDCl_3)

Hub³-Eg₃₆-OH (75)



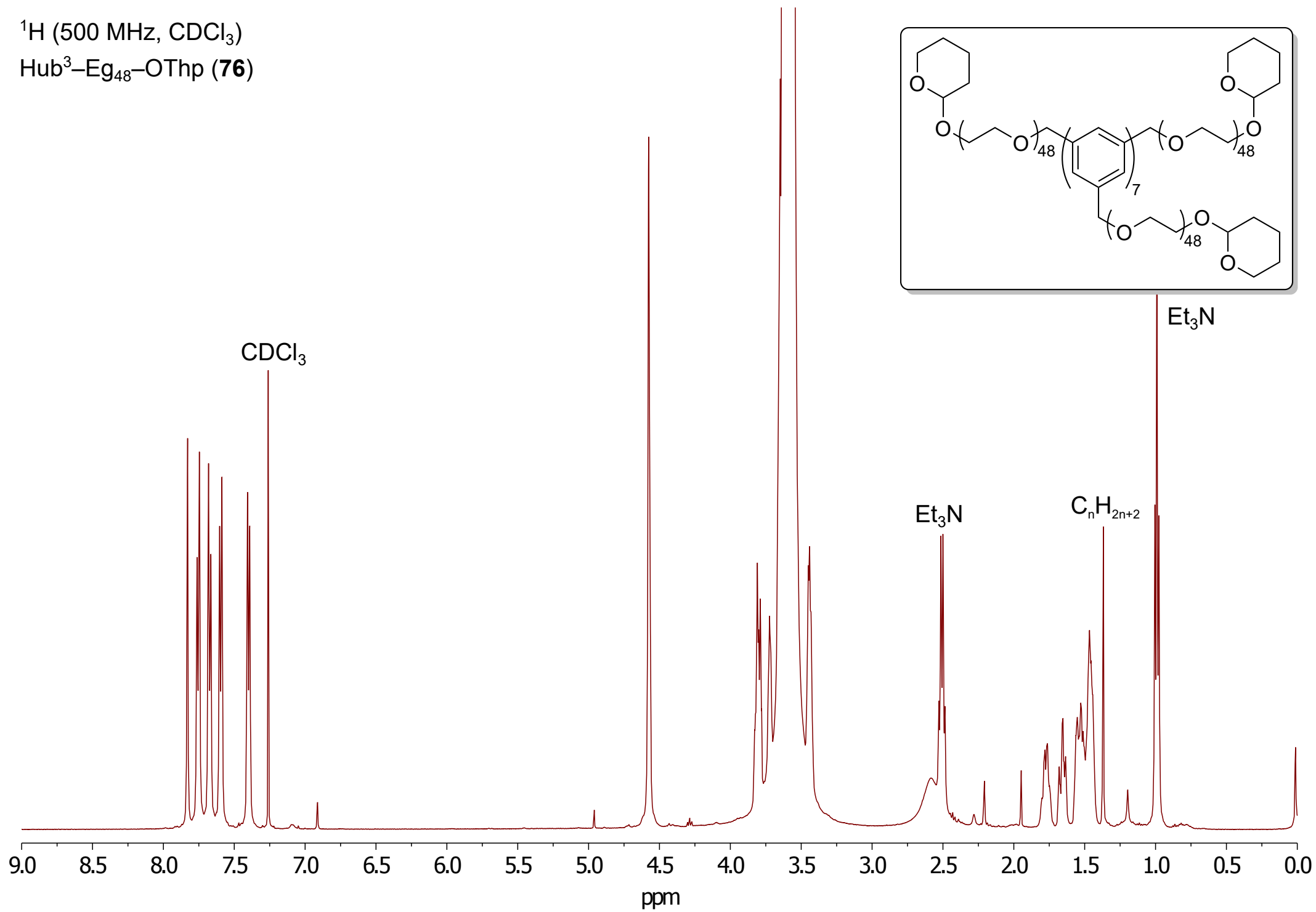
^{13}C (126 MHz, CDCl_3)

Hub³-Eg₃₆-OH (**75**)

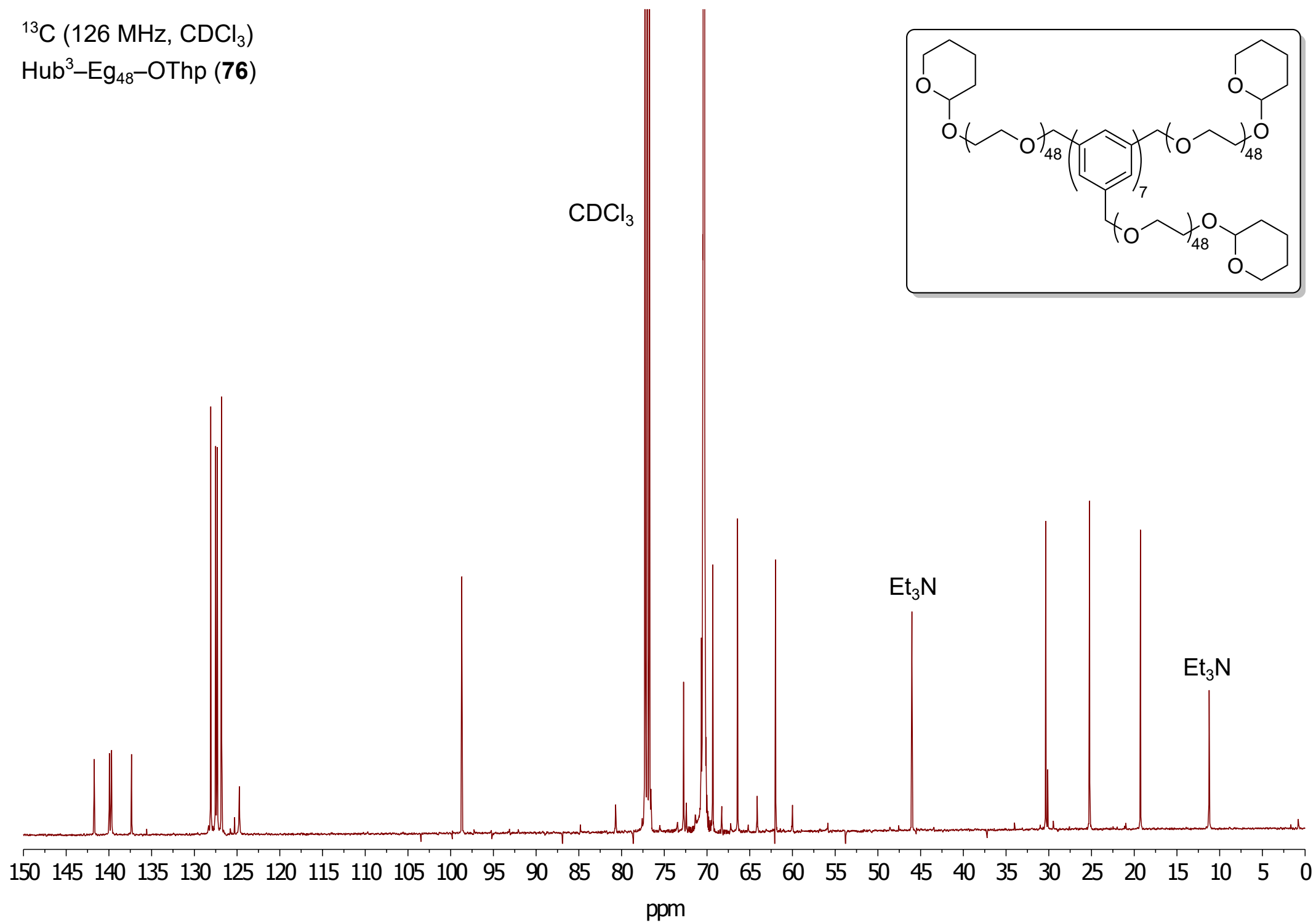
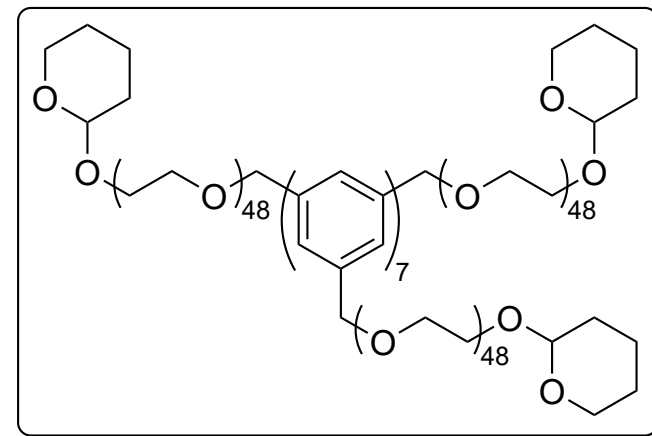


^1H (500 MHz, CDCl_3)

Hub³-Eg₄₈-OThp (**76**)

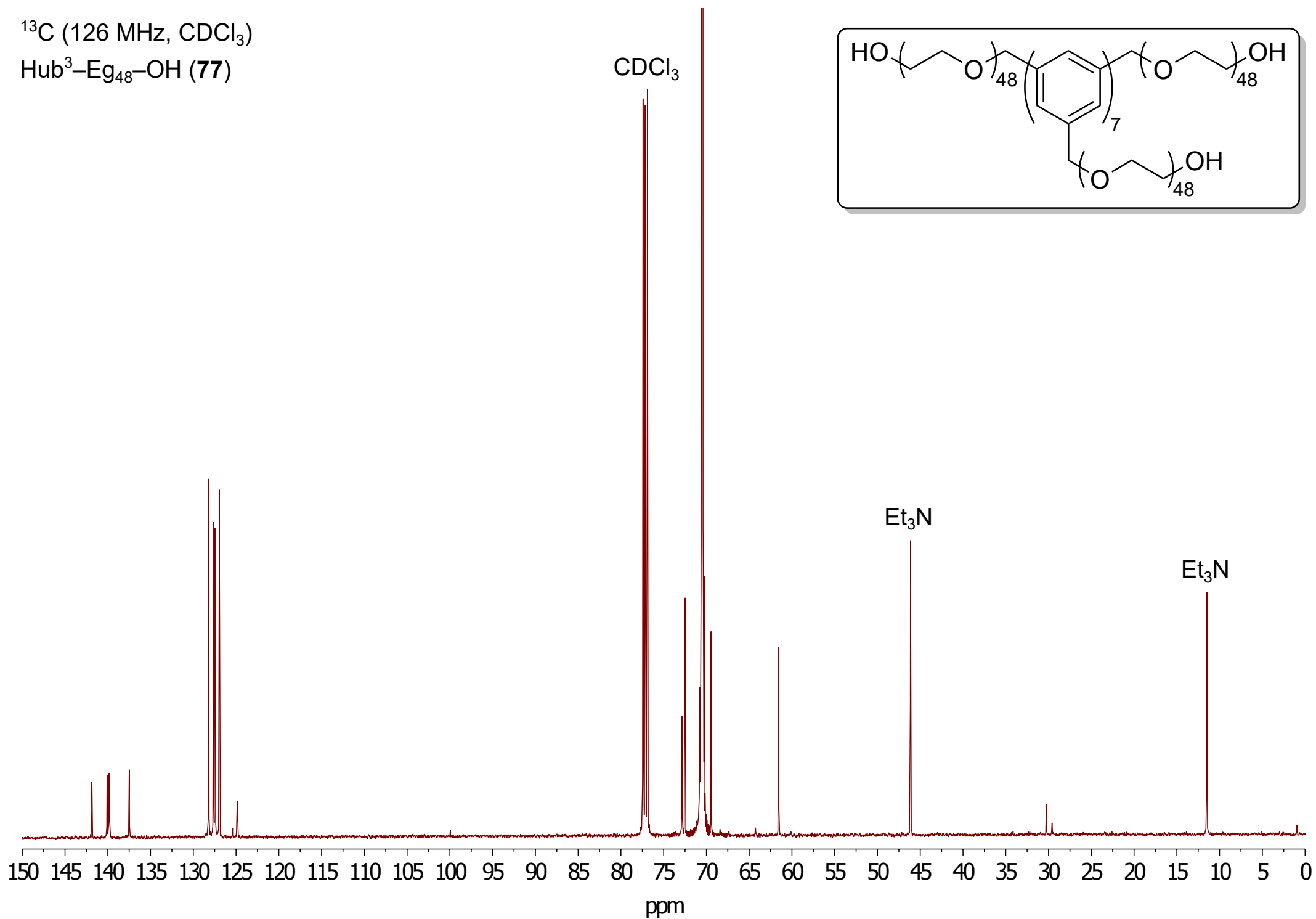
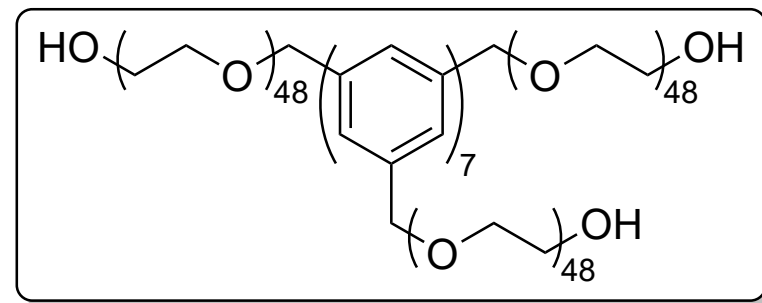


^{13}C (126 MHz, CDCl_3)
Hub³-Eg₄₈-OThp (**76**)



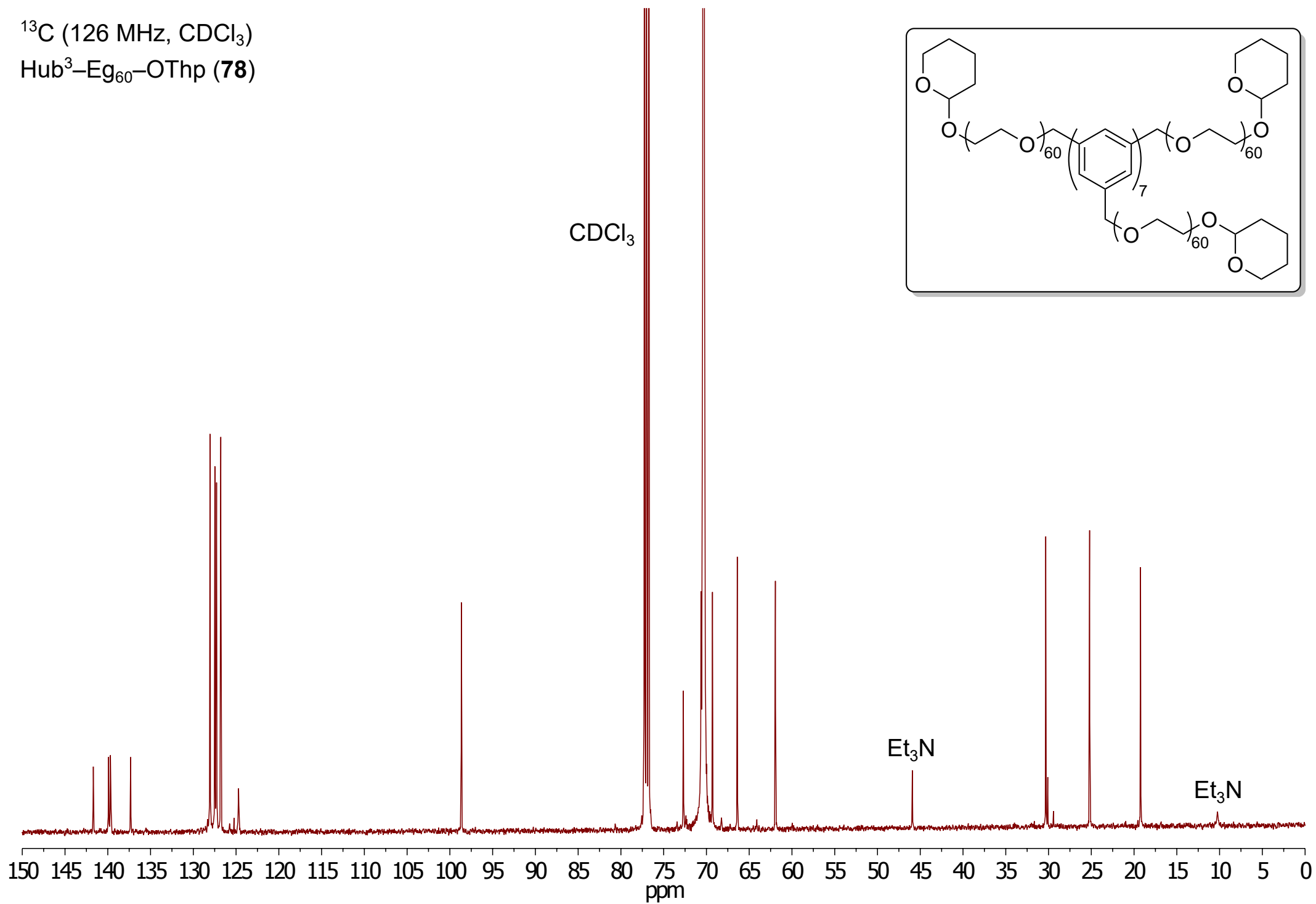
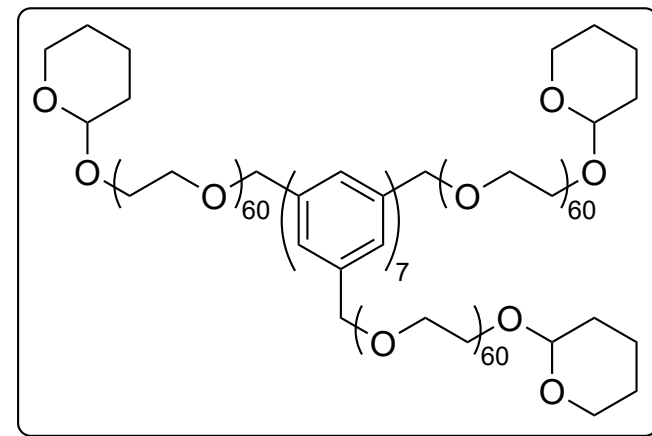
^{13}C (126 MHz, CDCl_3)

Hub³-Eg₄₈-OH (77)



^{13}C (126 MHz, CDCl_3)

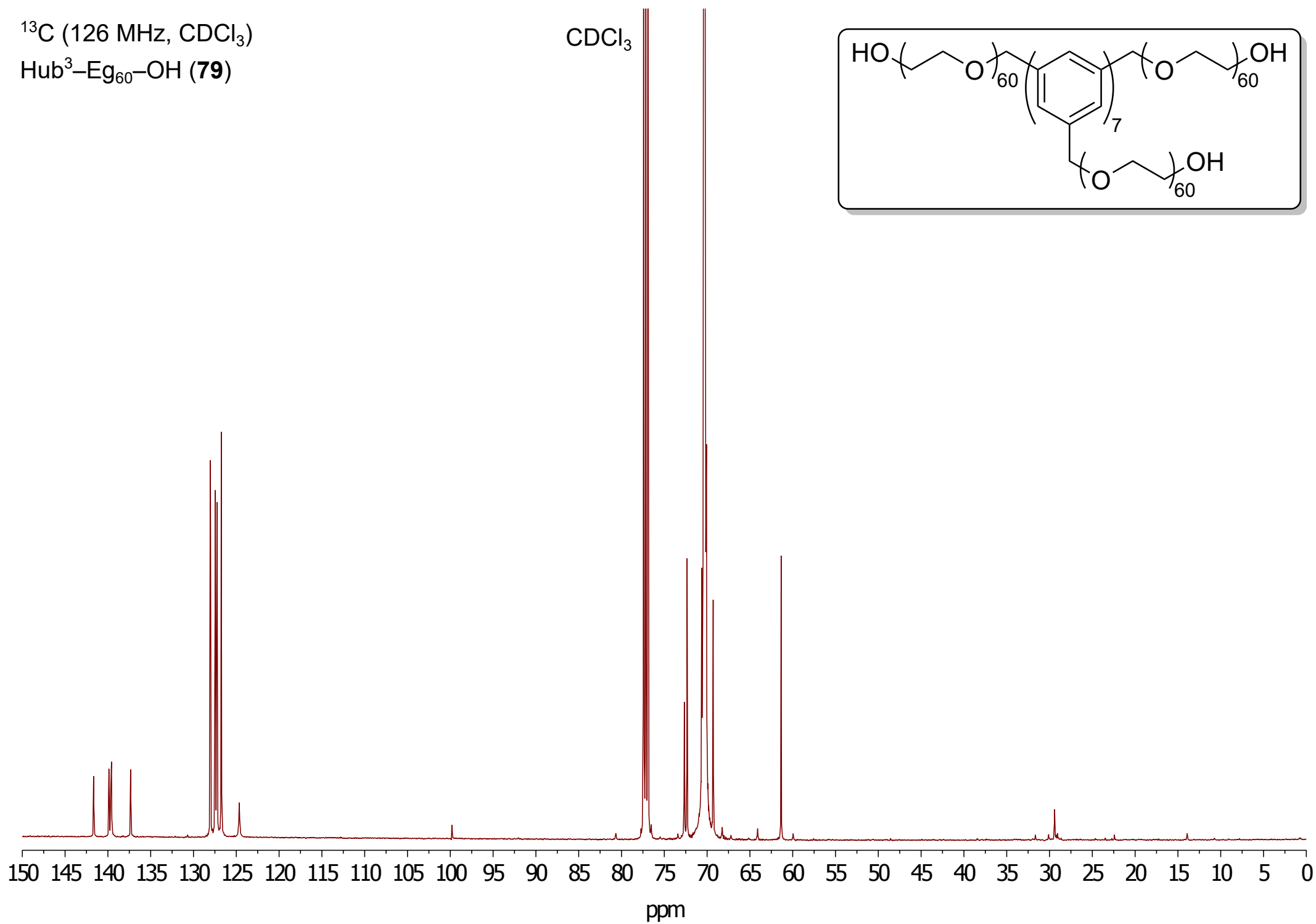
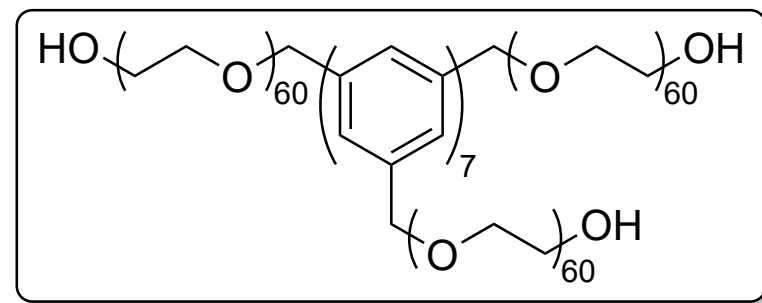
Hub³-Eg₆₀-OThp (**78**)



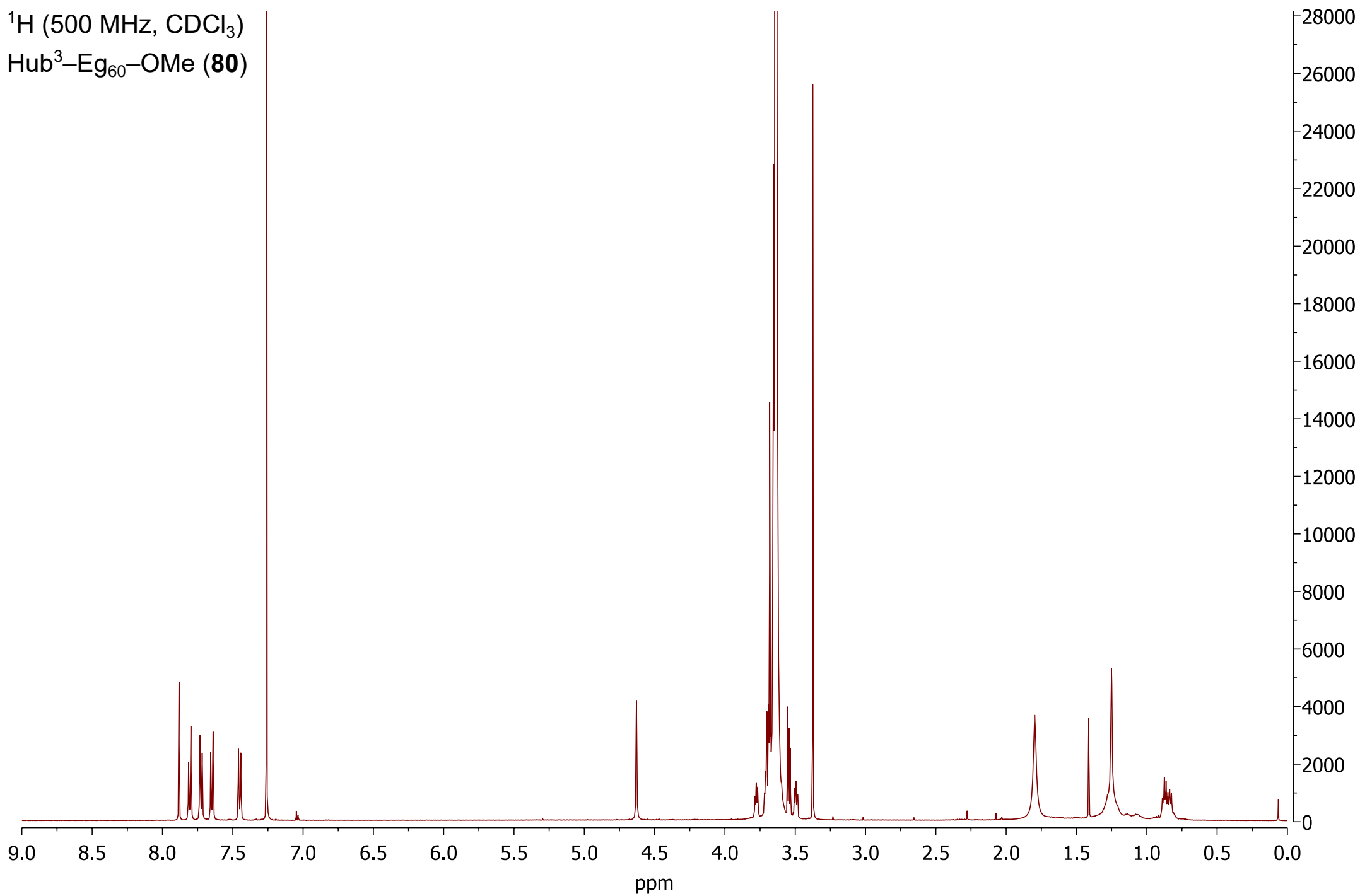
^{13}C (126 MHz, CDCl_3)

Hub³-Eg₆₀-OH (**79**)

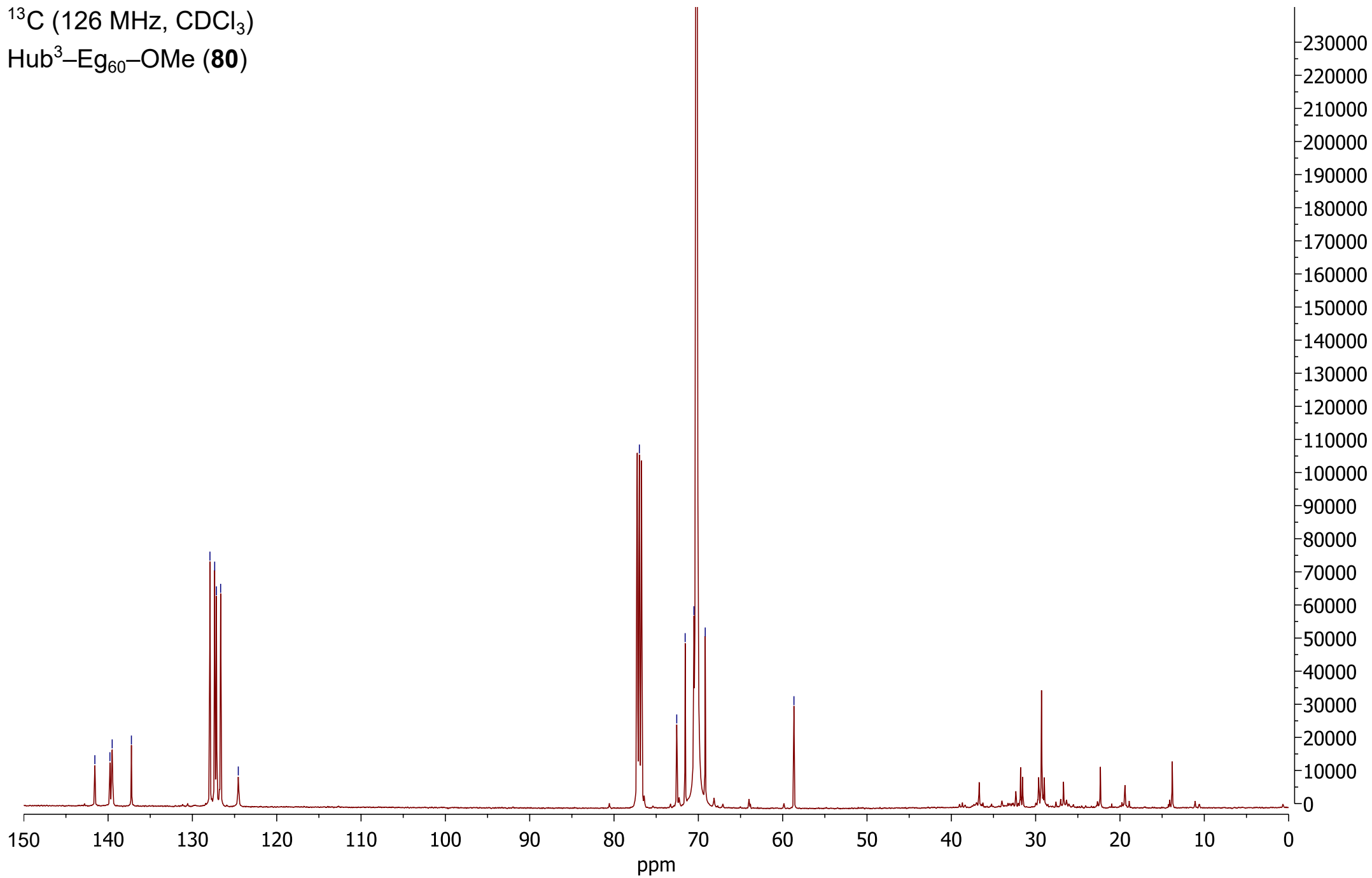
CDCl_3



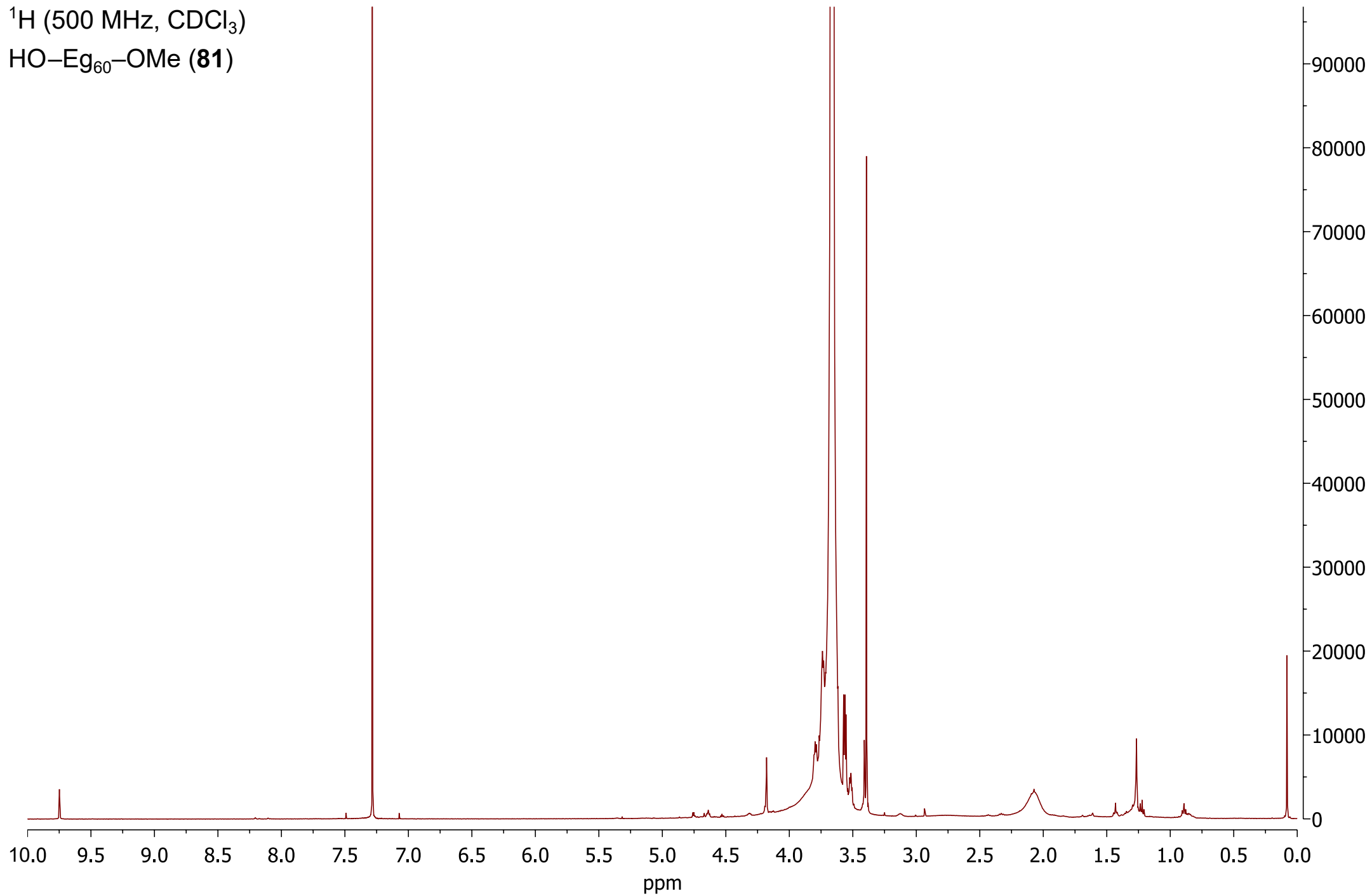
^1H (500 MHz, CDCl_3)
Hub³-Eg₆₀-OMe (**80**)



^{13}C (126 MHz, CDCl_3)
Hub³-Eg₆₀-OMe (**80**)

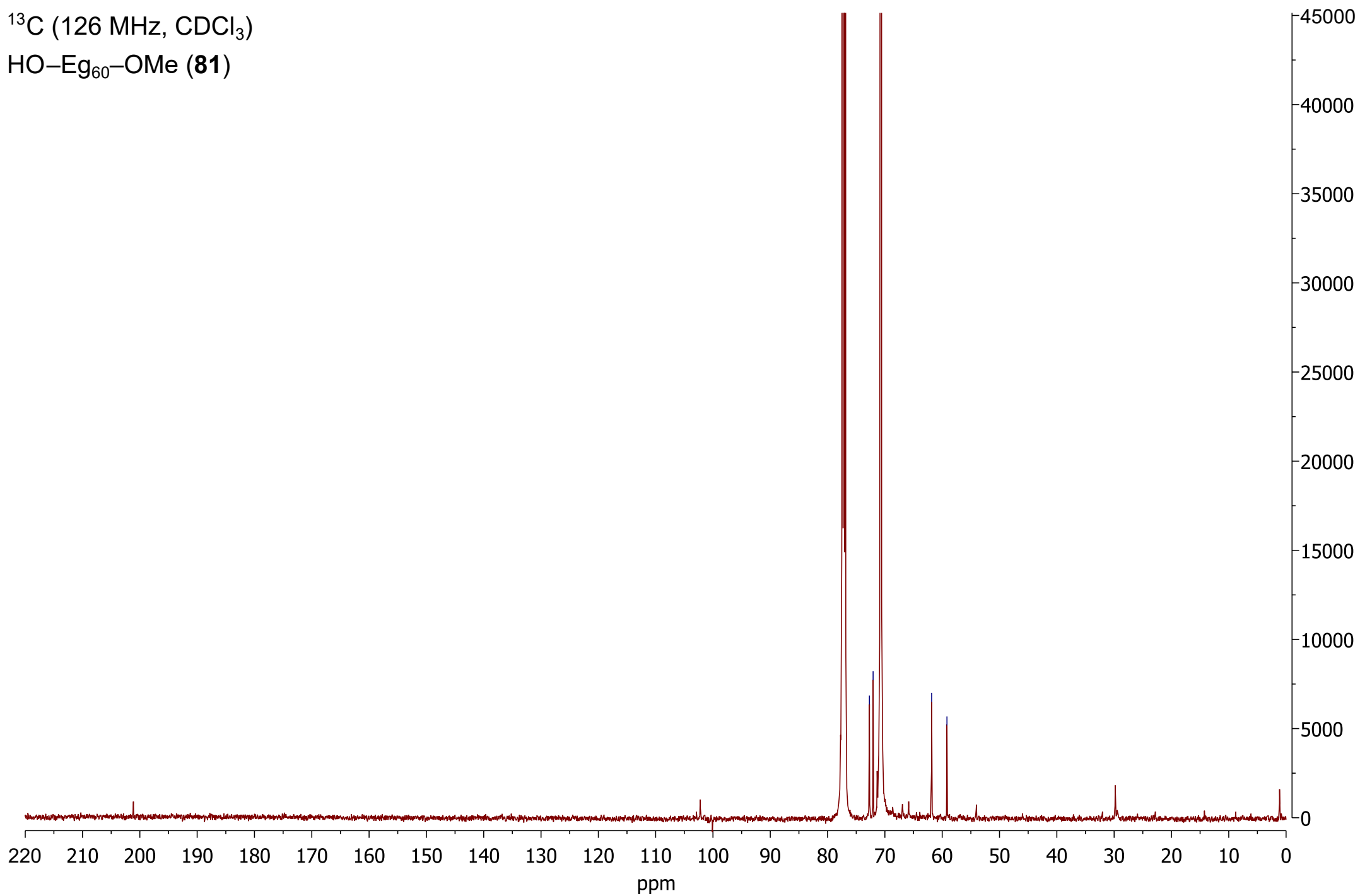


^1H (500 MHz, CDCl_3)
HO-Eg₆₀-OMe (**81**)



^{13}C (126 MHz, CDCl_3)

HO-Eg₆₀-OMe (**81**)



Permissions for use of figures and tables

Used content	Licence number	Licence date	Content Publisher	Content Publication	Reference
Figure 2 Figure 37 Figure 38 Figure 40 Figure 126 Figure 41	4195920932371	Sep 25, 2017	John Wiley & Sons	Chemistry - A European Journal	⁴
Figure 8	4195940604807	Sep 25, 2017	Royal Society of Chemistry	Chemical Communications	⁷
Figure 11 Figure 12	4195960371571	Sep 25, 2017	Nature Publishing Group	Nature	¹⁰
Figure 14	N/A (permission granted via letter)	13.02.2019	Polypure AS, Oslo Science Park, Gaustadalleen 21, NO-0349 Oslo, Norway	N/A (website content)	²⁴
Figure 20 Figure 27	4574960328518	Apr 23, 2019	John Wiley & Sons	Angewandte Chemie International Edition	²⁷
Figure 24 Figure 25	4577091124911	Apr 27, 2019	Georg Thieme Verlag KG	Synthesis	³⁷

Used content	Licence number	Licence date	Content Publisher	Content Publication	Reference
Figure 32 Table 7 Table 8 Figure 33 Figure 34	4196030683551	Sep 25, 2017	John Wiley & Sons	Angewandte Chemie International Edition	47
Figure 53	4596681135930	May 26, 2019	Elsevier	Tetrahedron Letters	34
Table 18	4604800210784	Jun 09, 2019	John Wiley & Sons	Wiley Books	61
Figure 54	4578741162263	Apr 30, 2019	Springer Nature	Nature	74
Figure 55	4578751046989	Apr 30, 2019	Royal Society of Chemistry	Chemical Communications	75
Figure 56	4578760355530	Apr 30, 2019	John Wiley & Sons	Chemistry - A European Journal	79
Figure 59	4578840447743	Apr 30, 2019	John Wiley & Sons	Wiley Books	82
Figure 63 Figure 65	4581240136905	May 03, 2019	Elsevier	Separation and Purification Technology	111
Figure 122 Table 26	4593190601904	May 20, 2019	Elsevier	Journal of Chromatography A	169
Figure 123 Figure 125	4593231381200	May 20, 2019	Elsevier	European Polymer Journal	173
Figure 127 Figure 128	4593240307854	May 20, 2019	John Wiley & Sons	Wiley Books	178

References

- 1 J. F. Kim, P. R. J. Gaffney, I. B. Valtcheva, G. Williams, A. M. Buswell, M. S. Anson and A. G. Livingston, *Org. Process Res. Dev.*, 2016, **20**, 1439–1452.
- 2 R. G. Gilbert, M. Hess, A. D. Jenkins, R. G. Jones, P. Kratochvíl and R. F. T. Stepto, *Pure Appl. Chem.*, 2009, **81**, 351–353.
- 3 S. Jevševar, M. Kunstelj and V. G. Porekar, *Biotechnol. J.*, 2010, **5**, 113–128.
- 4 G. Székely, M. Schaepertoens, P. R. J. Gaffney and A. G. Livingston, *Chem. - Eur. J.*, 2014, **20**, 10038–10051.
- 5 Jenkins A. D., Kratochvíl P., Stepto R. F. T. and Suter U. W., *Pure Appl. Chem.*, 1996, **68**, 2287.
- 6 T. T. Trinh, C. Laure and J.-F. Lutz, *Macromol. Chem. Phys.*, 2015, **216**, 1498–1506.
- 7 P. R. L. Malenfant and J. M. J. Frechet, *Chem. Commun.*, 1998, 2657–2658.
- 8 O. Renaudet and J.-L. Reymond, *Org. Lett.*, 2004, **6**, 397–400.
- 9 J. W. Grate, K.-F. Mo and M. D. Daily, *Angew. Chem. Int. Ed.*, 2016, **55**, 3925–3930.
- 10 M. Burns, S. Essafi, J. R. Bame, S. P. Bull, M. P. Webster, S. Balieu, J. W. Dale, C. P. Butts, J. N. Harvey and V. K. Aggarwal, *Nature*, 2014, **513**, 183–188.
- 11 J. Staunton and K. J. Weissman, *Nat. Prod. Rep.*, 2001, **18**, 380–416.
- 12 C. S. Fishburn, *J. Pharm. Sci.*, 2008, **97**, 4167–4183.
- 13 J. M. Harris and R. B. Chess, *Nat Rev Drug Discov*, 2003, **2**, 214–221.
- 14 J. Herzberger, K. Niederer, H. Pohlit, J. Seiwert, M. Worm, F. R. Wurm and H. Frey, *Chem. Rev.*, 2016, **116**, 2170–2243.
- 15 K. Knop, R. Hoogenboom, D. Fischer and U. S. Schubert, *Angew. Chem. Int. Ed.*, 2010, **49**, 6288–6308.
- 16 M. C. Parrott and J. M. DeSimone, *Nat Chem*, 2012, **4**, 13–14.
- 17 F. M. Veronese and A. Mero, *BioDrugs*, 2008, **22**, 315–329.
- 18 F. M. Veronese and G. Pasut, *Drug Discov. Today*, 2005, **10**, 1451–1458.
- 19 F. M. Veronese, P. Caliceti and O. Schiavon, *J. Bioact. Compat. Polym.*, 1997, **12**, 196–207.
- 20 M. S. Thompson, T. P. Vadala, M. L. Vadala, Y. Lin and J. S. Riffle, *Polymer*, 2008, **49**, 345–373.
- 21 P. L. Turecek, M. J. Bossard, F. Schoetens and I. A. Ivens, *J. Pharm. Sci.*, 2016, **105**, 460–475.
- 22 A. Weber, A. Engelmaier, G. Mohr, S. Haindl, H. P. Schwarz and P. L. Turecek, *J. Pharm. Biomed. Anal.*, 2017, **132**, 207–214.
- 23 S. P. Povoski, P. D. Davis, D. Colcher and E. W. Martin Jr, *Expert Rev. Mol. Diagn.*, 2013, **13**, 315–319.
- 24 Polypure AS (Norway), Monodispersity & PDI, <https://polypure.com/sites/default/files/Monodispersity%20%26%20PDI.pdf>, (accessed 18 April 2019).
- 25 P. Rittmeyer and U. Wietelmann, *Hydrides in Ullmann's Encyclopedia of Industrial Chemistry*, American Cancer Society, 2000.
- 26 A. Williamson, *Philos. Mag. Ser. 3*, 1850, **37**, 350–356.
- 27 A. C. French, A. L. Thompson and B. G. Davis, *Angew. Chem. Int. Ed.*, 2009, **48**, 1248–1252.
- 28 S. A. Ahmed and M. Tanaka, *J. Org. Chem.*, 2006, **71**, 9884–9886.
- 29 D. Niculescu-Duvaz, J. Getaz and C. J. Springer, *Bioconjug. Chem.*, 2008, **19**, 973–981.
- 30 K. Maranski, Y. G. Andreev and P. G. Bruce, *Angew. Chem. Int. Ed.*, 2014, **53**, 6411–6413.
- 31 N. Boden, R. J. Bushby, S. Clarkson, S. D. Evans, P. F. Knowles and A. Marsh, *Tetrahedron*, 1997, **53**, 10939–10952.
- 32 E. M. D. Keegstra, J. W. Zwikker, M. R. Roest and L. W. Jenneskens, *J. Org. Chem.*, 1992, **57**, 6678–6680.
- 33 Y. Chen and G. L. Baker, *J. Org. Chem.*, 1999, **64**, 6870–6873.
- 34 D. Lumpi, C. Braunschier, C. Hametner, E. Horkel, B. Zachhuber, B. Lendl and J. Fröhlich, *Tetrahedron Lett.*, 2009, **50**, 6469–6471.
- 35 C. M. Gothard and B. A. Grzybowski, *Synthesis*, 2012, **2012**, 717–722.

- 36 Ouchi Mikio, Inoue Yoshihisa, Liu Yu, Nagamune Satoshi, Nakamura Satoko, Wada Kazuhito and Hakushi Tadao, *Bull. Chem. Soc. Jpn.*, 1990, **63**, 1260–1262.
- 37 B. A. Burkett and T. H. Chan, *Synthesis*, 2004, **2004**, 1007–1010.
- 38 F. A. Loiseau, K. K. (Mimi) Hii and A. M. Hill, *J. Org. Chem.*, 2004, **69**, 639–647.
- 39 T. Ikawa, H. Sajiki and K. Hirota, *Tetrahedron*, 2004, **60**, 6189–6195.
- 40 L. H. Kaisalo and T. A. Hase, *Tetrahedron Lett.*, 2001, **42**, 7699–7701.
- 41 H. Sajiki, T. Ikawa and K. Hirota, *Tetrahedron Lett.*, 2003, **44**, 7407–7410.
- 42 T. C. Wabnitz, J.-Q. Yu and J. B. Spencer, *Chem. – Eur. J.*, 2004, **10**, 484–493.
- 43 A. M. Wawro, T. Muraoka, M. Kato and K. Kinbara, *Org. Chem. Front.*, 2016, **3**, 1524–1534.
- 44 A. M. Wawro, T. Muraoka and K. Kinbara, *Polym. Chem.*, 2016, **7**, 2389–2394.
- 45 Y. Li, Q. Guo, X. Li, H. Zhang, F. Yu, W. Yu, G. Xia, M. Fu, Z. Yang and Z.-X. Jiang, *Tetrahedron Lett.*, 2014, **55**, 2110–2113.
- 46 W. Zhang and D. P. Curran, *Tetrahedron*, 2006, **62**, 11837–11865.
- 47 H. Zhang, X. Li, Q. Shi, Y. Li, G. Xia, L. Chen, Z. Yang and Z.-X. Jiang, *Angew. Chem. Int. Ed.*, 2015, **54**, 3763–3767.
- 48 Y. Li, X. Qiu and Z.-X. Jiang, *Org. Process Res. Dev.*, 2015, **19**, 800–805.
- 49 D. Ormerod, B. Noten, M. Dorbec, L. Andersson, A. Buekenhoudt and L. Goetelen, *Org. Process Res. Dev.*, 2015, **19**, 841–848.
- 50 M. Huibers, Á. Manuzi, F. P. J. T. Rutjes and F. L. van Delft, *J. Org. Chem.*, 2006, **71**, 7473–7476.
- 51 G. Lapienis, *Prog. Polym. Sci.*, 2009, **34**, 852–892.
- 52 G. Szekely, M. Schaeperstoens, P. R. J. Gaffney and A. G. Livingston, *Polym. Chem.*, 2014, **5**, 694–697.
- 53 K. B. Sharpless, A. O. Chong and J. A. Scott, *J. Org. Chem.*, 1975, **40**, 1252–1257.
- 54 A. Bouzide and G. Sauvé, *Org. Lett.*, 2002, **4**, 2329–2332.
- 55 H. Nakatsuji, K. Ueno, T. Misaki and Y. Tanabe, *Org. Lett.*, 2008, **10**, 2131–2134.
- 56 C. B. Reese, H. T. Serafinowska and G. Zappia, *Tetrahedron Lett.*, 1986, **27**, 2291–2294.
- 57 B. Trathnigg and H. Ahmed, *Anal. Bioanal. Chem.*, 2011, **399**, 1523–1534.
- 58 R. E. Gawley and D. D. Hennings, *Sodium Hydride in Encyclopedia of Reagents for Organic Synthesis*, American Cancer Society, 2006.
- 59 C. Reichardt, *Chem. Rev.*, 1994, **94**, 2319–2358.
- 60 C. Reichardt, *Pure Appl. Chem.*, 2008, **80**, 1415–1432.
- 61 C. Reichardt and T. Welton, *Solvents and Solvent Effects in Organic Chemistry*, Wiley-VCH Verlag GmbH & Co. KGaA, Weinheim, 4th edition., 2011.
- 62 U. Wietelmann, M. Felderhoff and P. Rittmeyer, *Hydrides in Ullmann's Encyclopedia of Industrial Chemistry*, American Cancer Society, 2016, pp. 1–39.
- 63 J. Buckley, R. Lee Webb, T. Laird and J. Ward, *Chem. Eng. News*, 1982, **60**, 4–5.
- 64 G. DeWall, *Chem. Eng. News*, 1982, **60**, 4–5.
- 65 D. Heseck, M. Lee, B. C. Noll, J. F. Fisher and S. Mobashery, *J. Org. Chem.*, 2009, **74**, 2567–2570.
- 66 E. Filali, G. Lloyd-Jones and D. Sale, *Synlett*, 2009, **2009**, 205–208.
- 67 D. Nasipuri, A. Bhattacharyya and B. G. Hazra, *Chem. Commun.*, 1971, 660–661.
- 68 J. C. Powers, R. Seidner and T. G. Parsons, *Tetrahedron Lett.*, **22**, 1713–1716.
- 69 C. H. Jin, H. Y. Lee, S. H. Lee, I. S. Kim and Y. H. Jung, *Synlett*, 2007, **2007**, 2695–2698.
- 70 R. B. Merrifield, *J. Am. Chem. Soc.*, 1963, **85**, 2149–2154.
- 71 B. Merrifield, *Science*, 1986, **232**, 341.
- 72 Nobel Media AB, The Nobel Prize in Chemistry 1984 - Robert Bruce Merrifield 'for his development of methodology for chemical synthesis on a solid matrix.', <https://www.nobelprize.org/prizes/chemistry/1984/summary/>, (accessed 18 April 2019).
- 73 US3772264 (A), 1973.
- 74 E. Bayer and M. Mutter, *Nature*, 1972, **237**, 512–513.
- 75 S. So, L. G. Peeva, E. W. Tate, R. J. Leatherbarrow and A. G. Livingston, *Chem. Commun.*, 2010, **46**, 2808–2810.

- 76 S. So, L. G. Peeva, E. W. Tate, R. J. Leatherbarrow and A. G. Livingston, *Org. Process Res. Dev.*, 2010, **14**, 1313–1325.
- 77 D. J. Gravert and K. D. Janda, *Chem. Rev.*, 1997, **97**, 489–510.
- 78 WO2011148177 (A2), 2011.
- 79 P. R. J. Gaffney, J. F. Kim, I. B. Valtcheva, G. D. Williams, M. S. Anson, A. M. Buswell and A. G. Livingston, *Chem. – Eur. J.*, 2015, **21**, 9535–9543.
- 80 R. Dong, R. Liu, P. R. J. Gaffney, M. Schaeperstoens, P. Marchetti, C. M. Williams, R. Chen and A. G. Livingston, *Nat. Chem.*, 2019, **11**, 136–145.
- 81 R. Rautenbach, *Membranverfahren: Grundlagen der Modul- und Anlagenauslegung*, Springer, 1996.
- 82 R. W. Baker, *Membrane Technology and Applications*, John Wiley & Sons, 2004.
- 83 P. Marchetti, M. F. Jimenez Solomon, G. Szekely and A. G. Livingston, *Chem. Rev.*, 2014, **114**, 10735–10806.
- 84 P. Vandezande, L. E. M. Gevers and I. F. J. Vankelecom, *Chem. Soc. Rev.*, 2008, **37**, 365–405.
- 85 G. Szekely, M. F. Jimenez-Solomon, P. Marchetti, J. F. Kim and A. G. Livingston, *Green Chem.*, 2014, **16**, 4440–4473.
- 86 H. K. Lonsdale, U. Merten and R. L. Riley, *J. Appl. Polym. Sci.*, 1965, **9**, 1341–1362.
- 87 E. A. Mason and H. K. Lonsdale, *J. Membr. Sci.*, 1990, **51**, 1–81.
- 88 G. M. Geise, D. R. Paul and B. D. Freeman, *Prog. Polym. Sci.*, 2014, **39**, 1–42.
- 89 J. Wang, D. S. Dlamini, A. K. Mishra, M. T. M. Pendergast, M. C. Y. Wong, B. B. Mamba, V. Freger, A. R. D. Verliefe and E. M. V. Hoek, *J. Membr. Sci.*, 2014, **454**, 516–537.
- 90 M. M. M. Abdulsalam Ebrahim, Imperial College London, 2018.
- 91 R. Abejón, A. Garea and A. Irabien, *AIChE J.*, 2014, **60**, 931–948.
- 92 A. Caus, L. Braeken, K. Boussu and B. Van der Bruggen, *J. Chem. Technol. Biotechnol.*, 2009, **84**, 391–398.
- 93 A. Caus, S. Vanderhaegen, L. Braeken and B. Van der Bruggen, *Desalination*, 2009, **241**, 111–117.
- 94 S. S. Gunderson, W. S. Brower, J. L. O’Dell and E. N. Lightfoot, *Sep. Sci. Technol.*, 2007, **42**, 2121–2142.
- 95 J. C.-T. Lin and A. G. Livingston, *Chem. Eng. Sci.*, 2007, **62**, 2728–2736.
- 96 F. P. McCandless, *J. Membr. Sci.*, 1994, **89**, 51–72.
- 97 F. P. McCandless, *J. Membr. Sci.*, 1999, **154**, 15–23.
- 98 N. V. Patil, A. E. M. Janssen and R. M. Boom, *Chem. Eng. Sci.*, 2014, **106**, 86–98.
- 99 N. V. Patil, T. Schotel, C. V. Rodríguez Gómez, V. Aguirre Montesdeoca, J. J. W. Sewalt, A. E. M. Janssen and R. M. Boom, *J. Chem. Technol. Biotechnol.*, 2016, **91**, 1478–1484.
- 100 L. Peeva, J. da S. Bural, I. Valtcheva and A. G. Livingston, *Chem. Eng. Sci.*, 2014, **116**, 183–194.
- 101 L. Peeva, J. Da Silva Bural, Z. Heckenast, F. Brazy, F. Cazenave and A. Livingston, *Angew. Chem.*, 2016, **128**, 13774–13777.
- 102 W. E. Siew, A. G. Livingston, C. Ates and A. Merschaert, *Sep. Purif. Technol.*, 2013, **102**, 1–14.
- 103 P. Kreis and A. Górak, *Chem. Ing. Tech.*, 2005, **77**, 1737–1748.
- 104 J. Micovic, K. Werth and P. Lutze, *Chem. Eng. Res. Des.*, 2014, **92**, 2131–2147.
- 105 T. Roth, P. Kreis and A. Górak, *Chem. Eng. Res. Des.*, 2013, **91**, 1171–1185.
- 106 L. S. White and A. R. Nitsch, *J. Membr. Sci.*, 2000, **179**, 267–274.
- 107 Patrizia Marchetti, Ludmila Peeva and Andrew Livingston, *Annu. Rev. Chem. Biomol. Eng.*, 2017, **8**, 473–497.
- 108 W. R. Bowen and J. S. Welfoot, *Chem. Eng. Sci.*, 2002, **57**, 1121–1137.
- 109 W. R. Bowen and J. S. Welfoot, *Chem. Eng. Sci.*, 2002, **57**, 1393–1407.
- 110 W. M. Deen, *AIChE J.*, 1987, **33**, 1409–1425.
- 111 J. F. Kim, A. M. Freitas da Silva, I. B. Valtcheva and A. G. Livingston, *Sep. Purif. Technol.*, 2013, **116**, 277–286.
- 112 J. Stawikowska and A. G. Livingston, *J. Membr. Sci.*, 2012, **413–414**, 1–16.
- 113 D.-Y. Koh, B. A. McCool, H. W. Deckman and R. P. Lively, *Science*, 2016, **353**, 804–807.

- 114 M. Schaepertoens, C. Didaskalou, J. F. Kim, A. G. Livingston and G. Szekely, *J. Membr. Sci.*, 2016, **514**, 646–658.
- 115 J. F. Kim, G. Szekely, I. B. Valtcheva and A. G. Livingston, *Green Chem.*, 2014, **16**, 133–145.
- 116 N. V. Patil, X. Feng, J. J. W. Sewalt, R. M. Boom and A. E. M. Janssen, *Sep. Purif. Technol.*, 2015, **146**, 261–267.
- 117 W. E. Siew, A. G. Livingston, C. Ates and A. Merschaert, *Chem. Eng. Sci.*, 2013, **90**, 299–310.
- 118 G. Nasser, T. Renouard, S. Shahane, C. Fischmeister, C. Bruneau and M. Rabiller-Baudry, *ChemPlusChem*, 2013, **78**, 728–736.
- 119 L. Peeva, J. da Silva Burgal, S. Vartak and A. G. Livingston, *J. Catal.*, 2013, **306**, 190–201.
- 120 M. Priske, K.-D. Wiese, A. Drews, M. Kraume and G. Baumgarten, *J. Membr. Sci.*, 2010, **360**, 77–83.
- 121 J. da Silva Burgal, L. G. Peeva, S. Kumbharkar and A. Livingston, *J. Membr. Sci.*, 2015, **479**, 105–116.
- 122 J. da Silva Burgal, L. Peeva, P. Marchetti and A. Livingston, *J. Membr. Sci.*, 2015, **493**, 524–538.
- 123 I. B. Valtcheva, S. C. Kumbharkar, J. F. Kim, Y. Bhole and A. G. Livingston, *J. Membr. Sci.*, 2014, **457**, 62–72.
- 124 I. B. Valtcheva, P. Marchetti and A. G. Livingston, *J. Membr. Sci.*, 2015, **493**, 568–579.
- 125 WO2017212246 (A1), .
- 126 P. G. M. Wuts and T. W. Greene, *Greene's protective groups in organic synthesis*, Wiley-Interscience, Hoboken, N.J, 4th ed., 2007.
- 127 M. A. Tius, *Benzyl Isopropenyl Ether* in *Encyclopedia of Reagents for Organic Synthesis*, ed. John Wiley & Sons, Ltd, John Wiley & Sons, Ltd, Chichester, UK, 2001.
- 128 T. Mukaiyama, M. Ohshima and M. Murakami, *Chem. Lett.*, 1984, **13**, 265–266.
- 129 T. Mukaiyama, M. Ohshima, H. Nagaoka and M. Murakami, *Chem. Lett.*, 1984, **13**, 615–618.
- 130 N. B. Lorette and W. L. Howard, *Org. Synth.*, 1962, **42**, 1–3.
- 131 C. B. Reese, R. Saffhill and J. E. Sulston, *J. Am. Chem. Soc.*, 1967, **89**, 3366–3368.
- 132 K. S. Whitaker and D. T. Whitaker, *2-Methoxypropene* in *Encyclopedia of Reagents for Organic Synthesis*, American Cancer Society, 2001.
- 133 J. Tian, Y.-D. Ding, T.-Y. Zhou, K.-D. Zhang, X. Zhao, H. Wang, D.-W. Zhang, Y. Liu and Z.-T. Li, *Chem. – Eur. J.*, 2014, **20**, 575–584.
- 134 P. Schmidt and P. Lutze, *J. Membr. Sci.*, 2013, **445**, 183–199.
- 135 C. Andecochea Saiz, S. Darvishmanesh, A. Buekenhoudt and B. Van der Bruggen, *J. Membr. Sci.*, 2018, **546**, 120–127.
- 136 Y. Thiermeyer, S. Blumenschein and M. Skiborowski, *J. Membr. Sci.*, 2018, **567**, 7–17.
- 137 A. Böcking, V. Koleva, J. Wind, Y. Thiermeyer, S. Blumenschein, R. Goebel, M. Skiborowski and M. Wessling, *J. Membr. Sci.*, 2019, **575**, 217–228.
- 138 F.-X. Felpin and E. Fouquet, *Synthesis*, 2011, **2011**, 2893–2896.
- 139 S. Nimmig and M. Kaspereit, *Chem. Eng. Process. Process Intensif.*, 2013, **67**, 89–98.
- 140 J. F. Kim, G. Szekely, M. Schaepertoens, I. B. Valtcheva, M. F. Jimenez-Solomon and A. G. Livingston, *ACS Sustain. Chem. Eng.*, 2014, **2**, 2371–2379.
- 141 I. Sereewatthanawut, F. W. Lim, Y. S. Bhole, D. Ormerod, A. Horvath, A. T. Boam and A. G. Livingston, *Org. Process Res. Dev.*, 2010, **14**, 600–611.
- 142 E. M. Rundquist, C. J. Pink and A. G. Livingston, *Green Chem.*, 2012, **14**, 2197–2205.
- 143 R. M. Gould, L. S. White and C. R. Wildemuth, *Environ. Prog.*, 2001, **20**, 12–16.
- 144 C. Didaskalou, S. Buyuktiryaki, R. Kecili, C. P. Fonte and G. Szekely, *Green Chem.*, 2017, **19**, 3116–3125.
- 145 T. Fodi, C. Didaskalou, J. Kupai, G. T. Balogh, P. Huszthy and G. Szekely, *ChemSusChem*, 2017, **10**, 3435–3444.
- 146 T. Bednaříková, Z. Tošner, J. Horský and J. Jindřich, *J. Incl. Phenom. Macrocycl. Chem.*, 2015, **81**, 141–152.
- 147 S. D. Walker, C. J. Borths, E. DiVirgilio, L. Huang, P. Liu, H. Morrison, K. Sugi, M. Tanaka, J. C. S. Woo and M. M. Faul, *Org. Process Res. Dev.*, 2011, **15**, 570–580.
- 148 J.-N. Zhang, H. Li, W. Zhou, S.-L. Yu, D.-H. Qu and H. Tian, *Chem. – Eur. J.*, 2013, **19**, 17192–17200.

- 149 H. Jiang, J. Jia, A. Shkurenko, Z. Chen, K. Adil, Y. Belmabkhout, L. J. Weselinski, A. H. Assen, D.-X. Xue, M. O’Keeffe and M. Eddaoudi, *J. Am. Chem. Soc.*, 2018, **140**, 8858–8867.
- 150 D. Sun, Y. Ke, T. M. Mattox, S. Parkin and H.-C. Zhou, *Inorg. Chem.*, 2006, **45**, 7566–7568.
- 151 H. Furukawa, N. Ko, Y. B. Go, N. Aratani, S. B. Choi, E. Choi, A. Ö. Yazaydin, R. Q. Snurr, M. O’Keeffe, J. Kim and O. M. Yaghi, *Science*, 2010, **329**, 424–428.
- 152 H. C. Brown, S. Krishnamurthy and J. L. Hubbard, *J. Am. Chem. Soc.*, 1978, **100**, 3343–3349.
- 153 D. Peng, M. Zhang and Z. Huang, *Chem. – Eur. J.*, 2015, **21**, 14737–14741.
- 154 P. Belser, A. von Zelewsky, M. Frank, C. Seel, F. Vogtle, L. De Cola, F. Barigelletti and V. Balzani, *J. Am. Chem. Soc.*, 1993, **115**, 4076–4086.
- 155 C. Steinem, A. Janshoff, K. von dem Bruch, Karsten Reihls, J. Goossens and H.-J. Galla, *Bioelectrochem. Bioenerg.*, 1998, **45**, 17–26.
- 156 M. Glaser, H. Karlsen, M. Solbakken, J. Arukwe, F. Brady, S. K. Luthra and A. Cuthbertson, *Bioconjug. Chem.*, 2004, **15**, 1447–1453.
- 157 N. Khiar, R. Navas, E. Elhalem, V. Valdivia and I. Fernández, *RSC Adv.*, 2013, **3**, 3861–3864.
- 158 N. Khiar, M. P. Leal, R. Baati, C. Ruhlmann, C. Mioskowski, P. Schultz and I. Fernández, *Chem. Commun.*, 2009, 4121–4123.
- 159 M. P. Leal, M. Assali, I. Fernández and N. Khiar, *Chem. – Eur. J.*, 2011, **17**, 1828–1836.
- 160 D. Liu, L. A. Gugliotti, T. Wu, M. Dolska, A. G. Tkachenko, M. K. Sipton, B. E. Eaton and D. L. Feldheim, *Langmuir*, 2006, **22**, 5862–5866.
- 161 C. A. Hurley, J. B. Wong, J. Ho, M. Writer, S. A. Irvine, M. J. Lawrence, S. L. Hart, A. B. Tabor and H. C. Hailes, *Org. Biomol. Chem.*, 2008, **6**, 2554–2559.
- 162 Q. Zhang, H. Ren and G. L. Baker, *Tetrahedron Lett.*, 2014, **55**, 3384–3386.
- 163 C. Kim, B. A. Ondrusek and H. Chung, *Org. Lett.*, 2018, **20**, 736–739.
- 164 Q. Zhang, H. Ren and G. L. Baker, *J. Org. Chem.*, 2014, **79**, 9546–9555.
- 165 C. Kim and H. Chung, *J. Org. Chem.*, 2018, **83**, 9787–9794.
- 166 S. Z. Perry and H. Hibbert, *Can. J. Res.*, 1936, **14b**, 77–83.
- 167 R. Fordyce, E. L. Lovell and H. Hibbert, *J. Am. Chem. Soc.*, 1939, **61**, 1905–1910.
- 168 V. K. J. Rauterkus, H. G. Schimmel and W. Kern, *Makromol. Chem.*, 1961, **50**, 166–178.
- 169 B. Bömer, W. Heitz and W. Kern, *J. Chromatogr. A*, 1970, **53**, 51–54.
- 170 C. Booth, J. M. Bruce and M. Buggy, *Polymer*, 1972, **13**, 475–478.
- 171 V. P. Privalko and A. P. Lobodina, *Eur. Polym. J.*, 1974, **10**, 1033–1038.
- 172 F. Davis and S. Higson, *Macrocycles: Construction, Chemistry and Nanotechnology Applications*, John Wiley & Sons, Ltd., 2011.
- 173 A. Marshall, R. H. Mobbs and C. Booth, *Eur. Polym. J.*, 1980, **16**, 881–885.
- 174 Y. Kuroda and M. Kubo, *J. Polym. Sci.*, 1959, **36**, 453–459.
- 175 P. H. Elworthy and C. B. Macfarlane, *J. Chem. Soc. Resumed*, 1962, 537–541.
- 176 R. Fordyce and H. Hibbert, *J. Am. Chem. Soc.*, 1939, **61**, 1910–1911.
- 177 The Dow Chemical Company, CARBOWAX Polyethylene Glycols, http://msdssearch.dow.com/PublishedLiteratureDOWCOM/dh_0865/0901b8038086527b.pdf?filepath=polyglycols/pdfs/noreg/118-01789.pdf&fromPage=GetDoc, (accessed 26 May 2019).
- 178 S. Rebsdatt and D. Mayer, *Ethylene glycol* in *Ullmann’s Encyclopedia of Industrial Chemistry*, American Cancer Society, 2000.
- X1 SHELXTL v5.1, Bruker AXS, Madison, WI, 1998.
- X2 SHELX-2013, G.M. Sheldrick, *Acta Crystallographica* **2015**, C71, 3–8.
- X3 A.L. Spek (2003, 2009) PLATON, A Multipurpose Crystallographic Tool, Utrecht University, Utrecht, The Netherlands. See also A.L. Spek, *Acta Crystallographica* **2015**, C71, 9–18.